SOFT COMPARTMENTALIZED POLYMER COLLOIDS:

JANUS PARTICLES, MULTICOMPARTMENT STRUCTURES,

INORGANIC-ORGANIC HYBRIDS AND APPLICATIONS

DISSERTATION

zur Erlangung des akademischen Grades eines

Doktors der Naturwissenschaften (Dr. rer. nat.)

im Fach Chemie der Fakultät für Biologie, Chemie und Geowissenschaften

der Universität Bayreuth

vorgelegt von

Andreas Walther

Geboren in Coburg / Deutschland

Bayreuth, 2008

Die vorliegende Arbeit wurde in der Zeit von Februar 2006 bis Juni 2008 in Bayreuth am Lehrstuhl Makromolekulare Chemie II unter der Betreuung von Herrn Prof. Dr. Axel H. E. Müller angefertigt.

Dissertation eingereicht am: 08.07.2008

Zulassung durch die Promotionskommission: 23.07.2008

Wissenschaftliches Kolloquium: 29.10.2008

Amtierender Dekan: Prof. Dr. A. H. E. Müller (Erstgutachter)

Prüfungsausschuss: Prof. H. Alt (Vorsitz)

Prof. Dr. A. Böker (Zweitgutachter)

Prof. Dr. T. Hellweg

„Ob man die Wüste auch lieben kann, weiss ich nicht, aber sie ist es die meinen Schatz birgt."

Paulo Coelho
Der Alchimist

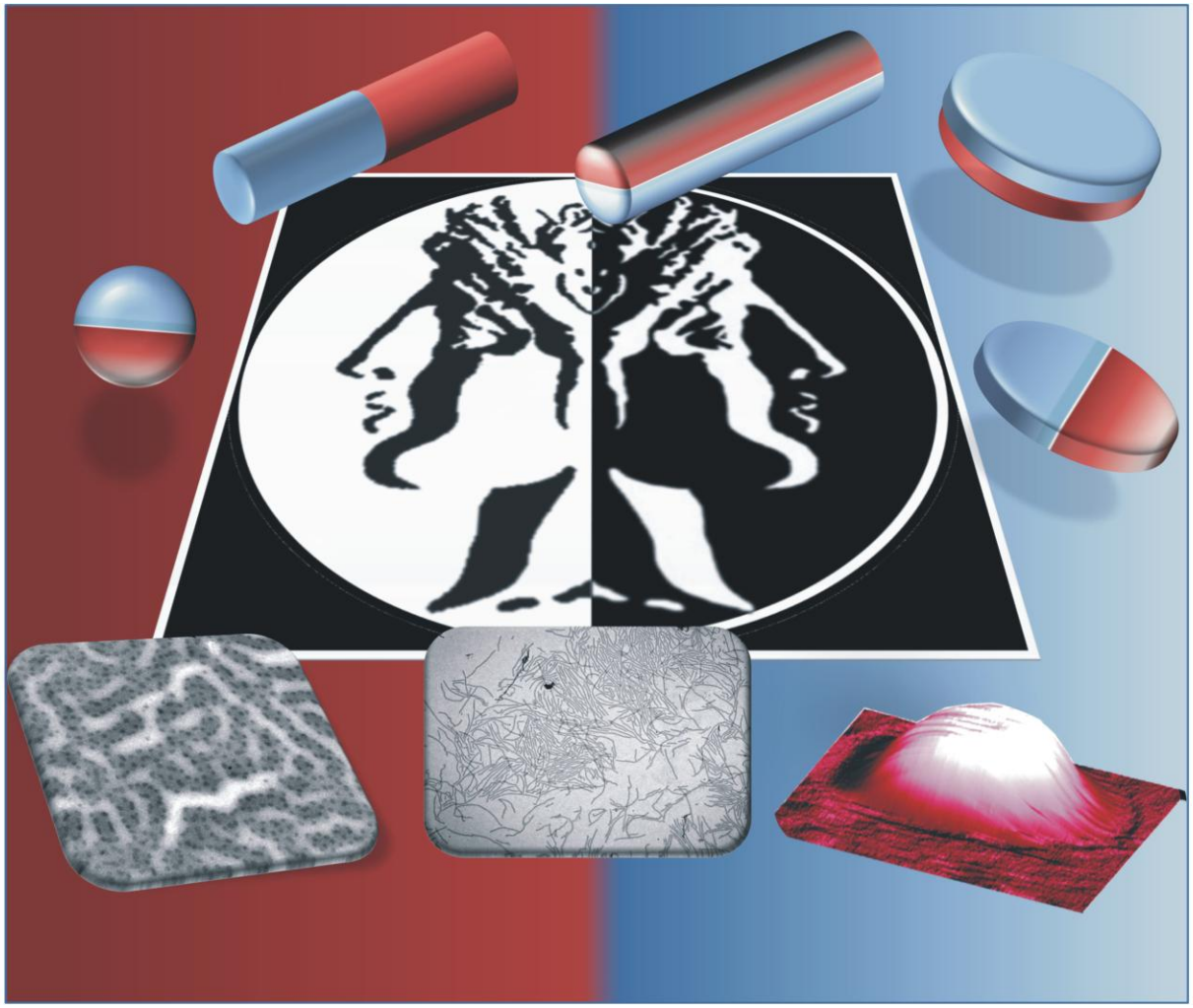

Meiner Familie

Summary

Compartmentalized polymer-based colloids with nanoscopic dimensions and different topologies were prepared based on various block copolymer architectures. The polymers were prepared via anionic polymerization or a controlled radical polymerization technique (RAFT). Self-assembly both in solution and in bulk were rigorously exploited to create the multicompartment architectures. Several new crosslinking strategies, in bulk and in solution, were thoroughly investigated to allow a controlled preservation and a high shape-persistence of the colloidal particles even when exposed to non-selective solvents.

Cylindrical and disc-like Janus particles were investigated according to their self-assembly behavior into superstructures. The Janus discs undergo back-to-back stacking in organic solvent. In aqueous solution, a size-dependent aggregation was found. While the smaller Janus discs are unimolecularly dissolved with a significant polystyrene surface exposed to the water, the larger Janus sheets can shield the insoluble side by a large bending in an intramolecular fashion. Janus cylinders self-assemble on two hierarchical levels. Upon exposure to a selective solvent, they self-organize into fibers. The length of these fibers depends on the concentration and a critical aggregation concentration exists below which self-assembly is absent. Secondly, the Janus cylinders form fibrillar networks with tunable pore sizes when deposited from more concentrated solution.

The surface-active properties of spherical Janus particle were exploited for the investigation of two possible applications of both academic and industrial relevance. In Pickering emulsion polymerization, extremely well-defined latexes with long-term stability could be prepared in a very facile fashion. A control of the particle size by changing the concentration of Janus particles could easily be achieved. Secondly, the nanostructuring of polymer blends was shown for a PS/PMMA model system. The system exhibits a control on two length scales. The first is the controlled decrease of the domains of the dispersed phase and the second is the controlled spacing between the particles at the interface. The particles are exclusively located at the interface and the nanostructuring can be obtained while matching macroscopic processing constraints, i.e. high-shear blending in a mini mixer.

The self-assembly of bis-hydrophilic triblock terpolymers with two outer hydrophobic blocks was investigated for a variety of different hydrophilic end blocks. The overall architecture of the solution structures could be tailored by changing the hydrophobic-to-hydrophilic balance. Additionally, the interaction between the corona-forming blocks has an influence on the particle shapes as well. The micelles possess coronas with appealing and tunable properties, due to the presence of a hydrophobic core and hydrophilic biocompatible and stimuli-responsive segments.

The self-assembly of miktoarm star terpolymers, bearing arms of polystyrene (PS), polybutadiene (PB) and poly(2-vinylpyridine) (P2VP), was analyzed both in solution as well as in the bulk state. In solution, the miktoarm star terpolymers form multicompartment micelles with a glassy (PS) and a soft compartment (PB), all rendered water-soluble by the P2VP corona. Strikingly, the soft PB compartments show hydrophobic bridges in aqueous medium which is of high interest as they can be used as a second motif for sensing, adhesion control or interaction with cellular membranes.

The transfer of a hexagonally ordered cylindrical bulk phase via crosslinking of the PB domain of a bulk structure of a similar miktoarm star terpolymer allowed the preparation of novel multicompartment cylinders. The structures possess perfectly parallel aligned compartments. Two symmetric and opposing PS and P2VP compartments surround a central ribbon-like PB compartment. The P2VP compartments could be used to generate perfectly aligned bi-axial nanowires inside spatially separated compartments within close proximity. Due to the presence of an amphiphilic corona, the extent of the compartmentalization can be tuned from separated nanowires into one homogenous nanowire simply by exchanging the solvent. The complexity and high control of the structure of this multicompartment cylinder is unmatched and can most likely not be obtained by solution based self-assembly.

In a third part, the controlled crosslinking of polybutadiene-*block*-poly(2-vinylpyridine) (PB-*b*-P2VP) block copolymers was investigated towards the preparation of shape-persistent templates for inorganic-organic hybrid materials. The in-depth analysis of the self-assembly behavior of several diblock copolymers in dioxane/water mixtures revealed the presence of a multitude of colloidal aggregates, and to the discovery of a new mechanism for the phase transition from cylindrical micelles to vesicles. The shapes of the aggregates could be locked via a simple photo-crosslinking procedure and allowed their transfer into non-selective solvents under retention of their shape.

In a second approach, a cylindrical bulk phase of the PB-*b*-P2VP block copolymers was crosslinked, yielding core-crosslinked compartmentalized nanorods. These nanorods were used for the conjugation with keggin-type polyoxometalates. The resulting hybrid materials show very well-defined rod-like structures and possess high surface-areas. They serve as catalyst carriers in current investigations.

Zusammenfassung

Kompartimentierte Polymerkolloide von nanoskopischer Größenordnung und mit verschiedenen Topologien wurden auf der Grundlage verschiedenartiger Blockcopolymerarchitekturen synthetisiert. Die Polymere wurden über anionische Polymerisation oder eine kontrollierte radikalische Polymerisationstechnik (RAFT) synthestisiert. Die Selbstorganisation sowohl in Lösung als auch im Festkörper wurde ausgenutzt um die Multikompartimentstrukturen zu erzeugen. Mehrere neue Vernetzungsmethoden, im Festkörper und in Lösung, wurden sorgfältig untersucht um eine kontrollierte Bewahrung und eine hohe Formbeständigkeit der kolloidalen Partikel zu ermöglichen, selbst wenn sie unselektiven Lösungsmitteln ausgesetzt werden.

Die Selbstorganisation zylindrischer und scheibchenförmiger Janus-Partikel in Superstrukturen wurde untersucht. Die Janusscheibchen zeigen „back-to-back stacking“ in organischen Lösungsmitteln. In wässriger Lösung konnte eine größenabhängige Aggregation festgestellt werden. Während die kleineren Janusdisks auf unimolekulare Art und ungestappelt dispergiert sind, können die größeren Janusplättchen die unlösliche Seite auf intramolekulare Art durch eine ausgeprägte Biegung abschirmen. Januszylinder zeigen Selbstorganisation auf zwei hierarchischen Ebenen. Werden sie einem selektiven Lösungmittel ausgesetzt, findet eine Selbstorganisation in Fasern statt, deren Länge konzentrationsabhängig ist. Außerdem existiert eine kritische Aggregationskonzentration unterhalb derer eine Selbstorganisation nicht zu beobachten ist. Als zweite Möglichkeit bilden die Januszylinder fibrillare Netzwerke mit einstellbaren Porengrößen im Falle der Abscheidung aus einer konzentrierteren Lösung.

Die oberflächenaktiven Eigenschaften sphärischer Janus-Partikel wurden für die Untersuchung zweier möglicher Anwendungen, die sowohl von akademischer als auch industrieller Relevanz sind, genutzt. Im Falle der Pickering-Emulsionspolymerisation konnten überaus gut definierte Latexpartikel, die eine gute Langzeitstabilität aufweisen, auf sehr einfache Art und Weise synthetisiert werden. Eine Kontrolle der Partikelgröße über die Änderung der Konzentration an Janus-Partikeln konnte problemlos erreicht werden. Zweitens wurde die Nanostrukturierung von Polymer-Blends für ein PS/PMMA Modellsystem gezeigt. Das System weist eine Kontrolle auf zwei Längenskalen auf. Erstens die kontrollierte Abnahme der Domänengrößen der dispergierten Phase und zweitens die kontrollierte Anordnung der Partikel an der Grenzfläche. Die Partikel befinden sich ausschließlich an der Grenzfläche und die Nanostrukturierung kann auch unter Berücksichtigung makroskopischer Prozesseinschränkungen, d.h. beim Mischen unter hoher Scherung in einem Doppleschneckenminimixer, erreicht werden.

Die Selbstorganisation bis-hydrophiler Triblockterpolymere mit zwei äußeren hydrophilen Blöcken wurde für eine Auswahl verschiedener hydrophiler Endblöcke untersucht. Die Gesamtarchitektur der Strukturen in Lösung konnte durch Änderung des Verhältnisses von hydrophilem zu hydrophobem Anteil angepasst werden. Zusätzlich haben die Wechselwirkungen zwischen den die Korona bildenden Blöcken einen Einfluss auf die Partikelform. Aufgrund des Vorhandenseins eines hydrophoben Kerns und hydrophiler biokompatibler und auf äußere Stimuli ansprechender Segmente, besitzen die Mizellen Koronen mit attraktiven und einstellbaren Eigenschaften.

Die Selbstorganisation von Miktoarm-Sternterpolymeren, mit Armen aus Polystyrol (PS), Polybutadien (PB) und Poly(2-vinyl pyridin) (P2VP), wurde sowohl in Lösung als auch im

Festkörper ausgenutzt. In Lösung bilden die Miktoarm-Sternterpolymere Multikompartimentmizellen mit einem glasartigen (PS) und einem weichen Kompartiment (PB), alle wasserlöslich aufgund der P2VP Korona. Auffallenderweise zeigen die weichen PB Kompartimente hydrophobe Härchen im wässrigen Medium, was von großem Interesse ist, da sie als ein zweites Strukturmotiv, neben der hydrophilen Korona, für die Sensorik, Adhäsionskontrolle oder für Wechselwirkungen mit zellulären Membranen dienen können.

Der Transfer einer wohlgeordneten hexagonalen zylindrischen Volumenphase durch Vernetzung der PB Domäne einer Morphologie eines ähnlichen Miktoarm-Sternterpolymer ermöglichte die Präparation neuartiger Multikompartimentzylinder. Die Strukturen besitzen vollkommen parallel angeordnete Kompartimente. Jeweils zwei symmetrische und gegenüberliegende PS- und P2VP-Kompartimente umgeben ein zentrales bandförmiges PB-Kompartiment. Die P2VP-Kompartimente konnten für die Generierung vollkommen linear angeordneter bi-axialer Nanodrähte innerhalb räumlich separierter Kompartimente, und doch in nächster Nähe zueinander befindlich, genutzt werden. Aufgrund der Anwesenheit einer amphiphilen Korona kann das Ausmaß der Kompartimentierung von separierten Nanodrähten hin zu einem homogenen Nanodraht auf einfache Weise durch Austausch des Lösungsmittels eingestellt werden. Die Komplexität und hohe Kontrolle der Struktur dieser Multikompartimentzylinder sucht ihresgleichen und kann mit hoher Wahrscheinlichkeit nicht ausgehend von Selbstorganisation in Lösung erhalten werden.

Im dritten Teil wurde die kontrollierte Vernetzung von Polybutadiene-*block*-Poly(2-vinyl pyridin) (PB-*b*-P2VP) Blockcopolymeren im Hinblick auf die Synthese formbeständiger Template für anorganisch-organische Hybridmaterialien untersucht. Die eingehende Analyse des Selbstorganisationsverhaltens mehrerer Diblockcopolymere in Dioxan/Wasser-Mischungen zeigte die Anwesenheit einer Vielzahl von kolloidalen Aggregaten und führte zur Entdeckung eines neuen Mechanismus für den Phasenübergang von zylindrischen Mizellen zu Vesikeln. Die Formen der Aggregate konnten durch einen einfachen Photovernetzungsvorgang fixiert werden, wodurch ihr Transfer in nichtselektive Lösungsmittel unter Beibehaltung ihrer Form ermöglicht wurde.

In einem zweiten Ansatz wurde eine zylindrische Volumenphase eines PB-*b*-P2VP Blockcopolymers vernetzt. Dies resultierte in kernvernetzten kompartimentierten Nanostäbchen. Diese Nanostäbchen wurden für die Konjugation mit Polyoxometalaten vom Keggin-Typ verwendet. Die resultierenden Hybridmaterialien zeigten wohldefinierte stäbchenförmige Strukturen und besitzen eine große Oberfläche. Sie dienen als Katalysatorträger in derzeit laufenden Untersuchungen.

Introduction

The discovery and introduction of block copolymers had a seminal effect on developments in polymer, colloidal and materials science. Block copolymers are composed of at least two polymers which are covalently linked together and thus enable the combination of decisive properties for multicomponent systems. The properties of this unique class of materials are of fundamental and academic, as well as of industrial interest. Together with a broader and deeper fundamental understanding of the thermodynamics and kinetics involved in the complex self-assembly processes, it has been possible to apply block copolymers to a multitude of demanding problems regarding the development of novel materials in all fields of science. The application areas may reach from tunable photonic band gap materials,[1, 2] nano-sized lithographic masks,[3, 4] inorganic-organic hybrid materials,[5-14] membrane science[15, 16] to advanced drug delivery systems[17-29] or tissue scaffolds, thus bridging all fields of science starting from physics over materials science to biomedical applications. All of these applications are only possible, when researchers make clever use of the precise self-organization of these soft matter systems. The developments have so far been possible due to major advances in the controlled/living polymerization techniques, allowing for the precise synthesis of well-defined tailor-made polymers. The precise macromolecular engineering enables the realization of more complex polymeric topologies which translates into a higher sophistication of self-assembled systems, exceeding the relatively simple structures from common diblock copolymers largely.

One of the inherent and most fascinating structural motifs in block copolymers is the presence of segments of different chemistry and physical properties within close proximity. By means of self-assembly, either concentration driven or induced by solvent selectivity, these polymer chains can be self-organized into compartmentalized structures. Due to their unlike properties, the compartments can be individually addressed and further functionalized to yield highly sophisticated delivery devices, catalyst carriers or building blocks for further directed self-assembly into hierarchical superstructures. With growing complexity of the polymer topology, the complexity and the structural variety of the self-assembled structures, both in solution and bulk, increase. The aim of this thesis is centered on the generation of compartmentalized polymeric nanoparticles, the evaluation of their self-assembly behavior, the generation of inorganic-organic hybrid materials and the application of those for current topics in materials science such as catalysis, emulsion technology and nanocomposite materials. Within the scope of this thesis, I made use of a variety of polymerization techniques such as living anionic, controlled radical, emulsion polymerization and crosslinking reactions in the bulk and solution state. Likewise, both self-assembly in solution as well as in the bulk state was rigorously exploited with the aim of utilizing these as tools for the generation of novel materials with advanced properties. Therefore, the following introduction will not contain extensive reviews on polymerization techniques and self-assembly, not the least as they are fundamentally understood to a large extent. On the contrary, I will stress the current state-of-the-art of compartmentalized polymeric particles and their applications. Some of the structures researched within this thesis (e.g. Janus particles and multicompartment micelles) are of unmatched complexity and their applications led to the discovery of novel properties both relevant for academic research as well as for industrial applications.

Compartmentalized Particles

General Remarks

The generation of polymeric colloidal particles with dimension and compartments in the sub-micron size region remains a challenging task. Most of the so-called “top-down” approaches, in which a structure is imposed onto a material, stay behind with limited success. Whereas lithography has proven to be a highly efficient technique for the formation of precisely structured dimensions on surfaces and also to some extent in the bulk state (via the two photon excitation technique) the transfer of this technique into the preparation of significant quantities of nano-sized compartmentalized polymeric particles still has limitations. The best lithographic patterning devices, within microfluidic channels, achieve micron-sized compartments and particles.[30-35] Despite further expected developments in this promising field, some limitations will certainly persist as lithography in hard contact mode is hardly possible for microfluidic devices. Similarly, the second important patterning approach via electrospinning using multifaceted tips has so far at its best led to particles in size ranges starting from several hundred nanometers to many micrometers.[36, 37] In general, both techniques have a great potential of being refined to higher structural resolution and represent certainly very versatile methods, especially when it comes to large-scale parallel synthesis.

However, many applications, no matter whether they are conceived in body fluids or in material science, require the preparation of very small nanoscopic particles. For instance, it is not reasonable to inject micrometer sized drug carriers into the vesicular system of a human body as they can clog small blood vessels. Likewise, when thinking about materials science, a structuring of emulsions, block copolymers or polymer blends with micron-sized particles is not useful as the desired domain sizes clearly range in the nanometer region. Consequently, there is a strong need for the development of processes leading to stable, nanometer-sized particles with internal organization and functionality.

The structuring of polymeric particles with compartments exhibiting nanoscopic features remains a clear key domain of self-assembly processes, representing “bottom-up” approaches. Among those, block copolymers are an ideal system for the generation of compartmentalized particles. They are not only relatively readily accessible via the on-going progress in synthetic techniques, but also their self-assembly behavior, both in bulk and solution, are sufficiently understood. Furthermore, the typical structural features are in the size range of tens to a few hundreds of nanometer, rendering them ideally suited for applications in the mesotechnology. Together with the tunability of the composition of the block copolymers, triggered by recent progress in controlled polymerization techniques, a large range of desired physical and chemical properties is accessible. This substantially broadens the range of applications.

Preparation of Compartmentalized Particles with Block Copolymers

Due to the inherent immiscibility of most polymers and the accompanying energetic penalties, block copolymers are known to undergo microphase segregation in the bulk state into highly organized and complex morphologies. Similarly, amphiphilic block copolymers self-assemble in selective solvents into well-defined micellar aggregates.[38-41]

In the simplest case, the structures formed by diblock copolymers in solution are two types of spherical micelles (star-like and crew-cut), cylindrical micelles and vesicles (see Scheme 1 - 1). The appearance of a certain morphology depends on the volume fractions of the blocks and the environmental parameters, such as temperature, salinity and pH.

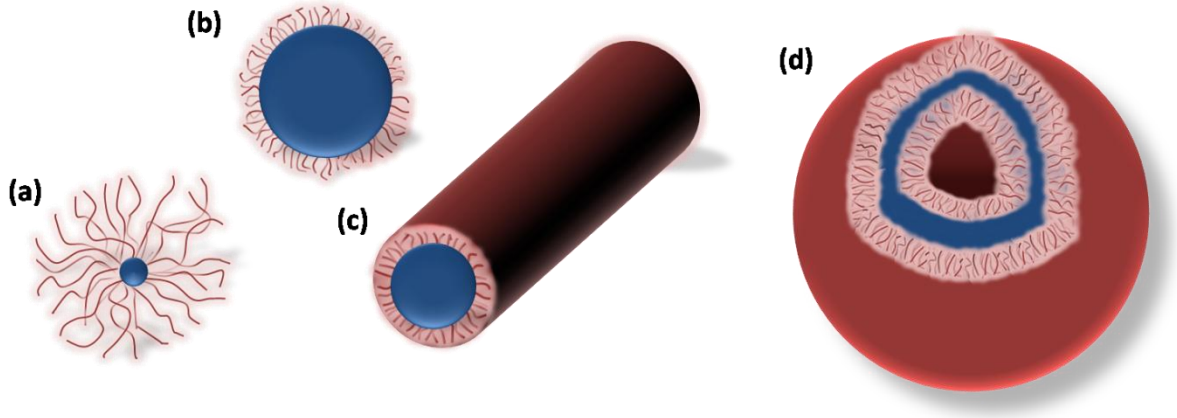

Scheme 1 - 1. Four major types of self-assembled colloidal aggregates formed by amphiphilic diblock copolymers in aqueous solution. Spherical star-like (a), spherical crew-cut micelles (b), cylindrical micelles (c) and vesicles (d).

Many researchers, e.g. Eisenberg, Discher, Armes, Wooley and Förster,[6, 11, 12, 42-62] only to name a few, have conducted in-depth studies of the preparation and stability of these systems. The structures typically possess a hydrophobic and a hydrophilic compartment. The hydrophilic compartment is sub-divided into one interior and one exterior in case of vesicles. One major drawback inherent to these self-assembled structures is their limited stability in non-selective solvents and their tendency to undergo morphological changes depending on the environmental conditions. In particular with respect to applications this has some major consequences. For instance in catalysis, the application of such micelles as carrier for inorganic nanoparticles is limited to solvents where the carrier structure persists. The tendency of forming defined aggregates is low when the block copolymer is exposed to a good solvent for both blocks, thus limiting the application range as nanoreactors or nanocontainers. For instance, micelles with polystyrene as inner block disassemble in most organic solvents and are thus not of wide applicability. Many catalytic reactions are however carried out in relatively non-selective solvents to provide sufficient solubility for a wide range of educts and products. Likewise, the utilization of non-crosslinked structures as templates for the preparation of mesoporous inorganic materials is restricted as structural rearrangements are possible. In order to overcome these problems, significant efforts have been undertaken to crosslink the shell or the core of

self-assembled nanoobjects.[63-69] Mostly, the approaches use considerable synthetic efforts in modifying parts of the structures for the crosslinks or require facilities that are not readily available, as e.g. γ-sources.[69] Therefore, a need for facile crosslinking strategies of general applicability still exists.

A different approach for overcoming the problems related to crosslinking dynamic micelles is the transfer of polymer bulk structures into solution via the selective crosslinking of a non-continuous phase of microphase-segregated block copolymer morphologies. Additionally, the variety in microphase-segregated morphologies provides another efficient and excellent tool for the preparation of polymeric multicompartment particles. In general, the variety of structures increases with rising complexity of the polymer architecture. Whereas diblock copolymers usually only exhibit five different morphologies (spherical, cylindrical, gyroidal, perforated lamella and lamella), triblock terpolymer and three or four arm miktoarm star polymers provide a vast multitude of structures. Figure 1 - 1 displays the theoretical phase diagram of a typical diblock copolymer, as well as the experimental ternary phase diagrams of polystyrene-*block*-polybutadiene-*block*-poly(methyl methacrylate) (SBM) triblock terpolymers as developed in a pioneering work by Stadler and coworkers, and the bulk morphologies of a miktoarm star terpolymer system, bearing arms of polystyrene, polybutadiene and poly(2-vinylpyridine).[70-72] It can be seen that a slight variation in the weight fractions of the constituents leads to significant changes in the microphase morphologies.

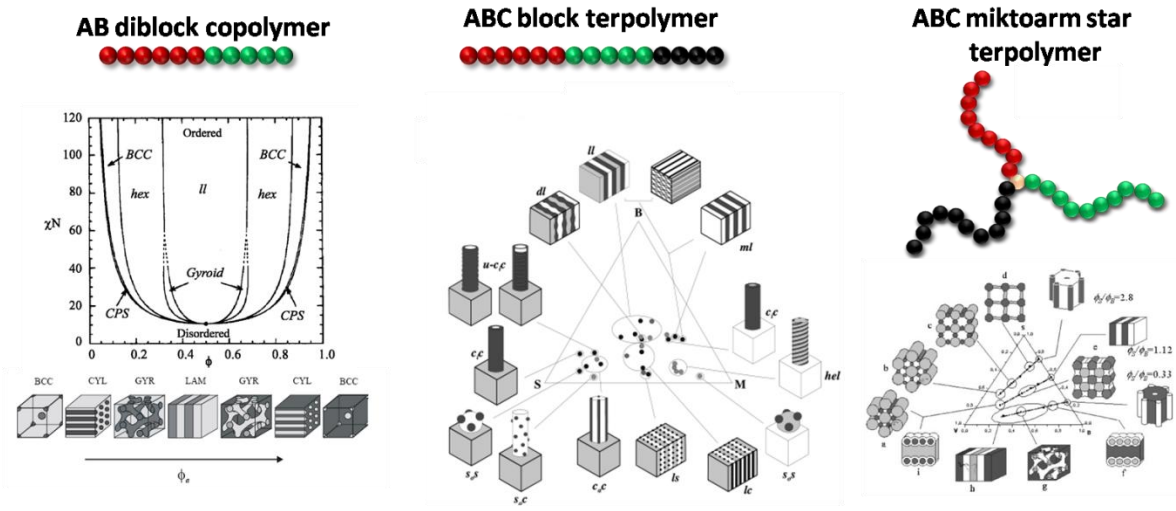

Figure 1 - 1. Theoretical binary phase diagram of diblock copolymers (left). Ternary phase diagram of linear SBM triblock terpolymers (center). The color code corresponds to the observed grey shades obtained from TEM images of thin films after staining with OsO_4: polystyrene - grey, polybutadiene - black and poly(methyl methacrylate) – white. Ternary phase diagram of SBV miktoarm star terpolymers (right). The color code corresponds to the observed grey shades obtained from TEM images of thin films after staining with OsO_4 and I_2: polystyrene - white, polybutadiene - black and poly(2-vinylpyridine) – grey.

Just for monitoring one example, the changes in morphology are shown for increasing the fraction of the inner polybutadiene block, while keeping the end blocks symmetric (see Figure 1 - 2). Five different morphologies can be observed, from which the first three can be used to create Janus particles.

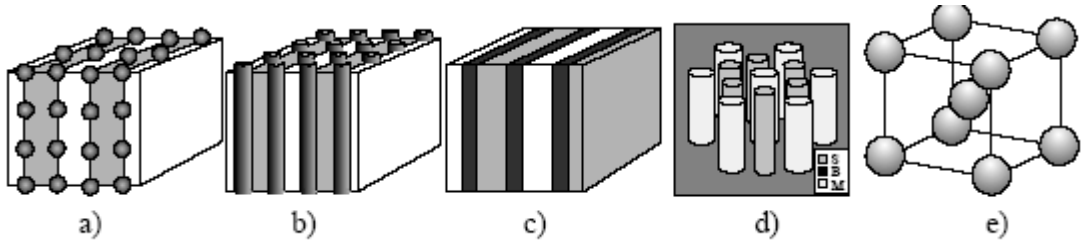

Figure 1 - 2. SBM-morphologies for terpolymers with symmetric end blocks. The polybutadiene volume fraction increases from left to right. a) ls = lamella sphere ($S_{45}B_6M_{49}^{225}$), b) lc = lamella cylinder($S_{48}B_{17}M_{35}^{238}$), c) ll = lamella lamella ($S_{24}B_{38}M_{38}^{245}$), d) cylinders in PB-matrix ($S_{23}B_{57}M_{20}^{215}$), e) mixed sphere of PS and PMMA in PB-matrix ($S_{11}B_{84}M_5^{97}$).[73]

The essential principle behind transferring polymeric bulk structures into solution is rather straight-forward, convincing and can lead to particles of unmatched complexity. In a first step, a polymer has to be designed which is capable of undergoing crosslinking by any kind of means. The only prerequisite is that the segment does not form the major, continuous phase. Secondly, to target a specific structure, the weight fractions of the block copolymer need to be adjusted and the interaction parameters between the various blocks need to be considered. Whereas this is fairly simple for diblock copolymers, the complexity rises for triblock terpolymers etc. Not every morphology shown in Figure 1 - 1 can be obtained for every triblock terpolymer. In a last step the morphology in the bulk state is crosslinked and transferred into solution. Depending on the target structure, ultrasound may assist the dissolution, in particular for cylindrical or lamellar structures. Depending on the crosslinking method, which may involve swelling solvents and reactive chemicals to be introduced or co-casted, the morphological transitions have to be monitored at all stages of the process. Slight variations in solvent quality may especially have an influence in case of the various morphologies of triblock terpolymers, reacting very sensitively to changes in the environment.

Keeping all these factors in mind, the transfer of block copolymer structures from the bulk state into solution via crosslinking represents a unique and astonishingly simple methodology to create multicompartment particles of unprecedented complexity. The particles are not only internally structured in a complex way, moreover their structures may in some cases never be accessible with self-assembly processes of the even most complex amphiphiles in solution. Thus this way represents a very powerful strategy and is surprisingly rare in literature as compared to self-assembly processes of amphiphilic polymers into colloids.

To further illustrate this procedure, the preparation of Janus particles and helical cylinders is shown in the following. In all cases linear triblock terpolymers are used as starting materials. The strategy is schematically outlined for the Janus particles and experimental results are shown for the helixes. The latter example demonstrates the powerful capabilities as even the most complex structures with limited thermodynamic stability, such as the helical morphology of SBM terpolymers, can easily be transferred.

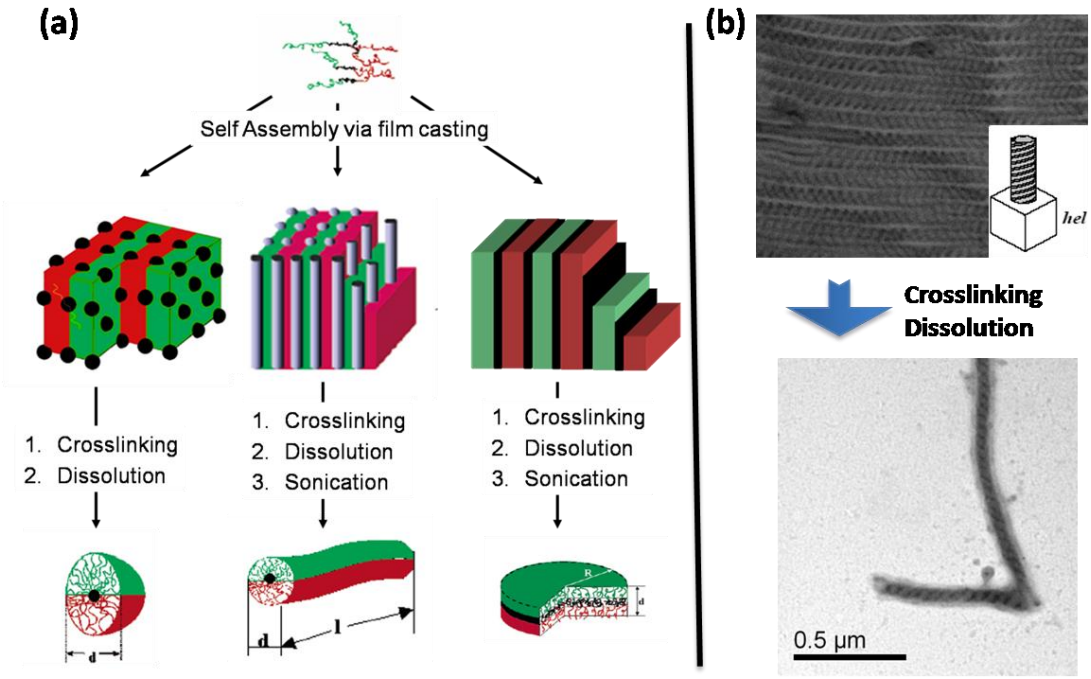

Scheme 1 - 2. (a) Preparation of spherical, cylindrical and disc-like Janus particles based on the selective crosslinking of triblock terpolymer structures. (b) Synthesis of cylinders with a helical arrangement of the middle block, PB (unpublished results by Walther et al.).

Aside the complex, internally structured particles available via the selective crosslinking of block copolymer microphase structures, a further substantial broadening of the accessible morphologies of self-assembled aggregates by block copolymers in solution was only very recently possible by either changing the type of interaction or significantly changing the type of polymer architecture.

For instance, Winnik and coworkers could show that a living type of micellization can be obtained for polyferrocenylsilane (PFS) based block copolymers.[74-79] These polymers undergo self-aggregation upon crystallization of the PFS into a cylindrical core. Due to the high reactivity and nucleation potential of the exposed crystal surfaces, a further addition of more block copolymer "monomers" leads to a living type extension of the structure into ABA type cylindrical co-micelles (see Scheme 1 - 3a).[75] These structures were furthermore used for the site-selective decoration with inorganic nanoparticles to render hybrid materials.

A different approach by Pochan and Wooley[80-85] aims at the kinetically controlled aggregation of triblock copolymer micelles via polyelectrolyte condensation and selective swelling (see Scheme 1 - 3b). The spherical micelles first transform into disc-like structures which self-assemble into long cylindrical micelles with time. In similar systems also the formation of toroidal micelles was observed. The methodology used appears to have some generality in terms of the selection of the complexing agent as cationic gold nanoparticles can be used as well.

Regarding the change of the polymer topology, fundamentally new structures where investigated by Lodge and coworkers (see Scheme 1 - 3c).[86-90] They used miktoarm star polymers, i.e. a terpolymer bearing three arms of hydrophilic, hydrophobic and fluorinated polymers, to construct multicompartment micelles with different structures and phase-segregated cores. Utilizing this approach, various kinds of spherical, cylindrical and bilayer-like

structures could be constructed by changing the lengths of the various arms. These studies are not only triggered by scientific curiosity but also by the possibility of reaching novel structures with advanced properties. For instance, multicompartment micelles can provide interesting possibilities in terms of multicomponent storage and release.[87, 91-93] An intrinsic prerequisite for the preparation of multicompartment micelles is the utilization of three different blocks for the creation of the micellar aggregate.

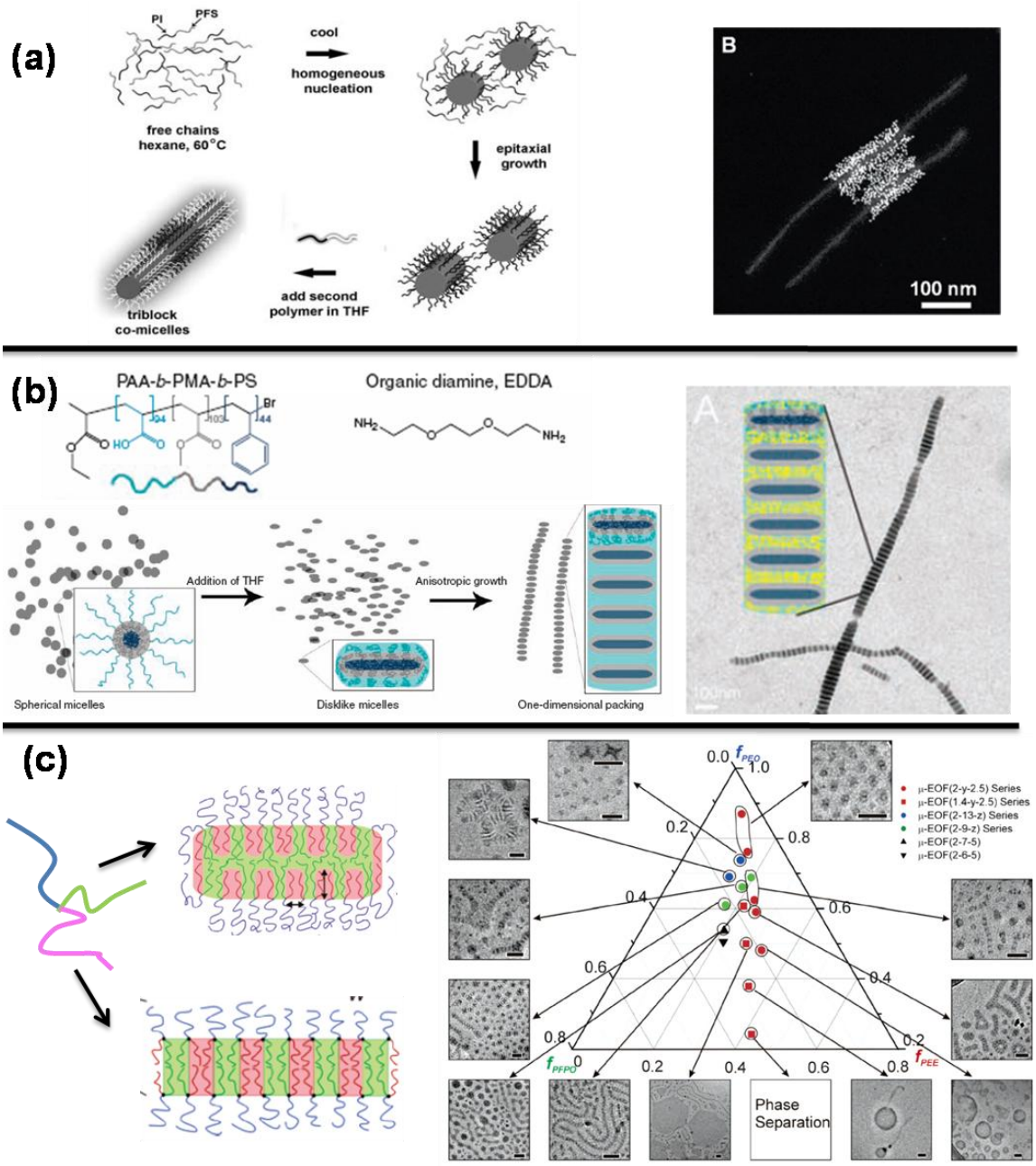

Scheme 1 - 3. (a) Formation of triblock co-micelles based on crystallization induced aggregation and living self-assembly of PFS containing block copolymers. A dark-field TEM image of an ABA co-micelle after decoration of the inner block with silver nanoparticles is shown on the right-hand side. (b) Kinetically controlled self-assembly of triblock terpolymer micelles via selective swelling and polyelectrolyte condensation of the corona. The right-hand side displays a TEM image of such cylinders using cationic gold nanoparticles as complexing agent. (c) The aggregation of miktoarm star terpolymers into multicompartment structures. Shown are two types of multicompartment cylinders and a partial phase diagram.

All of these fascinating and sophisticated structures have one feature in common, which is the structuring perpendicular to the major axis of the cylinder. Even by changing to very complex aggregation mechanism and very advanced polymer architectures, some limitations in terms of assembly formation persist. However, thinking about some special applications, such as nanowires for 1D charge transport, artificial nerves and for the orientation in external fields, a organization parallel the major axis with compartments would be highly desirable.[18] Block copolymer bulk morphologies provide these features to a large extent. In addition to the exploration of Janus cylinders in this thesis, the creation of multicompartment cylinders with multiple, perfectly parallel domains along the major axis of the cylinders will be elaborated in one of the following chapters.

Janus Particles

In recent years, Janus particles have emerged as a new division of colloidal structures. They represent one of the most promising sub-division of multicompartment particles which allow tackling present problems in bioscience, physics and materials science. Janus particles were initially named after the double-faced roman god Janus[94] and the first paper – though thoroughly overlooked in the following years – was published in the late 90'ies.[94b] The terminology is based on the special architectural feature of having two sides or at least two surfaces of different chemistry and/or polarity. As in many cases of modern material research, we can find an analogue to the Janus particles in nature. In many fungi, so-called hydrophobin proteins can be found.[95] This class of proteins has a structural motif in common, which is a characteristic sequence of eight cysteine residues with conserved spacings in their primary sequence. Due to this pattern, hydrophobins are surface-active proteins with a non-centrosymmetric arrangement of the hydrophilic and hydrophobic patches. As a consequence, these proteins undergo self-assembly processes into aggregates in aqueous solution.

Coming back to synthetic Janus systems, the lack of centrosymmetry has led to the discovery of novel material properties as well as to interesting aggregation behavior into superstructures on different length scales, and has opened up a wide field of conceivable applications. These application areas range from medicine, biochemistry, and physics to colloidal chemistry and thus define this research area as an interdisciplinary field. The synthetic access to those non-centrosymmetric structures had been limited to extremely small amounts in the beginning, thus also limiting the utilization of the particles in further studies. However, nowadays, new approaches have overcome those limitations and the generation of significant quantities is possible.

In general, Janus particles can be divided into several classes according to their architecture and dimensionality (see Scheme 1 - 4). Most commonly, spherical (3D) Janus particles can be imagined. In addition, two types of cylinders (1D) and two types of disc-like particles (2D) are conceivable. The lack of centrosymmetry is inherent to all of these particles and is the major challenging aspect in their preparation. Nevertheless, various groups have reported on the successful preparation of different kinds of Janus particles using various synthetic techniques.

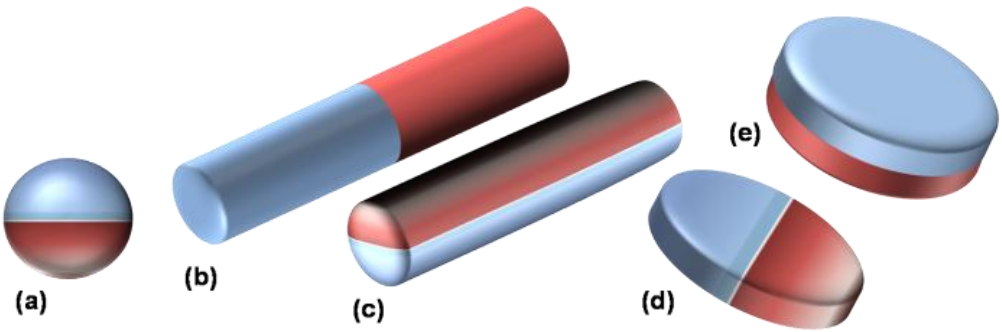

Scheme 1 - 4. Overview of possible Janus particle architectures. (a) Sphere , (b+c) cylinders, and (d+e) discs.

Preparation Pathways

At this point I will review the different approaches leading to Janus particles, focusing the interest on synthetic strategies showing scientific originality as well as technological importance. In particular in the last two to three years, some major developments took place, allowing for the reliable synthesis of significant quantities of Janus particles within a reasonable range of both synthetic effort as well as potential price. Schemes 1 - 2 and 1 - 5 give an overview of the preparation methods.

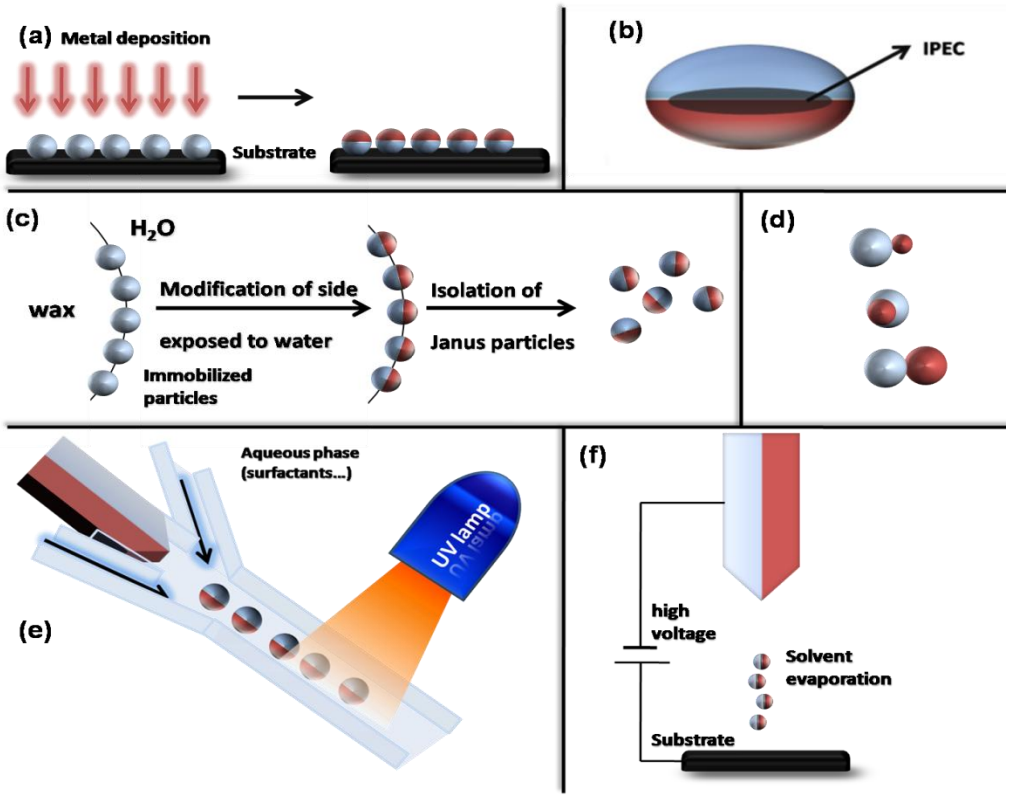

Scheme 1 - 5. Overview of approaches towards the preparation of Janus particles. (a) Classical two-dimensional technique involving shading of one particle side after their immobilization. (b) Ellipsoidal complex core coacervate micelle with an interpolyelectrolyte complex core (IPEC). (c) Pickering emulsion route. (d) Janus particles with two inorganic compartments, snowman-, acorn-, dumbbell-like nanoparticles (top to bottom). (e) Microfluidic photopolymerization system. (f) Electrospinning using a bi-phasic nozzle.

In the very beginning however, the most traditional technique to obtain Janus particles was based on a two-dimensional approach. In a first step, particles are deposited onto a substrate and then the above-lying surface is coated with metals (Scheme 1 - 5a). This methodology is one of the simplest, safest, and most convincing approaches to obtain well-defined Janus particles. For instance, in the early eighties Vessyié and coworkers[96, 97] published data about the hydrophobization of commercially available glass beads, leading to so-called “Janus pearls”. The major drawback of this strategy is that the amount of particles is extremely limited and does not allow their use to larger scale application studies. Nevertheless, due to its simplicity, this approach is still in use as can be seen by recent work by Paunov and Craye[98] or Ryan’s group.[99]

An extension of this concept was recently undertaken by Granick and coworkers,[100] who used a Pickering emulsion route to obtain larger quantities of Janus beads (Scheme 1 - 5c). The concept essentially transfers the two-dimensional technique into a solution phase and uses the high internal interface of an oil(wax)/water interface to achieve higher mass fractions of Janus particles. In a first step, they created a Pickering emulsion of wax and water using silica particles as stabilizers at high temperature. After cooling down the emulsion and a purification step, the particles are immobilized at the solidified interface. The key step of this process is the immobilization of the particles at the interface and the suppressed rotational diffusion of the particles at the solidified interface. The Janus particles can then be obtained after a functionalization of one side with aqueous phase chemistry and filtration at higher temperatures (see Scheme 1 - 5c).

Another approach for the preparation of significant quantities of Janus particles was presented by Lahann and coworkers.[36] They employed electrohydrodynamic jetting in combination with a two-phase side-by-side spinneret tip to generate spherical and cylindrical Janus particles with submicron dimensions (Scheme 1 - 5f). The electrospinning approach offers reliable control and allows an easy incorporation of metallic particles, ligands or dyes into the two sides. More recently, the concept had also been extended to the preparation of biphasic fully inorganic nanofibers made up of TiO_2 and SnO_2, representing the versatility of this methodology (see Scheme 1 - 5f).[101]

A further control and increase of the structural variety of Janus particles was only very recently possible with the development of photopolymerizations or photolithographic polymerizations within microfluidic devices.[30-35] Several research groups succeeded in the preparation of differently shaped colloidal particles with biphasic or triphasic substructures simply by applying a lithographic mask or changing the channel geometry of the microfluidic device. The microfluidic preparation is sketched in Scheme 1 - 5e. The tip releases a two-phase stream from its top, which is then cut into small particles and solvated by the aqueous phase crossflow. The aqueous phase also contains some surfactants to stabilize the resultant droplets. Subsequently, the photopolymerization locks the shape of the two phases and leads to biphasic particles. Although an excellent control of the shape could be achieved, the submicron region is not readily accessible by this method.

Additionally, efforts have been reported to generate purely inorganic Janus particles, e.g. dumbbell-, acorn- or snowman-shaped particles (see Scheme 1 - 5d). The formation of those biphasic particles is assisted by nucleation processes during the growth of the second material or

reaction induced phase separation.[102] Various compositions have been achieved so far and the particles are appealing as some of them combine optical properties for sensing with magnetic properties, which could allow an external manipulation. The different crystal surfaces of the two connected nanoparticles also enable a further highly selective functionalization of the two sides of the inorganic Janus particles.

Concerning a high control of the particle shape and nanoscopic size, an approach based on the self-organization of triblock terpolymers plays a significant role.[66-68, 103] This approach makes use of some unique bulk morphologies of triblock terpolymers[104] and has been intensely pursued in our group. Upon selective crosslinking of polybutadiene (PB) segments of various polymer microphase-separated structures, it is possible to obtain spherical, cylindrical and disc-like Janus particles (see Scheme 1 - 2). The crosslinking preserves the predestined orientation of the outer blocks and unambiguously yields the desired non-centrosymmetric particles. This method, introduced in the beginning of this decade, was the first technique to actually allow the preparation of truly nanometer-sized Janus particles on the gram scale. The precise control of the dimensions of the cross-sections is unmatched due to the utilization of the extremely well-defined triblock terpolymer templates.

In an approach purely based on self-assembly, Voets et al.[105] were able to prepare “double-faced” complex core coacervate micelles (C3M) using the forced co-assembly of two block copolymers, each possessing an oppositely charged polyelectrolyte segment (see Scheme 1 - 5b). The polyelectrolyte blocks formed a water-insoluble interpolyelectrolyte complex (IPEC) as the micellar core, whereas the two other block segments, poly(ethylene oxide) and polyacrylamide, underwent phase separation due to their incompatibility. The overall shape of these C3M micelles was discoidal. The important issue of evidencing the demixing of the corona was most elegantly tackled by NOESY NMR, a technique suitable for probing inter-chain interactions.

Some of the methods presented indeed possess the potential of scaling-up to industrial scale while keeping the price of the materials within a moderate region. Certainly, an industrial production of the particles will only be of interest if significant advantageous in the material properties of Janus particles over standard colloids or surfactants are discovered. This is discussed below.

Fascinating Superstructures

The ability of a material to self-assemble into complex hierarchical structures is encoded into its architecture, proteins being the best example. Since Janus particles possess the unique and novel feature of being non-centrosymmetric, many investigations have been concerned with the evaluation of the solution properties and self-assembly behavior of these particles.[34, 67, 68, 103, 106, 107] As some techniques allow the preparation of non-spherical particles, it is also possible to study the effect of the geometry on the types of aggregates formed. Indeed, it turned out that Janus particles exhibit a variety of complex and partially unexpected aggregates.

In the case of spherical Janus micelles, having hemispheres of polystyrene (PS) and poly(methyl methacrylate) (PMMA), aggregation into clusters is observed in various organic solvents, e.g. THF.[67] Similarly, Janus discs composed of two sides of PS and poly(*tert*-butyl methacrylate) (P*t*BMA) undergo back-to-back stacking into superstructures in organic solvents.[68] The self-

assembly behavior could be strikingly demonstrated with various imaging and scattering techniques. For instance, Figure 1 - 3 (a and c) shows Transmission Electron Microscopy (TEM) images of back-to-back stacked Janus discs. The images were obtained from ultrathin sections after embedding the superstructures from THF or acetone into a crosslinkable silicone oil, microtome cutting and staining. A stacking of the PS sides of the Janus discs can clearly be seen and the multicompartment architecture can be visualized (see Figure 1 - 3c for a schematic representation of the layers).

Furthermore, Figure 1 - 3d exhibits a scanning force microscopy (SFM) image of individual Janus micelles (small isolated particles) and superstructured surface clusters composed out of supermicelles (clustered large “fried-egg”-like structures). Each supermicelle is constituted of several individual Janus micelles. The Scheme 1 - in Figure 1 - 3e serves as a cartoon of the proposed aggregation pattern of individual Janus micelles into the supermicelles. This aggregation of the Janus particles into superstructures is surprising to some extent as both sides of the particles alone, as well as the base terpolymer, are well soluble in the organic solvent used. It appears though that the very slight selectivity of the solvent is sufficient to induce a self-assembly of the particles into defined discrete clusters of Janus particles. Such kind of an aggregation can be expected neither for standard block copolymers nor for homogeneous particles and thus represents one of the unique features of Janus particles.

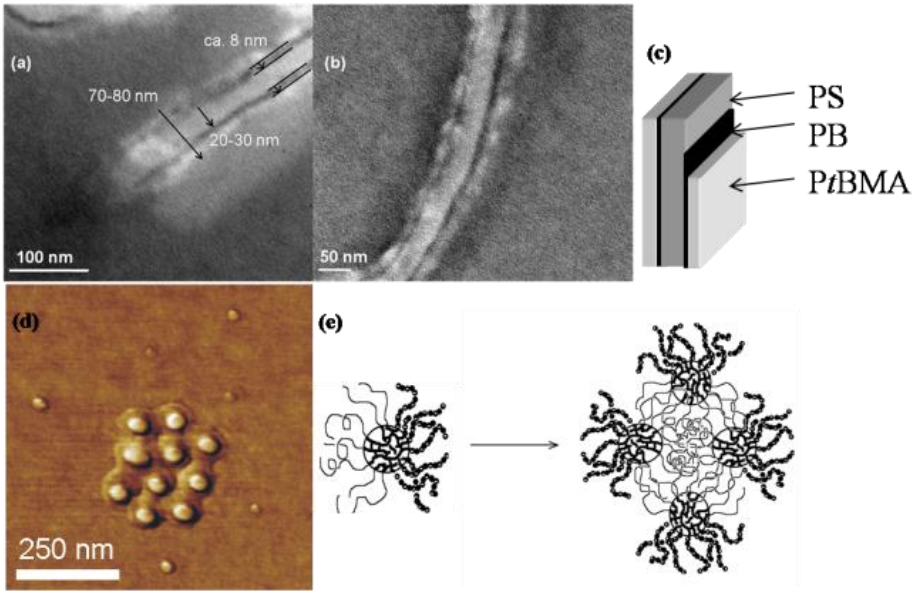

Figure 1 - 3. Superstructures formed by Janus discs, possessing one PS and one PtBMA side, in THF (a) and acetone (b). TEM images taken after embedding. (d) SFM height image (z-range = 30 nm) of single Janus micelles, composed of one PS and one PMMA side, and their supermicelles. The latter form ordered surface assemblies after deposition from THF onto mica. Scheme 1 -s (c) and (e) show the proposed aggregation patterns (polybutadiene = PB).

Turning to aqueous medium, the situation becomes even more complex and interesting. At first, we can distinguish two kinds of biphasic particles. The first ones are particles which are truly amphiphilic and possess one hydrophobic and one hydrophilic side. The second class has two completely water-soluble, yet unlike sides. In the first case, extensive studies have been carried out with spherical Janus particles composed of one hemisphere of water-soluble poly(methacrylic acid) (PMAA) and another side of PS.[103] The detailed investigations revealed that the Janus particles aggregate on two hierarchical levels (see Figure 1 - 4). The first one is the

assembly of single Janus particles into defined clusters, similar as in organic solution. The second is the aggregation into even larger aggregates, so-called giant micelles. The supermicelles and the giant micelles can be seen in the SFM and SEM (scanning electron microscopy) images below as small and very large structures, respectively. The structure of the very large supermicelles is unknown so far, however, it was suggested that they may be similar to multilamellar vesicles.

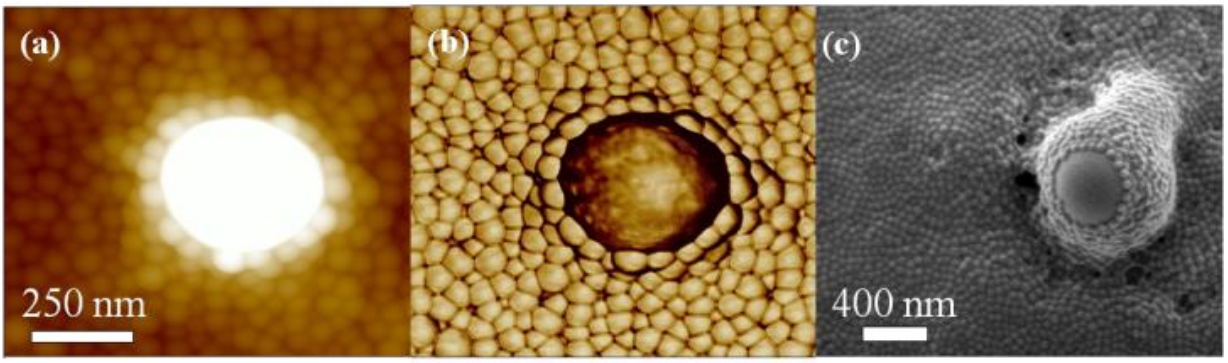

Figure 1 - 4. SFM height (a; z-range = 100 nm) and phase image (b), and SEM image (c) of amphiphilic Janus micelles, having one PS and one PMAA side, after deposition from aqueous solution.

Interestingly, the critical aggregation concentration of the amphiphilic Janus micelles (PS-PMAA) in water is higher than for the Janus particles in organic solution. This again comes as a surprise as water is a much stronger selective solvent than the organic solvents used and thus a lower critical aggregation concentration is anticipated.

Secondly, I consider the work of Granick's group dealing with the clustering of dipolar ("zwitterionic") micron-sized Janus particles, which serve as an example for fully water-soluble Janus particles.[107] Zwitterionic Janus particles do not behave like classical dipoles, as their size significantly exceeds the electrostatic screening length and thus the electrostatic interactions have a much shorter range than the particle size. The microscopic observations in this work are supported by Monte-Carlo calculations and reveal an assembly of the dipolar spherical Janus particles into defined clusters. The aggregation towards larger and larger structures is energetically favored as each cluster still carries a macroscopic dipole and would thus allow the assembly of already formed clusters into even larger assemblies. Many of the shapes found differ from aggregates expected from homogeneous particles which exclusively cluster due to van der Waals interactions. Generally, the differences are expected to be more pronounced for larger clusters and the clusters possess a less dense packing and a higher asymmetry.

Looking to the future, it is obvious that among surprising and novel aggregates found so far, Janus particles of different architectures are certainly useful for directional self-assembly towards complex hierarchical structures and novel materials.

Applications of Janus Particles

Due to the presence of various compartments of different chemistry and physical properties, a variety of specific applications are under discussion and exploration currently. Some of these studies have been triggered by theoretical predictions of certain advanced properties in particular of Janus colloids. In several examples in the literature, it is evident that when researchers make clever use of the inherent multicompartment character, the non-

centrosymmetric nature and the resulting physical characteristics, new materials with novel properties can be obtained. However, only some of those will be commercialized and make their way to real industrial applications or specialized product.

A first example for an interesting switchable device was shown by Nisisako et al., who made use of the electrical anisotropy of Janus particles filled with white and black pigments in both hemispheres.[31] In order to create a switchable display panel, they placed a thin layer of these spheres between two electrodes. Upon switching on an electric field, the particles orient their black sides to the negative electrode and vice versa. The orientation and the color of the display can be flipped simply by reversing the electrical field. With this method, very thin, robust and environmentally stable displays could be created.

Besides, Janus particles can be used as efficient and unique optical probes for biological interactions or rheological measurements in confined space. In recent years, this concept has been brought forward by Behrend and coworkers[108-112] who used Janus beads coated on one side with metal. These so-called (magnetically) modulated optical nanoprobes reflect and transmit light or emit fluorescence anisotropically, i.e. depending on their orientation with respect to the observer. Being placed into a specific environment, these particles blink on and off depending on the surrounding conditions. Precisely speaking, the frequency of the flickering can be used to draw detailed conclusions of the microenvironment and the viscoelastic properties, simply because the rotational diffusion of the particles experiences viscous drag. With this strategy it is possible to create devices ranging from precise nanoviscosimeters to nanothermometers. Further development of these particles has aimed at the incorporation of highly selective receptor sites or magnetic coatings on one side of the particles in order to use them as (bio)chemical nanosensors. Thus the flickering of the particles is not only sensitive to viscous drag, but also to electric and magnetic fields as well as to chemical attraction and biochemical forces.[113] For sensor applications, Janus particles could allow an independent biochemical conjugation with the possibility of imaging (microscopy or magnetic resonance tomography) based on dyes or contrast agents located within the other side. Thus, an interference of the two sides is minimized and the sensing functions could be optimized.

Another interesting effect which potentially finds application in nanoscience is the self-propulsion induced by catalytically active Janus beads with a spatially asymmetric distribution of the reaction site.[99, 114] Generally, self-motile particles are of interest in nanomedicine as they exhibit an increased diffusion coefficient compared to standard particles. This allows them to screen a larger volume for docking sites within less time and would make drug-delivery vehicles more efficient. Such devices had been recently described by Ryan and coworkers[99] They used micron-sized polystyrene particles coated on one side with a thin platinum layer and studied their diffusion by tracking experiments in dependence of the concentration of hydrogen peroxide. The latter served as “fuel” in these experiments as it is catalytically degraded by platinum into two reaction products and leads to an asymmetric distribution of reaction products and an accompanying osmotic potential (see Figure 1 - 5).

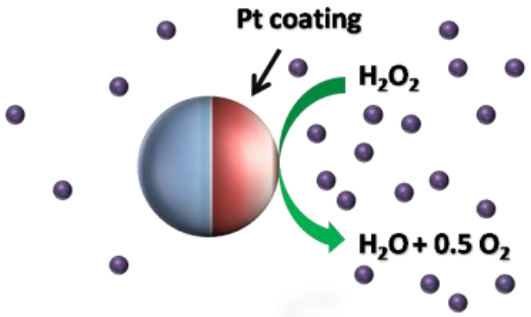

Figure 1 - 5. Self-propulsion of a Janus particle via the asymmetric distribution of reaction products in case of the catalytic degradation of hydrogen peroxide by platinum into two reaction products.

This nanoscale chemical locomotion leads to enhanced directed diffusion on a short time scale and is randomized for longer time-scales. The overall diffusion coefficient is substantially larger in the presence of fuel. By changing the catalytic centre to an active enzyme, the propulsion mechanism would mimic to some extent a bacterial flagellum.

From an industrial point of view, the surface activity of Janus particles is of fundamental interest. Due to the corona segregation, amphiphilic Janus particles are expected to strongly adsorb at interfaces. These particles uniquely combine the so-called Pickering effect, known for particles, with the amphiphilicity of classical surfactants. In recent years, several publications have appeared describing theoretically the remarkably high adsorption strength of Janus particles at interfaces.[115, 116] For instance, in case of spherical particles, the adsorption energy at a liquid/liquid interface is predicted to be up to three times higher for particles with corona segregation than for particles with a uniform surface. Therefore, Janus particles may be ideally suited as strong future emulsifiers. Following the predictions, Glaser et al.[117] recently used pendant drop tensiometry to show that bi-metallic Janus particles indeed lead to a significant reduction of the oil/water interfacial tension as compared to uniform metallic nanoparticles (iron oxide or gold) of similar size (see Figure 1 - 6).

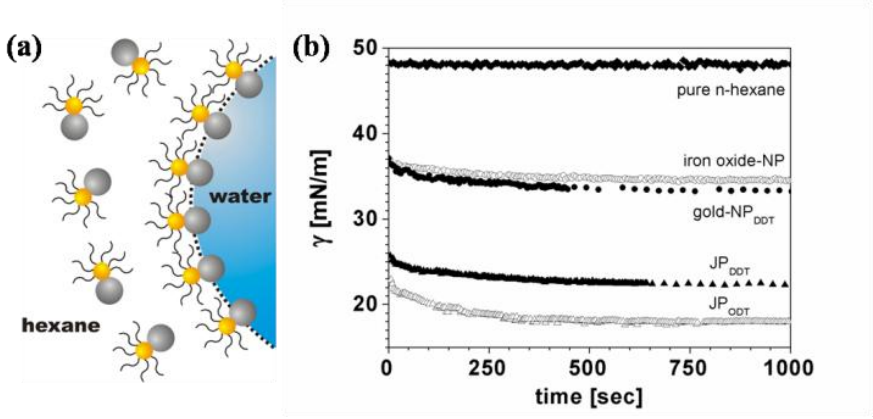

Figure 1 - 6. (a) Schematic representation of bimetallic Janus particles at the hexane/water interface (gold: gold part with surfactant; gray: iron oxide part). (b) Interfacial tension vs time as measured by pendant drop tensiometry (NP: homogeneous nanoparticles; JP: Janus particles).

This means that by changing the architecture, stronger and hence better surfactant particles can be created. The application of nano-sized Janus colloids to the stabilization of interfaces will be demonstrated in two chapters of this thesis.

Objective of this Thesis

The objective of this thesis is to broaden the scope of polymeric multicompartment particles with respect to their architecture, accessibility and possible applications in materials science. In addition, the generation of inorganic-organic hybrid materials based on these developed structures is of interest. One focus of this thesis is certainly the generation of novel Janus particles and the exploration of their solution properties. This is however not the sole objective as tailor-made compartmentalized colloids based on diblock copolymers are to be explored for a joint project with the chair of inorganic chemistry as well. Moreover, the structure formation of miktoarm star terpolymers in solution and the utilization of their bulk phase morphology for the preparation of multicompartment particles is a key topic of this thesis. We aim at the generation of fundamentally new particles and hybrid materials of very sophisticated organization using miktoarm star terpolymers.

For all structures prepared, the investigation of their self-assembly behavior as a function of the architecture or molecular structure is one key element of this thesis. This is of particular importance as applications of such colloidal particles can only be reliably realized when the solution behavior is well understood and characterized. To further push compartmentalized colloids into applications e.g. in materials science, ways for up-scaling the synthesis of such particles were to be explored as well. After having completed these tasks, the application of compartmentalized colloids as for instance as catalyst carriers and for the stabilization of interfaces is to be pursued. With preparation pathways in the multi-gram scale at hand, we want to show that compartmentalized colloids and Janus particles in particular are useful nanoscopic building blocks for the generation of novel materials with advanced properties.

References

1. Valkama, S.; Kosonen, H.; Ruokolainen, J.; Haatainen, T.; Torkkeli, M.; Serimaa, R.; ten Brinke, G.; Ikkala, O. *Nat. Mater.* **2004,** 3, 872.
2. Kang, Y.; Walish Joseph, J.; Gorishnyy, T.; Thomas Edwin, L. *Nat. Mater.* **2007,** 6, 957.
3. Park, M.; Harrison, C.; Chaikin, P. M.; Register, R. A.; Adamson, D. H. *Science* **1997,** 276, 1401.
4. Bang, J.; Kim, S. H.; Drockenmuller, E.; Misner, M. J.; Russell, T. P.; Hawker, C. J. *J. Am. Chem. Soc.* **2006,** 128, 7622.
5. Lysenko, E. A.; Bronich, T. K.; Slonkina, E. V.; Eisenberg, A.; Kabanov, V. A.; Kabanov, A. V. *Macromolecules* **2002,** 35, 6351.
6. Klingelhöfer, S.; Heitz, W.; Greiner, A.; Oestreich, S.; Förster, S.; Antonietti, M. *J. Am. Chem. Soc.* **1997,** 119, 10116.
7. Förster, S.; Antonietti, M. *Adv. Mater.* **1998,** 10, 195.
8. Tsutsumi, K.; Funaki, Y.; Hirokawa, Y.; Hashimoto, T. *Langmuir* **1999,** 15, 5200-5203.

9. Platonova, O. A.; Bronstein, L. M.; Solodovnikov, I. M.; Yanovskaya, I. M.; Obolonkova, P. M.; Valetsky, P. M.; Wenz, E.; Antonietti, M. *Coll. Pol. Sci.* **1997,** 275, 426.
10. Lu, J.; Yi, S. S.; Kopley, T.; Qian, C.; Liu, J.; Gulari, E. *J. Phys. Chem. B* **2006,** 110, 6655.
11. Massey, J. A.; Winnik, M. A.; Manners, I.; Chan, V. Z. H.; Ostermann, J. M.; Enchelmaier, R.; Spatz, J. P.; Möller, M. *J. Am. Chem. Soc.* **2001,** 123, 3147.
12. Lu, X.; Manners, I.; Winnik, M. A. *Macromolecules* **2001,** 34, 1917.
13. Chan, V. Z. H.; Hoffman, J.; Lee, V. Y.; Latrou, H.; Avgeropoulos, A.; Hadjichristidis, N.; Miller, R. D. *Science* **1999,** 286, 1716.
14. Lee, J.; Orilall, M. C.; Warren, S. C.; Kamperman, M.; DiSalvo, F. J.; Wiesner, U. *Nat. Mater.* **2008,** 7, 222.
15. Ludwigs, S.; Böker, A.; Voronov, A.; Rehse, N.; Magerle, R.; Krausch, G. *Nat. Mater.* **2003,** 2, 744.
16. Peinemann, K.-V.; Abetz, V.; Simon, P. F. W. *Nat. Mater.* **2007,** 6, 992.
17. Liu, J.; Zhang, Q.; Remsen, E. E.; Wooley, K. L. *Biomacromolecules* **2001,** 2, 362.
18. Guerin, G.; Raez, J.; Wang, X.-S.; Manners, I.; Winnik, M. A. *Prog. Coll. Pol. Sci.* **2006,** 132, 152.
19. Gu, J.; Cheng, W.-P.; Liu, J.; Lo, S.-Y.; Smith, D.; Qu, X.; Yang, Z. *Biomacromolecules* **2008,** 9, 255.
20. Zhang, L.; Nguyen, T. L. U.; Bernard, J.; Davis, T. P.; Barner-Kowollik, C.; Stenzel, M. H. *Biomacromolecules* **2007,** 8, 2890.
21. Sawant, R. M.; Hurley, J. P.; Salmaso, S.; Kale, A.; Tolcheva, E.; Levchenko, T. S.; Torchilin, V. P. *Bioconjugate Chem.* **2006,** 17, 943.
22. Giacomelli, C.; Le Men, L.; Borsali, R.; Lai-Kee-Him, J.; Brisson, A.; Armes, S. P.; Lewis, A. L. *Biomacromolecules* **2006,** 7, 817.
23. Rosler, A.; Vandermeulen, G. W. M.; Klok, H.-A. *Adv. Drug Delivery Rev.* **2001,** 53, 95.
24. Kataoka, K.; Harada, A.; Nagasaki, Y. *Adv. Drug Delivery Rev.* **2001,** 47, 113.
25. Wakebayashi, D.; Nishiyama, N.; Itaka, K.; Miyata, K.; Yamasaki, Y.; Harada, A.; Koyama, H.; Nagasaki, Y.; Kataoka, K. *Biomacromolecules* **2004,** 5, 2128.
26. Hoffman, A. S.; Stayton, P. S. *Prog. Polym. Sci.* **2007,** 32, 922.
27. Bontempo, D.; Li, R. C.; Ly, T.; Brubaker, C. E.; Maynard, H. D. *Chem. Commun.* **2005**, 4702.
28. Shimoboji, T.; Ding, Z. L.; Stayton, P. S.; Hoffman, A. S. *Bioconjugate Chem.* **2002,** 13, 915.
29. Rapoport, N. *Prog. Polym. Sci.* **2007,** 32, 962.
30. Nisisako, T.; Torii, T. *Adv. Mater.* **2007,** 19, 1489.
31. Nisisako, T.; Torii, T.; Takahashi, T.; Takizawa, Y. *Adv. Mater.* **2006,** 18, 1152.
32. Shepherd, R. F.; Conrad, J. C.; Rhodes, S. K.; Link, D. R.; Marquez, M.; Weitz, D. A.; Lewis, J. A. *Langmuir* **2006,** 22, 8618.
33. Dendukuri, D.; Pregibon, D. C.; Collins, J.; Hatton, T. A.; Doyle, P. S. *Nat. Mater.* **2006,** 5, 365.
34. Nie, Z.; Li, W.; Seo, M.; Xu, S.; Kumacheva, E. *J. Am. Chem. Soc.* **2006,** 128, 9408.
35. Seo, M.; Nie, Z.; Xu, S.; Mok, M.; Lewis, P. C.; Graham, R.; Kumacheva, E. *Langmuir* **2005,** 21, 11614.
36. Roh, K.-H.; Martin, D. C.; Lahann, J. *Nat. Mater.* **2005,** 4, 759.
37. Roh, K.-H.; Martin, D. C.; Lahann, J. *J. Am. Chem. Soc.* **2006,** 128, 6796.
38. Li, C.; Buurma, N. J.; Haq, I.; Turner, C.; Armes, S. P.; Castelletto, V.; Hamley, I. W.; Lewis, A. L. *Langmuir* **2005,** 21, 11026.
39. Antonietti, M.; Förster, S. *Adv. Mater.* **2003,** 15, 1323.
40. Reiss, G. *Prog. Pol. Sci.* **2003,** 28, 1107.
41. Förster, S.; Plantenberg, T. *Angew. Chem.* **2002,** 114, 712.
42. Selb, J.; Gallot, Y. *Makromol. Chem.* **1980,** 181, 809.
43. Selb, J.; Gallot, Y. *Makromol. Chem.* **1981,** 182, 2523.

44. Peng, H. S.; Chen, D. Y.; Jiang, M. *J. Phys. Chem. B* **2004,** 108, 5225.
45. Antonietti, M.; Heinz, S.; Schmidt, M.; Rosenauer, C. *Macromolecules* **1994,** 27, 3276.
46. Park, S.-Y.; Chang, Y.-J.; Farmer, B. L. *Langmuir* 22, 11369.
47. Calderara, F.; Riess, G. *Macromol. Chem. Phys.* **2003,** 197, 2115.
48. Peng, H. S.; Chen, D. Y.; Jiang, M. *Langmuir* **2003,** 19, 10989.
49. Choucair, A. A.; Kycia, A. H.; Eisenberg, A. *Langmuir* **2003,** 19, 1001.
50. Burke, S. E.; Eisenberg, A. *Langmuir* **2001,** 17, 6705.
51. Yu, K.; Bartels, C.; Eisenberg, A. *Langmuir* **1999,** 15, 7157.
52. Zhang, L.; Eisenberg, A. *Macromolecules* **1999,** 32, 2239.
53. Gao, Z.; Varshney, S. K.; Wong, S.; Eisenberg, A. *Macromolecules* **1994,** 27, 7923.
54. Yu, Y.; Eisenberg, A. *J. Am. Chem. Soc.* **1997,** 119, 8383.
55. Kukula, H.; Schlaad, H.; Antonietti, M.; Förster, S. *J. Am. Chem. Soc.* **2002,** 124, 1658.
56. Zhang, L.; Eisenberg, A. *J. Am. Chem. Soc.* **1996,** 118, 3168.
57. Zhang, L.; Eisenberg, A. *Science* **1995,** 268, 1728.
58. Liu, S.; Armes, S. P. *Langmuir* **2003,** 19, 4432.
59. Cai, Y.; Armes, S. P. *Macromolecules* **2004,** 37, 7116.
60. Lee, A. S.; Buetuen, V.; Vamvakaki, M.; Armes, S. P.; Pople, J. A.; Gast, A. P. *Macromolecules* **2002,** 35, 8540.
61. Lee, A. S.; Gast, A. P.; Buetuen, V.; Armes, S. P. *Macromolecules* **1999,** 32, 4302.
62. Baines, F. L.; Armes, S. P.; Billingham, N. C.; Tuzar, Z. *Macromolecules* **1996,** 29, 8151.
3. Prochazka, K.; Baloch, M. K.; Tuzar, Z. *Makromolekulare Chemie* **1979,** 180, 2521.
64. Guo, A.; Liu, G. J.; Tao, J. *Macromolecules* **1996,** 29, 2487.
65. O'Reilly, R. K.; Hawker, C. J.; Wooley, K. L. *Chem. Soc. Rev.* **2006,** 35, 1068.
66. Liu, Y.; Abetz, V.; Müller, A. H. E. *Macromolecules* **2003,** 36, 7894.
67. Erhardt, R.; Böker, A.; Zettl, H.; Kaya, H.; Pyckhout-Hintzen, W.; Krausch, G.; Abetz, V.; Müller, A. H. E. *Macromolecules* **2001,** 34, 1069.
68. Walther, A.; André, X.; Drechsler, M.; Abetz, V.; Müller, A. H. E. *J. Am. Chem. Soc.* **2007,** 129, 6187.
69. Maskos, M. *Polymer* **2006,** 47, 1172.
70. Breiner, U.; Krappe, U.; Abetz, V.; Stadler, R. *Macromol. Chem. Phys.* **1997,** 198, 1051.
71. Breiner, U.; Krappe, U.; Thomas, E. L.; Stadler, R. *Macromolecules* **1998,** 31, 135.
72. Stadler, R.; Auschra, C.; Beckmann, J.; Krappe, U.; Voigt-Martin, I.; Leibler, L. *Macromolecules* **1995,** 28, 3080.
73. Brinkmann, S. PhD Thesis, Mainz, **1997**.
74. Wang, X.; Wang, H.; Frankowski, D. J.; Lam, P. G.; Welch, P. M.; Winnik, M. A.; Hartmann, J.; Manners, I.; Spontak, R. J. *Adv. Mater.* **2007,** 19, 2279.
75. Wang, X.; Guerin, G.; Wang, H.; Wang, Y.; Manners, I.; Winnik, M. A. *Science* **2007,** 317, 644.
76. Wang, X.; Liu, K.; Arsenault, A. C.; Rider, D. A.; Ozin, G. A.; Winnik, M. A.; Manners, I. *J. Am. Chem. Soc.* **2007,** 129, 5630.
77. Guerin, G.; Raez, J.; Manners, I.; Winnik, M. A. *Macromolecules* **2005,** 38, 7819.
78. Raez, J.; Barjovanu, R.; Massey, J. A.; Winnik, M. A.; Manners, I. *Angew. Chem. Int. Ed.* **2000,** 39, 3862.
79. Massey, J. A.; Temple, K.; Cao, L.; Rharbi, Y.; Raez, J.; Winnik, M. A.; Manners, I. *J. Am. Chem. Soc.* **2000,** 122, 11577.
80. Cui, H.; Chen, Z.; Zhong, S.; Wooley, K. L.; Pochan, D. J. *Science* **2007,** 317, 647.
81. Li, Z.; Chen, Z.; Cui, H.; Hales, K.; Wooley, K. L.; Pochan, D. J. *Langmuir* **2007,** 23, 4689.
82. Cui, H.; Chen, Z.; Wooley, K. L.; Pochan, D. J. *Macromolecules* **2006,** 39, 6599.
83. Li, Z.; Chen, Z.; Cui, H.; Hales, K.; Qi, K.; Wooley, K. L.; Pochan, D. J. *Langmuir* **2005,** 21, 7533.

84. Chen, Z.; Cui, H.; Hales, K.; Li, Z.; Qi, K.; Pochan, D. J.; Wooley, K. L. *J. Am. Chem. Soc.* **2005,** 127, 8592.
85. Pochan, D. J.; Chen, Z.; Cui, H.; Hales, K.; Qi, K.; Wooley, K. L. *Science* **2004,** 306, 94.
86. Lodge, T. P.; Rasdal, A.; Li, Z.; Hillmyer, M. A. *J. Am. Chem. Soc.* **2005,** 127, 17608.
87. Li, Z.; Kesselman, E.; Talmon, Y.; Hillmyer Marc, A.; Lodge Timothy, P. *Science* **2004,** 306, 98.
88. Li, Z.; Hillmyer, M. A.; Lodge, T. P. *Macromolecules* **2006,** 39, 765.
89. Li, Z.; Hillmyer, M. A.; Lodge, T. P. *Langmuir* **2006,** 22, 9409.
90. Li, Z.; Hillmyer, M. A.; Lodge, T. P. *Nano Lett.* **2006,** 6, 1245.
91. Lodge, T. P.; Rasdal, A.; Li, Z.; Hillmyer, M. A. *J. Am. Chem. Soc.***2005,** 127, 17608.
92. Kubowicz, S.; Baussard, J.-F.; Lutz, J.-F.; Thuenemann, A. F.; von Berlepsch, H.; Laschewsky, A. *Angew. Chem. Int. Ed.* **2005,** 44, 5262.
93. Lutz, J.-F.; Laschewsky, A. *Macromol. Chem. Phys.* **2005,** 206, 813.
94. Walther, A.; Müller, A. H. E. *Soft Matter* **2008,** 4, 663.
94b. Rossmy, G. *Progr. Coll. Polym. Sci.*, **1998**, 111, 17.
95. Hektor Harm, J.; Scholtmeijer, K. *Curr. Opin. Biotechnol.* **2005,** 16, 434.
96. Casagrande, C.; Veyssié, M. C. *R. Acad. Sci. (Paris)* **1988,** II-306, 1423.
97. Casagrande, C.; Fabre, P.; E, R.; Veyssié, M. C. *Europhys. Lett.* **1989,** 9, 251.
98. Paunov, V. N.; Cayre, O. J. *Adv. Mater.* **2004,** 16, 788.
99. Howse, J. R.; Jones, R. A. L.; Ryan, A. J.; Gough, T.; Vafabakhsh, R.; Golestanian, R. *Phys. Rev. Lett.* **2007,** 99, 048102.
100. Hong, L.; Jiang, S.; Granick, S. *Langmuir* **2006,** 22, 9495.
101. Liu, Z.; Sun, D. D.; Guo, P.; Leckie, J. O. *Nano Lett.* **2007,** 7, 1081.
102. Perro, A.; Reculusa, S.; Ravaine, S.; Bourgeat-Lami, E.; Duguet, E. *J. Mat. Chem.* **2005,** 15, 3745.
103. Erhardt, R.; Zhang, M.; Böker, A.; Zettl, H.; Abetz, C.; Frederik, P.; Krausch, G.; Abetz, V.; Müller, A. H. E. *J. Am. Chem. Soc.* **2003,** 125, 3260.
104. Abetz, V.; Simon, P. F. W. *Adv. Pol. Sci.* **2005,** 189, 125.
105. Voets, I. K.; de Keizer, A.; De Waard, P.; Frederik, P. M.; Bomans, P. H. H.; Schmalz, H.; Walther, A.; King, S. M.; Leermakers, F. A. M.; Cohen Stuart, M. A. *Angew. Chem. Int. Ed.* **2006,** 45, 6673.
106. Dendukuri, D.; Hatton, T. A.; Doyle, P. S. *Langmuir* **2007,** 23, 4669.
107. Hong, L.; Cacciuto, A.; Luijten, E.; Granick, S. *Nano Lett.* **2006,** 6, 2510.
108. Behrend, C. J.; Anker, J. N.; McNaughton, B. H.; Kopelman, R. *J. Magn. Magn. Mater.* **2005,** 293, 663.
109. Anker, J. N.; Behrend, C. J.; Huang, H.; Kopelman, R. *J. Magn. Magn. Mater.* **2005,** 293, 655.
110. Behrend, C. J.; Anker, J. N.; McNaughton, B. H.; Brasuel, M.; Philbert, M. A.; Kopelman, R. *J. Phys. Chem. B* **2004,** 108, 10408.
111. Behrend, C. J.; Anker, J. N.; Kopelman, R. *Appl. Phys. Lett.* **2004,** 84, 154.
112. Anker, J. N.; Behrend, C.; Kopelman, R. *J. Appl. Phys.* **2003,** 93, 6698.
113. Choi, J.; Zhao, Y.; Zhang, D.; Chien, S.; Lo, Y. H. *Nano Lett.* **2003,** 3, 995.
114. Golestanian, R.; Liverpool, T. B.; Ajdari, A. *Phys. Rev. Lett.* **2005,** 94, 220801.
115. Binks, B. P.; Fletcher, P. D. I. *Langmuir* **2001,** 17, 4708.
116. Nonomura, Y.; Komura, S.; Tsujii, K. *Langmuir* **2004,** 20, 11821.
117. Glaser, N.; Adams, D. J.; Böker, A.; Krausch, G. *Langmuir* **2006,** 22, 5227.

Overview of this Thesis

This dissertation contains 12 publications, 10 presented from chapter 3 to 12 and two more in the appendix (13 and 14).

The thesis is connected by the common theme of studying compartmentalized, soft (polymeric) nanoparticles. My research efforts focused on new preparation pathways, the evaluation of the self-assembly behavior of the synthesized nanoparticles into superstructures, the realization of organic-inorganic hybrid materials and the application of compartmentalized particles to current problems in materials science.

In general, the synthesis of the required block copolymers was accomplished via two controlled/living polymerization techniques, anionic polymerization and Radical Addition Fragmentation Transfer (RAFT) polymerization. For the preparation of the compartmentalized colloids, self-assembly strategies in solution as well as in the bulk state were rigorously exploited. Since many of the used approaches and pursued applications require kinetically stabilized systems, facile crosslinking strategies for the bulk state and solution based assemblies were investigated. The evaluation of the solution properties was accomplished by combined light scattering and imaging techniques (*cryo*-TEM, TEM, SFM) to allow a monitoring of the ensemble behavior and an assessment of the individual structure on a single molecule level at the same time. The application studies were focused on utilizing the surface-active properties of bi-phasic Janus particles and the preparation of catalytically active hybrid materials with high surface areas. The formation of inorganic-organic hybrid materials involved the conjugation of metal salts as precursor onto designed moieties of selected compartments and their subsequent reaction into conducting, semi-conducting and catalytically active inorganic nanoparticles.

The chapters can to some extent be subdivided into three topics. Chapters 3 - 8 deal with Janus particles based on triblock terpolymers. Chapters 9 and 10 are comprised of investigations concerning the self-assembly behavior and structure formation of miktoarm star terpolymers in solution and in the bulk. The last two chapters (11 and 12) of the main part of this thesis explore the controlled crosslinking of diblock copolymers in solution and the bulk state and the creation of polyoxometalate grafted polymeric nanorods. The two publications in the appendix serve to put the finishing touch on this dissertation in terms of showing results majorly obtained during my preceding diploma thesis which are in close conjunction with this PhD thesis. Furthermore, a recent highlight article concerning the fascinating prospects of Janus particles is included therein.

In the following, I will present a summary of the key results obtained within the scope of this thesis. A complete coverage of the experimental results and conclusions can be found in the respective chapters.

Janus Particles

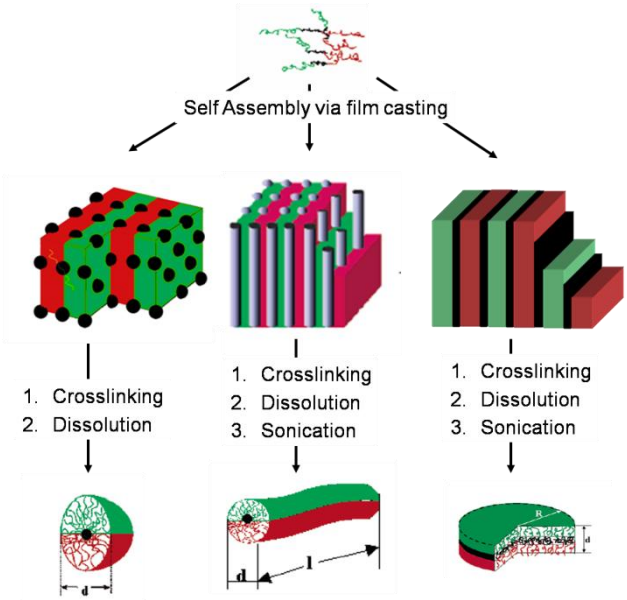

Scheme 2 - 1. Preparation of Janus particles with different architectures based on crosslinking the polybutadiene segments of various triblock terpolymers in the bulk.

Three different architectures of Janus particles (spherical, cylindrical and disc-like) were synthesized based on the selective crosslinking of microphase-segregated block terpolymer templates of suitable compositions (see Scheme 2 - 1). The block terpolymers, polystyrene-*block*-polybutadiene-*block*-poly(methyl methacrylate) (SBM) and polystyrene-*block*-polybutadiene-*block*-poly(tert.-butyl methacrylate) (SBT) were synthesized via living anionic polymerization using the sequential monomer addition technique. In order to allow a controlled crosslinking taking place and for obtaining sufficiently crosslinked networks, various strategies were explored. The results demonstrate that a careful monitoring of the microphase-segregated morphology during the addition of chemicals (swelling solvents and crosslinking agents) is necessary to allow a controlled crosslinking taking place. In particular, more labile morphologies, such as the lamella-lamella morphology of the SBT terpolymers with a very thin or discontinuous lamella of polybutadiene in the center, require a careful adjustment of the crosslinking conditions. Otherwise unwanted morphological transitions cannot be excluded, leading to the preparation of undesired products and low yields. A high control of the crosslinking strategies is one important prerequisite leading to a significant up-scaling of the yield of polymeric nanoparticles. The results concerning the controlled crosslinking are shown in Chapter 5.

Supramolecular Aggregation

The initial part of my thesis was devoted to investigations of the self-assembly behavior of Janus cylinders and Janus discs. These studies are fundamentally different to studies of other self-assembling systems, as we can for the first time study the effect of a sophisticated and unique architecture on the type of aggregate formed.

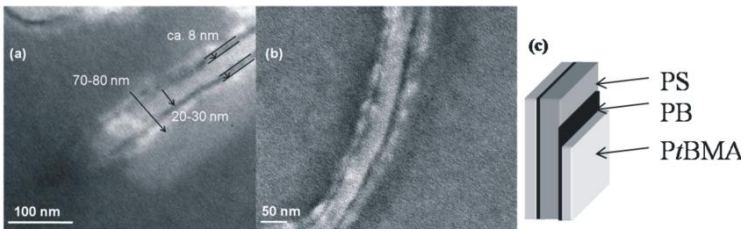

Figure 2 - 1. Superstructures formed by Janus discs, possessing one PS and one P*t*BMA side, in THF (a) and acetone (b). TEM images taken after embedding into a photo-crosslinkable silicon-oil. Thus the images show cross sections according to the drawing in (c).

Some key results in this part were the findings that Janus discs spontaneously form superstructures in organic solvents, which are good solvents for both sides. The Janus discs composed of two sides of polystyrene (PS) and poly(*tert*-butyl methacrylate) (P*t*BMA) undergo back-to-back

stacking into superstructures (see Chapter 14). The self-assembly behavior could be strikingly demonstrated with various imaging techniques. For instance, Figure 2 – 1a-c) show Transmission Electron Microscopy (TEM) images of back-to-back stacked Janus discs. The images were obtained from ultrathin sections after embedding the superstructures from THF or acetone into a crosslinkable silicone oil, microtome cutting and staining. A stacking of the PS sides of the Janus discs can clearly be seen and the multicompartment architecture can be visualized (see Figure 2 - 1c for a schematic representation of the layers). This aggregation of the Janus particles into superstructures is surprising to some extent as both sides of the particles alone, as well as the base terpolymer, are well soluble in the organic solvent used. It appears though that the very slight selectivity of the solvent is sufficient to induce a self-assembly of the Janus discs into defined discrete clusters. Such kind of an aggregation can neither be expected for standard block copolymers nor for homogeneous particles and thus represents one of the unique features of Janus particles.

Truly amphiphilic Janus discs (Chapter 4), which can be obtained by selective hydrolysis of the PtBMA side into PMAA (poly(methacrylic acid)), show somewhat different structures. Herein, a strong influence of the size of the Janus discs on the solution behavior can be deduced. The following picture emerges from the experimental results. Small Janus discs are mostly unimolecularly dissolved in water, as shown by *cryo*-TEM and SFM (Scanning Force Microscopy). According to the *cryo*-TEM images, the discs have a tendency to loosely bind at the edges (Figure 2 – 2a). An aggregation via back-to-back stacking and shielding of the interior of the PS side is widely absent. The height profiles of the SFM images (Figure 2 – 2c-d) show single Janus discs, confirming an absence of stacking. A very small fraction of back-to-back stacked Janus discs can be unambiguously identified in *cryo*-TEM (Figure 2 – 2b), however this motif of stabilization is mostly lacking. Strikingly, this is an unexpected finding and a unique feature of Janus particles. In case of very small discs it is reasonable to assume that the PMAA arms, protruding out on one side, can sufficiently shield the hydrophobic PS side (Figure 2 – 2g). The PMAA arms have an estimated counter length of ca. 110 nm and are thus sufficiently long. With increasing disc size, the steric and electrostatic repulsion of the PMAA brush hairs increases and presumably induces a slight bending of the structure. A further increase of the disc size to large Janus discs leads to a bending along major lines. Bending along major lines can for example be observed in the SEM (Scanning Electron Microscopy) images of the aggregates formed by the large Janus discs (Figure 2 – 2e) and can thus be seen as a main motif for the self-stabilization and the protection of the PS sides with increasing disc diameter. Due to the intrinsic stiffness of the crosslinked layer, large bending is favored with increasing size of the particle.

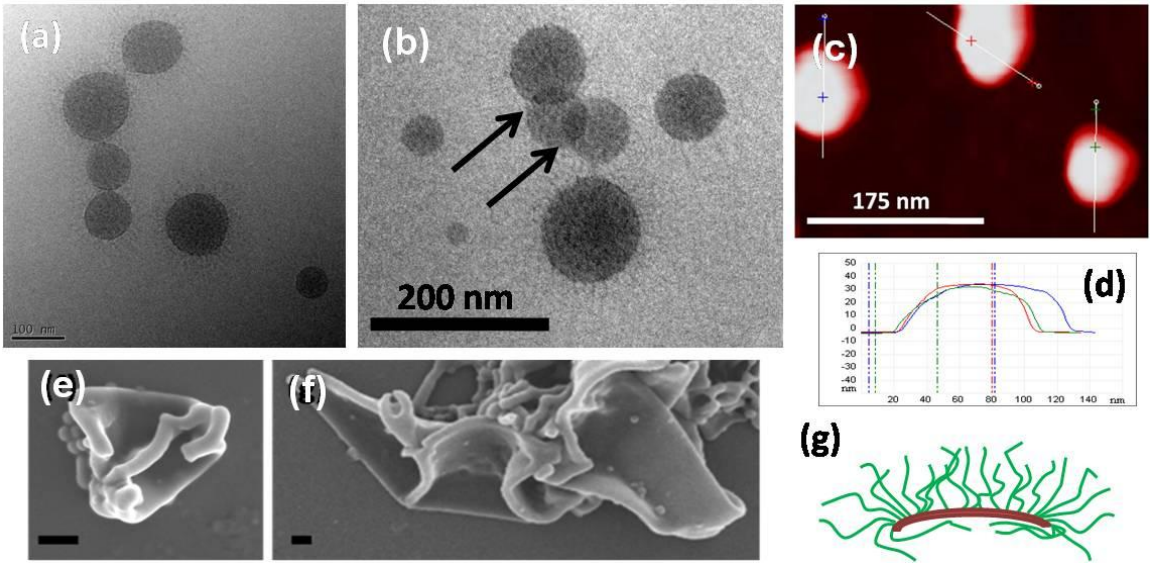

Figure 2 - 2. Cryo-TEM (a+b) and SFM (c) images of small Janus discs. Image (d) shows the section analyses of the lines shown in (c). Image (b) shows slight aggregation via back-to-back stacking of the PS side. (e+f) SEM images of large Janus discs in water (scale bar = 200 nm). (g) Schematic representation of unimolecularly stabilized Janus discs with PMAA arms (green), shielding the red PS side (the PB layer is omitted for clarity).

In case of the Janus cylinders (Chapter 3) having sides of PS and PMMA (poly(methyl methacrylate)), the aggregation can be induced using a selective solvent for one side (i.e. acetone = non-solvent for PS). In a common solvent for both sides, the Janus cylinders are well dispersed as can be seen in the *cryo*-TEM image of a THF solution (Figure 2 - 3a). However, when the solvent is exchanged to acetone, a clustering of the cylinders into fibrils can be observed. The fibrils are composed of 3-5 Janus cylinders which assemble with the PS side in the center (Figure 2 - 3d-e). The aggregation pattern is similar for different lengths of the Janus cylinders and leads to fibers which are significantly longer than the initial Janus cylinders. The length of the fibers can be tuned simply by the concentration. At very low concentrations, a critical aggregation concentration (cac) exists under which the Janus cylinders are unimolecularly dissolved with the PMMA side shielding the PS side. Interestingly, when a solution of Janus cylinders is deposited onto a substrate, a network-like pattern is formed (Figure 2 - 3b-c). Hence, the aggregation takes place on two hierarchical levels. The size of the pores can be tuned in a facile way by changing the concentration of the solution and the aspiration time. Furthermore, since the Janus cylinders can be assembled into fibrils with chemically different surfaces (by selecting the correct selective solvent), a tailoring of the surface chemistry of the networks can be achieved. This represents a very facile approach towards chemo-selective membranes, when higher functionalized Janus cylinders are used.

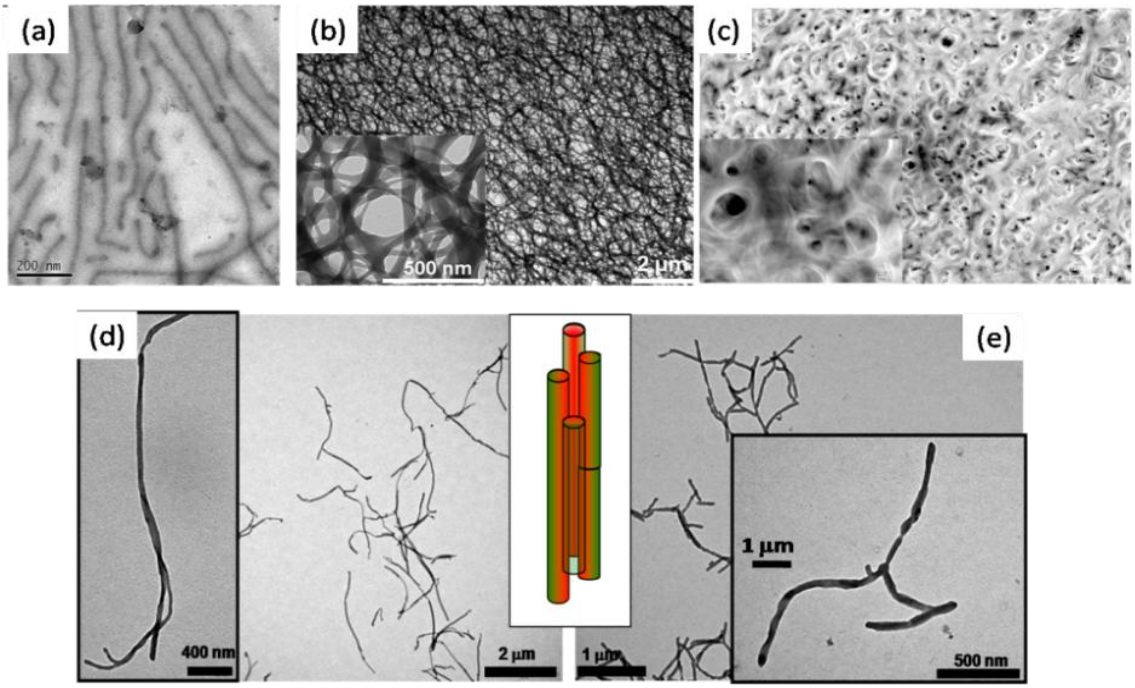

Figure 2 - 3. (a) Cryogenic-TEM image of non-aggregated Janus cylinders in THF. (b+c) TEM and SEM images of network-like structures obtained by drop-casting. (d+e) TEM images of fibrillar superstructures of long (left) and short (right) Janus cylinders.

Self-Assembly of Block Terpolymers in Solution: Toward a Control of the Corona Structure

This project aimed at a facile tunability of the corona structure and the aggregate morphologies formed by bis-hydrophilic triblock terpolymers in aqueous solution (Chapter 6). The triblock terpolymers were designed to have two hydrophilic outer blocks and one inner hydrophobic block with a very low glass transition temperature (PnBuA) to allow structural rearrangements. Polyethylenoxide and various (meth)acrylamide derivatives (NIPAAm, DEAAm, HPMA, AAm) were chosen as outer blocks in order to tailor the interaction parameter of the two hydrophilic blocks located in the micellar corona. Poly(meth)acrylamide derivatives exhibit different solution characteristics depending on the substitution pattern at the amide functions. Polyacrylamide (PAAm) without any hydrophobic substitutes is an extremely polar, highly water-soluble polymer, which does not show any lower critical solution temperature (LCST) behavior. It is known to undergo phase-separation with PEO, thus leading to Janus micelles.[1] Upon addition of hydrophobic substituents to the amide function, e.g. N-(isopropyl)acrylamide (NIPAAm) or N,N-(diethyl)acrylamide (DEAAm), the polymers PDEAAm and PNIPAAm exhibit an appealing stimuli-responsive LCST behavior with different LCSTs. Poly(*N*-(2-hydroxypropyl)methacrylamide) (PHPMA) is a non-immunogenic polymer and has an addressable hydroxyl function which allows the conjugation to drugs or units for cell recognition. Depending on the interaction parameter between the two blocks mixed and phase-segregated (patchy or Janus-type) coronas could be expected. In the case of the structures with mixed coronas, a facile tunability of the corona is possible by changing the degrees of polymerization of the two end blocks. In addition, both blocks can be used for sensing the environment, which is not possible for core-shell-corona structures. The synthesis of these triblock terpolymers was accomplished via Radical Addition Fragmentation Chain Transfer (RAFT) polymerization. Very well defined polymers could be

obtained by this process and a facile adjustment of all blocks allowed a precise tailoring of the overall hydrophilic-to-hydrophobic balance and of the ratio of the two outer blocks. With these features a large diversity of different multicompartment particles can be imagined and tailored for specific applications as for instance in biomedical or sensor applications.

Indeed, the resulting triblock terpolymers exhibit an interesting dynamic behavior in water and allow an adjustment of the corona properties. Interestingly, the aggregates can undergo structural transitions, i.e. from spherical into worm-like structures upon heating. Such a high dynamics cannot be seen for many other micellar systems. The responsiveness to heat involves both the corona structure due to the presence of the LCST segments and the overall architecture of the micelle, that can rearrange because of the low T_g properties of the hydrophobic block, PnBuA. By tuning the hydrophobic to hydrophilic balance, a large variety of structures, i.e. spherical and worm/like micelles as well as vesicles, can be obtained (see Figure 2 - 4).

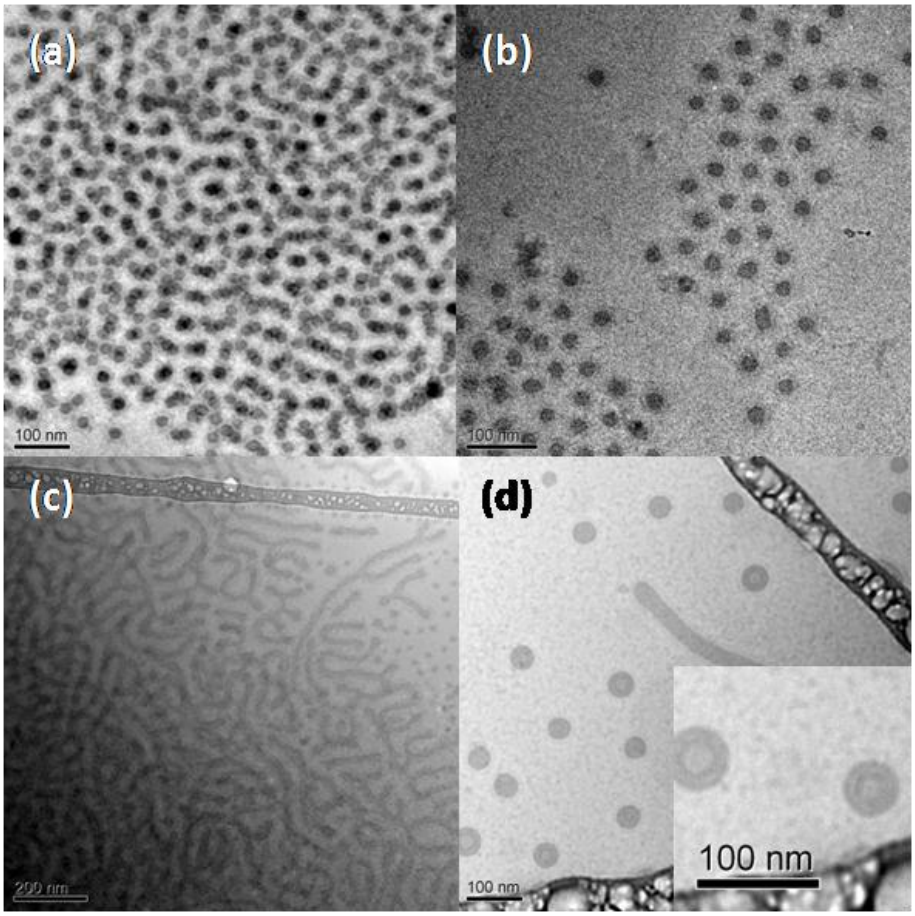

Figure 2 - 4. *Cryo*-TEM images of aggregates formed by PEO114-*block*-PnBuA105-*block*-PDEEAm181 (a+b).*Cryo*-TEM images of the major populations of aggregates found for (a+b), PEO114-*block*-PnBuA250-*block*-PAAm120 (c) and PEO114-PnBuA105-PHPMA101 (d).

Strikingly, a strong effect of the chemistry of the third block and thus the interaction between the various blocks on the type of aggregates formed can be deduced. At similar composition the PNIPAAm and PDEAAm based triblock terpolymers exhibit spherical micelles in water, whereas the PAAm ones exhibit spherical and worm-like micelles and the PHPMA based polymers form mainly vesicles. The decrease in curvature with changing the third block most likely originates from a rising incompatibility of the end blocks. By changing the architecture from spherical to

worm-like and in particular to vesicles, for a given volume fraction of hydrophobic and hydrophilic material, an unfavorable interfacial area between demixed areas of the corona can be minimized. For a variety of samples an aggregation of the micelles into string-like, non-random patterns (see Figure 2 - 4a) could be observed. This phenomenon possibly originates from a sticky interaction of patchy particles. Although the issue of the degree of demixing is a very complicated analytical issue and not fully solved at this point, the triblock terpolymers synthesized clearly provide a platform for the creation of novel multicompartment particles.

Applications of Janus Particles

After controlling the architecture of the Janus particles and gaining in-depth knowledge of their self-assembled structures, the attention was drawn to possible applications of Janus particles. From a scientific, as well as from an industrial point of view, the advanced surface-active properties of particles with a segregated corona over particles with a uniform wettability are very interesting. It was calculated that the surface activity of a Janus particle is up to three times higher at an oil/water interface than that of a uniform particle, leading to an enhanced adsorption at the interface. Janus particles uniquely combine the so-called Pickering effect, known from particles, with amphiphilicity - similar to block copolymers - induced by the Janus character. This combination enables a firm attachment at interfaces and may lead to advanced stabilizing properties in dispersions. Unwanted coalescence of domains of the dispersed phase are thus expected to be diminished using this highly surface-active particles. Thus, the surface active properties are highly interesting for industrial application.

In a first approach, Pickering emulsion polymerization of standard monomers was explored using amphiphilic Janus particles as stabilizers (Chapter 7). The polymerizations could be performed with a simple conventional technique and no pre-homogenization to a miniemulsion was necessary as it is the case for Pickering emulsion polymerizations using homogeneous particles. The reactions led to extremely well-defined latex particles with very narrow size distributions, independently of the monomer used (Figure 2 - 5).

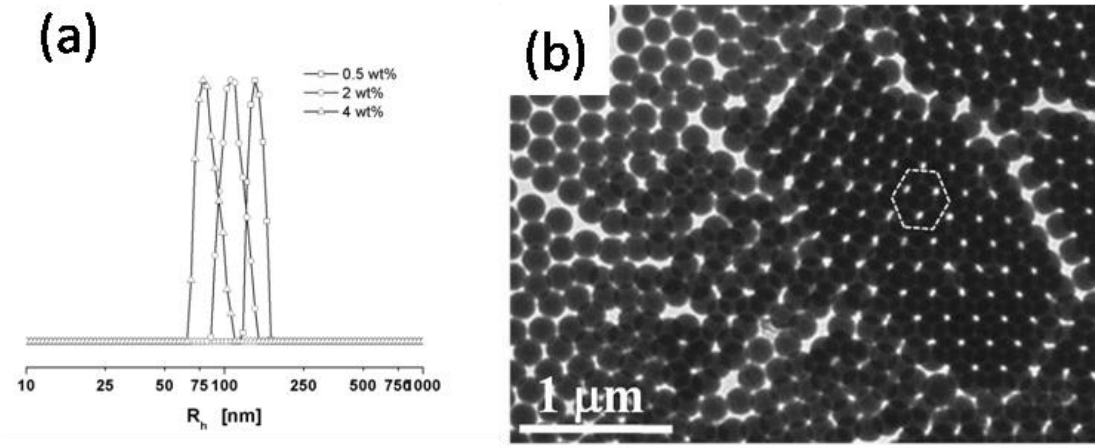

Figure 2 - 5. CONTIN plots (dynamic light scattering) for PS latexes obtained at different contents of Janus particles. (b) TEM micrograph for a PS latex with a stabilizer content of 4 wt%. A double layer of particles can be seen in the micrograph. The hexagon guides the eye for a better recognition of the well ordered pattern.

A control of the latex particle size could easily be achieved by changing the concentration of the stabilizer. After the polymerization, the latex is stabilized by amphiphilic Janus particles, which can, due to their size, not be easily removed from the interface by thermal energy. Thus, a significant improvement of the long-term stability is found.

A second application study dealt with the utilization of Janus particles for the engineering of nanostructured polymer blends with controlled nanoparticle location (Chapter 8). The combination of polymer properties by blending and the introduction of inorganic particles are the most attractive ways for obtaining new products with superior material performances, such as for tailoring the electronic, mechanical or optical features. This does not only hold for large-scale industrial applications, but also for scientific problems as for instance in the case of polymer blend solar cells. In both fields, there is a constant search for better ways of compatibilization. In analogy to colloidal science, we conceived of a novel concept for blending polymers using surfactant-like particles.

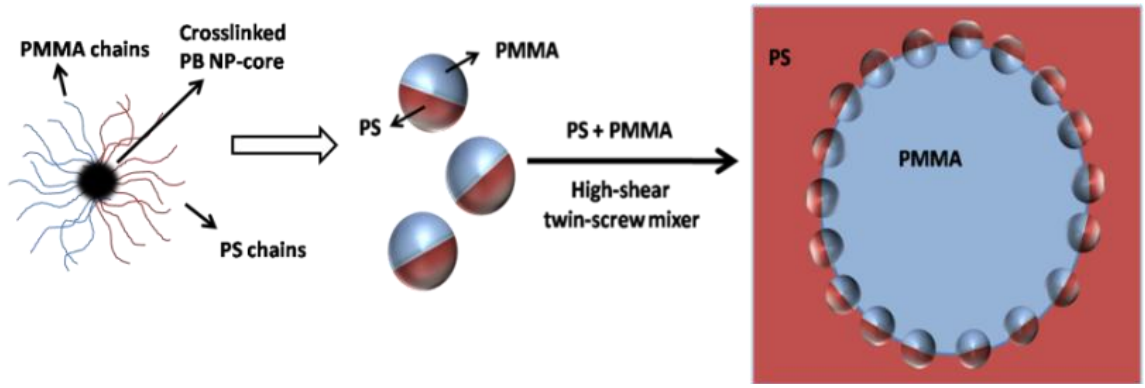

Scheme 2 - 2. Schematic representation of Janus particles and their adsorption at the blend interface of a PS/PMMA blend.

Therefore, we applied Janus particles on a *multi-gram* scale for the blend compatibilization of two model polymers in a twin screw mini-mixer (Scheme 2 - 2). It could be shown that the Janus particles can be located exclusively at the interface of the two polymer phases despite the high temperature and shear conditions. The domain sizes of the dispersed phase decrease with increasing content of Janus particles. The decrease is yet ongoing for high contents of Janus particles (Figure 2 - 6).

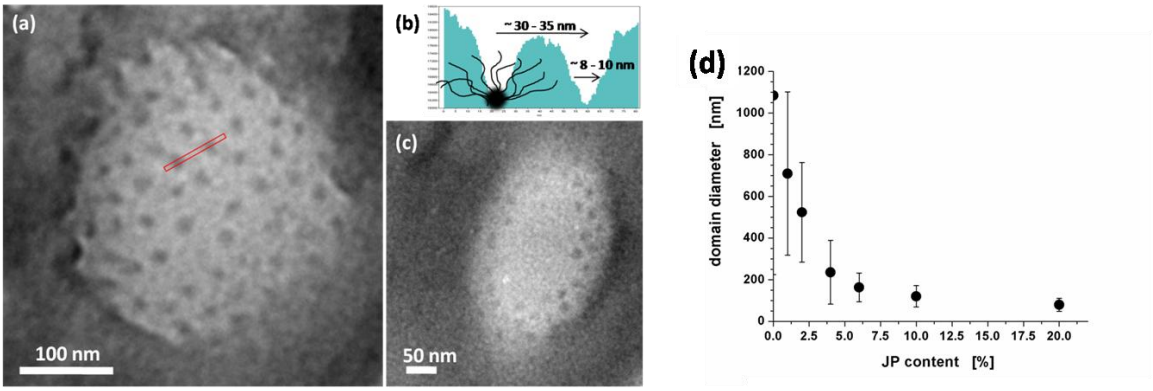

Figure 2 - 6. Endcaps of PMMA droplets in a PS matrix with Janus particles located at the interface (dark dots). (b) Section analysis of the red bar shown in image (a). One side of a Janus particle is schematically sketched to show its brush-like character and the location of the polybutadiene nanoparticle core. (d) Evolution of the PMMA domain size as a function of the Janus particle (JP).

Furthermore, the biphasic particles exhibit an ordered arrangement at the interface, which may be a way of a lateral structuring of polymer interfaces. The strong adsorption at the interface is explained in terms of the increased desorption energy of Janus particles. A similarly high control of the nanoscopic structuring of polymer blends with homogenous nanoparticles has not yet been shown in the literature and is thus of tremendous interest. Furthermore, the compatibilization efficiency was critically compared to state-of-the-art compatibilizers such as block copolymers. It was found that the efficiency of the Janus particles is superior as compared to block copolymer based compatibilizers. This approach demonstrates convincingly that Janus particles are a very promising tool for nanostructuring blend and block copolymer interfaces. Moreover, Janus particles provide a mean for the nanoscopic engineering of blend systems, while matching some macroscopic processing constraints. We are strongly convinced that the results will have an impact on materials science in general and will open up new ways of structuring nanocomposites and high-performance materials, thus bridging academic and industrial research. Developments based on modified Janus particles may take place in important fields like electro-optical polymeric devices (e.g. solar cells), nanocomposites with increased thermo-conductivity or improved crack characteristics and for self-healing materials.

Multicompartment Particles based on Miktoarm Star Terpolymers

At present, miktoarm star terpolymers provide some of the most fascinating and new ways to create multicompartment particles. Their utilization has so far been only restricted to the use of solution based self-assembly of miktoarm star terpolymers with one hydrophobic, one fluorinated and one hydrophilic block. Within the scope of my thesis, I investigated the aggregates formed by SBV miktoarm star terpolymers in acidic solution (Chapter 9), as well as their use for the preparation of novel multicompartment particles based on the selective crosslinking of the microphase-segregated bulk structures (Chapter 10).

SBV Miktoarm Star Terpolymers in Water

Some key results for the self-assembly of the SBV star terpolymers are shown in Figure 2 - 7. Mainly spherical particles with an internal structure can be found. The internal structure is invisible in the absence of OsO_4 staining. Thus the dark domains clearly originate from the stained double bonds of the polybutadiene and confirm the multicompartment character of the micelles. The intrinsic incompatibility between PB and PS is obviously sufficient to induce a phase-segregation in the multicompartment micelles. The corona of P2VP chains cannot be seen in TEM. The multicompartment micelles as found here are composed of two hydrophobic core entities, a soft PB domain and a hard PS domain. A more detailed observation of the particles reveals that the amount of dark domains varies. Unimers, dimers, trimers, tetramers and higher aggregates can be found. We expect that the initially formed unimers with a Janus type segregation into two hydrophobic and demixed cores self-assemble into higher aggregates due to the necessity of shielding some of the hydrophobic parts against the water. Interestingly, the PB domains sizes are different, depending on the size of the overall structure. The larger the PS core, the larger are also the PB domains located on it.

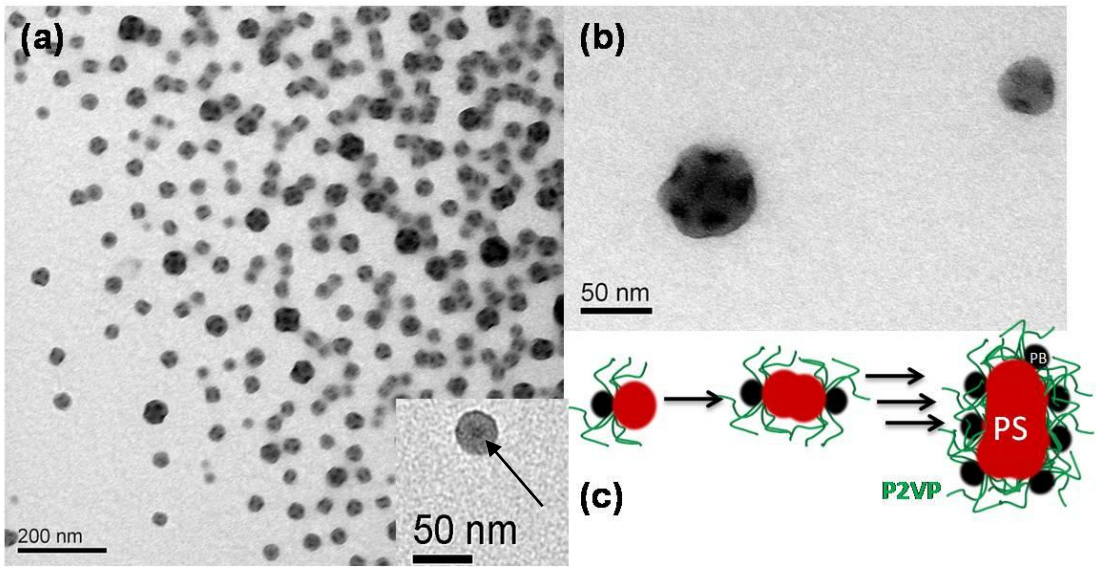

Figure 2 - 7. Low and high magnification TEM images after deposition of an aqueous solution (pH = 2) onto a carbon coated grid and subsequent staining with OsO_4. The inset in image (a) shows a unimeric multicompartment micelle (stained part highlighted by the arrow). The schematic drawing in (c) shows the proposed aggregation pattern. The sample was measured five days after dialysis.

The *cryo*-TEM images revealed a striking and, to the best of our knowledge, previously never seen feature, which is the connection of the micelles via hydrophobic bridges in water (Figure 2 - 8). In all images, several micelles are connected via protrusions extending from the participating micelles. In the upper two images a clear core-corona structure can be found. Note that the P2VP corona cannot be seen in the lower right image, thus confirming the bridges as hydrophobic material.

The implications of these findings are widespread. On the one hand it gives a plausible explanation for the aggregation of initially formed aggregates of multicompartment micelles. The red arrows in the upper two *cryo*-TEM images show all stages of the fusion process with an initially formed bridge, subsequent broadening, fusion and the still persisting nick after the fusion process. More importantly, the unique self-assembled aggregates formed by miktoarm star polymers possess a fair amount of hydrophobic patches exposed to water. For soft, fluid-like polymers with low glass transition temperatures (e.g. PB) forming these exposed domains, this has striking consequences. The

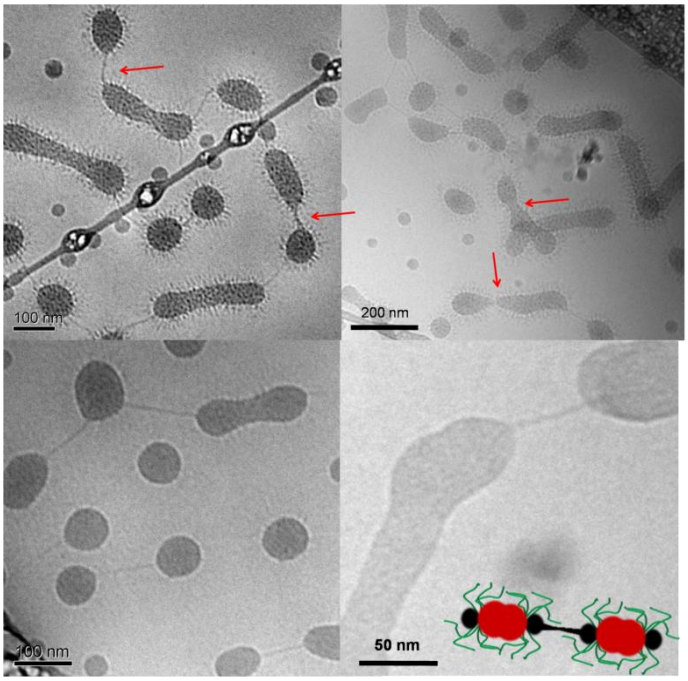

Figure 2 - 8. Cryo-TEM images of aggregates fromed by an aqueous solution (pH = 2) showing the presence of hydrophobic whiskers and a core-corona structure.

dynamic character of such polymers leads to an interaction of the hydrophobic material with its aqueous environment. The material cannot be pictured as hard and non-usable bulk material as for instance in the case of polystyrene. The bridges found in the *cryo*-TEM images resemble to some extent eukaryotic cilia and suggest their utilization as a second mean for sensing, adhesion control or recognition of cell patterns when aiming at controlled delivery. Furthermore, the hydrophobic nature leads to a different interaction with lipid bilayers or cell walls. Usually, hydrophobic moieties can easily penetrate cell walls and thus the hydrophobic parts could be used to enhance cell penetration of micelles. Based on these findings, the unique multicompartment micelles based on miktoarm star terpolymers are not only appealing for drug delivery due to the multicomponent storage but also due to the possibilities of enhanced uptake, adhesion control and advanced sensing.

Structure-Tunable Biaxial Hybrid Nanowires

Since PB is present as one arm in the SBV star terpolymers, the controlled crosslinking of a designated bulk structure was used in order to create biaxial inorganic-organic hybrid nanowires with tunable corona properties. The schematic synthesis and the experimental verification of the concept is given in Figure 2 - 9.

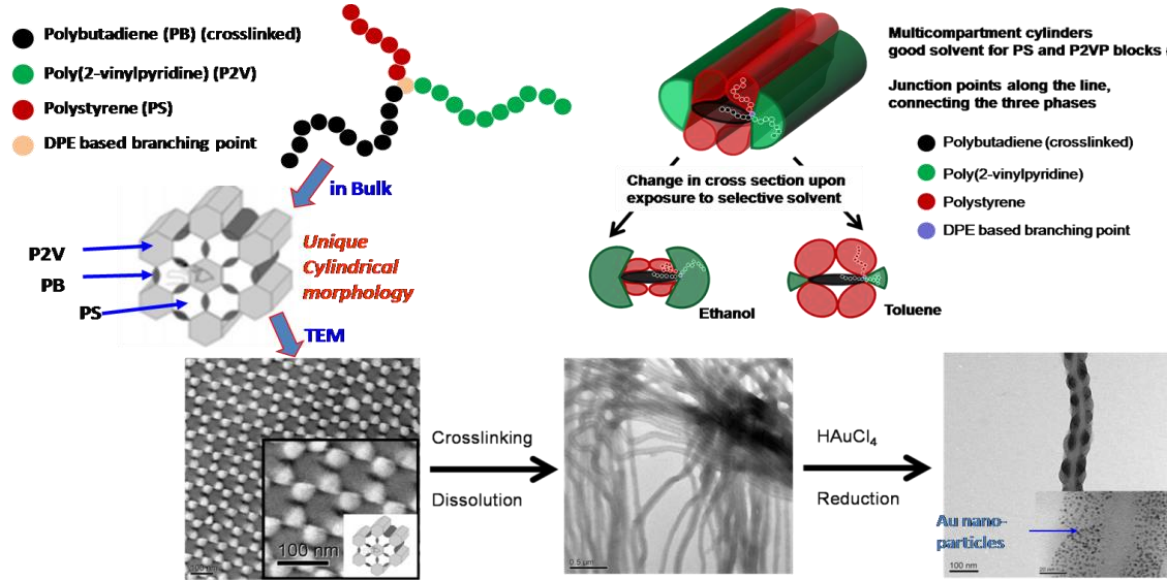

Figure 2 - 9. Strategy for the preparation of multicompartment cylinders and bi-directional nanowires. The TEM images show the bulk structure of the miktoarm star polymer, the cylinders obtained after crosslinking and a bidirectional nanowire after in-situ reduction of gold nanoparticles (from left to right).

Due to the star-shaped architecture, this polymer forms a unique cylindrical morphology in the bulk state, which cannot be obtained for linear triblock terpolymer. A TEM micrograph of a microtome-cut ultrathin section together with its schematic representation is shown in Scheme 2 - 1. The asymmetric, ribbon-like PB domains (black) are centered by two symmetric and opposing PS (red), and two P2VP (green) domains, respectively. The crosslinking of the polybutadiene domains essentially preserves the micro-orientation of the outer compartments and yields the cylinders as shown in Figure 2 - 9.

Due to the presence of P2VP on the two sides of the ribbon-like cylinder, the conjugation of metal salts can be used to create (semi-)conducting inorganic nanoparticles. Some major results concerning the conjugation are exhibited in Figure 2 - 10.

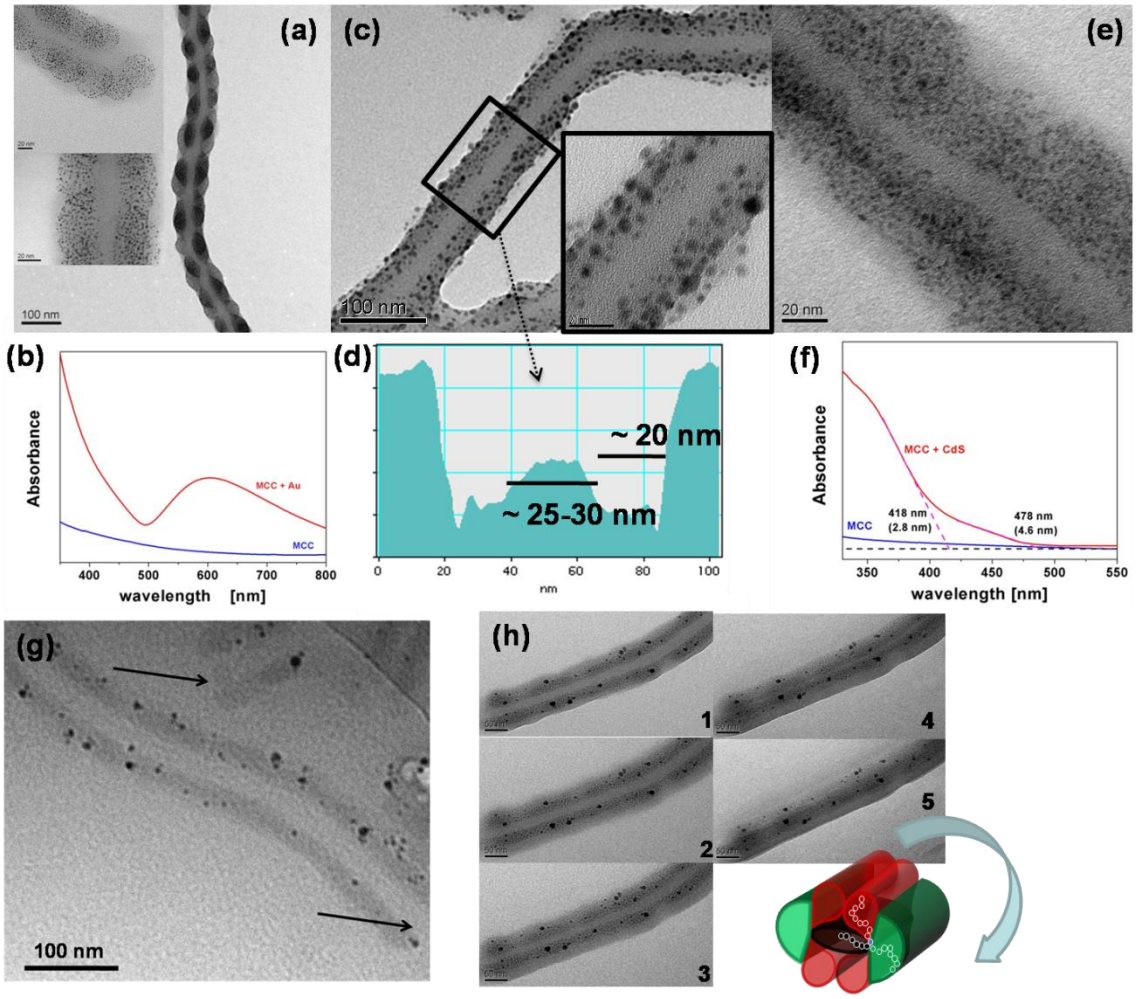

Figure 2 - 10. TEM micrographs of hybrid MCCs as prepared by reduction/reaction of various salts in toluene. (a) Au-loaded MCCs after reduction using a UV-Lamp. (b) UV-Vis spectrum of Au-loaded MCC in toluene. (c) Ag-loaded MCCs after reduction using sunlight. (d) Grey-scale section analysis of the area shown in (c). (e) CdS-loaded hybrid MCCs and its UV-Vis spectrum (f). *Cryo*-TEM image (g) and tilt series (h) of Ag-loaded MCCs after reduction using a UV-lamp. The schematic drawing shows the sequence of recording during the tilt series (1 = lowest angle, 5 = highest tilt angle).

All TEM micrographs exhibit the same feature, being the segregation of the nanoparticles at the two sides of the multicompartment cylinders. This compartmentalization can be nicely amplified by the grey-scale section analysis of the Ag-loaded MCC. Nanoparticles are completely absent in the centre of the structure (ca. 25-30 nm), which also confirms the absence of nanoparticles above and below the MCC. All nanoparticles are confined within the compartments (ca. 20 nm) located at the two sides of the ribbon-like structure and are perfectly aligned in a parallel fashion. Further evidence for the presence of two parallel and spatially separated nanowires is provided by a tilt series, allowing the recording of TEM micrographs at various observation angles. Some images of the tilt series are displayed in Figure 2 - 10 . At zero angle, the center appears lighter with a maximum diameter. With increasing angle up to 60°, the brighter center disappears continuously and the segregation into two parallel compartments cannot be seen anymore, as the rear compartment starts to be partially covered by the front one. In order to

further exclude any drying artifacts occurring during the TEM specimen preparation, we additionally recorded *cryo*-TEM of a different Ag-loaded sample in toluene. In contrast to the *cryo*-TEM image without coordinated NPs, the cylinders now exhibit two dark grey compartmentss on the two sides of the structure. The contrast originates from many small Ag nanoparticles, which cannot be resolved in *cryo*-TEM due to their very small size. Some of the larger Ag particles can however be nicely seen and confirm their coordination to the two sides of the cylinder. Note that the difference in contrast between the center of the MCC and the solvent almost vanishes because of the strong contrast originating from the Ag nanoparticles.

Due to the amphiphilic character of the corona (PS and P2VP) and its accompanying responsiveness to changes in the solvent quality a tuning of the distribution of the nanoparticles in the corona could be achieved. Figure 2 - 11 displays the redistribution of the Ag NPs upon changing the solvent from a common solvent (THF) to selective solvents (toluene and ethanol).

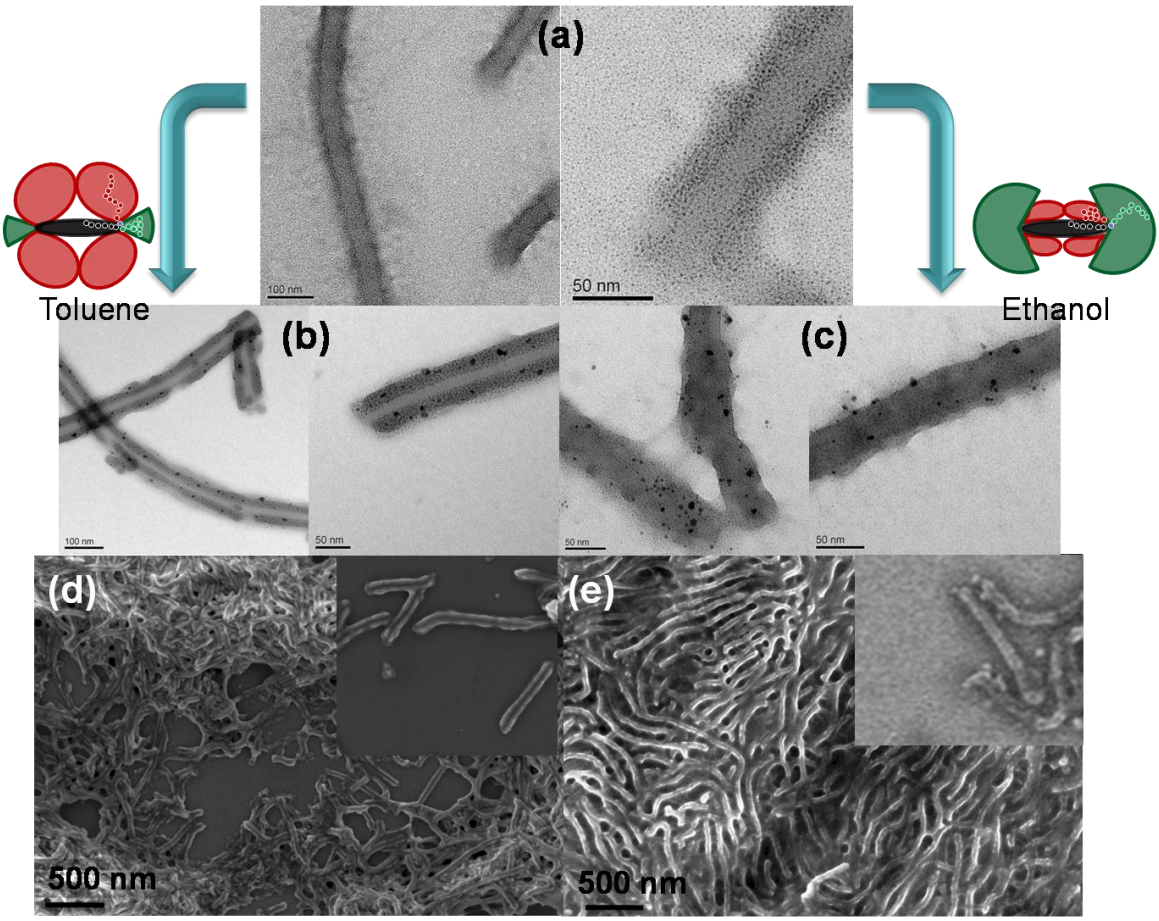

Figure 2 - 11. Structural changes of the corona upon exposure to selective solvents. TEM micrographs of Ag-loaded hybrid MCCs as deposited from THF (a), toluene (b) and ethanol (c). The solvent exchange was performed via dialysis from the THF solution. Low and high magnification non-stained SEM images of Ag-loaded MCCs obtained after deposition from toluene (d) and ethanol (e). The aggregation happens during drying of a droplet onto the silicon wafer.

Initially, the Ag nanoparticles as prepared in THF are predominantly located within the two side-compartments of the structure. Nevertheless, a certain amount (< 10 %) resides in the center of the MCC, meaning above or below. The appearance of particles in the center is caused by the incomplete phase-segregation of the P2VP and the PS compartments in THF. Striking changes can be observed upon exchange of the solvent to toluene and ethanol. In toluene, a non-solvent

for P2VP, the NPs undergo a drastic rearrangement. The hybrid MCCs exhibit a strong compartmentalization and confinement of the NPs within the two compartmentss at the sides. On the contrary, the Ag NPs get redistributed within the full corona of the MCCs in ethanol. This is caused by the collapse of the PS arms and the P2VP arms spreading around the full corona and shielding the full cylinder. The SEM images confirm the compartmentalization in toluene and the redistribution within the full corona for ethanol. Whereas, two distinct bright parallel lines can be found for toluene, a homogeneously bright cylinder can be found for ethanol. Brightness in SEM originates here from the Ag NPs, thus further proving the suggested structure. Consequently, the extent of compartmentalization can be tuned by the solvent choice and manipulated by changing the solvent quality. The two limiting cases are completely separated bi-axial and parallel nanowires and a homogeneous distribution in the corona.

The structure and hybrid materials obtained with this polymer are of such a complexity that it can hardly be imagined to create them with solution based self-assembly of even the most complex amphiphiles. This example demonstrates the powerful capabilities of transferring polymeric bulk structures into solution via crosslinking in order to create most complex multicompartment particles.

Compartmentalized Particles based on Diblock Copolymers

This part of my PHD originated from a joint project together with the chair of Inorganic Chemistry I, that required compartmentalized core-crosslinked cationically charged colloids which could be used for templating mesoporous materials and for the formation of inorganic-organic hybrid materials.

Crosslinking of Crew-Cut Micellar Aggregates of BV diblock copolymers

One way of preparing these materials was envisaged via crosslinking self-assembled aggregates of polybutadiene-*block*-poly(2-vinyl pyridine) (BV) block copolymers in aqueous solution. A careful investigation of various BV block copolymers with varying block lengths of the second block revealed a multitude of crew-cut micellar aggregates (Chapter 11). Depending on the block ratios and the fraction of water added into a dioxane solution of polymer, spherical micelles, branched cylindrical micelles and vesicles could be found (Figure 2 - 12). It was found that these aggregates can be crosslinked in a very facile fashion using a UV photoinitiator. Intermicellar crosslinking and side-reactions could fully be prevented, yielding core-stabilized colloids, stable to changes in environmental conditions and solvent exchange. The photo-crosslinking approach developed herein, shall be applicable to a wide variety of micelles carrying unsaturated moieties and it benefits from its simplicity. The introduction of reactive groups and the use of sophisticated equipment such as gamma sources is not necessary.

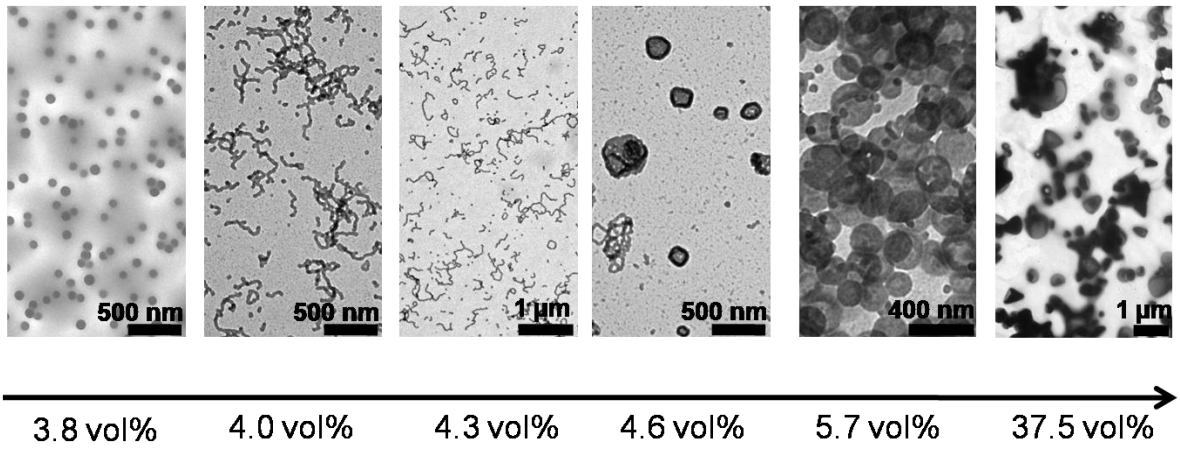

Figure 2 - 12. Phase evolution of crew-cut aggregates during the addition of water to a dioxane solution of B90V10 (c =0.5 wt%). The TEM images were obtained after crosslinking.

Of fundamental interest for colloid science was the observation of a new phase-transition from worm-like micelles to vesicles. The cylinders assemble into large network-like structures and hollow globules and then release smaller vesicles upon completion of the phase transition. This mechanism is essentially different compared to the common mechanism found for block copolymers, proceeding via cup-like intermediates. The results demonstrate that the phase-transition in block copolymers may follow significantly different pathways. The appearance of a certain pathway may depend on the individual system.

Keggin-type Polyoxomethalate Grafted BV Nanorods

An alternative approach for the creation of stabilized cationically charged polymeric nanoparticles was furthermore pursued in this project (Chapter 12). Similar to the preparation of Janus cylinders, microphase-segregated BV diblock copolymers films with a cylindrical morphology of PB in P2VP were crosslinked. The herewith obtained BV nanorods possess different characteristics as the self-assembled cylinders shown in Figure 2 - 13. The weight fractions of the corresponding blocks are almost inverse, as the solution based self-assembly is changed to self-assembly in the bulk. The BV nanorods obtained with the second approach are significantly better defined with respect to their diameter, are much stiffer and the corona block is much longer, compared to the core block. Due to these advantageous features, the BV nanorods were used for the conjugation with Keggin-type polyoxometalates (POM), yielding POM grafted core-shell cylinders, having a core of crosslinked PB and a corona of POM@P2VP.

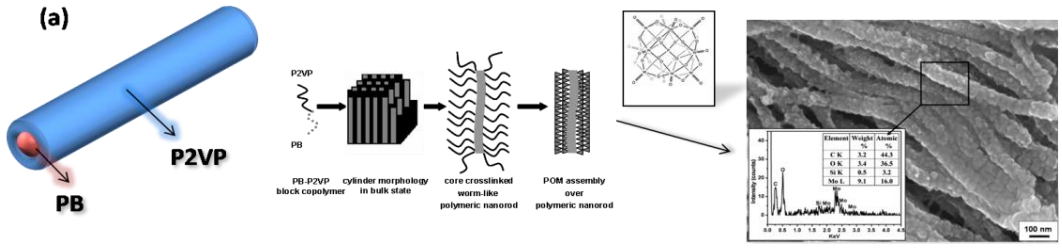

Figure 2 - 13. Synthetic access towards keggin-type POM grafted onto PB-P2VP core-shell nanorods. The right-hand side shows an SEM image with an EDX analysis serving as a confirmation of the structure.

Keggin ions are very attractive for catalytic applications, however, the commercially available materials have the disadvantage of showing very low surface areas and are thus cost ineffective.

With this conjugation, high surface areas can be achieved and the catalytic performance can be increased significantly. Furthermore, since shape-persistent nanorods are used, a large variety of different catalytic nanoparticles can be incorporated while the shape of the hybrid is retained. This is a considerable advantage to many other preparations of hybrid materials that use self-assembled templates, which always have the uncertainty of undergoing undesired structural changes.

Individual Contributions to Joint Publications

The results presented in this thesis were obtained in collaboration with others and published as indicated below. In the following, the contributions of all the coauthors to the different publications are specified. The asterisk denotes the corresponding author.

Chapter 3

This work is submitted to the JOURNAL OF THE AMERICAN CHEMICAL SOCIETY under the title:

"Self-Assembly of Janus Cylinders into hierarchical Superstructures"

by Andreas Walther,* Markus Drechsler, Sabine Rosenfeldt, Ludger Harnau, Matthias Ballauff, Volker Abetz and Axel H. E. Müller*

I conducted all experiments and wrote the publication.

Exceptions are stated in the following:

M. Drechsler performed some cryo-TEM measurements.

S. Rosenfeldt, L.Harnau and M. Ballauff treated the SANS data.

V. Abetz and A. Müller were involved in scientific discussion and correcting the manuscript.

Chapter 4

This work is published in SOFT MATTER (on the web) under the title:

"Superstructures of Amphiphilic Janus Discs in Aqueous Medium"

by Andreas Walther,* Markus Drechsler and Axel H. E. Müller*

I conducted all experiments and wrote the publication.

Exceptions are stated in the following:

M. Drechsler performed some cryo-TEM measurements.

A. Müller was involved in scientific discussion and correcting the manuscript.

Chapter 5

This work is published in POLYMER (**2008**, 49, 3217-3227) under the title:

"Controlled Crosslinking of Polybutadiene Containing Block Terpolymer Bulk Structures: A Facile Way towards Complex and Functional Nanostructures"

by Andreas Walther,* Astrid Göldel and Axel H. E. Müller*

I conducted all experiments and wrote the publication.

Exceptions are stated in the following:

A. Göldel performed the microtome cutting and some TEM measurements.

A. Müller was involved in scientific discussion and correcting the manuscript.

Chapter 6

This work is published in MACROMOLECULES (on the web) under the title:

"Bis-Hydrophilic Triblock Terpolymers via RAFT Polymerization: Towards Dynamic Micelles with Tunable Corona Properties"

by Andreas Walther,* Pierre-Eric Millard, Anja S. Goldmann, Tara M. Lovestead, Felix Schacher, Christopher Barner-Kowollik* and Axel H. E. Müller*

I conducted all experiments and wrote the publication.

Exceptions are stated in the following:

P.-E. Millard performed the LACCC measurements.

A. Goldmann performed the MALDI-ToF MS measurements.

T. Lovestead performed the ESI-MS measurements.

F. Schacher performed the 2D NMR measurement.

C. Barner-Kowollik and A. Müller were involved in scientific discussion and correcting the manuscript.

Chapter 7

This work is published in ANGEWANDTE CHEMIE INTERNATIONAL EDITION IN ENGLISH (**2008**, 47, 711-714) under the title:

"Towards Application of Janus Particles: Emulsion Polymerization using Janus Particles as Stabilizers"

by Andreas Walther,* Martin Hoffmann and Axel H. E. Müller*

I conducted experiments, the TEM measurements, wrote the publication and supervised M. Hoffmann during his advanced lab course doing further experiments.

A. Müller was involved in scientific discussion and correcting the manuscript.

Chapter 8

This work is published in ACS NANO (**2008**, 2, 1167-1178) under the title:

"Engineering Nanostructured Polymer Blends with Controlled Nanoparticle Location using Janus Particles"

by Andreas Walther,* Kerstin Matussek and Axel H. E. Müller*

I conducted all experiments, most of the analytical experiments and wrote the publication.

Exceptions are stated in the following:

K. Matussek operated the twin-screw mini mixer and performed microtome cutting of the samples.

A. Müller was involved in scientific discussion and correcting the manuscript.

Chapter 9

This work is accepted for publication in CHEMICAL COMMUNICATIONS under the title:

"Formation of Hydrophobic Bridges between Multicompartment Micelles in Water"

by Andreas Walther,* Axel H. E. Müller*

I conducted the experiments and wrote the publication.

A. Müller was involved in scientific discussion and correcting the manuscript.

Chapter 10

This work is submitted to NATURE NANOTECHNOLOGY under the title:

"Structure-Tunable Bidirectional Hybrid Nanowires Templated by Polymeric Multicompartment Cylinders"

by Andreas Walther,* Jiayin Yuan, Volker Abetz and Axel H. E. Müller*

I conducted all experiments and wrote the publication.

J. Yuan was involved in discussion and performed some UV-Vis and photoluminescence experiments.

V. Abetz and A. Müller were involved in scientific discussion and correcting the manuscript.

Chapter 11

This work is published in MACROMOLECULES (**2008**, 41, 3245-3260) under the title:

"Multiple Morphologies, Phase Transitions and Crosslinking of Crew-Cut Aggregates of Polybutadiene-*block*-Poly(2-vinylpyridine) Diblock Copolymers"

by Andreas Walther,* Anja S. Goldmann, Ram Sai Yelamanchili, Markus Drechsler, Holger Schmalz, Adi Eisenberg, Axel H. E. Müller*

I conducted most experiments and wrote the publication.

A. Goldmann performed the MALDI-ToF MS measurements.

R. Yelamanchilli was involved in discussion.

M. Drechsler performed some cryo-TEM measurements.

A. Eisenberg was involved in scientific discussion.

H. Schmalz and A. Müller were involved in scientific discussion and correcting the manuscript.

Chapter 12

This work is published in CHEMICAL COMMUNICATIONS (**2008**, 489-491) under the title:

"Core-Crosslinked Block Copolymer Nanorods as Novel Templates for the Assembly of Polyoxometalates"

by Ram Sai Yelamanchili, Andreas Walther, Axel H. E. Müller* and Josef Breu *

This is a joint project between the chairs of AC 1 and MC 2.

I conducted all experiments concerning the preparation of the core-crosslinked nanorods, assisted in the analytics, was involved in the discussion and wrote parts of the publication.

R. Yelamanchili performed all conjugation experiments with the inorganic compounds and most characterization of the hybrid materials.

A. Müller and J. Breu were involved in scientific discussion and correcting the manuscript.

Chapter 13 (Appendix)

This work is published as highlight article in SOFT MATTER (**2008**, 4, 663 - 668) under the title:

"Janus Particles"

By Andreas Walther* and Axel H. E. Müller*

I wrote the manuscript which was corrected by A. Müller.

Chapter 14 (Appendix)

This work is published in the JOURNAL OF THE AMERICAN SOCIETY (**2007**, 129, 6187-6198) under the title:

"Janus Discs"

by Andreas Walther,* Xavier André, Markus Drechsler, Volker Abetz, Axel H. E. Müller*

This publication is based on my preceding diploma thesis, but contains further key results obtained during my PhD studies.

I conducted all experiments and wrote the publication.

Exceptions are stated in the following:

X. André introduced me to anionic polymerization.

M. Drechsler performed some cryo-TEM measurements.

V. Abetz and A. Müller was involved in scientific discussion and correcting the manuscript.

References

1. Voets, I. K.; de Keizer, A.; De Waard, P.; Frederik, P. M.; Bomans, P. H. H.; Schmalz, H.; Walther, A.; King, S. M.; Leermakers, F. A. M.; Cohen Stuart, M. A. *Angew. Chem. Int. Ed.* **2006,** 45, 6673-6676.

3. SELF-ASSEMBLY OF JANUS CYLINDERS INTO HIERARCHICAL SUPERSTRUCTURES

Andreas Walther, Markus Drechsler, Sabine Rosenfeldt[&], Ludger Harnau[$], Matthias Ballauff[&], Volker Abetz[‡], Axel H. E. Müller

Makromolekulare Chemie II and Bayreuther Zentrum für Kolloide und Grenzflächen, Universität Bayreuth, D-95440 Bayreuth, Germany

Andreas.Walther@uni-bayreuth.de; *Axel.Mueller@uni-bayreuth.de*

[&] Physikalische Chemie I and Bayreuther Zentrum für Kolloide und Grenzflächen, Universität Bayreuth, D-95440 Bayreuth, Germany

[$] Max-Planck-Institut für Metallforschung and Institut für Theoretische und Angewandte Physik, Universität Stuttgart, D-70569 Stuttgart, Germany

[‡] Institut für Polymerforschung, GKSS-Forschungszentrum Geesthacht GmbH, D-21502 Geesthacht, Germany

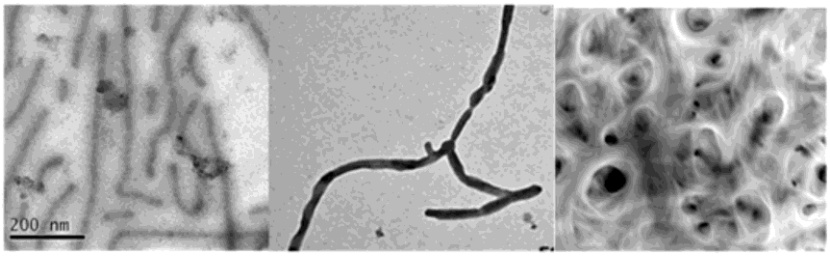

Submitted to the *Journal of the American Chemical Society*

Abstract

We present in-depth studies of the size-tunability and the self-assembly behavior of Janus cylinders showing a phase-segregation into two hemi-cylinders. The cylinders are prepared by crosslinking the lamella-cylinder morphology of a polystyrene-*block*-polybutadiene-*block*-poly(methyl methacrylate) block terpolymer. The length of the Janus cylinders can be adjusted both by the amplitude and the duration of a sonication treatment from the micro- to the nanometer length. The corona segregation into a biphasic particle is evidenced by selective staining of the PS domains with RuO_2 and subsequent imaging. The self-assembly behavior of these facial amphiphiles on different length scales is investigated combining dynamic light scattering (DLS), small-angle neutron scattering (SANS) and imaging procedures. Cryogenic transmission electron microscopy images of the Janus cylinders in THF, which is a good solvent for both blocks, exhibit unimolecularly dissolved Janus cylinders with a core-corona structure. These results are corroborated by SANS measurements. Supramolecular aggregation takes place in acetone, which is a non-solvent for polystyrene, leading to the observation of fiber-like aggregates. The length of these fibers depends on the concentration of the solution. A critical aggregation concentration is found, under which unimolecularly dissolved Janus cylinders exist. The fibers are composed of 2 – 4 Janus cylinders, shielding the inner insoluble polystyrene hemi-cylinder against the solvent. Thus, the SANS data reveal a core-shell structure of the aggregates. Upon deposition of the Janus cylinders from more concentrated solution, a second type of superstructure is formed on a significantly larger length scale. The Janus cylinders form fibrillar networks, in which the pore size depends on the concentration and the deposition time of the sample.

Introduction

In recent years, Janus particles have attracted much attention in nanoscience due to their interesting properties, both for academic as well as for technological reasons.[1-7] In general, Janus structures can be divided into three classes according to their architecture – spherical micelles (3D), two types of cylinders (1D) and sheets or discs (2D),[8] representing the intermediate case of dimensionality (see Scheme 3 - 1). The synthesis of such non-centrosymmetric structures with compartmentalized coronas is a demanding task for the synthetic chemist. Hence, only a few real nanosized polymer-based Janus structures are known in literature.

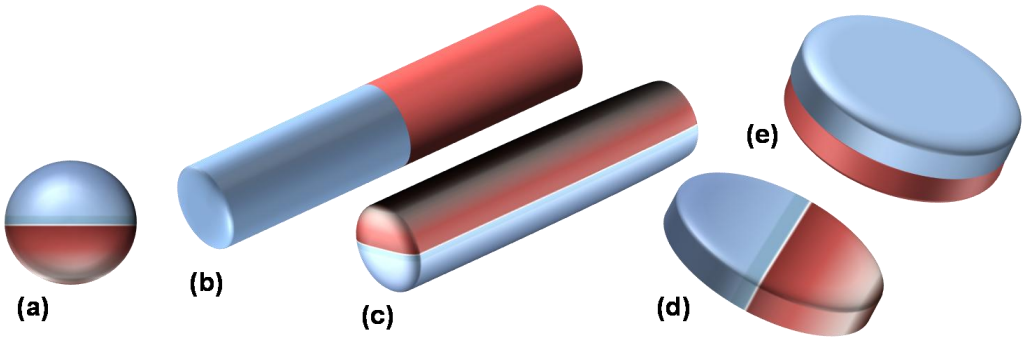

Scheme 3 - 1. Possible Janus architectures with phase-segregated shells: (a) spherical Janus micelle, (b+c) two types of Janus cylinders, (d+e) two types of Janus sheet/disc.

One of the most intensively studied systems is the one concerning the spherical Janus micelles, which are based on template-assisted synthesis using polystyrene-*block*-polybutadiene-*block*-poly(methyl methacrylate) (SBM) block terpolymers. The SBM Janus micelles, as well as their amphiphilic pendants, the hydrolyzed SBMA Janus micelles (MA: methacrylic acid) show interesting hierarchical organization on different length scales. The SBM micelles form larger aggregates in non-selective organic solvents, on a silicon surface,[9] and at the air/water interface.[10] The amphiphilic SBMA micelles, obtained after hydrolysis of the PMMA ester groups, also exhibit superstructures and giant particles.[11] Recently, we succeeded in the preparation of disc-shaped Janus particles which exhibit unexpected back-to-back stacked superstructures in good solvents.[1]

Concerning Janus cylinders, the most promising approach was described by Liu et al., who synthesized Janus cylinders based on the selective crosslinking and subsequent sonication of a lamella-cylinder phase of suitable SBM block terpolymers (see Scheme 3 - 1c).[12] Cylindrical Janus structures in the nanometer range are unknown in literature except of this approach. However, some efforts have been made aiming at the creation of AB type polymer brushes (see Scheme 3 - 1b). For instance, Ishizu et al.[13] synthesized amphiphilic brush-*block*-brush AB-type polymer brushes by a combined grafting through and grafting from process. After polymerizing a PEO macromonomer via ATRP, a second monomer (2-hydroxyethyl methacrylate, HEMA) was added to form the second block. Subsequent esterification with an ATRP initiator and an additional ATRP of HEMA rendered a Janus type polymer brush with PEO and PHEMA side chains. The polymer brush showed an ellipsoidal shape rather than a cylindrical one, as the degree of polymerization of the backbone was relatively low. Besides, Dendukuri et al. reported on the preparation of AB-type microparticles via continuous-flow lithography.[14] This preparation strategy can however not access nanometer-sized particles.

Janus structures are interesting for a variety of reasons. For instance, they may be used as nanorheological probes, highly specific chemical sensors for immunoassays and molecular interactions or may be employed for devices which require switching with an electric or magnetic field.[15-22] Furthermore, applications are conceivable in fields like nanomedicine. Janus particles with a catalytically active hemisphere exhibit propulsion induced by reactions on one side, resembling to some extent the bacterial flagella.[23] In addition, amphiphilic Janus particles could provide an ideal "repair and go" system for cracks within microfluidic channels such as blood vessels and act similar as artificial leukocytes.[24]

Herein, we present results concerning the size tunability of Janus structures with compartmentalized corona. Furthermore, structural details of the self-assembly properties of the Janus cylinders will be demonstrated by cryo-TEM, TEM, DLS and SANS, thus combining scattering and imaging techniques. The studies are fundamentally different to usual self-assembly studies known in literature. Herein we analyze the influence of a unique architectural feature, the Janus type segregation of the cylinder, on the type of aggregates formed. Only by knowing and being able to control the aggregation patterns of subdivided colloids, we will be able to transfer their unique properties into future applications. Aside of that, Janus cylinders can be considered as a large synthetic analogue of facial amphiphiles, which are of fundamental importance in bioscience. Due to their unique distribution of functional groups on the two sides, they have intriguing properties which result in the formation of distinct colloidal aggregates and foldamers.[25] Thus studying the aggregate behaviour of Janus cylinders can also shine further light on the self-assembly processes in much smaller systems of facial amphiphiles.

Results and Discussion

Size Tunability

Scheme 3 - 2 depicts the synthetic procedure towards the preparation of Janus cylinders. The Janus cylinders are produced by the selective crosslinking of the lamella-cylinder morphology, formed by a $S_{41}B_{14}M_{45}^{110}$ block terpolymer (polystyrene-*block*-polybutadiene-*block*-poly(methyl methacrylate)). The indices represent the weight fractions, whereas the superscript shows the overall molecular weight in kg/mol. The crosslinking of the polybutadiene domains can be accomplished via cold vulcanization using S_2Cl_2 in a well-ordered solvent-swollen bulk morphology.[26]

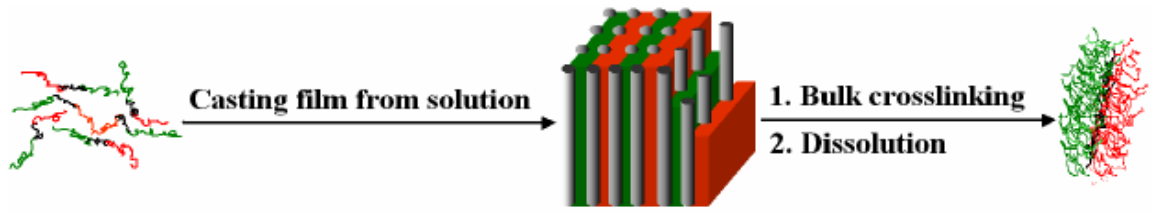

Scheme 3 - 2. Schematic synthesis of Janus cylinders.

Since sonication is used to create soluble cylinders from the tightly crosslinked block terpolymer template, it is possible to adjust their length by the duration of the homogenization procedure. Dynamic Light Scattering (DLS) and Transmission Electron Microscopy (TEM) were used to characterize the size evolution of the Janus cylinders with time and with varying power (see Figure 3 - 1).

The size distributions obtained by DLS show a characteristic shift towards smaller hydrodynamic radii with increasing sonication time (see Figure 3 - 1). Besides, the curves exhibit a significant narrowing for longer sonication times, indicating a decrease in polydispersity of the system. The second cumulant, which can be considered as an estimation of the polydispersity of the samples, decreases from 1.3 to 1.1. This indicates a fairly low or acceptable polydispersity. A detailed look at the evolution of the z-averaged hydrodynamic radius, $\langle R_h \rangle_z$, with sonication time and sonication power reveals a rapid decay. The curves follow an exponential decrease, indicating that in the beginning of the ultrasound treatment the large cylinders are fragmented into significantly smaller ones. After a certain time the curves show a more asymptotical behaviour with a slower decay of the cylinder length. Consequently, there is some higher resistance to the introduced sonication energy. This resistance is presumably due to the higher mobility of the smaller structures, an accompanying higher resistance and more flexible adaptation to the shock waves produced by the ultrasound. An increase in the sonication amplitude from 10 % to 70 % leads to a faster disruption, which is due to the higher energy introduced into the system. The observed decrease of the hydrodynamic radius can be correlated convincingly to a shortening of the Janus cylinders as observed by TEM (see Figure 3 - 1 c-e). The consecutive series of TEM images were obtained from Janus cylinder samples at different sonication times. Whereas the left image shows cylindrical molecules exceeding the 2 µm scale bar, the right image displays cylinders significantly smaller than 2 µm. The image in the centre exhibits cylinders of intermediate length corresponding to intermediate sonication time.

The results demonstrate convincingly the facile tunability of the size of the Janus cylinders. The cylindrical Janus particles can be adjusted from the micrometer range down to the nanometer level, thus covering a large mesoscopic length scale.

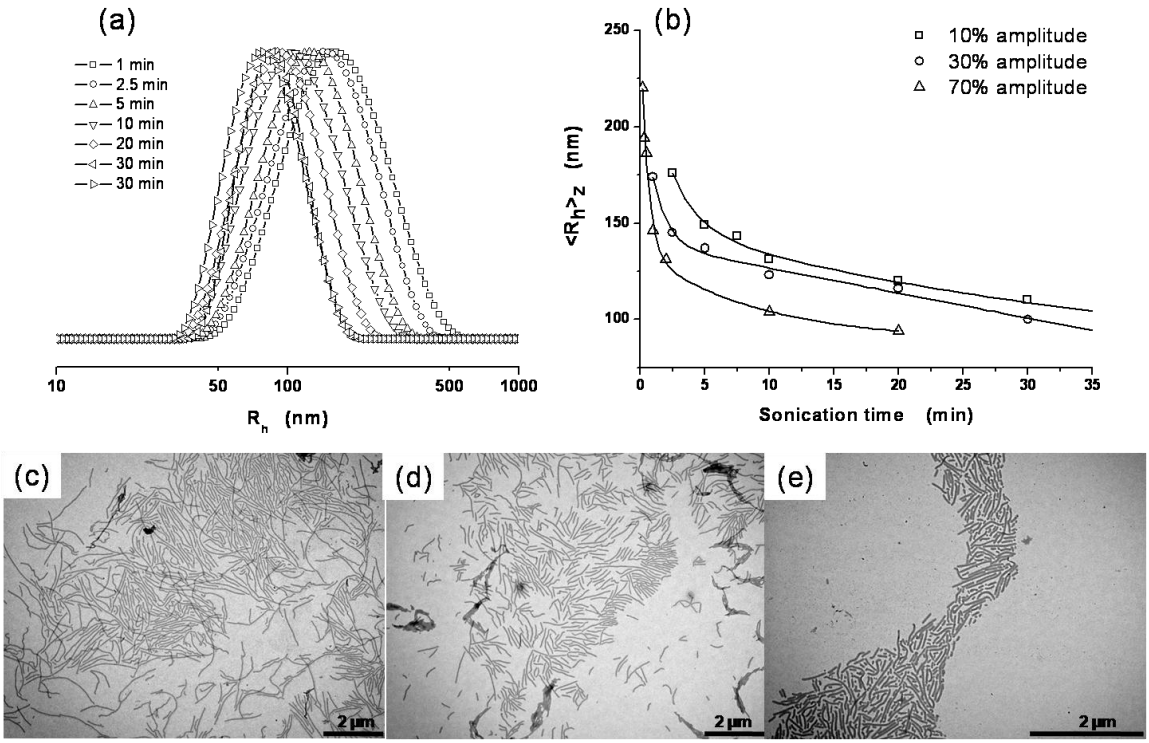

Figure 3 - 1. Size evolution of Janus cylinders: (a) DLS CONTIN plots at various states of sonication at 30% sonication amplitude and 80° scattering angle. (b) Time-dependence of the z-average hydrodynamic radius, obtained after extrapolating to $q^2 = 0$, at different sonication amplitudes as indicated in the image. (c), (d) and (e) TEM images obtained for different sonication times at 30% amplitude (1 min, 5 min, 20 min).

Janus Character

After being able to tune the size by means of sonication, it is of interest to give an evidence for the Janus character of the synthesized cylinders. To draw comprehensive conclusions about the self-assembly behavior, knowledge of the cross-section is an important prerequisite. Figure 3 - 2 shows several TEM images of Janus cylinders after staining with RuO_2. RuO_2 preferentially stains interfaces and aromatic moieties such as polystyrene, which is one hemi-cylinder of the Janus cylinders. The image presented in Figure 3 - 2a shows individual cylinders with a symmetric appearance of the cross section. This is caused by a thermodynamically preferred adsorption of one side of the Janus cylinders (PS) onto the carbon film. The diameter of the structure is ca. 75 nm (outer dark lines as margin). The two dark parallel lines indicate the presence of the major amount of polystyrene due to the strong selective staining. The PMMA does not lead to any contrast in TEM, as it is non-stained and additionally degrades upon e-beam exposure. Note that a slight dark corona can be seen surrounding the cylinders, which is caused by PS chains adsorbed onto the grid (ca. 20 - 25 nm). Note that a strong adsorption and the introduction of chemical stains (bulky molecules) also alter the dimensions of the particles and thus the dimension found may differ from the real ones in solution. The dimensions in solution as obtained by SANS and cryo-TEM will be discussed below. To be able to visualize the desymmetrized corona, we have to take advantage of the aggregation tendency of Janus cylinders on the surface of the TEM grid. Figure 3 - 2b shows a magnified section in which two Janus cylinders are aggregated on the right-hand side of the image. This aggregation of two Janus cylinders induces a rotation of the cylinders on the substrate. The aggregation hinders a preferred adsorption of one of its sides onto the TEM grid. The observation direction is now in plane with the interface of the phase segregation (see schematic drawings at the bottom of Figure 3 - 3-2). The cross-section in Figure 3 - 2d corresponds in term of the diameter to an individual Janus cylinder (~ 75 nm) and clearly exhibits a biphasic cross section. The white part (~ 17 nm) corresponds to the PMMA part. This white part is almost doubled (~ 27 nm, Figure 3 - 2d) for the two aggregated Janus cylinders on the right-hand side of Figure 3 - 2b. The overall diameter increases to ca. 130 nm, corresponding to two Janus cylinders. In conclusion, the selective staining of the PS domain of the cylinders clearly confirms the biphasic segregation into a Janus cylinder. This result also represents one of the first direct real space proofs for the Janus character of nano-sized polymeric colloids, which is also of fundamental importance.

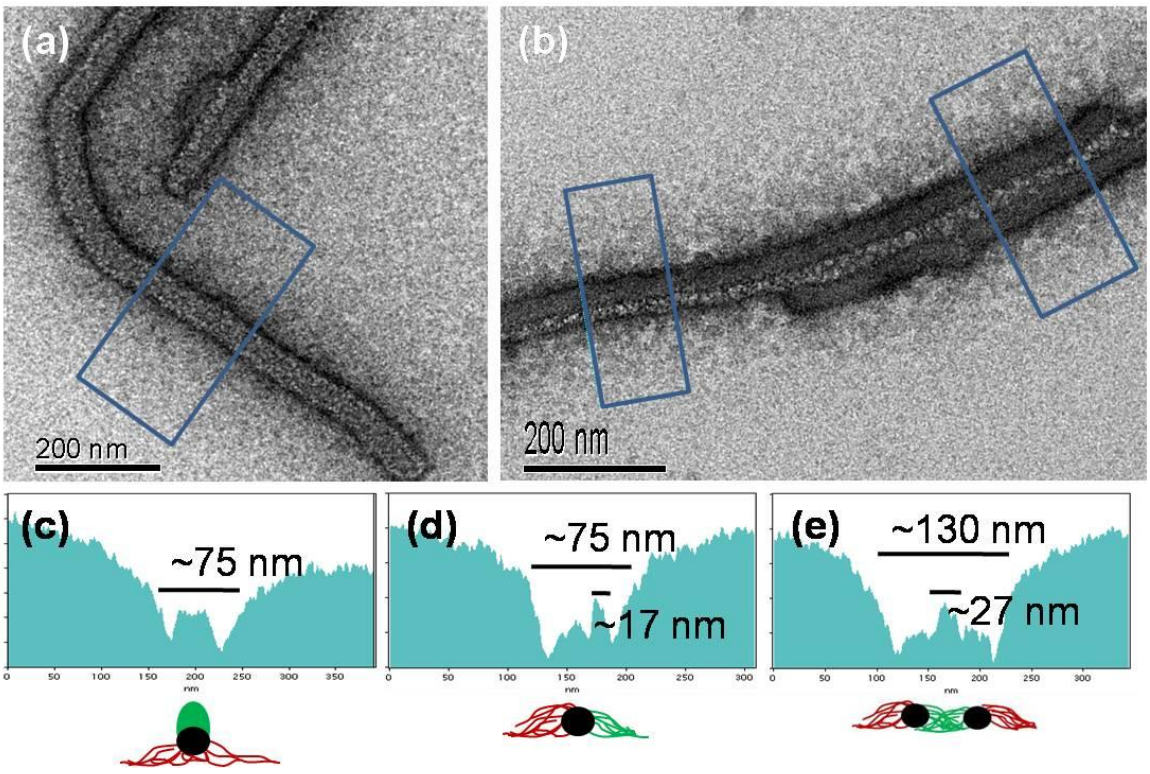

Figure 3 - 2. TEM images of single (a) and aggregated (b) Janus cylinders on a carbon-coated TEM grid after staining with RuO_2 for 2h. Grey scale analyses (c-e) correspond to the section analyses as shown in the images from left to right. The schematic drawings at the bottom exhibit the orientation of the Janus cylinders within the cross-sections (PB = black, PS = red, PMMA = green).

Solution Properties and Self-Assembly Behavior

Janus particles are known to undergo unexpected self-aggregation, even in good solvents. Earlier, Erhard et al. demonstrated convincingly that spherical Janus micelles assemble into discrete clusters above a certain critical aggregation concentration.[9] Recently, we published results on Janus discs indicating a back-to-back stacking of the particles in THF.[8] During the investigation of the disc-like Janus particles it turned out that cryo-TEM in THF is a very powerful technique to investigate the aggregation behavior of labile aggregates in organic solvents.[27] Compared to standard imaging techniques like scanning force microscopy (SFM) or scanning electron microscopy, this in-situ technique has major advantages. The first is the fact that the accessible concentration range is typically much higher. In particular, when analyzing the self-aggregation behavior of particles which are supposedly well soluble in the solvent (like a PS-PMMA Janus micelle in THF), the expected critical aggregation concentrations may be rather high. Moreover, the particles may only be loosely bound together. Usually, it is not possible to deposit single and well-separated molecules from more concentrated solution onto grids or wafers for imaging. However, cryo-TEM can directly image relatively high concentrations, and in combination with e.g. SFM for lower concentrations, a larger concentration range can be covered, leading to the possibility to determine larger aggregation concentrations. The second important advantage is the absence of drying artifacts for cryo-TEM.

Due to these advantages, cryo-TEM images of two batches of Janus cylinders with different lengths were acquired (see Figure 3 - 3). The images clearly exhibit numerous cylindrical molecules with a random orientation of their major axis. The Janus cylinders are well separated, despite the

crowdedness visible in the images. An organization into superstructures is not visible and thus not taking place. This is in contrast to the results obtained for spherical and disk-shaped Janus particles, which showed unexpected aggregates in non-selective organic solvents.

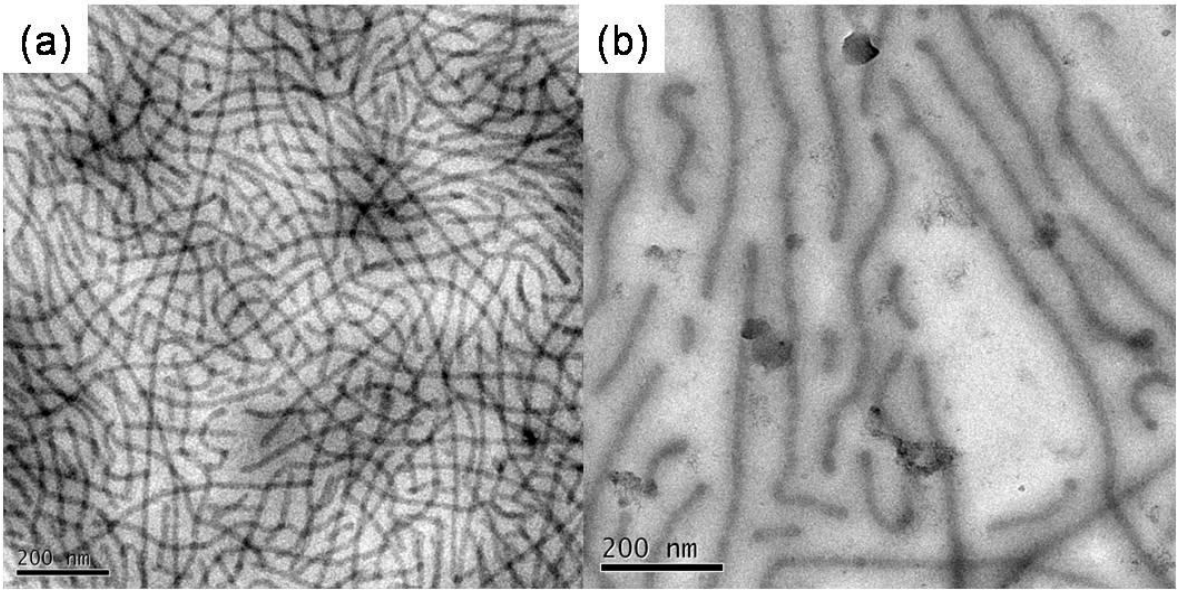

Figure 3 - 3. Cryo-TEM images obtained from Janus cylinders in THF at a concentration of 10 mg/ml. The samples were sonicated for 5 min (a) or 2.5 min (b), respectively.

The dark cylinders in all images correspond to the core of the Janus cylinder only. Note that the core has the highest contrast due to the incorporation of a large amount of S_2Cl_2 during the crosslinking procedure. The average core diameter is around 18 nm. The polybutadiene core is slightly swollen by the solvent as TEM investigations of the crosslinked terpolymer bulk structure had yield a value of 16 nm for the crosslinked core diameter. In addition, the Janus cylinders do not show a very strong bending and resemble stiff rods. The stiffness originates from the strong crosslinking of the well-defined initial block terpolymer bulk structure which contained 14 wt% polybutadiene. Note that bending is however restricted into two dimensions as the cylinders are confined within a thin film of vitrified THF. A careful inspection of the cylinders in Figure 3 - 3b reveals a core-corona contrast of the Janus cylinders. The cylinders are surrounded by a diffuse corona of side chains. The corona is around 20-25 nm thick and explains the relatively equal spacing between parallel cylinders, which are obviously confined in a very thin vitrified film of THF. Figure 3 - 3b gives the indication that the organization into superstructures is prevented by an efficient repulsion of the brush hairs.

The absence of any critical aggregation concentration could furthermore be confirmed by dynamic light scattering (DLS) and small angle neutron scattering (SANS). DLS shows a constant diffusion coefficient ($3.25 \cdot 10^{-15}$ m^2/ms) in a very large concentration range (10^{-3} - 1 g/L). The SANS data are shown in Figure 3 - 4 and can provide further insights in the solution behavior.

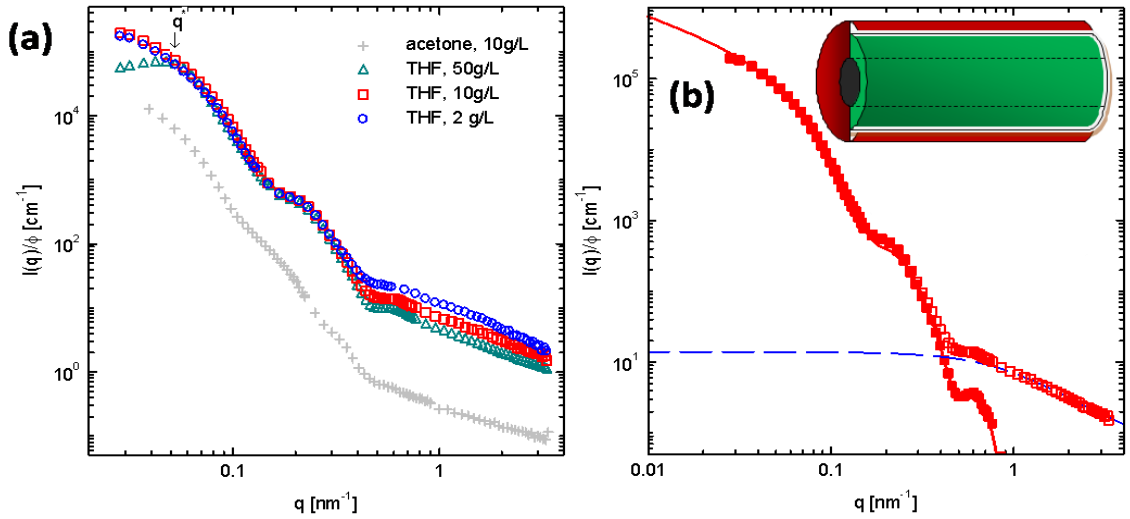

Figure 3 - 4. (a) Scattering intensities of the Janus particles in THF normalized to the volume fraction Φ. The scattering pattern of the Janus cylinders in acetone is shown for comparison and will be discussed below. It is shifted down by a factor of 10. (b) Scattering intensity of Janus cylinders (10 g/L) in THF before (open squares) and after (filled squares) subtraction of the contributions due to concentration fluctuations and incoherent scattering (blue dashed line). The solid line gives the description of the data based on the form factor of Janus cylinders. The inset shows a schematic drawing of the form factor model used.

Figure 3 - 4a shows the scattering intensities of the system in different solvents. We will first focus on the THF solutions; the scattering pattern in acetone will be shown to allow a direct and easy comparison later on. All intensities are normalized to the volume fraction, $\Phi = \rho V_p$ (ρ is the number density and V_p is the particle volume), of the particles. We attempted to describe the scattering intensity with a model of non-interacting Janus cylinders, as schematically sketched in Figure 3 - 4b.

In detail, the scattering intensity of Janus cylinders $I(q,\rho)$ as function of the scattering vector q ($q=|q|=(4\pi/\lambda)\sin(\Theta/2)$, λ is the incident wavelength, and Θ is the scattering angle) and the number density, ρ, of the dissolved particles is given by: [28-33]

$$I(q,\rho) = \rho I_0(q) S(q,\rho) + I_F(q,\rho) + I_{incoh} \qquad (1)$$

Here $I_0(q)$ describes how the scattering intensity is modulated by interference effects between radiation scattered by different parts of the same particle. Consequently, it is sensitive to the shape of the particle. The structure factor $S(q,\rho)$ is determined by the mutual interactions between different particles. Thus, it depends on the degree of local order in the sample. The contribution to the scattering intensity due to concentration fluctuations of the polymer chains is denoted by $I_F(q,\rho)$. I_{incoh} is the contribution of the incoherent scattering due to the protons. In the present study, the two last contributions become important only for large scattering vectors. I_{incoh} can be assumed to be constant in the given q range.[28,29] The contribution of the concentration fluctuations may be treated within a Gaussian approximation, as follows:

$$I_F(q,\rho) = \frac{I_F(0,\rho)}{1+\xi^2 q^2} \qquad (2)$$

where the correlation length ξ decreases upon increasing the particle number density according to $\xi \propto \rho^{-1/2}$.[29]

As suggested by the cryo-TEM images (Figure 3 - 3), the form factor may be best described by a core-shell cylinder with phase-separated shell as shown schematically in Figure 3 - 3b. Therefore we derived an expression for the scattering intensity of a randomly orientated non-interacting monodisperse Janus cylinder. It is given by :

$$I_0(q) = \frac{1}{4\pi} \int_0^{2\pi} d\phi \int_0^{\pi} d\theta \sin\theta F(q,\theta,\phi) F^*(q,\theta,\phi) \qquad (3)$$

with

$$\begin{aligned} F(q,\theta,\phi) &= 2\pi\Delta\rho_c \frac{L_c \sin\left(q\cos\theta(L_c/2)\right)}{q\cos\theta(L_c/2)} \frac{R_c^2 J_1\left(qR_c\sin\theta\right)}{qR_c\sin\theta} + \frac{L_s \sin\left(q\cos\theta(L_s/2)\right)}{q\cos\theta(L_s/2)} \\ &\times \left[\Delta\rho_{sL} \int_0^{\pi} d\phi_r \frac{1}{A^2} \left(e^{iAR_{sL}}[1-iAR_{sL}] - e^{iAR_c}[1-iAR_c] \right) \right. \\ &+ \left. \Delta\rho_{sR} \int_{\pi}^{2\pi} d\phi_r \frac{1}{A^2} \left(e^{iAR_{sR}}[1-iAR_{sR}] - e^{iAR_c}[1-iAR_c] \right) \right] \\ A &= q\sin\theta\cos(\phi_r - \phi) \end{aligned}$$

The model accounts for a core-shell cylindrical structure with a core radius (R_c) a biphasic shell, which has different extensions of the hemi-cylinders (R_{sL} and R_{sR}) and unlike scattering length densities ($\Delta\rho_c$, $\Delta\rho_{sL}$ and $\Delta\rho_{sR}$).

The grafting nature of the semi-shells of the particle leads to a significant smaller scattering length densities, $\Delta\rho_{sL}$ and $\Delta\rho_{sR}$, as compared to the bulk phases. This was considered in the fitting of the data. On basis of the TEM images and well-defined bulk structures used for the preparation of the Janus cylinders, we initially did not expect any significant polydispersity in the radius. However, in solution the soft hemi-cylinder shells fluctuate significantly and thus, we had to take a distribution of the radii into account. A Schulz-Zimm distribution is used to adapt the model to characterize the size distribution of the overall radius.

The scattering intensities of the Janus cylinders in THF exhibit two oscillations in the intermediate q range. The upturn of the intensity at $q^* \approx 0.05$ nm^{-1} for the concentration of 50 g/L can be attributed to intermolecular correlations between the particles. The mean distance d between two Janus cylinders can be approximated to d = 130 nm ($2\pi/q^* = d$). This value is in good agreement with the distance between two particles seen in the cryo-TEM pictures. At intermediate scattering vectors, the scattering intensities measured in THF nearly merge and thus predominantly describe the cross section of the Janus cylinders. After subtraction of the contributions due to concentration fluctuations and incoherent scattering, the coherent scattering intensity pattern could be recovered (filled symbols in Figure 3 - 4b).[30,32]

Due to the polydispersity in the overall radius and the very similar scattering length densities of the two solvent-swollen hemi-cylinders, we do not detect any difference between R_{sR} and R_{sL}. The best description for a single non-aggregated Janus cylinders in a good solvent was obtained for R_c = 8 nm,

$R_{sL} = R_{sR} = R_s$ = 27 nm. A Schulz-Zimm distribution was used to characterize the size distribution of the overall radius (σ_s = 3 nm in THF). Unfortunately, it is not possible to deduce the length of the Janus cylinders due to the limited *q*-range accessible with SANS.[29] The modeling of the SANS data and the deduced length scales corroborate the imaging data and prove that the Janus cylinders are unimolecularly dissolved in good solvents over a wide concentration regime. This is a striking difference as compared to spherical and disk-like Janus particles[8,9], which showed aggregation patterns in good solvents for both sides.

In order to introduce a stronger driving force for the self-assembly, the aggregation behavior in acetone was studied. Acetone is a non-solvent for polystyrene and thus promotes an increase in facial amphiphilicity of the Janus cylinders. Figure 3 - 5 shows the concentration-dependent diffusion coefficient of a sample of Janus cylinders, the corresponding CONTIN plots, as well as SANS data and TEM images of the aggregates formed. In contrast to typical DLS measurements in THF, a clear kink at $c \approx 0.2$ g/L is present for the concentration dependence of the diffusion coefficient. Below this concentration, the diffusion coefficient stays constant. Furthermore, the value coincides with the diffusion coefficient obtained for the same sample in THF at high dilution ($3.25 \cdot 10^{-15}$ m^2/ms). The drop of the diffusion coefficient above $c \approx 0.2$ mg/mL indicates that aggregation of the cylinders into significantly longer structures must take place above this critical aggregation concentration (cac). The clustering of the cylinders into larger aggregates is also evident from the CONTIN plots shown in Figure 3 - 5b. The main peak shows a strong shift towards longer decay times and even becomes bimodal for higher concentrations, showing the presence of very large structures. The more concentrated solutions show a visible, but not a too strong sedimentation after several weeks, meaning that the large structures are reasonably stable.

The SANS intensities, measured in acetone, show a distinct shift of the characteristic oscillations to smaller scattering vectors (Figure 3 - 4a) and accordingly an increase of the cross-sectional diameter of the investigated structure. Considering that the PS side is insoluble and no longer solvent swollen in acetone leads to the conclusion that the scattering length densities of the PB core and the PS part become virtually indistinguishable in the experiment. The PS parts shrinks into a much more compact substructure and fuses in terms of scattering contrast with the PB core. Thus R_c should be is significantly higher as compared to the Janus particles dissolved in THF. Modeling of the scattering intensity leads to R_c = 14 nm and R_s = 34 nm (see solid and dotted white line in the Scheme 3 - in Figure 3 - 5c). The fitting includes a polydispersity of σ_s = 7 nm. Hence, the data must be interpreted as an aggregation of several Janus cylinders into a superstructured fiber as sketched within Figure 3 - 5c. The moderate expansion of the core diameter R_c, is caused by the collapse of the PS part onto it. The radius of the shell increases due to the clustering of several Janus cylinders.

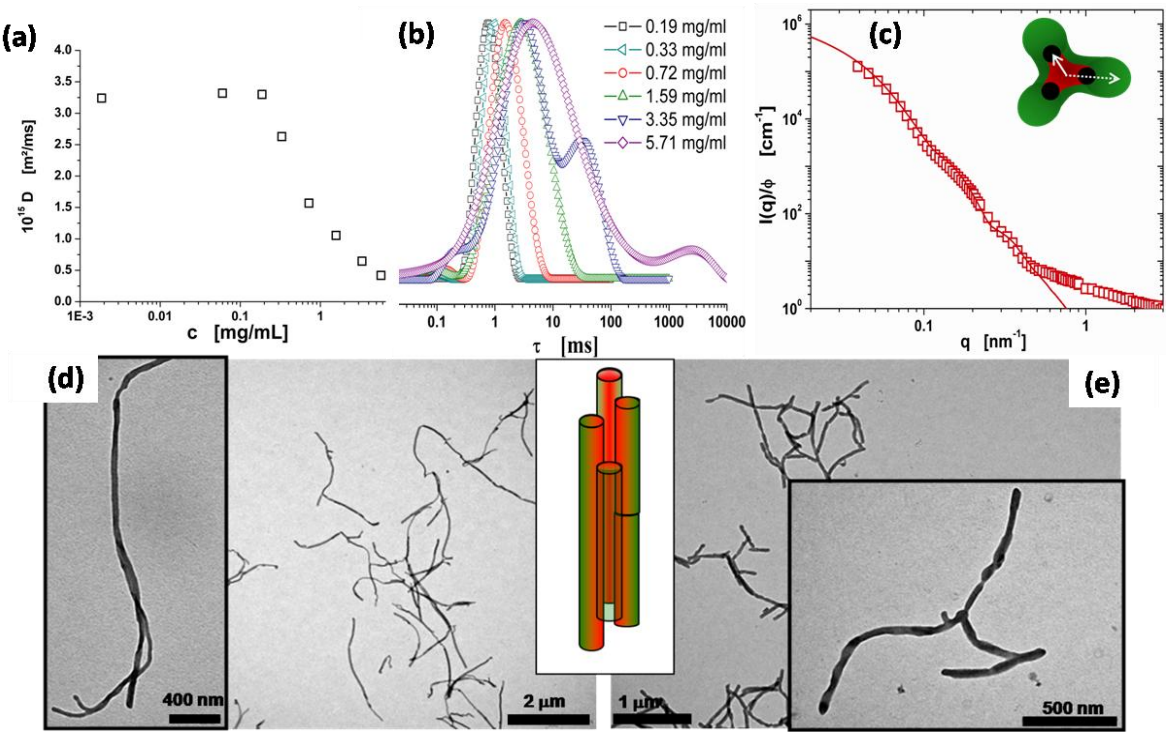

Figure 3 - 5. (a) Concentration dependence of the diffusion coefficients of a sample of Janus cylinders (sonication at 30% amplitude for 2.5 min). (b) CONTIN plots at 80° scattering angle at various concentrations, as indicated. CONTIN plots for c < 0.19 mg/ml are omitted, as they coincide with the one of 0.19 mg/ml. (c) SANS data, modeling and a schematic cartoon depicting the deduced length scales of a cross section of one possible aggregate (PS = red, PB core = black, PMMA = green). (d+e) TEM images obtained after deposition from a 0.5 mg/ml acetone solution of Janus cylinders onto carbon coated grids after 2.5 min (d) and 30 min (e) sonication at 30% amplitude. The two insets show magnified images. The Scheme 3 - in the centre highlights the occurring aggregation. The polystyrene part (red) is hidden within the centre of a fiber-like aggregate.

Unfortunately, we failed to obtain cryo-TEM images from acetone solutions. This is probably due to the fast evaporation and poor film-forming properties of acetone. Therefore, standard TEM analysis of the acetone solution of the Janus cylinders was performed. Figure 3 - 5 shows a selection of TEM images obtained from self-assembled Janus cylinders at different sonication times, deposited from a 0.5 mg/mL solution. The images exhibit superstructures formed by the solvent induced self-assembly. The aggregates remain intact during deposition on the TEM grid, indicating a strong association of the cylindrical Janus particles. The Janus cylinders form fiber-like aggregates with the PS part hidden in the centre of the aggregate. The fibers are longer than the initial cylinders in THF but are of finite size. The images reveal that 2 – 4 Janus cylinders participate in the formation of one super-structured fiber at a given point. The diameters determined by TEM (50 – 80 nm) are in agreement with the shell thickness derived by modeling the SANS data. The aggregation pattern is independent of the Janus cylinder length as similar aggregates can be found as shown in Figure 3 - 5. An increase in the height profile of Janus cylinders deposited from acetone solutions in scanning force microscopy investigations was reported by Liu et al.[12] However, here we look in much more detail at the aggregation patterns, concentrations and structures formed. TEM images at higher concentration show slightly thicker and much longer fibers, which can explain the further decrease of the diffusion coefficient for solutions with increasing concentration. At very low concentrations, below the cac, unimolecularly and slightly aggregated Janus cylinders can be found (see Supporting Information for TEM images). A longitudinal extension of the Janus cylinders is not found.

Consequently, since the PS is collapsed in acetone, the PMMA part shields the complete structure and prevents aggregation at such low concentrations. Above the cac, the cylinders are clearly fused together into one homogeneous structure.

The overall picture emerging from the experimental results of the solvent induced self-assembly of the Janus cylinders in selective solvent is as follows: The aggregation is concentration dependent and shows a critical aggregation concentration. Therefore, the stabilization occurs with two different mechanisms. At very low concentrations, below the cac, the Janus cylinders exist unimolecularly dissolved with a collapsed PS part, which is shielded by the well soluble PMMA arms in an intramolecular fashion. Around the cac, aggregation takes place by clustering of Janus cylinders, first into aggregates with increased diameter and without significant longitudinal extension. At this point a strong drop in the diffusion coefficient is not expected as an increased diameter has only a minor influence on the overall diffusion coefficient. For energetic reasons, it is favored to start the aggregation with a maximum of contact surface between the PS parts of different cylinders. Above the cac, or more precisely above the kink in Figure 3 - 5a, a concentration triggered fiber-like aggregation into longitudinally extended superstructured fibers takes place. The fibers become longer with increasing concentration. Above the cac, the stabilization involves an intermolecular process in which several cylinders come together and cooperatively shield the inner PS domain.

Surface Structures

Aside these fiber-like aggregates found in selective solvents, a formation of networks was observed upon depositing Janus cylinders from more concentrated solution. The length scales involved here significantly exceed the one of the superstructures formed in dilute and semi-concentrated acetone solution. Consequently, the Janus cylinders can be considered to be able to assemble on a second hierarchical level into considerably larger structures than those formed in selective solvents in dilute and semi-dilute solution. The aggregation patterns develop in non-selective solvent (THF) as well as in selective solvent (acetone). They can be created in a very facile fashion. Figure 3 - 6a and 6b show representative images obtained by TEM.

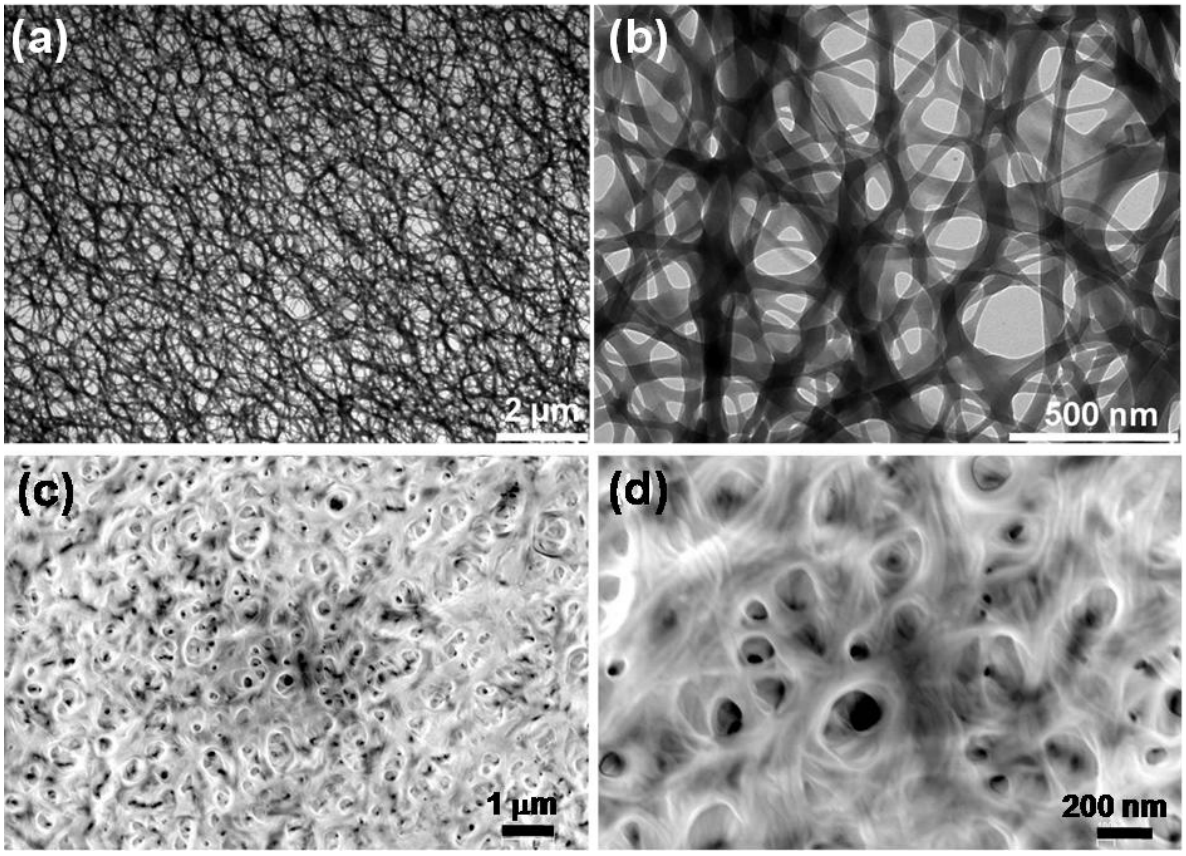

Figure 3 - 6. TEM images (a and b) of network-like aggregation patterns formed by deposition of Janus cylinders onto a TEM grid from THF solution (c = 5 mg/mL). SEM images obtained by drying a solution of Janus cylinders in THF on a mica substrate. Image (d) shows a magnified section of image (c).

The network shows polydisperse pores in the range of a few hundred nanometers, which can be developed over a large micron-sized area. Thus the nanoscopic pores can be created over mesoscopic length scales. The pore sizes of these patterns can be tuned in a very simple fashion by increasing the concentration of the solution or the aspiration time. The SEM images shown in Figure 3 - 6c and 6d were obtained by drying a droplet of a Janus cylinder solution in THF on a mica substrate. The pores are significantly smaller, in the range of 100 – 200 nm, and the polymer matrix is more continuous, leading to a higher mechanical strength. Strikingly, a continuous film formation is not observed and the stabilization of the network-like pattern is favored. Reptation of the large cylinders is prevented on these time-scales of drying.

Due to the fiber formation in acetone, with PS being in the center of the superstructured fibers, it is furthermore possible to tune the surface energy of the networks. Whereas a mixed surface of PS and PMMA should be present when creating these patterns with a THF solution, the surface presumably consists exclusively of PMMA when using an acetone solution. This shows a way of how to tune the surface energy and the chemoselectivity of the structure, which would for instance play a role when using these membrane-like structures as templates for atomic layer deposition (ALD) or for further chemical modifications. Furthermore, these structures are appealing when thinking about creating them in polymer matrixes. The networks could be valuable for reinforcing mechanical properties of certain polymers or could be used to create bicontinuous patterns. Selective etching as for instance for PMMA with UV irradiation may even be a tool to create nanoscopic channels within a polymer host material (e.g. PS).

Conclusions

We have presented a thorough investigation of the size-tunability and the self-assembly properties of Janus cylinders, synthesized by selectively crosslinking SBM block terpolymer bulk phases. This is the first time that the effect of hemicylindrical segregation of a nanosized cylinder, a unique architectural feature attributed to the Janus character, on the self-assembled structures is shown. The Janus cylinders investigated are large synthetic analogues of facial amphiphiles. The biphasic character of the Janus cylinder could clearly be proven by a selective staining of the PS hemi-cylinder of the Janus cylinders.

The size of the Janus cylinders can be tuned from the micrometer range down to the nanometer range by a simple sonication treatment. The evolution of the particle size follows an exponential decay and the size distribution narrows during this process. The size can be tuned both by the duration and the energy of the sonication treatment.

The Janus cylinders are unimolecularly dissolved in good organic solvents as observed by cryo-TEM, DLS and SANS in THF. Cryo-TEM shows a core-corona structure with an extended corona, indicating an efficient repulsion of the brush hairs, which prevents the aggregation into superstructures. The SANS data corroborates the imaging data and yields further insights into the solution structure and fluctuations of the Janus cylinders. The form-factor for a core-shell Janus cylinder was developed for the fitting process.

Self-assembly of Janus cylinders can be induced in selective solvents such as acetone. The stabilization of the collapsed sides occurs with two mechanisms, an intramolecular and an intermolecular one. DLS demonstrates that the aggregation is concentration dependent, exhibiting a critical aggregation concentration (cac), and that the size of the aggregates increases with increasing concentration above the cac. Above the cac, the Janus cylinders cluster and form superstructured fibers with a PS domain in its center. The modeling of the SANS data reveals a collapse of the PS part onto the PB core and an aggregation into larger diameters. These data are corroborated by TEM images showing that 2 – 4 Janus cylinders form one fiber at a given point. The fibers progressively extended in length with increasing concentration. Below the cac, the stabilization occurs via an intramolecular mechanism. The collapsed PS side is shielded by the PMMA arms extending around large parts of the cylinder and minimizing the contact between PS and solvent.

Aggregation on a second hierarchical level can be obtained when depositing Janus cylinders on surfaces. It is possible to form network-like pattern upon deposition from concentrated solution, independent of the solvent used. These fibrillar networks can be obtained with different pore sizes and different surface compositions simply by changing the concentration and the solvent quality, respectively. The aggregation patterns found are promising candidates for the generation of bicontinuous structures within host materials via self-assembly, the reinforcement and channel creation within those, and for the facile preparation of membranes or templates.

Acknowledgments

This work was supported by European Science Foundation within the EUROCORES SONS program (BioSONS) and by the EU within the Marie Curie RTN POLYAMPHI. Andreas Walther thanks the Bavarian Graduate Support Program for a scholarship. We are also indebted to the Institut Laue-Langevin (ILL) Grenoble and Peter Lindner for providing beam time and support at the SANS instrument D11.

References

(1) Walther, A.; Matussek, K.; Müller, A. H. E. *ACS Nano* **2008**, *2*, 1167-1178.
(2) Walther, A.; Müller, A. H. E. *Soft Matter* **2008**, *4*, 663-668.
(3) Roh, K.-H.; Martin, D. C.; Lahann, J. *Nat. Mater.* **2005**, *4*, 759-763.
(4) Roh, K.-H.; Yoshida, M.; Lahann, J. *Langmuir* **2007**, *23*, 5683-5688.
(5) Binks, B. P.; Fletcher, P. D. I. *Langmuir* **2001**, *17*, 4708-4710.
(6) Nonomura, Y.; Komura, S.; Tsujii, K. *Langmuir* **2004**, *20*, 11821-11823.
(7) Walther, A.; Hoffmann, M.; Müller, A. H. E. *Angew. Chem., Int. Ed.* **2008**, *47*, 711-714.
(8) Walther, A.; André, X.; Drechsler, M.; Abetz, V.; Müller, A. H. E. *J. Am. Chem. Soc.* **2007**, *129*, 6187-6198.
(9) Erhardt, R.; Böker, A.; Zettl, H.; Kaya, H.; Pyckhout-Hintzen, W.; Krausch, G.; Abetz, V.; Müller, A. H. E. *Macromolecules* **2001**, *34*, 1069-1075.
(10) Xu, H.; Erhardt, R.; Abetz, V.; Müller, A. H. E.; Gödel, W. A. *Langmuir* **2001**, *17*, 6787-6793.
(11) Erhardt, R.; Zhang, M.; Böker, A.; Zettl, H.; Abetz, C.; Frederik, P.; Krausch, G.; Abetz, V.; Müller, A. H. E. *J. Am. Chem. Soc.* **2003**, *125*, 3260-3267.
(12) Liu, Y.; Abetz, V.; Müller, A. H. E. *Macromolecules* **2003**, *36*, 7894-7898.
(13) Ishizu, K.; Satoh, J.; Toyoda, K.; Sogabe, A. *J. Mater. Sci.* **2004**, *39*, 4295-4300.
(14) Dendukuri, D.; Pregibon, D. C.; Collins, J.; Hatton, A. T.; Doyle, P. S. *Nat. Mater.* **2006**, *5*, 365-369.
(15) Behrend, C. J.; Anker, J. N.; McNaughton, B. H.; Kopelman, R. *J. Magn. Magn. Mater.* **2005**, *293*, 663-670.
(16) Choi, J.; Zhao, Y.; Zhang, D.; Chien, S.; Lo, Y.-H. *Nano Lett.* **2003**, *3*, 995-1000.
(17) Anker, J. N.; Behrend, C.; Raoul, K. *J. Appl. Phys.* **2003**, *93*, 6698-6700.
(18) Anker, J. N.; Kopelman, R. *Appl. Phys. Lett.* **2003**, *82*, 1102-1104.
(19) Behrend, C. J.; Anker, J. N.; McNaughton, B. H.; Brasuel, M.; Philbert, M. A.; Kopelman, R. *J. Phys. Chem. B* **2004**, *108*, 10408-10414.
(20) Behrend, C. J.; Anker, J. N.; Kopelman, R. *Appl. Phys. Lett.* **2004**, *84*, 154-156.
(21) Nisisako, T.; Torii, T.; Takahashi, T.; Takizawa, Y. *Adv. Mater.* **2006**, *18*, 1152-1156.
(22) Roh, K.-H.; Yoshida, M.; Lahann, J. *Langmuir* **2007**, *23*, 5683-5688.
(23) Golestanian, R.; Liverpool, T. B.; Ajdari, A. *Phys. Rev. Lett.* **2005**, *94*, 220801.
(24) Verberg, R.; Dale, A. T.; Kumar, P.; Alexeev, A.; Balazs, A. C. *J. R. Soc. Interface* **2007**, *4*, 349-357.
(25) Zhao, Y. *Curr. Opin. Colloid Interface Sci.* **2007**, *12*, 92-97.
(26) Walther, A.; Goldel, A.; Müller, A. H. E. *Polymer* **2008**, *49*, 3217-3227.
(27) Walther, A.; Goldmann, A. S.; Yelamanchili, R. S.; Drechsler, M.; Schmalz, H.; Eisenberg, A.; Müller, A. H. E. *Macromolecules* **2008**, *41*, 3254-3260.
(28) Benoit, H. C.; Higgins, J. S. *Polymers and Neutron Scattering*; Clarendon Press: Oxford, 1994.
(29) Yan, L.; Harnau, L.; Cohen Stuart, M. A.; Rosenfeldt, S. *Soft Matter* **2008**, *4*, 2207-2212.
(30) Rosenfeldt, S.; Dingenouts, N.; Ballauff, M.; Lindner, P.; Likos, C. N.; Werner, N.; Vögtle, F. *Macromol. Chem. Phys.* **2002**, *203*, 1995-2004.

Supporting Information

Experimental Section

Materials

All solvents and reagents were obtained from Merck or Aldrich in p.a. grade and used without further treatment except for the following ones. Acetonitrile (Aldrich) was obtained in HPLC grade and used directly.

Synthesis

The anionic polymerization of the polystyrene-*block*-polybutadiene-*block*-poly(methyl methacrylate) (SBM) terpolymer was conducted in a similar way as reported elsewhere.[1, 2] In this study $S_{41}B_{14}M_{45}^{110}$ is used as Janus cylinder precursor polymer. The subscript numbers denote the mass fraction in percent, and the superscripts give the number average molecular weight in kg/mol.

Cold vulcanization

A solvent-cast film was introduced into a reaction vessel and swollen in acetonitril for a certain period of time (typically: 12 – 48 h). Afterwards, the calculated amount of S_2Cl_2 (typically: 5 vol%) was introduced with a syringe and the crosslinking was allowed to take place for 24 h at room temperature. After the reaction, the film was washed with several aprotic non-solvents, e.g. acetonitrile and isooctane. Subsequently, the film was purified by Soxhlet extraction with THF for 24 h yielding a soluble and an insoluble fraction. The insoluble fraction was subjected to a sonication treatment.

Sonication

The product underwent ultrasonic treatment using a Branson model-250 digital sonifier, equipped with 1/8 in. diameter tapered microtip, at various amplitudes (200 watt at 100% amplitude). For this purpose, a dispersion of insoluble crosslinked material (c = 0.3 - 1 mg/mL) in THF was allowed to stand at room temperature for several hours to ensure good swelling of the material. Afterwards, it was subjected to the sonication treatment in a special cell, cooled with water, at room temperature. The on/off cycle times were typically in the range of 2s/2s and 2s/10s, depending on the amplitude.

Dynamic Light Scattering (DLS)

Dynamic light scattering was performed on an ALV DLS/SLS-SP 5022F compact goniometer system with an ALV 5000/E cross-correlator and a He–Ne laser (λ_0 = 632.8 nm). Prior to the light scattering measurements the sample solutions were filtered using Millipore or Roth filters (housing: polypropylene, membrane: polytetrafluoroethylene) with a pore size of 5 μm. All samples were analyzed at high dilution. The data evaluation of the dynamic light scattering measurements was performed with the CONTIN algorithm[3] and the values of the hydrodynamic radii were obtained after extrapolating the angle-dependent scattering data to $q^2 \rightarrow 0$.[4]

Transmission Electron Microscopy (TEM)

Bright-field TEM was performed on Zeiss CEM 902 and LEO 922 OMEGA electron microscopes operated at 80 kV and 200 kV, respectively. The specimens were prepared by placing a droplet of

solution onto a carbon-coated TEM grid, waiting for a certain time (10 – 300 s) and subsequent blotting of the residual liquid using filter paper. RuO_2 staining was done in the gas phase by placing a TEM specimen in a closed chamber with a vial containing $RuCl_3$ and NaOCl solution.

For **cryogenic transmission electron microscopy (cryo-TEM)** studies, a drop of the sample dissolved in THF was put on a lacey carbon transmission electron microscopy (TEM) grid, where most of the liquid was removed with blotting paper, leaving a thin film stretched over the lace. The specimens were instantly vitrified by rapid immersion into liquid nitrogen in a temperature controlled freezing unit (Zeiss Cryobox, Zeiss NTS GmbH, Oberkochen, Germany). The temperature was monitored and kept constant in the chamber during all of the sample preparation steps. After freezing the specimens, the specimen was inserted into a cryo-transfer holder (CT3500, Gatan, München, Germany) and transferred to a Zeiss EM 922 OMEGA FE-TEM. Examinations were carried out at temperatures around 90 K. The transmission electron microscope was operated at an acceleration voltage of 200 kV. Zero-loss filtered images (ΔE = 0 eV) were taken under reduced dose conditions (100-1000 e/nm^2). All images were registered digitally by a bottom mounted CCD camera system (Ultrascan 1000, Gatan) combined and processed with a digital imaging processing system (Gatan Digital Micrograph 3.9 for GMS 1.4).

Scanning Electron Microscopy (SEM)

SEM was performed using a LEO 1530 Gemini instrument equipped with a field emission cathode with a lateral resolution of approximately 2 nm. The acceleration voltage was chosen between 0.5 and 3 kV.

Small Angle Neutron Scattering (SANS)

The Janus particles were dissolved in deuterated solvent (2g/L, 10g/L and 50g/L in THF-d_8 99.5%, and 10 g/L in acetone-d_6 99.5% Deutero GmbH). The specific volume of the particles was determined in THF to 0.78 cm^3/g using a DMA-60 densitometer (Paar, Graz, Austria). Small-angle neutron scattering experiments were performed using the instrument D11 at the Institut Laue-Langevin (ILL) in Grenoble. All data discussed were converted to absolute intensities using standard software provided by the instrument.[5-6] The scattering of the solvent $I_{LM}(q)$ and the empty capillary $I_{cap}(q)$ were subtracted from the intensity of each sample $I_{sample}(q)$. The scattering intensity of the pure particles $I(q)$ is given by $I(q) = I_{sample}(q) - (1-\phi)I_{LM}(q) - I_{cap}(q)$ (where ϕ is the volume fraction of the particles). [6]

TEM images of Janus cylinders from acetone solutions at low to intermediate concentrations

At very low concentrations, below the cac, unimolecularly and slightly aggregated Janus cylinders can be found (Figure Sup-1). A longitudinal extension of the Janus cylinders is not found. The slight aggregation is presumably even caused by the sample preparation process which requires prolonged aspiration times. A rapid blotting is not possible as otherwise no material can be found on the grid. The accompanying drying during the long aspiration times induces a concentration change and thus a slight aggregation. The extension into longer fibers is evident when comparing images b and c of Figure Sup - 1.

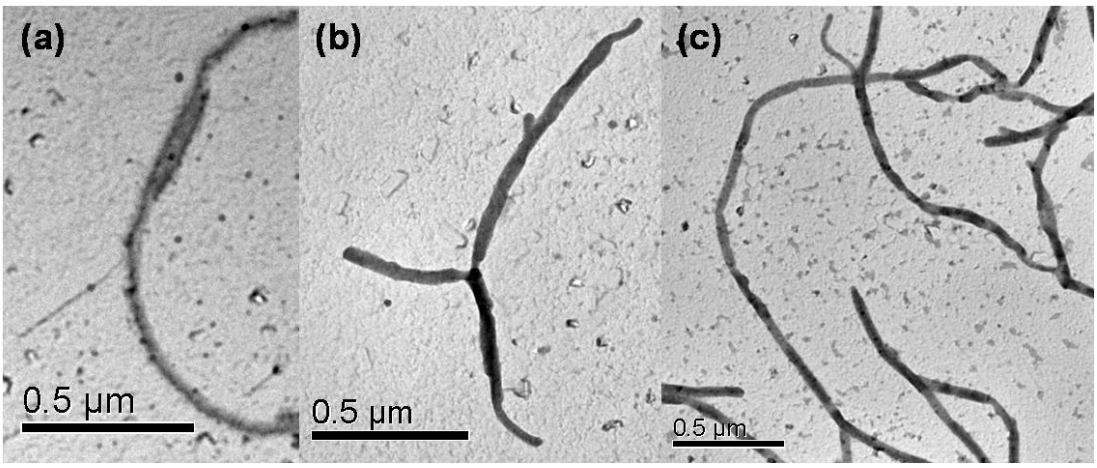

Figure Sup 3 - 1. Typical TEM images obtained from Janus cylinder solutions in acetone at different concentrations (a = 0.019 mg/mL, b = 0.186 mg/mL, c = 0.72 mg/mL). The sample was sonicated for 2.5 min at 30% amplitude.

1. Goldacker, T.; Abetz, V.; Stadler, R.; Erukhimovich, I.; Leibler, L. *Nature* **1999,** 398, (6723), 137-139.
2. Auschra, C.; Stadler, R. *Polymer Bulletin* **1993,** 30, (3), 257-264.
3. Provencher, S. W. *Makromol. Chem.* **1979,** 180, 201-209.
4. Berne, B. J.; Pecora, R., *Dynamic Light Scattering*. John Wiley & Sons: New York, 1976.
5. P. Lindner, Scattering experiments: experimental aspects, initial data reduction & absolute calibration. In Neutrons, X-Rays and Light: Scattering methods applied to soft condensed matter, P. Lindner, T. Zemb, Eds.; Elsevier North Holland Delta Series: Amsterdam, 2002; p. 23-48.
6. Rosenfeldt, S; Karpuk, E.; Lehmann, M.; Meier, H.; Lindner, P.; Harnau, L.; Ballauff, M. *Chem. Phys. Chem.* **2006**, 7, 2097-2104.

4. SUPERSTRUCTURES OF AMPHIPHILIC JANUS DISCS IN AQUEOUS MEDIUM

Andreas Walther, Markus Drechsler, Axel H. E. Müller

Makromolekulare Chemie II and Bayreuther Zentrum für Kolloide und Grenzflächen, Universität Bayreuth, D-95440 Bayreuth, Germany

Andreas.Walther@uni-bayreuth.de; *Axel.Mueller@uni-bayreuth.de*

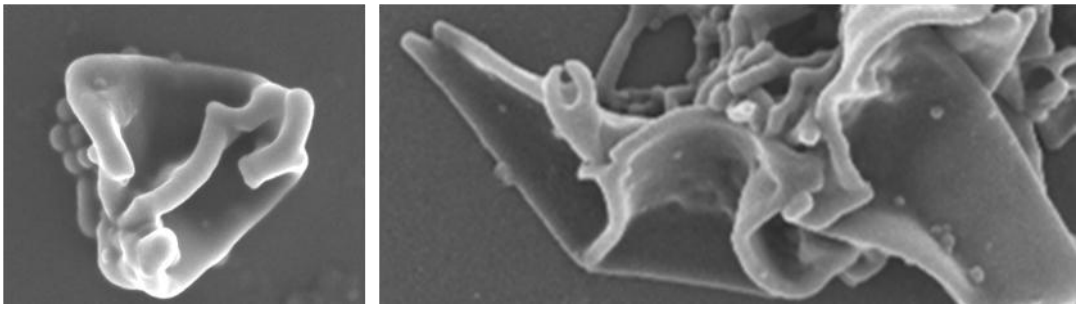

Accepted for *Soft Matter*

Introduction

Colloidal aggregates with sub-micron sized compartmentalized structures are increasingly gaining scientific interest, which is mainly due to their advanced properties making them attractive for various applications.[1-10] Among these multicompartment structures, Janus particles receive special attention for their unique non-centrosymmetric character.[11-23] This distinctive feature enables these particles to undergo fascinating aggregation behavior and furthermore leads to the possibility for the particles to align and strongly adsorb at interfaces. [24-27] In general, Janus particles can be divided into several classes according to their architecture or dimensionality (see Scheme 4 - 1).

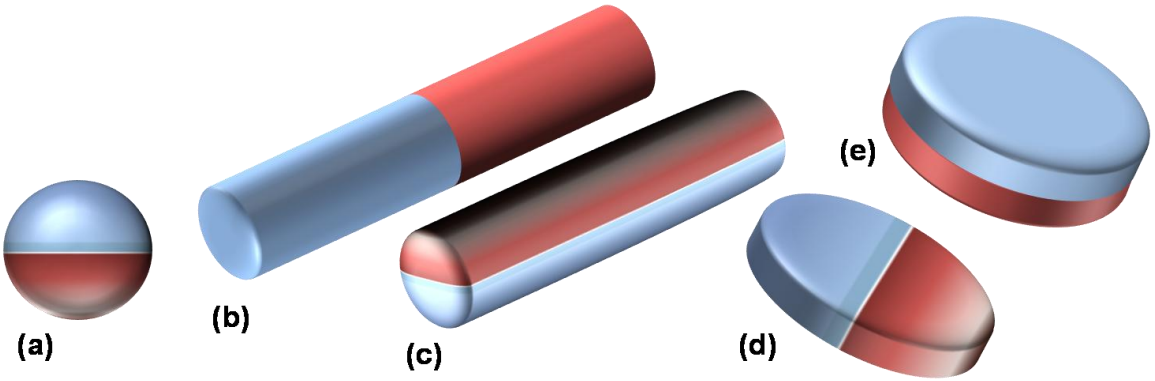

Scheme 4 - 1. Overview of possible Janus particle architectures. (a) spherical Janus particle, (b + c) two types of Janus cylinder and (d + e) two types of Janus discs.

Nowadays, the preparation of significant quantities of spherical particles can be accomplished via several ways, as recently reviewed in a highlight article.[11] However the preparation of non-spherical nanometer-sized ones remains a challenging task. Mainly, a block terpolymer assisted synthetic pathway via crosslinking of well-ordered bulk phases enables their preparation.[28] With this approach it had been possible to create spherical, cylindrical and disc-like Janus particles. Truly amphiphilic Janus micelles, composed of one polystyrene (PS) and one poly(methacrylic acid) (PMAA) side were thoroughly investigated with respect to their supramolecular aggregation behavior. It was found that aggregation takes place on two levels. Firstly, the Janus micelles cluster into supermicelles upon reaching a certain critical aggregation concentration (cac). This cac is surprisingly high with a value of 0.1 mg/mL. Furthermore, the initially clustered Janus micelles can undergo a second aggregation into so-called supramicelles, which are significantly larger in size.

The Janus particle used for this study are shown in Scheme 4 - 1e and are composed of a polystyrene side and one poly(methacrylic acid) side. The preparation of those Janus discs can be accomplished via selectively crosslinking the butadiene lamella of the lamella-lamella (ll) morphology of a well-defined microphase-segregated bulk template of a polystyrene-*block*-polybutadiene-*block*-poly(*tert*.-butyl methacrylate) (SBT) triblock terpolymer and subsequent transformation of the hydrophobic poly(*tert*.-butyl methacrylate) PtBMA into PMAA via acid catalyzed elimination of the t-butyl group (see Scheme 4 - 2). The solution behavior of the non-hydrolyzed PS-PtBMA Janus discs in organic solution and their interfacial activity were recently

described by us.[19] It may be useful to recall some of the key results of the earlier publication. Firstly, the disc thickness was shown to be in the range of 30 – 35 nm. The Janus discs underwent a fascinating aggregation into back-to-back stacked superstructures, even in organic solvents which are good solvents for both blocks and thus only slightly selective.[19] The back-to-back stacking could be clearly proven by cryogenic transmission electron microscopy (cryo-TEM).

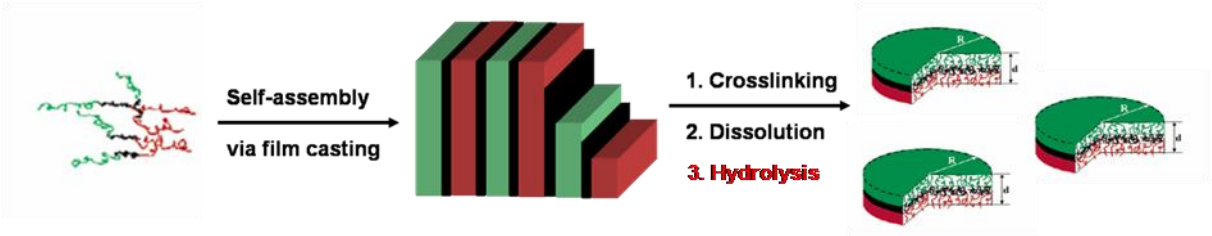

Scheme 4 - 2. Schematic synthesis of flat Janus particles, based on the selective crosslinking of PB domains of a SBT terpolymer with lamellar-lamellar (ll) morphology and subsequent acidic hydrolysis.

These two examples regarding the superstructure formation serve to show the interest in studying this fascinating class of compartmentalized colloids. In general, in the field of self-assembling amphiphilic block copolymer systems, much research has been devoted to the study of the influence of environmental parameters or the effect of block lengths or monomer variation. The increasing understanding has opened a broad field of applications for such amphiphiles in both science and industry. On the contrary, there are only very limited studies of the self-assembly behavior of amphiphilic Janus particles.[12, 13, 19, 20, 29, 30] Those investigations are almost exclusively concerned with spherical particles. However, if one aims at future applications of these promising colloidal structures, the investigation of their aggregation mechanism, especially in dependence of the particle architecture, is of fundamental importance to be able of achieving a high control for applications later on. Therefore, we herein present results on the self-assembly behavior of truly amphiphilic polymeric Janus discs of different sizes in aqueous medium. The results are obtained by combining several imaging techniques with dynamic light scattering.

Results and Discussion

For the investigations presented here, two different samples of disc-like Janus particles were chosen. These discs are composed of one PS side and one PMAA side. Hence, they are of true amphiphilic character and can be dissolved in aqueous medium via step-wise dialysis from a common solvent, dioxane. Both samples are obtained via acidic hydrolysis of the P*t*BMA sides of the original Janus discs. The PS and the PtBMA/PMAA arms have an average length of 550 and 450 repeating units. The size distributions of the two samples before hydrolysis of the P*t*BMA side were analyzed by dynamic light scattering (DLS, see Supporting Information). After extrapolation of the angular dependent scattering data for this kinds of non-spherical particles, z-average apparent hydrodynamic radii, $\langle R_h \rangle_{z,app}$, of 330 nm and 105 nm for SBT_{large} and SBT_{small} can be obtained before hydrolysis, respectively. In terms of the actual discs size, that means that SBT_{small} only contains nanometer sized particles, whereas SBT_{large} has sizes reaching up to a few microns in discs diameter. Thus, the two batches of Janus particles allow a study of the influence

of the particle size on the types of aggregates formed. To further distinguish the aggregates and the effect of the different geometrical shape, the colloidal structures formed by a simple linear triblock terpolymer, polystyrene-*block*-polybutadiene-*block*-poly(methacrylic acid) (SBMA), of similar composition as the Janus discs were also investigated for comparison.

The hydrolysis of the *tert*-butyl protected sides of the Janus discs and the linear triblock terpolymer was achieved via acidic hydrolysis in dichloromethane using trifluoroacetic acid as catalyst for isobutene elimination. The extent of hydrolysis as analyzed by FT-IR and ^{1}H-NMR is larger than 95%. Figure 4 - 1 shows the FT-IR spectra of $SBMA_{small}$ before and after hydrolysis. The CH deformation of the *tert*-butyl group at 1368 cm^{-1} vanishes almost completely for the hydrolyzed sample. Note that some other CH deformations of other alkyl groups are located in this region as well. Furthermore, the characteristic carbonyl peak shifts from 1732 (ester) to 1706 cm^{-1} (acid) and broadens and a shoulder appears around 1680 - 1690 cm^{-1}. Additionally, typical broad bands of the O-H valence vibration of the acid between 3700 and 2400 cm^{-1} appear. At 2600 cm^{-1} the O-H stretching vibration of carboxylic acid dimers can be observed.

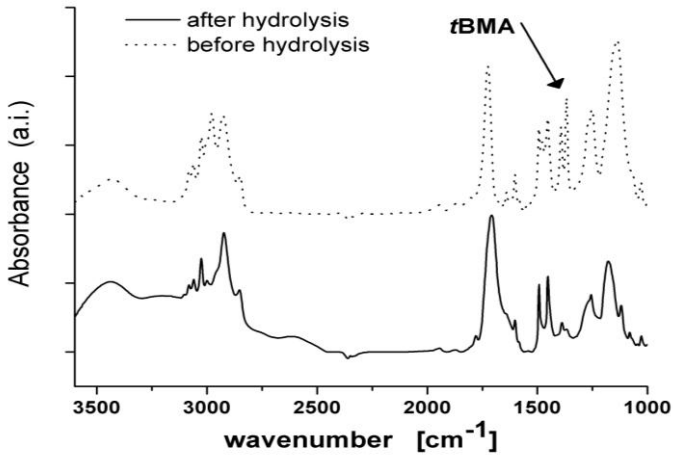

Figure 4 - 1. FT-IR spectra of Janus discs before and after hydrolysis.

Since the truly amphiphilic Janus particles and the SBMA triblock terpolymer, obtained after hydrolysis, contain ca. 50 wt% PS, a direct dissolution into water is not possible due to the high glass transition temperature of the polystyrene. Therefore, step-wise dialysis of the structures from a good solvent (dioxane) for both blocks into the selective solvent water was used at a concentration of 1 mg/mL. After complete dialysis, a macroscopic difference in the behavior of the three samples can be observed. Whereas the aqueous solution of linear block terpolymer only shows a slight turbidity (SBMA), the solution of the small Janus discs ($SBMA_{small}$) exhibits a higher turbidity. An even higher turbidity and a visible sedimentation, after leaving the sample non-agitated for a while, can be observed for $SBMA_{large}$, containing the largest flat Janus particles. Clearly, the macroscopic observations already demonstrate a different aggregation behavior of the various amphiphiles present in the solutions. To further quantify this behavior, the sizes and size distributions of the aggregates present in solution were analyzed by DLS of the micellar solution of SBMA and the well dissolved particles of the small Janus discs. A striking difference between the hydrodynamic sizes of the two colloidal structures can be found.

Whereas SBMA leads to aggregate sizes of $<R_h>_{z,app}$ = 96 nm, $SBMA_{small}$ exhibits much larger apparent hydrodynamic radii ($<R_h>_{z,app}$ = 195 nm). Figure 4 - 2 shows the angular dependent dynamic light scattering data of SBMA and $SBMA_{small}$ aggregates in water. In general, the occurrence of angular dependence in DLS may have several origins, such as large flexible molecules, anisotropic shapes and polydispersity. For large anisotropic molecules, like rods and disc-shaped molecules, flexion, bending and rotational diffusion occur in addition to the standard translational diffusion. Their contributions to the scattered light are dependent on the wave vector, q, thus inducing an angular dependence. Neither much theoretical nor much experimental work has been reported in the case of disc-like scatterers, which is mainly due to the limited access to free disc-like molecules. A formulation of the dynamic form factor for the intensity of scattered light from thin discs was proposed by Fujime and Kubota and applied to the study of membrane fragments.[31-33] Regarding the angular dependence of the plots in Figure 4 - 2, a strong difference can be observed. Whereas the SBMA micelles do not show any significant angular dependence, $SBMA_{small}$ shows a curved increase at low to intermediate scattering vector and a more asymptotical behavior at higher scattering vector. Due to the absence of any angular dependence, a spherical structure can be unambiguously assigned to the SBMA aggregates. The behavior of $SBMA_{small}$ strongly indicates an anisometric shape and is moreover in agreement with the theoretical expectations according to the dynamic form factor for a disc-like particle.

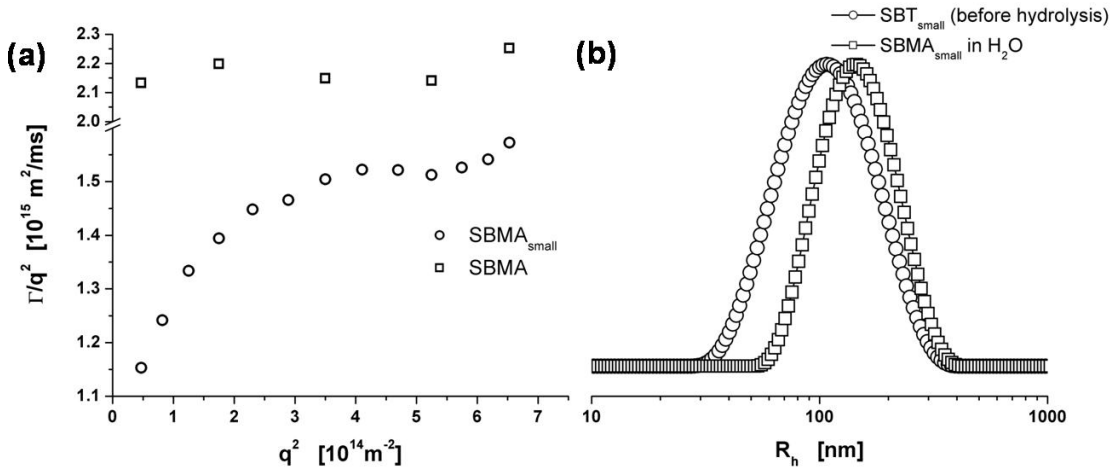

Figure 4 - 2. (a) Angular dependent dynamic light scattering data of SBMA micelles and $SBMA_{small}$ aggregates in aqueous solution (100 mM NaCl, pH = 8). Note the break in the y-axis. (b) CONTIN plots at 90° obtained for SBT_{small} before hydrolysis (in THF) and of the aggregates formed by the hydrolyzed Janus discs, $SBMA_{small}$, in aqueous solution.

A comparison of the CONTIN plots of SBT_{small} before hydrolysis in organic media and of the aggregates formed in water of the hydrolyzed $SBMA_{small}$ is shown in Figure 4 - 2b. A moderate shift of the maximum towards higher radii can be observed. The overall apparent z-average hydrodynamic radius, obtained after extrapolating the angular dependent scattering data to $q^2 \rightarrow 0$ almost doubles. This demonstrates that the amphiphilic Janus discs show somewhat larger structures, however, are still of finite size.

Clearly, after assessing the sizes and the size-distribution, the most important question to answer for these novel colloidal particles is what type of aggregate structures is formed. In

comparison to linear block copolymers a significant geometrical constraint is encoded into the structure of the Janus discs. Since the Janus discs possesses a certain stiffness or bending modulus for the disc-plane, the formation of highly curved aggregates such as spherical particles is expected to be limited.

A very elegant way of determining the structure of colloidal aggregates is to analyze their shapes *in-situ* by cryogenic transmission electron microscopy (cryo-TEM). For this technique a very thin film of liquid, spanning over holes in a TEM grid, is vitrified and the structures are thus preserved. The vitrified film is typically thinner than 100 nm,[34] which is of significance when imaging disc-like structures larger. Usually side-on views onto discs are only possible if the disc diameters are significantly smaller than 100 nm, typically at around 50 nm.[35] Even at this small diameter most of the disc are nonetheless oriented in plane and viewed in a face-on fashion in *cryo*-TEM. Most probably, shearing forces during the blotting procedure help to induce this order.

Figure 4 - 3 shows some representative images obtained for the micelles of SBMA and the aggregates of the small Janus discs, $SBMA_{small}$. All structures are surrounded by an additional corona of PMAA chains of ca. 50 nm, which can be well seen in the insert in Figure 4 - 3b and 4 - 3c. The most obvious difference is the increase of the core sizes of the structures. For the non-crosslinked SBMA micelles the core diameter is ca. 46 nm. This core diameter is significantly exceeded by the Janus disc which have average core diameters larger than 100 nm. Additionally, some of those structures are slightly anisometric as shown in Figure 4 - 3c.

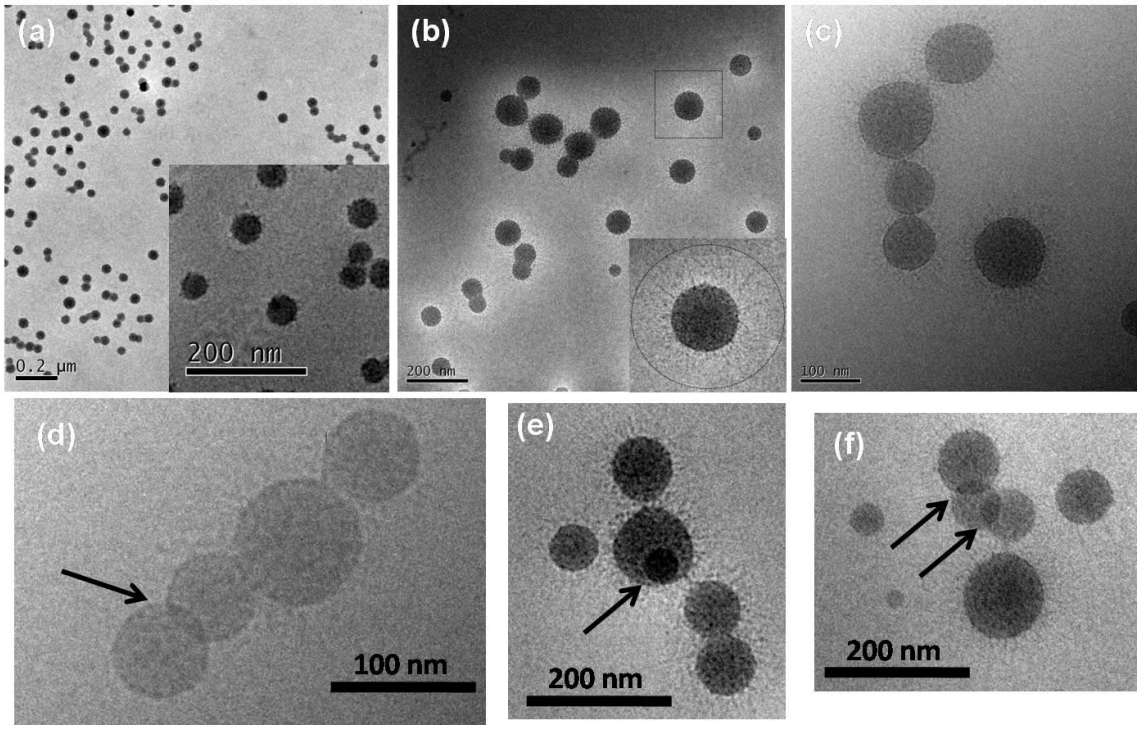

Figure 4 - 3. Cryo-TEM of micelles formed by SBMA (a) and structures of $SBMA_{small}$ (b+c). The insert in (b) shows a magnified aggregate with its circled corona of PMAA chains. Images (d-f) show Janus discs which aggregate via back-to-back stacking at some boundaries as highlighted by the arrows. The images were obtained at 100 mM CsCl and pH = 10, adjusted by CsOH. The concentration is 1 mg/mL for all samples.

In agreement with the DLS data, the structure of the SBMA micelles can be unambiguously assigned to a spherical micelle. For the small Janus discs the situation is less clear. They could either be bilayer-like superstructures in face-on view or could be unimolecularly dissolved Janus discs. As mentioned in the section above, *cryo*-TEM of such large structures with diameters above 200 nm does not allow an edge-on imaging of disc-shaped particles. The anisometry of some particles, as for instance in Figure 4 - 3c, gives an indication that these structures are not spherical. Moreover, a non-spherical shape of the particles is also strongly suggested by the appearance of a distinct angular dependence in DLS. The structures tend to be loosely connected at their boundaries, but a clear stacking is not found for the large majority of the structures. The particles are very homogenous in their center and are thus not composed of several back-to-back stacked discs. Back-to-back stacking results in clear steps in the grey scale profile within the interior of the particles, as found earlier for the non-hydrolyzed particles.[19] A consequent size match for all structures is impossible. Indeed, Figure 4 – 3 (d-f) show some particles, which overlap at their edges via back-to-back stacking. The arrows highlight areas where the stacking can be observed easily. Thus this structural motif can be unambiguously identified. However, it is widely absent for the system. Thus the stabilization is mainly provided via an unimolecular fashion.

In order to further draw conclusions about the particle structure, scanning force microscopy was performed for the sample composed of Janus discs. To allow a spatial separation of the aggregates after deposition onto freshly cleaved mica, a highly diluted solution (0.01 mg/mL) was used for dip-coating of the samples. Figure 4 - 4 shows a summary of the SFM images obtained.

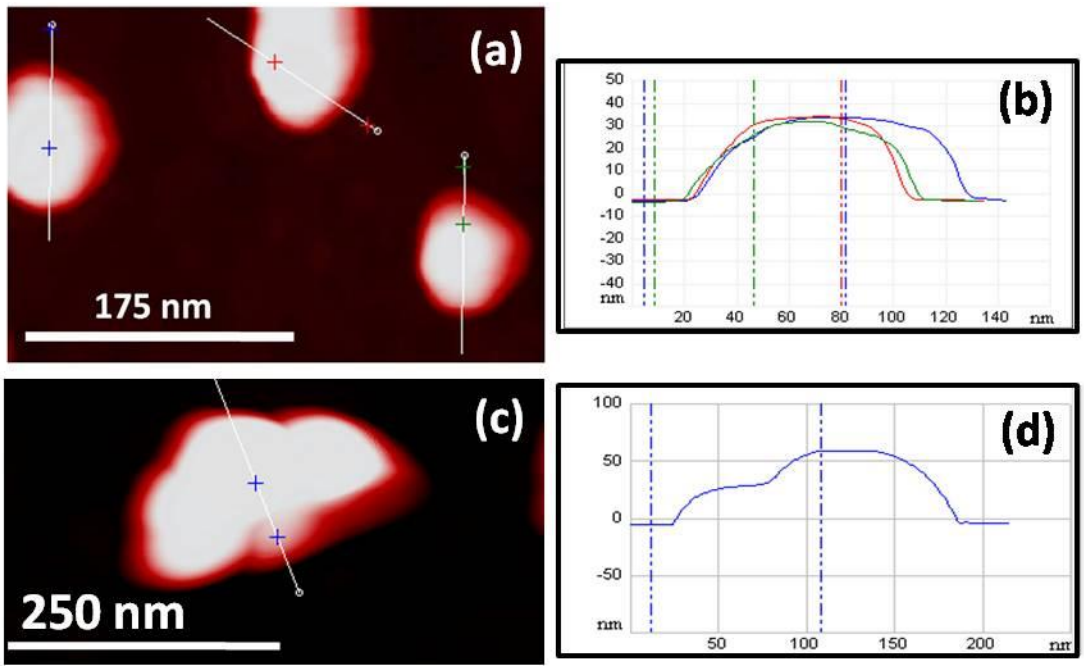

Figure 4 - 4. High-Resolution Tapping Mode Scanning Force Microscopy (SFM) images obtained from $SBMA_{small}$ after deposition from highly diluted aqueous media (c = 0.01 mg/mL) onto freshly cleaved mica. Image (a) and (c) are height images with a z-scale of 100 nm. Section analyses (b) and (d) correspond to the lines shown in (a) and (c), respectively.. All images were acquired using a super-sharp SFM tip (R_{apex} < 2 nm) under very soft tapping conditions.

A thorough examination of many images reveals a similar height profile for most particles. The step is in the range of 25 - 35 nm and the profiles are flat in the centre of the particles, thus confirming a disc-like particle character. By comparing the step height with the thickness values obtained for the non-hydrolyzed Janus discs and the triblock terpolymer template,[19] which was used for initially synthesizing the disc-shaped Janus particles, it can be concluded that the height corresponds to the thickness of one single Janus disc. A very limited number of particles can be found, exhibiting a two-step height profile. The second step is around 60 – 75 nm, thus pointing to a stacking of two Janus discs. These results coincide with the cryo-TEM data and confirm the unimolecular stabilization of the Janus discs in water. Strikingly, both cryo-TEM and SFM demonstrate the absence of aggregation of the small Janus discs. The PS side is exposed to water, which is a surprising finding attributable to the unique architecture of the particle.

After having analyzed the aggregation pattern of the small Janus discs, the attention is now focused on the aggregation behavior of larger flat Janus particles in $SBMA_{large}$. This sample contains a fraction of very large micron-sized flat Janus particles. The sample already behaves macroscopically different as it shows visible sedimentation after transfer into water. From a mechanistic point of view larger particles are interesting as bending of a disc-like structure starts playing a role. Very similar to a persistence length for cylindrical molecules, the disc stiffness (i.e. the bending modulus) of a freely diffusing disc manifests itself in a persistence area. This local stiffness is only of minor importance when the disc plane gets larger and larger. Thus a stiff unbendable small disc converts into a readily bendable one when its dimension significantly exceeds the persistence area. This can be seen in analogy to stiff polymer chains which undergo a transition from rods to worm-like molecules when they are much longer than their persistence length.

The initial attempts to visualize the aggregates of $SBMA_{large}$ by *cryo*-TEM only gave unsatisfactory results as most of the structures are too large and thus cannot be analyzed in transmission mode. Therefore, scanning electron microscopy was used to visualize the structure of the formed aggregates. Drying of PS-containing aggregates from water is considered to not alter their structure significantly, as PS possesses a high glass transition temperature and the aggregates are in the so-called “frozen” state. Figure 4 - 5 gives an overview of various SEM images obtained for the aggregates formed by large flat Janus particles of $SBMA_{large}$.

The aggregates formed by this material are strikingly different as compared to $SBMA_{small}$. Bending of the structure plays a significant role and the aggregation is beyond simple back-to-back stacking. Due to their large size, the single Janus discs can bend sufficiently and thus shield the inner polystyrene part against the non-solvent water. For instance the image in the top left corner of Figure 4 - 5 is mainly composed on one single Janus disc and shows a collapsed and wrinkled-up structure in water. These images demonstrate a way of how a single Janus disc, if it is large enough can be solubilized unimolecularly into water, simply by flipping over a part of it (see e.g. top left image in Figure 4 -) or collapsing and wrinkling up.

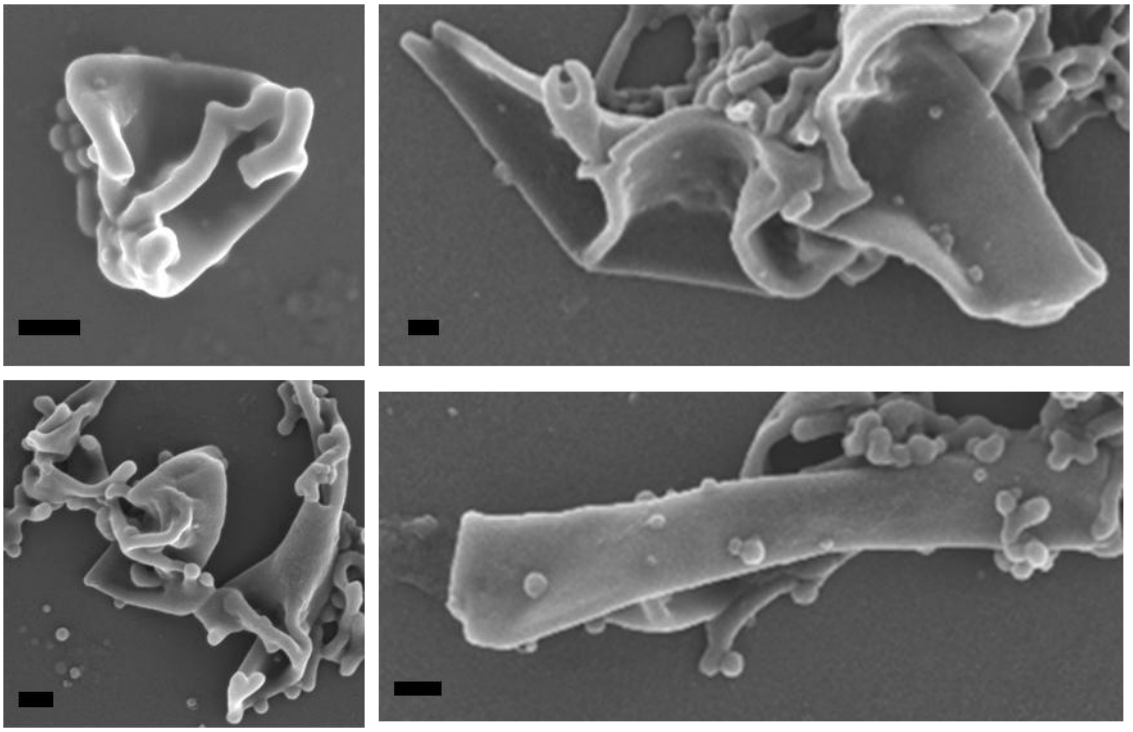

Figure 4 - 5. Scanning Electron Microscopy (SEM) images obtained after deposition of $SBMA_{large}$ onto a silicon wafer (c = 0.1 mg/mL) and subsequent sputtering with a thin platinum coating. The scale bar is 200 nm in each image.

Mechanism of Stabilization

The following picture emerges from the experimental results. Small Janus discs are mostly unimolecularly dissolved in water, as shown by *cryo*-TEM and SFM. According to the *cryo*-TEM images, the discs have a tendency to loosely aggregate at the edges. An aggregation via back-to-back stacking and shielding of the interior of the PS side is widely absent. Strikingly, this is an unexpected finding and a unique feature of Janus particles. In case of very small discs it is reasonable to assume that the PMAA arms, protruding out on one side, can sufficiently shield the hydrophobic PS side. The PMAA arms have an estimated counter length of ca. 110 nm and are thus sufficiently long. With increasing disc size, the steric and electrostatic repulsion of the PMAA brush hairs increases and presumably induces a slight bending of the structure (see Scheme 4 - 3.

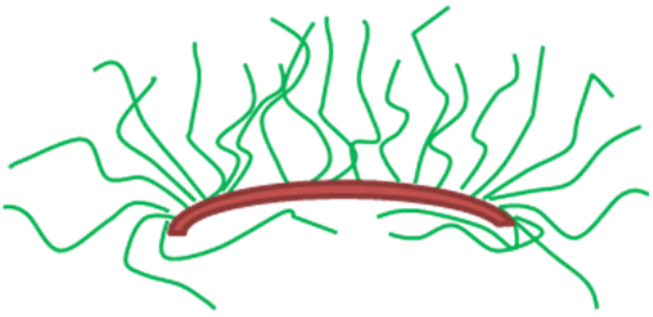

Scheme 4 - 3. Single particle stabilization mechanism for small Janus discs. The PMAA brush hairs are shown in green and the PS layer is drawn in red. The thin PB layer (< 10 nm) is omitted for clarity.

A further increase of the disc size to large Janus discs leads to a bending along one major line. Bending via one dominant line into a bilayer structure should be energetically favored as compared to bending the disc over one central focal point, leading to something like a “mushroom head”. Bending along major lines can for example be observed in the images of the aggregates formed by the large structures of $SBMA_{large}$ and can thus be seen as a main motif for the self-stabilization and the protection of the PS sides.

Some future investigations shall be dedicated to the fundamentally interesting behavior of isolated Janus discs. Certainly, Janus discs with a uniform size, as for instance obtained by lithographic approaches, would be very beneficial.

Conclusion

The solution behavior of a novel class of amphiphilic particles, so-called Janus discs, in aqueous medium has been explored by a variety of imaging techniques and dynamic light scattering. The Janus discs consist of one polystyrene and one poly(methacrylic acid) side. Two batches with differently sized flat Janus particles were compared. Significant differences can be observed for both samples. Small Janus discs are stabilized by the long PMAA chains, protruding out of one side and shielding the PS side against water. They are not aggregated via back-to-back stacking. The structures are of disc-like shape. The larger Janus particles exhibit a second stabilization mechanism. Apart from interparticle aggregation via stacking, they can undergo bending and stabilize the PS side via an intraparticle mechanism, e.g. by flipping over one part of the structure. Due to the intrinsic stiffness of the crosslinked layer, large bending is favored with increasing size of the particle.

Acknowledgments

This work was supported by the European Science Foundation within the EUROCORES SONS-AMPHI, BioSONS and the MC RTN Polyamphi programs. A. Walther acknowledges a fellowship from the Bavarian Elite Support Program.

References

1. Li, Z.; Hillmyer, M. A.; Lodge, T. P. *Langmuir* **2006,** 22, 9409.
2. Lodge, T. P.; Rasdal, A.; Li, Z.; Hillmyer, M. A. *J. Am. Chem. Soc.* **2005,** 127, 17608.
3. Li, Z.; Kesselman, E.; Talmon, Y.; Hillmyer, M. A.; Lodge, T. P. *Science* **2004,** 306, 98.
4. Laschewsky, A. *Current Opinion in Colloid & Interface Science* **2003,** 8, 274.
5. Cui, H.; Chen, Z.; Zhong, S.; Wooley, K. L.; Pochan, D. J. *Science* **2007,** 317, 647.
6. Li, Z.; Chen, Z.; Cui, H.; Hales, K.; Qi, K.; Wooley, K. L.; Pochan, D. J. *Langmuir* **2005,** 21, 7533.
7. Pochan, D. J.; Chen, Z.; Cui, H.; Hales, K.; Qi, K.; Wooley, K. L. *Science* **2004,** 306, 94.
8. Wang, X.; Wang, H.; Frankowski, D. J.; Lam, P. G.; Welch, P. M.; Winnik, M. A.; Hartmann, J.; Manners, I.; Spontak, R. J. *Adv. Mater.* **2007,** 19, 2279.
9. Wang, X.; Liu, K.; Arsenault, A. C.; Rider, D. A.; Ozin, G. A.; Winnik, M. A.; Manners, I. *J. Am. Chem. Soc.* **2007,** 129, 5630.
10. Wang, X.; Guerin, G.; Wang, H.; Wang, Y.; Manners, I.; Winnik, M. A. *Science* **2007,** 317, 644.
11. Walther, A.; Müller, A. H. E. *Soft Matter* **2008,** 4, 663.
12. Erhardt, R.; Zhang, M.; Böker, A.; Zettl, H.; Abetz, C.; Frederik, P.; Krausch, G.; Abetz, V.; Müller, A. H. E. *J. Am. Chem. Soc.* **2003,** 125, 3260.
13. Erhardt, R.; Böker, A.; Zettl, H.; Kaya, H.; Pyckhout-Hintzen, W.; Krausch, G.; Abetz, V.; Müller, A. H. E. *Macromolecules* **2001,** 34, 1069.
14. Förster, S.; Abetz, V.; Müller, A. H. E. *Adv. Polym. Sci.* **2004,** 166, 173.
15. Shepherd, R. F.; Conrad, J. C.; Rhodes, S. K.; Link, D. R.; Marquez, M.; Weitz, D. A.; Lewis, J. A. *Langmuir* **2006,** 22, 8618.
16. Roh, K.-H.; Martin, D. C.; Lahann, J. *Nat. Mater.* **2005,** 4, 759.
17. Liu, Y.; Abetz, V.; Müller, A. H. E. *Macromolecules* **2003,** 36, 7894.
18. Glaser, N.; Adams, D. J.; Böker, A.; Krausch, G. *Langmuir* **2006,** 22, 5227.
19. Walther, A.; André, X.; Drechsler, M.; Abetz, V.; Müller, A. H. E. *J. Am. Chem. Soc.* **2007,** 129, 6187.
20. Hong, L.; Cacciuto, A.; Luijten, E.; Granick, S. *Nano Lett.* **2006,** 6, 2510.
21. Nisisako, T.; Torii, T.; Takahashi, T.; Takizawa, Y. *Adv. Mater.* **2006,** 18, 1152.
22. Dendukuri, D.; Pregibon, D. C.; Collins, J.; Hatton, T. A.; Doyle, P. S. *Nat. Mater.* **2006,** 5, 365.
23. Howse, J. R.; Jones, R. A. L.; Ryan, A. J.; Gough, T.; Vafabakhsh, R.; Golestanian, R. *Phys. Rev. Lett.* **2007,** 99, 048102.
24. Walther, A.; Hoffmann, M.; Müller, A. H. E. *Angew. Chem. Int. Ed.* **2007,** 120, 723.
25. Walther, A.; Matussek, K.; Müller, A. H. E. *ACS Nano* **2008,** 2, 1167.
26. Binks, B. P.; Fletcher, P. D. I. *Langmuir* **2001,** 17, 4708.
27. Nonomura, Y.; Komura, S.; Tsujii, K. *Langmuir* **2004,** 20, 11821.
28. Walther, A.; Goldel, A.; Müller, A. H. E. *Polymer* **2008,** 49, 3217.
29. Nie, Z.; Li, W.; Seo, M.; Xu, S.; Kumacheva, E. *J. Am. Chem. Soc.* **2006,** 128, 9408.
30. Dendukuri, D.; Hatton, T. A.; Doyle, P. S. *Langmuir* **2007,** 23, 4669.
31. Marque, J.; Ikegami, A.; Kubota, K.; Tominaga, Y.; Fujime, S. *Biophys. J.* **1986,** 50, 139.
32. Fujime, S.; Kubota, K. *Biophys. Chem.* **1985,** 23, 1.
33. Kubota, K.; Tominaga, T.; Fujime, S.; Otomo, J.; Ikegami, A. *Biophys. Chem.* **1985,** 23, 15.
34. Karlsson, G. *J. Micr.* **2001,** 203, 326.
35. Johnsson, M.; Edwards, K. *Biophys. J.* **2003,** 85, 3839.
36. Provencher, S. W. *Makromol. Chem.* **1979,** 180, 201.
37. Berne, B. J.; Pecora, R., *Dynamic Light Scattering*. John Wiley & Sons: New York, 1976.

Supporting Information

Experimental Section

Preparation of Janus discs

The preparation of the Janus discs, their triblock terpolymer precursors, crosslinking and sonication is extensively described in a preceding publication.

Hydrolysis

Hydrolysis of the Janus discs was achieved via treatment of 10 mg/mL solutions with 5 v/v trifluoroacetic acid (p.a. grade, Aldrich) in dichloromethane for 24 – 48 hours. In order to dissolve the particles into water, step-wise dialysis from dioxane into water was performed.

Dynamic Light Scattering (DLS)

Dynamic light scattering was performed on an ALV DLS/SLS-SP 5022F compact goniometer system with an ALV 5000/E cross-correlator and a He–Ne laser (λ_0 = 632.8 nm). Prior to the light scattering measurements the sample solutions were filtered using Millipore or Roth filters (housing: polypropylene, membrane: polytetrafluoroethylene) with a pore size of 5 μm. All samples were analyzed at high dilution. The data evaluation of the dynamic light scattering measurements was performed with the CONTIN algorithm[36] and the values of the hydrodynamic radii were obtained after extrapolating the angle-dependent scattering data to $q^2 \rightarrow 0$.[37]

Scanning Electron Microscopy (SEM)

SEM was performed using a LEO 1530 Gemini instrument equipped with a field emission cathode with a lateral resolution of approximately 2 nm. Prior to imaging, the surfaces were coated with a thin layer of platinum. The acceleration voltage was chosen between 0.5 and 3 kV.

For **cryogenic transmission electron microscopy (cryo-TEM)** studies, a drop of the sample dissolved in warter was put on a lacey transmission electron microscopy (TEM) grid, where most of the liquid was removed with blotting paper, leaving a thin film stretched over the lace. The specimens were instantly vitrifed by rapid immersion into liquid ethane and cooled to approximately 90 K by liquid nitrogen in a temperature controlled freezing unit (Zeiss Cryobox, Zeiss NTS GmbH, Oberkochen, Germany). The temperature was monitored and kept constant in the chamber during all of the sample preparation steps. After freezing the specimens, the specimen was inserted into a cryo-transfer holder (CT3500, Gatan, München, Germany) and transferred to a Zeiss EM922 EF-TEM instrument. Examinations were carried out at temperatures around 90 K. The transmission electron microscope was operated at an acceleration voltage of 200 kV. Zero-loss filtered images (ΔE = 0 eV) were taken under reduced dose conditions (100-1000 e/nm^2). All images were registered digitally by a bottom mounted CCD camera system (Ultrascan 1000, Gatan) combined and processed with a digital imaging processing system (Gatan Digital Micrograph 3.9 for GMS 1.4).

Scanning Force Microscopy (SFM)

SFM images were taken on a Veeco Multimode operated in Tapping Mode. Super-sharp probes with finite tip sizes with radii of 2 nm were used. Offline data processing was done using the Nanoscope Software (V6r2.1).

Size distributions (CONTIN plots) of non-hydrolyzed Janus discs

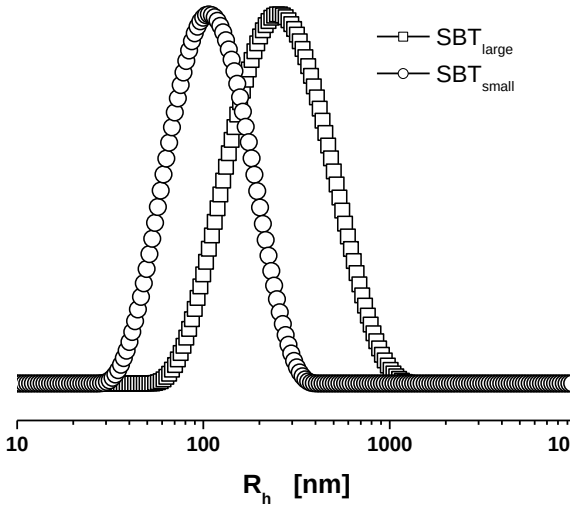

Figure Sup 4 - 1. CONTIN plots at 90^0 for the non-hydrolyzed Janus disc precursors leading to the samples SBT_{large} and SBT_{small} after acidic hydrolysis (in THF).

5. Controlled Crosslinking of Polybutadiene Containing Block Terpolymer Bulk Structures: A Facile Way towards Complex and Functional Nanostructures

Andreas Walther, Astrid Göldel, Axel H. E. Müller

Makromolekulare Chemie II and Bayreuther Zentrum für Kolloide und Grenzflächen, Universität Bayreuth, D-95440 Bayreuth, Germany

Andreas.Walther@uni-bayreuth.de; *Axel.Mueller@uni-bayreuth.de*

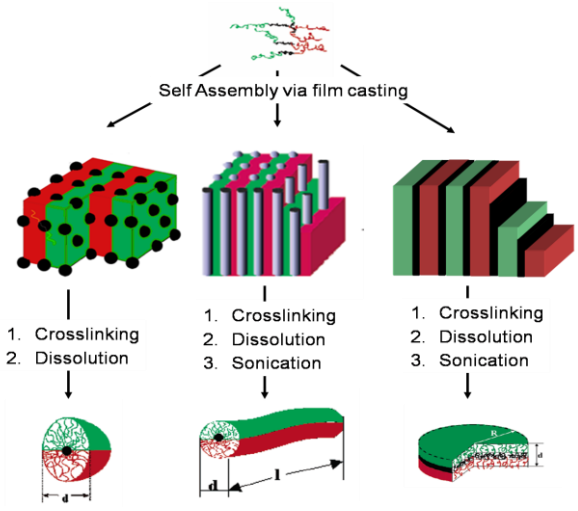

Published in *Polymer*, **2008**, 49, 3217

Abstract

The controlled crosslinking of polystyrene-*block*-polybutadiene-*block*-poly(*tert*-butyl methacrylate) (SBT) block terpolymers in their microphase-segregated bulk state is investigated. Two different methods, cold vulcanization and free radical crosslinking as well as its optimized procedure, the thiol-polyene method, are applied for crosslinking the lamellar polybutadiene microdomains within the lamella-lamella (ll) morphology of SBT bulk structures. It was found that the microphase-separated structures of the block terpolymers react very sensitively towards the addition of swelling solvents and crosslinking agents. The changes in the microphase-segregated morphologies are followed at all stages with transmission electron microscopy to give an in-depth view of the nanoscopic transformations. These partially unexpected changes in the morphologies make a careful adjustment and optimization of the reaction conditions necessary. For cold vulcanization, i.e. the reaction of double bonds with sulphur monochloride, several swelling solvents and concentrations of crosslinking agents are explored. In the case of free radical crosslinking, it is found that an increase of the radical initiator concentration above 5 wt% does not lead to an increase of insoluble material as radical chain cleavages occur as side reactions, thus limiting the amount of the desired gel fraction. However, the addition of a trifunctional thiol can further increase the desired network formation. By means of this procedure and a subsequent homogenization, it is possible to create novel disc-like Janus particles. Dynamic light scattering and scanning force microscopy are used to highlight the flat nanoparticle structure and to demonstrate the influence of the crosslinker on the formed structures.

Introduction

Widespread research in polymer science has been devoted to the field of block copolymers in the past decades. Block copolymers represent a fascinating class of material as they can combine the properties of several different polymers in a unique fashion. Block copolymers have found applications in nanoelectronics, biotechnology and industry. Due to the mutual incompatibility of different polymers with each other, block copolymers exhibit microphase-segregated morphologies in the bulk. The appearance of a certain morphology is mainly determined by the following parameters: the Flory-Huggins interaction parameter between the blocks (□), the volume fractions and the degree of polymerization. The phase diagrams of diblock copolymers are theoretically and experimentally well explored.[1-6]

Generally, several structural transitions can be observed when increasing the volume fraction of one block from zero to fifty percent, starting from a mixed system, via a spherical phase, a cylindrical phase, a gyroidal phase and finally ending up in a lamellar phase. In addition, perforated lamellar structures were found in some diblock copolymer systems between the gyroidal and the lamellar phase[7-9].

However, upon introduction of a third block to the block copolymer system, the situation becomes fairly complicated and much more morphologies can be found. Furthermore, the prediction of the stability of a certain morphology is difficult as all interactions between the different blocks must be considered.[10-13] Pioneering work in the field of block terpolymers was done by Stadler et al.[14-16], who performed in depth investigations of the polystyrene-*block*-polybutadiene-*block*-poly(methyl methacrylate) (SBM) system. The phase diagram of SBM block terpolymers and other block terpolymers comprise a multitude of fascinating phase-segregated structures on the nanometer scale.[17]

It was found that even a slight variation in the volume fractions, or a simple change in the interaction parameters between the different blocks, e.g. by hydrogenation of the inner polybutadiene block, can result in significant changes of the microphase-segregated morphologies found. For instance, an increase of the inner PB fraction, while keeping the endblocks of PS and PMMA symmetric, can already lead to five different morphologies. Low fractions of PB lead to spherical domains of PB at the lamellar interface of PS and PMMA (so-called lamella-sphere, ls), which are followed by PB cylinders (lamella-cylinder, lc) upon further increase. A completely lamellar phase with alternating layers of PS, PB and PMMA (lamella-lamella, ll) is present for fully symmetric SBM block terpolymers. For SBM block terpolymers, having PB as major component, cylindrical and spherical domains of PS and PMMA can be found in a PB matrix.

Clearly, given the wide variety of complex structures formed by block copolymer systems, it would be desirable to be capable of stabilizing those in order to be able of transferring those complex architectures into solution. First attempts for crosslinking a block copolymer domain were performed by Ishizu et al.[18, 19], who reported about the successful synthesis of polymer microspheres. For this purpose they crosslinked the spherical domains of a polystyrene-*block*-poly(4-vinyl pyridine) (PS-*b*-P4VP or SV) and of a polystyrene-*block*-polybutadiene (PS-*b*-PB or SB) diblock copolymer using 1,4-dibromobutane[18] or sulphur monochloride.[19] Decker et al. reported on the aspects of the radical crosslinking of SB and SBS block copolymers.[20-24] The focus of these

investigations was drawn to the kinetic and mechanistic aspects and not to the potentially resulting nanostructures.

Concerning the crosslinking of ABC block terpolymer nanostructures towards the preparation of functional nanostructures, the literature is limited to a few approaches. Certainly, the strategy by Liu et al, utilizing the UV crosslinking of cinnamoyl moieties, is worth mentioning. By means of this process it was for example possible to generate PS-PCHEMA-PAA (polystyrene-*block*-poly(2-cinnamoyloxy-ethyl methacrylate)-*block*-poly(*tert*-butyl acrylate)) core-shell-corona nanofibres.[25] For this purpose, block terpolymer films, exhibiting core-shell cylinders, were irradiated with UV and sonicated. Morphological rearrangements are unlikely as the UV irradiation proceeds within the rigid block terpolymer nanostructure and does not involve further chemical additives. However, one of the major drawbacks of this process is the chemistry involved. The introduction of the cinnamoyl moities requires the synthetically demanding polymerization of silyl-protected HEMA, the deprotection of it and the polymer analogues modification with cinnamoyl chloride. Furthermore, the monomer choice is limited according to the reactivity behaviour of monomers in anionic polymerization.

In contrast, polybutadiene or polyisoprene may serve as alternatives as they are extremely easy to polymerize in a wide variety of solvents and furthermore, a large amount of microphase-segregated structures of its block copolymers is already known. A few attempts of crosslinking SBM block terpolymers with lamella-sphere and lamella-cylinder morphologies have already led to fascinating spherical and cylindrical Janus particles.[26-28]

Janus structures are colloids which posses two phase-segregated compartments of different chemistry or polarity. Their preparation on the nanometer scale is very difficult and has so far most convincingly been accomplished via the selective crosslinking of SBM block terpolymer nanostructures.

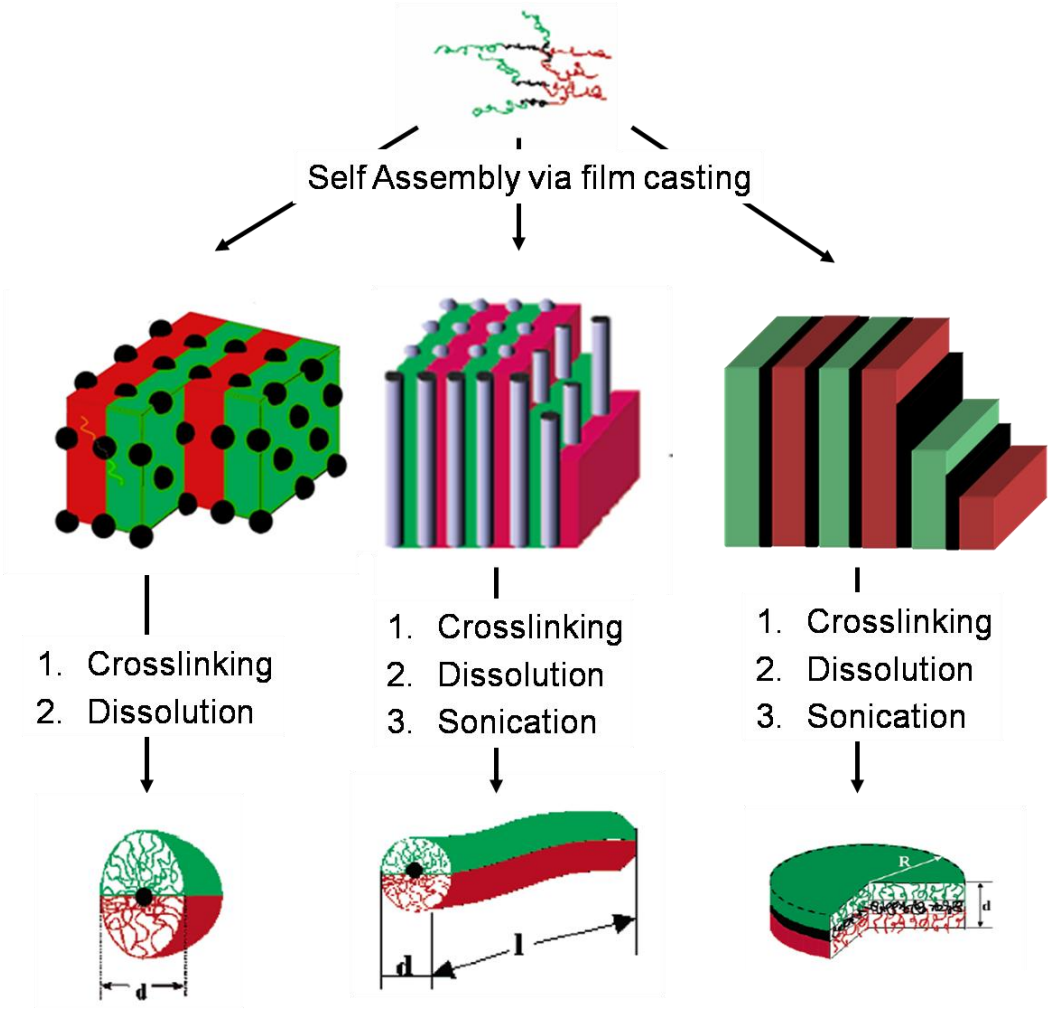

Scheme 5 - 1. Overview of the pathway for the preparation of different Janus particles via selective crosslinking of microphase-segregated structures of block terpolymers.

Janus structures are an intense field of our research due to the fact that they exhibit unique self-assembly behaviour and may serve as future surfactants, owing to their high surface activities predicted. However, a detailed investigation of the crosslinking process itself and the precautions required to carry it out in the fragile environment of block terpolymer bulk nanostructures is lacking. Since additives need to be co-casted while the film formation or swelling agents and reactive chemicals are necessary, morphological rearrangements are most likely.

Herein we report on the controlled crosslinking of polybutadiene microdomains of a series of polystyrene-*block*-polybutadiene-*block*-poly(tert-butyl methacrylate) block terpolymers. The compositions of the block terpolymers were tailored to be at the morphological boundary of the lamella-lamella morphology, as will be shown below. Cold vulcanization, the reaction between S_2Cl_2 and double bonds, and the thermally initiated free radical polymerization, as well as its optimization, the thiol-polyene reaction were employed as crosslinking reactions and thoroughly investigated. These reaction conditions can easily be applied in standard laboratories, in contrast to γ-irradiation with cobalt sources which represents another way of crosslinking polybutadiene.

Several unexpected problems concerning morphological rearrangements encountered during the crosslinking will be discussed in the following. The finally developed procedures can be applied to a large variety of block copolymers and should stimulate further work in the direction of crosslinking

block terpolymer bulk structures, containing polybutadiene or polyisoprene, towards internally structured nanoparticles.

Since the crosslinking of the inner polybutadiene layer preserves the preorientation of the PS and P*t*BMA part, sheet- or disc-like Janus particles can be obtained after a homogenization procedure (see Scheme 5 - 1). Some experimental results of the characterization of the Janus discs will be highlighted at the end to show the influence of the different crosslinking methods on the obtained material.

Experimental Section

Materials

All solvents and reagents were obtained from Merck or Aldrich in p.a. grade and used without further treatment except for the following ones. Decane (p.a., Aldrich) and Isooctane (p.a., Aldrich) were treated with sec-butyl lithium and distilled. THF (p.a. Merck) was treated with sec-butyl lithium at low temperatures and distilled. Cyclohexane (Merck) and acetonitrile (Aldrich) were obtained in HPLC grade and used directly.

Synthesis

The anionic polymerization of the polystyrene-*block*-polybutadiene-*block*-poly(*tert*-butyl methacrylate) (SBT) block terpolymers was conducted in a similar way as reported elsewhere.[29, 30]

Crosslinking with AIBN / Thiol-Polyene process

AIBN (5 wt%, relative to the mass of the SBT block terpolymer), trimethylolpropane mercaptopropionate (TRIS, 0 - 5 wt%) and SBT block terpolymer were dissolved in $CHCl_3$ and the film casting process was allowed to take place in a solvent vapour filled desiccator for about two weeks, yielding films with thicknesses between 0.5 – 2 mm. Afterwards, the film was dried in vacuo at RT for 24 h and crosslinked at 80 °C for 48 h. Subsequently, the film was purified by Soxhlet extraction with THF for 24 h yielding a soluble fraction and an insoluble fraction. The insoluble fraction was subjected to a sonication treatment.

Cold vulcanization

A solvent-cast film (typical thickness between 0.5 – 2 mm) was introduced into a reaction vessel and swollen in solvent (decane or isooctane) for a certain period of time (typically: 12 – 48 h). Afterwards, the calculated amount of S_2Cl_2 (typically: 1.5 – 5 vol%) was introduced with a syringe and the crosslinking was allowed to take place for 12 - 48 h at room temperature. After the reaction, the film was washed with several aprotic non-solvents, e.g. acetonitrile and isooctane. Subsequently, the film was purified by Soxhlet extraction with THF for 24 h yielding a soluble and an insoluble fraction. The insoluble fraction was subjected to a sonication treatment.

Sonication

The product underwent ultrasonic treatment using a Branson model-250 digital sonifier, equipped with 1/8 in. diameter tapered microtip, at various amplitudes (200 watt at 100% amplitude). For this purpose, a dispersion of insoluble crosslinked material (c = 0.3 - 1 mg/ml) in THF was allowed to

stand at room temperature for several hours to ensure good swelling of the material. Afterwards, it was subjected to the sonication treatment in a temperature controlled cell. The on/off cycle times were typically in the range of 2s/2s and 2s/10s, depending on the amplitude used.

GPC-viscosity measurements were conducted using the following column and detector setup: 5µ PSS SDV gel, 10^3 Å, 10^5 Å and 10^6 Å, 30 cm each; Shodex RI-71 refractive index detector; Jasco Uvidec-100-III UV detector (λ = 254 nm); Viscotek viscosity detector H 502B. The molecular weights were determined by the universal calibration principle[31] using the viscosity module of the PSS-WinGPC scientific V 6.1 or V 7.12 software package. Linear PMMA standards (PSS, Mainz) were used to construct the universal calibration. Prior to measurements the samples were filtrated using 3 µm PTFE filters.

GPC-MALS measurements were performed at room temperature using a GPC equipped with a Wyatt Technology DAWN DSP-F multi-angle light scattering detector (He-Ne Laser; λ = 632.8 nm) and a Shodex-RI-71 refractive index detector. Three 30 cm PSS SDV columns (10^4, 10^5, and 10^6 Å) were used with THF as eluent at a flow rate of 1 mL/min. Data evaluation was performed with the Astra Software package.

NMR

^{1}H- and ^{13}C-NMR spectra were obtained on a Bruker AC 250 at an operating frequency of 250 MHz and 62.5 MHz, respectively. Various deuterated solvents (Deutero GmbH) were used depending on the solubility of the samples. As an internal standard, the residual proton signal of the deuterated solvent was used.

Transmission Electron Microscopy (TEM)

The bulk morphologies of the SBT triblock terpolymer were examined using TEM. Films (around 1 mm thick) were cast from 5% (w/w) solutions in $CHCl_3$ and allowed to evaporate slowly for 2 weeks. The as-cast films were dried for 1 day in vacuum at room temperature and then annealed at 80 °C for 1 - 5 days. Thin sections were cut at room temperature using a Reichert-Jung Ultracut E microtome equipped with a diamond knife. To enhance the electron density contrast between the three blocks, the sections were exposed to OsO_4 vapour for 60 s, which leads to a preferential staining of the polybutadiene block appearing black. Bright-field TEM was performed on Zeiss CEM 902 and LEO 922 OMEGA electron microscopes operated at 80 kV and 200 kV, respectively.

Scanning Force Microscopy (SFM)

SFM images were taken on a Digital Instruments Dimension 3100 microscope or on a Veeco Multimode operated in Tapping Mode. Standard silicon nitride probes were driven at 3 % offset below their resonance frequencies in the range of 250 - 350 kHz. According to the distributor of the tips, the normal tips possess finite tip sizes with radii of 10 - 20 nm. Offline data processing was done using the Nanoscope Software (V 5.13r10sr1 and V6r2.1).

Results and Discussion

Synthesis and Characterization of SBT Block Terpolymers

Several polystyrene-*block*-polybutadiene-*block*-poly(*tert*-butyl methacrylate) (SBT) block terpolymers were prepared by living anionic polymerization in THF using the sequential monomer addition technique. The weight fractions of the different blocks were targeted towards symmetric fractions of the endblocks in order to form lamellar microphase-separated structures in the bulk. Due to the synthetic pathway in THF in the presence of lithium counterions, the block terpolymers are constituted of a high 1,2-butadiene content. From the ^{1}H NMR spectra (see Figure 5 - 1) the exact weight fractions of the three blocks, as well as the fraction of 1,2-butadiene can be calculated.

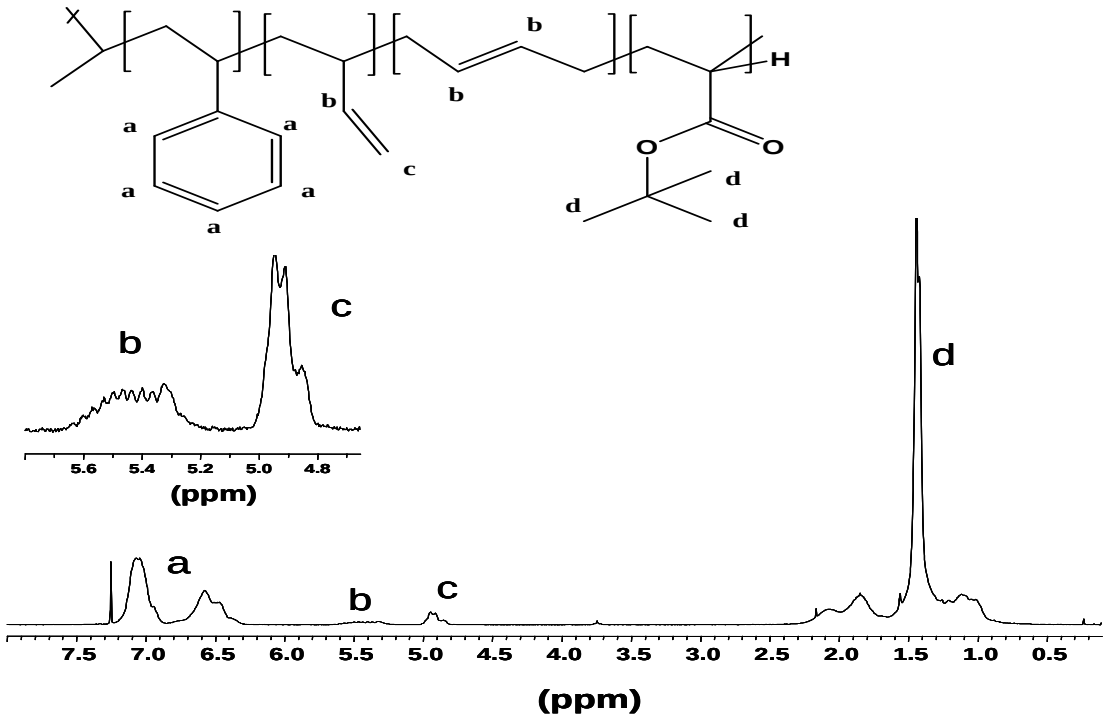

Figure 5 - 1. ^{1}H NMR spectrum of a SBT block terpolymer, recorded in $CDCl^{3}$. All unassigned peaks of the backbone are located in the broad peak area ranging from 0.7 – 2.4 ppm.

All three SBT block terpolymers possess a 1,2-vinyl content of 90 - 95 %, a controlled molecular weight distribution and an almost symmetric composition regarding the endblocks. The polybutadiene fraction was varied in a range from 4 – 10 wt%. A high 1,2-vinyl content of the polybutadiene is preferred as it facilitates the later radical crosslinking process using AIBN. The molecular characteristics of all the three SBT block terpolymers used in this study are summarized in Table 5 - 1.

Table 5 - 1. Molecular Characterization of the SBT block terpolymers.

	Composition[a]	10^3 x M_n (M_w/M_n)	10^3 x $M_{n,\ MALS}$ (M_w/M_n)
SBT-1	S42B10T48	138 (1.09)[b]	133 (1.06)
SBT-2	S45B5T50	134 (1.07)[b]	133 (1.03)
SBT-3	S46B4T50	171 (1.06)[b]	171 (1.06)

[a] Weight fractions of the three blocks as calculated from the ^{1}H NMR spectra (S = polystyrene, B = polybutadiene, T = *tert*-butyl methacrylate). [b] Calculated value for the number average molecular weight, M_n, based on calculation of the exactly determined M_n of the polystyrene precursor and the determined weight fractions of the blocks. The M_n of the PS precursor and the polydispersity of the block terpolymers were evaluated with standard THF GPC and calibration against linear PS standards.

Microphase Structure

Since this study aims at the controlled crosslinking of lamella-lamella block terpolymer morphologies towards the preparation of sheet- or disc-like Janus structures, it is important to ensure the presence of fully lamellar morphologies of the SBT block terpolymers in the bulk. Transmission electron microscopy is a powerful technique for investigating the microphase separation of block copolymers and was hence used in this study. In order to enhance the electron density contrast of the material, the measured ultrathin sections were stained with OsO_4 prior to measurement. This method preferentially stains the polybutadiene domains, leading to a black appearance in the bright field imaging mode. Figure 5 - 2 shows TEM micrographs of SBT-1, prepared by solution casting from a chloroform solution.

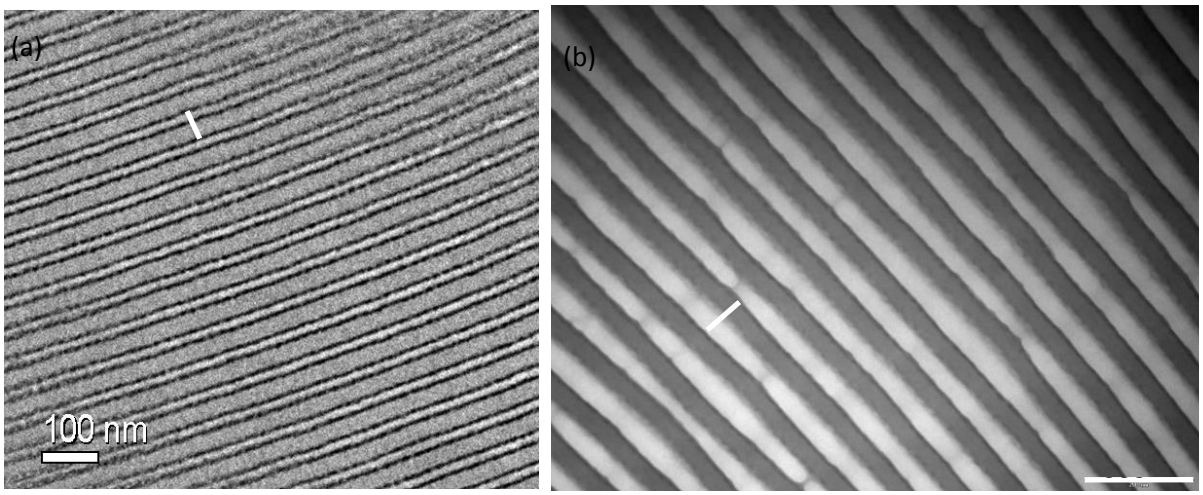

Figure 5 - 2. Transmission electron micrographs of ultrathin sections of a SBT-1 film after staining with OsO_4. The ultrathin film was imaged using a normal (a) and a carbon coated (b) TEM grid. The insert in (a) shows a magnified part of the image. The white bars indicate the long period of the periodicity of the structure.

A continuous polybutadiene layer (black) can be clearly seen between the polystyrene (grey) and the poly(*tert*-butyl methacrylate) (white) lamellae, indicating the presence of fully lamellar morphology. Interestingly, the SBT block terpolymer forms still a fully lamellar morphology despite the low fraction of polybutadiene. In the case of SBM block terpolymers of similar composition, the lamellar phase is not sTable 5 - for PB contents smaller approximately 25 wt%. This reflects nicely the earlier mentioned strong influence of the interaction parameters between the different blocks.

The thickness of the inner polybutadiene phase can be calculated to ca. 6 nm. This value may however be slightly overestimated as the incorporation of the staining agent can lead to an increase of the volume fraction. The polybutadiene layer is only visible on one side of the polystyrene lamella in Figure 5 - 2, which is probably due to a tilting of the structure with respect to the cut of the ultrathin section. This is a quite frequently observed phenomenon in TEM images for block copolymer structures with very thin features.[32]

An interesting peculiarity is the observation of two different long periods, depending on the grid type used. The smaller long period in Figure 5 - 2a (53 nm) in contrast to the longer one, observed in Figure 5 - 2b (80 nm), can be explained by a shrinkage of the structure. It was already shown earlier that in block copolymers containing poly(methyl methacrylate) as one phase, the apparent micrograph does not necessarily reflect the real dimensions of the specimen, i.e. the thickness of the lamella is underestimated from the micrograph.[15, 33] This is due to the easy degradation of poly(meth)acrylates upon exposure to an electron beam.[15, 33] On the contrary, aromatic structures, like polystyrene, are much less sensitive to radiation damage as they undergo delocalized excitations.[34] The standard TEM grid (holey Cu-grid) is unable of providing sufficient mechanical stability to the film and thus the structures shrinks, which as consequence results in a wrong representation of the actual volume fractions of the two end blocks, PS and P*t*BMA. On the right hand side, though, the volume fractions are represented as expected and the herein determined long period is closer to the real value, which can e.g. be determined by SAXS.

In contrast to the clear lamellar (ll) morphologies of SBT-1, the SBT block terpolymers with polybutadiene fractions smaller 6 wt%, SBT-2 and SBT-3, show different microphase-segregated structures. Figure 5 - 3 shows a TEM image of SBT-2, in which localized discontinuities of the butadiene lamella can be observed (highlighted by the arrows).

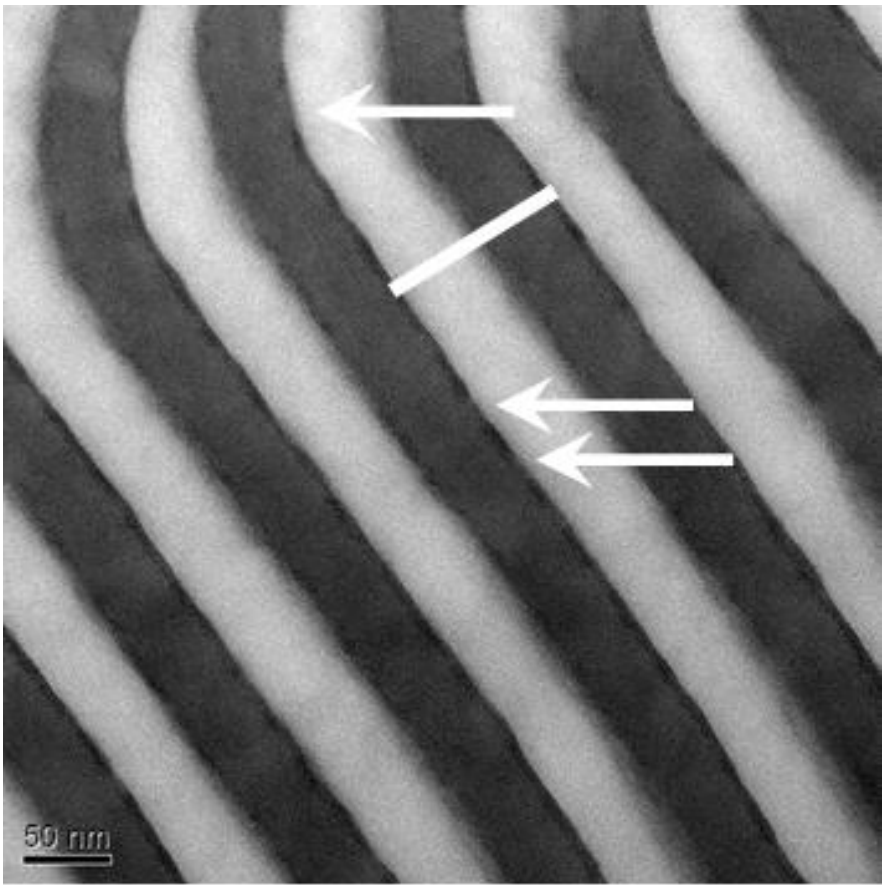

Figure 5 - 3. Transmission electron micrograph of an ultrathin section of a SBT-2 film after staining with OsO_4. The ultrathin film was imaged using a carbon coated TEM grid. The white bar indicates the long period of the periodicity of the structure.

These discontinuities seem to be randomly distributed and do not exhibit any higher three-dimensional order or periodicity. A clear transition to the lamella-sphere (ls) or lamella-cylinder (lc) morphology cannot be observed. This morphology is thus best described as an irregularly perforated lamella (ipl). Perforated lamellar structures of diblock copolymers, such as the hexagonally perforated lamella (hpl), are considered to be metasTable 5 - long-living transition states.[35-37] Consequently, the ipl structure found here will certainly react very sensitive to the presence of crosslinking and swelling agents. The thickness of the polybutadiene lamella is less than 5 nm and the long period can be calculated to 86 nm.

Despite the discontinuities, this SBT block terpolymer may still serve as a material for the synthesis of flat Janus particles. The perforations may only act as kind of desirable predetermined breaking point, leading to a decrease of the duration of the homogenization procedure using sonication.

A transmission electron microscopy investigation of the third SBT block terpolymer, SBT-3, with an even lower content of polybutadiene (4 wt%) reveals a clear break-up of the ll morphology. The TEM images below show comparable morphologies, mainly independent of the solvent used for the film casting.

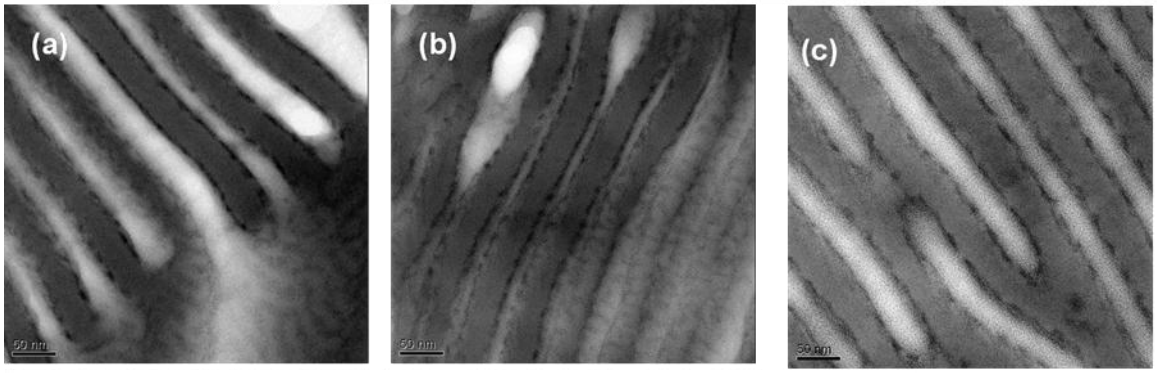

Figure 5 - 4. Transmission electron micrographs of ultrathin sections of SBT-3 films after film casting from different solvents, dichloromethane (a), dioxane (b) and 2-butanone (c). The ultrathin sections were stained with OsO_4 and imaged using standard TEM grids.

In all cases, only short cylinders or elongated spheres can be seen at the interface of PS and P*t*BMA. The morphologies itself are not very well developed in the complete samples, indicating a strong competition of the chain conformational entropy and the interfacial energies of the system. Due to the small domain size of the polybutadiene, SBT-3 is not suitable for the synthesis of Janus discs. However, a clear transition to a defined lamella-cylinder or lamella-sphere morphology does not take place, which unfortunately prevents the usage of this block terpolymer for the synthesis of spherical Janus micelles as well. Even the polar solvent dioxane cannot induce the clear transition to a lamella-sphere morphology.

In consequence of the microphase-separated structures found, only SBT-1 and SBT-2 were investigated for the controlled crosslinking as only those bulk nanostructures may result in disc-like Janus particles.

Crosslinking of the SBT Block Terpolymer Bulk Nanostructures

Two strategies were employed for the crosslinking of the SBT block terpolymer morphologies. Cold vulcanization, radical crosslinking using AIBN and its optimization – the thiol-polyene procedure – have proven to be effective routes for crosslinking polybutadiene microdomains. Cold vulcanization is the reaction of double-bonds with sulphur monochloride (S_2Cl_2) in the swollen state and leads to the coupling of two vinyl moieties. In contrast to the free radical crosslinking via e.g. AIBN, this reaction leads to a significant volume increase of the crosslinked material. The agent does not react in a chain reaction, but in a defined molar ratio.

Cold Vulcanization with Sulphur Monochloride (S_2Cl_2)

As a first step, the swelling ability of several solvents in combination with the SBT block terpolymer films needs to be analyzed. The choice of solvents is limited to aprotic solvents, because protic solvents react with S_2Cl_2 and thus prevent a crosslinking. The conditions were optimized for the SBT-2 block terpolymer, as this polymer was expected to react more sensitively to changes in solvent quality. This assumption is based on the fact that perforated lamellar structures may not be in full thermal equilibrium, as mentioned above. The investigations revealed that only a small number of organic solvents is able to swell the polymer film under retention of the desired morphology. Many solvents from polar to non-polar tend to dissolve the polymer film completely, which is probably

due to the high solubility of the poly(*tert*-butyl methacrylate). Figure 5 - 5 shows the corresponding TEM images of the swollen block terpolymer films after one day of swelling, subsequent rapid drying, microtome cutting and staining with OsO_4.

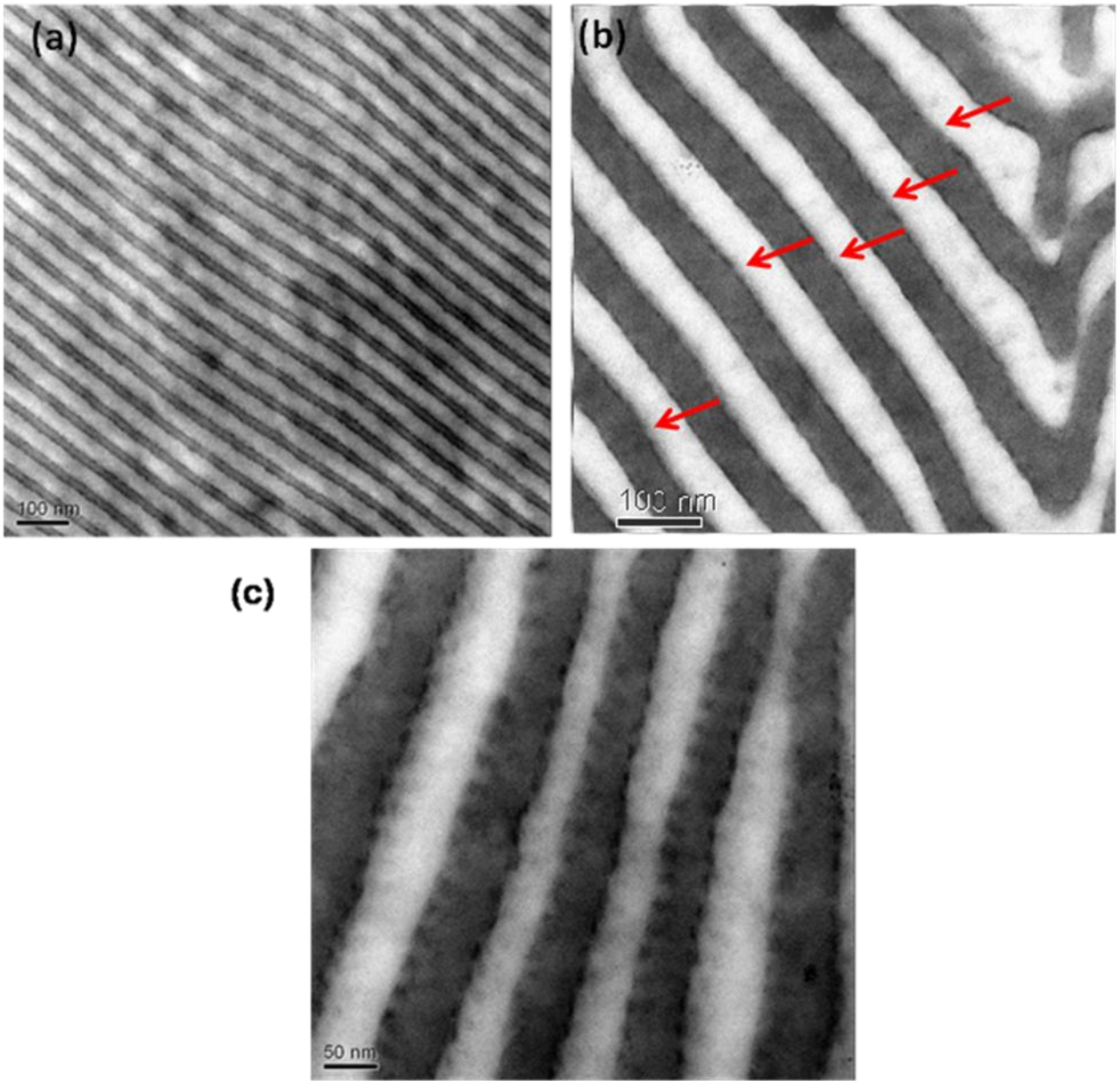

Figure 5 - 5. Transmission electron micrographs of ultrathin sections of SBT-2 films after swelling in isooctane (a), decane (b) and acetonitrile/THF (95/5 vol%, c) and rapid drying. Prior to imaging the films were stained with OsO4.

Among the suitable solvents only decane and isooctane can be used as they do not alter the microphase-separated structure in any undesired fashion. Whereas the discontinuities remain in the polybutadiene layer upon swelling with decane (Figure 5 - 5b), a continuous lamella can be observed when using isooctane as swelling agent (Figure 5 - 5a). The latter solvent promotes a "healing" of the perforations of the butadiene layer, which is due to the good swelling of the polybutadiene in isooctane. In contrast, a mixture of acetonitrile with 5 vol% THF induces an undesired transition of the lamella-lamella morphology to a microphase-segregated structure with small cylindrical or disc-shaped domains of polybutadiene at the interface. This is caused by the high polarity of the acetonitril, leading to a minimization of the surface area of the polybutadiene

domains. Consequently, the latter solvent combination is not suitable for the preparation of large disc-shaped Janus particles with high aspect ratios. These results confirm the expected sensitivity of the irregularly perforated lamella towards a change in the solvent quality and show how careful the solvent choice needs to be done. The differences in the morphologies, which develop upon swelling in the three different solvents, have an influence on the kind of Janus particles, which can be created during the cold vulcanization.

Another point which needs attention to be paid to is, whether the crosslinking agent itself can have an influence on the microphase-separated structure. Therefore, a detailed TEM investigation was performed after crosslinking the swollen films with different concentrations of sulphur monochloride (see Figure 5 - 6). The images are somewhat blurry, which is related to the fluffy appearance and the related difficulties in cutting the ultrathin sections of the highly swollen and crosslinked films. This is also one of the reasons why the crosslinked polybutadiene layer is not clearly visible in all micrographs. Additionally, the butadiene phase is distributed in an extremely thin three-dimensional lamella and the contrast, evolving from the reaction of the thin crosslinked polybutadiene with S_2Cl_2 layer is not always high enough to give sufficient contrast during the TEM imaging. A clear dark appearance of the PB phase can however be seen for the crosslinked lamella in Figure 5 - 6d (SBT-1). Indications for a crosslinked PB phase can be seen in the magnified inset in Figure 5 - 6b (SBT-2). Reasonably, it is easier to visualize the slight electron density contrast after crosslinking with S_2Cl_2 in isooctane for the block terpolymer with the higher polybutadiene content, i.e. SBT-1 (Figure 5 - 6d). Additional staining of some remaining double bonds with OsO_4 after crosslinking a SBT-1 bulk structure in isooctane gives a clear evidence for the persistence of the lamellar morphology (compare Figure 5 - 6e and 6f).

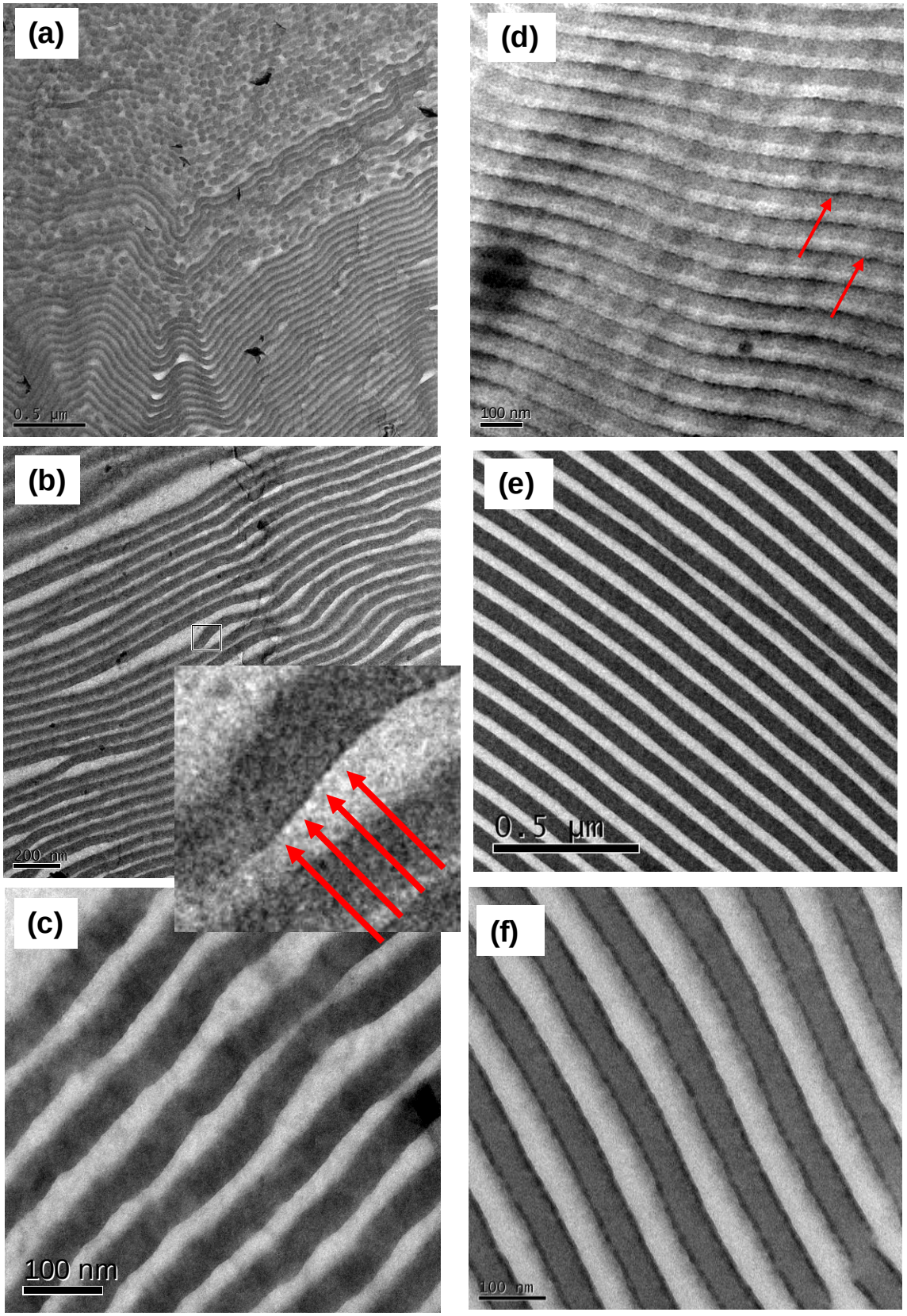

Figure 5 - 6. Transmission electron micrographs of different polymer films after crosslinking with S_2Cl_2. SBT-2 crosslinked with 5 vol% (a) and 3 vol% (b) S_2Cl_2 after swelling in isooctane. (c) SBT-2 crosslinked with 5 vol% S_2Cl_2 after swelling in decane. (d) SBT-1 crosslinked with 5 vol% S_2Cl_2 after swelling in isooctane. SBT-1 crosslinked with 1.5 vol% S_2Cl_2 after swelling in isooctane (e) and after additional staining with OsO_4 (f).

Considering the concentration effect of the crosslinking agent on the microphase-separated structure, a dramatic effect can be observed. The TEM image in Figure 5 - 6a (SBT-2, isooctane, 5 vol% S_2Cl_2) shows a break-up of the PS lamella into cylinders and the P*t*BMA phase becomes continuous. A transition to a core-shell cylindrical morphology occurs. The change in the morphology is definitely induced by the crosslinking agent, S_2Cl_2, as it was observed earlier that swelling in isooctane does not lead to a break-up of the PS phase (see Figure 5 - 5a). This strong effect was unexpected in the first place, as sulphur monochloride is an extremely reactive chemical and was only used in relatively small quantities (< 5 vol%). However, the morphological reorientation acts on a faster time-scale than the crosslinking. Consequently, the crosslinking of complex block terpolymer bulk nanostructures and metasTable 5 - morphologies needs to be verified at every step of the crosslinking process. A similar transition cannot be observed for the reaction in decane (Figure 5 - 6c), which is due to the unlike solvent quality and the different swelling behaviour of the three block terpolymer phases. Generally, decane is a worse swelling solvent and thus reduces the mobility of the phase towards structural rearrangements. On the other hand, it also limits diffusion of the S_2Cl_2 and may thus be not advantageous for a tight crosslinking. In the case of the crosslinking of SBT-1 with 5 vol% S_2Cl_2 in isooctane (Figure 5 - 6d), the breakup of the polystyrene lamella can only be seen for a small part of the imaged sample (hence not shown here), but the major parts remain intact. The ordinary lamellar morphology of SBT-1 obviously exhibits a higher stability towards a change in the solvent quality as it represents the thermodynamic equilibrium structure. Consequently, the crosslinking of the SBT-1 bulk films after swelling with isooctane and crosslinking with 1.5 vol% S_2Cl_2 proceeds smoothly as can be seen in Figure 5 - 6e and 6f.

In conclusion, concerning the structural integrity of the microphase-segregated structure, decreasing the concentration of the crosslinking agent (1.5 – 3 vol%) has a positive influence for all samples. A breakup of the polystyrene layer can no longer be observed, neither for SBT-1 nor for SBT-2, allowing the desired crosslinking process in the lamellar morphology to take place. Isooctane is to be preferred as swelling solvent, as it promotes a desirable continuous layer formation of the polybutadiene phase even at very low volume fractions of PB. Furthermore, the high degree of swelling ensures a fast and efficient crosslinking reaction to take place.

Aside the structural evolution during swelling and crosslinking, the focus was also set on the extent of the crosslinking. Table 5 - 2 summarizes the results of the purification of the SBT-2 polymer films after swelling and crosslinking with S_2Cl_2 using three different solvents and varying concentrations of crosslinking agent.

Table 5 - 2. Results of the purification after cold vulcanization of SBT-2.

Swelling Solvent	S_2Cl_2 (vol%)	Fraction of insoluble material [%]	Degree of crosslinking [%][b]
Decane	5	89.4	ca. 61
Isooctane	5	94.5	ca. 96
Isooctane	3	93.2	ca. 73
Isooctane	1.5	95.2	ca.73
ACN + THF 95/5 vol%	5	6.3	not measured

[a] Crosslinking was performed for 24h, using S_2Cl_2 as crosslinking agent, after swelling of the film in the corresponding solvent for 24h. Soxhlet extraction was conducted for 24 h using THF as eluent. [b] Based on elemental analysis of the sulphur and/or the chlorine content of the insoluble material after soxhlet extraction.

The cold vulcanization after swelling in the ACN/THF (95/5 vol%) mixture leads to mainly soluble Janus particles, reflecting the morphological transition to a completely discontinuous polybutadiene layer during swelling. The two other solvents, decane and isooctane, show a small difference for the fractions of insoluble and soluble materials. The major part is insoluble for both procedures. However, the insoluble fraction is always higher using isooctane as swelling solvent, even for low concentrations of sulphur monochloride. The extent of crosslinking, as determined by elemental analysis, indicates a slight difference in the extent of crosslinking for the two methods, meaning that the degree of crosslinked polybutadiene bonds is higher for isooctane. This is due to a higher extent of swelling in the case of isooctane, which facilitates the diffusion of the crosslinking agent into the polybutadiene lamella. The purification results reflect directly the solvent induced changes of the morphologies (see Figure 5 - 5 and 6). Based on the TEM results regarding the structural transitions, the S_2Cl_2 content needs to be reduced in case of isooctane. Nevertheless, its good swelling ability still ensures a high degree of crosslinking and a large fraction of insoluble material. Note that the morphologies and the extent of crosslinking are much more sensitive to the type of solvent and the crosslinking agent used than to the times for swelling and reaction.

In order to obtain flat Janus particles in the end of the process, the cold vulcanization has to be performed in decane or in isooctane with 1.5 - 3 vol% of crosslinking agent. This ensures the integrity of the microphase-separated structure and the presence and persistence of a lamellar (ll) morphology. Isooctane has some advantages as it leads to a “healing” of the holes in the ipl structure of the polybutadiene layer and to a better crosslinking even at lower contents of crosslinking agent.

Concerning an up-scaling of this reaction up to the gram scale, it is recommended performing the cold vulcanization using larger samples with similar thicknesses. Although we did not find differences for the crosslinking of films with thicknesses ranging from 0.5 – 2 mm, some problems could be anticipated if a big bulk plastic sample was introduced. With increasing ratio of volume to

surface area, i.e. increased sample size, the diffusion rate of swelling solvent and crosslinking agent starts playing a larger role.

Crosslinking with AIBN and the Thiol-Polyene Procedure

The radical crosslinking processes using AIBN or the thiol-polyene method have one important advantage over the cold vulcanization, which is the stability of the linking bonds in acidic media. This allows a subsequent facile hydrolysis of the poly(*tert*-butyl methacrylate) part using strong acids for the preparation of novel water-soluble disc-like Janus particles. On the contrary however, radical crosslinking usually does not proceed with the same efficiency as the cold vulcanization, leading to a lower degree of crosslinking.

According to the work of Decker et al.[20-24], the crosslinking of AIBN in combination with TRIS, a trifunctional thiol, is expected to lead to an increased fraction of insoluble material (thiol-polyene reaction). This is due to the fact, that TRIS can act as transfer agent and is also able to react with the 1,4-polybutadiene moieties which are usually not attacked during a normal radical crosslinking. Hence, this additive should lead to a stronger and more complete crosslinking and undesired side reactions, like radical transfer to the polymer backbone and radical chain scission should additionally be decreased due to the high chain transfer constants known for thiols. Therefore, the beneficial influence of this additive was also investigated in the present study.

Before carrying out the crosslinking, TEM images were recorded in order to assure the presence of lamellar morphologies. It can be seen in Figure 5 - 7 that film casting in presence of AIBN and TRIS has no influence on the development of the lamellar (ll) morphology. The morphologies are of long range order and the black polybutadiene layers can be seen nicely in all cases. It is worth noting that a further increase of the TRIS concentration above 10 wt% results in a preferential swelling of the P*t*BMA phase. Despite the swelling of this phase, the lamellar block terpolymer morphology mainly remains unaffected.

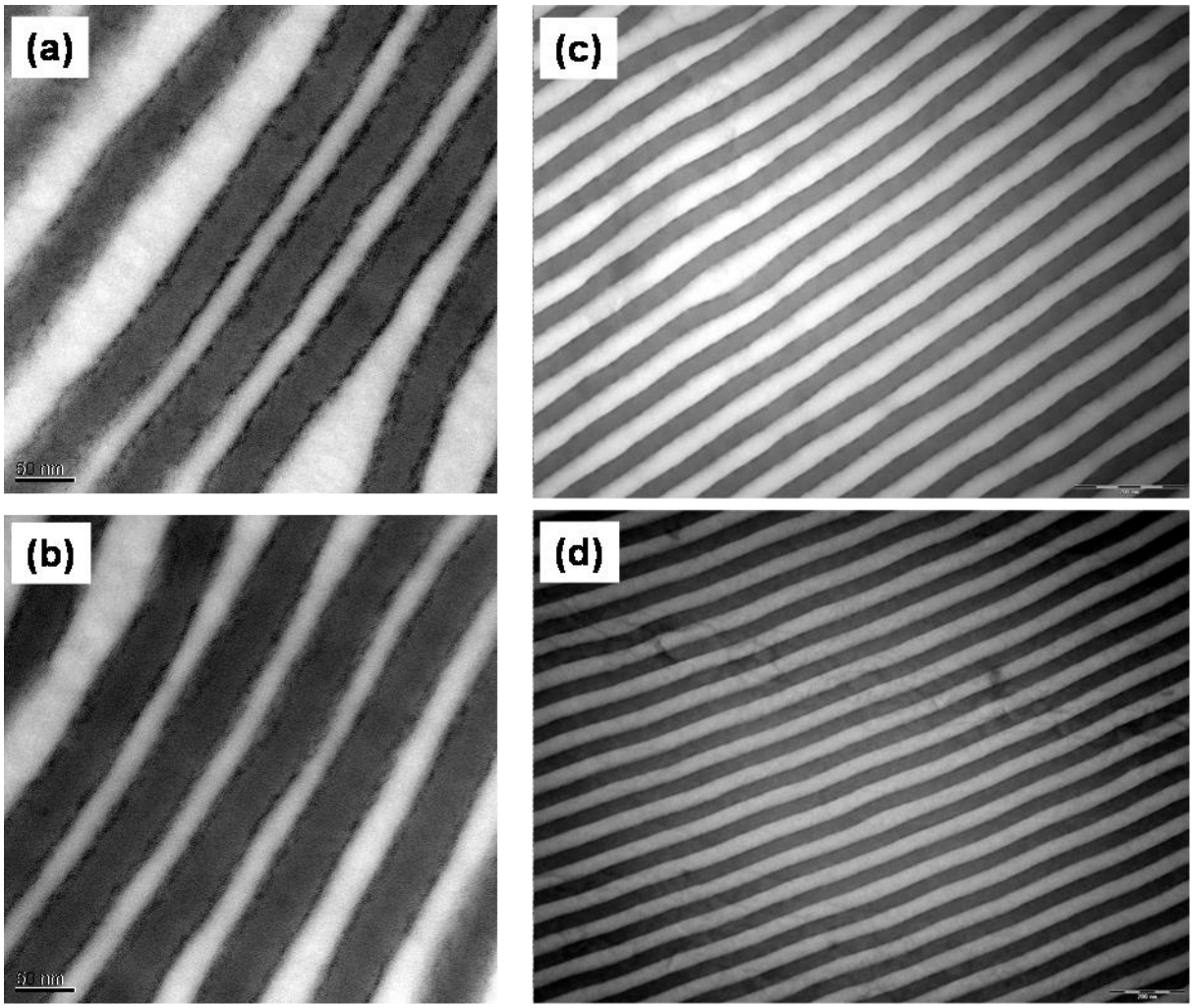

Figure 5 - 7. Transmission electron micrographs after staining with OsO_4. Ultrathin sections of SBT-2 with 5 wt% AIBN (a), SBT-1 with 5 wt% AIBN and 5 wt% TRIS (b), SBT-1 with 5 wt% AIBN (c) and SBT-1 with 5 wt% AIBN and 5 wt% TRIS (d).

An initially performed variation of the AIBN concentration from 3 - 10 wt% showed only a small influence on the ratio of insoluble to soluble material after purification with soxhlet extraction (see Table 5 - 3). The fraction of insoluble material increases for higher concentrations of AIBN, but reaches a kind of plateau with further increase. It will be seen later that the never occurring complete crosslinking, even at high AIBN concentration, might be due to radical chain cleavages. Therefore, in order to ensure a sufficient crosslinking with an acceptable amount of side reactions, the simple radical crosslinking procedure can be carried out at a concentration of 5 wt% AIBN.

Table 5 - 3. Influence of the AIBN concentration and the addition of TRIS on the crosslinking behaviour of SBT block terpolymer films.

Entry	Terpolymer	AIBN [wt%]	TRIS [wt%]	Fraction of insoluble material [%][a]
1	SBT-2	3.2	-	26
2	SBT-2	5	-	48
3	SBT-2	5.9	-	51
4	SBT-2	9.8	-	55
5	SBT-2	5	5	63
6	SBT-1	5	-	72
7	SBT-1	5	5	91

[a] Soxhlet extraction with THF for 24h.

Table 5 - 3 also compares the influence of TRIS on the ratio of soluble to insoluble material. It can be seen from entries 2 and 5, as well as 6 and 7, that an addition of 5 wt% TRIS results in a clear increase of the crosslinked insoluble fraction, representing a beneficial influence of this additive. Generally, the fraction of insoluble material is much higher for SBT-1 than for SBT-2, which is due to the higher content of polybutadiene, facilitating the crosslinking procedure. Unfortunately, it was not possible to determine the exact extent of crosslinking of the polybutadiene bonds, e.g. by infrared spectroscopy, as the content of polybutadiene is too low to allow a sufficient resolution of the signals. However, a rough estimation, also based on NMR spectra, indicates a degree of crosslinking of around 60 – 80 %. The extent of crosslinking is in a similar range compared to the cold vulcanization process.

In order to investigate the occurring side reactions during the radical crosslinking procedures, GPC-viscosity measurements of the soluble parts were performed (Figure 5 - 8). The measurements revealed the presence of a strong peak at about half of the molecular weight of the block terpolymer precursors. The appearance of this peak is independent of the crosslinking method (AIBN, AIBN+TRIS) as well as of the block terpolymer used. The molecular weight indicates that the chain scission must take place at the inner block segment, i.e. polybutadiene. This may be caused by a radical chain transfer with subsequent chain cleavage. It can be seen that the addition of TRIS cannot fully prevent the radical chain cleavage, as a peak corresponding to roughly half of the molecular weight of the precursor remains. However, since the fraction of soluble material is much lower in the case of the thiol-polyene procedures, the radical chain scission reactions are at least significantly reduced.

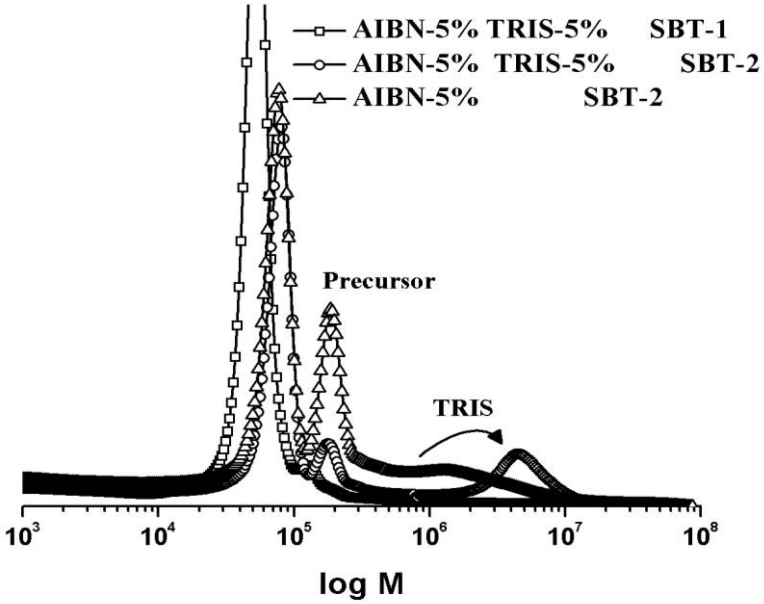

Figure 5 - 8. RI traces for the molecular weight distribution as obtained by GPC-viscosity measurements for the soluble fractions after soxhlet extraction of the crosslinked block terpolymer samples.

At the higher molecular weight side, two shoulders in the range of 10^6 -10^7 g/mol can be observed for the crosslinking of the SBT-2 samples, whereas no shoulder is visible for the soluble fraction of the crosslinked SBT-1 sample. The soxhlet extraction obviously has an estimated molecular weight cut-off of 10^7 g/mol. The absence of high molecular weight shoulders in the latter case is due to the facilitated crosslinking at higher PB content, leading to the rapid formation of high molecular weight gel networks. Comparing the peak values of the two shoulders for the two SBT-2 fractions leads to the conclusion that the crosslinking with the thiol-polyene system leads to higher crosslinked aggregates, whereas the reaction with pure AIBN results in a considerable amount of only lightly crosslinked oligomers of the block terpolymers. The high transfer efficiency of the thiols are responsible for this behaviour as the addition of those introduces trifunctional crosslinking points and thus a more continuous crosslinking. Oligomeric structures are undesired as they can only be considered as fragments of the targeted nanostructures.

In conclusion, two different kinds of crosslinking methods for polybutadiene microdomains were studied. It was clearly proven that the crosslinking can be accomplished via two ways, the cold vulcanization and the radical crosslinking process in combination with the thiol-polyene process. For performing the cold vulcanization the conditions need to be adjusted carefully as the morphologies react very sensitive to changes in the solvent quality. The addition of the crosslinking agent, sulphur monochloride has a remarkable und unexpectedly strong influence on the microphase-segregated morphology. The radical crosslinking process and the thiol-polyene process can be performed more easily and the resulting material has the benefit of possessing bonds which are stable to acidic conditions. Therefore, this material is the ideal precursor for the acidic hydrolysis towards amphiphilic water-soluble Janus sheets. On the contrary, the radical crosslinking suffers from some side reaction and generally leads to lower gel-fractions. Both methods provide suitably crosslinked material for the preparation of sheet- or disc-like Janus structures.

Characterization of Resulting Soluble Nanostructures

Soluble internally structured flat nanoparticles can be obtained after sonication of the crosslinked block terpolymer bulk nanostructures (see Scheme 5 - 1). As mentioned earlier, these kind of nanoscopic Janus discs are widely unknown in literature, although theoretical calculations exist, dealing with their remarkable surface activities. Clearly, this demonstrates the limited synthetic accessibility. Detailed investigations concerning size and shape evolution, angular dependent scattering behaviour, supramolecular aggregation and behaviour at oil/water interfaces were recently published by us elsewhere.[38] Therefore, herein a result regarding the influence of the crosslinking method will be highlighted.

Figure 5 - 9 compares the influence of the crosslinking method, cold vulcanization or thiol-polyene process, by means of the particle sizes obtained by dynamic light scattering. The two differently crosslinked SBT-2 samples were sonicated under exactly the same conditions for five minutes at 30% of the maximum amplitude, leading to the observation of nanometer-sized particles.

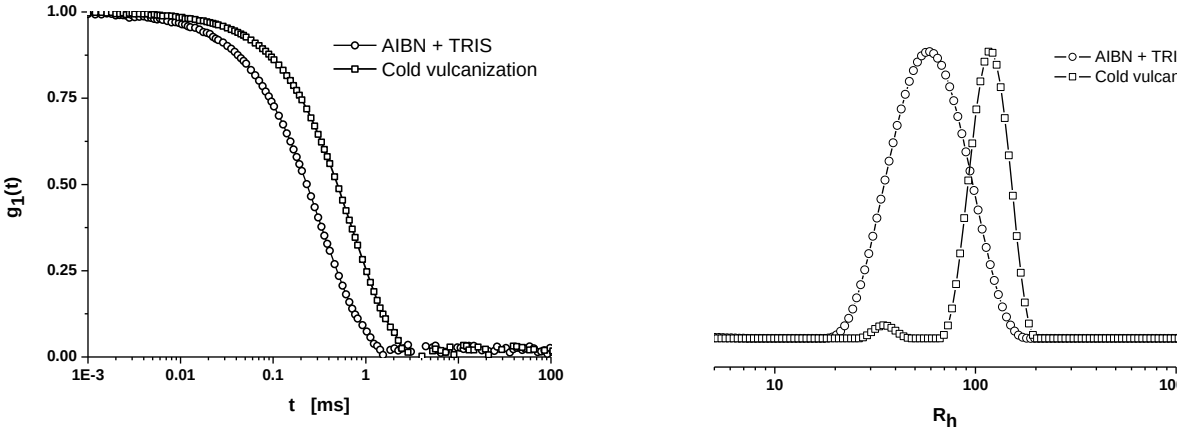

Figure 5 - 9. Normalized field auto-correlation functions (left) and their corresponding CONTIN plots (right) for differently crosslinked SBT-2 bulk structures. The crosslinking method is indicated within the Figure. After crosslinking, the samples were sonicated for 5 min at 30% amplitude. The small peak in the Contin plot of the sample obtained by cold vulcanization may arise from small fragments, which were cut off during the homogenization.

It can be seen that the sample, crosslinked with the cold vulcanization, leads to significantly larger particle sizes. The average hydrodynamic radius is larger by a factor of two as compared to the sample, which had been crosslinked via the thiol-polyene method. Consequently, the crosslinking with S_2Cl_2 leads to a more continuous crosslinking throughout the material and may have some advantages if very large structures are required for specific applications. On the contrary, the crosslinking with the thiol-polyene method can experimentally be achieved more easily as it only involves co-casting of the component and simple heating of the microphase-segregated bulk structure. Hence, depending on the requirements, the appropriate crosslinking method needs to be selected.

The ultimate success of this strategy to prepare flat Janus-type nanostructures can be shown by scanning force microscopy. Figure 5 - 10 shows a representative SFM image with two circular objects. The objects possess disc-like character as can be seen in the high aspect ratios deduced from the section analysis and the 3D surface plot of the larger structure. The particles are indeed completely flat in their centre.

The results convincingly demonstrate, how the unique bulk morphologies of polybutadiene containing ABC block terpolymers can be transformed into novel internally structured nanoparticles.

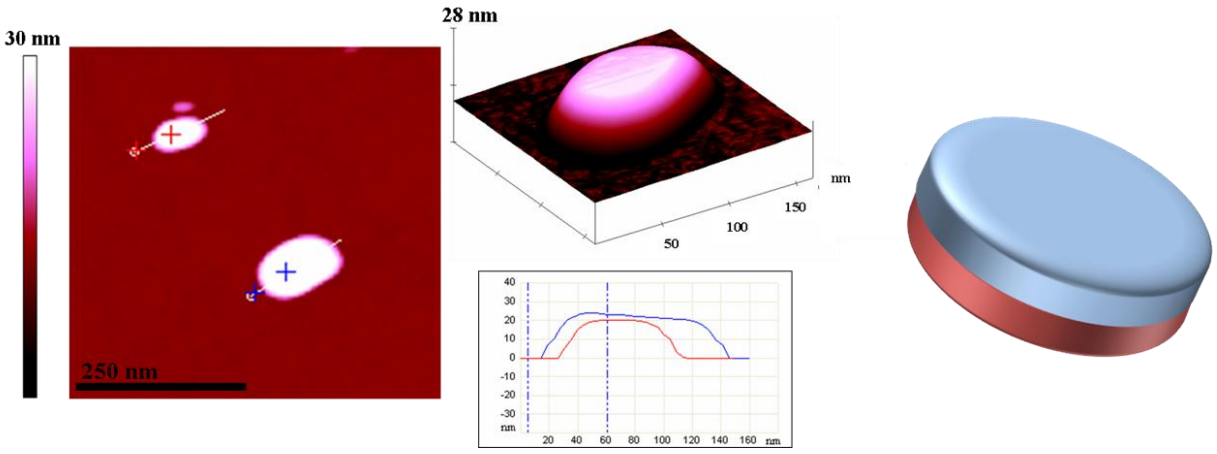

Figure 5 - 10. Scanning force microscopy height image (left) obtained from a dip-coated sample (0.1 mg/L) of Janus discs, based on SBT-2 (crosslinked with S_2Cl_2 and sonicated for 10 min at 30% amplitude). Corresponding section analyses and 3D surface plot (larger particle) are shown in the center. Schematic representation of a Janus disc is shown on the right.

Conclusions

The controlled crosslinking of polybutadiene microdomains of polystyrene-*block*-polybutadiene-*block*-poly(*tert*-butyl methacrylate) block terpolymers has been explored. Despite the low fractions of polybutadiene of only 5 – 10 wt%, lamellar (ll) morphologies are formed, contrary to polystyrene-*block*-polybutadiene-*block*-poly(methyl methacrylate) block terpolymers.

The microphase-segregated morphologies of the block terpolymers react very sensitively towards additives, which are necessary for the crosslinking. This is due to the accompanying instability related to the low PB content. Careful optimization of the conditions is necessary in order to successfully crosslink the desired morphologies. The morphologies developed upon addition of chemicals were thoroughly investigated at all stages of the crosslinking. The addition of swelling solvents and crosslinking agent partially caused severe, unexpected and undesired changes in the bulk morphologies, thus requiring careful adjustment of the crosslinker concentration and the type of swelling solvent. Generally, the cold vulcanization leads to a higher extent of crosslinking and a larger fraction of desired crosslinked material. The free radical crosslinking can be performed more easily and can be improved by the thiol-polyene process, which leads to a higher fraction of crosslinked material. GPC-viscosity measurements indicate that radical chain cleavage at the inner block takes place as side-reaction. This side-reaction prevents a further increase of the fraction of crosslinked material with increasing concentration of radical crosslinker, however, it can be suppressed to some extent by the addition of thiols for the thiol-polyene process.

Both methods, cold vulcanization and radical crosslinking, provide facile and highly effective routes for the crosslinking of polybutadiene containing block terpolymer microphase-segregated structures. Moreover, the shown procedures may serve as guidelines for future investigations for the preparation of functional nanoparticles via crosslinking microphase-segregated block terpolymers in the bulk.

Finally, some properties of the obtained Janus discs are highlighted to demonstrate the effectiveness and usefulness of crosslinking block terpolymer bulk structures towards the preparation of internally structured nanostructures. The size of the resultant nanoparticles was shown to depend on the crosslinking method, i.e. larger structures can be obtained by the cold vulcanization, representing a more continuous crosslinking. Additionally, the flat shape of the novel Janus discs can be confirmed by scanning force microscopy.

Acknowledgments

The authors would like to acknowledge Thorsten Goldacker for the synthesis of SBT-2. This work was supported by the ESF SONS-AMPHI, BIOSONS Programs and the Marie Curie RTN Polyamphi. Andreas Walther thanks the Bavarian Graduate Support Program for a scholarship.

References

1. Aranda-Espinoza, H.; Bermudez, H.; Bates, F. S.; Discher, D. E. *Phys. Rev. Lett.* **2001,** 87, 208301.
2. Semenov, A. N. *Sov. Phys. JETP* **1985,** 61, 733.
3. Nonobe, T.; Tsuge, S.; Ohtani, H.; Kitayama, T.; Hatada, K. *Macromolecules* **1997,** 30, 4891.
4. Matsen, M. W.; Bates, F. S. *J. Chem. Phys.* **1997,** 106, 2436.
5. Matsen, M. W.; Bates, F. S. *Macromolecules* **1996,** 13, 1091.
6. Leibler, L. *Macromolecules* **1980,** 18, 1602.
7. Hajduk, D. A.; Takenouchi, H.; Hillmyer, M. A.; Bates, F. S.; Vigild, M. E.; Almdal, K. *Macromolecules* **1997,** 30, 3788.
8. Vigild, M. E.; Almdal, K.; Mortensen, K.; Hamley, I. W.; Fairclough, J. P. A.; Ryan, A. J. *Macromolecules* **1998,** 31, 5702.
9. Hajduk, D. A.; Ho, R. M.; Hillmyer, M. A.; Bates, F. S.; Almdal, K. *Macromolecules* **1998,** 102, 1356.
10. Spontak, R. J.; Zielinski, J. M. *Macromolecules* **1992,** 25, 663.
11. Spontak, R. J.; Kane, L. *Macromolecules* **1994,** 27, 1267.
12. Nakazawa, K.; Ohta, T. *Macromolecules* **1993,** 26, 5503.
13. Mogi, Y.; Mori, K.; Kotsuji, H.; Matsushita, Y.; Noda, I.; Han, C. C. *Macromolecules* **1993,** 26, 5169.
14. Breiner, U.; Krappe, U.; Abetz, V.; Stadler, R. *Macromolecular Chemistry and Physics* **1997,** 198, 1051.
15. Yang, S.; Chen, J.-S.; Koerner, H.; Breiner, T.; Ober, C. K.; Poliks, M. D. *Chem. Mater.* **1998,** 10, 1475.
16. Mannebach, G.; Bieringer, R.; Morschhaeuser, R.; Stadler, R. *Macromol. Symp.* **1998,** 132, 245.
17. Abetz, V.; Goldacker, T. *Macromol. Rapid Commun.* **2000,** 21, 16.
18. Ishizu, K.; Fukutomi, T. *J. Polym. Sci., Polym. Letters Ed.* **1988,** 26, 281.
19. Ishizu, K.; Onen, A. *J. Polym. Sci. Polym. Chem. Ed.* **1989,** 27, 3721.
20. Decker, C.; Viet, T. N. T. *J. Appl. Polym. Sci.* **1999,** 77, 1902.
21. Decker, C.; Viet, T. N. T. *Polymer* **2000,** 41, 3905.
22. Decker, C.; Nguyen Thi Viet, T. *Macromol. Chem. Phys.* **1999,** 200, 358.
23. Decker, C.; Nguyen Thi Viet, T. *Macromol. Chem. Phys.* **1999,** 200, 1965.
24. Decker, C. *Prog. Polym. Sci.* **1996,** 21, 593.
25. Liu, G. J.; Yan Xiaohu, L. Z.; Zhou, J. Y.; Duncan, S. *J. Am. Chem. Soc.* **2003,** 125, 14039.
26. Erhardt, R.; Böker, A.; Zettl, H.; Kaya, H.; Pyckhout-Hintzen, W.; Krausch, G.; Abetz, V.; Müller, A. H. E. *Macromolecules* **2001,** 34, 1069.

27. Erhardt, R.; Zhang, M.; Böker, A.; Zettl, H.; Abetz, C.; Frederik, P.; Krausch, G.; Abetz, V.; Müller, A. H. E. *J. Am. Chem. Soc.* **2003,** 125, 3260.
28. Liu, Y.; Abetz, V.; Müller, A. H. E. *Macromolecules* **2003,** 36, 7894.
29. Goldacker, T.; Abetz, V.; Stadler, R.; Erukhimovich, I.; Leibler, L. *Nature* **1999,** 398, 137.
30. Auschra, C.; Stadler, R. *Polym. Bull.* **1993,** 30, 257.
31. Benoit, D.; Groubisic, Z.; Rempp, P.; Decker, D.; Zilliox, J. G. *J. Chem. Phys.* **1966,** 63, 1507.
32. Goldacker, T. PhD Thesis, Universität Bayreuth, Bayreuth, 1999.
33. Bieringer, R.; Abetz, V. *Polymer* **2000,** 41, 7981.
34. Pullman, B.; Pullman, A., *Quantum Biochemistry*. Interscience: New York, **1963**.
35. Qi, S.; Wang, Z. G. *Phys. Rev. E* **1997,** 55, 1682.
36. Laradji, M.; Shi, A.-C.; Noolandi, J.; Desai, R. C. *Phys. Rev. Lett.* **1997,** 78, 2577.
37. Laradji, M.; Shi, A.-C.; Noolandi, J.; Desai, R. C. *Macromolecules* **1997,** 73, 86.
38. Walther, A.; André, X.; Drechsler, M.; Abetz, V.; Müller, A. H. E. *J. Am. Chem. Soc.* **2007,** 129, 6187.

6. Bis-Hydrophilic Triblock Terpolymers via RAFT Polymerization: Towards Dynamic Micelles with Tunable Corona Properties

Andreas Walther,[1] Pierre-Eric Millard,[1] Anja S. Goldmann,[1] Tara M. Lovestead,[2] Felix Schacher,[1] Christopher Barner-Kowollik,[2,3] Axel H. E. Müller[1]

[1]Makromolekulare Chemie II and Bayreuther Zentrum für Kolloide und Grenzflächen, Universität Bayreuth, D-95440 Bayreuth, Germany,

Andreas.Walther@uni-bayreuth.de; *Axel.Mueller@uni-bayreuth.de*

[2]Centre for Advanced Macromolecular Design, School of Chemical Sciences and Engineering, The University of New South Wales, NSW 2052, Australia

[3]current address: Preparative Macromolecular Chemistry, Institut für Technische Chemie und Polymerchemie, Universität Karlsruhe, Engesserstr. 18, 76128 Karlsruhe, Germany,

christopher.barner-kowollik@polymer.uni-karlsruhe.de

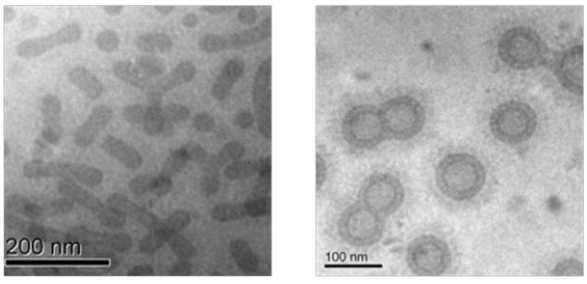

Published in: Macromolecules, **2008**, DOI: 10.1021/ma801215q

Abstract

We present the synthesis of well-defined bis-hydrophilic block terpolymers with two outer hydrophilic blocks and an inner hydrophobic block together with studies concerning their colloidal aggregates formed in water. The investigations aim at the preparation of dynamic micelles with tunable corona properties. Highly functionalized poly(ethylene oxide) macro-chain transfer agents (PEO-CTAs) of two molecular weights (2 and 5 kDa) are used as mediating agents in Radical Addition Fragmentation Chain Transfer (RAFT) polymerization: The synthesis is accomplished by first polymerizing n-butyl acrylate as hydrophobic block and then chain extending the diblock copolymers further with various (meth)acrylamide derivatives, acrylamide (AAm), N-isopropylacrylamide (NIPAAm), N,N-diethylacrylamide (DEAAm,) and N-(2-hydroxypropyl)-methacrylamide (HPMA). Due to the high degree of functionalization of the PEO-CTA, the blocking efficiency is near quantitative and the diblock copolymers can be obtained easily in a wide range of compositions and with an excellent control of the molecular weights and polydispersities (< 1.15). Similarly, the chain extensions with the different (meth)acrylamide proceeds with very high blocking efficiencies to obtain well-defined block terpolymers. The hydrophilic-to-hydrophobic balance as well as the chain lengths of the hydrophilic blocks can be adjusted as desired. The second part of this study describes the aqueous solution characteristics of the micellar aggregates of the block terpolymers. A significant effect of the preparation pathway (direct dissolution or dialysis from a common solvent) on the type of formed aggregates is found, indicating a strong influence of the dissolution kinetics. The self-assembled aggregates are of dynamic character as they can undergo fusion and fission processes, induced both by temperature and time. Large-scale rearrangement of the architectures are possible as ensured by the low glass transition temperature of the hydrophobic block, poly(n-butyl acrylate). Depending on the hydrophilic-to-hydrophobic balance and the pair of hydrophilic end blocks employed, spherical micelles, worm-like micelles and vesicles can be found. The corona structure of the micelles can be tuned by changing the length and the type of hydrophilic polymers used.

Keywords: Bis-hydrophilic block terpolymers, RAFT polymerization, dynamic micelles, multicompartment micelle, LCST.

Introduction

Block copolymers are able to self-assemble into discrete and well-defined colloidal aggregates in the mesoscopic size range. The significant interest in these structures originates from their potential applications in a variety of fields, such as in nanotechnology and biomedicine. Great effort has been directed at the exploration of the aggregate structures of diblock copolymers. In particular with the introduction of advanced polymerization techniques such as controlled radical polymerization methods, it was possible to substantially broaden the accessible structures. At the same time, the concept of "smart" nanoparticles was introduced and led to the discovery of tunable structures as in the case of so-called "schizophrenic micelles".[1-7] "Smart" nanoparticles undergo structural changes while sensing environmental stimuli, such as changes in temperature, pH or ionic strength.[8-21] With these properties, clearly, applications in the biomedical field have come into the focus and represent some promising approaches for tackling problems in controlled delivery and controlled release of active compounds.[11-13, 22-26]

In very recent time, efforts have been undertaken to obtain a further subdivision of the micellar structures as in the case of Janus particles[27, 28] or other multicompartment micelles.[29-34] These studies are not only triggered by scientific curiosity but also by the possibility of reaching novel structures with advanced properties. For instance, multicompartment micelles can provide interesting possibilities in terms of multicomponent storage.[35-39] An intrinsic prerequisite for the preparation of multicompartment micelles is the utilization of three different blocks for the creation of the micellar aggregate. Whereas anionic polymerization still has its reputation in producing most well-defined block terpolymers or miktoarm star terpolymers, the controlled radical polymerization techniques have emerged as a second mean for the preparation of sophisticated sub-divided colloidal structures. The higher tolerance towards functional groups is the particular benefit of the latter techniques.

Interestingly, in the field of bis-hydrophilic block terpolymers, a dominant interest was so far placed on the preparation of ABC block terpolymers with a hydrophobic A block and two hydrophilic blocks connected to each other (B+C). Typically, these polymers lead to core-shell-corona micelles and were investigated by a variety of groups.[40-47] Surprisingly, the preparation of terpolymers with two outer hydrophilic blocks and one inner hydrophobic block has not yet been subjected to intense research.[15, 17] Some success has been reported by Eisenberg and Meier who prepared vesicles with asymmetric walls based on specifically tailored block terpolymers.[48-50] The use of these vesicles as nanocontainers with different internal and external wall was suggested, demonstrating the interest in these structures. Moreover, depending on the interaction of the two outer blocks, A and B, mixed and phase-segregated structures within the corona can be anticipated.[51] In the case of the structures with mixed coronas, a facile tunability of the corona is possible by changing the degrees of polymerization of the two end blocks. In addition, both blocks can be used for sensing the environment, which is not possible for core-shell-corona structures. Additional modification of the structures is possible via incorporating stimuli-sensitive blocks and the access to different particle architectures is feasible by changing the hydrophilic-to-hydrophobic balance. With these features a large diversity of different multicompartment particles can be imagined and tailored for specific applications. Some results were recently reported concerning the creation of similar desired structures using the co-assembly of two diblocks, either by forcing them into a complex-core coacervate micelle (C3M)

or simple undirected co-micellization.[52, 53] Depending on the corona-forming blocks, C3Ms can undergo phase-separation in the corona.[54] However, both approaches have some disadvantages. Firstly, C3Ms are only stablein medium of low salinity and moreover structures with high aspect ratios such as cylinders could not yet been achieved. For the co-micellization of two block copolymers having the same end block, the drawbacks are obvious. The co-micellization is only a statistical process and thus the micellar structure, in particular the corona composition, cannot be precisely controlled. Some theoretical considerations even suggest that two populations of homogeneous micelles, each just composed of one kind of the diblock copolymer mixture, can coexist.[55] Besides, studies so far only included core-forming blocks with high glass transition temperatures, which hinder structural rearrangements after the co-micellization and minimize the possibilities of structural rearrangements towards external stimuli.

Herein, we present the synthesis of novel bis-hydrophilic block terpolymers via RAFT polymerization[56-58] as well as results concerning the characterization of the solution behavior of the resulting polymers in water with respect to the dynamics of the core-forming block and the particle architecture. Poly(ethylene oxide) (PEO) and various poly(meth)acrylamide derivatives are used as hydrophilic blocks. Poly(meth)acrylamide derivatives exhibit different solution characteristics depending on the substitution pattern at the amide functions. Polyacrylamide (PAAm) without any hydrophobic substitutes is an extremely polar, highly water-soluble polymer, which does not show any lower critical solution temperature (LCST) behavior. It is known to undergo phase-separation with PEO, thus leading to Janus micelles.[54] Upon addition of hydrophobic substituents to the amide function, e.g. N-(isopropyl)acrylamide (NIPAAm) or N,N-(diethyl)acrylamide (DEAAm), the polymers PDEAAm and PNIPAAm exhibit an appealing stimuli-responsive LCST behavior with different LCSTs. Poly(*N*-(2-hydroxypropyl)methacrylamide) (PHPMA) is a non-immunogenic polymer and has an addressable hydroxyl function which allows the conjugation to drugs or units for cell recognition.[59-62] Poly(n-butyl acrylate)(PnBuA) serves as inner hydrophobic block ensuring high dynamics in the micellar core due to its low glass transition temperature (T_g ≈ - 46 °C). In terms of synthesis, the polymerization of (meth)acrylamides is a domain of Radical Addition Fragmentation Transfer (RAFT) polymerization. Therefore, RAFT polymerization was used as it also provides means to assess a library of different block terpolymers in a reasonable time frame. The synthetic strategy first involved the preparation of PEO based macro-chain transfer agents (macro-CTAs), which were subsequently used for the block copolymerization of n-butyl acrylate and different (meth)acrylamides. With this approach it is possible to obtain a series of very well-defined block terpolymers of different structures. It is shown that the hydrophilic-to-hydrophobic balance can be tuned over a large range and that the ratio of chain lengths of the two outer hydrophilic blocks can be adjusted. In a last section, we will highlight some micellar structures to demonstrate the feasibility of the concept and the arising possibilities.

Experimental Section

Materials. N,N-dimethylformamide (DMF, anhydrous), N,N-dimethylacetamide (DMAc, anhydrous), 1-Methyl-2-pyrrolidinone (NMP, anhydrous) and dimethylsulfoxide (DMSO, anhydrous) were purchased from Aldrich and used without further purification. Dichloromethane (DCM), diethyl ether, benzene and ethanol were obtained in p.a. grade and used as received. THF (p.a. grade) was cleaned by distillation from Na/K alloy. N,N-Azobisisobutyronitrile (AIBN), acrylamide (AAm) and N-isopropylacrylamide (NIPAAm) were ordered from Aldrich and recrystallized from ethanol. N,N-diethylacrylamide (DEAAm, ABCR chemicals), N-(2-hydroxypropyl)methacrylamide (HPMA, ABCR chemicals), monomethoxy poly(ethylene oxide) (M_n = 5000 – PDI = 1.04, M_n = 2000 – PDI = 1.04, Aldrich), 4-(dimethylamino)pyridine (DMAP, Aldrich), dicyclohexylcarbodiimide (DCC, Aldrich), phenylmagnesium bromide solution in diethyl ether 2.8 M (Acros), α-Bromophenylacetic acid (Aldrich, 98%) and carbon disulfide (Aldrich, reagent plus > 99.9%) were used as received. N-butyl acrylate (nBuA) was purchased from Aldrich in the highest purity available and purified by passing through a basic alumina column.

Polymer Characterization

SEC in THF. SEC in THF was conducted at an elution rate of 1 mL·min^{-1} using a Shodex RI-101 detector, a Waters 996 photodiode array detector (PDA), and PSS SDVgel columns (300 x 8 mm, 5µm): 10^5, 10^4, 10^3, and 10^2 Å. Polystyrene standards were used to calibrate the columns, and toluene was used as an internal standard.

SEC in NMP. Polymers were characterized by size exclusion chromatography (SEC) using a Waters 510 HPLC Pump, a Bischoff 8110 RI detector, a Waters 486 UV detector (λ = 270 nm), and a 0.05 M solution of LiBr in 2-*N*-methylpyrrolidone (NMP) as eluent. PSS GRAM columns (300 x 8 mm, 7µm): 10^3, 10^2 Å (PSS, Mainz, Germany) were thermostated at 70 °C. A 20µL of a 0.4 wt.-% polymer solution was injected at an elution rate of 1 mL·min^{-1}. Polystyrene standards were used to calibrate the columns, and methyl benzoate was used as an internal standard.

SEC in DMAc. For DMAc SEC measurements, dimethylacetamide/0.05% LiBr as the mobile phase (1 mL·min^{-1}), a column set consisted of a PL 5.0 µm bead size guard column and a set of 3x5 µm PL linear columns (10^3, 10^4, and 10^5 Å) (70 °C), a DRI detector, and linear polystyrene standards were used.

ESI-MS. Electrospray ionization mass spectrometry experiments were carried out using a Thermo Finnigan LCQ Deca quadrupol ion-trap mass spectrometer (Thermo Finnigan, San Jose, CA) in positive ion mode. The ESI-MS is equipped with an atmospheric pressure ionization source which operates in the nebulizer assisted electrospray mode. The instrument was calibrated with caffeine, MRFA, and Ultramark 1621 (all from Aldrich) in the mass range 195-1822 amu. All spectra were acquired over the mass to charge range (m/z) of 150 – 2000 Da with a spray voltage of 5kV, a capillary voltage of 39 V and a capillary temperature of 275 °C. Nitrogen was used as sheath gas (flow: 40 of maximum) while helium was used as auxiliary gas (flow: 5% of maximum). The solvent was a 6:4 v/v mixture of THF/methanol with polymer concentration ~ 0.4 mg·mL^{-1}. The instrumental resolution of the employed experimental set-up is 0.1 amu. The

theoretical isotopic patterns were generated using the Xcalibur™ program included with the Thermo Finnigan LCQ Deca ion trap mass spectrometer.

Liquid adsorption chromatography under critical conditions (LACCC). Liquid adsorption chromatography under critical conditions (LACCC) was conducted on a chromatographic system composed of a degasser ERC 3415α, a pump P4000 (TSP) and an autosampler AS3000 (TSP). Two detectors were used, a UV-detector UV6000LP (TSP) with two wavelengths (λ = 230 nm and 261 nm) and an evaporative light scattering detector (ELSD) EMD 960 (Polymer Laboratories) operating at 80 °C with a gas flow rate of 6.8 L/min. Two reversed phase column C18, 250x4.6 mm ID, with 5 µm average particle size were employed, one with 120 Å (YMC), and the other with 300 Å pore diameters (Macherey-Nagel). The solvents, acetonitrile (ACN) and water (H_2O), were HPLC grade and used freshly. The critical solvent composition for polyethylene glycol monomethyl ether (PEO-OH) determined for this system was ACN/H_2O 39.1/60.9 (v/v) at 23°C with a flow rate of 0.5 mL/min.

Samples were dissolved in the critical mix at a concentration of 0.2 wt %. Then 20 µL were injected. Modified PEO-OH appeared in adsorption mode due to the low polarity of the end group. To obtain a narrow and well defined peak, a gradient was used after the elution time of remaining PEO-OH. The composition sequence is detailed here. The critical composition was maintained for 16 min. Then, over 16 min, a linear gradient up to 60% of ACN was realized. This percentage was decreased directly to the critical composition over 1 min with also a linear gradient. Finally this proportion was kept for 60 min to equilibrate the system before a next measurement.

MALDI-ToF-MS. Matrix-Assisted Laser Desorption Time of Flight mass spectra were recorded on a Bruker Reflex III operated in linear mode using a nitrogen laser (337 nm) and an accelerating voltage of 20 kV. 2,5-Dihydroxybenzoic acid, 2,4,6-Trihydroxyacetophenone monohydrate, trans-2-[3-4-tert.-Butylphenyl-2methyl-2-propenyliden]-malononitrile, 3-Indoleacrylic acid, 2´-(4-hydroxyphenylazo)-benzoic acid or dithranol were used as matrix. Samples were prepared from DMAc or DMSO solution by mixing matrix (20 $mg \cdot mL^{-1}$) and sample (10 $mg \cdot mL^{-1}$) in a ratio 4:1 or by mixing matrix (20 $mg \cdot mL^{-1}$), sample (10 $mg \cdot mL^{-1}$) and salt (sodium trifluoracetate or potassium trifluoracetate, 10 $mg \cdot mL^{-1}$) in a ratio 20:5:1.

NMR. ^{1}H and ^{13}C NMR spectra were recorded on a Bruker AC-250 spectrometer in various solvents at room temperature. The 2D-HMBC spectrum of PEO-2k-CTA was acquired on a Bruker Avance 300.

Synthesis

α-Bromophenylacetate terminated Poly(ethylene oxide) (PEO-Br). 10 g PEO (M_n = 5000, 2 mmol) were dissolved in 50 mL DCM. Afterwards, DMAP (49 mg, 0.4 mmol), DCC (2.07 g, 10 mmol) and α-bromophenylacetic acid (1.29 g, 6 mmol) were added and the solution was stirred for 24h at room temperature under nitrogen atmosphere. After filtration, the product was precipitated into cold diethyl ether. Further purification was accomplished by several cycles of product redissolution in warm ethanol, precipitation at low temperatures and subsequent

centrifugation. Finally, the functionalized PEO derivative was dialyzed against benzene and freeze-dried with a final yield of around 80 – 90 %. NMR characterization is provided in the Supporting Information and elsewhere.[63]

Synthesis of PEO macro-chain transfer agents (PEO-CTA). 10 g of freeze-dried PEO-Br were heated to 60 °C in high vacuum overnight. Subsequently, 50 mL of anhydrous THF was added under a nitrogen flow and a clear solution was obtained by slight heating. In a second reaction flask, carbon disulfide (0.26 mL, 4.4 mmol) was added with a syringe to a degassed THF solution (10 mL) of phenylmagnesium bromide (1.43 mL of 2.8 M solution in diethyl ether, 4 mmol). This flask was allowed to stand at room temperature for 30 min and then heated to 50 °C for another 30 min. Afterwards, the dark-red solution was transferred with a syringe to an addition funnel connected to the flask containing the PEO-Br solution in degassed THF. The solution was added drop-wise at room temperature and the reaction was allowed to proceed for 3 h. After precipitation into cold hexane, the product, PEO-CTA, was purified in the same way as PEO-Br with a final yield of 80 – 90 %. NMR characterization is provided in the Supporting Information and elsewhere.[63]

PEO-*block*-PnBuA diblock copolymers. A representative example is as follows. A mixture of PEO-5k-CTA (0.3 g, 0.06 mmol), nBuA (5.76 g, 45 mmol) and DMF (3.29 g, 45 mmol) in a screw-cap flask, sealed with a rubber septum, was degassed by bubbling with nitrogen. In a second flask, a stock solution of AIBN (19.7 mg, 0.12 mmol) in DMF (10 mL) was degassed similarly. Afterwards, 1 mL of this stock solution was transferred to the reaction mixture with a syringe and the polymerization flask was placed into an oil bath at 60 °C. Samples were withdrawn to monitor the conversion and to obtain PEO-*block*-PnBuA diblock copolymers of desired compositions. The polymer was isolated from the samples via dilution with ethanol (rapid cooling) and subsequently dialyzed against benzene to remove residual solvent and monomer. Freeze-drying of the samples yielded the final pure diblock copolymers in near quantitative yields. NMR characterization is provided in the Supporting Information.

PEO-*block*-PnBuA-*block*-PNIPAAm, PEO-*block*-PnBuA-*block*-PDEAAm and PEO-*block*-PnBuA-*block*-PHPMA block terpolymers. All block terpolymers having PNIPAAm, PDEAAm or PHPMA end blocks can be synthesized in analogous fashion. In case of DEAAm (liquid monomer), only 50% of solvent of the following representative experiment was added. A representative example for PEO-*block*-PnBuA-*block*-PNIPAAm is as following. 1 g of PEO-*block*-PnBuA ($M_{n,calc}$ = 18700, 0.054 mmol) was dissolved in DMF (6.46 g, 88 mmol). After complete dissolution, NIPAAm (5 g, 44 mmol) was added and the mixture was degassed by bubbling with nitrogen. Subsequently, 0.5 mL of a degassed stock solution of AIBN (63.7 mg, 0.388 mmol) in 10 mL DMSO was introduced into the reaction mixture and the flask was placed into an oil bath thermostated at 60 °C. Samples were withdrawn to monitor the conversion and to obtain block terpolymers of desired compositions. The polymer was isolated from the samples via dilution with dioxane or DMSO (rapid cooling) and subsequently dialyzed against dioxane or water (for PHPMA based triblock copolymers) to remove residual solvent and monomer. Freeze-drying of the samples yielded the final pure triblock copolymers in near quantitative yields. NMR characterization is provided in the Supporting Information.

PEO-*block*-PnBuA-*block*-PAAm. All polymerizations were conducted in a mixed solvent system of DMF and DMSO. DMF is used to initially dissolve the PEO-*block*-PnBuA diblock copolymers, which do not readily dissolve in DMSO. DMSO is needed as solvent for the polymerization due to the solubility characteristics of PAAm. In a typical experiment, 1 g of PEO-*block*-PnBuA ($M_{n,calc}$ = 37000, 0.0272 mmol) was dissolved in 2 g DMF. Subsequently, 3 mL of DMSO and 1.1 g AAm (15.5 mmol) were added to this flask and the solution was deoxygenated by bubbling with nitrogen. Subsequently, 0.5 mL of a degassed stock solution of AIBN (8.9 mg, 0.054 mmol) in 5 mL DMSO was introduced into the reaction mixture and the flask was placed into an oil bath thermostated at 60 °C. Samples were withdrawn to monitor the conversion and to obtain block terpolymers of desired compositions. The polymer was isolated from the samples via dilution with DMSO (rapid cooling) and subsequently dialyzed against water to remove residual solvent and monomer. Freeze-drying of the samples yielded the final pure block terpolymers in near quantitative yields. NMR characterization is provided in the Supporting Information.

Solution Characterization of Aggregates

Formation of Aggregates. Micelles were prepared by dissolution of the polymers (c = 5 mg·mL^{-1}) in water at room temperature and prolonged stirring. In case of dialysis, the polymer solution in dioxane or DMSO (5 mg·mL^{-1}) was exchanged step-wise to water in a dialysis cell using dialysis membranes with a MWCO of 5000 – 10000 kDa.

For ***cryo*genic transmission electron microscopy (*cryo*-TEM)** studies, a drop of the sample dissolved in water was put on a lacey transmission electron microscopy (TEM) grid, where most of the liquid was removed with blotting paper, leaving a thin film stretched over the lace. The specimens were instantly vitrified by rapid immersion into liquid ethane and cooled to approximately 90 K by liquid nitrogen in a temperature controlled freezing unit (Zeiss *Cryo*box, Zeiss NTS GmbH, Oberkochen, Germany). The temperature was monitored and kept constant in the chamber during all of the sample preparation steps. After freezing the specimens, the specimen was inserted into a *cryo*-transfer holder (CT3500, Gatan, München, Germany) and transferred to a Zeiss EM922 EF-TEM instrument. Examinations were carried out at temperatures around 90 K. The transmission electron microscope was operated at an acceleration voltage of 200 kV. Zero-loss filtered images (ΔE = 0 eV) were taken under reduced dose conditions. All images were registered digitally by a bottom mounted CCD camera system (Ultrascan 1000, Gatan) combined and processed with a digital imaging processing system (Gatan Digital Micrograph 3.9 for GMS 1.4).

Dynamic Light Scattering (DLS). Dynamic light scattering was performed on an ALV DLS/SLS-SP 5022F compact goniometer system with an ALV 5000/E cross-correlator and a He–Ne laser (λ_0 = 632.8 nm). An automatic thermostating control system was used for the temperature sweeps. The heating steps were chosen to either 1 or 2 K. Prior to each measurement, the sample was allowed to equilibrate for 10 min. The data evaluation of the dynamic light scattering measurements was performed with the CONTIN algorithm.

Results and Discussion

Synthesis and Characterization of PEO-CTA

The most important prerequisite for the successful synthesis of block copolymers via RAFT using a macro-chain transfer agent (CTA) is the near quantitative coupling of the first block to the CTA.[64] Otherwise, a significant fraction of the first unmodified block contaminates the final block copolymers. The synthetic access towards poly(ethylene oxide) based CTAs is outlined in **Error! Reference source not found.** and was adapted similarly from Hawker and coworkers.[63] PEO-CTAs of this kind have not yet widely been used for the RAFT polymerization.[65] Herein, two poly(ethylene oxides) of different molecular weights (M_n = 2000 g·mol^{-1}= PEO-2k and M_n = 5000 g·mol^{-1} = PEO-5k) were used.

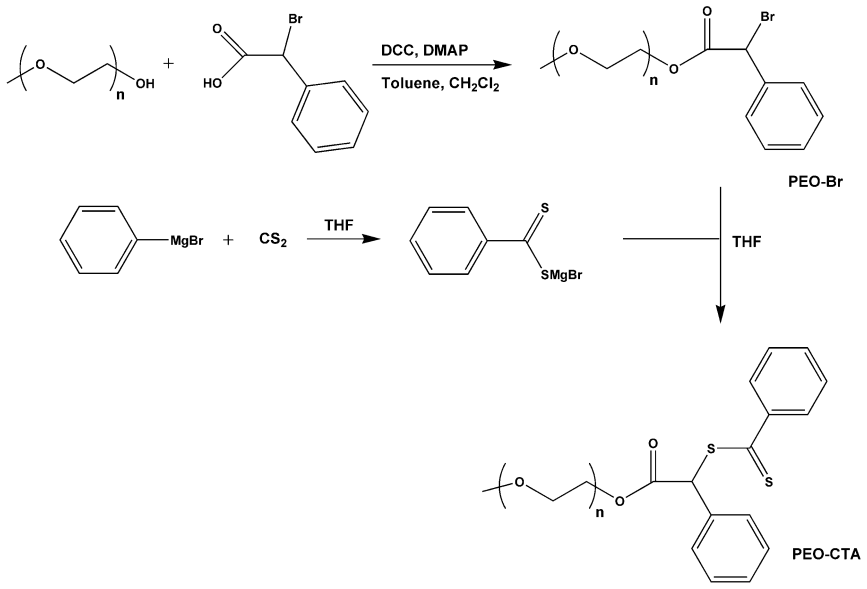

Scheme 6 - 1. Synthetic access to PEO based macro-chain transfer agents (PEO-CTAs).

Due to the necessity of ensuring sufficient conversion of the hydroxyl group of the PEO-OH, various techniques were used for the analysis. The product formation was monitored using NMR, ESI-MS (electrospray ionization mass spectrometry) and LACCC (liquid adsorption chromatography at critical conditions). The structure of PEO-2k-Br and the connection of the CTA moiety to the PEO chain within PEO-2k-CTA can be confirmed with a straight-forward assignment of the peaks in the ^{1}H, ^{13}C and a 2D-HMBC spectra (Supporting Information). A comparison of the signals of PEO and the CTA group indicates a near quantitative formation of the desired product. However, the estimation of the extent of end group functionalization based on ^{1}H-NMR loses reliability for higher degrees of polymerization (DP) of PEO, i.e. for PEO-5k-CTA having a DP of 114. The successful formation of the product and the intermediate was furthermore confirmed by ESI-MS, as shown in **Error! Reference source not found.**.[66] The isotopic patterns found correspond well to the simulated once of the target compounds. Some minor peaks can found for the PEO-2k-Br and PEO-2k-CTA. In case of PEO-2k-CTA, one minor peak pattern can be assigned to a K-species, induced by the ionization of the compound with potassium, or to PEO-2k-OH (1793-1796 amu). The other peaks may be caused by minor synthetic byproducts with good ionization capabilities, or by degradation processes during the

ESI process or sample preparation,[67] as they cannot be assigned with any charged species of neither PEO-OH nor PEO-Br.

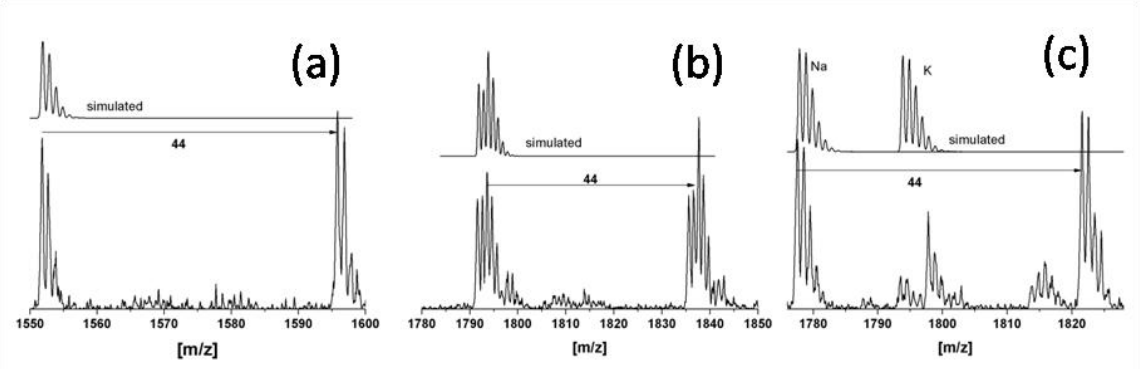

Figure 6 - 1. ESI-MS of PEO-2k-OH (a), PEO-2k-Br (b) and PEO-2k-CTA (c). Simulated spectra of the target compounds are shown for comparison (Na-species for (b) and (c), K-species for (c)) .

After the qualitative confirmation of the product structure by means of NMR and ESI-MS, LACCC was used to quantitatively analyze the end group modification starting from PEO-OH. LACCC is one of the only techniques that is exclusively sensitive to modifications of the end group of a polymer molecule when keeping the side groups or repeating units unreacted. For these conditions, the adsorption of the monomer units (HPLC mode) and the separation by the hydrodynamic volume (SEC mode) are exactly balanced and any change in the elution volume solely arises from chemical changes of the end group. LACCC can be applied for a wide range of molecular weights and is the technique of choice for the quantitative assessment of the extent of functionalization of the end groups. **Error! Reference source not found.** displays the LACCC traces for all steps of the functionalization and both molecular weights of the PEO. For both chain lengths of PEO, the modification with the α-bromophenylacetic acid proceeds quantitatively as can be seen from the full shift of the traces for PEO-OH (squares) to PEO-Br (circles). After careful optimization of the reaction from PEO-Br to PEO-CTA (triangles), this reaction is also almost fully quantitative. A slight cleavage of the initially formed ester function can be observed, leading to the reappearance of tiny peaks at the elution volume of PEO-OH. A small peak corresponding to the released PEO-OH can also be found in the ESI-MS data of PEO-2k-CTA (1793-1796 amu). This cleavage process was a major side reaction which needed to be suppressed during the optimization of the reaction conditions. It was accomplished by reducing the reaction time and temperature to 3 h at room temperature under our conditions. Refluxing for prolonged time was not necessary; on the contrary it led to an amplification of the cleavage process. Further significant side-products cannot be observed, which also confirms the additional peaks in the ESI-MS data to be mostly irrelevant for the following polymerizations.

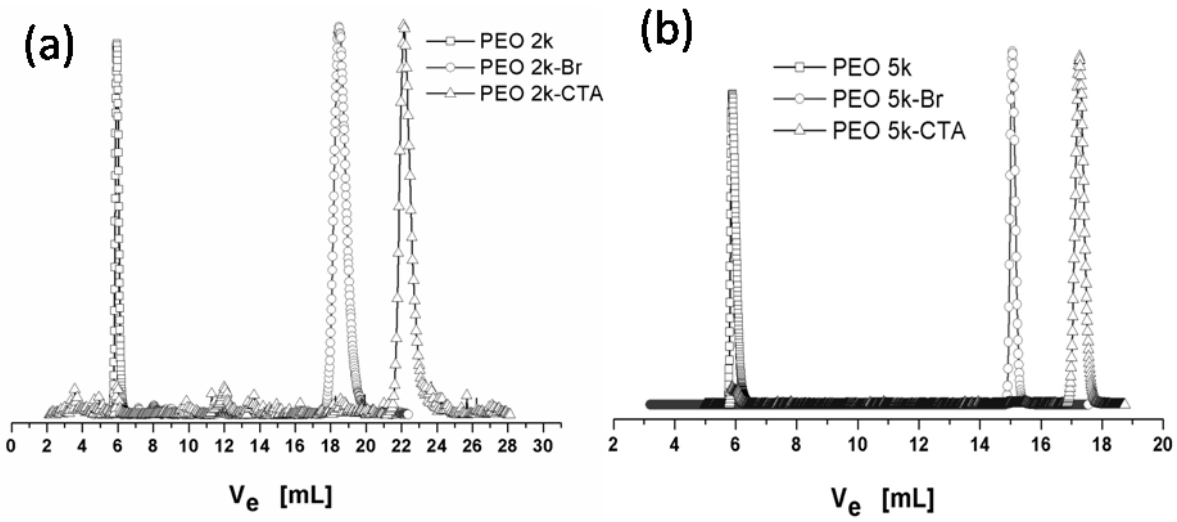

Figure 6 - 2. LACCC traces of various end group-modified PEOs as indicated in the graphs. A solvent gradient was applied after a certain time in order to force the elution of PEO-Br and PEO-CTA and to minimize the measurement time.

In conclusion, several analytical methods have been used to confirm the near quantitative preparation of PEO based macro-CTAs of different molecular weights. The developed reaction conditions allow the fast and straight-forward preparation of pure PEO-CTAs.

Synthesis and Characterization of PEO-*block*-PnBuA Diblock Copolymers

N-butyl acrylate (n-BuA) was chosen for the polymerization of the second block because of its low glass transition temperature. The low glass transition temperature facilitates the dynamic behavior of micelles in water. A hydrophobic block with a high glass transition temperature, e.g. poly(methyl methacrylate), polystyrene or poly(vinylpyridine), would lead to so-called frozen micelles and would limit a responsive behavior.

The polymerization kinetics for n-BuA using both PEO-CTAs are shown in **Error! Reference source not found.**. Note that all plots are composed of at least two reactions, demonstrating a very high reproducibility of the reactions. For both molecular weights of PEO-CTA, linear time-conversion plots, being indicative for a constant radical concentration, and an almost linear increase of the molecular weight with conversion can be observed, indicating a well-controlled RAFT process taking place. The deviation from exact linearity of the evolution of molecular weights in dependence of the conversion can be understood considering the different hydrodynamic dimensions as a function of the composition and the non-absolute calibration of the SEC system. The polydispersity indices remain very low (PDI < 1.1) within the investigated conversion range. The SEC elution traces show an onset of interchain coupling for conversions higher than 20 %. These expected,[68] but nevertheless unwanted termination reactions show the necessity of stopping the reactions at moderately low conversion of 20 – 25 %. Only under these circumstances, block copolymers are obtained which still carry the RAFT end group to a major extent and allow the sufficient block extension towards block terpolymers.

.

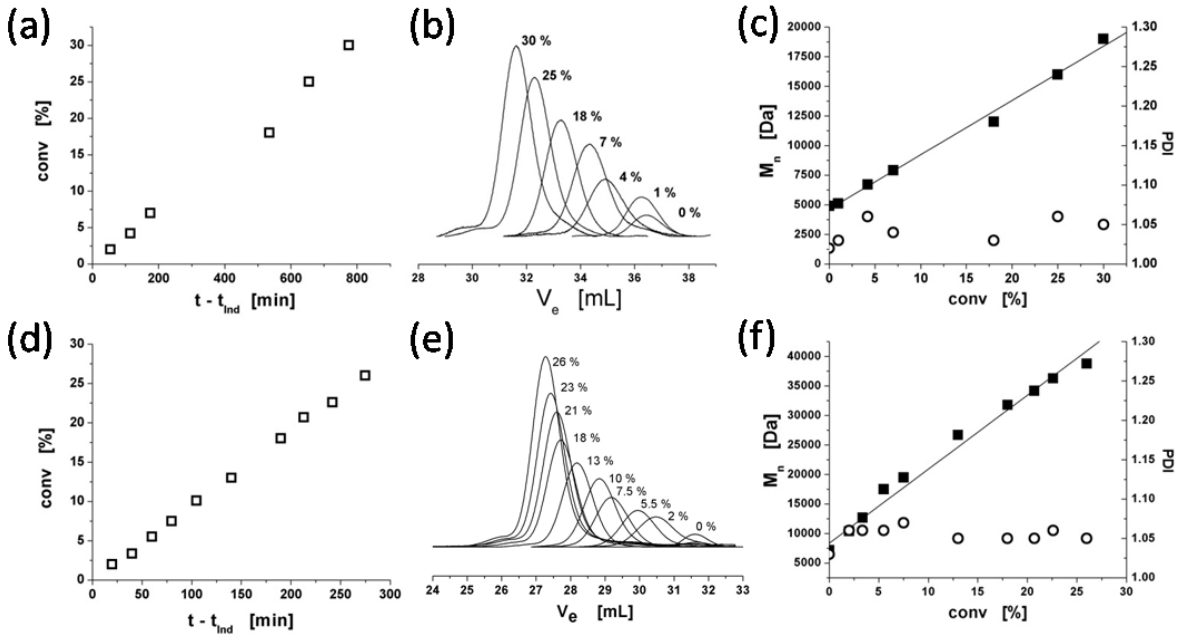

Figure 6 - 3. Results for the polymerization of n-BuA using PEO-2k-CTA (top, a - c) and PEO-5k-CTA (bottom, d – f). Time conversion plots (a & d), SEC elution traces (b & e) and evolution of molecular weights and polydispersity indices as a function of the conversion. The induction period[69] (30 min) was subtracted for the time conversion plots to allow a better display of the data points.

Strikingly, since great efforts were made to obtain quantitatively functionalized PEO-CTAs, almost no residual precursor can be found contaminating the diblock copolymers. The blocking efficiency is very high and a separation of residual homopolymer from the diblock copolymer is not necessary as it was in some other studies.[65] Table 6 - 1 summarizes the various polymers synthesized following the considerations mentioned above.

Table 6 - 1. Overview of PEO-*block*-PnBuA Diblock Copolymers.

Diblock Copolymers[a]	$M_{n,\,SEC}$[b] (PDI)	$M_{n,\,calc}$[c]	$M_{n,\,MALDI}$
PEO45-PnBuA29	7700 (1.07)	6000	6100 (1.13)
PEO45-PnBuA100	18500 (1.07)	18200	17400 (1.09)
PEO114-PnBuA105	20600 (1.05)	18700	16900 (1.11)
PEO114-PnBuA201	31800 (1.05)	31000	-
PEO114-PnBuA250	37300 (1.09)	37200	36500 (1.09)
PEO114-PnBuA778	82200 (1.08)	105000	-

[a] The numbers behind the individual blocks correspond to the degree of polymerization, as determined by ^{1}H-NMR. [b] SEC in THF calibrated with PS standards. [c] Calculation based on the weight fractions determined by ^{1}H-NMR and the true molecular weight of the PEO-CTA.

Independent of the PEO-CTA used, various degrees of polymerizations can be obtained for the second block, demonstrating the versatility of our approach. If the target is a very long second block, the monomer feed can easily be increased without losing control of the reaction or leading to unreasonably long reaction times. The experimentally determined values using SEC with a PS calibration curve only give apparent molecular weights. The calculated values were confirmed in several cases by MALDI-ToF measurements of some diblock copolymers which show a satisfying agreement (Supporting Information).

In conclusion, the RAFT polymerization of n-BuA in conjunction with highly functionalized PEO-CTAs provides very well-defined PEO-*block*-PnBuA diblock copolymers with tailored block ratios. A separation of homopolymer and diblock copolymer is unnecessary. Additionally, high molecular weights are accessible without the appearance of significant termination reactions. A key-step towards the synthesis of the desired bis-hydrophilic block terpolymers is based on limiting the conversion in order to obtain diblock copolymers with a high degree of CTA groups attached to their chain ends.

Synthesis and Characterization of Bis-Hydrophilic Block Terpolymers

Various (meth)acrylamide derivatives were chosen for the polymerization of the third block in order to obtain bis-hydrophilic terpolymers with two hydrophilic end blocks. In general, (meth)acrylamides are a very versatile class of monomer as they exhibit different solution behavior depending on the substitution pattern used. A main focus for the polymerization towards block terpolymers was set on the PEO-5k-CTA based block copolymers, as longer polymer chains lead to larger sizes of their micellar aggregates and thus facilitate later investigations with *cryo*-TEM. Furthermore, the tendency for two polymers to phase-segregate scales with their number of repeating units, which obviously increases for higher chain length of PEO. Nevertheless, one run was conducted for the shorter PEO based block copolymers to convincingly demonstrate the good control over the reaction parameters. For the analysis of the block terpolymers, one has to distinguish between two sets of terpolymers: The first group consists of PEO-*block*-PnBuA-*block*-PDEAAm and PEO-*block*-PnBuA-*block*-PNIPAAm copolymers which both carry thermo-responsive segments of moderate polarity. These block terpolymers can be analyzed in a rather straight-forward manner. The second set comprises PEO-*block*-PnBuA-*block*-PHPMA and PEO-*block*-PnBuA-*block*-PAAm block terpolymers. Those carry permanently water-soluble end blocks of very high polarity. Their extremely limited solubility in the unimolecular, non-associated form remains a challenging aspect in their characterization as will be pointed out below. Nevertheless, both polymers are very interesting as the PEO/PAAm system has a high tendency to phase-segregate and PEO/PHPMA is very interesting in terms of biomedical applications.

Considering the first group, the kinetic data of several runs for the preparation of PEO-*block*-PnBuA-*block*-PDEAAm and PEO-*block*-PnBuA-*block*-PNIPAAm are shown in **Error! Reference source not found.**. All polymerizations show characteristics of a controlled chain transfer reaction taking place. The time conversion plots are linear and there is a linear increase of molecular weight with increasing conversion. The extension of the third block can be performed independently of the PEO chain length as can be seen by comparing the two top rows, which list data for PEO-2k and PEO-5k based block terpolymers. Under similar conditions, the polymerization of DEAAm is almost five times faster than compared to NIPAAm, yet still exhibiting a high level of control. Whereas a significant recombination shoulder occurs around 20 – 25 % conversion in case of PEO-*block*-PnBuA-*block*-PNIPAAm block terpolymers, it is absent for all PEO-*block*-PnBuA-*block*-PDEAAm polymers until a conversion of up to 40 %. All SEC elution traces show a distinct shift towards shorter elution volumes with increasing conversion. The whole peak is displaced, indicating an almost complete blocking efficiency from the second to the third block. These good results obviously benefit from the fact that the polymerizations of the diblock copolymers, PEO-*block*-PnBuA, had been stopped at low conversions ensuring a high

extent of capping with the CTA. Note that the PEO-*block*-PnBuA-*block*-PDEAAm block terpolymers can also be analyzed with a standard THF SEC, whereas more polar eluents, such as NMP, are required for PEO-*block*-PnBuA-*block*-PNIPAAm.

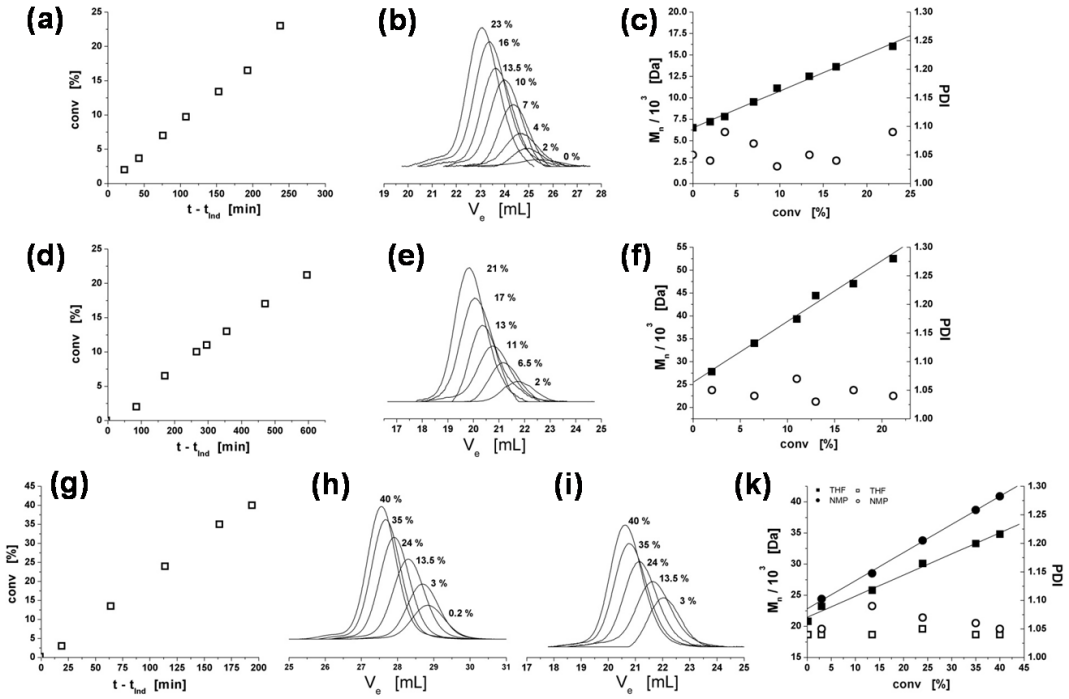

Figure 6 - 4. Time-conversion plots (a, d, g), SEC elution traces (b, e, h, i) and the evolution of molecular weights and polydispersities as a function of conversion (c, f, k) for the block extension of PEO45-PnBuA29 with NIPAAM (a-c) and PEO114-PnBuA105 with NIPAAm (d-f) and DEAAM (g-h). For DEAAM, both THF (h) and NMP (i) SEC traces and analysis are shown. The induction period[69] (20 – 25 min) was subtracted for the time conversion plots to allow a better display of the data points.

The most well-defined block terpolymers can again be obtained by limiting the conversion to a moderate degree, depending on the monomer used. For micellization studies the suppression of interchain coupling, leading to ABCCBA structures, is important as this could lead to intermicellar connections and flower-like micelles. The compositions of all block terpolymers, including the second group of PEO-*block*-PnBuA-*block*-PHPMA and PEO-*block*-PnBuA-*block*-PAAm, were confirmed by ^{1}H-NMR. The spectra including the peak assignments are shown in the Supporting Information, confirming the compositions of all block terpolymers. Due to the moderate speed and viscosity of the polymerizations, samples can easily be taken at various points to obtain block terpolymers with varying degrees of polymerization for the end block. This sampling allows a final tuning of the corona structure of the resulting micelles. To keep sufficient clarity, Table 6 - 2 only displays the final polymers (last samples) at high degree of polymerization for the last block and for some intermediate samples which were used for MALDI-ToF characterization. Note that MALDI-ToF analysis of amphiphilic block terpolymers is a challenging task. Due to the significantly different solubility characteristics, the polymers tend to form physical aggregates in a wide variety of solvents. Nevertheless, we were able to obtain several meaningful MALDI-ToF spectra for some selected PEO-*block*-PnBuA-*block*-PDEAAm and PEO-*block*-PnBuA-*block*-PNIPAAm polymers (Supporting Information). The MALDI-ToF data coincides well with the calculated molecular weights of the various polymers and convincingly demonstrates the

successful and controlled extension. Consequently, the block terpolymers can be tailored in their composition and molecular weights over a wide range.

Table 6 - 2. Overview of the Block Terpolymers Synthesized.

Block Terpolymer[a]	$M_{n,\,SEC}$ (PDI)[b]	$M_{n,\,calc}$[d]	$M_{n,\,MALDI}$ (PDI)
PEO114-PnBuA105-PDEAAm181	34800 (1.04) 40900 (1.05)[c]	41800	42700 (1.02)
PEO114-PnBuA250-PDEAAm200	54000 (1.06) 60500 (1.07)[c]	62600	69000 (1.02)
(PEO114-PnBuA250-PDEAAm99)	(46600 (1.06))	(49800)	(48400 (1.03))
PEO45-PnBuA29-PNIPAAm46	15900 (1.10)	11200	12600 (1.03)
PEO114-PnBuA105-PNiPAAm350	66200 (1.09)	58250	n.a.
(PEO114-PnBuA105-PNiPAAm275)	(56000 (1.12))	(49800)	(48400 (1.04))
(PEO114-PnBuA105-PNiPAAm195)	(52500 (1.04))	(40700)	(43500 (1.03))
PEO114-PnBuA250-PNIPAAm217	70000 (1.05)	61700	
(PEO114-PnBuA250-PNIPAAm82)	(51800 (1.05))	(46500)	(45928 (1.03))
PEO114-PnBuA105-PAAm195	-	30900	-
PEO114-PnBuA250-PAAm120	-	48200	-
PEO114-PnBuA105-PHPMA129	-	36700	-
PEO114-PnBuA250-PHPMA93	-	50300	-

[a] The numbers behind the individual blocks correspond to the degree of polymerization, as determined by ^{1}H-NMR [b] SEC was performed in NMP using a PS calibration curve. [c] SEC was performed in THF using a PS calibration curve. [d] Calculation based on the weight fractions determined by ^{1}H-NMR and the true molecular weight of the PEO-CTA.

The situation regarding the analysis of the second set of terpolymers, utilizing the very polar monomers HPMA and AAm, is different. Due to the presence of the extremely polar segments as end blocks, the solubility characteristics are altered in a very undesirable fashion. Even in solvents with a high solvating power, such as DMAc, DMF, NMP and DMSO, the polymers form aggregates or do not dissolve sufficiently, thus strongly complicating analytical techniques such as SEC or MALDI-ToF. The kinetic data and the SEC results are shown in Figure 6 - 5. Both polymerizations of HMPA (Figure 6 - 5b) and AAm (Figure 6 - 5a) show a linear behavior in the time conversion plot, indicating a controlled chain transfer reaction at a constant radical concentration taking place. In contrast to the block extension with HPMA, which exhibits a strictly linear behavior, all polymerizations with AAm show a decrease of the reaction rate at conversions exceeding 20 %. Such a behavior can be correlated with the discoloration of the reaction solution from pink to orange for conversions higher than 20 %, indicating an undesirable side reaction of the CTA. Most probably, the amide groups of the AAm undergo some side reactions with the dithioester function of the CTA moiety, leading to a decrease in the reaction rate. Consequently, the conversion shall be limited to values lower than 20% to minimize this effect and to obtain the most well-defined polymers of this type possible. A limited broadening of the molecular weight distribution cannot be excluded at higher conversions. Likewise, since HPMA is a methacrylamide derivative, which is used for the chain extension of an acrylate chain end, some increase in the polydispersity index can be anticipated.

Nevertheless, a controlled chain extension taking place is strongly indicated by (i) the continuous change in solubility of the various isolated block terpolymers with different chain lengths of the third block (see Supporting Information for comments), (ii) by the SEC results showing the

absence of any diblock precursor and (iii) by the appearance of different aggregate structures of the block terpolymers in water.

Particularly, the SEC data can be used to prove a high blocking efficiency. Both PHPMA and PAAm based block terpolymers do not dissolve readily at room temperature in NMP or DMAc, some heating is always required. The PAAm based block copolymers do even not dissolve in DMAc at elevated temperatures. Once dissolved at higher temperatures, SEC measurements in NMP and DMAc were conducted for several of those block terpolymers. The behavior is similar for all chain lengths of the third block. A peak corresponding to unimolecularly dissolved polymer molecules cannot be found, even not for the shortest chains of PAAm and PHPMA. The limited solubility of the end blocks in these solvents, as indicated by the temperature required for their dissolution, induces aggregate or micelle formation upon cooling. Consequently, the peak appears close to the exclusion volume resulting in unreasonably high molecular weights. Strikingly and most important for concluding a high blocking efficiency and successful chain extension is the absence of a peak corresponding to residual diblock copolymer, PEO-*block*-PnBuA. The diblock copolymer would not take part in the aggregate formation and would lead to peaks at much higher elution volumes as found here. For instance, for the SEC trace in NMP, the corresponding diblock elution trace is shown as comparison (Figure 6 - 5c). Similarly, for the DMAc SEC measurements (Figure 6 - 5d), the elution trace of a PEO-*block*-PnBuA-*block*-PNIPAAm terpolymer with almost the same degrees of polymerization is shown as an indication for where the PEO-*block*-PnBuA-*block*-PHPMA polymer would be expected. In the case of the block terpolymer, the signal is completely flat, proving the absence of significant amounts of the PEO-*block*-PnBuA diblock precursor. Furthermore, unimolecularly dissolved polymers cannot be found. Note that the polymer purification was accomplished via dialysis and thus the removal of any diblock precursor by selective precipitation is excluded. Additionally, a calculation of the theoretical block length of the third block, based on the apparent molecular weight of the SEC measurements (10^5-10^7 Da, Figure 6 - 5e), led to extremely high degrees of polymerizations for the third block, which do by no means coincide with the fraction determined by ^{1}H-NMR. If the molecular weight estimation of the SEC measurements were correct, the blocking efficiency would be significantly below 10% and thus a signal of the residual diblock copolymer precursor would be strongly visible. Since this is not the case, the only explanation is the presence of micellar aggregates during the SEC measurements. The strong aggregation tendency unfortunately prevents using MALDI-ToF, static light scattering or osmometry for the determination of the true molecular weights.

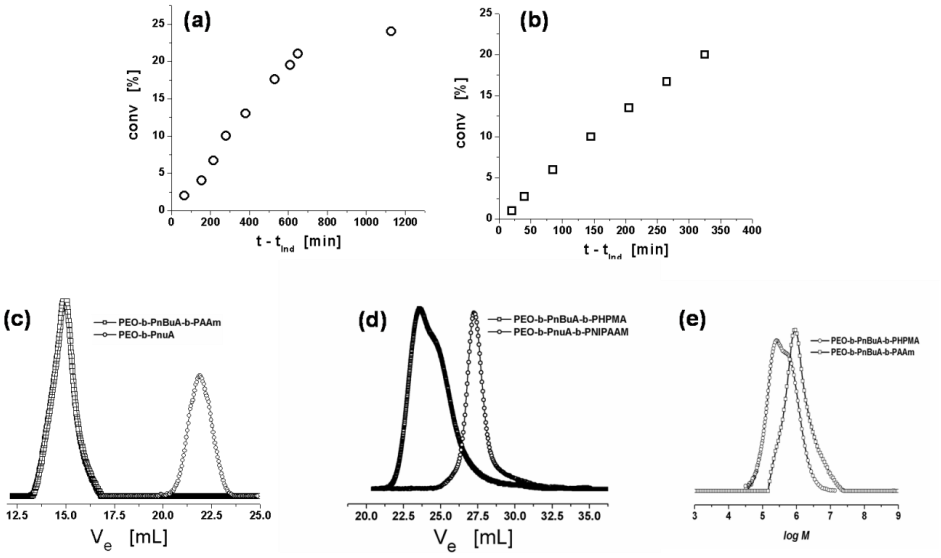

Figure 6 - 5. Typical time-conversion plots for the block extension of PEO-*block*-PnBuA diblock copolymers with AAm (a) and HPMA (b). The induction periods[69] (160 and 95 min) were subtracted for the time conversion plots to allow a better display of the data points. (c) NMP SEC elution traces of the PEO-*block*-PnBuA diblock copolymer precursor and the aggregates formed after block extension with AAm, as indicated in the graph. (d) DMAc SEC elution traces of the aggregates formed by PEO-*block*-PnBuA-*block*-PHPMA polymers. The elution trace of a PEO-*block*-PnBuA-*block*-PNIPAAm of similar degrees of polymerization for each block is shown for comparison. (e) Molecular weight distribution profiles for the PEO-*block*-PnBuA-*block*-PHPMA and PEO-*block*-PnBuA-*block*-PAAm triblock copolymers shown in (d) and (c).

In conclusion, the difficult solubility characteristics prevent the in-depth characterization of the second group of block terpolymers in the unimolecular state. However, the kinetic data in combination with the solubility behavior and the SEC results, revealing the presence of aggregates and a high blocking efficiency, strongly indicate a successful chain transfer reaction with a controlled increase of molecular weight taking place.

Colloidal Aggregates

Although a full coverage of the complex thermo-responsive behavior and the issue of corona phase-segregation is beyond the scope of this report, we nevertheless want to demonstrate the viability of the approach in terms of tuning the aggregate morphology, micellar dynamics and solution behavior.

Based on the selection of PnBuA as hydrophobic block possessing a low glass transition temperature far below room temperature, a dynamic behavior of the micelles is expected. Initially, attention was drawn to the dissolution behavior of the block terpolymers. Generally, all polymers do not dissolve instantaneously in water. Depending on the block length and type of the third block, several weeks are required to obtain turbid solutions which do not show any larger particles. The turbidity decreases to some extent during the weeks indicating dissolution of initially present, very large aggregates into smaller ones. Since dissolution times of weeks are not time efficient, the second most common way of preparing micellar solutions via dialysis from a common solvent into a selective solvent, water, was additionally explored.

Some representative *cryo*-TEM images for a PEO-*block*-PnBuA-*block*-PDEAAm terpolymer with a comparably long hydrophobic block are shown in **Error! Reference source not found.**. This

example nicely demonstrates the complex and kinetically governed dissolution behavior of the polymers.

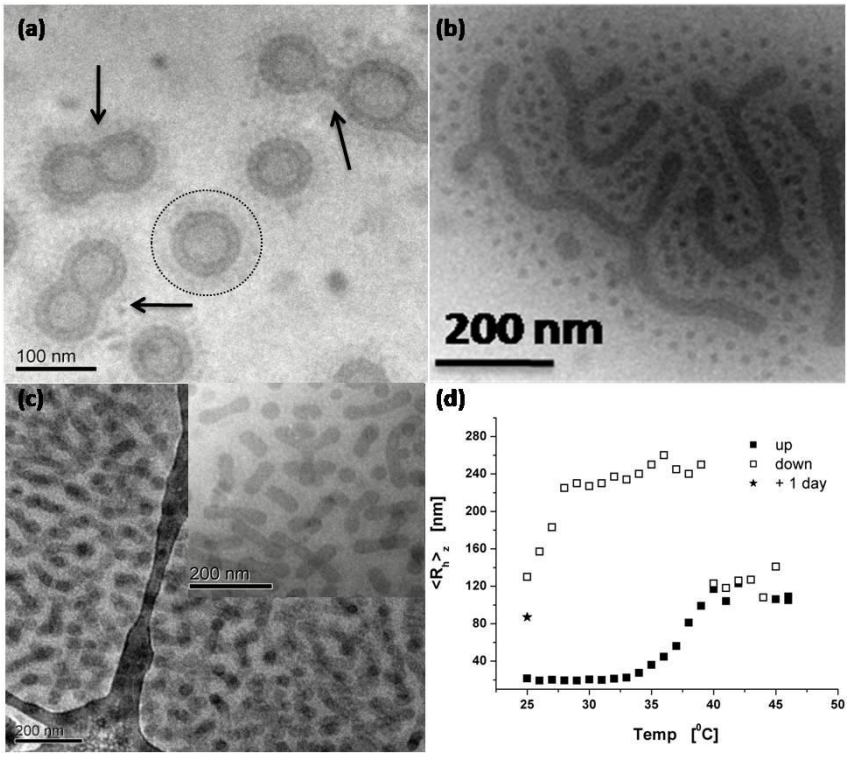

Figure 6 - 6. *Cryo*-TEM images of aggregates formed by PEO114-PnBuA250-PDEAAm135 after direct dissolution in water and stirring for four weeks (a), dialysis from dioxane into water (b) and a subsequent heating cycle of the aggregates to 45 °C (c). Temperature dependent DLS measurement of the spherical micelles in (b), obtained by filtration (220 nm pore size). The star indicates an ageing time of one day.

The direct dissolution of this polymer into water leads to a large fraction of vesicles (shown in **Error! Reference source not found.**a) and a small fraction of branched worm-like aggregates (not shown here). The image shows vesicles, surrounded by a corona of PEO or PDEAAm. Several fission processes of vesicles can be seen in the image, which coincide with the observed decrease of turbidity during the weeks of dissolution. On the contrary, dialysis from dioxane into water leads to fractions of smaller and larger spherical micelles and worm-like aggregates (**Error! Reference source not found.**b). Thus, direct dissolution favors the generation of aggregates of lower curvature. The appearance of several different morphologies depending on the preparation conditions used indicates a strong influence of the kinetics of the aggregate formation. The equilibriums state is not reached easily, a phenomenon known for block copolymer based aggregates.[70-72] A subsequent heating cycle of the latter solution to 45 °C and back to room temperature, hence above the LCST of the PDEAAm, induces a disappearance of the small micelles and a transition into branched worm-like micelles (**Error! Reference source not found.**c). This transition can be followed via a temperature sweep in a dynamic light scattering instrument (DLS, Figure 6 - 8d), after isolation of the population of the spherical micelles via filtration (pore size 220 nm). The isolated spherical micelles fuse into finite sized, larger aggregates upon reaching the cloud point during heating. When cooling down, the curve shows a strong hysteresis with larger, loosely bound aggregates being visible in the intermediate stage. After sufficient ageing, the aggregate size is constant, sufficiently larger than before the heating cycle and corresponds to a transition of the spherical micelles into branched worm-like

micelles. Consequently, a clear and distinct change in the micelle architecture can be induced by the temperature cycle. The main transition happens during the heating and is clearly assisted by the change (decrease) of the hydrophilic-to-hydrophobic ratio upon reaching the cloud point, favoring the formation of aggregates of lower curvature (i.e. worm-like micelles).[73-77] The utilization of the soft PnBuA provides the desired means for large-scale rearrangements in response to changes of the environmental conditions. The micelles are not only able to change their corona structure (first level) due to the presence of thermo-responsive segments, but also the overall structure of the micelles can be changed due to the low T_g of the hydrophobic block (second level). This represents a much higher degree of responsiveness that cannot be expected for high T_g polymers such as polystyrene or poly(2-vinylpyridine).The worm-like structure is stable upon further heating cycles in terms of the geometrical shape, indicating sufficient thermodynamic stability. An extension into longer cylindrical micelles can take place with further heating cycles. Hence, the spherical micelles are in kinetically frustrated state and the thermodynamically preferred architecture can be recovered via a heating cycle.

Similarly, *cryo*-TEM investigations of a block terpolymer with a significantly shorter hydrophobic block led to the images shown in **Error! Reference source not found.**. The hydrophobic block length (PnBuA = 105 units) is decreased to a little less than half of the preceding polymer (PnBuA = 250 units). The direct dissolution into water yields small slightly ill-defined aggregates, meaning their cores are not entirely spherical, neither of a distinct other shape, e.g. disc-like (**Error! Reference source not found.**a). Dialysis leads to the observation of two distinct populations of spherical micelles (**Error! Reference source not found.**b). The small spherical micelles fuse into larger spherical micelles after a heating cycle, representing the thermodynamically more stable structure (**Error! Reference source not found.**c). The temperature ramp monitored by DLS (**Error! Reference source not found.**d) shows first an increase of the hydrodynamic radius to a constant level and a further increase upon cooling. The first increase is presumably related to a fusion process of the small micelles and the second increase to an extension of the corona. The shape of the curve and the extent of hysteresis is independent of the heating steps used, owing to a defined thermodynamic pathway of the transition. The transition from small micelles into larger ones again shows that aggregates of smaller curvature are more stable in water, than what is obtained straight after dialysis.

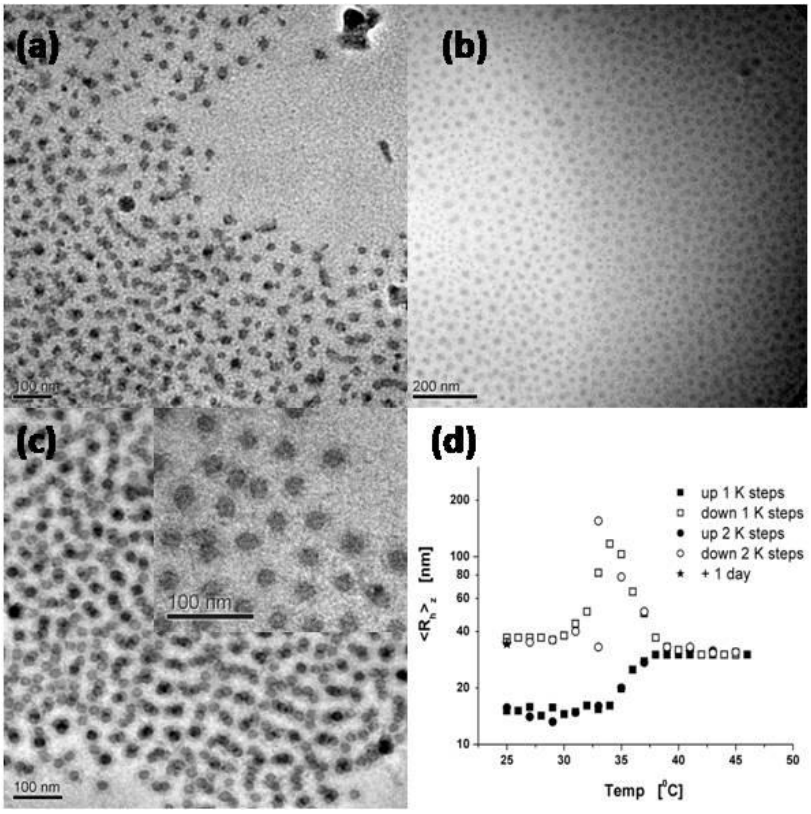

Figure 6 - 7. *Cryo*-TEM images of aggregates formed by PEO114-PnBuA105-PDEEAm181 after direct dissolution in water and stirring for four weeks (a), dialysis from dioxane into water (b) and a subsequent heating cycle of the aggregates (b) to 45 °C (c). Temperature dependent DLS measurement for two different heating rates (squares = 1K steps, circles = 2K steps).

Clearly, the shorter hydrophobic block of the latter polymer favors the formation of spherical micelles, whereas the longer block leads to the formation of aggregates of lower interfacial curvatures (rods and vesicles). This behavior can be understood in terms of adjusting the hydrophilic-to-hydrophobic balance. [73-77] Additionally, it can be concluded that the micelles obviously possess a dynamic character as they both undergo structural rearrangements and direct, yet time-consuming dissolution in water. The occurrence of a certain aggregate shape depends on the preparation pathway and demonstrates the strong influence of kinetic effects in this system.

Due to the dynamic behavior in combination with the incorporation of thermo-responsive segments, we expect an interesting behavior in terms of thermo-responsiveness of these structures. Indeed, the thermo-responsiveness and the effect of repeated heating cycles on the aggregate structures and corona phase-behavior will be addressed in a forthcoming publication.

In a last section we compare the influence of the last block on the morphology of the aggregates formed by PEO-*block*-PnBuA-*block*-PAAm and PEO-*block*-PnBuA-*block*-PHPMA (**Error! Reference source not found.**). The upper two *cryo*-TEM micrographs (Figure 6 - 8a and 8b) show spherical micelles of PEO-*block*-PnBuA-*block*-PAAm with a short segment of the hydrophobic block (PnBuA = 105 units). The core-corona morphology is well visible in both micrographs and further highlighted by the circle in Figure 6 - 8b. Upon further increase of the hydrophobic block length (PnBuA = 250 units), while keeping the fraction of PAAm almost constant, a full transition to cylindrical micelles occurs (Figure 6 - 8d). This behavior is similar to the PNIPAAm and PDEAAm

systems. However, the extension using HPMA as third block leads to the observation of very small vesicles and worm-like aggregates, even for very low fractions of PnBuA (PnBuA = 105 units, Figure 6 - 8e). This behavior is drastically different from the PNIPAAm and PDEAAm systems. Since the hydrophilic-to-hydrophobic balance is similar in all systems, the incompatibility of both end blocks starts playing a significant role. Aggregates of lower curvature are clearly preferred for rising incompatibility of the end blocks, as the interface between the two end blocks can be minimized, i.e. by creating an asymmetric vesicle walls. Although PEO and PAAm have shown to be incompatible in the case of the C3Ms,[54] the PHPMA/PEO system appears even more susceptible to the formation of microphase-segregation as concluded from the observation of the aggregates of lowest curvature. The colloidal structures based on both PAAm and PHPMA block terpolymers are stable to several heating cycles, as shown by the temperature dependent DLS measurements. Only slight expansions or contractions of the structures take place upon repeated heating. Consequently, the difference in aggregate structure does not originate from kinetic obstacles during the micelle preparation but from the chemically unlike end blocks and the different incompatibilities of them with PEO.

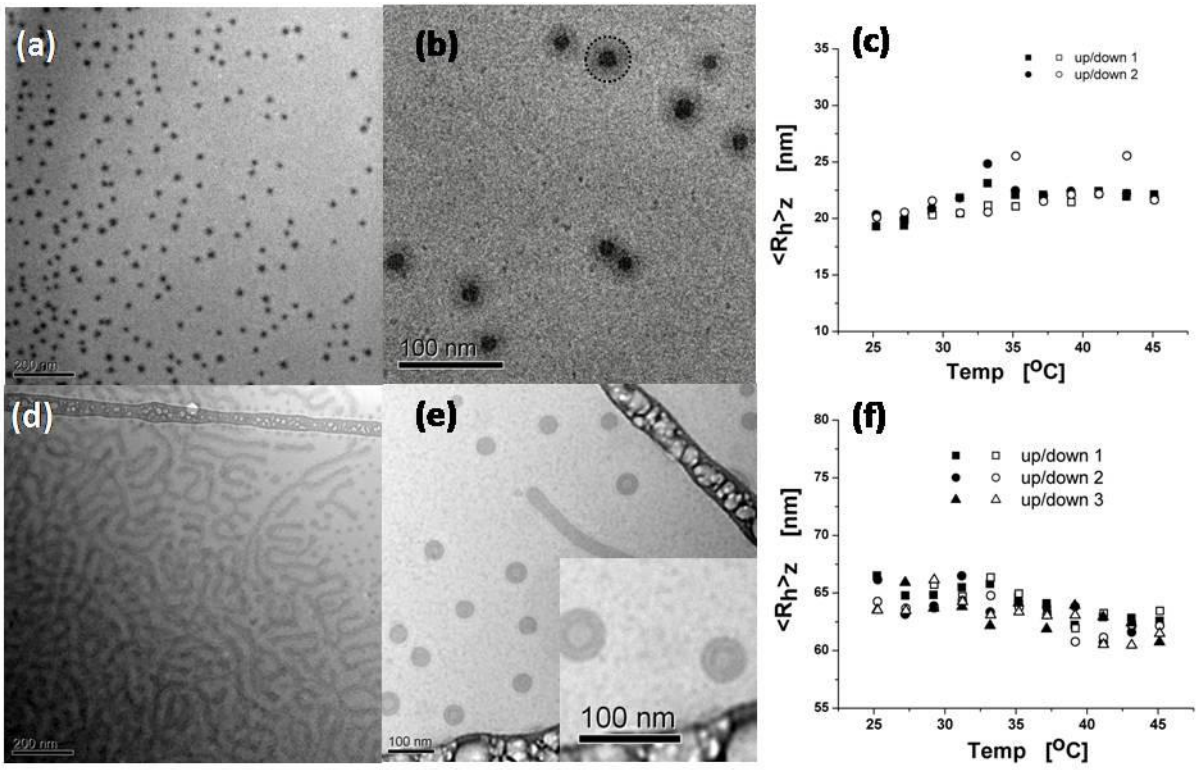

Figure 6 - 8. *Cryo*-TEM images of the major populations of aggregates found for PEO114-PnBuA105-PAAm103 (a+b), PEO114 -PnBuA250 -PAAm120 (d) and PEO114-PnBuA105-PHPMA101 (e). Repeated temperature sweep DLS measurements for PEO114-PnBuA105-PAAm103 (c) and PEO114-PnBuA105-PHPMA101 (f) after filtration with 220 nm filters.

Conclusions

We present the synthesis of well-defined bis-hydrophilic block terpolymers possessing two hydrophilic end blocks via RAFT mediated living/controlled radical polymerization. The strategy aims at a facile tunability of the corona structure and the aggregate morphologies formed by these polymers.

The optimization of the synthesis of the PEO-based macro-CTAs allowed the easy and straight-forward synthesis of amphiphilic PEO-*block*-PnBuA diblock copolymers of various compositions. The blocking efficiency is near quantitative, which makes complicated and time-consuming separation processes of homopolymer and diblock copolymer unnecessary. Similarly, the extension with NIPAAm and DEAAm proceeds almost quantitatively as the polymerizations of the diblock copolymers were stopped at moderate conversions in order to ensure a sufficient capping of the PEO-*block*-PnBuA with the CTA moiety. The block terpolymers with PDEAAm and PNIPAAm as well as the diblock copolymers where exhaustively characterized by SEC, MALDI-ToF and NMR. They exhibit very low polydispersities, typically below 1.15. The reactions allow a full control of the hydrophilic and hydrophobic block length. For the extension with AAm and HPMA, the characterization remained challenging due to the strongly amphiphilic character of the polymers and the accompanying tendency to form aggregates in all kinds of solvents. Despite using several state-of-the-art SEC systems for amphiphilic block copolymers, a unimolecularly dissolved and well-separated species could not be characterized. The complete disappearance of the SEC peak related to the diblock copolymer precursor in conjunction with the controlled reaction kinetics and the gradual change in the solution characteristics however strongly point towards a controlled chain extension.

Finally, the solution properties of the polymers in water are analyzed with respect to the corona block, the hydrophilic-to-hydrophobic balance and the kinetics involved during dissolution and phase transitions. A direct dissolution of the polymers is possible due to the low glass transition temperature of the hydrophobic block, however the process requires weeks. The structures found for the polymers directly dissolved in water may be significantly different from the ones obtained by dialysis from a common solvent (dioxane, DMSO) into water, indicating a strong influence of the solvation pathway and kinetics. Direct dissolution in water leads to aggregates with lower curvature of the interface. Once dissolved in water, the aggregates can undergo structural transitions, i.e. from spherical into worm-like structures upon heating. The responsiveness to heat involves both the corona structure due to the presence of the LCST segments and the overall architecture of the micelle, that can rearrange because of the low T_g properties of the hydrophobic block, PnBuA. By tuning the hydrophilic-to-hydrophobic balance, a large variety of structures, i.e. spherical and worm-like micelles as well as vesicles, can be obtained. A strong effect of the chemistry of the third block and thus the interaction between the various blocks on the type of aggregates formed can be deduced. At similar composition the PAAm based block terpolymers form spherical and worm-like micelles, whereas the PHPMA based polymers form mainly vesicles. The terpolymers synthesized provide a novel platform for the creation of multicompartment particles with tunable corona properties.

Acknowledgements

The authors are grateful for financial support from the Australian Research Council (ARC) and the Deutsche Forschungsgemeinschaft (DFG) for financial support in the form of a Linkage project. CBK acknowledges receipt of an Australian Professorial Fellowship (ARC). We thank Mr. E. H. H. Wong, S. Edinger, D. Danz and M. Schumacher for supporting mass spectrometry and size exclusion chromatography measurement. A. Walther acknowledges support from the Bavarian Elite Support Program. Dr. L. Barner and Mr. I. Jacenyik are thanked for their excellent management of the CAMD facilities.

References

1. Rao, J.; Luo, Z.; Ge, Z.; Liu, H.; Liu, S. *Biomacromolecules* **2007,** 8, 3871-3878.
2. Wang, D.; Wu, T.; Wan, X.; Wang, X.; Liu, S. *Langmuir* **2007,** 23, 11866-11874.
3. Wang, D.; Yin, J.; Zhu, Z.; Ge, Z.; Liu, H.; Armes, S. P.; Liu, S. *Macromolecules* **2006,** 39, 7378-7385.
4. Cai, Y.; Armes, S. P. *Macromolecules* **2005,** 38, 271-279.
5. Liu, S.; Armes, S. P. *Langmuir* **2003,** 19, 4432-4438.
6. Weaver, J. V. M.; Armes, S. P.; Bütün, V. *Chem. Commun.* **2002**, 2122-2123.
7. Liu, S.; Armes, S. P. *Angew. Chem. Int. Ed.* **2002,** 41, 1413-1416.
8. Zhang, L.; Bernard, J.; Davis, T. P.; Barner-Kowollik, C.; Stenzel, M. H. *Macromol. Rapid Commun.* **2008,** 29, 123-129.
9. Hsu, Y.-H.; Chiang, W.-H.; Chen, C.-H.; Chern, C.-S.; Chiu, H.-C. *Macromolecules* **2005,** 38, 9757-9765.
10. Topp, M. D. C.; Dijkstra, P. J.; Talsma, H.; Feijen, J. *Macromolecules* **1997,** 30, 8518-8520.
11. Gu, J.; Cheng, W.-P.; Liu, J.; Lo, S.-Y.; Smith, D.; Qu, X.; Yang, Z. *Biomacromolecules* **2008,** 9, 255-262.
12. Zhang, L.; Nguyen, T. L. U.; Bernard, J.; Davis, T. P.; Barner-Kowollik, C.; Stenzel, M. H. *Biomacromolecules* **2007,** 8, 2890-2901.
13. Sawant, R. M.; Hurley, J. P.; Salmaso, S.; Kale, A.; Tolcheva, E.; Levchenko, T. S.; Torchilin, V. P. *Bioconjugate Chem.* **2006,** 17, 943-949.
14. Giacomelli, C.; Le Men, L.; Borsali, R.; Lai-Kee-Him, J.; Brisson, A.; Armes, S. P.; Lewis, A. L. *Biomacromolecules* **2006,** 7, 817-828.
15. Zhang, W.; Shi, L.; Ma, R.; An, Y.; Xu, Y.; Wu, K. *Macromolecules* **2005,** 38, 8850-8852.
16. Rodriguez-Hernandez, J.; Lecommandoux, S. *J. Am. Chem. Soc.* **2005,** 127, 2026-2027.
17. Sfika, V.; Tsitsilianis, C.; Kiriy, A.; Gorodyska, G.; Stamm, M. *Macromolecules* **2004,** 37, 9551-9560.
18. Gil, E. S.; Hudson, S. M. *Prog. Polym. Sci.* **2004,** 29, 1173-1222.
19. Sumerlin, B. S.; Lowe, A. B.; Thomas, D. B.; McCormick, C. L. *Macromolecules* **2003,** 36, 5982-5987.
20. Yusa, S.; Shimada, Y.; Mitsukami, Y.; Yamamoto, T.; Morishima, Y. *Macromolecules* **2003,** 36, 4208-4215.
21. Liu, S.; Weaver, J. V. M.; Save, M.; Armes, S. P. *Langmuir* **2002,** 18, 8350-8357.
22. Rosler, A.; Vandermeulen, G. W. M.; Klok, H.-A. *Adv. Drug Delivery Rev.* **2001,** 53, 95-108.
23. Kataoka, K.; Harada, A.; Nagasaki, Y. *Adv. Drug Delivery Rev.* **2001,** 47, 113-131.
24. Hoffman, A. S.; Stayton, P. S. *Prog. Polym. Sci.* **2007,** 32, 922-932.
25. Bontempo, D.; Li, R. C.; Ly, T.; Brubaker, C. E.; Maynard, H. D. *Chem. Commun.* **2005**, 4702-4704.
26. Rapoport, N. *Prog. Polym. Sci.* **2007,** 32, 962-990.

27. Walther, A.; André, X.; Drechsler, M.; Abetz, V.; Müller, A. H. E. *J. Am. Chem. Soc.* **2007,** 129, 6187-6198.
28. Walther, A.; Müller, A. H. E. *Soft Matter* **2008,** 4, 663-668.
29. Li, Z.; Kesselman, E.; Talmon, Y.; Hillmyer Marc, A.; Lodge Timothy, P. *Science* **2004,** 306, 98-101.
30. Li, Z.; Hillmyer, M. A.; Lodge, T. P. *Langmuir* **2006,** 22, 9409-9417.
31. Cui, H.; Chen, Z.; Zhong, S.; Wooley, K. L.; Pochan, D. J. *Science* **2007,** 317, 647-650.
32. Cui, H.; Chen, Z.; Wooley, K. L.; Pochan, D. J. *Macromolecules* **2006,** 39, 6599-6607.
33. Li, Z.; Chen, Z.; Cui, H.; Hales, K.; Qi, K.; Wooley, K. L.; Pochan, D. J. *Langmuir* **2005,** 21, 7533-7539.
34. Wang, X.; Guerin, G.; Wang, H.; Wang, Y.; Manners, I.; Winnik, M. A. *Science* **2007,** 317, 644-647.
35. Li, Z.; Hillmyer, M. A.; Lodge, T. P. *Macromolecules* **2006,** 39, 765-771.
36. Lodge, T. P.; Rasdal, A.; Li, Z.; Hillmyer, M. A. *J. Am. Chem. Soc.* **2005,** 127, 17608-17609.
37. Kubowicz, S.; Baussard, J.-F.; Lutz, J.-F.; Thuenemann, A. F.; von Berlepsch, H.; Laschewsky, A. *Angew. Chem. Int. Ed.* **2005,** 44, 5262-5265.
38. Lutz, J.-F.; Laschewsky, A. *Macromol. Chem.Phys.* **2005,** 206, 813-817.
39. Li, Z.; Kesselman, E.; Talmon, Y.; Hillmyer, M. A.; Lodge, T. P. *Science* **2004,** 306, 98-101.
40. Willet, N.; Gohy, J.-F.; Auvray, L.; Varshney, S.; Jerome, R.; Leyh, B. *Langmuir* **2008,** 24, 3009-3015.
41. Willet, N.; Gohy, J.-F.; Lei, L.; Heinrich, M.; Auvray, L.; Varshney, S.; Jerome, R.; Leyh, B. *Angew. Chem. Int. Ed.* **2007,** 46, 7988-7992.
42. Khanal, A.; Inoue, Y.; Yada, M.; Nakashima, K. *J. Am. Chem. Soc.* **2007,** 129, 1534-1535.
43. Zhang, W.; Jiang, X.; He, Z.; Xiong, D.; Zheng, P.; An, Y.; Shi, L. *Polymer* **2006,** 47, 8203-8209.
44. Li, G.; Shi, L.; An, Y.; Zhang, W.; Ma, R. *Polymer* **2006,** 47, 4581-4587.
45. Lei, L.; Gohy, J.-F.; Willet, N.; Zhang, J.-X.; Varshney, S.; Jerome, R. *Polymer* **2004,** 45, 4375-4381.
46. Lei, L.; Gohy, J.-F.; Willet, N.; Zhang, J.-X.; Varshney, S.; Jerome, R. *Macromolecules* **2004,** 37, 1089-1094.
47. Gohy, J.-F.; Willet, N.; Varshney, S.; Zhang, J.-X.; Jerome, R. *Angew. Chem. Int. Ed.* **2001,** 40, 3214-3216.
48. Liu, F.; Eisenberg, A. *J. Am. Chem. Soc.* **2003,** 125, 15059-15064.
49. Stoenescu, R.; Graff, A.; Meier, W. *Macromol. Biosci.* **2004,** 4, 930-935.
50. Stoenescu, R.; Meier, W. *Chem. Commun.* **2002**, 3016-3017.
51. Charlaganov, M.; Borisov, O. V.; Leermakers, F. A. M. *Macromolecules* **2008,** 41, 3668-3677.
52. Li, G.; Shi, L.; Ma, R.; An, Y.; Huang, N. *Angew. Chem. Int. Ed.* **2006,** 45, 4959-4962.
53. Ma, R.; Wang, B.; Xu, Y.; An, Y.; Zhang, W.; Li, G.; Shi, L. *Macromol. Rapid Commun.* **2007,** 28, 1062-1069.
54. Voets, I. K.; de Keizer, A.; De Waard, P.; Frederik, P. M.; Bomans, P. H. H.; Schmalz, H.; Walther, A.; King, S. M.; Leermakers, F. A. M.; Cohen Stuart, M. A. *Angew. Chem. Int. Ed.* **2006,** 45, 6673-6676.
55. Halperin, A. *J. Phys. France* **1988,** 49, 131.
56. Chiefari, J.; Chong, Y. K.; Ercole, F.; Krstina, J.; Jeffery, J.; Le, T. P. T.; Mayadunne, R. T. A.; Meijs, G. F.; Moad, C. L.; Moad, G.; Rizzardo, E.; Thang, S. H. *Macromolecules* **1998,** 31, 5559-5562.
57. Barner, L.; Davis, T. P.; Stenzel, M. H.; Barner-Kowollik, C. *Macromol. Rapid Commun.* **2007,** 28, 539-559.
58. Perrier, S.; Takolpuckdee, P. *J. Polym. Sci. Part A: Polym. Chem.* **2005,** 43, 5347-5393.
59. Hong, C.-Y.; Pan, C.-Y. *Macromolecules* **2006,** 39, 3517-3524.

60. Scales, C. W.; Vasilieva, Y. A.; Convertine, A. J.; Lowe, A. B.; McCormick, C. L. *Biomacromolecules* **2005,** 6, 1846-1850.
61. Rihova, B.; Kubackova, K. *Curr. Pharma. Biotechnol.* **2003,** 4, 311-322.
62. Konak, C.; Oupicky, D.; Chytry, V.; Ulbrich, K.; Helmstedt, M. *Macromolecules* **2000,** 33, 5318-5320.
63. Bang, J.; Kim, S. H.; Drockenmuller, E.; Misner, M. J.; Russell, T. P.; Hawker, C. J. *J. Am. Chem. Soc.* **2006,** 128, 7622-7629.
64. Stenzel, M. H. 'Complex Architecture Design via the RAFT Process: Scope, Strengths and Limitations' in 'Handbook of RAFT Polymerization' Barner-Kowollik, C. Ed. Weinheim, Germany, **2008**, pp. 315-367
65. Li, Y.; Lokitz, B. S.; McCormick, C. L. *Macromolecules* **2006,** 39, 81-89.
66. Barner-Kowollik, C.; Davis, T. P.; Stenzel, M. H. *Polymer* **2004,** 45, 7791-7805.
67. Vana, P.; Albertin, L.; Barner, L.; Davis, T. P.; Barner-Kowollik, C. *J. Polym. Sci., Part A: Polym. Chem.* **2002,** 40, 4032-4037.
68. Barner-Kowollik, C.; Quinn, J. F.; Morsley, D. R.; Davis, T. P. *J. Polym. Sci., Part A: Polym. Chem.* **2001,** 39, 1353-1365.
69. Barner-Kowollik, C.; Buback, M.; Charleux, B.; Coote, M. L.; Drache, M.; Fukuda, T.; Goto, A.; Klumperman, B.; Lowe, A. B.; McLeary, J. B.; Moad, G.; Monteiro, M. J.; Sanderson, R. D.; Tonge, M. P.; Vana, P. *J. Polym. Sci., Part A: Polym. Chem.* **2006,** 44, 5809-5831.
70. Yu, K.; Zhang, L.; Eisenberg, A. *Langmuir* **1996,** 12, 5980-5984.
71. Zhang, L.; Eisenberg, A. *Polym. Adv. Technol.* **1998,** 9, 677-699.
72. Zhang, L.; Eisenberg, A. *Macromolecules* **1999,** 32, 2239-2249.
73. Zhang, L.; Eisenberg, A. *J. Am. Chem. Soc.* **1996,** 118, 3168-81.
74. Jain, S.; Bates, F. S. *Science* **2003,** 300, 460-464.
75. Zhang, L.; Eisenberg, A. *Science* **1995,** 268, 1728-1731.
76. Walther, A.; Goldmann, A. S.; Yelamanchili, R. S.; Drechsler, M.; Schmalz, H.; Eisenberg, A.; Müller, A. H. E. *Macromolecules* **2008,** 41, 3254-3260.
77. Rodriguez-Hernandez, J.; Checot, F.; Gnanou, Y.; Lecommandoux, S. *Prog. Polym. Sci.* **2005,** 30, 691-724.

Supporting Information

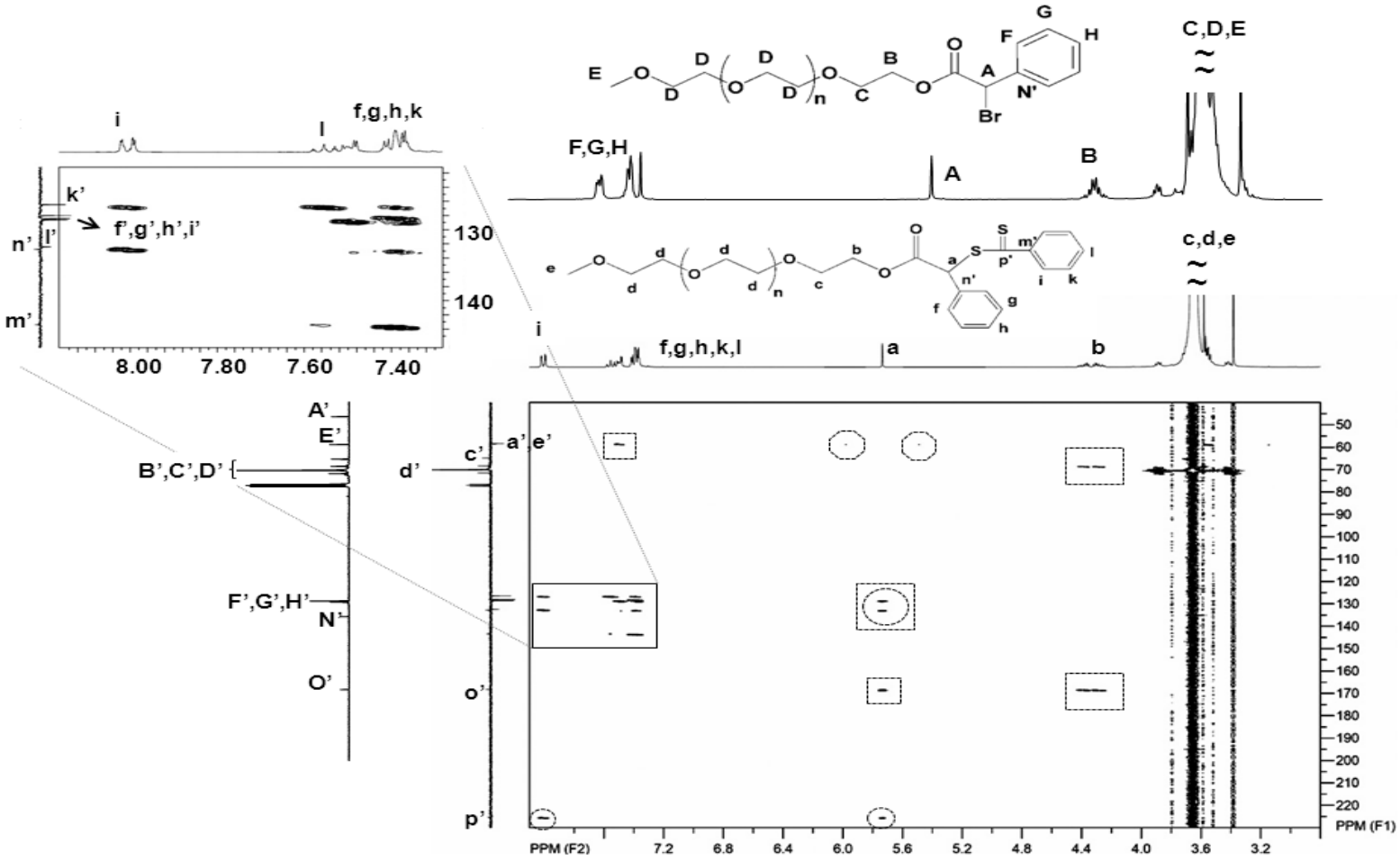

Figure Sup 6 - 9. Top and left are 1H and 13C NMR spectra of PEO-2k-Br, serving as comparison (capital letters). 2D-HMBC NMR is shown for PEO-2k-CTA in the lower right corner. The peaks are indexed as shown in the Figure. Primed letters (') represent carbon atoms. The octagons are sulphur satellites.

Comments to the NMR spectra:

The structure of PEO-2k-Br can be confirmed with a straight-forward assignment of the peaks according to the structure shown. All peaks of the α-bromophenylacetate group can be found and a comparison of the aromatic protons (F, G, H) or the methine proton adjacent to the bromine group (A) with the signals of PEO indicate a near quantitative formation of the desired product. It shall be noted that the estimation of the extent of end group functionalization based on ^{1}H-NMR loses reliability for higher degrees of polymerization (DP) of PEO. In this case, the reliability is insufficient for the PEO-5k-CTA, having a DP of 114. After the second reaction step, a distinct shift of the methine peak (A to a) can be observed upon the substitution of the bromine group with the dithiobenzoate group, leading to PEO-2k-CTA. The initial peak A disappears completely, indicating a high conversion into the desired macro-CTA. The 2D-HMBC spectrum is used to clearly prove the connection of the PEO to the two phenyl units of the chain transfer agent. The squares and circles are key peaks confirming the connection of the PEO to the R-group (phenyl, n', f, g, h) and the CS_2-Z-group moiety (i, k, l, m', p').

SEC and MALDI-ToF of diblock copolymers

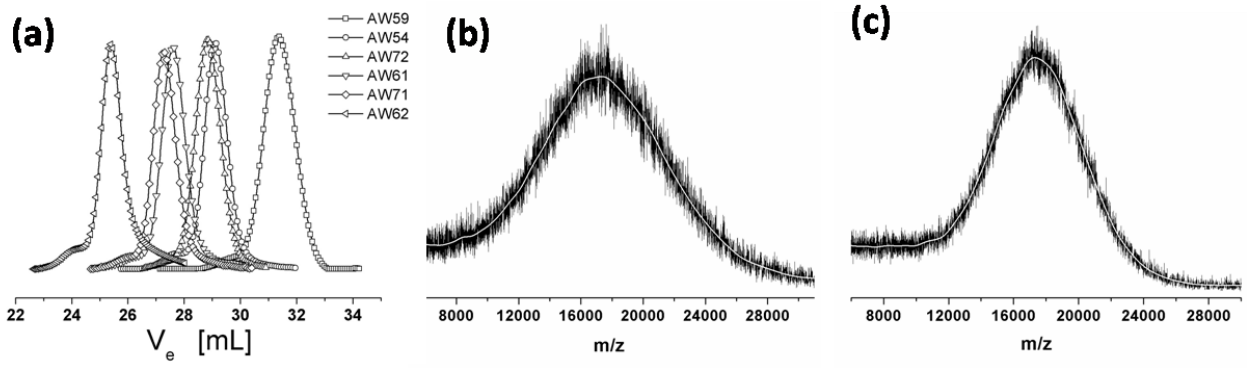

Figure Sup 6 - 2. SEC elution traces of PEO-*block*-PnBuA block copolymers. MALDI-ToF spectra of AW-72 (b) and AW-54 (c)

Samplec code	Composition
AW-59	PEO45-PnBuA29
AW-54	PEO45-PnBuA100
AW-72	PEO114-PnBuA105
AW-61	PEO114-PnBuA201
AW-71	PEO114-PnBuA250
AW-62	PEO114-PnBuA778

.

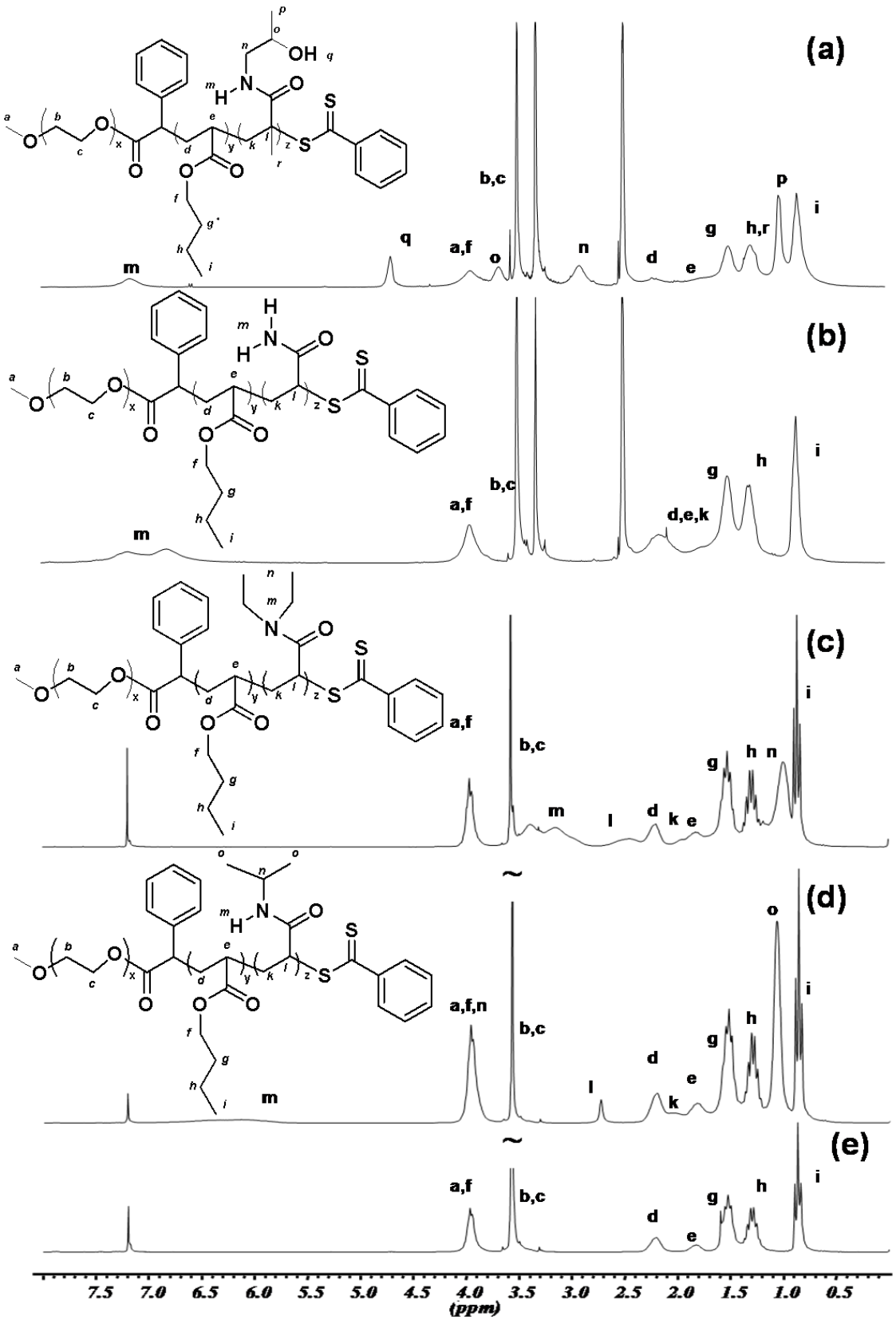

Figure Sup 6 - 3. Representative ^{1}H-NMR spectra of PEO-*block*-PnBuA-*block*-PHPMA (a), PEO-*block*-PnBuA-*block*-PAAm (b), PEO-*block*-PnBuA-*block*-PDEAAm (c), PEO-*block*-PnBuA-*block*-PNIPAAm (d) triblock terpolymers and PEO-*block*-PnBuA diblock (e) copolymers. Spectra (a) and (b) were recorded in d_6-DMSO due to the limited solubility of the block terpolymers in $CDCl_3$.

MALDI-ToF spectra of block terpolymers

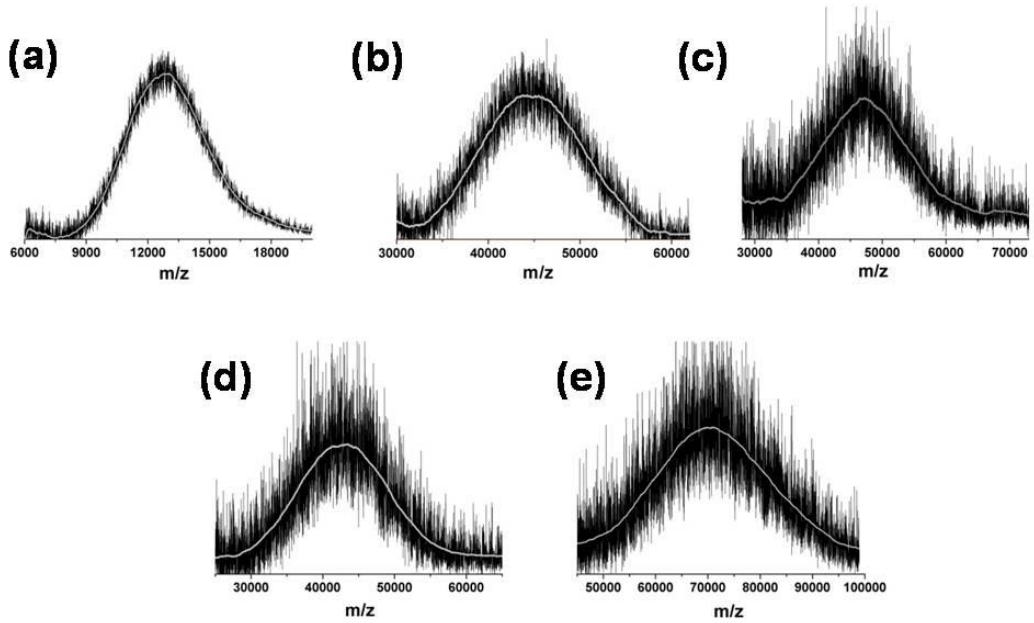

Figure Sup 6 - 4. MALDI-ToF spectra of PEO45-PnBuA29-PNIPAAm46 (a), PEO114-PnBuA105-PNiPAAm195 (b), PEO114-PnBuA250-PNIPAAm82 (c), PEO114-PnBuA105-PDEAAm181 (d), PEO114-PnBuA250-PDEAAm200 (e).

Continuous solubility change with increasing length of the third block

Due to the polymerization of a highly polar block, the solubility is changed progressively with increasing length of the third block and can thus be used an indicator for the successful block extension. For instance, whereas the diblock copolymers (PEO-*block*-PnBuA) of any composition are perfectly soluble in THF, $CHCl_3$ and dioxane, an increase in the block length of the third block leads to prolonged times for dissolution or simply results in insolubility for longer blocks of PHPMA and PAAm. Similarly, the diblock copolymers hardly dissolve in DMSO, mostly as a highly viscous liquid or a gel, requiring several hours, days or even weeks for complete dissolution. With increasing degree of polymerization of the third block, the triblock terpolymers dissolve more rapidly for the longest PHPMA and PAAm blocks. Consequently, this continuous change in the solubility behavior points to a controlled chain extension with a controlled growth of the third block with increasing conversion.

7. TOWARDS APPLICATION OF JANUS PARTICLES: EMULSION POLYMERIZATION USING JANUS PARTICLES AS STABILIZERS

Andreas Walther, Martin Hoffmann, Axel H. E. Müller

Makromolekulare Chemie II and Bayreuther Zentrum für Kolloide und Grenzflächen, Universität Bayreuth, D-95440 Bayreuth, Germany

Andreas.Walther@uni-bayreuth.de; *Axel.Mueller@uni-bayreuth.de*

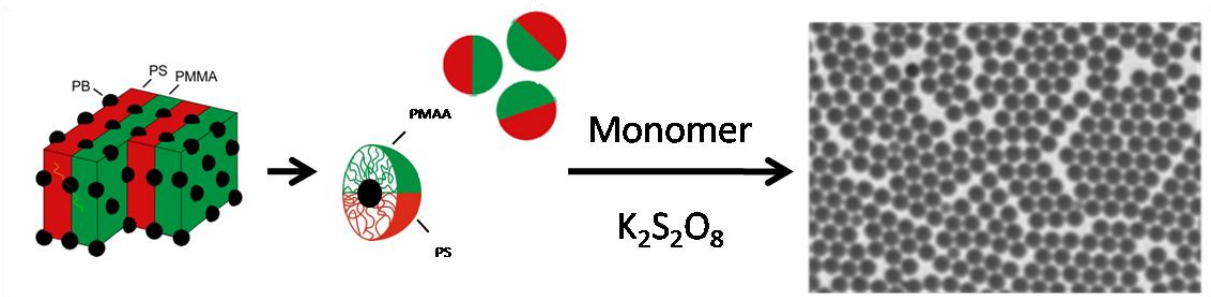

Published in *Angewandte Chemie International Edition,* **2008**, 47, 711.

Janus particles (JP) are compartmentalized colloids which possess two sides of different chemistry or polarity. These particles have moved into the focus of various research groups ranging from physics, chemistry to biological science. One of the major challenging aspects regarding the synthesis of such particles still is the production of larger quantities in order to allow investigations of their application possibilities. Several two-dimensional techniques such as sputtering or micro-contact printing only lead to a small amount.[1, 2] On the contrary, the template-assisted pathway using well-defined microphase segregated block terpolymer templates yields JP of different architectures in considerable quantities.[3-6] More recently, site-specific modification of Pickering emulsions, electro-spinning and up-scaled microfluidic devices may be used to create larger amounts.[7-11] Thus, major synthetic challenges in the production of JP may be overcome in the near future.

JP are interesting for a variety of reasons, one of them being the self-organization into complex and well-defined assemblies. Possible applications range from physics, biophysics and medicine to display technology.[8, 12-17-18] However, the advanced surface-active properties of particles with a segregated corona over particles with a uniform wettability are most interesting. Binks et al. calculated that the surface activity of a JP is up to three times higher at an oil/water interface than that of a uniform particle, leading to a strengthened adsorption at the interface.[19] Recently, Glaser et al. found that bimetallic JP lead to a significant reduction of the oil/water interfacial tension as compared to similar uniform particles.[20] Thus, the predictions were verified, rendering the surface active properties highly interesting for industrial application.

Herein, we report on the first successful emulsion polymerization using JP as stabilizers. This is the first time that JP are used for application studies which are very close to industrial desire. In recent years much work within the field of emulsion polymerization has been devoted to the introduction of novel polymerization techniques, the generation of novel latex architectures or to the variation of the architecture of the polymeric stabilizer.[21-33] Generally, electrosteric stabilization of polymers is superior to the electrostatic stabilization alone, induced by classical low-molecular weight surfactants such as SDS.[34] However, particles with Janus character have not been used in these studies so far, mainly due to the difficult accessibility of these structures. The application of JP to emulsion stabilization is yet very interesting. These particles uniquely combine the so-called Pickering effect,[35-37] known from particles, with amphiphilicity - similar to block copolymers - induced by the Janus character. Since polymeric star-like JP are used in this study, even the electrosteric stabilization effect is present. The adsorption energy at the interface is expected to be significantly higher than for similar standard particles of uniform wettability or standard polymeric surfactants. Therefore, JP are expected to suppress unwanted aggregation and coalescence more efficiently. This is certainly highly beneficial for a long-term stability as desorption of the stabilizer is minimized.

We prepared the amphiphilic JP by selectively crosslinking the spherical polybutadiene microdomains within a lamella-sphere morphology of a microphase-separated template of a polystyrene-*block*-polybutadiene-*block*-poly(methyl methacrylate) triblock terpolymer (PS-PB-PMMA) and subsequent hydrolysis of PMMA to poly(methacrylic acid) (see Scheme 7 - 1).[3, 4]

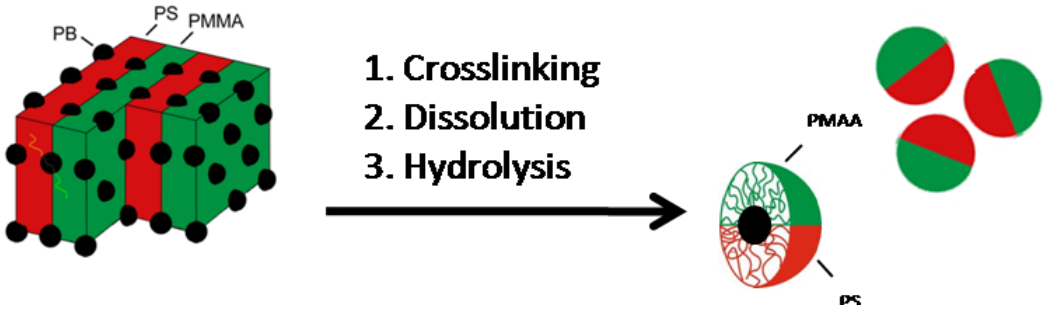

Scheme 7 - 1. Schematic representation of the template-assisted synthesis of spherical JP and their aggregation into superstructures according to their compartmentalization. PB = polybutadiene, PS = polystyrene, PMMA = poly(methyl methacrylate), PMAA = poly(methacrylic acid).

Conventional emulsion polymerizations were carried out in a process adapted from Charleux et al.[33], using $K_2S_2O_8$ as thermal initiator in slightly basic solution (K_2CO_3). Styrene and n-butyl acrylate (nBuA) were selected as monomers, due to the possibility of studying the influence of the glass transition temperature and the interaction between stabilizer and latex particle. PnBuA ($T_g \approx$ - 46 °C) has an unfavorable interaction with the PS part of the stabilizer. To allow a meaningful comparison, the amount of stabilizer was varied, whereas the initiator and monomer concentrations were kept constant. Furthermore, all emulsion polymerizations were allowed to proceed to full conversion as followed by gravimetry and the absence of monomer odor at the end of the polymerization. Note that the JP aggregate into micelle-like assemblies in aqueous solution in the concentration regime used here.[33] The critical aggregation concentration is around 0.05 mg/mL and thus significantly higher than the critical micellization concentration (cmc) of linear amphiphilic block copolymers.

After complete polymerization, the resulting latexes were characterized by transmission electron microscopy (TEM) and dynamic light scattering (DLS, see Table 7 - 1).All reactions containing JP are well controlled and lead to well-defined latexes with long-term stability. In comparison with the soap-free emulsion polymerization (ref.), a striking decrease of the particle size and polydispersity can be observed. The good control is also expressed by the decreasing particle size with increasing amount of stabilizer present in the system, as expected.

Table 7 - 1. Overview of Latex Characterization

Entry	Monomer	JP content [wt%][a]	$\langle R_h \rangle_z$ (PDI)[b] [nm]	R_n R_w/R_n[c] [nm]	A_{JP}[d] [nm^2]	$N_{ad,JP}$[e]
Ref.	Styrene	0	-	987 (1.15)	-	-
1	Styrene	0.51	147 (1.02)	129 (1.010)	16900	12
2	Styrene	1.96	112 (1.01)	95 (1.005)	6210	18
3	Styrene	3.88	91 (1.01)	81 (1.010)	3750	22
4	n-BuA	0.51	198 (1.01)	-	-	-
5	n-BuA	1.96	189 (1.01)	-	-	-
6	n-BuA	3.97	163 (1.05)	-	-	-

[a] Relative percentage of JP to monomer. [b] Obtained by DLS. [c] Statistical calculation based on the TEM micrographs. [d] Average surface area, which is stabilized by one JP (see exp. section). [e] Number of JP adsorbed onto one latex particle.

For instance, in the case of PS, the hydrodynamic radius decreases from ca. 147 nm for 0.5 wt% to 91 nm for 4 wt% of JP stabilizer (Figure 7 - 1). The hydrodynamic radii are smaller for the polymerization of styrene as compared to n-butyl acrylate. This indicates a better performance of the stabilizer for styrene as monomer, which is expected as polystyrene is a high T_g material, thus enabling a firm attachment of the PS part of the JP. Furthermore, the resulting PS latex particles do not have any unfavorable interaction with the PS side of the JP as it is the case for PnBuA. This also leads to a lower tendency for the JP to desorb from the interface. The difference in the radii obtained by DLS and TEM can be understood considering the polyelectrolyte character of the stabilizer. The polyelectrolyte chains are partially extended under the conditions of the DLS measurements (high pH, moderate salinity), whereas they are collapsed in the dried state. Thus, the values obtained by TEM are closer to the real radius of an actual PS latex sphere

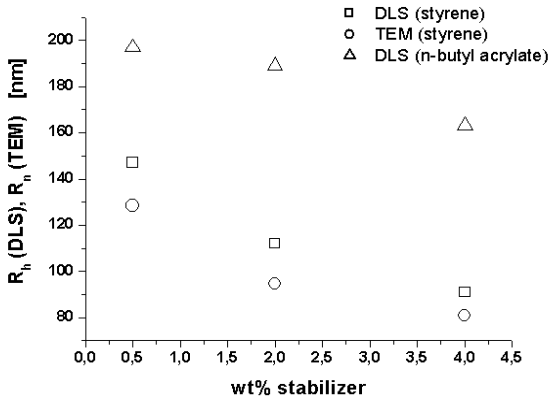

Figure 7 - 1. Dependence of the hydrodynamic radius (DLS) and the number average-radius (TEM) of the latex particles as a function of the stabilizer amount. The data are given for styrene and n-butyl acrylate as monomers as indicated within the Figure.

The polydispersity of an emulsion system is another measure to estimate the efficiency of a stabilizer. Figure 7 - 2 displays the autocorrelation functions and CONTIN plots for the PS latexes obtained at three different amounts of JP (0.5 wt%, 2 wt%, 4 wt%). The CONTIN plots show very narrow unimodal peaks and the polydispersities of the samples can be estimated by the cumulant analysis of the samples to yield very low values of 1.01 – 1.02, indicating the generation of nearly monodisperse particles.

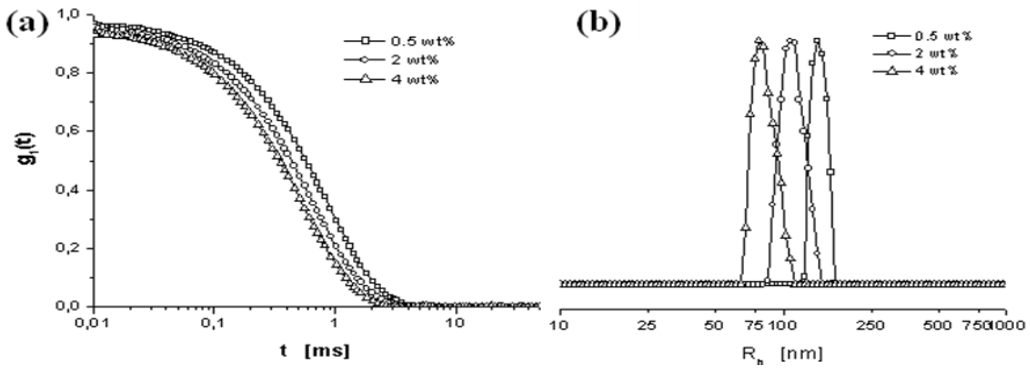

Figure 7 - 2. Autocorrelation functions and CONTIN plots obtained for the emulsion polymerizations of styrene after full conversion.

Statistical TEM analysis of the PS latexes verifies the monodispersity with values of R_w/R_n = 1.005 – 1.01. The PnBuA latexes cannot be reliably analyzed via TEM due to their soft constitution. The results confirm an exceptionally good performance of the JP in the emulsion polymerization of styrene and n-butyl acrylate. Strikingly, the particles assemble into regularly packed assemblies, although the liquid is blotted away fast and not evaporated slowly, as it is usually done for the creation of 2D colloidal crystals. This observation confirms the high monodispersity of the latex particles. (see Figure 7 - 3).

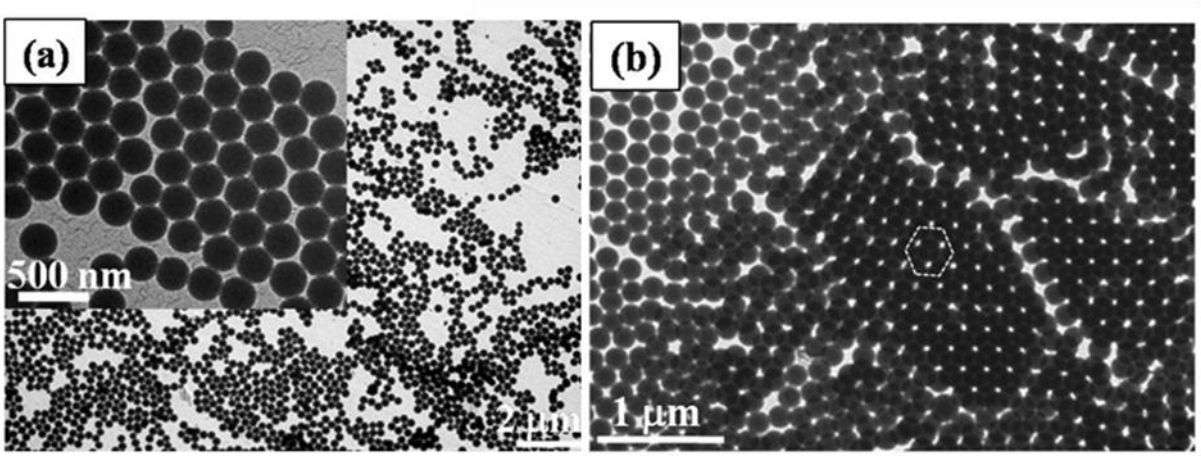

Figure 7 - 3. TEM micrographs for polystyrene latexes with a stabilizer content of 0.5 wt% (a) and 4 wt% (b). A double layer of particles can be seen in the lower micrograph. The hexagon guides the eye for a better recognition of the well ordered pattern.

From the radii of the actual PS latex beads, we calculated the average surface area, A_{JP}, stabilized by one JP (Table 7 - 1 and Figure 7 - 4). Interestingly, A_{JP} decreases with increasing amount of stabilizer. The value obtained at very low stabilizer content (~ $1.7 \cdot 10^4$ nm^2) is remarkably high, considering that the JP possess a cross section of only ca. 1300 nm^2 ($R_h \approx 10$ nm).[3, 4] Consequently, the area which is stabilized by one JP significantly exceeds the cross section, independent of the stabilizer concentration used. This leads to the conclusion that all JP are adsorbed at the interface, which is not always the case for standard Pickering emulsions.[38] Certainly this positive effect of enhanced adsorption can be ascribed to the amphiphilic Janus character of the stabilizing particles and the accompanying high adsorption energy at the interface. The particle coverage on the latexes is loose with a fair amount of uncovered surface. A comparison of the latex particle size with the average surface area per particle, A_{JP}, shows that only 12 to 22 JP per latex particle are necessary for stabilizing the dispersion at the lowest content of stabilizer. Since stable dispersions can be obtained, the JP act as excellent stabilizers.

The number of adsorbed JP per latex particle, $N_{ad,JP}$, lies within the range of the number of JP which form a micellar superstructure in water (28 – 38).[3, 4] Thus, the number of latex particles produced is similar to the number of supermicelles. Therefore, a first indication on the mechanism can be deduced. Most likely, in a first step, the superstructures act as a seed for the emulsion polymerization. Since $N_{ad,JP}$ varies and is slightly lower than for the supermicelles, the system has a dynamic character as well.

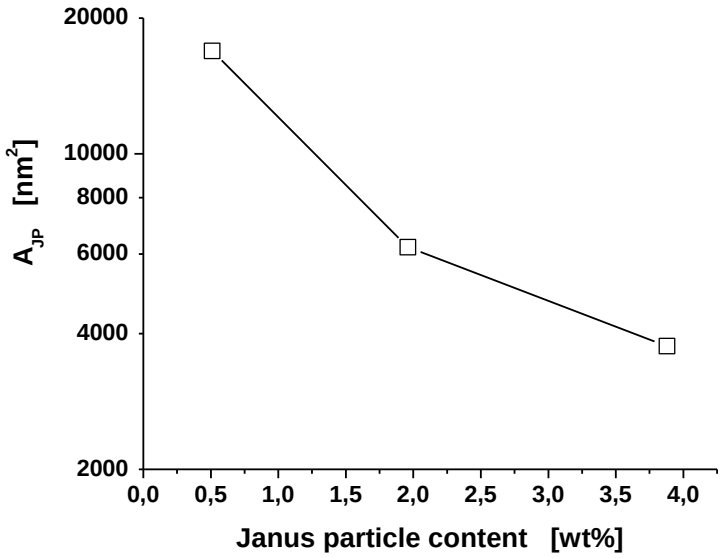

Figure 7 - 4. Dependence of the average surface area, AJP, which is stabilized by one JP as a function of the stabilizer content for polystyrene latexes. The line serves to guide the eye.

A comparison of the good performance of the JP with known systems is desired, however not straightforward due to the novelty. Similar work concerning Pickering emulsion polymerization was for instance performed by Landfester et al.[39] and Bon et al.,[40] who employed silica particles or clay platelets with similar sizes as the JP used. Their emulsion polymerizations suffered from coagulation and the miniemulsion technique was required to obtain stable dispersions. In the case of silica, successful emulsion polymerizations were only possible in the presence of 4-vinylpyridine as comonomer in order to ensure some attractive interaction between polymerizing latex particle and silica beads. In this case, using JP as stabilizers, stable dispersions can be obtained easily with simple conventional emulsion polymerization independently of the monomer used. Concerning a comparison with amphiphilic block copolymers, a scientifically correct and fair assessment of the performance can be made by comparing the molar concentrations of stabilizer used with the obtained particle sizes. Due to the high molar mass of the polymeric JP, the emulsion polymerizations were conducted at extremely low molar concentrations of stabilizer (~10^{-7} mol/L). In the field of block copolymers, such low concentrations are uncommon for the emulsion polymerization and reference values thus hardly exist. The typical concentration range of standard stabilizers is in the region of ~10^{-4} mol/L.[28, 33] Hence, it is highly doubtful that emulsion polymerizations with block copolymer stabilizers might be able to yield comparable particle sizes and low polydispersities, even if similarly low concentrations of block copolymer stabilizer were used and led to stable dispersions at all.

The development of a reference system for the JP, investigations of their performance in the emulsion polymerization, as well as of the complex mechanism of the Pickering emulsion polymerization using JP are underway and will be reported separately in a full article.

In conclusion, for the first time, JP have been applied to the emulsion polymerization of different monomers, an industrially most relevant topic. The emulsion polymerizations can be conducted in a facile fashion and do not require additives or miniemulsion polymerization technique as other Pickering emulsion polymerizations. The resulting latex dispersions show very well controlled particle sizes with extremely low polydispersities. The particle size decreases with

increasing content of stabilizer. A detailed analysis of the surface coverage of the latex particles reveals a loose coverage of the latex surface by the JP. The surface area stabilized by one JP exceeds its cross section several times. A comparison with the literature strongly indicates a superior performance of the JP in emulsion polymerization and renders this material highly interesting for fundamental studies and for future wide-spread industrial applications.

References

1. Cayre, O.; Paunov, V. N.; Velev, O. D. *Chem. Commun.* **2003**, 2296.
2. Paunov, V. N.; Cayre, O. J. *Adv. Mater.* **2004,** 16, 788.
3. Erhardt, R.; Zhang, M.; Böker, A.; Zettl, H.; Abetz, C.; Frederik, P.; Krausch, G.; Abetz, V.; Müller, A. H. E. *J. Am. Chem. Soc.* **2003,** 125, 3260.
4. Erhardt, R.; Böker, A.; Zettl, H.; Kaya, H.; Pyckhout-Hintzen, W.; Krausch, G.; Abetz, V.; Müller, A. H. E. *Macromolecules* **2001,** 34, 1069.
5. Liu, Y.; Abetz, V.; Müller, A. H. E. *Macromolecules* **2003,** 36, 7894.
6. Walther, A.; André, X.; Drechsler, M.; Abetz, V.; Müller, A. H. E. *J. Am. Chem. Soc.* **2007,** 129, 6187.
7. Roh, K.-H.; Martin, D. C.; Lahann, J. *Nat. Mater.* **2005,** 4, 759.
8. Roh, K.-H.; Yoshida, M.; Lahann, J. *Langmuir* **2007,** 23, 5683.
9. Shepherd, R. F.; Conrad, J. C.; Rhodes, S. K.; Link, D. R.; Marquez, M.; Weitz, D. A.; Lewis, J. A. *Langmuir* **2006,** 22, 8618.
10. Nie, Z.; Li, W.; Seo, M.; Xu, S.; Kumacheva, E. *J. Am. Chem. Soc.* **2006,** 128, 9408.
11. Dendukuri, D.; Pregibon, D. C.; Collins, J.; Hatton, A. T.; Doyle, P. S. *Nat. Mater.* **2006,** 5, 365.
12. Behrend, C. J.; Anker, J. N.; McNaughton, B. H.; Kopelman, R. *J. Magn. Magn. Mater.* **2005,** 293, 663.
13. Choi, J.; Zhao, Y.; Zhang, D.; Chien, S.; Lo, Y. H. *Nano Lett.* **2003,** 3, 995.
14. Anker, J. N.; Behrend, C.; Kopelman, R. *J. Appl. Phys.* **2003,** 93, 6698.
15. Behrend, C. J.; Anker, J. N.; Kopelman, R. *Appl. Phys. Lett.* **2004,** 84, 154.
16. Behrend, C. J.; Anker, J. N.; McNaughton, B. H.; Brasuel, M.; Philbert, M. A.; Kopelman, R. *J. Phys. Chem. B* **2004,** 108, 10408.
17. Nisisako, T.; Torii, T.; Takahashi, T.; Takizawa, Y. *Adv. Mater.* **2006,** 18, 1152.
18. Golestanian, R.; Liverpool, T. B.; Ajdari, A. *Phys. Rev. Lett.* **2005,** 94, 220801.
19. Binks, B. P.; Fletcher, P. D. I. *Langmuir* **2001,** 17, 4708.
20. Glaser, N.; Adams, D. J.; Böker, A.; Krausch, G. *Langmuir* **2006,** 22, 5227.
21. Freal-Saison, S.; Save, M.; Bui, C.; Charleux, B.; Magnet, S. *Macromolecules* **2006,** 39, 8632.
22. Manguian, M.; Save, M.; Charleux, B. *Macromol. Rapid Commun.* **2006,** 27, 399.
23. Mock, E. B.; Bruyn, H. D.; Hawkett, B. S.; Gilbert, R. G.; Zukoski, C. F. *Langmuir* **2006,** 22, 4037.
24. Nicolas, J.; Charleux, B.; Guerret, O.; Magnet, S. *Macromolecules* **2005,** 38, 9963.
25. Pusch, J.; van Herk, A. M. *Macromolecules* **2005,** 38, 6909.
26. Ferguson, C. J.; Hughes, R. J.; Nguyen, D.; Pham, B. T. T.; Gilbert, R. G.; Serelis, A. K.; Such, C. H.; Hawkett, B. S. *Macromolecules* **2005,** 38, 2191.
27. Nicolas, J.; Charleux, B.; Guerret, O.; Magnet, S. *Angew. Chem. Int. Ed.* **2004,** 43, 6186.
28. Save, M.; Manguian, M.; Chassenieux, C.; Charleux, B. *Macromolecules* **2005,** 38, 280.
29. Smulders, W.; Monteiro, M. J. *Macromolecules* **2004,** 37, 4474.
30. Fujii, S.; Randall, D. P.; Armes, S. P. *Langmuir* **2004,** 20, 11329.

31. Detrembleur, C.; Debuigne, A.; Bryaskova, R.; Charleux, B.; Jerome, R. *Macromol. Rapid Commun.* **2006,** 27, 37.
32. Houillot, L.; Nicolas, J.; Save, M.; Charleux, B.; Li, Y.; Armes, S. P. *Langmuir* **2005,** 21, 6726.
33. Burguière, C.; Pascual, S.; Bui, C.; Vairon, J.-P.; Charleux, B.; Davis, K. A.; Matyjaszewski, K.; Bétrémieux, I. *Macromolecules* **2001,** 34, 4439.
34. Gilbert, R., *Emulsion Polymerization - A Mechanistic Approach*. Academic Press: London, **1995**.
35. Wamsdon, W. *Proc. R. Soc. London* **1903,** 72, 156.
36. Pickering, S. U. *J. Chem. Soc.* **1907,** 91, 2001.
37. Binks, B. P. *Curr. Opin. Coll. Int. Sci.* **2002,** 7, 21.
38. Saleh, N.; Sarbu, T.; Sirk, K.; Lowry, G. V.; Matyajeszewski, K.; Tilton, R. D. *Langmuir* **2005,** 21, 9873.
39. Tiarks, F.; Landfester, K.; Antonietti, M. *Langmuir* **2001,** 17, 5775.
40. Cauvin, S.; Colver, P. J.; Bon, S. A. F. *Macromolecules* **2005,** 38, 7887.
41. Zhang, L.; Barlow, R. J.; Eisenberg, A. *Macromolecules* **1995,** 28, 6055.

Supporting Information

Experimental Section

Materials

Styrene (S; Sigma-Aldrich, 99+%) and n-butyl acrylate (Sigma-Aldrich, 99+%) were destabilized by passing through a basic alumina column and purged with nitrogen for 30 minutes before use. Potassium persulfate ($K_2S_2O_8$; Sigma-Aldrich, 99+%) and potassium carbonate (K_2CO_3; Merck, >99%) were used without further purification. The Janus particles were obtained by free radical crosslinking of a lamella-sphere morphology of a polystyrene-*block*-polybutadiene-*block*-poly(methyl)methacrylate triblock terpolymer in the bulk state. After alkaline hydrolysis, the particles contain two hemispheres, polystyrene and polymethacrylic acid. The two sides consist each of ca. 13 chains which are attached to a central crosslinked particular polybutadiene core. They core is surrounded by about 13 chains each of PS (DP = 800) and PMMA (DP = 700), which are phase-separated. In order to dissolve the particles in water, dialysis from a good solvent for both blocks to the selective solvent water is required. After step-wise dialysis from dioxane/methanol = 8/2 v/v into water, the particles were freeze-dried. The behaviour of polystyrene containing block copolymers and their micelles were deeply investigated by Eisenberg et al.[41] Further details of the preparation of the Janus micelles can be found elsewhere.[3, 4]

Emulsion Polymerisation

For the preparation of the solutions, the Janus particles at the desired concentration were dissolved in an aqueous solution, containing K_2CO_3 (0.02 mol/L), degassed by N_2 bubbling and stirred for at least 12 hours at 70 °C in 10 – 15 ml glass bottles. Afterwards, styrene or n-butyl acrylate (10 wt%) as a monomer was added with a syringe and the system was allowed to equilibrate for 2 hours. Adding of $K_2S_2O_8$ solution to give a final concentration of c = 0.01 mol/L initiated the reaction, which was stopped no sooner than 24 hours to get full conversion.

Analytical Techniques

Dynamic light scattering (DLS) was performed on an ALV-CGS-8F goniometer with an ALV-5000/E WIN Multiple Tau Digital Correlator and a He-Ne laser (632.8 nm) at a scattering angle of 90° and room temperature. For sample preparation all emulsions were highly diluted with a 0.1 M sodium chloride solution at pH 10. Bright field transmission electron microscopy (TEM) was performed using Zeiss CEM 902 and LEO 922 OMEGA electron microscopes operating at 80 kV and 200 kV, respectively. For sample preparation, a droplet of diluted aqueous latex solution was deposited onto a hydrophilized carbon-coated Cu grid.

Calculations

The final density of particles N_p (dm^{-3}) was calculated according to equation (I) with the number average radius, R, obtained by TEM (ρ_p = 1.05 g cm^{-3}; density of polystyrene). τ_p reflects the content of solid after full polymerization of styrene.

$$(I) \qquad N_p = \frac{6\,\tau_p}{\pi\,\rho_p\,2R_p^3}$$

The average surface area stabilized by one Janus particle, A_{JP}, was calculated using equation (II), in which N_{JP} denotes the number of Janus beads per dm^3. N_{JP} can be calculated using the overall molecular weight of the JP and the concentration used.

$$(II) \qquad A_{JP} = 4\pi\,R^2\,N_p / N_{JP}$$

The average number of adsorbed Janus particles per latex particle, $N_{ad,JP}$ is calculated by dividing the surface area of a latex particle by the area stabilized by one Janus particle, A_{JP}.

8. Engineering Nanostructured Polymer Blends with Controlled Nanoparticle Location using Janus Particles

Andreas Walther, Kerstin Matussek, Axel H. E. Müller

Makromolekulare Chemie II and Bayreuther Zentrum für Kolloide und Grenzflächen, Universität Bayreuth, D-95440 Bayreuth, Germany

Andreas.Walther@uni-bayreuth.de; Axel.Mueller@uni-bayreuth.de

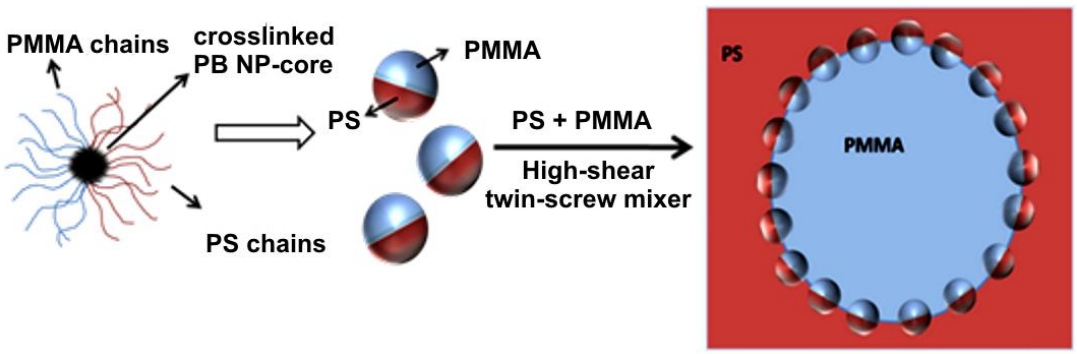

Published in *ACS NANO*, **2008**, 2, 1167.

Abstract

Janus particles are used on a multi-gram scale for the blend compatibilization of two polymers in a twin screw mini-mixer. It is shown that the Janus particles can be located exclusively at the interface of the two polymer phases despite the high temperature and shear conditions. The domain sizes of the dispersed phase decrease with increasing content of Janus particles. The decrease is yet ongoing for high contents of Janus particles. Furthermore, the biphasic particles exhibit an ordered arrangement at the interface. Thus, the approach demonstrates that a nanoscopic structuring of the interface can be achieved under macroscopic processing conditions. The structural order occurs on two levels. The first is the complete adsorption at the interface and the second is the lateral ordering at the interface. The strong adsorption at the interface is explained in terms of the increased desorption energy of Janus particles. Secondly, the compatibilization efficiency is critically compared to state-of-the-art compatibilizers. The efficiency of the Janus particles is found to be superior as compared to block copolymer based compatibilizers. The efficiency gap between Janus particles and block copolymer compatibilizers widens for larger amounts added.

Introduction

The combination of polymer properties by blending is one of the most attractive ways for obtaining new products with superior material properties, such as for tailoring the electronic, mechanical or optical properties. This does not only hold for large-scale industrial applications, but also for scientific problems as for instance in the case of polymer blend solar cells. In both fields, there is a constant search for novel and better ways of compatibilization [1, 2] The major challenging difficulty is to overcome the inherent immiscibility of polymers by using compatibilizing agents to allow for a sufficient mixing into nanoscopically sized domains of the dispersed phase. In industry, most commonly reactive blending or, similarly, the addition of block copolymers is used for compatibilizing the two components. One of the major drawbacks of this approach is that much of the block copolymer stabilizer does not adsorb at the interface and is lost during the high shear extrusion process, thus significantly increasing the cost of the polymer blend.[3-6]

In analogy to colloid science, we conceived of a novel concept of compatibilizing polymer blends and for controlling the location of the particles within the blend structure. In recent years, several publications have appeared discussing the superior surface-active properties of so-called Janus particles (JPs).[7] Janus particles are compartmentalized colloidal particles, which show segregation into two hemispheres. These particles uniquely combine the so-called Pickering effect with amphiphilicity and are thus known as surfactant particles.[8] It has been calculated and experimentally shown for liquid-liquid interfaces that these particles adsorb strongly at interfaces, in particular stronger than standard surfactants or homogeneous particles.[7, 9-11] Triggered by these stimulating results, we applied Janus particles, having one PS and one PMMA side, for the blend compatibilization of PS and PMMA.

Generally, nanocomposites, i.e. nanoparticle-filled block copolymers and homopolymers have been attracting increasing interest in the past years, which was triggered by several interesting theoretical and experimental contributions. Very important contributions for a fundamental understanding of nanocomposites were for instance published by Mackay and co-workers[12], who analyzed the miscibility of polymers with nanoparticles in dependence of their relative sizes, meaning radii of gyration. In essence, they found that polymeric nanoparticles are completely miscible with a matrix material as long as the particle radius is smaller than the radius of gyration of the polymer used as matrix. They proposed an enthalpic gain due to an increase in molecular contacts at the dispersed nanoparticle surfaces as compared with the surface of phase-segregated nanoparticles. With increasing the nanoparticle size above the coil dimensions of the polymeric materials, the particles are expelled from the matrix and large-scale phase separation occurs. In terms of block-copolymer nanoparticle composite materials, it was shown by Thompson *et al.* that in the absence of any specific (enthalpic) interactions, larger particles are expelled from the bulk phase.[13] This is caused by a loss of conformational entropy, because the polymer chains must stretch around the solid particles. This penalty increases with rising particles size. In the case of binary polymer blends containing polymers A and B, it should first be distinguished between blends containing particles, which are preferentially attracted by one component (*e.g.* polymer A) and particles which are attracted similarly to both components. For the first system, Ginzburg and co-workers stated that a decrease of the particle size, smaller

than the radius of gyration would have a beneficial effect on compatibilizing a mixture.[14, 15] However, in the latter case, when the interfacial tension between the polymers A and B, γ_{AB}, exceeds the difference of the interfacial tension of a colloid C with the two components, $\gamma_{AB} > |\gamma_{CA} - \gamma_{BC}|$, the situation is different. The system is then largely dominated by the interfacial tension between the two blend components. Hore *et al.*[16] found that large scale phase separation is favored for low interfacial tensions between the two mixture components, simply because of an insufficient adsorption of the nanoparticles. The tendency of a particle to migrate and stick to an interface scales with the interfacial tension of A and B, γ_{AB}, and with the square of the particle radius. Consequently, the compatibilization of the system is better for larger particles as they cannot be removed so easily from the interface once they are adsorbed.

In conclusion, a complex interplay between enthalpic and entropic contributions governs the dispersion and location of particles in polymers, block copolymers and polymer blends.

With respect to materials science, nanocomposites represent a very promising and also in some cases cost-effective way of structuring hybrid materials and obtaining high-performance properties.[17-19] For instance, nanoparticles can be used to positively alter processing conditions,[20] mechanical properties such as toughness[21] or crack characteristics,[22, 23] or to change the electronic[24-26] and optical properties.[27, 28] To achieve better materials, control in the precise location of the nanoparticles is essential.

Recently, Kramer and co-workers[29-35] showed that a control of the location and spatial distribution of homogeneously coated gold nanoparticles (polystyrene or poly(2-vinylpyridine chains as corona) within one phase of a polystyrene-*block*-poly(2-vinylpyridine) (PS-*b*-PVP) diblock copolymer can be achieved by changing the grafting density, the added volume fraction of particles as well as the block copolymer molecular weight. For small grafting densities of PS or in case of particles grafted with a mixture of PVP and PS polymers, the particles are predominantly located at the interface. The results suggested a redistribution of the coronal chains into a surfactant-like particle. However, in order to obtain these results very mild film casting processes were required that would allow for a suggested redistribution of the corona chains. Moreover, the process is limited to a small scale, both caused by the relatively limited film casting process and secondly by the complex nanoparticle synthesis.

Herein, we will demonstrate two major results. First, a superior performance of Janus particles for compatibilizing polymer blends under high-shear conditions in a twin-screw miniature mixer, utilizing Janus particles on a *multi-gram* scale. Secondly, we will show how to overcome problems in the precise positioning of particles in polymer blends. So far, success in the controlled and exclusive location of particles at interfaces under aggressive conditions remains limited. However, with this approach, we will illustrate that the location of the Janus particles can be effectively controlled on the nanoscale, whereas the processing parameters are applicable to macroscopic production constraints.

Results and Discussion

Janus Particles and their Behaviour in a Homopolymer

The Janus particles in this study were prepared by crosslinking the well-defined lamella-sphere bulk structure of a polystyrene-*block*-polybutadiene-*block*-poly(methyl methacrylate) triblock terpolymer (SBM), having symmetric end blocks and a very small fraction of polybutadiene. Details of this procedure were published earlier.[36] These Janus particles consist of a tightly crosslinked polybutadiene nanoparticle core with ca. 13 chains each of PMMA and PS protruding out of it. The two polymers are microphase segregated into two hemispheres, leading to a biphasic particle as shown in Scheme 8 - 1.

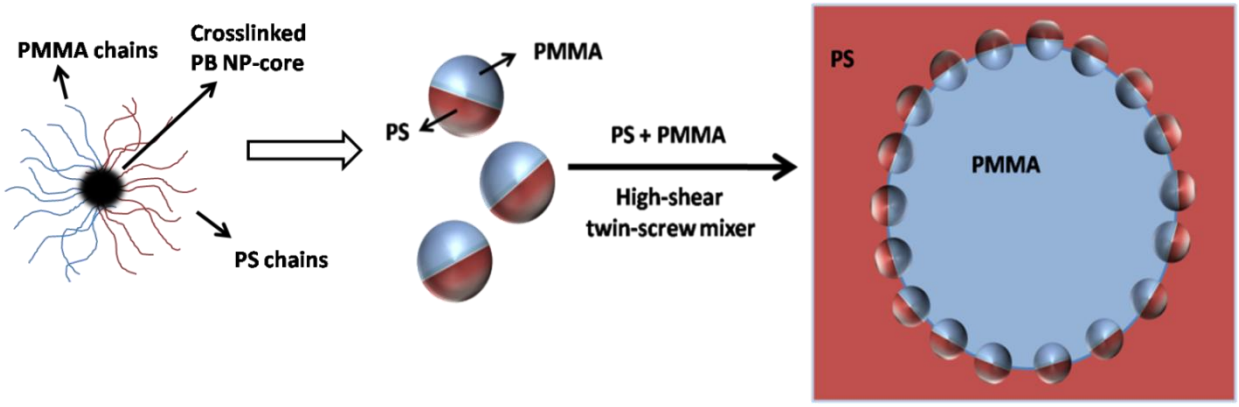

Scheme 8 - 1. Schematic representation of Janus particles and their adsorption at the blend interface of a PS/PMMA blend.

In organic solution, these particles have a number-average hydrodynamic radius of around 10 nm, as found by fluorescence correlation spectroscopy, and are thus of comparable dimensions as the polymers used in this study, PMMA (M_w = 120 kg/mol, PDI = 1.8, $R_g \approx 9.5$ nm) and PS (M_w = 230 kg/mol, PDI = 1.6 $R_g \approx 14.4$ nm). In order to allow drawing meaningful conclusions from the following blend results and from the influence of the Janus character onto their location in the blend, a sufficient mixing of the particles with the matrix component PS has to be assured. In particular, it needs to be shown that large-scale phase separation does not occur, as otherwise, the particles might be preferentially segregated to the blend interface because of their size and therefore less influence of the biphasic Janus character would dominate the results.

Figure 8 - 1 shows a representative non-stained TEM micrograph of Janus particles blended into the PS matrix. At low magnification the TEM images appear completely homogeneous and only for higher magnifications the well-dispersed Janus particles become distinguishable. Large-scale phase separation cannot be detected; in contrast, the Janus particles are predominantly unimolecularly dispersed. Note that also the formation of dimers, trimers or micelle-like aggregates is very limited. The Janus particles are thus well dispersed. The small black dots correspond to the polybutadiene nanoparticle core, which has the highest contrast in TEM, due to its crosslinking with S_2Cl_2. The white shadow on one side is caused by the PMMA side, which is degraded upon e-beam exposure. Apart from allowing a conclusion of the miscibility of the Janus particles with the homopolymer, these images also unambiguously confirm the non-centrosymmetric Janus character of these particles. An analysis of the dimensions of the

structures yields a radius of the polybutadiene nanoparticle core of 3 – 5 nm and a total radius, as judged from the white PMMA shadow, of 20 - 25 nm.

Although the total visible radius is larger than the radius of gyration of the PS matrix, the particles stay well dispersed. Apart from the applied shear, which certainly assists the dispersion, this can be rationalized considering several factors. First, the radius of gyration of the Janus particles is significantly smaller than the visible radius, deduced by TEM. Additionally, only one side is immiscible with the PS phase, which can be seen as a reduction of the radius to almost half of its total dimension. This goes along with a reduction of unfavorable contacts as compared to a homogeneous particle of similar size and different composition as the matrix material. Secondly, only the polybutadiene core is a densely crosslinked impenetrable nanoparticle core, having a radius smaller than the coil dimensions of the PS phase. Furthermore, a penetration of the PS side of the Janus particle by the PS chains of the matrix material is possible, thus further limiting an entropic penalty by chain conformational entropy loss. Another factor in this context, which might play a role, is the fact that the PS matrix material exhibits a high polydispersity, which presumably favors the miscibility.

In conclusion, the Janus particles are well dispersed in the matrix material and hence the influence of the Janus character on the location of the particles in a polymer blend and the compatibilization efficiency can be rationally investigated.

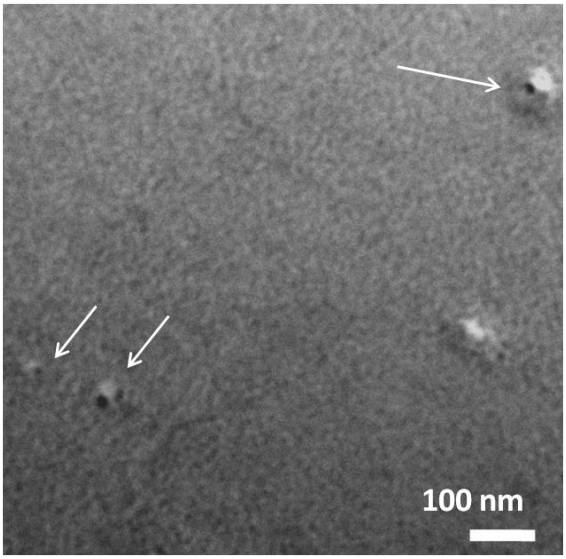

Figure 8 - 1. TEM of Janus particles blended into a PS matrix (2 wt% of Janus particles). The arrows highlight Janus particles.

Janus Particles in PS/PMMA Polymer Blends

Due to the unique combination of amphiphilicity combined with the particle character, Janus particles are expected to strongly adsorb and orient at the interface. The adsorption energy at the interface is significantly enhanced as compared to standard block copolymers, which are commonly used as stabilizers in polymer alloys. To the best of our knowledge, none of the theoretical studies has included Janus particles into their considerations. Note that Janus particles impose another significant enthalpic contribution to the free energy of the system. The interfacial tension between the sides and the respective polymers is negligibly small, whereas the interfacial tensions of the two sides with the unlike blend component is in the region of the interfacial tension of the mixture.

In order to apply this new concept and to study the effect of the Janus particles on the compatibilization of polymer blends, we prepared PS/PMMA blends at weight ratios of 6/4 and 8/2 with various amounts of Janus particles. To allow a meaningful estimation of the performance of the bead-like stabilizer, several polymer blends using linear block copolymers were prepared for comparison.

In a first step, the weight fraction of Janus particles was changed from one to 20 wt% to allow a monitoring of the morphological changes. The mixing parameters like temperature, shear rate and mixing period were kept constant for all mixtures to minimize the experimental errors during the blending and allowing a reliable comparison. Note that the statistical analysis of polymer blends with 8/2 blending ratio leads to more accurate values, as a thermal relaxation of the droplets after blending can be done in order to reduce the shear-induced asymmetry of the dispersed droplets. In case of a blend ratio of 6/4 this is not possible, because the morphology may relax into a co-continuous one after prolonged annealing[37], for which a straightforward droplet analysis cannot be applied anymore. The symmetric blend ratio was additionally chosen though for its significance in terms of tailoring mechanical properties or *e.g.* in polymer solar cells, which would in the best sense require co-continuous morphologies. Furthermore, it was theoretically shown that for different mixing ratios of polymers, the compatibilization efficiency of a given particle can be different.[14]

The SEM and TEM images shown in Figure 8 - 2 give a first overview of the development of the domain sizes of the dispersed phase. The SEM images (PS/PMMA = 6/4) are shown at the same magnification to allow a straightforward overview of the changes occurring with increasing Janus particle content. The magnification of the TEM images (PS/PMMA = 8/2) is changed progressively to allow a good display of the domain sizes. Clearly, the PMMA domains, appearing as dips or white domains in the PS matrix in the SEM and TEM images, respectively, show a distinct and rapid decrease in size. Initially, the number-average domain diameter, D_n, of the reference sample without addition of any stabilizer is in the micrometer range (D_n = 1.8 μm for 6/4 and D_n = 1.1 μm for 8/2). Upon addition of only one percent of Janus particles, a rapid decrease of the domain diameter to an average PMMA domain diameter of D_n = 1.2 μm (6/4) and D_n = 710 nm (8/2) can be observed. This decay steadily continues with increasing amount of compatibilizer and truly nanoscopically sized domains can be obtained. With a further increase of the Janus bead content, a continuous decreases of the domain sizes even below D_n = 140 nm (6/4) and D_n = 80 nm (8/2) for 20 wt% Janus particle content can be observed. Importantly, this

nanostructuring of the polymer blend can be achieved without special high-shear processing units or complex chemical reactions within the blend mixture. Moreover, no optimization of the blending conditions was done, demonstrating furthermore the efficiency of the stabilizer used.

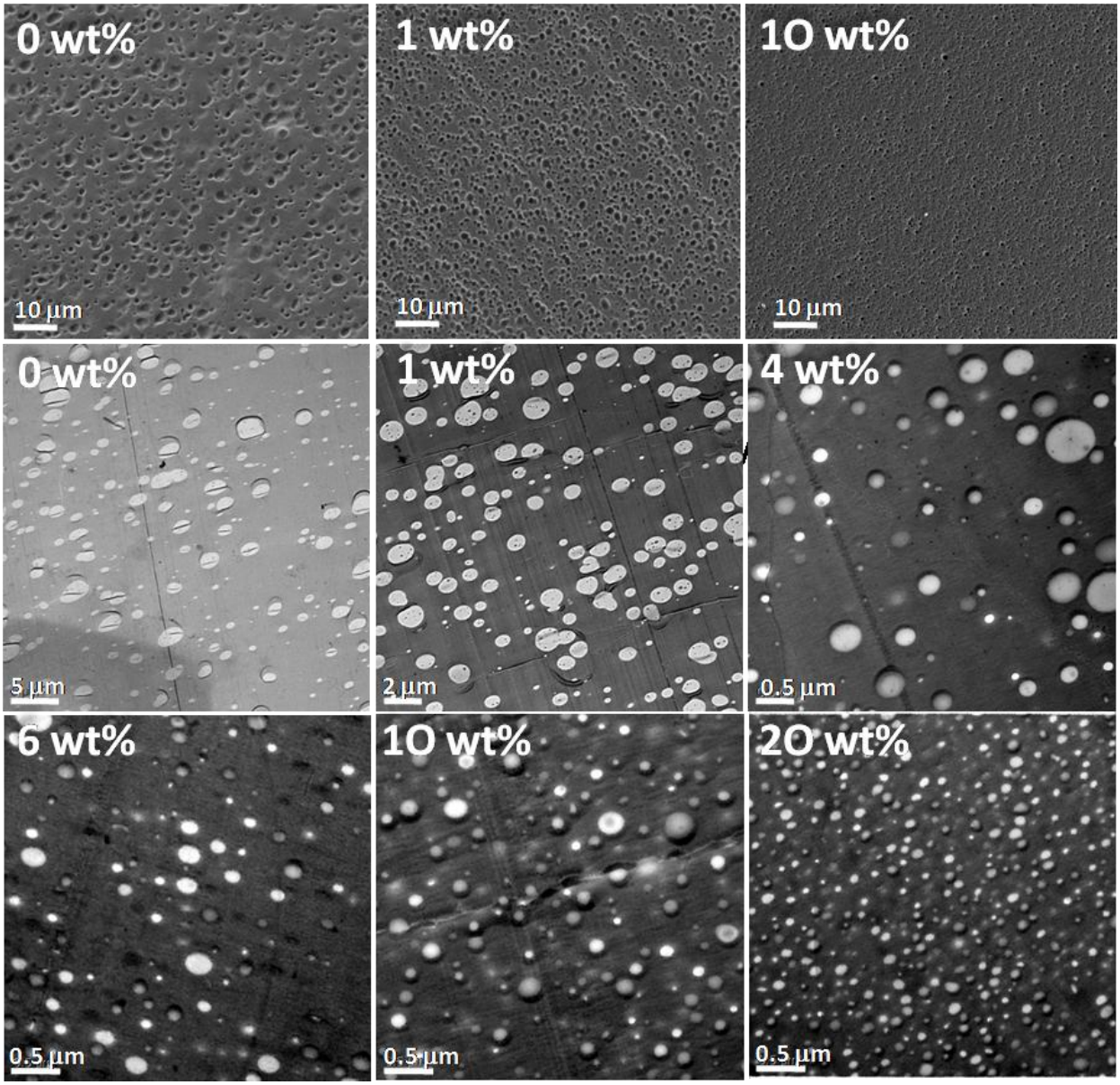

Figure 8 - 2. SEM images obtained for blends at a PS/PMMA ratio of 6/4 (top row). Non-stained TEM images obtained for blends at a PS/PMMA ratio of 8/2 (centre and lower row). The amount of compatibilizer is indicated in each image.

The decay of the number-average domain diameters of the PMMA droplets ($D_{n,PMMA}$), is shown in Figure 8 - 3.

A strong and strikingly rapid decay of the PMMA domain sizes can be observed. The decrease is yet ongoing for high concentrations, indicating an only insignificant loss of stabilizer in one of the blend components. The rapid decay itself is an indication for the presence of a compatibilizer of very high interfacial activity.

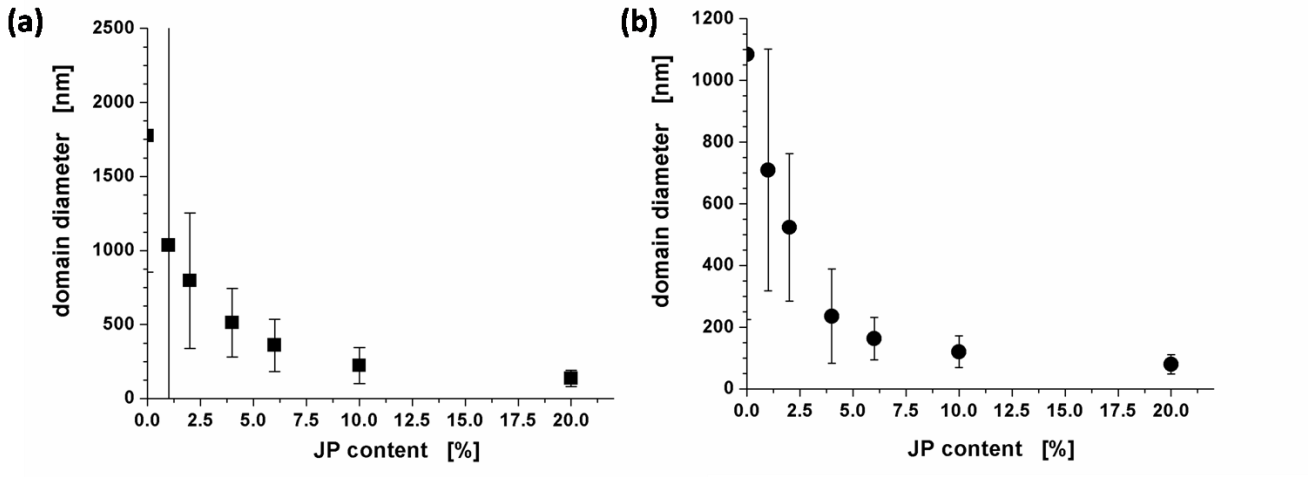

Figure 8 - 3. Decrease of the number-average PMMA domain diameter as a function of the content of Janus particles at PS/PMMA ratios of 6/4 (a) and 8/2 (b). The vertical bars show the standard deviation of the size distribution of the PMMA domains.

In conclusion of the observed decrease of the domain diameter with the increased addition of Janus particles, it is evident that the Janus particles act as stabilizers at the interface of the PS/PMMA blends. Figure 8 - 4 shows a representative overview of two selected TEM images at higher magnification for two different Janus particle contents and two different blending ratios of PS and PMMA. In both images, small black dots can be observed at the interface of the PMMA and PS phases. These small black particles can be identified, in terms of their size, as the cores of the Janus particles. Those cores consist of polybutadiene, which was crosslinked with S_2Cl_2, thus explaining the contrast in TEM. Furthermore, both domains, PS and PMMA, appear homogeneous and hardly any single or aggregated Janus particles within one phase can be found. Note that Janus particles can be clearly identified within the PS or PMMA phase (see *e.g.* Figure 8 - 1).

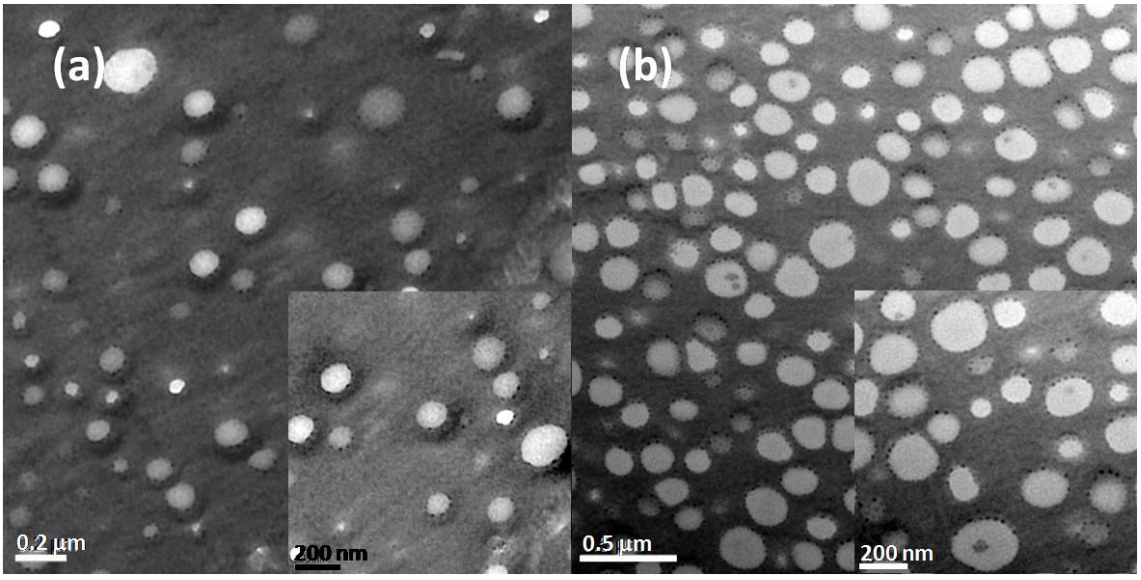

Figure 8 - 4. TEM images obtained for (a) 10 wt% JP in a 8-2 PS/PMMA blend and for (b) 20 wt% JP in a 6/4 PS/PMMA blend.

These observations give a first explanation of the excellent performance of Janus particles as stabilizers in polymer blends. Obviously, the Janus particles are almost exclusively located at the interface and only a negligibly small fraction is "lost" as unimers or micellar aggregates in one of the components, also representing a significant improvement as compared to block copolymer compatibilizers.[3-6] This is a direct consequence of the high interfacial activity and increased adsorption energy at interfaces of Janus particles.

The strong adsorption of Janus particles can be elucidated with an energetic consideration of the system. The surface activity of a particle can be expressed in terms of the desorption energy of the particle from an interface. Binks *et al.* derived an expression for the calculation of the desorption energy of an amphiphilic particle, adsorbed at an interface of two immiscible liquids, based on its surface free energy, E(β).[7]

$$E(\beta) = 2\pi R^2 \left[\gamma(S_{JP}S)(1+cos\alpha) + \gamma(M_{JP}S)(cos\beta - cos\alpha) + \gamma(M_{JP}M)(1-cos\beta) - \frac{1}{2}\gamma(SM)(sin^2\beta)\right]$$

for $\beta \leq \alpha$ (I)

The surface free energy (equation (I)) depends on the immersion depth of the particle at the interface, β , the asymmetry of the biphasic particle, α, and the radius, R, of the particle. A particle is completely immersed into one of the phases for $\beta = 0^o$ and $\beta = 180^o$, and adsorbed along its equator for $\beta = 90^o$. For completely symmetric hemispheres, α approaches 90^o. Furthermore, the equation depends on the various interfacial tensions between the PMMA (M_{JP}) and PS (S_{JP}) side of the Janus particle with the two bulk phases PS (S) and PMMA (M) ($\gamma(S_{JP}S)$, $\gamma(M_{JP}M)$, $\gamma(M_{JP}S)$), as well as on the interfacial tension of the blend components ($\gamma(MS)$). Note that this equation is valid under the condition that the Janus particles are sufficiently smaller than the stabilized domains, allowing the assumption of quasi-planar interfaces. The desorption energy, which is a measure for the interfacial activity of a particle, can be calculated from the energy which is necessary to transfer a particle from the interface to one of the bulk phases (E_{PS} - $E_{interface}$ or E_{PMMA} - $E_{interface}$). Assuming negligible interfacial tensions ($\gamma(S_{JP}S)$, $\gamma(M_{JP}M)$) for the sides of the Janus particle with their respective blend phases and an equatorial adsorption ($\beta = 90^o$) of the indeed completely symmetric Janus particle ($\alpha = 90^o$), the desorption energy for a Janus particle ($E_{JP,des}$) reads as:

$$E_{JP,des} = 2\pi R^2\gamma(SM) + \pi R^2\gamma(SM) = 3\pi R^2\gamma(SM) \quad \text{(II)}$$

Similarly, Pieranski derived an expression for the desorption energy of a homogeneous particle, P,[7, 38] ($\alpha = 0^o$, $E_{hom,des}$). Herein γ(PS), γ(PM) and γ(SM) are the interfacial tensions of the particle with PS and PMMA, and between the two polymers (PS & PMMA), respectively.

$$E_{hom,des} = \pi R^2\gamma(SM)(1-|cos\beta|)^2 \quad \text{with} \quad cos\beta = \frac{|\gamma(PS)-\gamma(PM)|}{\gamma(SM)} \quad \text{(III)}$$

The maximum of the desorption energy, $E_{hom,des}$, can be reached if $|\gamma(PS)-\gamma(PM)| << \gamma(SM)$ and reads as $\pi R^2\gamma(SM)$.

Clearly, these considerations show the stronger adsorption of the Janus particles as compared to homogeneous particles of similar size. The desorption energy of an ideal Janus particle is three

times higher than for a standard particle. This gap widens for asymmetrically (non-equatorially) adsorbed homogeneous particles, which are preferentially wetted by one blend component. In particular for small nanoparticles and higher temperatures, the energetic difference between biphasic and normal particles matters most. Note that the probability of the displacement of a particle from the interface scales with $p \sim exp(-E/kT)$. Therefore, the probability of a Janus particle to desorb from the interface is lower by a factor of $e^3 \approx 20$. Consequently, the biphasic nature of the Janus particles is the origin of a crucial additional energetic contribution and is the reason for a complete adsorption in combination with a firm attachment of the particles at the interface.

In terms of a general applicability of this approach for other polymer blend systems, the Flory-Huggins interaction parameter, χ, can be used rationalize the effect of changing the polymer blend components. This interaction parameter is related to the interfacial tension, γ, of a binary blend system via $\gamma \sim \chi^{1/2}$.[39, 40] *Thus, t*he Flory-Huggins parameter can be directly related to the desorption energies in equations (II) and (III). Following these considerations, the adsorption is favored and simplified for polymer systems with larger unfavorable interaction, χ. Herein, we used a PS/PMMA polymer blend model system with a relatively low incompatibility (χ(SM) ≈ 0.036 at 210 °C,[41] γ(SM) ≈ 1.12 mN/m at 210 °C[42]). Note that a complete particle adsorption at the interface could even be achieved for such a system with relatively low incompatibility for which the location of the particles at the interface is less favored. Most polymer blend systems show a higher incompatibility and would thus lead to a strengthened adsorption at the interface.

In this context, a comparison with previous results in literature is appropriate. Kramer and co-workers[29-35] could show a control of the location of homogeneous particles and mixed (possibly biphasic) particles in block copolymers in one of the phases or predominantly at the interface, respectively. However, they required extremely mild film casting processes in their preparation of the composite materials, which is thus not representative of the conditions used here. Concerning high shear blending, this is the first time that Janus particles are used and so any comparison with literature can be made. For homogeneous particles, it is known that the exclusive location of particles at the interface remains challenging. Often only a fraction of the particles can be located at the interface or there is an incomplete coverage of the interface.[43, 44] Therefore, the order at the interface is low as well and a significant fraction of particles is “lost” in one of the phases and may contaminate the properties of a nanocomposite material. For instance, Vermont *et al.*[44] demonstrated that they could obtain some compatibilization of polyisobutylene /polydimethylsiloxane (PIB/PDMS) blends with silica particles. However, the particles were also located in both phases, particularly in the PDMS phase, thus altering the properties of all phases and resulting in ill-defined nanocomposites. Additionally, the particles did not exhibit any order at the interface. An inversion of the weight fractions of the polymer blend resulted in an unsatisfying compatibilization, demonstrating the need of tailoring the surface chemistry of the particles. Some further success was recently reported by Chung *et al.*[45], who showed that nanoparticles with specifically tailored surface chemistry assembled to a large extent at a polymer blend interface after a soft annealing step in a thin film. After casting of the film, the particles were located in all components. Whether the interfacial adsorption would persist during high shear blending could not be shown, but is at least uncertain.

Aside the strong adsorption of the Janus particles, even an ordering of the particles could be observed. Due to the yet finite thickness of 70 – 90 nm of the ultrathin sections used for the TEM investigations, several circular endcaps of the PMMA droplets can be identified at closer observation of the TEM images. Two of those caps are shown in Figure 8 - 5.

The section analysis in Figure 8 - a shows a core diameter of around 8 – 10 nm, which confirms the black points as the diameter of individual Janus particles. The particles adsorb strongly at the interfaces, but are yet separated from each other by the repellence of their polymer brush-like corona. Both TEM images exhibit an ordered arrangement of the Janus particles (dark dots) at the interface. All Janus particles are separated from each other by a similar centre-to-centre distance of around 30 – 35 nm and are closely packed. The efficient repellence of the Janus particles along the PS/PMMA interface also goes along with a strong reduction of the coalescence of Janus particle stabilized PMMA droplets during the blending process. The exhibited order at the interface is a very interesting observation that would allow a lateral two-dimensional nanoscopic structuring of the interface

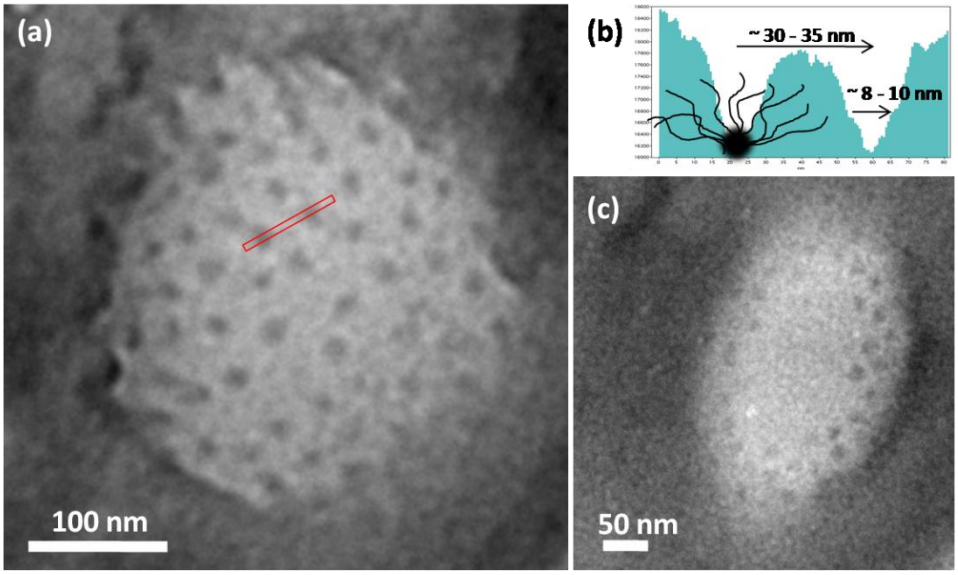

Figure 8 - 5. Endcaps of PMMA droplets with Janus particles located at the interface. (a) and (c) are representative examples at 10 wt% and 6 wt% of JP content in a 6/4 PS/PMMA blend. (b) Section analysis of the red bar shown in image (a). One side of a Janus particle is schematically sketched to show its brush-like character and the location of the polybutadiene core.

These results additionally demonstrate that desired functionalities based on modified Janus particles (*e.g.* bimetallic Janus particles[46]) could be precisely and exclusively located at the blend interface even under the strong shear and high temperature conditions of the twin-screw mini-mixer. In a next step, this implies that particles can be selectively located in the two phases or at the interface, just depending on the fact whether they are homogeneous in their corona or phase-segregated into two hemispheres. This offers a high control for engineering nanocomposite polymer blends of desired compositions and properties.

Comparison with state-of-the-art compatibilizers

Apart from the structuring of the interface, a comparison with existing polymer blend stabilizers is very desirable. In the competitive field of polymer engineering and in particular in polymer blend processing, a novel type of stabilizer will only be of scientific and economic interest if a considerable improvement in the compatibilization can be achieved. Currently, block and graft copolymers are state of the art compatibilizers for polymer blends. The effectiveness of a block copolymer to adsorb and stabilize a polymer blend interface against coalescence depends mainly on its molecular weight, the block ratios and the molecular weights of the blend components. The tendency of migrating to an interface is highest for low-molecular weight polymers, whereas the suppression of coalescence is often best for high molecular weight polymers. Additionally, low molecular weight polymers have a high solubility in the blend components and high molecular weight polymers tend to form micelles, thus representing an obstacle for the compatibilization. This controversy is also expressed in the fact that self-consistent field modeling suggested on the one hand that the interfacial tension of an A/B blend is best reduced for high molecular weight diblocks, thus leading to a strong emulsification.[47] On the other hand, experimental studies find that high molecular weight block copolymers do not give the best results, simply because they are not able to diffuse to the interface in an appropriate time and are trapped in micelles.[5, 48] Therefore, these counteracting forces always need to be balanced carefully for the development of efficient stabilizers.

Generally, the PS/PMMA blend system is a well explored system and thus would, in principal, allow a comparison with the literature.[3, 47, 49-51] However, due to the different experimental conditions for the preparation and the different compatibilizers used, we decided to establish our own reference system, for which we can apply exactly the same blending conditions as for the Janus particles. Therefore, we prepared two series of PS/PMMA blends using a linear SBM (polystyrene-*block*-polybutadiene-*block*-poly(methyl methacrylate)) block copolymer as stabilizer. Note that SBM triblock terpolymers are very efficient blend compatibilizer.[52-55] The linear triblock terpolymer used is exactly the same polymer, which is employed for the preparation of the Janus particles. It is of the same composition and has a similar radius of gyration as compared to the Janus particles. Thus, partitioning effects because of different radii of gyration are similar. Therefore, it can be considered as a scientifically correct and fair assessment of the compatibilization efficiency. Similarly to the polymer blends prepared with the Janus particles, the amount of SBM stabilizer was varied for the polymer blends to follow the decay of the domain size of the dispersed PMMA phase in dependence of the compatibilizer content. The fraction of added SBM terpolymer was corrected for the slight mass increase, caused by the cold vulcanization, during the crosslinking reaction yielding the Janus particles. Hence, the blends were prepared at exactly the same molar amount of SBM, either in the form of linear polymer or crosslinked in a Janus particle, and thus allow a scientifically correct assessment of the stabilizer performance. A first overview can be obtained by comparing the TEM images and the frequency distributions of the dispersed PMMA droplets at a given concentration of stabilizer. Figure 8 - 6 displays data for PS/PMMA blends at 4 wt%, 10 wt% and 20 wt% of compatibilizer and blending ratios of 8/2 and 6/4, respectively.

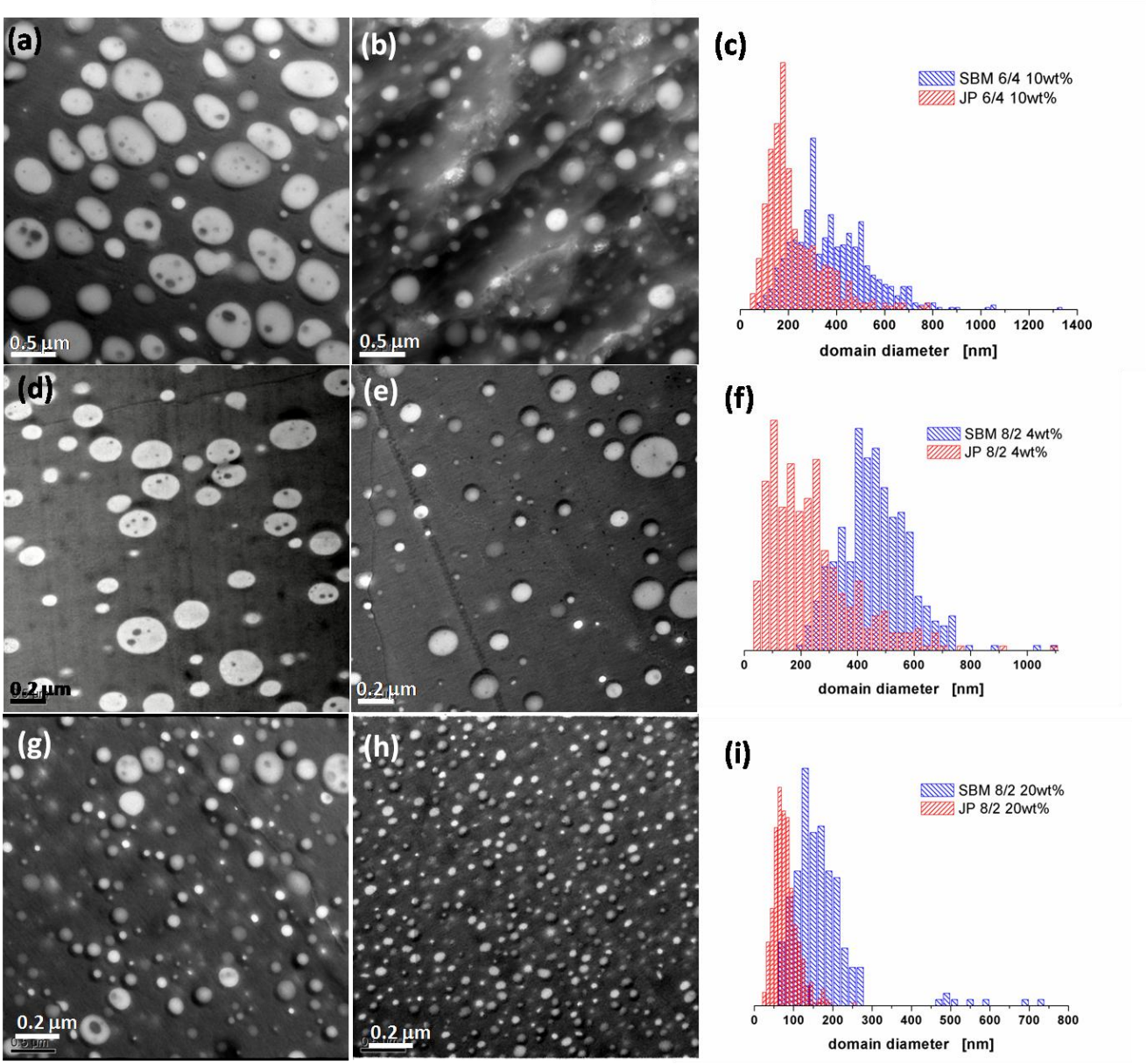

Figure 8 - 6. TEM images for polymer blends stabilized with SBM (a, d, g) and Janus particles (b, e, h) for different PS/PMMA ratios of 6/4 (first row) and 8/2 (second and third row). The concentration of the compatibilizer is 10 wt% (a), 4 wt% (b) and 20 wt%. The right side shows histograms of the statistical analysis of the PMMA domains.

A striking difference can be observed from the images straightaway. At any given concentration, the addition of Janus particles leads to significantly smaller domain diameters, indicating a superior stabilization of the polymer blend system. A more detailed conclusion can be drawn by analyzing the frequency distribution of the domain sizes as shown on the right-hand side in Figure 8 - 6. The maximum of the size distribution of the PMMA domains is shifted towards higher diameter when using the block copolymer instead of the Janus particles. The effect is present independently of the stabilizer content and blend ratios used. Consequently, the Janus particles outperform the standard block copolymer tremendously.

A completely quantitative picture can be obtained by comparing the number-average PMMA domain sizes for both compatibilizers over the full range of stabilizer content and the different

blending ratios. Figure 8 - 7a shows the evolution of the domain diameters as a function of the stabilizer content.

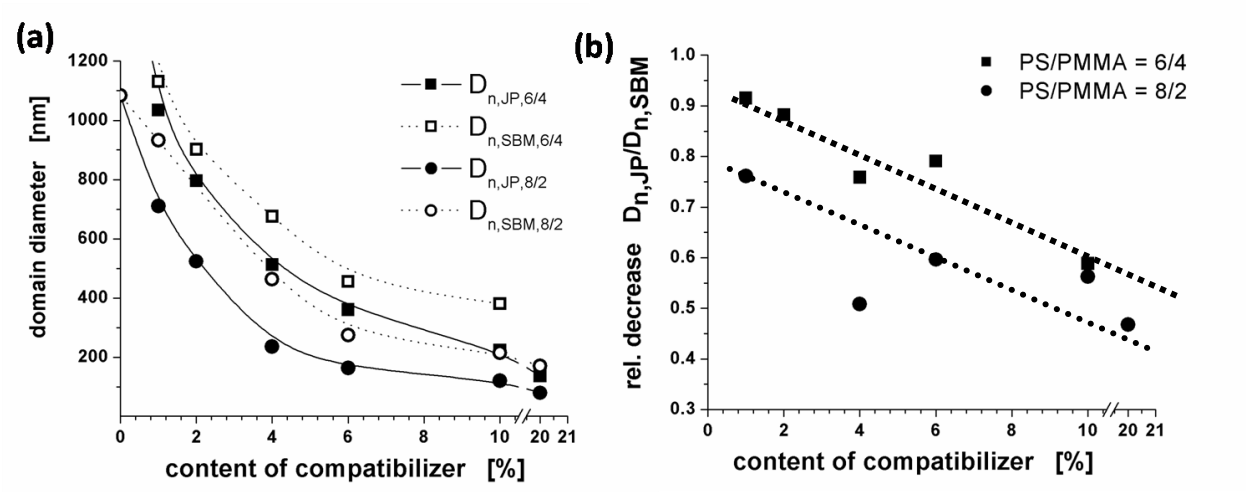

Figure 8 - 7. (a) Evolution of the PMMA domain diameter as a function of the content of compatibilizer for different types of stabilizers, SBM and Janus particles, and varying blending ratios as indicated in the graph. (b) Relation between the number average PMMA domain sizes of polymer blends compatibilized with SBM and Janus particles. Both blend ratios are shown as indicated in the graph. The lines serve to guide the eye.

Comparing the filled (Janus particles) with the open symbols (SBM) leads to the conclusion that under any blending ratio, the Janus particles lead to smaller domain sizes. Additionally, the Janus particles lead to a more rapid decay than the block copolymer, which is also a typical feature of a compatibilizer with a higher efficiency. Moreover, the SBM block copolymer shows a leveling off for higher concentrations and the addition of more block copolymer does not further decrease the domain sizes. Domain sizes in the region below 100 nm or 250 nm for the different blending ratios of 8/2 and 6/4, respectively, may not be reached. The block copolymer stabilizer loses its efficiency, a phenomenon seen for other systems already.[3, 6] In accordance with the TEM images, a significant fraction of the block copolymer stabilizer is lost as micellar aggregates. Those aggregates can be found at most of the concentrations and appear to be increasingly dominant for higher concentrations. Figure 8 - 8 shows some of these aggregates after selectively staining the remaining olefinic polybutadiene bonds with OsO_4. The structures embedded into the PMMA droplets are very small and often darker than the matrix phase composed of PS. Bearing in mind that the contrast in TEM evolves from thickness in combination with mass density, it is evident that these structures are significantly stained with OsO_4, thus confirming the presence of polybutadiene and henceforth of SBM block copolymer micelles. A dark ring can be seen surrounding the PMMA domain at the interface to the PS matrix. This ring originates from the SBM block copolymer acting as stabilizer of the phase boundary. The micellar aggregates are too small to contain significant amounts of polystyrene homopolymer. Consequently, they do not participate in the compatibilization process and thus the limited compatibilization efficiency of the SBM block copolymer can be reasonably understood. Note that micelles within the PS matrix cannot be identified easily as the micelles cannot be unambiguously distinguished from small dispersed and stabilized PMMA domains. Therefore, in order to not underestimate the performance of the block copolymer, those small structures were counted as domains. Presumably, a fair amount of those might be micelles though, which would increase the number average domain size, $D_{n,SBM}$.

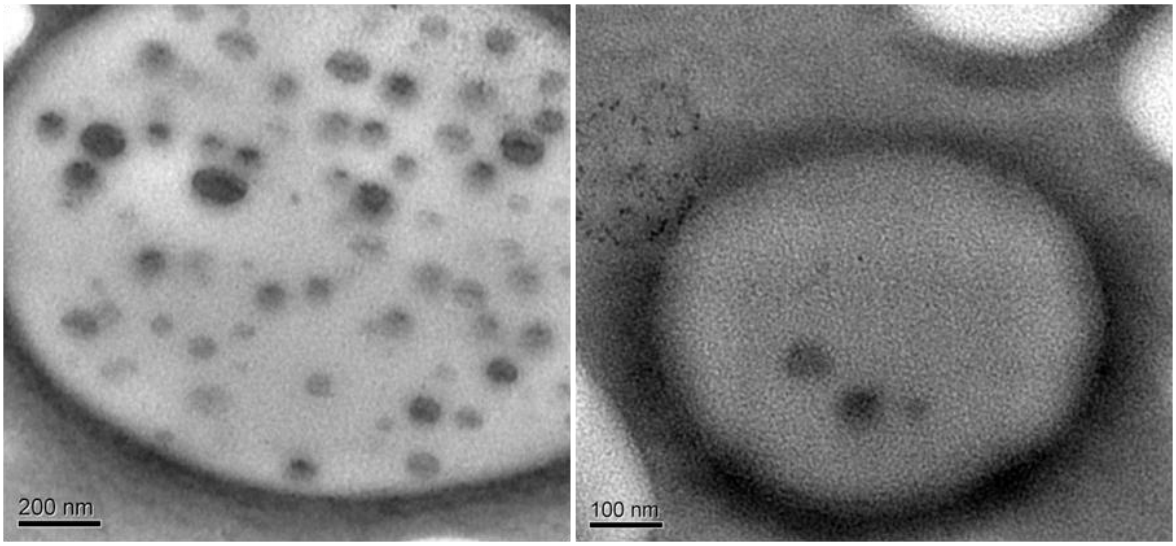

Figure 8 - 8. TEM micrographs for a polymer blend (PS/PMMA = 8/2) stabilized with 10 wt% SBM, after staining of the polybutadiene double bonds with OsO_4.

Concerning the blends compatibilized with Janus particles, the domain sizes continue to decrease even for high contents of stabilizer. This is a direct consequence of the Janus character of the particles. Due to the unique combination of the Pickering effect with amphiphilicity, the biphasic particles adsorb strongly at the interface and do not lose their efficiency for higher concentrations. This is also the reason why with increasing content of stabilizer, the relative gap between the domain sizes for blends stabilized with block copolymers or Janus particles, respectively, widens. Figure 8 - 7b displays the ratio of the two values $D_{n,JP}$ over $D_{n,SBM}$, which can be best used to demonstrate this behavior. A decrease of this ratio can be observed. This means that the SBM block copolymer is outperformed at all times, but the effect and the efficiency gap becomes more and more pronounced for increasing compatibilizer content. Already at moderate compatibilizer concentrations at a blending ratio of 8/2, the Janus particles lead to domains of half the size as when using the block copolymer. This is a tremendous boost in the performance and nicely demonstrates the powerful capabilities of Janus particles for stabilizing block copolymer interfaces and homogenizing polymer blends.

Depending on the targeted or desired diameter of the dispersed phase, the mass fraction of the stabilizer can be cut back by even fifty percent. All of this can be realized in this case by a relatively simple synthetic transformation of the block copolymer into a Janus particle. The resulting physical characteristics of the Janus particles, i.e. the strengthened adsorption based on the combination of Pickering effect with amphiphilicity, lead to the superior performance observed here. Note that in this first study of the PS/PMMA model system, no further optimization of the blending conditions or special high shear blending apparatuses were used[56], and we could nonetheless obtain very promising results.

Looking out to the future, with the growing number of preparation pathways to Janus particles in the chemists' and material scientists' hand (electrospinning, microfluidic devices, Pickering particle route, bimetallic nanoparticles, triblock terpolymer based route[57]), it appears likely to increasingly obtain tailor-made Janus particles. With these particles, it would be possible to blend a large variety of different polymers. Although Janus particles may not find widespread

application for blending standard commodity plastics, they are very promising candidates for the nanostructuring of high performance materials of strongly immiscible components, for self-healing composites, increased thermo-conductivity or for optoelectronic devices. It appears possible, for instance, that adequately functionalized inorganic nanoparticle do light harvesting in combination with compatibilizing polymer blend solar cells.

Additionally, due to the strong adsorption, Janus particles can overcome energetic boundaries, which were theoretically calculated for homogeneous particles and are thus another efficient mean in the nanoparticle toolbox for the controlled positioning of nanoparticles in polymer blends and block copolymers. Therefore, it may be possible to locate particles of a large size range at the interface, in particular those particles, which, if they were be homogeneous, would not adsorb at the interface due their size. Additionally, with our results, we also hope to promote some theoretical work, treating the behavior of Janus particles in polymer blends and homopolymers in order to gain further insights into the system.

Conclusion

We present the first application study using Janus particles on a *multi-gram* scale, which can be seen as a demonstration of the capabilities of the synthesis of complex nanoparticles. It is shown that Janus particles can be used to efficiently compatibilize polymer blends under high shear conditions. A constant decay of the domain size of the dispersed phase can be observed, independent of the blend composition used. The performance of the Janus particles in compatibilizing the polymer blend is significantly superior to other state-of-the-art compatibilizers, such as linear block copolymers. Common problems like micellization of the stabilizer and insufficient adsorption at the interface can be overcome to a major extent. The origin of this continuous decrease is the strengthened adsorption of the Janus particles at the interface, which is in turn caused by their biphasic particle character. In contrast to block copolymers or homogeneous particles, the Janus particles are located at the interface, even at high temperature and shear. The adsorption energy of a Janus particle at an interface at processing conditions is almost as high as for a homogeneous particle at room temperature. This can be explained by an additional enthalpic contribution to the adsorption energy. The Janus particles, adsorbed to the polymer blend interface, exhibit an ordered arrangement. Consequently, the structural order occurs on two levels. The first is the complete adsorption at the interface and the second is the lateral ordering at the interface. This renders them an interesting tool for the nanostructuring of blend and block copolymer interfaces. Therefore, Janus particle provide a mean for the nanoscopic engineering of polymer blend systems, while matching some macroscopic processing constraints.

Methods

Materials

Poly(methyl methacrylate) (PMMA, M_w = 120000, PDI = 1.8) and Polystyrene (PS, M_w = 230000, PDI = 1.6) were purchased from Aldrich. The SBM polymer used for blending and for the preparation of the Janus particles is a polystyrene-*block*-polybutadiene-*block*-poly(methyl methacrylate) (SBM) triblock terpolymer, which was prepared by anionic polymerization. The Janus particles were obtained by crosslinking the lamella-sphere morphology of the SBM triblock terpolymer in the bulk state *via* cold vulcanization with sulphur monochloride (S_2Cl_2). The two sides consist each of ca. 13 chains, which are attached to a central crosslinked particular polybutadiene core. They core is surrounded by about 13 chains each of PS (DP = 800) and PMMA (DP = 700), which are phase-separated.

Blend preparation

In order to prepare a homogenous polymer powder, the calculated amounts of PS, PMMA and Janus particles were dissolved in THF, precipitated into methanol and dried in vacuo for 2 days. The blends were prepared in a Haake MiniLab Twin Screw extruder at 210^{o}C and 40 rpm. The duration of melt blending was 3 min. After blending the material was extruded and the center of the released strand was microtomed at half of its length. The microtom cut sections were imaged with TEM, whereas the cut material area was exposed to deep UV for etching away the PMMA domains. The latter one was used for SEM imaging after covering with a thin layer of platinum.

Scanning Electron Microscopy (SEM)

SEM was performed using a LEO 1530 Gemini instrument equipped with a field emission cathode with a lateral resolution of approximately 2 nm. The acceleration voltage was chosen between 0.5 and 3 kV.

Transmission Electron Microscopy (TEM)

For TEM, thin sections were cut at room temperature using a Reichert-Jung Ultracut E microtome equipped with a diamond knife. Bright-field TEM was performed on Zeiss CEM 902 and LEO 922 OMEGA electron microscopes operated at 80 kV and 200 kV, respectively.

Acknowledgments

The authors acknowledge financial support from the DFG and the ESF within the EUROCORES-BioSONS program. We are also indebted to J. Rockser and B. Goßler for their skilful work with the microtome, as well as with the TEM and SEM measurements. A. Walther thanks the Bavarian Elite Support Program for a fellowship and Prof. E. Kramer for an inspiring conversation. H. Ruckdäschel is acknowledged for the discussions in an early stage of this project.

References

1. Kietzke, T.; Neher, D.; Landfester, K.; Montenegro, R.; Guentner, R.; Scherf, U. *Nat. Mater.* **2003,** 2, 408.
2. Kietzke, T.; Neher, D.; Kumke, M.; Montenegro, R.; Landfester, K.; Scherf, U. *Macromolecules* **2004,** 37, 4882.
3. Adedeji, A.; Lyu, S.; Macosko, C. W. *Macromolecules* **2001,** 34, 8663.
4. Noolandi, J.; Hong, K. M. *Macromolecules* **1982,** 15, 492.
5. Lyu, S.; Jones, T. D.; Bates, F. S.; Macosko, C. W. *Macromolecules* **2002,** 35, 7845.
6. Zhao, H.; Huang, B. *J. Polym. Sci., Part B: Polym. Phys.* **1998,** 36, 85.
7. Binks, B. P.; Fletcher, P. D. I. *Langmuir* **2001,** 17, 4708.
8. Walther, A.; Hoffmann, M.; Müller, A. H. E. *Angew. Chem. Int. Ed.* **2007,** 120, 723.
9. Nonomura, Y.; Komura, S.; Tsujii, K. *Langmuir* **2004,** 20, 11821.
10. Glaser, N.; Adams, D. J.; Böker, A.; Krausch, G. *Langmuir* **2006,** 22, 5227.
11. Walther, A.; André, X.; Drechsler, M.; Abetz, V.; Müller, A. H. E. *J. Am. Chem. Soc.* **2007,** 129, 6187..
12. Mackay, M. E.; Tuteja, A.; Duxbury, P. M.; Hawker, C. J.; Van Horn, B.; Guan, Z.; Chen, G.; Krishnan, R. S. *Science* **2006,** 311, 1740.
13. Thompson, R. B.; Ginzburg, V. V.; Matsen, M. W.; Balazs, A. C. *Science,* **2001,** 292, 2469.
14. He, G.; Ginzburg, V. V.; Balazs, A. C. *J. Polym. Sci., Part B: Polym. Phys.* **2006,** 44, 2389.
15. Ginzburg, V. V. *Macromolecules* **2005,** 38, 2362.
16. Hore, M. J. A.; Laradji, M. *J. Chem. Phys.* **2007,** 126, 244903.
17. Balazs, A. C.; Emrick, T.; Russell, T. P. *Science* **2006,** 314, 1107.
18. Lee, J. Y.; Shou, Z.; Balazs, A. C. *Macromolecules* **2003,** 36, 7730.
19. Lee, J. Y.; Thompson, R. B.; Jasnow, D.; Balazs, A. C. *Macromolecules* **2002,** 35, 4855.
20. Hong, Y.; Cooper-White, J. J.; Mackay, M. E.; Hawker, C. J.; Malmstroem, E.; Rehnberg, N. A. *J. Rheol.* **1999,** 43, 781.
21. Yang, H.; Zhang, X.; Qu, C.; Li, B.; Zhang, L.; Zhang, Q.; Fu, Q. *Polymer* **2007,** 48, 860.
22. Gupta, S.; Zhang, Q.; Emrick, T.; Balazs, A. C.; Russell, T. P. *Nat. Mater.* **2006,** 5, 229.
23. Lee, J.-Y.; Zhang, Q.; Emrick, T.; Crosby, A. J. *Macromolecules* **2006,** 39, 7392.
24. Peng, G.; Qiu, F.; Ginzburg, V. V.; Jasnow, D.; Balazs, A. C. *Science* **2000,** 288, 1802.
25. Buxton, G. A.; Balazs, A. C. *Mol. Simul.* **2004,** 30, 249.
26. Liu, J.; Tanaka, T.; Sivula, K.; Alivisatos, A. P.; Frechet, J. M. J. *J. Am. Chem. Soc.* **2004,** 126, 6550.
27. Buxton, G. A.; Lee, J. Y.; Balazs, A. C. *Macromolecules* 2003, 36, 9631.
28. Bockstaller, M. R.; Thomas, E. L. *Phys. Rev. Lett.* 2004, 93, 166106.
29. Kim, B. J.; Fredrickson, G. H.; Kramer, E. J. *Macromolecules* 2008, 41, 436.
30. Park, S. C.; Kim, B. J.; Hawker, C. J.; Kramer, E. J.; Bang, J.; Ha, J. S. *Macromolecules* 2007, 40, 8119.
31. Kim, B. J.; Fredrickson, G. H.; Hawker, C. J.; Kramer, E. J. *Langmuir* **2007,** 23, 7804.
32. Chiu, J. J.; Kim, B. J.; Yi, G.-R.; Bang, J.; Kramer, E. J.; Pine, D. J. *Macromolecules* **2007,** 40, 3361.
33. Kim, B. J.; Bang, J.; Hawker, C. J.; Kramer, E. J. *Macromolecules* **2006,** 39, 4108.
34. Kim, B. J.; Chiu, J. J.; Yi, G.-R.; Pine, D. J.; Kramer, E. J. *Adv. Mater.* **2005,** 17, 2618.
35. Chiu, J. J.; Kim, B. J.; Kramer, E. J.; Pine, D. J. *J. Am. Chem. Soc.* **2005,** 127, 5036.
36. Erhardt, R.; Böker, A.; Zettl, H.; Kaya, H.; Pyckhout-Hintzen, W.; Krausch, G.; Abetz, V.; Müller, A. H. E. *Macromolecules* **2001,** 34, 1069.
37. Stratford, K.; Adhikari, R.; Pagonabarraga, I.; Desplat, J.-C.; Cates, M. E. *Science* **2005,** 309, 2198.
38. Pieranski, P. *Phys. Rev. Lett.* **1980,** 45, 569.
39. Helfand, E.; Tagami, Y. *J. Chem. Phys.* **1972,** 56, 3592.

40. Helfand, E.; Sapse, A. M. *J. Chem. Phys.* **1975,** 62, 1327.
41. Russell, T. P.; Hjelm, R. P, Jr.; Seeger, P. A. *Macromolecules*, **1990**, 23, 890.
42. Rundqvist, T.; Cohen, A.; Klason, C. *Rheol. Acta* **1996,** 35, 458.
43. Elias, L.; Fenouillot, F.; Majeste, J. C.; Cassagnau, P. *Polymer* **2007,** 48, 6029.
44. Vermant, J.; Cioccolo, G.; Golapan Nair, R.; Moldenaers, P. *Rheol. Acta.* **2004,** 43, 529.
45. Chung, H.-j.; Ohno, K.; Fukuda, T.; Composto, R. J. *Nano Lett.* **2005,** 5, 1878.
46. Xu, C.; Xie, J.; Ho, D.; Wang, C.; Kohler, N.; Walsh, E. G.; Morgan, J. R.; Chin, Y. E.; Sun, S. *Angew. Chem. Int. Ed.* **2008,** 47, 173.
47. Israels, R.; Jasnow, D.; Balazs, A. C.; Guo, L.; Krausch, G.; Sokolov, J.; Rafailovich, M. *J. Chem. Phys.* **1995,** 102, 8149.
48. Galloway, J. A.; Jeon, H. K.; Bell, J. R.; Macosko, C. W. *Polymer* **2005,** 46, 183.
49. Yin, Z.; Koulic, C.; Pagnoulle, C.; Jerome, R. *Macromolecules* **2001,** 34, 5132.
50. Schulze, J. S.; Cernohous, J. J.; Hirao, A.; Lodge, T. P.; Macosko, C. W. *Macromolecules* **2000,** 33, 1191.
51. Jeon, H. K.; Zhang, J.; Macosko, C. W. *Polymer* **2005,** 46, 12422.
52. Lach, R.; Grellmann, W.; Weidisch, R.; Altstädt, V.; Kirschnick, T.; Ott, H.; Stadler, R.; Mehler, C. *J. Appl. Polym. Sci.* **2000,** 78, 2037.
53. Kirschnick, T.; Gottschalk, A.; Ott, H.; Abetz, V.; Puskas, J.; Altstädt, V. *Polymer* **2004,** 45, 5653.
54. Ruckdäschel, H.; Sandler, J. K. W.; Altstädt, V.; Schmalz, H.; Abetz, V.; Müller, A. H. E. *Polymer* **2007,** 48, 2700.
55. Ruckdäschel, H.; Sandler, J. K. W.; Altstädt, V.; Rettig, C.; Schmalz, H.; Abetz, V.; Müller, A. H. E. *Polymer* **2006,** 47, 2772
56. Shimizu, H.; Li, Y.; Kaito, A.; Sano, H. *Macromolecules* **2005,** 38, 7880.
57. Walther, A.; Müller, A. H. E. *Soft Matter* **2008,** 4, 663.

9. Formation of Hydrophobic Bridges between Multicompartment Micelles in Water

Andreas Walther and Axel H. E. Müller

Makromolekulare Chemie II and Bayreuther Zentrum für Kolloide und Grenzflächen, Universität Bayreuth, D-95440 Bayreuth, Germany

Andreas.Walther@uni-bayreuth.de; *Axel.Mueller@uni-bayreuth.de*

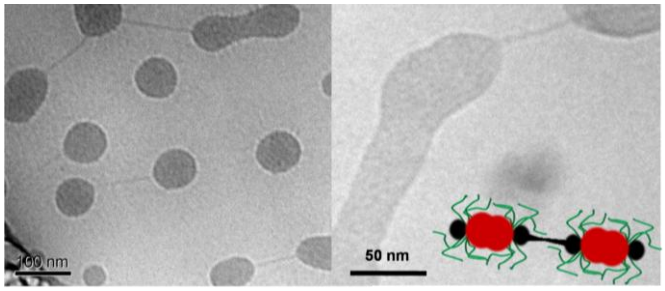

Accepted for *Chemical Communication*

We report on the unexpected finding of the formation of hydrophobic bridges between polybutadiene patches of multicompartment micelles based on amphiphilic miktoarm star terpolymers in water.

The introduction of soft matter systems such as block copolymers into the field of controlled drug delivery, sensing and adhesion control has led to a rapid development of new and specific vehicles for the controlled administration of active compounds.[1] Many synthetic colloids are aimed to mimic biological entities in a very simplified fashion as for instance in case of phospholipid or block copolymer vesicles, resembling to some extent a simple cell.[2] To allow a higher diversification in terms of mimicking cell functions, transmembrane channels or small vesicles were incorporated into the vesicle wall or the vesicle interior, respectively.[3] Both strategies aim at a higher control of functionality regarding mediated transport or hierarchical structure formation.

The recent discovery of so-called multicompartment micelles (MCMs), i.e. colloids possessing several compartments of different properties, has enriched the possibilities for sequential or multicomponent delivery.[4] Lodge and coworkers recently showed that fluoro- and hydrocarbons can be selectively entrapped into fluorinated and hydrophobic domains of MCMs based on miktoarm star terpolymers.[4c] A phenomenon inherent to these novel MCMs based on miktoarm stars, as compared to those composed of linear triblock copolymers is the fact that the hydrophobic domains can be rather exposed to the surrounding water, being one major difference. In general, MCMs are not only appealing due to the possibility of multicomponent storage, but also of having multicomponent sensing or significantly changing the micelles substrate adhesion interactions. Precisely speaking, not only the hydrophilic block, as in case of colloids formed by linear polymers, is sufficiently accessible from the aqueous phase, even the hydrophobic blocks can be in sufficient contact.

In biological systems, sensing and molecular recognition can be performed with a variety of methods. In eukaryotic cells for instance, hair-like protrusions, so-called cilia, can be found, which are key features for interactions with its surrounding.[5] For polymer-based controlled drug administration systems, it was recently revealed that hydrophobic patches of Janus particles or MCMs can be the decisive feature for desired interactions with cell membranes or hydrophobic areas within injured blood vessels.[6] Hydrophobic parts of MCMs can interact with cell membranes or surfaces in a completely different fashion than hydrophilic polymers found in the coronas of standard micelles. This is also one of the reasons why amphiphilic particles and amphiphilic proteins are currently explored as drug or gene delivery agents.[7] These examples serve to show the great importance of controlling and developing accessible hydrophobic motifs in polymeric MCMs.

In this communication, we report on the surprising finding of bridge formation between hydrophobic domains of MCMs composed of amphiphilic miktoarm star polymers. These bridges seem to provide an understanding for the aggregation of MCMs into higher ordered cylinders. Moreover, the results demonstrate that hydrophobic compartments of polymer based MCMs are not non-dynamic, shape persistent entities which can only be used for storage. They may however be used to perform tasks which require dynamics, such as for molecular recognition, sensing, adhesion control and enhanced cell penetration.

The polymer used herein is a SBV* miktoarm star terpolymer bearing one arm each of polystyrene (PS), polybutadiene (PB) and poly(2-vinyl pyridine) (P2VP).[8] The exact polymer used is a $S_{54}B_{18}V_{28}^{182}$, where subscript and superscripts denote the weight fractions and the overall molecular weight in kg/mol, respectively. In terms of number average degree of polymerization this corresponds to $S_{944}B_{605}V_{485}$. P2VP ensures sufficient aqueous solubility of the aggregates at low pH. The two hydrophobic polymers, PS and PB, are incompatible and possess significantly different glass transition temperatures and are thus very different in terms of their dynamic behavior. PS with its typical glass transition temperature around 100°C leads to non-dynamic behavior of so-called frozen micelles, whereas the soft PB part has a glass transition temperature significantly below room temperature and allows a dynamic behavior. After dialysis of the SBV* polymer from dioxane into water (c = 5 mg/mL, pH 2), the resulting self-assembled aggregates were characterized with TEM (see Figure 9 - 1) after staining the PB double bonds with OsO_4.

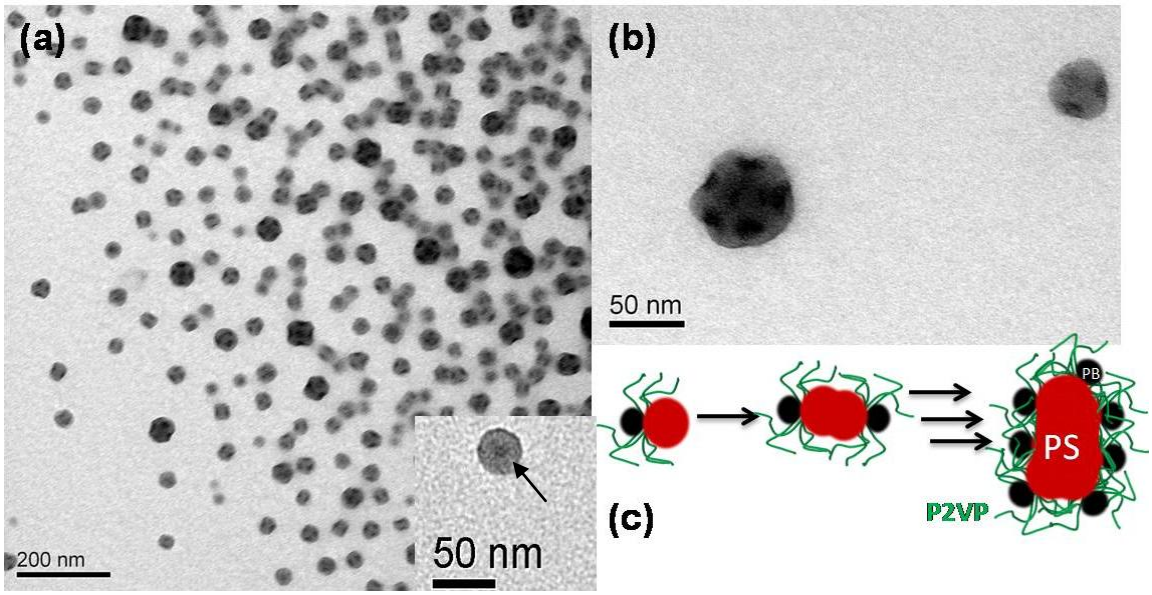

Figure 9 - 1. TEM images of MCMs deposited onto a carbon-coated TEM grid after staining the PB bonds with OsO_4, thus appearing black. The inset in image (a) shows a unimeric MCM (stained part highlighted by the arrow). The schematic drawing in (c) shows the proposed aggregation pattern (PS = red, PB = black, P2VP = green). The sample was measured five days after dialysis.

Mainly spherical particles with an internal structure can be found. The internal structure is invisible in the absence of OsO_4 staining. Thus the dark domains clearly originate from the stained double bonds of the polybutadiene and confirm the multicompartment character of the micelles. The intrinsic incompatibility between PB and PS is obviously sufficient to induce a phase-segregation in the MCMs. The corona of P2VP chains cannot be seen in TEM. The MCMs as found here are composed of two hydrophobic core entities, a soft PB domain and a hard PS one. A more detailed observation of the particles reveals that the amount of dark domains varies. Unimers, dimers, trimers, tetramers and higher aggregates can be found. In accordance with the observation by Lodge, we expect that the initially formed unimers with a Janus type segregation of the core into two hydrophobic and demixed cores self-assemble into higher aggregates due to the necessity of shielding some of the hydrophobic parts against water. The time-dependent assembly of the initially formed aggregates can be followed by dynamic light

scattering (DLS). The CONTIN plots, corresponding to the radii distribution functions, are shown in Figure 9 - 2 for certain aging times. With increasing aging the structures grow in size. Thus, the initially formed small aggregates slowly fuse into larger ones. A slight bimodality of the size distribution can be observed upon aging for extended time. This may originate from fusion of already built up large MCMs. It should however not be overinterpreted as the intensity in the unweighted CONTIN plots scales with r^6 and thus the true number fraction is rather small. The fusion process can be significantly enhanced by annealing the solution at higher temperature, e.g. 60°C. The temperature assists the aggregation by additional softening of the polymeric components and increased collision events.

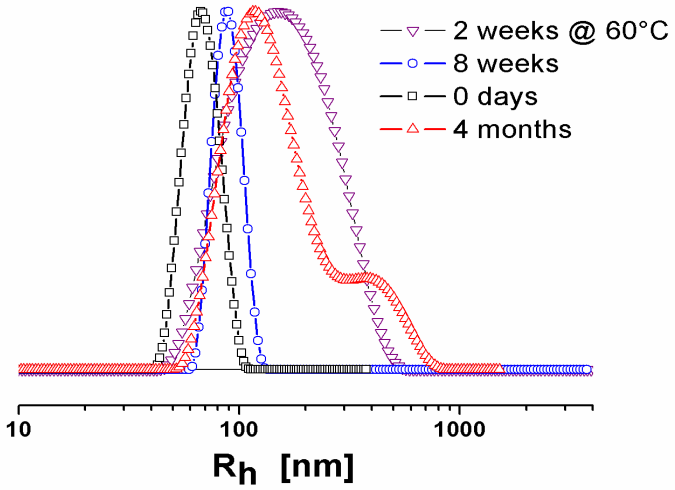

Figure 9 - 2. Intensity-weighted DLS CONTIN plots for different aging times of aqueous solutions of SBV at room temperature or at 60°C as indicated within the figure (2 mg/mL, pH = 2, 80 mM NaCl).

Given that PS is present as larger volume fraction, a PS core is formed that is decorated with PB domains, coinciding with the observations in TEM. Since we use very high molecular weight polymers as compared to Lodge's studies, the structural features of the MCMs are much larger and thus we have the possibility of looking into more detail at the small textures. Interestingly, the PB domains sizes are different, depending on the size of the overall structure. The larger the PS core, the larger are also the PB domains located on it. This indicates that some PB domains can fuse on the surface, minimizing the energetically unfavorable interface between PB and water.

To further explore the structure, we performed cryo-TEM measurements of the micelles. Cryo-TEM is a method, in which a thin film of the micellar solution, stretching over a TEM grid, is rapidly vitrified in liquid ethane. Afterwards, the film is transferred into the microscope, while maintaining the cryogenic temperatures and subsequently imaged in transmission mode. All structures within the film are preserved and even complex and very fragile assemblies can be imaged in a quasi in-situ fashion. Figure 9 - 3 gives an overview of the aggregates found. The cryo-TEM images reveal a striking and, to the best of our knowledge, previously never seen feature, which is the connection of the micelles via hydrophobic bridges in water.

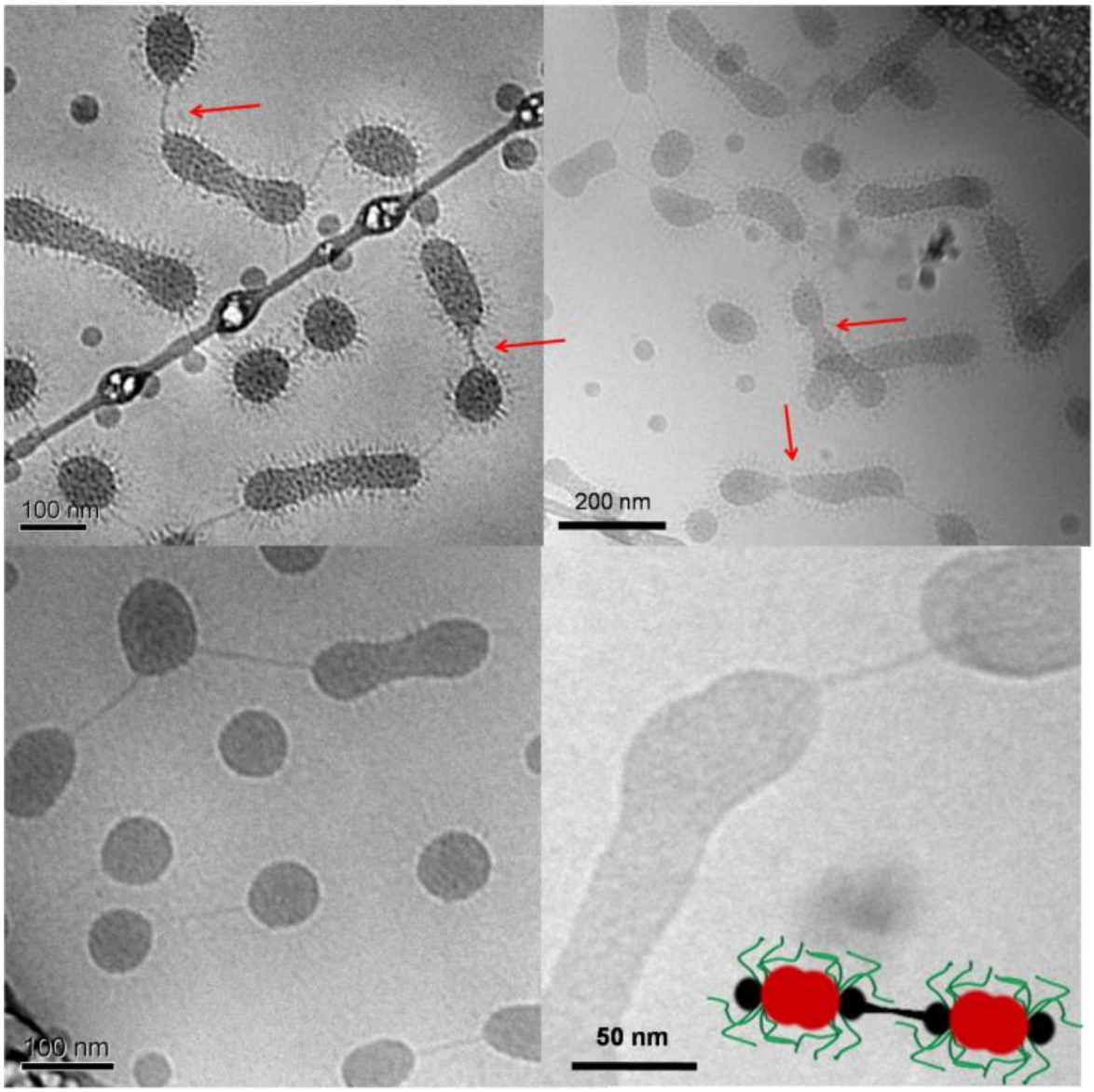

Figure 9 - 3. Cryo-TEM images showing hydrophobic bridge formation between various multicompartment micelles or cylinders. The sample was allowed to age for three weeks.

In all images, several micelles are connected via protrusions extending from the participating micelles. In the upper two images a clear core-corona structure can be found. The corona consists of highly solvated P2VP chains, surrounding the multicompartment core. The internal structure of the PB domains on the PS core cannot be visualized due to insufficient contrast between the two hydrocarbons. The imaging of a highly solvated corona structure usually requires slight defocusing and an optimum thickness of the specimen film. In the two lower images, the imaging conditions do not allow a resolution of the P2VP corona, thus hydrophobic material with high contrast to the water can exclusively be seen. Since the bridges can still be clearly seen with a similar contrast as the hydrophobic core, they consequently have to be composed of hydrophobic material as well. Note, that similar bridges cannot be found in dynamic micelles of a linear PB-P2VP polymer ($B_{11}V_{89}^{100}$, cryo-TEM images can be found in the supplementary information). Consequently, the bridges are neither formed by P2VP nor can their formation be attributed to experimental procedures in cryo-TEM. They clearly originate from the unique architecture and structure of the MCMs. The bridges are also not strong enough

to allow visualization with standard TEM which involves strong shearing forces during blotting and drying. Only the quasi in-situ technique cryo-TEM allows the imaging of such fragile assemblies. Due to the low glass transition temperature of the PB and its accompanying dynamic character, the bridges must be formed by PB. This is a somewhat astonishing finding as the bridge formation involves the creation of a significantly unfavorable interface of PB and water. It shall be noted that the length of the bridges is absolutely in agreement with the chain dimensions of the PB. Its high degree of polymerization, (605 units), corresponds to a contour length of ca. 150 nm (for 1,2-PB), easily allowing the formation of bridges of up to twice that length. In fact, we do not find whiskers exceeding the double contour length, which would be unreasonably long. A large fraction of the aggregates are connected via their end-caps, indicating a higher exposure of the PB domains and susceptibility of bridge formation at these points.

The thermodynamic stability of these bridges cannot be readily understood. Certainly, two requirements for the formation of the bridges are (i) fluid-like polymers and (ii) a sufficiently low interfacial tension. Clearly, with increasing glass transition temperature and interfacial tension between a given polymer and water, the stability or the tendency to build such bridges decreases significantly. The mechanism for the formation of these bridges is presumably related to collision of several PB domains of the aggregates, leading to a sticky interaction and a prolonged adhesion of the micelles. Thus we attribute the formation of the bridges more to a kinetic phenomenon, than a thermodynamically stable structure. Nevertheless, the structures are sufficiently metastable to allow aggregation and imaging.

The impact of this finding is widespread. On the one hand it shines light on the aggregation of initially formed aggregates of MCMs. The red arrows in the upper two cryo-TEM images show all stages of the fusion process with an initially formed bridge, subsequent broadening, fusion and the still persisting nick after the fusion process. This fusion processes can explain the increase in hydrodynamic radii of the aggregates as found by DLS. More importantly, the unique self-assembled aggregates formed by miktoarm star polymers possess a fair amount of hydrophobic patches exposed to water. For soft, fluid-like polymers with low glass transition temperatures (like PB) forming these exposed domains, this has striking consequences in terms of adhesion to substrates. The dynamic character of such polymers leads to an interaction of the hydrophobic material with its aqueous environment. The material cannot be pictured as hard and non-usable bulk material as for instance in the case of polystyrene.

Looking out to the future, the bridges found in the cryo-TEM suggest their utilization as a second mean for sensing and particularly for adhesion control, especially when aiming at controlled delivery. Furthermore, the hydrophobic nature leads to a different interaction with lipid bilayers or cell walls. Usually, hydrophobic moieties can more effectively penetrate cell walls and thus the hydrophobic parts could be used to enhance cell penetration of micelles. Based on these findings, the unique multicompartment micelles based on miktoarm star terpolymers are not only appealing for multicomponent delivery but also due to the rising possibilities of increased adhesion control.

Conclusions

MCMs based on SBV* miktoarm star terpolymers form bridges between the hydrophobic PB patches. This previously never seen phenomenon occurs due to the low glass transition temperature of the PB, its accompanying dynamics and the significant exposure of the PB domains to water. It shows a unique way of how MCMs, an emerging class of colloids, can interact with the environment via hydrophobic interactions and can regulate cell interaction or adhesion control. Furthermore, the brides provide an understanding for the occuring fusion processes in self-assembled aggregates of miktoarm star terpolymers.

Acknowlegments

The authors thank H. Hückstädt for the polymer synthesis and the European Science Foundation for financial support within the EUROCORES SONS program (project BioSONS). A. Walther acknowledges a fellowship from the Bavarian Elite Support Program.

References

1 (a) K. Kataoka, A. Harada and Y. Nagasaki, *Adv. Drug Delivery Rev.*, 2001, **47**, 113; (b) M. Sauer, D. Streich and W. Meier, *Adv. Mater.*, 2001, **13**, 1649.

2 (a) T. Lian and R. J. Y. Ho, *J. Pharm. Sci.*, 2001, **90**, 667; (b) A. Choucair, P. L. Soo and A. Eisenberg, *Langmuir*, 2005, **21**, 9308.

3 (a) Y. Ma, W.-F. Dong, M. A. Hempenius, H. Möhwald and G. J. Vancso, *Nat. Mater.*, 2006, **5**, 724; (b) M. Kumar, M. Grzelakowski, J. Zilles, M. Clark and W. Meier, *Proc. Natl. Acad. Sci.*, 2007, **104**, 20719; (c) H.-C. Chiu, Y.-W. Lin, Y.-F. Huang, C.-K. Chuang and C.-S. Chern, *Angew. Chem. Int. Ed.*, 2008, **47**, 1875.

4. (a) Z. Li, E. Kesselman, Y. Talmon, A. M. Hillmyer and P. Lodge Timothy, *Science*, 2004, **306**, 98; (b) S. Kubowicz, J.-F. Baussard, J.-F. Lutz, A. F. Thünemann, H. von Berlepsch and A. Laschewsky, *Angew. Chem. Int. Ed.*, 2005, **44**, 5262; (c) T. P. Lodge, A. Rasdal, Z. Li and M. A. Hillmyer, *J. Am. Chem. Soc.*, 2005, **127**, 17608; (d) J.-F. Lutz and A. Laschewsky, *Macromol. Chem. Phys.*, 2005, **206**, 813; (e) Z. Li, M. A. Hillmyer and T. P. Lodge, *Langmuir*, 2006, **22**, 9409; (f) F. Schacher, A. Walther, M. Ruppel and A. H. E. Müller, *Pol. Mater.Sci. Eng.*, 2007, **96**, 94.

5. (a) J. F. Reiter and K. Mostov, *Proc. Natl. Acad. Sci.*, 2006, **103**, 18383; (b) V. Singla and J. F. Reiter, *Science*, 2006, **313**, 629; C. Ainsworth, *Nature*, 2007, **448**, 638; (c) R. D. Sloboda and J. Rosenbaum, L., *J. Cell Biol.*, 2007, **179**, 575.

6. (a) R. Verberg, A. T. Dale, P. Kumar, A. Alexeev and A. C. Balazs, *J. R. Soc. Interface*, 2007, **4**, 349-357; (b) A. Alexeev, W. E. Uspal and A. C. Balazs, *ACS Nano*, 2008, **2**, 1117.

7. M. A. Kostiainen, G. R. Szilvay, J. Lehtinen, D. K. Smith, M. B. Linder, A. Urtti and O. Ikkala, *ACS Nano*, 2007, **1**, 103.

8. H. Hückstädt, A. Göpfert and V. Abetz, *Macromol.Chem.Phys.*, 2000, **201**, 296.

Supporting Information

Methods

The polymer used in this study is a miktoarm star terpolymer, bearing three arms of polystyrene (S), poly(2-vinyl pyridine) (V) and polybutadiene (B) , $S_{54}B_{18}V_{28}^{182}$. The subscripts and superscript denote the weight fractions and the overall molecular weight in kg/mol of the terpolymer.

Dynamic Light Scattering (DLS)

Dynamic light scattering was performed on an ALV DLS/SLS-SP 5022F compact goniometer system with an ALV 5000/E cross-correlator and a He–Ne laser (λ_0 = 632.8 nm). Prior to the light scattering measurements the sample solutions were filtered using Millipore or Roth filters (housing: polypropylene, membrane: nylon) with a pore size of 5 μm. All samples were analyzed at high dilution. The data evaluation of the dynamic light scattering measurements was performed with the CONTIN algorithm.

Transmission Electron Microscopy (TEM)

Bright-field TEM was performed on Zeiss LEO 922 OMEGA electron microscope operated at 200 kV. Contrast enhancement of PB over PS was achieved by OsO_4 staining. The sample was deposited by placing a droplet onto a plasma-treated carbon coated TEM grid. Residual liquid was blotted after 15 sec.

For **cryogenic transmission electron microscopy (cryo-TEM)** studies, a drop of the sample dissolved in THF was put on a lacey TEM grid, where most of the liquid was removed with blotting paper, leaving a thin film stretched over the lace. The specimens were instantly vitrifed by rapid immersion into liquid ethane and cooled to approximately 90 K by liquid nitrogen in a temperature controlled freezing unit (Zeiss Cryobox, Zeiss NTS GmbH, Oberkochen, Germany). The temperature was monitored and kept constant in the chamber during all of the sample preparation steps. Afterwards, the specimen was inserted into a cryo-transfer holder (CT3500, Gatan, München, Germany) and transferred to a Zeiss EM922 EF-TEM instrument. Examinations were carried out at temperatures around 90 K. The transmission electron microscope was operated at an acceleration voltage of 200 kV. Zero-loss filtered images (ΔE = 0 eV) were taken under reduced dose conditions (100-1000 e/nm^2). All images were registered digitally by a bottom mounted CCD camera system (Ultrascan 1000, Gatan) combined and processed with a digital imaging processing system (Gatan Digital Micrograph 3.9 for GMS 1.4).

Additional cryo-TEM images of $B_{11}V_{89}^{100}$ (measured at pH = 2)

The images show core-corona micelles that are not connected by hydrophobic bridges despite their close proximity. The imaging conditions are exactly the same as for the multicompartment micelles.

The micelles can be obtained by direct dissolution in acidic water and are thus of high dynamic nature. Dialysis of the polymer from a common solvent (dioxane) into water leads to similar results.

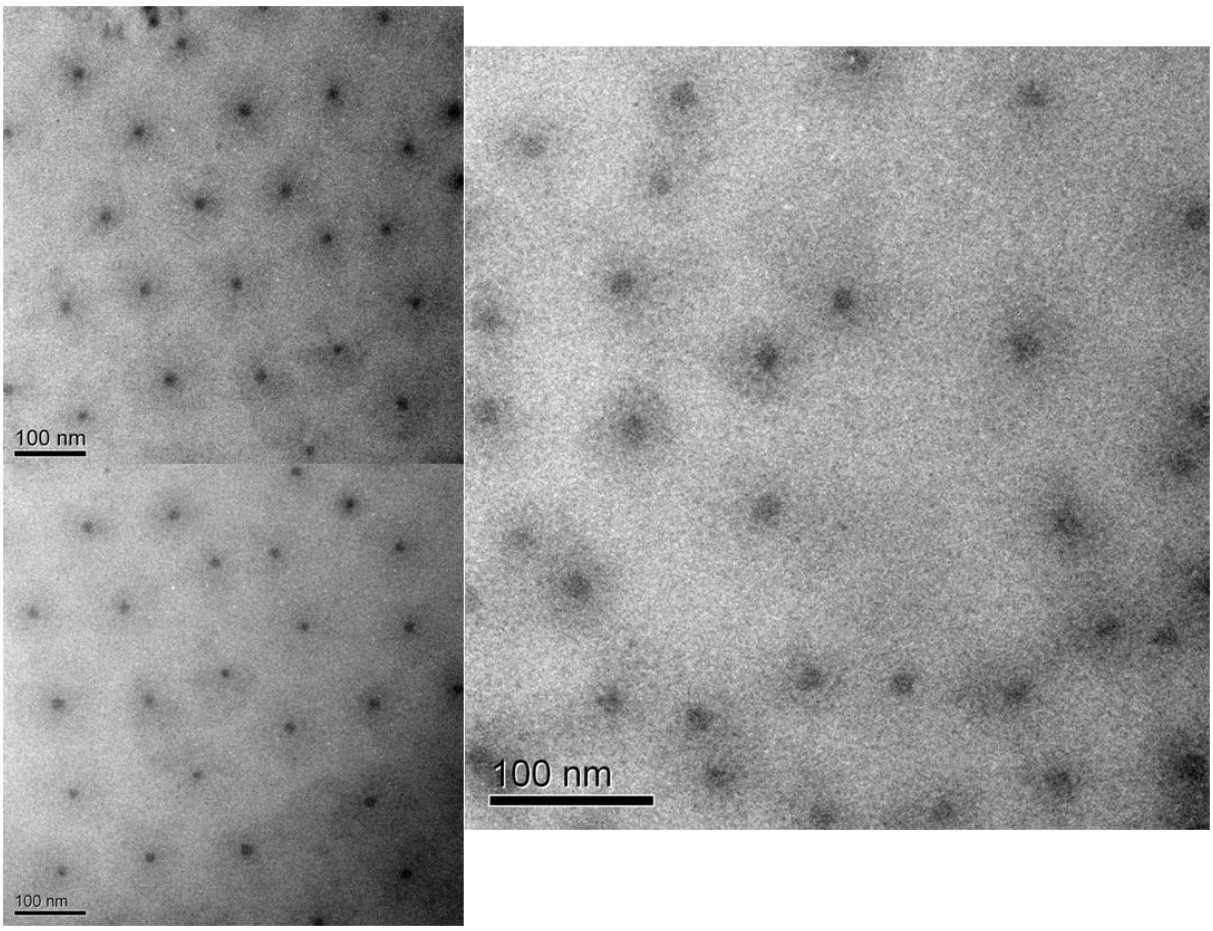

Figure Sup 9 – 1. Cryo-TEM images of $B_{11}V_{89}^{100}$ at pH = 2.

10. Structure-Tunable Bidirectional Hybrid Nanowires Templated by Polymeric Multicompartment Cylinders

Andreas Walther, Jiayin Yuan, Volker Abetz‡, Axel H. E. Müller

Makromolekulare Chemie II and Bayreuther Zentrum für Kolloide und Grenzflächen, Universität Bayreuth, D-95440 Bayreuth, Germany

‡ Institut für Polymerforschung, GKSS-Forschungszentrum Geesthacht GmbH, D-21502 Geesthacht, Germany

Andreas.Walther@uni-bayreuth.de; *Axel.Mueller@uni-bayreuth.de*

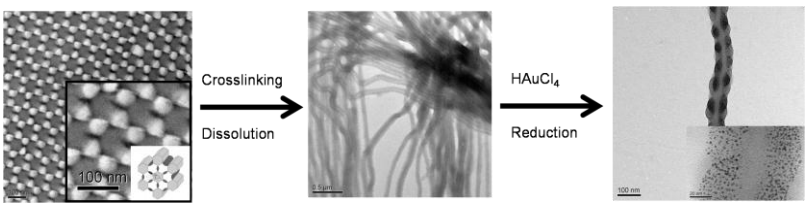

Submitted to *Nature Nanotechnology*

The precise organization of matter on the meso- and nanoscale is of great importance for generating materials with superior properties.[1-8] For soft matter, block copolymers underwent a tremendous success story. The complexity of structures and their potential applications are encoded into the polymer architecture. The control in functionality allows the utilization of non-covalent bonds to achieve inorganic-organic hybrid materials[9-11] with desired electric, magnetic and optical properties.[12, 13] Herein we show that crosslinking of a miktoarm star terpolymer bulk structure overcomes limitations of solution-based self-assembly and leads to novel multicompartment cylinders (MCCs) and hybrid nanowires of unmatched sophistication. The MCCs exhibit a desirable 1D-distribution of the compartments parallel to the cylinder axis. The selective generation of inorganics allows the preparation of perfectly aligned biaxial nanowires whose spatial compartmentalization can be tuned. The inorganic-organic hybrids are interesting as novel building blocks for nanotechnology, e.g. in opto-electronic devices, molecular junctions or nanoelectronics.

In general, ABC block terpolymers have substantially broadened the range of accessible self-assembled nanostructures. However, the development of miktoarm stars, i.e. star polymers bearing three or more different polymeric arms, enables even more complex structures, paving the way to new classes of functional particles. In bulk, novel cylindrical morphologies of unprecedented complexity are preferred as they can accompany the junction points at the phase boundary most easily.[14, 15] Cylindrical morphologies should be perfectly suited for multicomponent transport or membrane structures. In solution, Lodge and coworkers described the formation of new self-assembled multicompartment aggregates which cannot be found for linear polymers.[16, 17] This demonstrates that an increase in architectural complexity leads to advanced structures. Although these nanostructures are very fascinating, they are limited when thinking about applications, which often require 1D structures. Aside some concentric core-shell-corona structures, the major part of segmented cylindrical aggregates known are transversely structured, meaning that the compartments are perpendicular to the main axis, or only composed of small subdivisions.[1, 16-18] The MCCs described herein are fundamentally different as they possess the unique feature of having several different parallel aligned 1D compartments. This structure can only be realized by crosslinking a well-defined bulk structure of a miktoarm star terpolymer. So far, the crosslinking of block terpolymer morphologies has, at its best, led to core-shell particles[19] or Janus particles having a non-centrosymmetric corona. The experimental discovery of the latter nanomaterials has promoted the exploration of a variety of highly distinct applications in all fields of science, ranging from biomedicine to physics.[20] The side-selective decoration of desired compartments of the MCCs with inorganic nanoparticles renders hybrid nanowires, possessing the unique feature of having two longitudinally aligned compartments hybridized with inorganics via non-covalent interactions. Those structures principally allow the conductance of two signals within the same molecular device and may thus be ideally suited for nanoelectronics or as artificial nerves. Furthermore, the extent of compartmentalization can be tuned by the solvent polarity. Such a sophisticated and well-defined organization of hybrid nanowires is unmatched und thus of great importance for further developments in nanotechnology. The concept demonstrates that an increase in complexity of polymeric architectures can promote significant advances for hybrid materials with novel nanoscopic structures.

Results and Discussion

Our strategy is based on crosslinking the polybutadiene microdomain of a miktoarm star in bulk (Scheme 10 - 1). The SBV miktoarm star bears three different arms of polystyrene (PS), polybutadiene (PB) and poly(2-vinylpryidine) (P2VP), all connected in one branching point.[14] The polymer used is $S_{34}B_{11}V_{55}^{288}$, where subscripts and superscripts denote the weight fractions and the molecular weight in kg/mol, respectively. The asymmetric, ribbon-like PB domains (black) are surrounded by two symmetric and opposing PS (red), and two P2VP (green) domains, respectively.

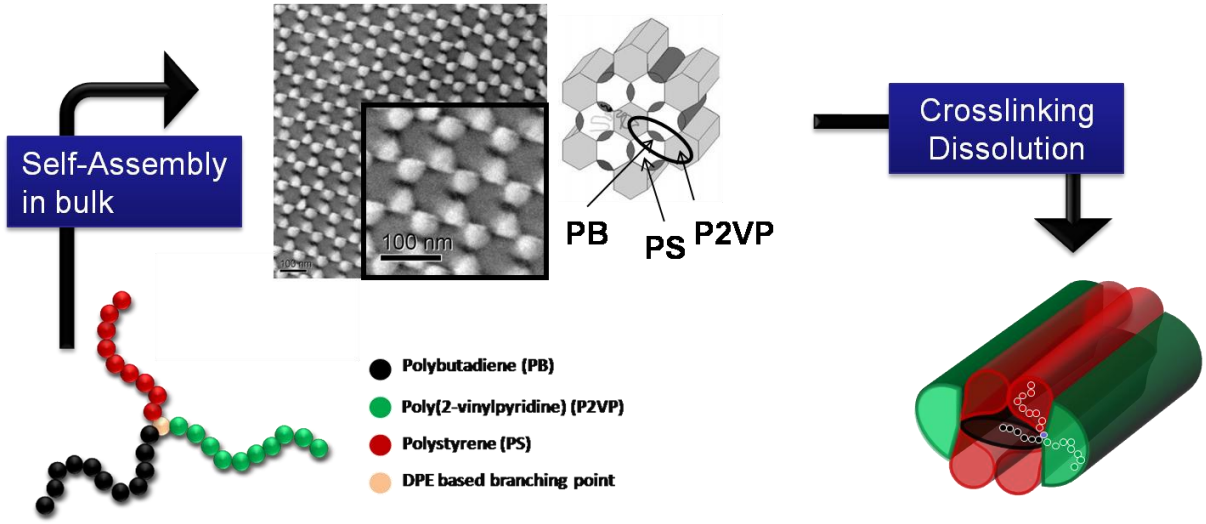

Scheme 10 - 1. Preparation of MCCs via crosslinking the polybutadiene phase (black) of a bulk structure of a SBV miktoarm star. The center shows a TEM micrograph and the schematic representation of the hexagonal bulk structure stained with OsO_4 and I_2. Therein polybutadiene, poly(2-vinylpyridine) and polystyrene appear black, grey and white.

Free-radical crosslinking of the PB domains, using a co-cast UV photo-initiator, preserves the micro-orientation of the bulk domains. Subsequent dissolution using sonication allows the transfer of this distinctive morphology into solution and yields our MCCs.

Most importantly, in contrast to core-shell-corona particles or Janus particles obtained by crosslinking linear block terpolymers, these MCCs cannot be obtained in similar precision by solution-based self-assembly of most complex amphiphiles.[16, 17]

The cylinders are several micrometers in length (Figure 10 - 1), tunable by the sonication time. Upon deposition of the cylinders onto a TEM grid, an internal structure of the particles is observed using toluene or tetrahydrofuran (THF) as solvents, but not for ethanol. Since ethanol and toluene are selective solvents for P2VP and PS, respectively, the cylinders undergo structural transformations within their corona. In ethanol, the P2VP chains surround the complete structure and lead to an almost homogenous cylinder. In toluene, the P2VP chains are collapsed and strongly compartmentalized into the two sides. In both selective solvents, a sufficient stabilization of the cylinders against aggregation occurs, confirming the presence of P2VP and PS in the corona. In THF, a common solvent for both corona blocks, the cylinders are partly phase-segregated due to the geometrical constraints imposed during the crosslinking in the bulk.

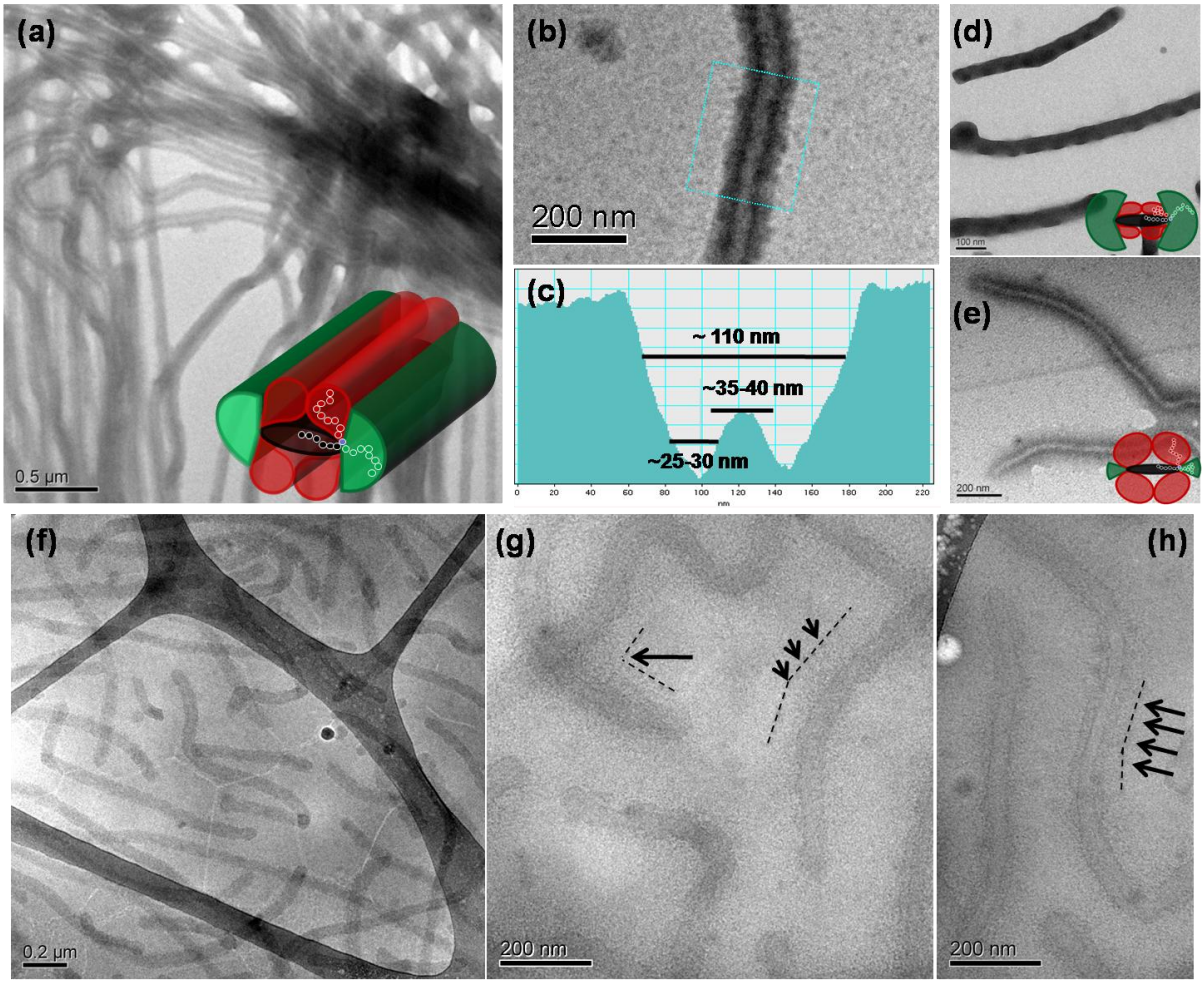

Figure 10 - 1. TEM micrographs of MCCs in THF (a,b), ethanol (d) and toluene (e). Image (c) shows a grey scale analysis of the area shown in image (b). Schematic drawings visualize the structural changes of the corona upon exposure to selective solvents. Low and higher magnification cryo-TEM images MCCs (1 g/L) in THF (f,g). Brush-like corona and an almost side-on view (h) of the MCCs are highlighted by arrows.

We now turn to the internal structure visible for THF and toluene. According to the bulk morphology, the PB phase forms a ribbon-like domain with an aspect ratio of 3 – 4 that is preserved during the crosslinking. Therefore, the cylinders, possessing an asymmetric cross-section, deposit with the broader side onto the grid. The P2VP cylinders are located at the two sides and PS is mainly above and below. Since contrast in TEM evolves from mass thickness, the darker parts at the side can be explained by the slightly larger mass density of the P2VP in contrast to the other components. The inner light grey cylinder has a diameter of ca. 35 – 40 nm, corresponding to the longer side of the PB ribbon in the bulk. The overall structure has a diameter of ca. 110 nm and is thus in a very reasonable region when bearing the dimensions of the microphase structure in mind.

Cryogenic TEM in THF provided further information on the structure of the cylinders in solution. Unimolecularly dissolved cylinders with moderate bending can clearly be identified. Only the core of the cylinders is visible. At higher magnification, a core-corona structure can be visualized. A slight grey shadow (highlighted by arrows) is visible surrounding the darker center of the structure. Since cryo-TEM images the structures embedded in a very thin vitrified film (< 100 nm), mainly the top view onto the ribbon-like cylinder can be found (see Supporting Information). The core diameter is mostly homogenous and slightly larger than the microphase structure and the TEM micrographs obtained in the dried state.

In a next step, we exploited the strong coordination ability of P2VP toward metal salts to generate inorganic-organic hybrid nanowires. Figure 10 - 2 shows compartmentalized hybrid cylinders obtained by the reduction/reaction of metal salts of (semi-)conducting Au, Ag and CdS nanoparticles in toluene.

All TEM micrographs exhibit the same feature, being the segregation of the nanoparticles at the two sides of the MCCs as amplified by the grey-scale section analysis of the Ag-loaded MCC. Nanoparticles are completely absent in the center (PS and PB phases) of the structure (ca. 25-30 nm), but are confined within the lateral compartments (P2VP phase at two sides of MCC, ca. 20 nm) and perfectly aligned in a parallel fashion. Further evidence for the presence of two parallel and spatially separated nanowires is provided by a tilt series, allowing the recording of TEM micrographs at various angles. Some images are displayed in Figure 10 - 2h and a movie is provided as Supporting Information. At zero angle, the center appears lighter with a maximum diameter. With increasing angle up to 60°, the brighter center disappears continuously and the segregation into two parallel compartments cannot be seen anymore, as the rear compartment starts to be partially covered by the front one. To exclude any drying artifacts during the TEM specimen preparation, we additionally recorded cryo-TEM of a different Ag-loaded sample in toluene (Figure 10 - 2g). In contrast to the image without metal nanoparticles (Figure 10 - 1f-h), the cylinders now exhibit two dark grey lateral compartments. The contrast originates from many tiny Ag nanoparticles, which cannot be resolved in cryo-TEM due to their extremely small size. Only some larger ones can be seen and confirm their coordination into the two sides of the cylinder. Note that the difference in contrast between the center of the MCC and the solvent almost vanishes because of the strong contrast originating from the Ag nanoparticles. In conclusion, the nanoparticles, when generated in toluene, are exclusively confined within the two P2VP sides (green in Scheme 10 - 1) and lead to the formation of perfectly aligned bi-axial inorganic-organic hybrid nanowires. Another interesting observation can be made at the end of the MCCs. The ends are “open”, meaning that the two hybridized sides are not connected. This feature, inaccessible from solution based crosslinking, is desired as it would allow an individual access of the nanowire compartments.

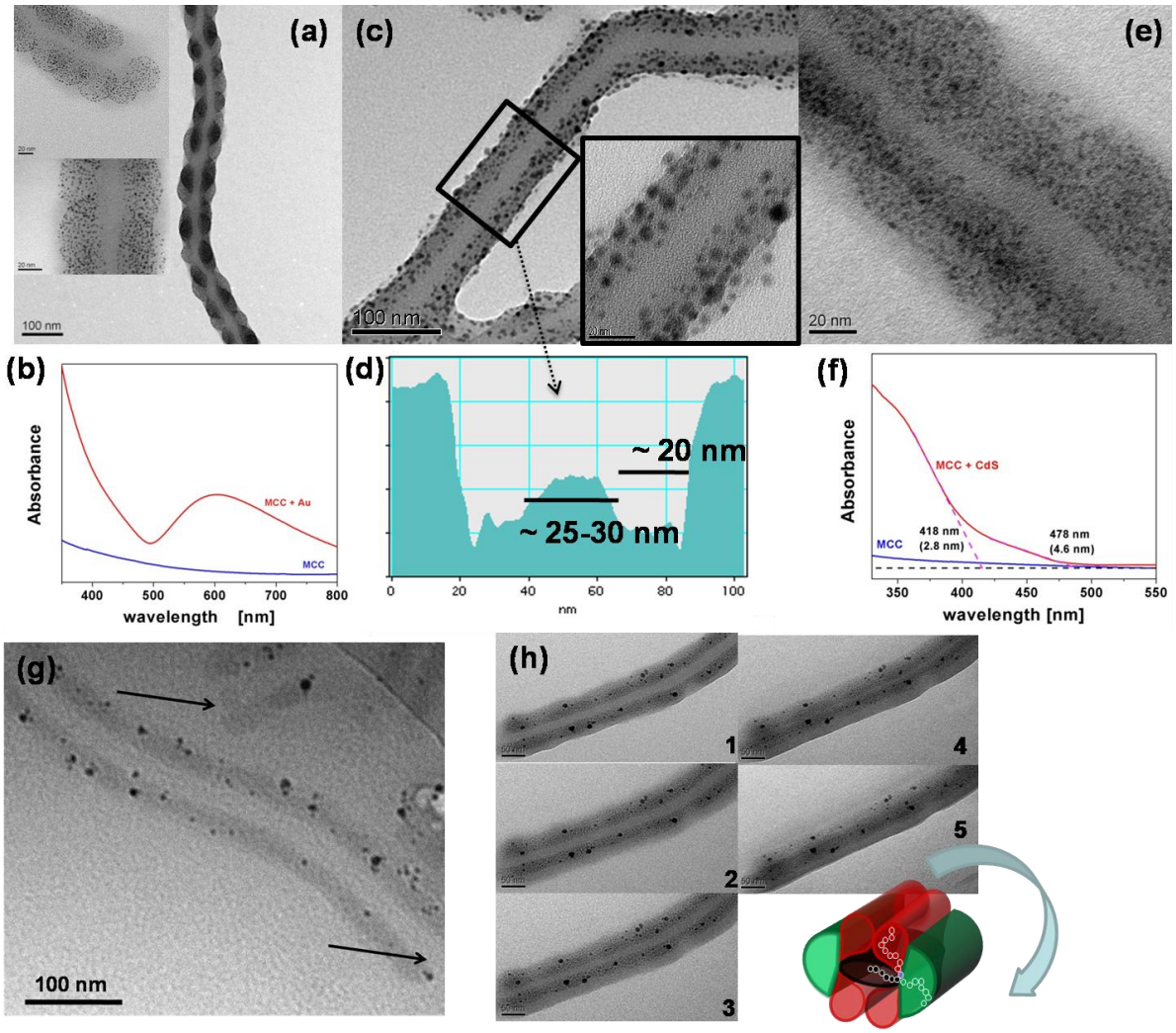

Figure 10 - 2. TEM micrographs of hybrid MCCs as prepared by reduction/reaction of various salts in toluene. (a) Au-loaded MCCs after UV reduction. (b) UV-Vis spectrum of Au-loaded MCC in toluene. (c) Ag-loaded MCCs after reduction using sunlight. (d) Grey-scale section analysis of the area shown in (c). (e) CdS-loaded hybrid MCCs and its UV-Vis spectrum (f). Cryo-TEM image (g) and tilt series (h) of Ag-loaded MCCs after UV reduction. The schematic drawing shows the sequence of recording during the tilt series (1 = 0°, 5 = 60°).

The optical properties of the hybrid MCC were investigated for the Au and CdS-loaded particles. In case of Au (diameter ≈ 2.5 nm), the UV-vis absorption band of the surface plasmon is found at ca. 600 nm (Figure 10 - 2b), significantly higher than for spherical gold nanoparticles (~ 520 nm).[21] It is characteristic of nanoparticles interacting in a string-like fashion.[22] Due to the strong insolubility of the P2VP·$HAuCl_4$ complex, an undulated structure is found (Figure 10 - 2a).[23] Interestingly, the coordination with Ag and Cd ions leads to very homogeneous compartments because an acid-base reaction with protonation is absent therein (Figure 10 - 2c and 2e). For CdS, the UV-vis spectrum illustrates two transition bands with thresholds at 418 and 478 nm (Figure 10 - 2f), corresponding to 2.8 nm (coinciding well with the TEM observation) and 4.6 nm (resulting from the coalescence of two nanoparticles due to their close proximity), respectively.

Due to the amphiphilic and solvent-responsive character of the corona, a tuning of the distribution of the nanoparticles in the corona has been achieved (Figure 10 - 3).

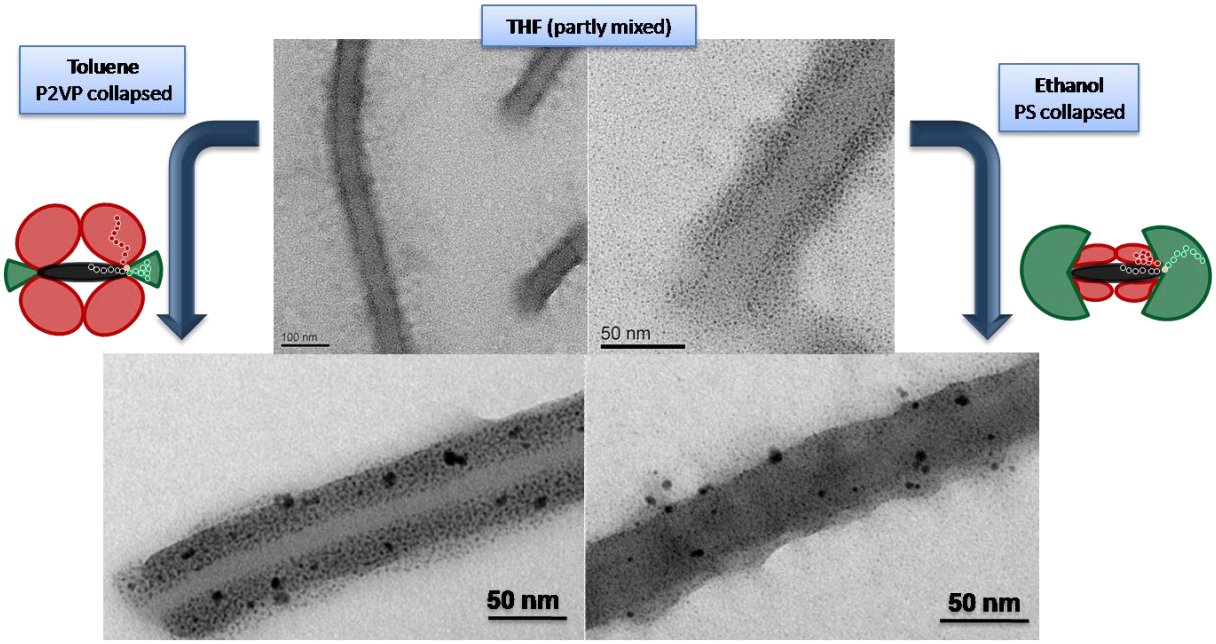

Figure 10 - 3. Structural changes of the corona upon exposure to selective solvents. TEM micrographs of Ag-loaded hybrid MCCs deposited from THF (a), toluene (b) and ethanol (c).

Initially, the Ag nanoparticles (d = 1 – 3 nm) prepared in THF are predominantly located within the two side compartments, whereas a certain amount (< 10 %) appears to reside in the center, meaning above or below. The appearance of particles in the center is caused by the incomplete phase segregation of the compartments in THF. Striking changes can be observed upon exchange of the solvent to toluene and ethanol via dialysis. In toluene, the nanoparticles undergo a drastic rearrangement. The hybrid MCCs exhibit a strong compartmentalization and confinement of the nanoparticles within the two cylindrical domains at the sides. On the contrary, the nanoparticles get redistributed within the full corona of the MCCs in ethanol as the PS arms collapse and the P2VP arms spread around the full corona. Importantly, the extent of compartmentalization can be tuned by the solvent choice and manipulated by changing the solvent quality. The two limiting cases are completely separated bi-axial and parallel nanowires and a homogeneous distribution in the corona.

In conclusion, we have demonstrated that sophisticated bulk structures of complex polymer architectures can be locally preserved and then transferred into novel and unique tunable cylindrical multicompartment structures in solution. Those are of such a high complexity that it can hardly be imagined to create them by solution-based self-assembly with a similar precision. This is of fundamental importance as it demonstrates that the research in direction of more sophisticated polymer topologies can indeed result in the formation of colloidal structures of unprecedented properties.

Herein crosslinking of a miktoarm star leads to MCCs. Their corona is subdivided into four solvent-tunable compartments, which can host (semi-)conducting inorganic nanoparticles. This allows the preparation of inorganic-organic bi-axial nanowires with a parallel arrangement. The compartments are completely separated. The particles can be redistributed within the corona of the hybrid-MCCs by changing the solvent quality. The two distinct structures possible are two separated but aligned nanowires within the same MCC or a single nanowire covering the full corona. This tunability, although only reached by a solvent exchange at the moment, can be of high importance when thinking about signal conductance in nanowires in general.

Looking out to the future, we expect developments taking place both in synthetic efforts towards functional polymers with complex architectures as well as in the improvement of novel functional structures based on most complex polymer topologies. Hybrid-MCCs, as presented here, are ideal candidates for conducting signals within two directions, in soft optoelectronic devices, nanoelectronics or as artificial nerves. Moreover, an improved responsive behavior may result in sensors or responsive junctions just by switching from a biphasic to a monophasic nanowire.

Our results demonstrate that structural restrictions for colloids, based on self-assembly of linear block copolymers can be overcome. Substantially new particles with very sophisticated and desirable architectures are accessible utilizing the bulk structures of miktoarm star terpolymers, quaterpolymers, etc. In terms of some device applications, these structures are more desirable than what could so far be obtained by solution based self-assembly of even the most complex polymeric amphiphiles and we believe to promote further research in this emerging area.

Acknowledgments

The authors acknowledge H. Hückstadt for the polymer synthesis and the DFG (DFG SPP 1165, Mu896/22) for financial support. A.W. thanks the Bavarian Elite Support Program for a fellowship.

Financial Interest Statement

The authors declare no competing financial interests.

References

1. Cui, H.; Chen, Z.; Zhong, S.; Wooley, K. L.; Pochan, D. J. *Science* 2007, 317, 647.
2. Nie, Z.; Kumacheva, E. *Nat. Mater.* 2008, 7, 277.
3. Geblinger, N.; Ismach, A.; Joselevich, E. *Nat. Nano.* 2008, 3, 195.
4. Wang, X.-S.; Winnik, M. A.; Manners, I. *Angew. Chem. Int. Ed.* 2004, 43, 3703.
5. van Hameren, R.; Schon, P.; van Buul, A. M.; Hoogboom, J.; Lazarenko, S. V.; Gerritsen, J. W.; Engelkamp, H.; Christianen, P. C. M.; Heus, H. A.; Maan, J. C.; Rasing, T.; Speller, S.; Rowan, A. E.; Elemans, J. A. A. W.; Nolte, R. J. M. *Science* 2006, 314, 1433.
6. Stupp, S. I.; LeBonheur, V.; Walker, K.; Li, L. S.; Huggins, K. E.; Keser, M.; Amstutz, A. *Science* 1997, 276, 384.
7. Huang, Y.; Duan, X.; Wei, Q.; Lieber, C. M. *Science* 2001, 291, 630.
8. Walther, A.; André, X.; Drechsler, M.; Abetz, V.; Müller, A. H. E. *J. Am. Chem. Soc.* 2007, 129, 6187.
9. Chai, J.; Buriak, J. M. *ACS Nano* 2008, 2, 489.
10. Valkama, S.; Kosonen, H.; Ruokolainen, J.; Haatainen, T.; Torkkeli, M.; Serimaa, R.; ten Brinke, G.; Ikkala, O. *Nat. Mater.* 2004, 3, 872.
11. Ruokolainen, J.; Makinen, R.; Torkkeli, M.; Makela, T.; Serimaa, R.; Ten Brinke, G.; Ikkala, O. *Science* 1998, 280, 557.
12. Balazs, A. C.; Emrick, T.; Russell, T. P. *Science* 2006, 314, 1107.
13. Lin, Y.; Böker, A.; He, J.; Sill, K.; Xiang, H.; Abetz, C.; Li, X.; Wang, J.; Emrick, T.; Long, S.; Wang, Q.; Balazs, A.; Russell, T. P. *Nature* 2005, 434, 55.
14. Hückstadt, H.; Göpfert, A.; Abetz, V. *Macromol. Chem. Phys.* 2000, 201, 296.
15. Wang, R.; Xu, T. *Polymer* 2007, 48, 4601.
16. Li, Z.; Kesselman, E.; Talmon, Y.; Hillmyer Marc, A.; Lodge Timothy, P. *Science* 2004, 306, 98.
17. Li, Z.; Hillmyer, M. A.; Lodge, T. P. *Langmuir* 2006, 22, 9409.
18. Wang, X.; Guerin, G.; Wang, H.; Wang, Y.; Manners, I.; Winnik, M. A. *Science* 2007, 317, 644.
19. Yan, X.; Liu, G.; Liu, F.; Tang, B. Z.; Peng, H.; Pakhomov, A. B.; Wong, C. Y. *Angew. Chem. Int. Ed.* 2001, 40, 3593.

20. Walther, A.; Müller, A. H. E. *Soft Matter* 2008, 4, 663.
21. Gao, J.; Bender, C. M.; Murphy, C. J. *Langmuir* 2003, 19, 9065.
22. Djalali, R.; Chen, Y. f.; Matsui, H. *J. Am. Chem. Soc.* 2002, 124, 13660
23. Polotsky, A.; Charlaganov, M.; Xu, Y.; Leermakers, F. A. M.; Daoud, M.; Müller, A. H. E.; Dotera, T.; Borisov, O. *Macromolecules* 2008, 41, 4020.

Supporting Information

Methods

The polymer used in this study is a miktoarm star terpolymer, bearing three arms of polystyrene (S), poly(2-vinyl pyridine) (V) and polybutadiene (B) , $S_{34}B_{11}V_{55}^{288}$. The subscripts and superscript denote the weight fractions and the overall molecular weight in kg/mol of the terpolymer.[14]

For the **crosslinking**, film casting was performed in the presence of 20 – 40 wt% of a UV photo-initiator (Lucirin TPO, courtesy of BASF). The addition of the photo-initiator did not alter the microphase segregated structure, indicating a low selectivity. Afterwards, the solvent cast films were annealed (100 ^{0}C for 2 days) and crosslinked in the bulk state using a standard UV lamp (cut-off < 320 nm). Subsequently, the crosslinked films were purified by soxhlet extraction with THF for 2 days. The insoluble fraction was then subjected to a sonication treatment utilizing a Branson digital sonifier until a semi-transparent solution was obtained (c = 1 – 10 mg/mL in THF, 1 min at 30% amplitude). In order to remove small cylinders, the solution underwent repeated centrifugation and redispersion cycles (each run at 13000 rpm for 50 min). Final dispersion in dioxane and freeze-drying yielded the product.

Coordination of inorganic salts. $AgPF_6$ (Aldrich, 99.99 %), silver acetate (Aldrich, 99.99 %), Cadmium cyclohexanebutyrate (Acros), and $HAuCl_4$ (Aldrich, 99.999 %) were used as precursors for the preparation of inorganic nanoparticles. In a typical experiment, a 1 mg/mL solution of multicompartment cylinders in toluene (THF or ethanol) was mixed with the desired salt under nitrogen atmosphere. The ratio of amine function to metal salt was kept in the range of 2-3, thus ensuring a high degree of loading. Afterwards, the mixtures were stirred for 24 h and sonicated for 15 min to allow a full coordination of the salt to the amine functions. Reduction was achieved by exposure to sunlight or using a UV lamp (cut-off < 350 nm) in the case of Ag and Au nanoparticles. CdS nanoparticles were prepared by reaction of cadmium ion coordinated multicompartment cylinders with hydrogen sulfide gas, which was introduced by bubbling through the solution.

Scanning Electron Microscopy (SEM). SEM was performed using a LEO 1530 Gemini instrument equipped with a field emission cathode with a lateral resolution of approximately 2 nm. The samples were uncoated and secondary electron detection was used. The acceleration voltage was chosen between 0.5 and 3 kV.

Transmission Electron Microscopy (TEM). The bulk morphology of the miktoarm star terpolymer were examined using TEM. Films (around 1 mm thick) were cast from 5% (w/w) solutions in $CHCl_3$ and allowed to evaporate slowly for two weeks. The as-cast films were dried for one day in vacuum at room temperature and then annealed at 100 °C for 2 days. Thin sections were cut at room temperature using a Reichert-Jung Ultracut E microtome equipped with a diamond knife. To enhance

the electron density contrast between the three blocks, the sections were exposed to OsO_4 and I_2 vapour for 60 s and overnight, respectively. This leads to a preferential staining of the polybutadiene block appearing black and the poly(2-vinylpyridine) block appearing grey. Bright-field TEM was performed on Zeiss LEO 922 OMEGA electron microscopes operated at 200 kV.

For **cryogenic transmission electron microscopy (cryo-TEM)** studies, a drop of the sample dissolved in THF was put on a lacey TEM grid, where most of the liquid was removed with blotting paper, leaving a thin film stretched over the lace. The specimens were instantly vitrifed by rapid immersion into liquid nitrogen and cooled to approximately 90 K by liquid nitrogen in a temperature controlled freezing unit (Zeiss Cryobox, Zeiss NTS GmbH, Oberkochen, Germany). The temperature was monitored and kept constant in the chamber during all of the sample preparation steps. Afterwards, the specimen was inserted into a cryo-transfer holder (CT3500, Gatan, München, Germany) and transferred to a Zeiss EM922 EF-TEM instrument. Examinations were carried out at temperatures around 90 K. The transmission electron microscope was operated at an acceleration voltage of 200 kV. Zero-loss filtered images (ΔE = 0 eV) were taken under reduced dose conditions (100-1000 e/nm^2). All images were registered digitally by a bottom mounted CCD camera system (Ultrascan 1000, Gatan) combined and processed with a digital imaging processing system (Gatan Digital Micrograph 3.9 for GMS 1.4).

UV/visible absorption spectra of samples were recorded on a Perkin-Elmer Lambda 15 UV/visible spectrophotometer. **Photoluminescence** spectra of samples were collected on a Shimadzu RF-5301 PC spectrofluorometer.

Cryo-TEM

In cryo-TEM, a thin film of a liquid, stretching over a hole of a suitable TEM grid, is vitrified by rapidly plunging into liquid ethane (for water) or liquid nitrogen (for organic solvents). This preserves the structure embedded inside the thin films and allows a quasi in-situ imaging of biological molecules or colloids. Due to the very thin film thicknesses of much below 100 nm, asymmetric particles are embedded with preferential orientations. This orientation behavior is schematically shown for a cylinder with an asymmetric, ellipsoidal cross section. The side-on view and the top view as used in the manuscript are shown to clarify the terminology.

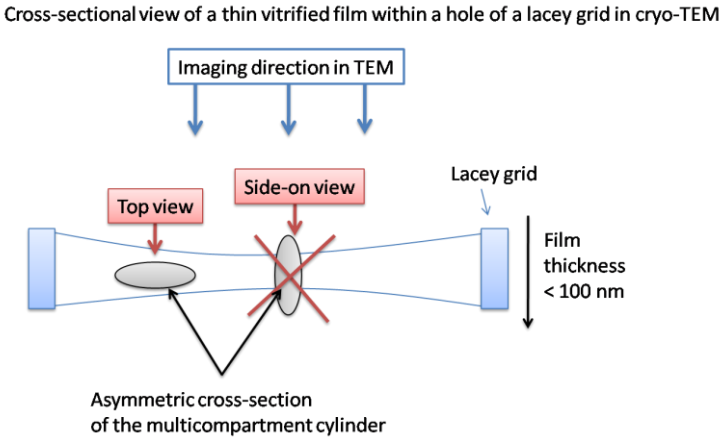

Scheme Sup 10 - 1: Preferential orientation of asymmetric particles within thin film during cryo-TEM investigations.

11. Multiple Morphologies, Phase Transitions and Crosslinking of Crew-Cut Aggregates of Polybutadiene-*block*-Poly(2-vinylpyridine) Diblock Copolymers

Andreas Walther, Anja S. Goldmann, Ram Sai Yelamanchili[#], Markus Drechsler, Holger Schmalz, Adi Eisenberg[&], Axel H. E. Müller

Makromolekulare Chemie II and Bayreuther Zentrum für Kolloide und Grenzflächen, Universität Bayreuth, D-95440 Bayreuth, Germany

[#]Anorganische Chemie I, Universität Bayreuth, D-95440 Bayreuth, Germany

[&] Department of Chemistry, McGill University, 801 Sherbrooke Street West, Montreal, Quebec H3A 2K6, Canada

Andreas.walther@uni/bayreuth.de, axel.mueller@uni-bayreuth.de

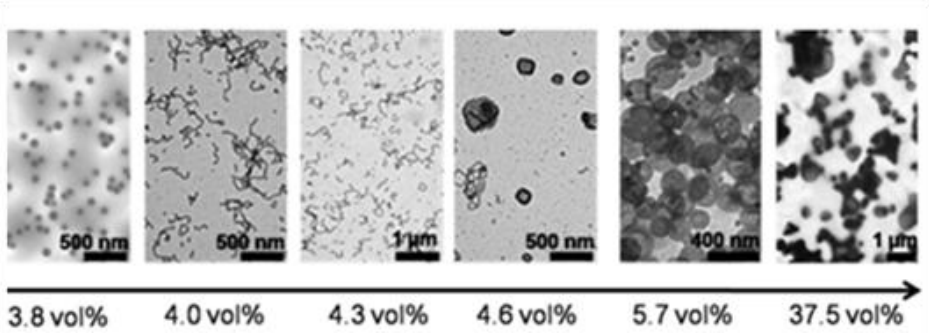

Published in: Macromolecules, **2008**, 41, 3254.

Abstract

We describe detailed investigations on the self-assembly of polybutadiene-*block*-poly(2-vinylpyridine) diblock copolymers into so-called crew-cut micellar aggregates in aqueous media. Three analogous diblock copolymers with different short segments of poly(2-vinylpyridine) were synthesized via anionic polymerization. The self-assembled aggregates are studied in dioxane/water mixtures by means of dynamic light scattering and transmission electron microscopy. Depending on the added volume fraction of water, spherical micelles, branched cylindrical micelles and vesicles can be found. These aggregates can be crosslinked in a facile fashion using a UV photoinitiator. The structures of the crew-cut aggregates remain intact during crosslinking, yielding stabilized polymeric nanoparticles. A transfer of these nanoparticles into common, only slightly selective solvents, in which no aggregates or different type of aggregates would exist without crosslinking, is possible. The crosslinked nanoparticle structures remain unchanged during this process. Moreover, a new pathway for the phase transition of cylindrical micelles to vesicles was found and is elucidated.

Introduction

Amphiphilic block copolymers are able to self-assemble into discrete well-defined nanoarchitectures upon exposure to selective solvents.[1-4] The properties and the aggregate structures can be modified via, e.g., changing the chemical composition of the constituting blocks.[5-9] Pioneering work by Eisenberg and others has given a deep insight in the formation mechanism[10-13], structural variety[9, 14, 15] and application possibilities of self-assembled aggregates.[16-19] A major interest in this research has been devoted to anionic polyelectrolyte systems, such as the polystyrene-block-poly([meth]acrylic acid) (PS-*b*-P[M]AA) systems.

In the field of cationically charged block copolymers and their self-assembly, in particular Förster and Armes[20-24] have reported results on micellar aggregation and properties. For instance, Förster et al. studied the fusion of micelles of polybutadiene-block-poly(2-vinylpyridine) (PB-*b*-P2VP) on different substrates via scanning force microscopy.[25] Furthermore, spherical aggregates were used for the templated synthesis of nanoporous silica.[26] Spherical micelles of quaternized PS-*b*-P4VP type in aqueous solution were reported by Selb[27, 28] and Eisenberg.[29, 30] In addition to that, pH induced phase transitions of PS-*b*-P4VP in DMF/H2O mixtures were investigated.[31] In general however, the solution studies of block copolymers containing vinylpyridine segments were mainly focused on inverse micelles in organic solvents based on polystyrene as hydrophobic block.[32-36] Concerning applications, inverse micelles were, for instance, used for templating inorganic nanoparticles inside the micellar core and subsequent catalytic reactions.[37] Very high turnover rates, high activities and long-term stability were found for the Pd catalyzed Heck reactions using Pd nanoparticles embedded into the P4VP core of inverse PB-b-P4VP micelles.[37] Vinylpyridine has extremely good coordination properties for metal ions and was used to create various catalytically active nanoparticles, such as Au[38], Pd[39], Co[40]. Recently, arrays of PS-b-P4VP micelles were used to create single-walled carbon nanotubes, demonstrating the versatility of the structures.[41]

One of the major drawbacks of self-assembled systems when aiming at applications, for instance in catalysis, is the fact that the structures depend on the type of solvent used. The tendency of forming defined aggregates is low when the block copolymer is exposed to a good solvent for both blocks, thus limiting the application range of nanoreactors or nanocontainers. For instance, micelles with polystyrene as inner block disassemble in most organic solvents and are thus not of wide applicability. Therefore, the crosslinking of block copolymer micelles and vesicles may serve as an alternative. Various efforts have been undertaken to crosslink the shell or the core of self-assembled nanoobjects.[42-44] In the case of polybutadiene containing block copolymers, the crosslinking is generally possible via γ -irradiation, radical reactions or 'cold vulcanization' using S_2Cl_2.[45-47] Recently, Maskos[48] reported on the crosslinking of micelles based on polybutadiene-block-poly(ethylene oxide) block copolymers using γ-irradiation.

Here, we present a systematic investigation of the phase transitions, morphological variety and facile UV crosslinking of PB-*b*-P2VP diblock copolymer aggregates. The two blocks of this diblock copolymer combine two advantageous features, i.e. the ability to crosslink the structure and the chelating properties of P2VP. Thus, the formed structures and their crosslinked analogues may be of wide applicability.

We demonstrate that crosslinking of the PB domains in various kinds of aggregates based on PB-*b*-P2VP diblock copolymers can be easily accomplished with a UV photoinitiator. In contrast to a γ-source, photoinitiators are readily available and can thus find widespread use, resembling a major advantage. Additionally, detailed investigations of the aggregate morphologies of PB-b-P2VP diblock copolymers crew-cut systems in aqueous solvent mixtures will be reported. Furthermore, a new pathway for the phase transition from branched cylindrical micelles to vesicles will be described, which is of fundamental importance for the study of diblock copolymer aggregates.

Experimental Section

Materials

Tetrahydrofuran (Merck, p.a.) was purified by successive distillation over CaH_2 and potassium and kept under dry nitrogen before usage. 2-Vinylpyridine (Acros, 97%) was distilled from CaH_2 under nitrogen. Subsequently, 2-vinylpyridine was degassed three times via freeze pump thaw cycles using a high vacuum line (10^{-4} - 10^{-5} mbar), stirred over Et_3Al for 2 h and condensed into storage ampoules. Butadiene (Linde) was passed over columns with molecular sieve and activated alumina, followed by storage over Bu_2Mg under purified nitrogen before use. Dioxane (Aldrich, p.a.), Lucirin TPO (BASF), s*ec*-BuLi (Acros, 1.3 M in cyclohexane/hexane: 92/8), Bu_2Mg (Aldrich, 1 M in heptane), Et_3Al (Aldrich, 1 M in hexanes) were used as received. Lucirin TPO is courtesy of BASF AG.

Synthesis

The synthesis of the polybutadiene-*block*-poly(2-vinylpyridine) diblock copolymers was accomplished via sequential living anionic polymerization of the corresponding monomers in THF using *sec*-BuLi as initiator. Prior to the reaction the used THF was treated with *sec*-BuLi at -40 °C followed by stirring over night at room temperature in order to produce alkoxides to stabilize the living polybutadiene. Butadiene polymerization was initiated with *sec*-BuLi at -70 °C, and butadiene was allowed to polymerize at -10 °C for 8 h. After subsequent cooling to -70 °C 2-vinylpyridine was added to the reaction mixture. After 1h reaction time the polymerization was terminated with degassed methanol, and the product precipitated in a water/methanol mixture. In order to produce a series of diblock copolymers with identical PB block but varying P2VP block lengths, samples were taken during 2VP polymerization at different conversions.

Mass spectrometry

MALDI-TOF MS analysis was performed on a Bruker Reflex III equipped with a 337-nm N2 laser in the reflector mode and 20 kV acceleration voltage. The number-average molecular weight, M_n, of the sample was determined in the linear mode.

Preparation of micellar aggregates

The micellar solutions were usually prepared by step-wise dialysis of dioxane solutions against water/dioxane mixtures of desired compositions. Only in case of studying the phase transition,

slow addition of water instead of dialysis was used. This allows a higher accuracy in terms of concentration and solvent composition. In all case Millipore water was used.

Crosslinking

Crosslinking of the micellar solutions (0.025 wt% - 0.5 wt%) in dioxane/water mixtures of any composition was accomplished by a UV initiator (0.2 – 5 mg/mL), Lucirin TPO. Prior to crosslinking with a Standard UV Lamp (cut-off < 350 nm) for 2 – 6 h, the sample was allowed to equilibrate for 6 – 24 h at room temperature.

Size Exclusion Chromatogrpahy (SEC)

SEC measurements were performed at room temperature on a system with PSS SDVgel columns (30 x 8 mm, 5 μm particle size) with 10^2, 10^3, 10^4, and 10^5 Å pore sizes using RI and UV detection (λ = 254 nm). THF was used as eluent (flow rate 1.0 mL/min) and the WinGPC software was used for data evaluation. Prior to measurements the samples were filtrated using 0.2 μm PTFE filters.

Dynamic Light Scattering (DLS)

Dynamic light scattering was performed on an ALV DLS/SLS-SP 5022F compact goniometer system with an ALV 5000/E cross-correlator and a He–Ne laser (λ_0 = 632.8 nm). Prior to the light scattering measurements the sample solutions were filtered using Millipore or Roth filters (housing: polypropylene, membrane: polytetrafluoroethylene) with a pore size of 0.45 - 1 μm. All samples were analyzed at high dilution. The data evaluation of the dynamic light scattering measurements was performed applying the CONTIN algorithm[49], which yields an intensity-weighted distribution of decay times after an inverse Laplace transformation of the intensity auto-correlation function. The polydispersities were determined from unimodal peaks via the cumulant method.

Transmission Electron Microscopy (TEM)

A droplet of the crosslinked micellar solution was placed on a formvar coated copper grid and most of the liquid was removed by blotting with a filter paper. Subsequently, bright-field TEM was performed on Zeiss CEM 902 and Zeiss EM 922 OMEGA FE-TEMs operating at 80 kV and 200 kV, respectively.

For **cryogenic transmission electron microscopy (cryo-TEM)** studies, a drop of the sample dissolved in THF was put on a lacey carbon transmission electron microscopy (TEM) grid, where most of the liquid was removed with blotting paper, leaving a thin film stretched over the lace. The specimens were instantly vitrified by rapid immersion into liquid nitrogen in a temperature controlled freezing unit (Zeiss Cryobox, Zeiss NTS GmbH, Oberkochen, Germany). The temperature was monitored and kept constant in the chamber during all of the sample preparation steps. After freezing the specimens, the specimen was inserted into a cryo-transfer holder (CT3500, Gatan, München, Germany) and transferred to a Zeiss EM 922 OMEGA FE-TEM. Examinations were carried out at temperatures around 90 K. The transmission electron microscope was operated at an acceleration voltage of 200 kV. Zero-loss filtered images (ΔE = 0 eV) were taken under reduced dose conditions (100-1000 e/nm^2). All images were registered digitally by a bottom mounted CCD camera system (Ultrascan 1000, Gatan) combined and processed with a digital imaging processing system (Gatan Digital Micrograph 3.9 for GMS 1.4).

Results and Discussion

Polymer Synthesis and Molecular Characterization

Three different polybutadiene-*block*-poly(2-vinylpyridine) (PB-*b*-P2VP) diblock copolymers were synthesized via sequential living anionic polymerization in THF using the same polybutadiene precursor with a predominant 1,2-structure (89% according to ^{1}H NMR). During the polymerization of the second block several samples were taken in order to obtain diblock copolymers with varying block lengths for the P2VP block. With this method it was possible to obtain a series of diblock copolymers, allowing a systematic study of the influence of the chain length on the aggregate structures formed. Table 11 - 1 shows a summary of the molecular characteristics of the different block copolymers.

Table 11 - 1. Polymer Characterization.

Sample code [a]	DP_n	$M_{n,NMR}$ [b] (kg/mol)	$M_{n,GPC}$ [c] (kg/mol)
B80V20	PB_{721}-$P2VP_{93}$	48.7	66.8 (1.02)
B87V13	PB_{721}-$P2VP_{56}$	44.9	66.4 (1.02)
B90V10	PB_{721}-$P2VP_{39}$	43.1	66.3 (1.02)

[a] The numbers denote the weight fractions in percent. [b] Molecular weight as calculated using the true molecular weight of the PB precursor, as determined by MALDI-ToF and the weight fractions as determined by ^{1}H-NMR. [b] Molecular weights as determined by THF GPC using a polystyrene calibration curve. The polydispersity index is given in brackets.

The molecular weights were calculated based on the absolute molecular weight of the PB precursor, determined by MALDI-TOF mass spectrometry (see Figure 11 - 1a), and the monomer unit weight fractions from ^{1}H-NMR spectra obtained for the different diblock copolymers. All polymers were designed to have a relatively short P2VP block in order to access the crew-cut regime for the micellar aggregates and to create a large variety of different structures. The polybutadiene precursor and the block copolymers exhibit both narrow molecular weight distributions as can be judged from the GPC elution traces in THF (see Figure 11 - 1b). Upon addition of the second monomer a distinct shift in the elution peak can be observed, corresponding to an increase in molecular weight and an extension of the polybutadiene to a diblock copolymer. Only a moderate shift of the peaks can be found within the series of the PB-*b*-P2VP diblock copolymers, which is however expected due to the interdependency of the increase in hydrodynamic radius and the adsorption of the poly(2-vinylpyridine) units onto the columns. The enlargement in hydrodynamic volume, caused by the increase in molecular weight, is somewhat counterbalanced by the rising adsorption. To further prove a complete blocking efficiency upon addition of the second monomer, a MALDI-TOF analysis of the diblock copolymer having the shortest P2VP chain was performed. The polybutadiene and the diblock copolymer B90V10 are structurally most analogous within the series and are thus expected to undergo ionization with a similar efficiency. The corresponding spectrum (see Figure 11 - 1c) shows a complete shift of the main peak of the polybutadiene precursor to higher molecular weights for the diblock copolymer, B90V10. Any remaining polybutadiene precursor cannot be identified and we can thus indeed conclude a full initiation of the second block. The determined number-average molecular

weight, M_n, changes to 43.7 kg/mol, which is in excellent agreement with the calculated molecular weight based on the ^{1}H-NMR of the diblock.

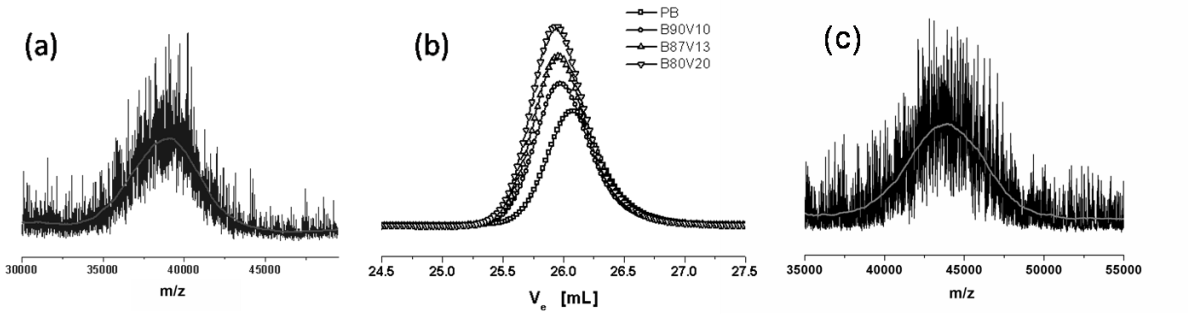

Figure 11 - 1. (a) MALDI-TOF spectrum obtained for the polybutadiene precursor after completion of the polymerization of the first block. (b) THF GPC elution traces of the polybutadiene precursor and the diblock copolymers. (c) MALDI-TOF spectrum obtained for B90V10.

Aggregate Morphologies

Despite the low glass transitions temperature of the polybutadiene, the diblock copolymers are not directly soluble in acidic water. This is presumably due to the large PB fraction in the diblock copolymers. Therefore, step-wise dialysis or slow addition of water was chosen to prepare the micellar aggregates. Due to the strong insolubility of polybutadiene in water, micellar aggregation can be induced by changing the solvent quality from a good solvent (i.e. dioxane) for both blocks to a selective solvent. Neutral water was used instead of acidic water in order to minimize charging of the P2VP chains during dialysis. It is expected that charged P2VP chains occupy more space due to electrostatic repulsion than uncharged ones, which may be unfavorable for the development of crew-cut aggregates, like worm-like micelles and vesicles. However, in the last stage of the process and if fully water-soluble structures are to be obtained, one has to dialyze against acidic water in order to allow for a sufficient stabilization of the P2VP chains, as P2VP is insoluble in water at neutral pH.

First investigations were focused on the kind of aggregates that can be found at high water concentrations. Results from Eisenberg and others had shown that the usual phase transitions start from unimers to spherical micelles to worm-like micelles and then to vesicles upon addition of water to dioxane solution of amphiphilic block copolymers. Hence, a variety of structures at low water concentration can only be expected for diblock copolymers forming vesicles at high water concentrations (here: dioxane/water = 1/1).

Figure 11 - 2 show dynamic light scattering data and transmission electron micrographs of the aggregates formed by the diblock copolymer. The TEM micrographs were acquired after crosslinking a 0.25 wt% solution of the diblock copolymer in dioxane/water (1/1 v/v or 5/3 v/v) mixtures. Crosslinking of the particles is necessary to allow an imaging of the structures, as uncrosslinked particles often tend to disassemble and form films upon deposition on the TEM grids. The successful crosslinking will be shown in the following section of this publication. At this point

it may just be mentioned that the aggregates remain structurally unaffected during the crosslinking process using a UV photoinitiator.

The plot of decay rates vs. squared scattering vector does not show any strong angular dependence and the linear fit of the data passes through the origin, indicating the observation of real diffusive spherical particles.[50] Viscosity and refractive index data from Nayak et al.[51] were used to correctly treat the DLS data in dioxane/water mixtures.

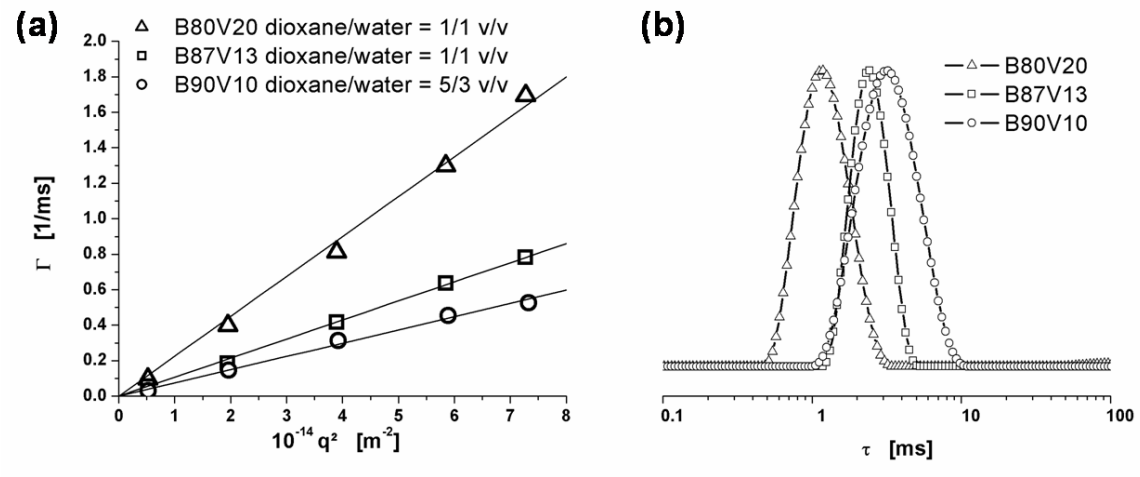

Figure 11 - 2. (a) Dependence of the decay rate on the scattering vector for the aggregates formed by the different diblock copolymers, as indicated in the graphs. The diffusion coefficients were determined from the slopes of the fitted lines. (b) Decay time distributions as obtained by CONTIN analysis at 90°. The measurements were conducted at 0.33 mg/mL in dioxane/water (1/1 and 5/3 v/v).

The DLS shows comparable slopes and diffusion coefficients (see Figure 11 - 2a) for B87V13 and B90V10 and correspondingly a similar distribution in the CONTIN plots (see Figure 11 - 2b). On the contrary, B80V20 has a significantly higher diffusion coefficient and a CONTIN plot shifted to lower decay times, indicating the presence of smaller aggregates.

The z-average hydrodynamic radius of B80V20 can be calculated from the slope of the linear fit to $\langle R_h \rangle_z$ = 64 nm using the Stokes-Einstein equation. Cumulant analysis yields a polydispersity index of 1.05. The TEM analysis of the crosslinked sample shows spherical type micelles which exhibit a similar size range compared to the hydrodynamic radius obtained from DLS. A statistical analysis yields number-average and z-average radii of $\langle R \rangle_n$ = 48 nm and $\langle R \rangle_z$ = 51 nm, which are slightly lower than the z-average hydrodynamic radius. A lower value for the radius obtained from the TEM is expected and the difference to the z-average hydrodynamic radius appears reasonable when bearing the fact in mind, that the P2VP chains are collapsed in the dried state and not extended as in solution. Furthermore, the polybutadiene core is not swollen with solvent (dioxane) in the dried state and may thus be shrunken to some extent as well.

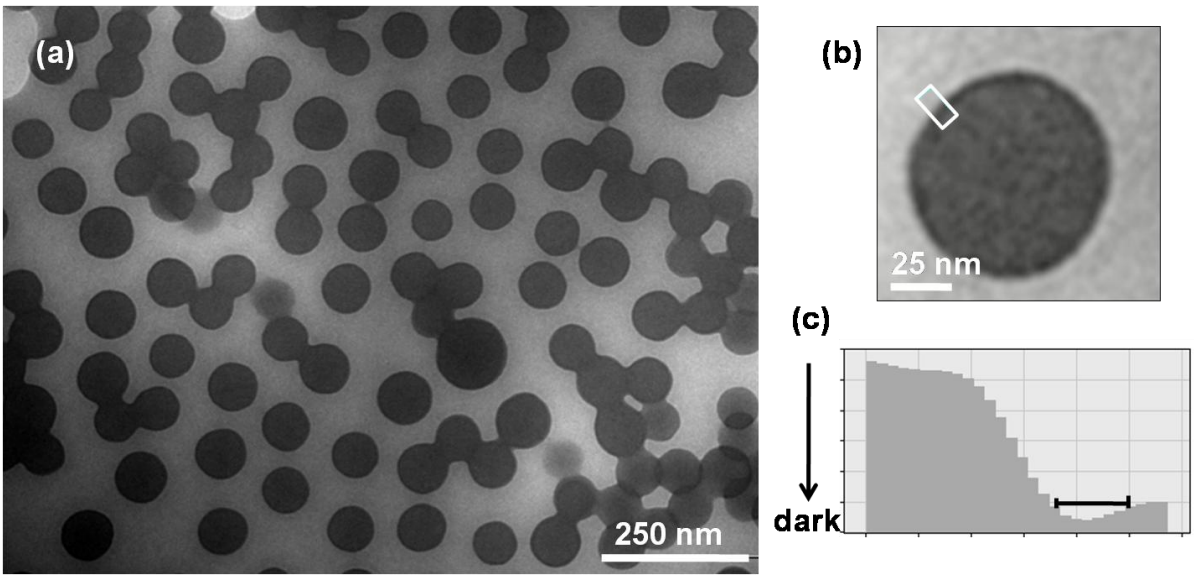

Figure 11 - 3. (a) TEM micrograph of B80V20 aggregates, which were photo-crosslinked in a dioxane/water (1:1) mixture (0.25 wt%). The sample was deposited onto a Formvar coated copper grid. (c) Section analysis of the white area of the magnified TEM image (b). The horizontal bar in image (c) indicates the presence of the dark ring surrounding the spherical micelle in image (b).

The micelles are well-defined and exhibit a moderately low polydispersity ($\langle R \rangle_w / \langle R \rangle_n$ =1.04). The magnified micelle in Figure 11 - 3b exhibits a dark ring surrounding the spherical micelle. This corona can be further elucidated by the section analysis, as presented in Figure 11 - 3c. The ring has an extension of ca 3 – 5 nm and originates from the collapsed P2VP corona shielding the PB core of the micelle. The slightly different contrast of P2VP and PB is sufficient to be directly imaged, even without further staining (e.g. by I_2). Due to the low fraction of P2VP in the corona, the structures can be considered as crew-cut micelles.

The other two block copolymers with even shorter P2VP blocks show a different aggregation behavior at high water concentrations. The DLS data again exhibit no significant angular dependence, which is indicative of spherical particles (see Figure 11 - 2).

The determined particle radii are $\langle R_h \rangle_z$ = 159 nm and 193 nm for B87V13 and B90V10, respectively. These aggregates are significantly larger than those formed by B80V20. B90V10 exhibits a broader distribution of decay times, reflecting the higher polydispersity with respect to B87V13. The polydispersities determined from the cumulant analysis (1.07 for B87V13 and 1.13 for B90V10) confirm this observation. The TEM micrographs (see Figure 11 - 4), obtained for both samples after crosslinking clearly show vesicles.

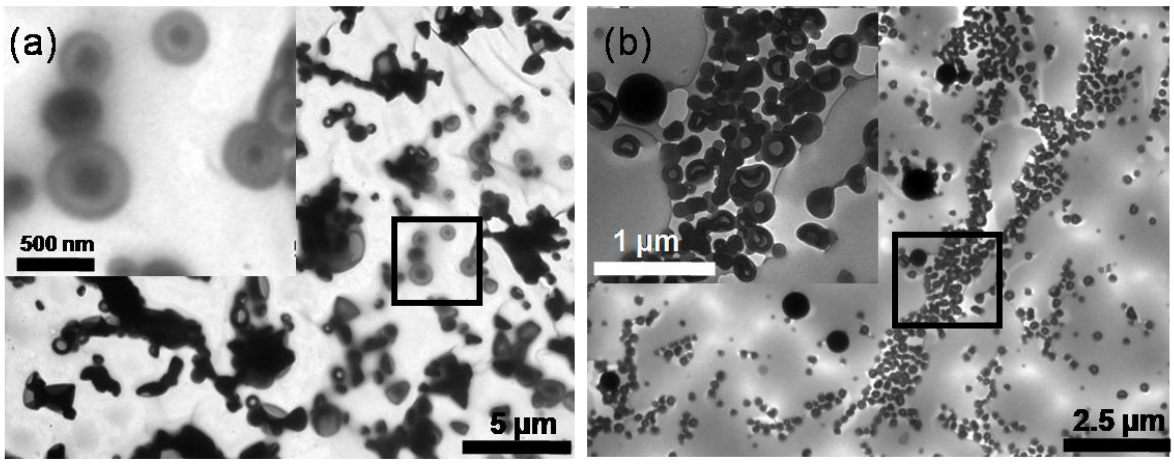

Figure 11 - 4. TEM micrographs of vesicles formed by B90V10 (a) and B87V13 (b) in dioxane/water mixtures (a = 5:3; b = 1:1). The particles were imaged on a Formvar coated copper grid after crosslinking of the solutions (c = 0.25 wt%). The insets represent magnifications corresponding to the squares shown.

B90V10 exhibits larger vesicles and a broader size distribution. Additionally, some vesicles appear to contain a core, which may be an indication for multilamellar vesicular aggregates. The larger aggregates present on the images seem to form during deposition, as they cannot be found in the DLS measurements. Aggregation of small particles into larger ones often occurs during the solvent evaporation process. This is why we always paid attention to the fact whether the structures found in TEM correspond to what can be found in DLS. It will be shown in the following section that the solution structures after crosslinking coincide with the ones before as concluded from the DLS data. B87V13, in contrast to B90V10, contains a small fraction of large compound micelles. Due to the appearance of vesicles in these two samples, one of them was selected for the later investigation of the phase-transitions which occur at lower water concentrations (see below).

Crosslinking

Before turning to the morphological transitions of the micellar system, the successful and facile crosslinking of different aggregate morphologies will be shown in the following. Generally, crosslinking of polybutadiene containing micellar aggregates can yield well-defined nanoobjects, which can find widespread use, i.e. as robust templates for inorganic materials. Herein, we present a new approach for the facile crosslinking of polybutadiene. Instead of γ-irradiation, which is a very non-invasive, however not a readily available and expensive technique, an oil-soluble photo crosslinker on phosphin oxide basis was used. The crosslinking can be conducted simply by mixing the micellar solution in dioxane/water mixtures with the photoinitiator and subsequent UV exposure. A coagulation of the structures and an intermicellar crosslinking was not observed, even not for higher concentrations of block copolymer up to 0.5 wt%. The hydrophobic UV-initiator is presumably located in the polybutadiene phase after a short equilibration time.

Dynamic Light Scattering was used in order to analyze whether the crosslinking has any effect on the type of micellar aggregate formed. Figure 11 - 5 displays a comparison of the angular dependent decay rates and several CONTIN plots before and after crosslinking of different samples.

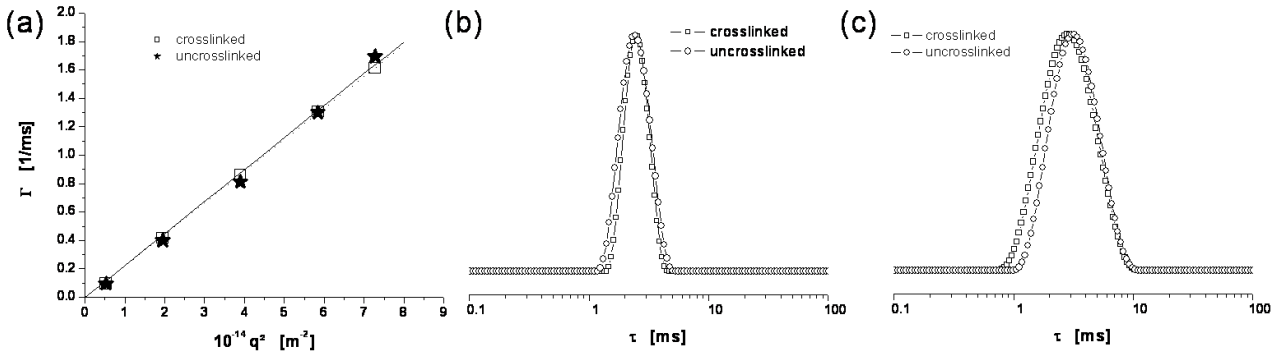

Figure 11 - 5. (a) Angular dependence of the decay rates of B80V20 before (c = 0.25 wt%) and after crosslinking (c = 0.1 wt%) in a dioxane/water mixture (1:1). (b) CONTIN plots (at 90o) before (c = 0.25 wt%) and after (c = 0.1 wt%) crosslinking of B87V13 in dioxane/water mixture (1:1). (c) CONTIN plots (at 90o) before (c = 0.25 wt%) and after (c = 0.1 wt%) crosslinking of B90V10 in dioxane/water mixture (5:3).

No major changes can be observed after crosslinking of the aggregates, independent of the aggregates shape, i.e. spherical micelle or vesicle. The decay rates for B80V20 essentially stay the same and the CONTIN plots for B87V13 and B90V10 neither exhibit significant changes. B90V10 shows a tiny shift towards smaller radii, indicating a slight contraction of the structures. Such small changes may however also be caused by the fitting procedure of the CONTIN algorithm in the evaluation of the autocorrelation functions.

After crosslinking, the particles were transferred into different solvents in order to prove the sufficient crosslinking and to explore their shape persistence upon changes in solvent quality. Figure 11 - 6 displays several TEM images obtained for the different diblock copolymers after crosslinking and transfer into ethanol or THF.

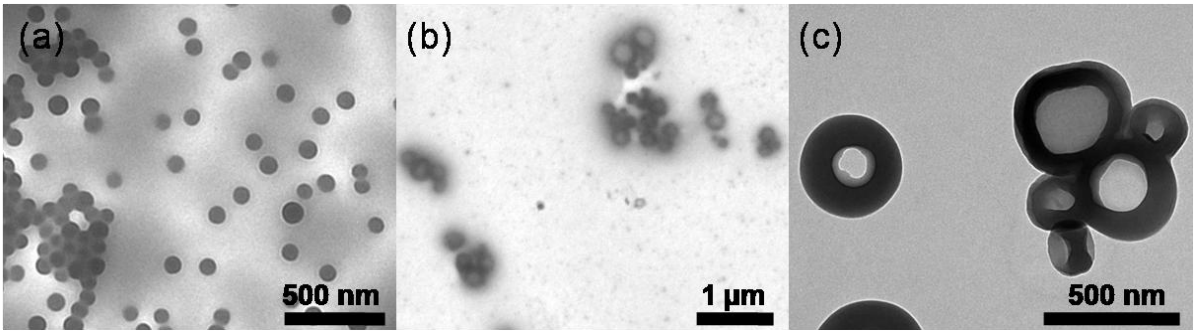

Figure 11 - 6. TEM micrographs of micelles and vesicles formed by B80V20 (a), B87V13 (b), and B90V10 (c). The aggregates were crosslinked and transferred into different solvents, then deposited on a Formvar coated copper grid. Images (a) and (b) were acquired from THF solution, whereas image (c) was acquired from ethanol.

The images convincingly show that the crosslinked structures of the aggregates remain intact after transfer into different solvents in which disassembly or a morphological transition is expected. After transfer, B80V20 still exhibits spherical micelles, whereas B87V13 and B90V10 show vesicles. The structures found coincide with the initial structures found in dioxane/water mixtures (Figure 11 - 3 & 4). The efficiency of the crosslinking can be ultimately confirmed by a comparison with the aggregates formed by uncrosslinked B80V20 in THF solution. DLS analysis of B80V20 in THF gave an indication for a fraction of larger aggregates. In order to analyze the

structures, *cryogenic* TEM (*cryo*-TEM) measurements were performed. The concept of *cryo*-TEM in THF has recently been applied by our group to study the self-assembly behavior of complex polymeric particles in organic solvents.[47, 52]

The *cryo*-TEM image in Figure 11 - 7 clearly exhibits cylindrical micelles of uncrosslinked B80V20 in THF. Similar results were obtained for B87V13 and B90V10. However, after crosslinking of certain micellar or vesicular aggregates in dioxane/water mixtures and subsequent transfer into THF, cylindrical micelles cannot be found anymore (see Figure 11 -s 6a & 6b). This ultimately confirms the successful crosslinking of the polymeric nanoparticles. The aggregation behavior of all PB-*b*-P2VP diblock copolymers in THF is unexpected in the first place as THF is a presumably good solvent for both blocks. Most probably, the slight selectivity of the "common" solvent THF towards the two block segments is sufficient to induce this aggregation.

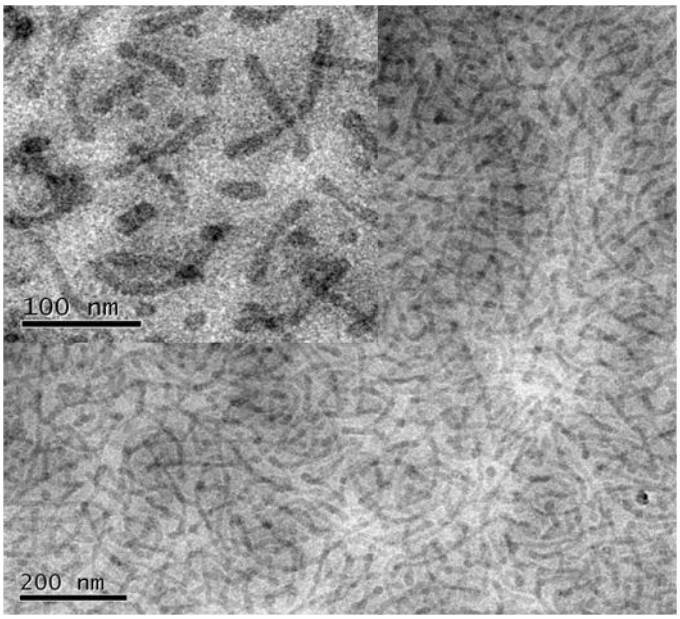

Figure 11 - 7. Cryo-TEM images obtained for a 1 wt% solution of B80V20 in THF. The inset shows a cryo-TEM image which was taken with a higher magnification at a different position.

In conclusion, the crosslinking of the particles can be easily performed for different kinds of aggregates. Additionally, the aggregates can be transferred into various solvents and the shape remains unaffected. Thus, the particles may, for instance, be applicable as catalyst carriers for inorganic nanoparticles in a wide range of solvents. In principle, the separation of crosslinked micelles or vesicles from a reaction mixture may be easily accomplished via ultrafiltration or centrifugation.

Phase Transitions

It is known from both experimental and theoretical work that block copolymers usually undergo phase transitions starting from spherical via cylindrical going to vesicular aggregates. In the case of PS-*b*-PAA block copolymers, the phase transitions can be induced by e.g. adding water to an initial solution of the diblock copolymer in an organic solvent,[5, 53-56] by changing the ionic strength,[57, 58] addition of base[57] or acid[57, 59] and to a small extent by temperature.[60]

B90V10 was selected for the investigation concerning the morphological transitions due to the observation of vesicles at high water concentrations and due to its composition, having the shortest P2VP block. Parallel DLS and TEM studies were conducted to identify the phase transitions. Figure 11 - 8 gives an overview of TEM micrographs obtained at different water contents.

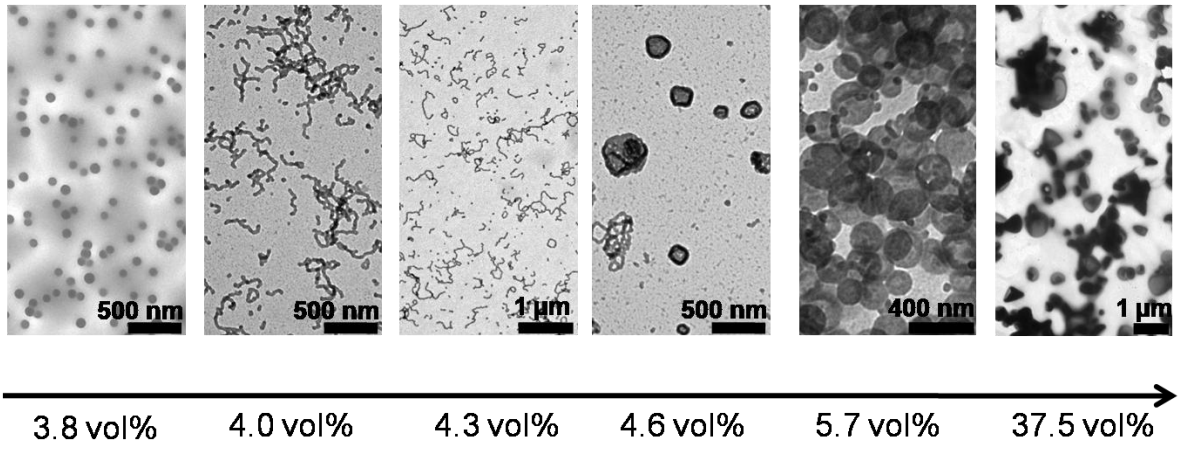

Figure 11 - 8. Phase evolution of crew-cut aggregates during the addition of water to a dioxane solution of B90V10 (c =0.5 wt%). The TEM images were obtained after crosslinking.

All phase transitions occur at very low water contents of less than 10 vol%. The system shows well developed spherical micelles for a very low water content of 3 vol%. A further increase induces a transition of the spherical micelles into branched worm-like micelles. The existence region of this type of aggregate is extremely narrow and worm-like micelles can only be found at water contents between 2 and 4 vol% in dioxane. The addition of more water to the system results in a transition of the branched worm-like micelles into vesicles. The transition occurs at a water content of 4.6 vol% under these particular conditions. At this point a coexistence of long worm-like micelles, with large globules and already developed vesicles can be found (see Figure 11 - 9). The coexistence of the different morphologies can be seen as an indication of a complex phase transition taking place at this point. The subsequently occurring vesicles still possess an internal structure inside their wall (see 4.6 and 5.7 vol% H_2O). This irregularly structured wall then disappears at higher water concentration and one ends up with standard vesicles at high water concentration. The polydispersity of the vesicles apparently increases with increasing water content, which might be caused by the decreasing solubility of the P2VP chains and its lower spatial requirement at higher water concentrations.

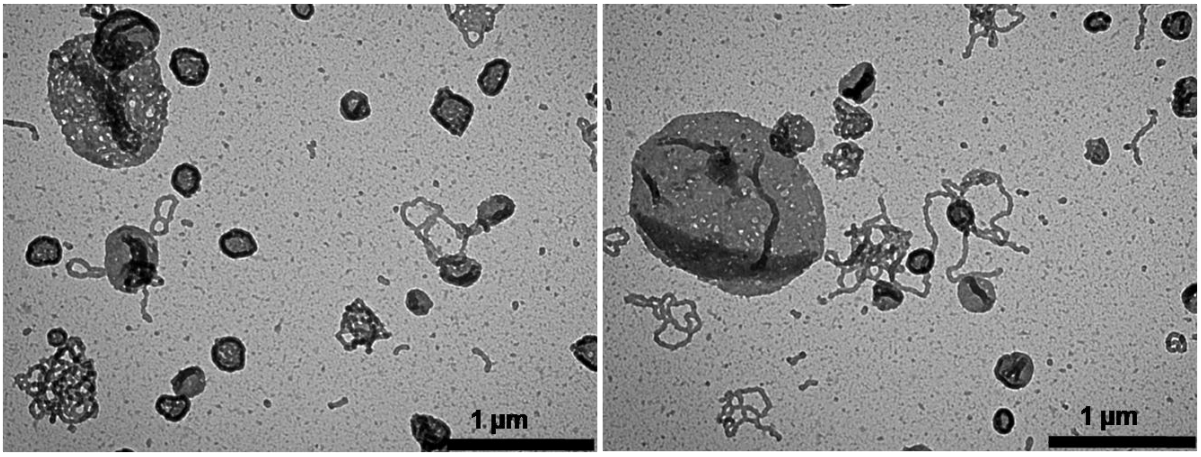

Figure 11 - 9. TEM micrographs obtained at the phase transition from branched cylindrical micelles to vesicles. The structures were crosslinked prior to imaging (c = 0.5 wt%, 4.6 vol% H2O).

Due to the appearance of large globules at the rod-vesicle transition and vesicles with internally structured walls, further attention was drawn to the phase transitions from branched cylindrical micelles to vesicles. The transition occurs in a completely different fashion than in the well-known crew-cut PS-*b*-PAA systems, investigated by Eisenberg and coworkers. In their case the transition follows a two step process. In the beginning, the cylinders transform into a lamellar structure, which then forms vesicles via a cup-like intermediate.[54] This mechanism finds some analogy with low-molecular weight amphiphiles which show a similar transition mechanism, involving a metastable disc-like bilayer structure.[61-63] Within this context it should also be mentioned that Discher et al. recently observed the network formation of worm-like micelles of a symmetric non-crew-cut PB-*b*-PAA diblock copolymer via fluorescence microscopy. They identified a network-like structure as last morphology before the observation of vesicles and higher ordered vesicles.[64]

In this case, we propose the following pathway: In the beginning of the transition, the branched cylinders assemble into larger globules, whereas distinct lamellar structures cannot be found. These globules may be very large in size as can be seen in the right-hand image of Figure 11 - 9. Importantly, a formation of the large globules during the deposition can be excluded as they can be observed everywhere on the TEM grid, even in very sparsely covered areas. The hollow globules still show the worm-like cylindrical micelle features in their walls. In a following step, the vesicles are formed out of these hollow globules. However, the question arises how these globules or larger structures are able to form vesicles of significantly smaller size. A more detailed look at many images helps to solve this question. Figure 11 - 10 exhibits several magnifications of larger globules.

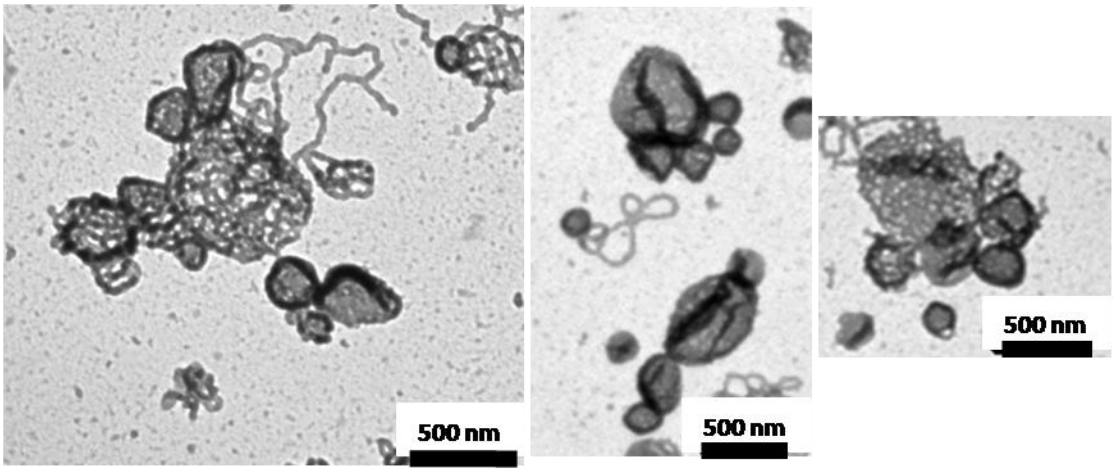

Figure 11 - 10. Magnification of TEM images obtained at the phase-transition from worm-like micelles to vesicles.

In the images presented, it can be seen that several smaller vesicles are connected to larger globules and network-like structures of worm-like micelles. Consequently, in order to complete the phase transition, these smaller vesicles must be released and completely separated from the larger globules and network-like aggregates. This observation can essentially explain how small vesicles are formed out of large globules. The large globules are unstable under the solvent conditions and do not lead to the formation of giant vesicles, but to the formation of small ones. The phase transition from worm-like micelles to vesicles can thus be reasonably understood. Upon further addition of water the rodlike features in the walls disappear and the cylinders in the walls of the small vesicles fuse to give unstructured vesicle walls in the end.

These results demonstrate that the phase-transition in block copolymers may follow significantly different pathways. The appearance of a certain pathway may depend on the individual system. The mechanism shown here may be a result of the branched nature of the cylindrical micelles, which certainly facilitates the formation of large hollow globules as compared to linear cylindrical micelles.

Conclusion

The phase-transitions and structures of crew-cut aggregates of polybutadiene-*block*-poly(2-vinylpyridine) were explored by combined DLS and TEM investigations. Depending on the block ratios and the added amount of water, differently shaped crew-cut aggregates are formed in dioxane/water mixtures. The morphologies change from spherical micelles via branched cylindrical micelles to vesicles with increasing water content. A new pathway for the transformation of cylindrical micelles into vesicles has been found. The cylinders assemble into large network-like structures and hollow globules and then release smaller vesicles upon completion of the phase transition.

The aggregates can be crosslinked via a simple photo-crosslinking method using a commercial UV photo-initiator, yielding stable nanoparticles of different architectures. It was shown that the stabilized nanoparticles can be transferred into different solvents under persistence of their shape, rendering them interesting for further applications in a large variety of solvents.

Acknowledgments

Denise Danz is acknowledged for the MALDI-ToF measurements and her help in the synthesis of the block copolymers. This work was supported by the European Union within the Marie Curie RTN POLYAMPHI and by the DFG within the EUROCORES project BIOSONS. A. Walther acknowledges financial support from the Bavarian Elite Support Program. R. S. Yelamanchili thanks the Bavarian Elite Network for a fellowship.

References

1. Li, C.; Buurma, N. J.; Haq, I.; Turner, C.; Armes, S. P.; Castelletto, V.; Hamley, I. W.; Lewis, A. L. *Langmuir* **2005,** 21, 11026.
2. Antonietti, M.; Förster, S. *Adv. Mat.* **2003,** 15, 1323.
3. Reiss, G. *Prog. Pol. Sci.* **2003,** 28, 1107.
4. Förster, S.; Plantenberg, T. *Angew. Chem.* **2002,** 114, 712.
5. Shen, H.; Eisenberg, A. *Macromolecules* **2000,** 33, 2561.
6. Yu, K.; Eisenberg, A. *Macromolecules* **1996,** 29, 6359.
7. Choucair, A.; Lavigueur, C.; Eisenberg, A. *Langmuir* **2004,** 20, 3894.
8. Terreau, O.; Luo, L.; Eisenberg, A. *Langmuir* **2003,** 19, 5601.
9. Zhang, L.; Eisenberg, A. *J. Am. Chem. Soc.* **1996,** 118, 3168.
10. Choucair, A. A.; Kycia, A. H.; Eisenberg, A. *Langmuir* **2003,** 19, 1001.
11. Burke, S. E.; Eisenberg, A. *Langmuir* **2001,** 17, 6705.
12. Yu, K.; Bartels, C.; Eisenberg, A. *Langmuir* **1999,** 15, 7157.
13. Zhang, L.; Eisenberg, A. *Macromolecules* **1999,** 32, 2239.
14. Kukula, H.; Schlaad, H.; Antonietti, M.; Förster, S. *J. Am. Chem. Soc.* **2002,** 124, 1658.
15. Zhang, L.; Eisenberg, A. *Science* **1995,** 268, 1728.
16. Borchert, U.; Lipprandt, U.; Bilang, M.; Kimpfler, A.; Rank, A.; Peschka-Suess, R.; Schubert, R.; Lindner, P.; Förster, S. *Langmuir* **2006,** 22, 5843.
17. Choucair, A.; Soo, P. L.; Eisenberg, A. *Langmuir* **2005,** 21, 9308.
18. Soo, P. L.; Luo, L.; Maysinger, D.; Eisenberg, A. *Langmuir* **2002,** 18, 9996.
19. Luo, L.; Tam, J.; Maysinger, D.; Eisenberg, A. *Bioconjugate Chem.* **2002,** 13, 1259.
20. Liu, S.; Armes, S. P. *Langmuir* **2003,** 19, 4432.
21. Cai, Y.; Armes, S. P. *Macromolecules* **2004,** 37, 7116.
22. Lee, A. S.; Buetuen, V.; Vamvakaki, M.; Armes, S. P.; Pople, J. A.; Gast, A. P. *Macromolecules* **2002,** 35, 8540.
23. Lee, A. S.; Gast, A. P.; Butun, V.; Armes, S. P. *Macromolecules* **1999,** 32, 4302.
24. Baines, F. L.; Armes, S. P.; Billingham, N. C.; Tuzar, Z. *Macromolecules* **1996,** 29, 8151.
25. Regenbrecht, M.; Akari, S.; Förster, S.; Möhwald, H. *Surf. Interface Anal.* **1999,** 27, 418.
26. Krämer, E.; Förster, S.; Göltner, C.; Antonietti, M. *Langmuir* **1998,** 14, 2027.
27. Selb, J.; Gallot, Y. *Makrom. Chem.* **1980,** 181, 809.
28. Selb, J.; Gallot, Y. *Makrom. Chem.* **1981,** 182, 1513.
29. Gao, Z.; Varshney, S. K.; Wong, S.; Eisenberg, A. *Macromolecules* **1994,** 27, 7923.
30. Yu, Y.; Eisenberg, A. *J. Am. Chem. Soc.* **1997,** 119, 8383.
31. Shen, H.; Zhang, L.; Eisenberg, A. *J. Am. Chem. Soc.* **1999,** 121, 2728.
32. Peng, H. S.; Chen, D. Y.; Jiang, M. *J. Phys. Chem. B* **2004,** 108, 5225.
33. Antonietti, M.; Heinz, S.; Schmidt, M.; Rosenauer, C. *Macromolecules* **1994,** 27, 3276.
34. Park, S.-Y.; Chang, Y.-J.; Farmer, B. L. *Langmuir* 22, 11369.
35. Calderara, F.; Riess, G. *Macromol. Chem. Phys.* **2003,** 197, 2115.
36. Peng, H. S.; Chen, D. Y.; Jiang, M. *Langmuir* **2003,** 19, 10989.

37. Klingelhöfer, S.; Heitz, W.; Greiner, A.; Oestreich, S.; Förster, S.; Antonietti, M. *J. Am. Chem. Soc.* **1997,** 119, 10116.
38. Förster, S.; Antonietti, M. *Adv. Mater.* **1998,** 10, 195.
39. Tsutsumi, K.; Funaki, Y.; Hirokawa, Y.; Hashimoto, T. *Langmuir* **1999,** 15, 5200.
40. Platonova, O. A.; Bronstein, L. M.; Solodovnikov, I. M.; Yanovskaya, I. M.; Obolonkova, P. M.; Valetsky, P. M.; Wenz, E.; Antonietti, M. *Colloid Pol. Sci.* **1997,** 275, 426.
41. Lu, J.; Yi, S. S.; Kopley, T.; Qian, C.; Liu, J.; Gulari, E. *J. Phys. Chem. B* **2006,** 110, 6655.
42. Prochazka, K.; Baloch, M. K.; Tuzar, Z. *Makrom. Chem.* **1979,** 180, 2521.
43. Guo, A.; Liu, G. J.; Tao, J. *Macromolecules* **1996,** 29, 2487.
44. O'Reilly, R. K.; Hawker, C. J.; Wooley, K. L. *Chem. Soc. Rev.* **2006,** 35, 1068.
45. Liu, Y.; Abetz, V.; Müller, A. H. E. *Macromolecules* **2003,** 36, 7894.
46. Erhardt, R.; Böker, A.; Zettl, H.; Kaya, H.; Pyckhout-Hintzen, W.; Krausch, G.; Abetz, V.; Müller, A. H. E. *Macromolecules* **2001,** 34, 1069.
47. Walther, A.; André, X.; Drechsler, M.; Abetz, V.; Müller, A. H. E. *J. Am. Chem. Soc.* **2007,** 129, 6187.
48. Maskos, M. *Polymer* **2006,** 47, 1172.
49. Provencher, S. W. *Makrom. Chem.* **1979,** 180, 201.
50. Stepanek, P. *J. Chem. Phys.* **1993,** 99, 6384.
51. Nayak, J. N.; Aralaguppi, M. I.; Naidu, B. V. K.; Aminabhavi, T. M. *J. Chem. Eng. Data* **2004,** 49, 468.
52. Walther, A.; Drechsler, M.; Abetz, V.; Müller, A. H. E. *to be published.*
53. Shen, H.; Eisenberg, A. *J. Phys. Chem. B* **1999,** 103, 9473.
54. Chen, L.; Shen, H.; Eisenberg, A. *J. Phys. Chem. B* **1999,** 103, 9488.
55. Yu, Y.; Zhang, L.; Eisenberg, A. *Langmuir* **1997,** 13, 2578.
56. Terreau, O.; Bartels, C.; Eisenberg, A. *Langmuir* **2004,** 20, 637.
57. Zhang, L.; Eisenberg, A. *Macromolecules* **1996,** 29, 8805.
58. Zhang, L.; Shen, H.; Eisenberg, A. *Macromolecules* **1997,** 30, 1001.
59. Zhang, L.; Eisenberg, A. *J. Pol. Sci. B* **1999,** 37, 1469.
60. Desbaumes, L.; Eisenberg, A. *Langmuir* **1999,** 15, 36.
61. Farquhar, K. D.; Misran, M.; Robinson, B. H.; Steyltler, D. C.; Morini, P.; Garret, P. R.; Holzwarth, J. F. *J. Phys.: Condens. Matter* **1996,** 8, 9397.
62. Edward, K.; Almgren, M.; Bellare, J.; Brown, W. *Langmuir* **1989,** 5, 473.
63. O'Connor, A. J.; Hatton, A. T.; Bose, A. *Langmuir* **1997,** 13, 6931.
64. Geng, Y.; Ahmed, F.; Bhasin, N.; Discher, D. E. *J. Phys. Chem. B* **2005,** 109, 3772.

12. CORE-CROSSLINKED BLOCK COPOLYMER NANORODS AS NOVEL TEMPLATES FOR THE ASSEMBLY OF POLYOXOMETALATES

Ram Sai Yelamanchili,[a] Andreas Walther,[b] Axel H. E. Müller[b] and Josef Breu [a]

[a] Department of Inorganic Chemistry I, University of Bayreuth, 95447 Bayreuth, Germany.

[b]Department of Macromolecular Chemistry II, University of Bayreuth, 95447 Bayreuth, Germany.

josef.breu@uni-bayreuth.de, *axel.mueller@uni-bayreuth.de*

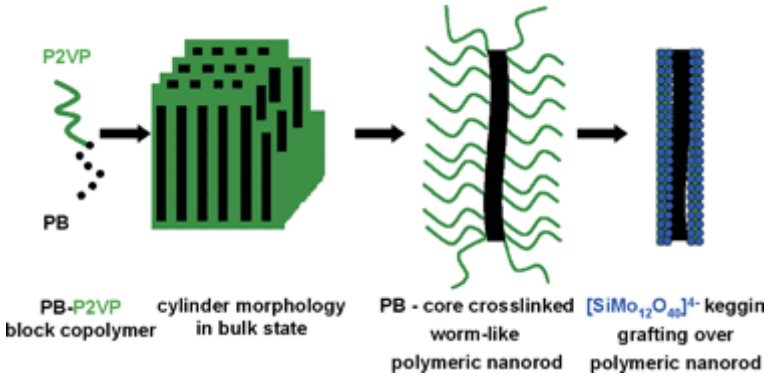

Published in *Chemical Communications*, **2008**, 489-491

Core-crosslinked PB-P2VP block copolymer nanorods are used as templates for the synthesis of keggin-type heteropolyoxometalate (POM) nanostructures by grafting $[SiMo_{12}O_{40}]^{4-}$ keggin ions on the template.

The organic template-directed synthesis of inorganic materials has attracted world wide attention due to the ability of organics to self-assemble into a variety of micelle nanostructures with well-defined shape and size.[1-3] An important class of organic templates used for the synthesis of materials is the amphiphilic block copolymers.[4] However, block copolymer micelles are very sensitive to the reaction conditions. Change in pH, temperature, solvent, or ionic strength can lead to micelle transformation or disintegration. For example, when polybutadiene-block-poly(2-vinylpyridine) (PB-P2VP) with 80% PB is dissolved in THF, worm-like micelles are formed in solution. Addition of water or protonation leads to a micelle transformation thus leading to undesired changes in the template morphology (see Supporting Information). Hence, the use of polymeric micelles to synthesize inorganic materials with desired morphologies is not always possible due to the dynamic nature of micelles. The micelle stability is especially important for the synthesis of materials which ask for changes in reaction conditions.

In this communication, we present a novel synthesis strategy for the development of inorganic nanostructures using core-crosslinked stable polymer templates. Scheme 12 - 1 summarizes this novel approach for the synthesis of desired inorganic nanostructures. Firstly, a block copolymer is synthesized which microphase-separates into a well-defined cylindrical bulk structure. Generally, adjusting the volume fractions and molecular weight of the block copolymer allows a facile tunability of the dimensions and shapes of the desired polymeric template. Secondly, it is possible to freeze the dynamics of the polymeric nanostructures by crosslinking the core, shell or even the surface.[5] In the present study, the core of the micelles is crosslinked and the resultant polymeric micelles are stable and resistant to changes in reaction conditions. Thirdly, protonation or quaternization can be performed at controllable rate to achieve charge matching between the polymer template and inorganic complexes. Fourthly, anionic inorganic precursors are grafted on the charged template and the inorganic/organic nanocomposite will precipitate. Please note, that when using an acidic inorganic precursor, quaternization of polymer template and grafting of the corresponding anion take place simultaneously.

Keggin-type heteropolyoxometalates (POM) were chosen as inorganic precursors due to the following reasons. Polyoxometalates (POM), the discrete metal-oxygen cluster compounds mainly of transition metals, exhibit fascinating properties and applications.[6] The properties of the POMs, particularly of the keggin-type, depend mainly on the nature of the counter cation and the composition of the POM anion.[7] POMs with high surface areas and controllable nanostructures are of interest in a variety of applications such as high performance catalysts (acid and redox), sensor devices and electrodes (due to their high ion conductivity, electron density, rapid and reversible oxidative-reductive processes).[7,8] But, POMs present relatively small surface areas, the surface area of commercial $H_4SiMo_{12}O_{40}$ is 4 m^2g^{-1}, which hinders accessibility to the active sites and as a result the applications of POMs are limited.[7] Hence, there is a great demand to develop POM materials with high surface area.

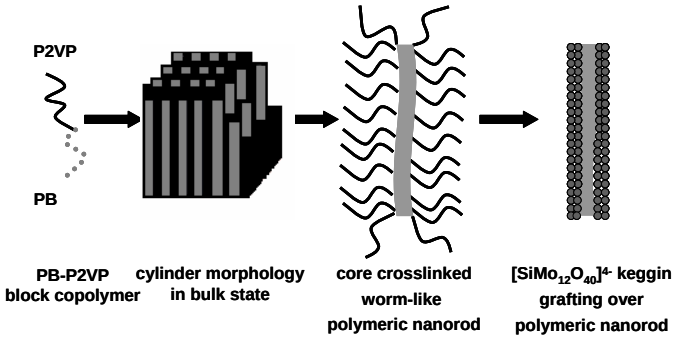

Scheme 12 - 1. Synthesis of $[SiMo_{12}O_{40}]^{4-}$ keggin nanostructures using core-crosslinked PB-P2VP worm-like polymer template and $H_4[SiMo_{12}O_{40}]$.

The efficiency of the POMs can be increased by two approaches. (1) using high surface area solids as supports to disperse POM and (2) developing composite materials with POMs as building blocks. Mesoporous silica materials like MCM-41 or SBA-15 have very high surface area (ca. 800–1000 m^2g^{-1}) and these materials were used as supports for the dispersion of POM.[9,10] There are also reports using carbon, silica gel, titanium gel, aluminium, etc. as solid supports for the dispersion of POM.[11] Even though, the accessible surface area for POMs can be increased by these methods, limitations rely on low POM loading, leaching of the active sites into the reaction medium and pore blocking in porous supports. Another approach involves the synthesis of POM nanocomposites using organic surfactants or polymers.[12,13] However, the accessible surface area is lower and organic templates need to be removed to have free access to the POM active sites but the hybrid structures tend to collapse during the template removal.[12] Neumann and co-workers used polymeric micelles to synthesize POM nanoparticles and observed improved catalytic activities for the developed POM nanostructures.[14] All together, these results indicate that the synthesis of chemically and physically well defined, discrete POM nanostructures with high accessible surface area is of great interest. But the synthesis of POM nanostructures requires control of various reaction parameters like pH, temperature, ionic strength, etc.. Hence, the templating micelles should be stable and resistant to changes in reaction parameters.

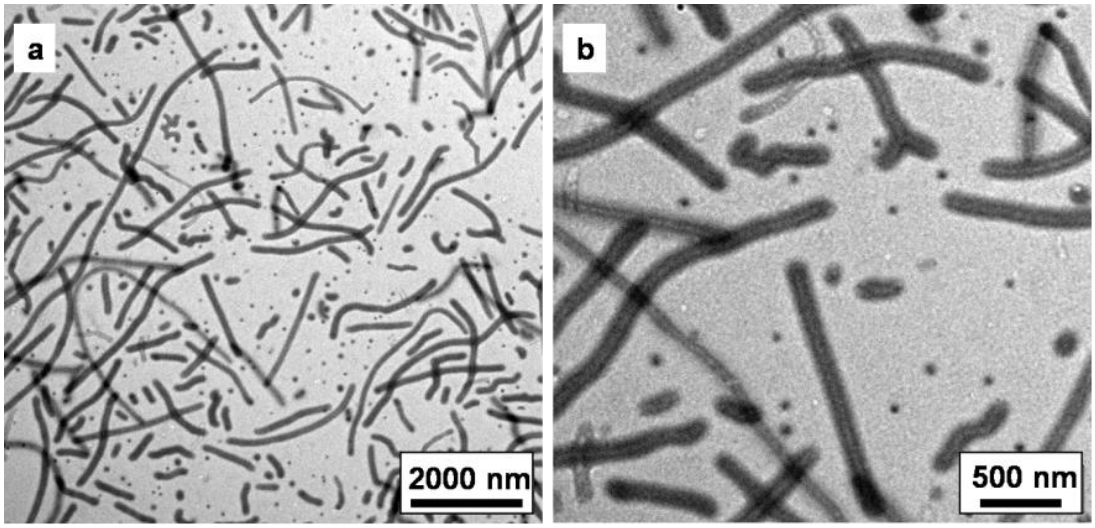

Figure 12 - 1. TEM images of the core-crosslinked PB-P2VP worm-like polymer template at different magnifications.

To prove our concept, a well-defined PB-P2VP block copolymer with 30 wt-% PB and a molecular weight of 2.0×10^5 g/mol was synthesized by anionic polymerization (see Supporting Information). The weight fractions are chosen in such a way that it forms a cylindrical morphology in the bulk state with PB-cylinders embedded in a P2VP matrix. The unsaturated PB-cores were crosslinked using a commercial photointiator to lock the cylindrical structure. The core-crosslinked cylinders exhibit worm-like morphologies when dissolved in THF or acetone. The block copolymer nanostructures were characterized using scanning electron microscopy (SEM), transmission electron microscopy (TEM), energy dispersive X-ray analysis (EDX), and Fourier transform infrared (FTIR) measurements.

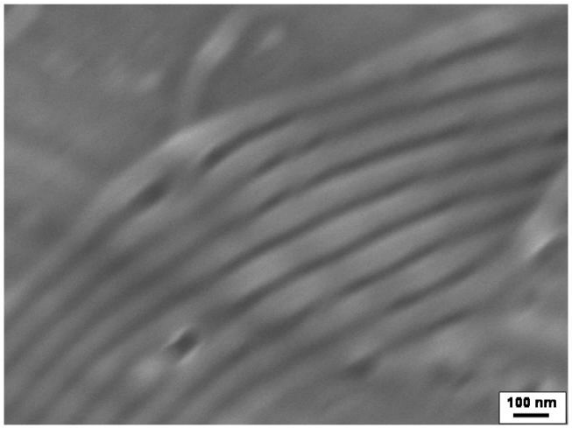

Figure 12 - 2. SEM image of the core-crosslinked PB-P2VP worm-like polymer template.

The TEM images of the core-crosslinked PB-P2VP worm-like polymer template are shown in Figure 12 - 1 (Zeiss CEM 902 microscope at an accelerating voltage of 80 kV). The core-corona structure of the worm-like polymer template is revealed due to the different electron penetrability of the PB core and P2VP corona. The diameter of the PB core is approximately 40 nm and the P2VP corona extends ca. 35 nm around the PB-core. The total diameter of the worm-like polymeric rods is ca. 110 nm. As sonication is necessary for the dissolution of the crosslinked PB-P2VP template, worm-like polymer rods with different lengths are observed. Figure 12 - 2 shows the SEM image of worm-like polymer rods (Leo 1530 FESEM), where the smooth surface of the polymer cylinders can be observed.

The keggin-type POM nanostructures can be synthesized by adding the PB-P2VP worm-like polymer solution to the $H_4SiMo_{12}O_{40}$ (POM) solution. Experimental details are provided in the Supporting Information. When neutral polymer rods in THF are added to the POM solution (which is a heteropolyacid) the 2-vinylpyridine units in the arms will be protonated, while the POM-anions are simultaneously grafted onto the template. Thus formation of the inorganic/organic nanocomposites is driven by strong Coulombic interactions between the 2-vinylpyridinium arms of the core-crosslinked PB-P2VP worm-like micelles and the inorganic POM anions. The polymer-POM nanocomposite is referred hereafter as POM-1. The produced POM-1 was characterized using SEM, EDX, TEM, FTIR, X-ray diffraction (XRD) and N_2 sorption measurements.

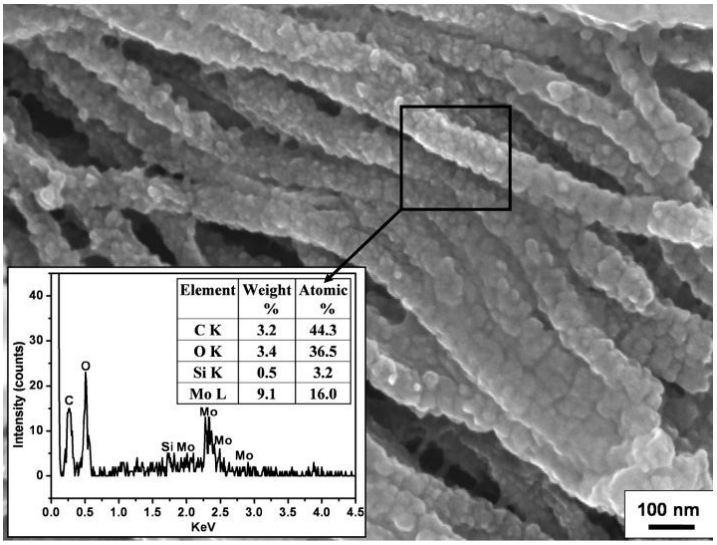

Figure 12 - 3. SEM image of the $[SiMo_{12}O_{40}]^{4-}$ keggin POM grafted onto core-crosslinked PB-P2VP worm-like polymer template (inset: EDX spectrum).

The formation of POM-1 can be directly observed by SEM and TEM. In comparison to the pure polymer nanorods (Figure 12 - 2), the surface of the POM-1 is rough (Figure 12 - 3). The surface roughness of the POM-1 is due to the grafting of $[SiMo_{12}O_{40}]^{4-}$ keggin around the polymer template. The selected area EDX spectrum clearly shows the presence of Si, Mo and C and confirms the grafting of $[SiMo_{12}O_{40}]^{4-}$ keggin around the template. The surface roughness due to the presence of $[SiMo_{12}O_{40}]^{4-}$ keggin POM around the polymer template becomes also obvious when comparing the TEM images of the pure polymer template (Figure 12 - 1) with POM-1 (Figure 12 - 4). The interaction of the inorganic $[SiMo_{12}O_{40}]^{4-}$ keggin POM with the P2VP block of the core-crosslinked PB-P2VP worm-like polymer template also changed the dimensions of the resultant composite nanostructures. In the absence of the $[SiMo_{12}O_{40}]^{4-}$ keggin POM anions, the P2VP corona of the core-crosslinked PB-P2VP worm-like polymer rods is stretched (ca. 35 nm around the core). Addition of $[SiMo_{12}O_{40}]^{4-}$ keggin POM caused the complexation of the 2-vinylpyridine units in the arms with the keggin anions and as a result the P2VP corona shrinks from initial ca. 35 nm to ca. 15-20 nm. The $[SiMo_{12}O_{40}]^{4-}$ keggin POM-grafted worm-like polymer rods exhibit overall diameters in the range of ca. 60-65 nm, thus significantly smaller than the initial pure worm-like polymer rod.

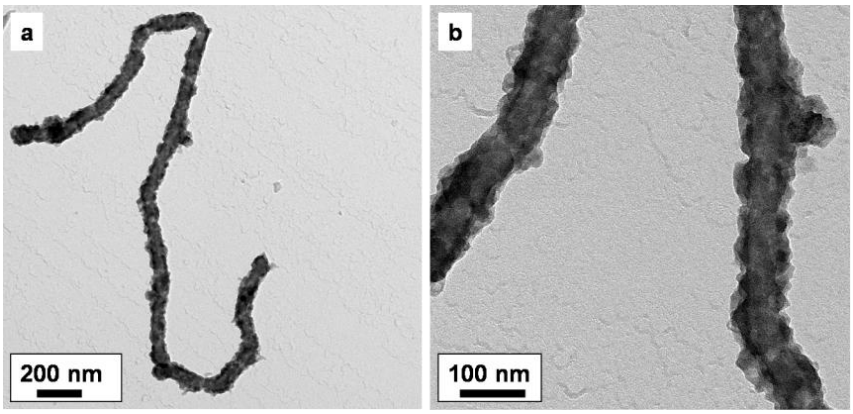

Figure 12 - 4. TEM images of the $[SiMo_{12}O_{40}]^{4-}$ keggin POM-grafted onto core-crosslinked PB-P2VP worm-like polymer template at different magnifications.

The grafting of $[SiMo_{12}O_{40}]^{4-}$ keggin POM over wormlike polymer rods was further verified by FTIR analysis. FTIR spectra (Bruker IFS66V using samples made with KBr pellets) of the pure $H_4SiMo_{12}O_{40}$ keggin POM, POM-1 and core-crosslinked polymer rod template are shown in Figure 12 - 5. It has been widely reported that the keggin-type heteropolyoxometalates show four characteristic bands, which are the fingerprint of the keggin structure.[15] There are four kinds of oxygen atoms in $H_4SiMo_{12}O_{40}$ (O_a – oxygen in SiO_4 tetrahedra, O_d – terminal oxygen atom to Mo, O_b – corner sharing oxygen and O_c – edge sharing oxygen) and these characteristic bands were observed at ν_{as} (Mo-O_d) – 952 cm^{-1}, ν_{as} (Mo-O_b-Mo) – 794 cm^{-1}, ν_{as} (Mo-O_c-Mo) – 864 cm^{-1} and ν_{as} (Si-O_a) – 902 cm^{-1}. The FTIR spectrum of the POM-1 corresponds well to the superposition of the spectra of the pure keggin type heteropolyoxometalates and PB-P2VP polymer rod template which is clear evidence that the keggin structure stayed intact when being grafted onto the worm-like polymer rods.

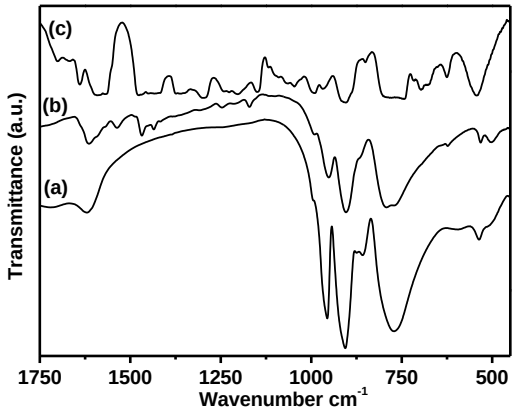

Figure 12 - 5. FTIR spectra of the (a) pure $H_4[SiMo_{12}O_{40}]$ keggin POM, (b) POM-1 and (c) core-crosslinked PB-P2VP worm-like polymer template.

In addition, wide-angle powder XRD patterns (PANalytical X-ray diffractometer with Ni-filtered Cu Kα radiation at 40 kv and 40 mA) of the pure $H_4[SiMo_{12}O_{40}]$ keggin POM, core-crosslinked worm-like polymer template and POM-1 were recorded (see Supporting Information). In contrast to the pure $H_4[SiMo_{12}O_{40}]$ keggin POM, XRD patterns of POM-1 do not show any characteristic peaks for $H_4[SiMo_{12}O_{40}]$. This amorpous nature is an indication of the very high degree of dispersion of keggin POM in the polymer matrix.[10d] The N_2 sorption measurements (at 77 K on a Quantachrome Autosorb 1) of POM-1 show that the developed keggin POM nanostructures have 37 m^2/g surface area, where as the commercially available POM ($H_4SiMo_{12}O_{40}$) only has 4 m^2/g surface area.

In conclusion, we presented a novel approach for the grafting of keggin-type heteropolyoxometalates around the core-crosslinked PB-P2VP worm-like polymer templates. The produced POM-1 exhibit high dispersion, improved surface area and are thus expected to be useful in catalytic, electrochemical and biotechnology related applications. An investigation of the properties of the POM-1 is ongoing together with steps aimed at the synthesis of other metal oxide nanostructures. The method appears to be generally applicable. For instance, $[PMo_{12}O_{40}]^{3-}$ keggin-type POM nanostructures can be synthesized following the same procedure (see Supporting Information).

Acknowledgment

This project is supported by Elite Network Bavaria (ENB). R. S. Y. and A. W. would like to acknowledge Elite Network Bavaria for a fellowship. We would like to thank Dr. Holger Schmalz and Dr. Markus Drechsler for their help with uncrosslinked polymer synthesis and *cryo*-TEM measurements, respectively.

References

1 F. Schüth, *Angew. Chem. Int. Ed.*, 2003, **42**, 3604.
2. R. Ulrich, A. D. Chesne, M. Templin and U. Wiesner, *Adv. Mater.* 1999, **11**, 141.
3. S. A. Davis, M. Breulmann, K. H. Rhodes, B. Zhang and S. Mann, *Chem. Mater.,* 2001, **13**, 3218.
4. S. Förster, in *Colloid Chemistry I Topics in Current Chemistry*, 2003, **226**, 1-28.
5. R. K. O'Reilly, C. J. Hawker and K. L. Wooley, *Chem. Soc. Rev.,* 2006, **35**, 1068.
6. M. T. Pope and A. Müller, *Polyoxometalate Chemistry From Topology via Self-Assembly to Applications,* Kluwer Academic Publishers, Netherlands, 2001.
7. J. B. Moffat, in *Metal-Oxygen Clusters - The Surface and Catalytic Properties of Heteropoly Oxometalates*, Kluwer Academic / Plenum Publishers, New York, 2001.
8. (a) K. Okamoto, S. Uchida, T. Ito and N. Mizuno, *J. Am. Chem. Soc.*, 2007, **129**, 7378; (b) K. Nomiya, H. Murasaki and M. Miwa, *Polyhedron*, 1986, **5**, 1031; (c) D. E. Katsolulis, *Chem. Rev.*, 1998, **98**, 359; (d) J. T. Rhule, C. L. Hill, D. A. Judd and R. F. Schinazi, *Chem. Rev.*, 1998, **98**, 327; (e) V. Kogan, Z. Aizenshtat and R. Neumann, *Angew. Chem. Int. Ed.*, 1999, **38**, 3331.
9. (a) C. T. Kresge, M. E. Leonowicz, W. J. Roth, J. C. Vartuli and J. S. Beck, *Nature* 1992, **359**, 710; (b) T. Blasco, A. Corma, A. Martinez and P. Martinez-Escolano, *J.Catal.,* 1998, **177**, 306; (c) Q. -H. Xia, K. Hidajat and S. Kawi, *J. Catal.,* 2002, **209**, 433.
10. (a) D. Zhao, J. Feng, Q. Huo, N. Melosh, G. H. Fredrickson, B. F. Chmelka and G. D. Stucky, *Science,* 1998, **279**, 548; (b) S.-Y. Yu, L. -P. Wang, B. Chen, Y.-Y. Gu, H. -M. Ding, and Y. -K. Shan, *Chem. Eur. J.*, 2005, **11**, 3894; (c) C. Shi, R. Wang, G. Zhu, S. Qiu and J. Long, *Eur. J. Inorg. Chem.,* 2005, **2005**, 4801; (d) L. Yang, Y. Qi, X. Yuan, J. Shen and J. Kim, *J. Mol. Catal. A: Chem.,* 2005, **229**, 199.
11. (a) P. M. Rao, A. Wolfson, S. Kababya, S. Vega and M. V. Landau, *J. Catal.*, 2005, **232**, 210; (b) L. R. Pizzio, C. V. Caceres and M. N. Blanco, *Appl. Catal. A: Gen.*, 1998, **167**, 283.
12. (a) A. Taguchi, T. Abe and M. Iwamoto, *Adv. Mater.,* 1998, **10**, 667; (b) A. Stein, M. Fendorf, T. P. Jarvie, K. T. Mueller, A. J. Benesi and T. E. Mallouk, *Chem. Mater.*, 1995, **7**, 304; (c) G. G. Janauer, A. Dobley, J. Guo, P. Zavalij and M. S. Whittingham, *Chem. Mater.*, 1996, **8**, 2096.
13. (a) H. Yun, M. Kuwabara, H. Zhou and I. Honma, *Thin Solid Films,* 2007, **515**, 2842; (b) A. Khanal, K. Nakashima, N. Kawasaki, Y. Oishi, M. Uehara, H. Nakamura and Y. Tajima, *Colloid Polym. Sci.,* 2005, **283**, 1226.
14. G. Maayan, R. Popovitz-Biro and R. Neumann, *J. Am. Chem. Soc.*, 2006, **128**, 4968.
15. C. Rocchiccioli-Deltcheff, M. Fournier, R. Frank and R. Thouvenot, *Inorg. Chem.*, 1983, **22**, 207.

Supporting Information

Experimental section

Synthesis of polymer and crosslinking reactions

The synthesis of the polybutadiene-*block*-poly(2-vinylpyridine) diblock copolymers (PB-P2VP) was accomplished via sequential living anionic polymerization. Butadiene polymerization was initiated with sec-BuLi at -70°C, and butadiene was allowed to polymerize at -10°C for 8 h. After subsequent cooling to -70°C, 2-vinylpyridine was added to the reaction mixture. After 1h reaction time the polymerization was terminated with degassed methanol, and the product precipitated in a water/methanol mixture. According to NMR and GPC, coupled to a multi-angle laser light scattering detector, the polymer synthesized is $PB_{30}P2VP_{70}^{200}$. The subscript numbers denote the mass fraction in percent, and the superscripts give the number-average molecular weight in kg/mol. For crosslinking of the block copolymer in the bulk state, a 10 wt% solution of PB-P2VP in THF was allowed to evaporate slowly in the presence of 40 wt% of Lucirin TPO, corresponding to the amount of polymer. After complete evaporation of the solvent and film annealing, the films were crosslinked on a UV lamp (cut-off < 350 nm) for 2 – 6 hours. Subsequently, soxhlet extraction was performed in THF and the insoluble product underwent ultrasonication in a THF dispersion in order to obtain soluble PB-P2VP core-crosslinked cylinders.

Synthesis of POM nanostructures

The template directed synthesis of the polyoxometalate nanostructures was carried out at room temperature. The core-crosslinked PB-P2VP polymer solution in THF (0.5 wt%) was added to 10 mL of 10^{-2} M $H_4[SiMo_{12}O_{40}]$ in THF with continuous stirring for 6h. With the addition of polymer solution, the yellow colour of the POM solution starts disappearing and when it reaches the neutralization point the yellow colour of the solution disappears completely. The resultant precipitate aged in the reaction mixture for 12 h. The precipitated was washed 3 times with deionized water and kept for overnight drying at 100^{o}C.

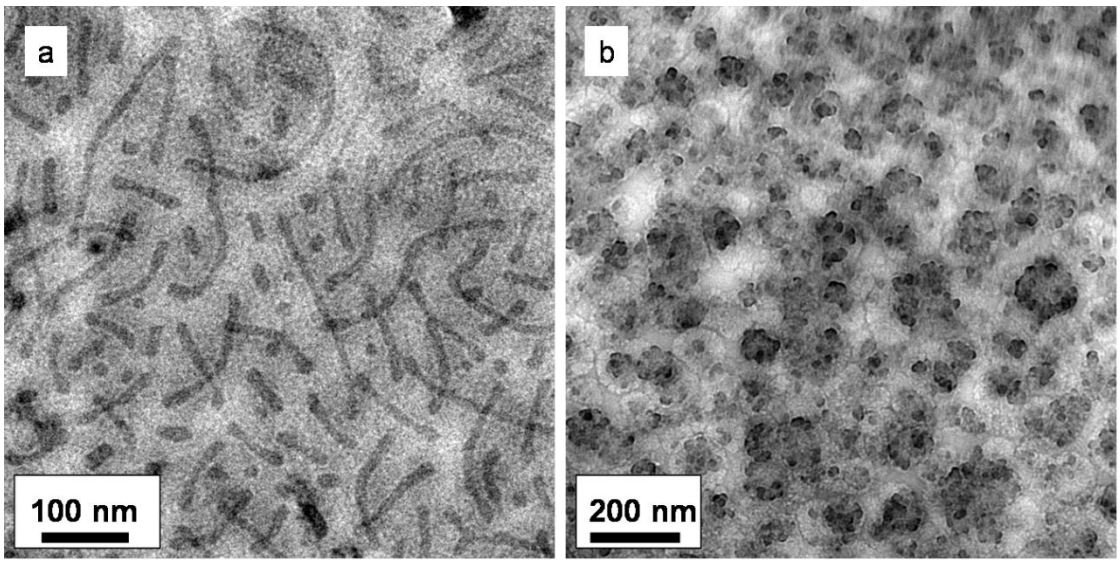

Figure Sup 12 - 1. Cryo-TEM images of the (a) 1 wt% of PB_{80}-$P2VP_{20}$ (64,900 g/mol) in THF wormlike micelles without core crosslinking, (b) 1 wt% of PB_{80}-$P2VP_{20}$ (64,900 g/mol) in THF acidified with 2M HCl.

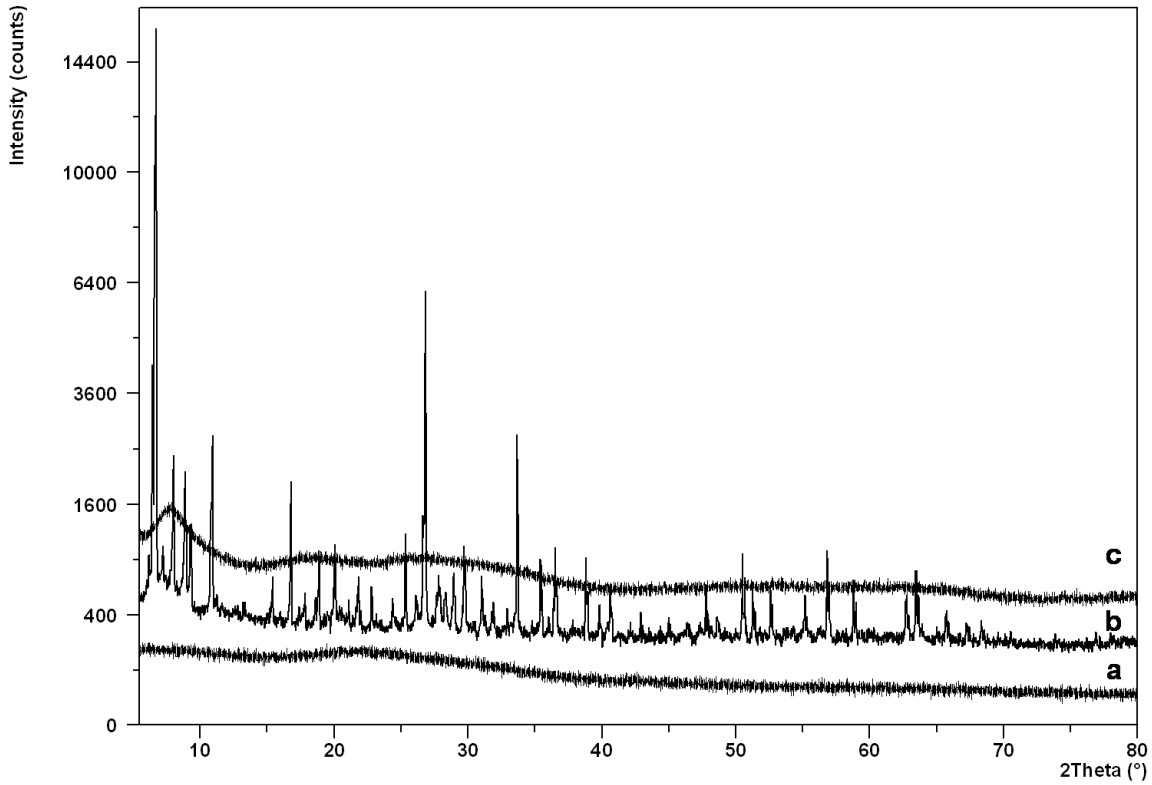

Figure Sup 12 - 2. Powder X-ray diffraction patterns of (a) core-crosslinked PB-P2VP polymeric nanorod template (b) pure POM and (c) POM-1.

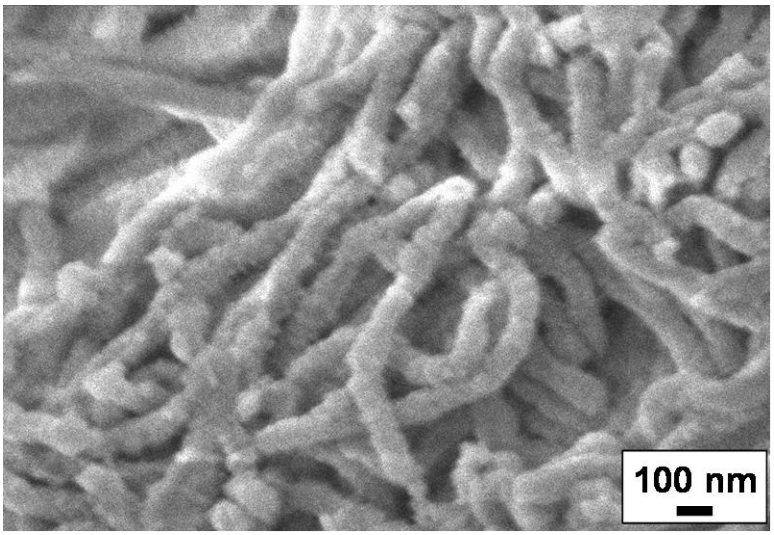

Figure Sup 12 - 3. SEM image of the $[PMo_{12}O_{40}]^{3-}$ keggin POM grafted over core-crosslinked PB-P2VP worm-like polymer template.

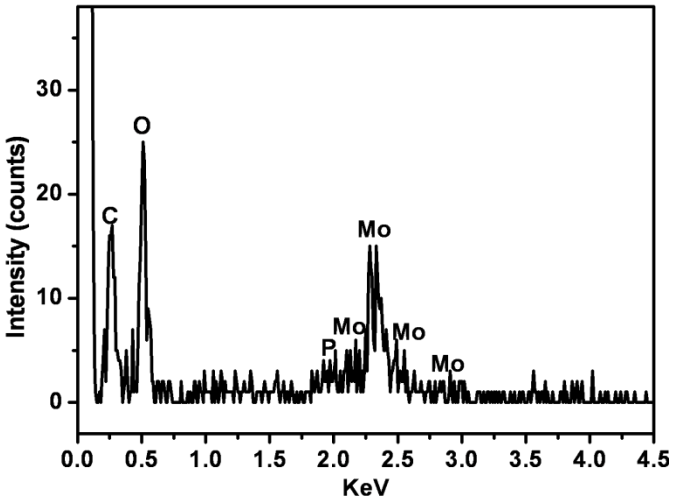

Figure Sup 12 - 4. EDX spectrun of the $[PMo_{12}O_{40}]^{3-}$ keggin POM grafted over core-crosslinked PB-P2VP worm-like polymer template.

13. JANUS PARTICLES

Andreas Walther, Axel H. E. Müller

Makromolekulare Chemie II and Bayreuther Zentrum für Kolloide und Grenzflächen, Universität Bayreuth, D-95440 Bayreuth, Germany

Andreas.Walther@uni-bayreuth.de; Axel.Mueller@uni-bayreuth.de

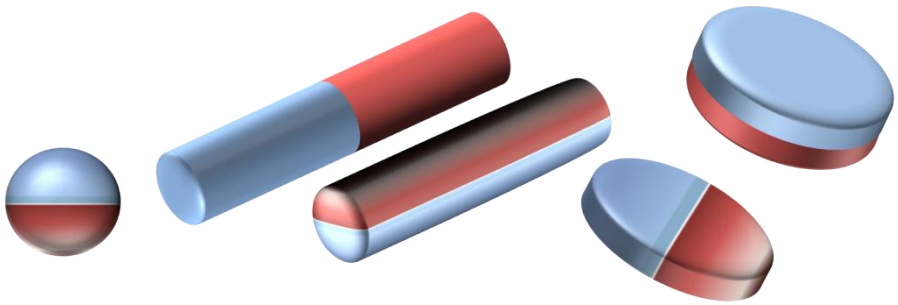

Published in *Soft Matter*, **2008**, 4, 663.

Introduction

In recent years, Janus particles have emerged as a new division of colloidal structures. Janus particles were initially named after the double-faced roman god Janus. The terminology is based on the special architectural feature of having two sides or at least two surfaces of different chemistry and/or polarity. As in many cases of modern material research, we can find an analogue to the Janus particles in nature. In many fungi, so-called hydrophobin proteins can be found.1 This class of proteins has a structural motif in common, which is a characteristic sequence of eight cysteine residues with conserved spacings in their primary sequence. Due to this pattern, hydrophobins are surface-active proteins with a non-centrosymmetric arrangement of the hydrophilic and hydrophobic patches. As a consequence, these proteins undergo self-assembly processes into aggregates in aqueous solution.

Coming back to synthetic Janus systems, the lack of centrosymmetry has led to the discovery of novel material properties as well as to interesting aggregation behavior into superstructures on different length scales, and has opened up a wide field of conceivable applications. These application areas range from medicine, biochemistry, and physics to colloidal chemistry and thus define this research area as an interdisciplinary field. The synthetic access to those non-centrosymmetric structures had been limited to extremely small amounts in the beginning, thus also limiting the utilization of the particles in further studies. However, nowadays, new approaches have overcome those limitations and the generation of significant quantities is possible.

In general, Janus particles can be divided into several classes according to their architecture and dimensionality (see Scheme 13 - 1). Most commonly, spherical (3D) Janus particles can be imagined. In addition, two types of cylinders (1D) and two types of disc-like particles (2D) are conceivable. The lack of centrosymmetry is inherent to all of these particles and is the major challenging aspect in their preparation. Nevertheless, various groups have reported on the successful preparation of different kinds of Janus particles using various synthetic techniques.

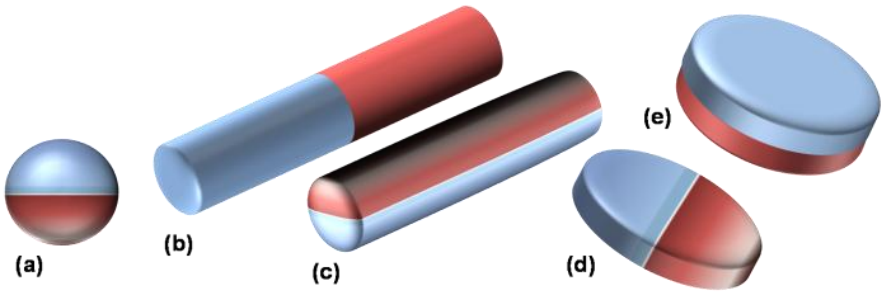

Scheme 13 - 1. Overview of possible Janus particle architectures. (a) Sphere , (b+c) cylinders, and (d+e) discs.

This article covers the synthetic strategies towards the preparation of Janus particles as well as their aggregation behavior into fascinating hierarchical superstructures. In another section we will highlight possible pursued applications, their partial realization and finish with future perspectives to give an outlook of where research in this fascinating area may lead. It should be noted that we also review research activities, which do not explicitly use the term *Janus* for their particles, but which make use of the same structural motif of non-centrosymmetric particles.

Preparation Pathways

At this point we consider the different approaches leading to Janus particles. We focus the interest on synthetic strategies showing scientific originality as well as technological importance. In particular in the last two to three years, some major developments took place, allowing for the reliable synthesis of significant quantities of Janus particles within a reasonable range of both synthetic effort as well as potential price. Scheme 13 - 2 and 13 - 3 give an overview of the preparation methods.

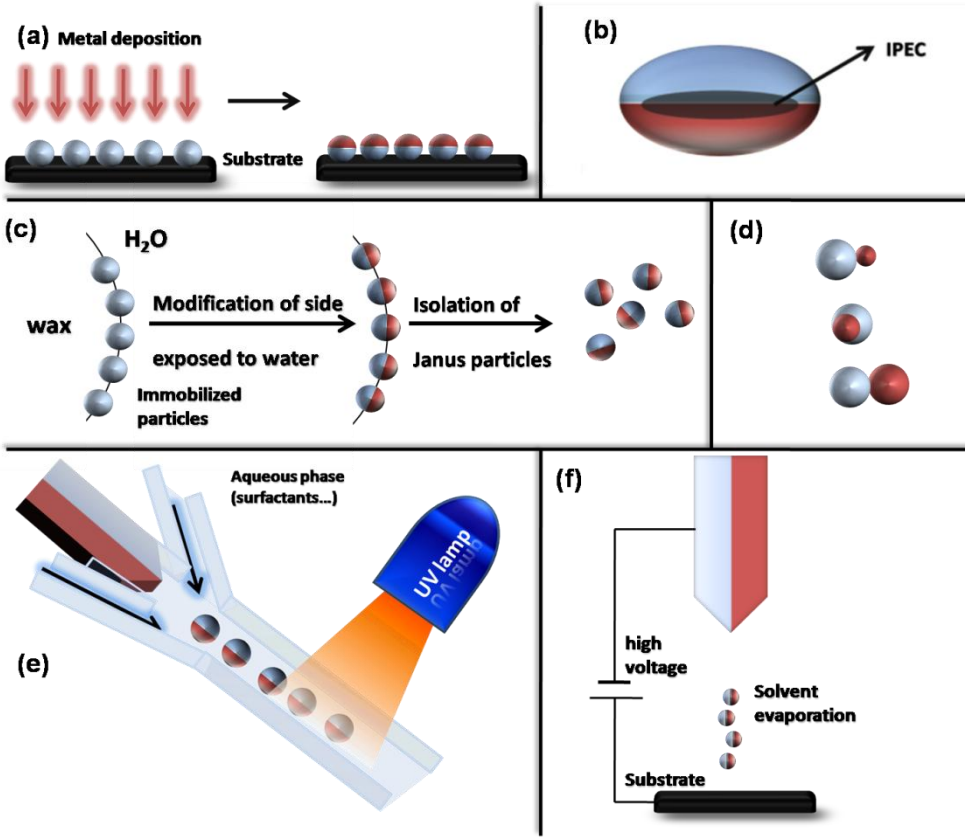

Scheme 13 - 2. Overview of approaches towards the preparation of Janus particles. (a) Classical two-dimensional technique involving shading of one particle side after their immobilization. (b) Ellipsoidal complex core coacervate micelle with an interpolyelectrolyte complex core (IPEC). (c) Pickering emulsion route. (d) Janus particles with two inorganic compartments, snowman-, acorn-, dumbbell-like nanoparticles (top to bottom). (e) Microfluidic photopolymerization system. (f) Electrospinning using a bi-phasic nozzle.

In the very beginning however, the most traditional technique to obtain Janus particles was based on a two-dimensional approach. In a first step, particles are deposited onto a substrate and then the above-lying surface is coated with metals (Scheme 13 - 2a). This methodology is one of the simplest, safest, and most convincing approaches to obtain well-defined Janus particles. For instance, in the early eighties Vessyié and coworkers[2, 3] published data about the hydrophobization of commercially available glass beads, leading to so-called “Janus pearls”. The major drawback of this strategy is that the amount of particles is extremely limited and does not allow their use to larger scale application studies. Nevertheless, due to its simplicity, this approach is still in use as can be seen by recent work by Paunov and Craye[4] or Ryan’s group.[5]

An extension of this concept was recently undertaken by Granick and coworkers[6], who used a Pickering emulsion route to obtain larger quantities of Janus beads. The concept essentially transfers the two-dimensional technique into a solution phase and uses the high internal interface of an oil(wax)/water interface to achieve higher mass fractions of Janus particles. In a first step, they created a Pickering emulsion of wax and water using silica particles as stabilizers at high temperature. After cooling down the emulsion and a purification step, the particles are immobilized at the solidified interface. The key step of this process is the immobilization of the particles at the interface and the suppressed rotational diffusion of the particles at the solidified interface. The Janus particles can then be obtained after a functionalization of one side with aqueous phase chemistry and filtration at higher temperatures (see Scheme 13 - 2c).

Another approach for the preparation of significant quantities of Janus particles was presented by Lahann and coworkers.[7] They employed electrohydrodynamic jetting in combination with a two-phase side-by-side spinneret tip to generate spherical and cylindrical Janus particles with submicron dimensions. The electrospinning approach offers reliable control and allows an easy incorporation of metallic particles, ligands or dyes into the two sides. More recently, the concept had also been extended to the preparation of biphasic fully inorganic nanofibers made up of TiO_2 and SnO_2, representing the versatility of this methodology (see Scheme 13 - 2f).[8]

A further control and increase of the structural variety of Janus particles was only very recently possible with the development of photopolymerizations or photolithographic polymerizations within microfluidic devices.[9-14] Several research groups succeeded in the preparation of differently shaped colloidal particles with biphasic or triphasic substructures simply by applying a lithographic mask or changing the channel geometry of the microfluidic device. The microfluidic preparation is sketched in Scheme 13 - 2e. The tip releases a two-phase stream from its top, which is then cut into small particles and solvated by the aqueous phase crossflow. The aqueous phase also contains some surfactants to stabilize the resultant droplets. Subsequently, the photopolymerization locks the shape of the two phases and leads to biphasic particles. Although an excellent control of the shape could be achieved, the submicron region is not readily accessible by this method.

Additionally, efforts have been reported to generate purely inorganic Janus particles, e.g. dumbbell-, acorn- or snowman-shaped particles (see Scheme 13 - 2d). The formation of those biphasic particles is assisted by nucleation processes during the growth of the second material or reaction induced phase separation.[15] Various compositions have been achieved so far and the particles are appealing as some of them combine optical properties for sensing with magnetic properties, which could allow an external manipulation. The different crystal surfaces of the two connected nanoparticles also enable a further highly selective functionalization of the two sides of the inorganic Janus particles.

Concerning a high control of the particle shape and nanoscopic size, an approach based on the self-organization of triblock terpolymers plays a significant role.[16-19] This approach makes use of some unique bulk morphologies of triblock terpolymers[20] and has been intensely pursued in our group. Upon selective crosslinking of polybutadiene (PB) segments of various polymer microphase-separated structures, it is possible to obtain spherical, cylindrical and disc-like Janus particles (see Scheme 13 - 3).

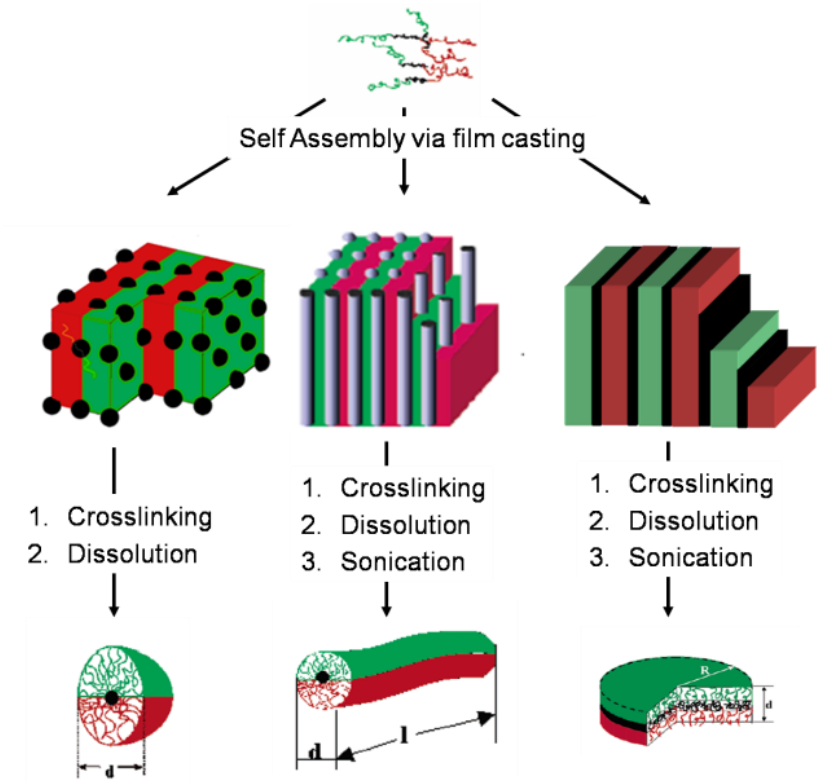

Scheme 13 - 3. Preparation of Janus particles with different architectures based on crosslinking the polybutadiene segments of various triblock terpolymers in the bulk.

The crosslinking preserves the predestined orientation of the outer blocks and unambiguously yields the desired non-centrosymmetric particles. This method, introduced in the beginning of this decade, was the first technique to actually allow the preparation of truly nanometer-sized Janus particles on the gram scale. The precise control of the dimensions of the cross-sections is unmatched due to the utilization of the extremely well-defined triblock terpolymer templates.

In an approach purely based on self-assembly, Voets et al.[21] were able to prepare “double-faced” complex core coacervate micelles (C3M) using the forced co-assembly of two block copolymers, each possessing an oppositely charged polyelectrolyte segment (see Scheme 13 - 2b). The polyelectrolyte blocks formed a water-insoluble interpolyelectrolyte complex (IPEC) as the micellar core, whereas the two other block segments, poly(ethylene oxide) and polyacrylamide, underwent phase separation due to their incompatibility. The overall shape of these C3M micelles was discoidal. The important issue of evidencing the demixing of the corona was most elegantly tackled by NOESY NMR, a technique suitable for probing inter-chain interactions.

Some of the methods presented indeed possess the possibility of scaling-up them to industrial scale while keeping the price of the materials within a moderate region. Certainly, an industrial production of the particles will only be of interest if significant advantageous in the material properties of Janus particles over standard colloids or surfactants are discovered. This is discussed below.

Fascinating Superstructures

The ability of a material to self-assemble into complex hierarchical structures is encoded into its architecture, proteins being the best example. Since Janus particles possess the unique and novel feature of being non-centrosymmetric, many investigations have been concerned with the evaluation of the solution properties and self-assembly behavior of these particles.[13, 16, 17, 19, 22, 23] As some techniques allow the preparation of non-spherical particles, it is also possible to study the effect of the geometry on the types of aggregates formed. Indeed, it turned out that Janus particles exhibit a variety of complex and partially unexpected aggregates.

In the case of spherical Janus micelles, having hemispheres of polystyrene (PS) and poly(methyl methacrylate) (PMMA), aggregation into clusters is observed in various organic solvents, e.g. THF.[17] Similarly, Janus discs composed of two sides of PS and poly(*tert*-butyl methacrylate) (P*t*BMA) undergo back-to-back stacking into superstructures in organic solvents.[19] The self-assembly behavior could be strikingly demonstrated with various imaging and scattering techniques. For instance, Figure 13 - 1 (a and c) shows Transmission Electron Microscopy (TEM) images of back-to-back stacked Janus discs. The images were obtained from ultrathin sections after embedding the superstructures from THF or acetone into a crosslinkable silicone oil, microtome cutting and staining. A stacking of the PS sides of the Janus discs can clearly be seen and the multicompartment architecture can be visualized (see Figure 13 - 1c for a schematic representation of the layers).

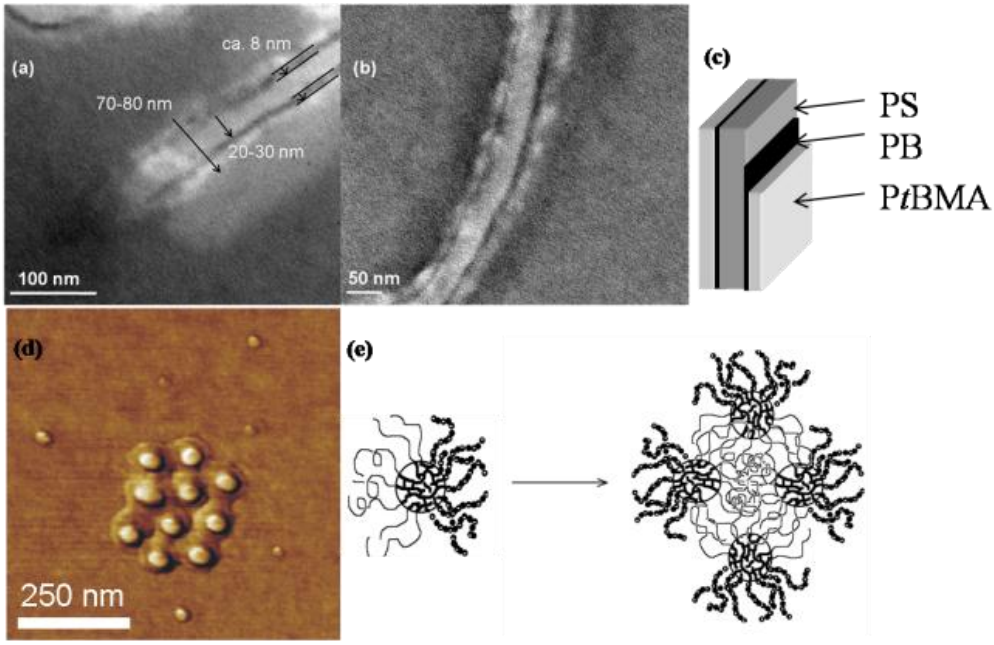

Figure 13 - 1. Superstructures formed by Janus discs, possessing one PS and one PtBMA side, in THF (a) and acetone (b). TEM images taken after embedding. (d) SFM height image (z-range = 30 nm) of single Janus micelles, composed of one PS and one PMMA side, and their supermicelles. The latter form ordered surface assemblies after deposition from THF onto mica. Scheme 13 -s (c) and (e) show the proposed aggregation patterns (polybutadiene = PB; images reprinted with permission ref. 17 and 19. Copyright (2001, 2007) American Chemical Society).

Furthermore, Figure 13 - 1d exhibits a Scanning Force Microscopy (SFM) image of individual Janus micelles (small isolated particles) and superstructured surface clusters composed out of

supermicelles (clustered large “fried-egg”-like structures). Each supermicelle is constituted of several individual Janus micelles. The scheme in Figure 13 - 1e serves as a cartoon of the proposed aggregation pattern of individual Janus micelles into the supermicelles. This aggregation of the Janus particles into superstructures is surprising to some extent as both sides of the particles alone, as well as the base terpolymer, are well soluble in the organic solvent used. It appears though that the very slight selectivity of the solvent is sufficient to induce a self-assembly of the particles into defined discrete clusters of Janus particles. Such kind of an aggregation can be expected neither for standard block copolymers nor for homogeneous particles and thus represents one of the unique features of Janus particles.

Turning to aqueous medium, the situation becomes even more complex and interesting. At first, we can distinguish two kinds of biphasic particles. The first ones are particles which are truly amphiphilic and possess one hydrophobic and one hydrophilic side. The second class has two completely water-soluble, yet unlike sides. In the first case, extensive studies have been carried out with spherical Janus particles composed of one hemisphere of water-soluble poly(methacrylic acid) (PMAA) and another side of PS.[16] The detailed investigations revealed that the Janus particles aggregate on two hierarchical levels (see Figure 13 - 2). The first one is the assembly of single Janus particles into defined clusters, similar as in organic solution. The second is the aggregation into even larger aggregates, so-called giant micelles. The supermicelles and the giant micelles can be seen in the SFM and SEM (Scanning Electron Microscopy) images below as small and very large structures, respectively. The structure of the very large supermicelles is unknown so far, however, it was suggested that they may be similar to multilamellar vesicles.

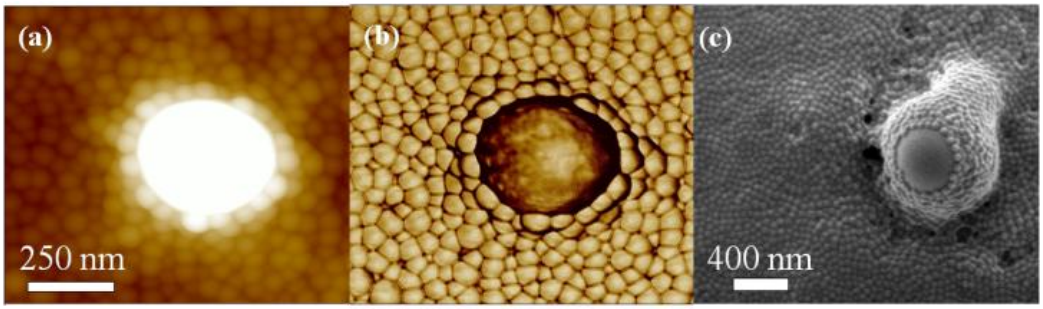

Figure 13 - 2. SFM height (a; z-range = 100 nm) and phase image (b), and SEM image (c) of amphiphilic Janus micelles, having one PS and one PMAA side, after deposition from aqueous solution. (images reprinted with permission from, ref. 16. Copyright (2003) American Chemical Society.)

Interestingly, the critical aggregation concentration of the amphiphilic Janus micelles (PS-PMAA) in water is higher than for the Janus particles in organic solution. This again comes as a surprise as water is a much stronger selective solvent than the organic solvents used and thus a lower critical aggregation concentration is anticipated.

Secondly, we consider the work of Grannik’s group dealing with the clustering of dipolar (“zwitterionic”) micron-sized Janus particles, which serve as an example for fully water-soluble Janus particles.[23] Zwitterionic Janus particles do not behave like classical dipoles, as their size significantly exceeds the electrostatic screening length and thus the electrostatic interactions have a much shorter range than the particle size. The microscopic observations in this work are supported by Monte-Carlo calculations and reveal an assembly of the dipolar spherical Janus

particles into defined clusters. The aggregation towards larger and larger structures is energetically favored as each cluster still carries a macroscopic dipole and would thus allow the aggregation of already formed clusters into larger assemblies. Many of the aggregate shapes found differ from aggregates expected from homogeneous particles which exclusively cluster due to van der Waals interactions. Generally, the differences are expected to be more pronounced for larger clusters and the clusters possess a less dense packing and a higher asymmetry.

Looking to the future, it is obvious that among surprising and novel aggregates found so far, Janus particles of different architectures are certainly useful for directional self-assembly towards complex hierarchical assemblies and novel materials.

Fields of Application

Since challenges in the synthesis of Janus particles are on the way to be overcome, researchers from various fields have turned to the investigation of possible applications. Some of these studies have been triggered by theoretical predictions of certain advanced properties of Janus colloids. In several examples in the literature, it is evident that when researchers make clever use of the inherent non-centrosymmetric character and the resulting physical characteristics, new materials with novel properties can be obtained. However, only some of those will be commercialized and make their way to real industrial applications or specialized product.

A first example for an interesting switchable device was shown by Nisisako et al., who made use of the electrical anisotropy of Janus particles filled with white and black pigments in both hemispheres.[10] In order to create a switchable display panel, they placed a thin layer of these spheres between to electrodes. Upon switching on an electric field, the particles orient their black sides to the negative electrode and vice versa. The orientation and the color of the display can be flipped simply by reversing the electrical field. With this method, very thin, robust and environmentally stable displays could be created.

Besides, Janus particles can be used as efficient and unique optical probes for biological interactions or rheological measurements in confined space. In recent years, this concept has been brought forward by Behrend and coworkers[24-28] who used Janus beads coated on one side with metal. These so-called (magnetically) modulated optical nanoprobes reflect and transmit light or emit fluorescence anisotropically, i.e. depending on their orientation with respect to the observer. Being placed into a specific environment, these particles blink on and off depending on the surrounding conditions. Precisely speaking, the frequency of the flickering can be used to draw detailed conclusions of the microenvironment and the viscoelastic properties, simply because the rotational diffusion of the particles experiences viscous drag. With this strategy it is possible to create devices ranging from precise nanoviscosimeters to nanothermometers. Further development of these particles has aimed at the incorporation of highly selective receptor sites or magnetic coatings on one side of the particles in order to use them as (bio)chemical nanosensors. Thus the flickering of the particles is not only sensitive to viscous drag, but also to electric and magnetic fields as well as to chemical attraction and biochemical forces.[29] For sensor applications, Janus particles could allow an independent biochemical conjugation with the possibility of imaging (microscopy or magnetic resonance tomography)

based on dyes or contrast agents located within the other side. Thus, an interference of the two sides is minimized and the sensing functions could be optimized.

Another interesting effect which potentially finds application in nanoscience is the self-propulsion induced by catalytically active Janus beads with a spatially asymmetric distribution of the reaction site.[5, 30] Generally, self-motile particles are of interest in nanomedicine as they exhibit an increased diffusion coefficient compared to standard particles. This allows them to screen a larger volume for docking sites within less time and would make drug-delivery vehicles more efficient. Such devices had been recently described by Ryan and coworkers[5] They used micron-sized polystyrene particles coated on one side with a thin platinum layer and studied their diffusion by tracking experiments in dependence of the concentration of hydrogen peroxide. Hydrogen peroxide served as “fuel” in these experiments as it is catalytically degraded by platinum into two reaction products and leads to an asymmetric distribution of reaction products and an accompanying osmotic potential (Figure 13 - 3).

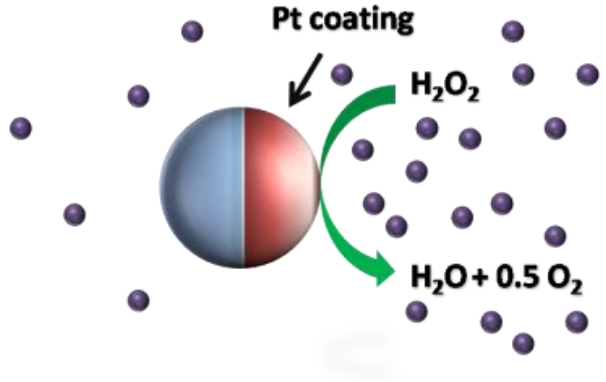

Figure 13 - 3. Self-propulsion of a Janus particle via the asymmetric distribution of reaction products in case of the catalytic degradation of hydrogen peroxide by platinum into two reaction products.

This nanoscale chemical locomotion leads to enhanced directed diffusion on a short time scale and is randomized for longer time-scales. The overall diffusion coefficient is substantially larger in the presence of fuel. By changing the catalytic centre to an active enzyme, the propulsion mechanism would mimic to some extent a bacterial flagellum.

From an industrial point of view, the surface activity of Janus particles is of fundamental interest. Due to the corona segregation, amphiphilic Janus particles are expected to strongly adsorb at interfaces. These particles uniquely combine the so-called Pickering effect, known for particles, with the amphiphilicity of classical surfactants. In recent years, several publications have appeared describing theoretically the remarkably high adsorption strength of Janus particles at interfaces.[31, 32] For instance, in case of spherical particles, the adsorption energy at a liquid/liquid interface is predicted to be up to three times higher for particles with corona segregation than for particles with a uniform surface. Therefore, Janus particles may be ideally suited as strong future emulsifiers. Following the predictions, Glaser et al.[33] recently used pendant drop tensiometry to show that bi-metallic Janus particles indeed lead to a significant reduction of the oil/water interfacial tension as compared to uniform metallic nanoparticles (iron oxide or gold) of similar size (Figure 13 - 4).

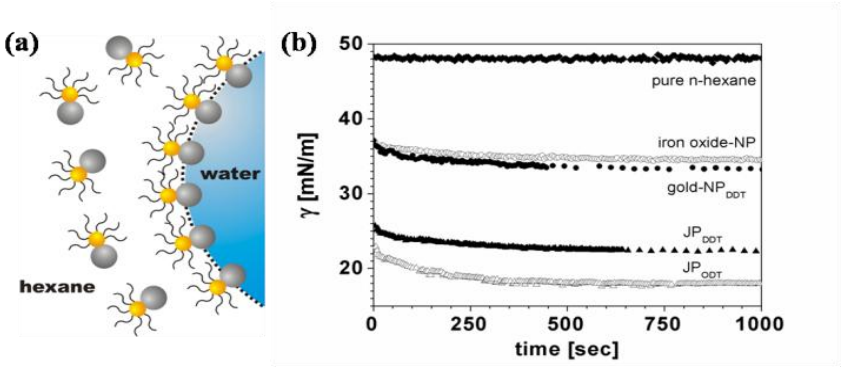

Figure 13 - 4. (a) Schematic representation of bimetallic Janus particles at the hexane/water interface (gold: gold part with surfactant; gray: iron oxide part). (b) Interfacial tension vs time as measured by pendant drop tensiometry (NP: homogeneous nanoparticles; JP: Janus particles). Reprinted with permission from ref. 33. Copyright (2006) American Chemical Society.

This means that by changing the particle architecture, stronger and hence better surfactant particles can be created. In order to further develop this application, we lately conducted emulsion polymerization of standard monomers using amphiphilic Janus particles as emulsifiers.[34] The polymerizations could be performed with a simple conventional technique and no pre-homogenization to a miniemulsion was necessary as it is the case for Pickering emulsion polymerizations using homogeneous particles. The reactions led to extremely well-defined latex particles independently of the monomer used. A control of the latex particle size could easily be achieved by changing the concentration of the stabilizer. After the polymerization, the latex is stabilized by amphiphilic Janus particles, which can, due to their size, not easily be removed from the interface by thermal energy. Thus, a significant improvement of the long-term stability can be anticipated.

Conclusions and Future Prospective

Current research has enabled the preparation of Janus particles with a variety of techniques. With this progress it is nowadays possible to produce significant quantities of well-defined Janus particles with a variety of architectures. Major initial challenges in the controlled production of these colloids are on a good way to be overcome. Some of the developed preparation methods even possess the capability of being extended to industrial scale, making technological applications of Janus particles conceivable. It was shown, that particles of different architectures exhibit the ability to self-assemble into complex hierarchically structured novel superstructures. Therefore, this new division of colloidal particles can serve as building blocks for novel superstructured devices. Along with the development of new methods to prepare Janus particles, scientists from various disciplines have started to look into the possible applications. Among those, especially applications as highly specific sensors, self-motile particles and for the stabilization of interfaces appear very promising. Certainly, the high costs currently associated with the production of Janus particles will limit some technological applications. On the contrary however, for fundamental research, they provide an ideal platform for the creation of novel nanodevices and for the exploration of new ways to tackle present problems, like directed self-assembly, controllable delivery vehicles or precise sensors for multicomponent systems. Looking out to the future, a wide research field is opened and we will certainly see a range of developments taking place based on the concept of Janus type non-centrosymmetric colloids.

References

1. Hektor Harm, J.; Scholtmeijer, K. *Curr. Opin. Biotechnol.* **2005,** 16, 434.
2. Casagrande, C.; Veyssié, M. C. *R. Acad. Sci. (Paris)* **1988,** II-306, 1423.
3. Casagrande, C.; Fabre, P.; E, R.; Veyssié, M. C. *Europhys. Lett.* **1989,** 9, 251.
4. Paunov, V. N.; Cayre, O. J. *Adv. Mater,* **2004,** 16, 788.
5. Howse, J. R.; Jones, R. A. L.; Ryan, A. J.; Gough, T.; Vafabakhsh, R.; Golestanian, R. *Phys. Rev. Lett.* **2007,** 99, 048102.
6. Hong, L.; Jiang, S.; Granick, S. *Langmuir* **2006,** 22, 9495.
7. Roh, K.-H.; Martin, D. C.; Lahann, J. *Nature Mat.* **2005,** 4, 759.
8. Liu, Z.; Sun, D. D.; Guo, P.; Leckie, J. O. *Nano Lett.* **2007,** 7, 1081.
9. Nisisako, T.; Torii, T. *Adv. Mater.* **2007,** 19, 1489.
10. Nisisako, T.; Torii, T.; Takahashi, T.; Takizawa, Y. *Adv. Mater.* **2006,** 18, 1152.
11. Shepherd, R. F.; Conrad, J. C.; Rhodes, S. K.; Link, D. R.; Marquez, M.; Weitz, D. A.; Lewis, J. A. *Langmuir* **2006,** 22, 8618.
12. Dendukuri, D.; Pregibon, D. C.; Collins, J.; Hatton, T. A.; Doyle, P. S. *Nature Mat.* **2006,** 5, 365.
13. Nie, Z.; Li, W.; Seo, M.; Xu, S.; Kumacheva, E. *J. Am. Chem. Soc.* **2006,** 128, 9408.
14. Seo, M.; Nie, Z.; Xu, S.; Mok, M.; Lewis, P. C.; Graham, R.; Kumacheva, E. *Langmuir* **2005,** 21, 11614.
15. Perro, A.; Reculusa, S.; Ravaine, S.; Bourgeat-Lami, E.; Duguet, E. *J. Mat. Chem.* **2005,** 15, 3745.
16. Erhardt, R.; Zhang, M.; Böker, A.; Zettl, H.; Abetz, C.; Frederik, P.; Krausch, G.; Abetz, V.; Müller, A. H. E. *J. Am. Chem. Soc.* **2003,** 125, 3260.
17. Erhardt, R.; Böker, A.; Zettl, H.; Kaya, H.; Pyckhout-Hintzen, W.; Krausch, G.; Abetz, V.; Müller, A. H. E. *Macromolecules* **2001,** 34, 1069.
18. Liu, Y.; Abetz, V.; Müller, A. H. E. *Macromolecules* **2003,** 36, 7894.
19. Walther, A.; André, X.; Drechsler, M.; Abetz, V.; Müller, A. H. E. *J. Am. Chem. Soc.* **2007,** 129, 6187.
20. Abetz, V.; Simon, P. F. W. *Adv. Pol. Sci.* **2005,** 189, 125.
21. Voets, I. K.; de Keizer, A.; De Waard, P.; Frederik, P. M.; Bomans, P. H. H.; Schmalz, H.; Walther, A.; King, S. M.; Leermakers, F. A. M.; Cohen Stuart, M. A. *Angew. Chem. Int. Ed.* **2006,** 45, 6673.
22. Dendukuri, D.; Hatton, T. A.; Doyle, P. S. *Langmuir* **2007,** 23, 4669.
23. Hong, L.; Cacciuto, A.; Luijten, E.; Granick, S. *Nano Lett.* **2006,** 6, 2510.
24. Behrend, C. J.; Anker, J. N.; McNaughton, B. H.; Kopelman, R. *J. Magn. Magn. Mater.* **2005,** 293, 663.
25. Anker, J. N.; Behrend, C. J.; Huang, H.; Kopelman, R. *J. Magn. Magn. Mater.* **2005,** 293, 655.
26. Behrend, C. J.; Anker, J. N.; McNaughton, B. H.; Brasuel, M.; Philbert, M. A.; Kopelman, R. *J. Phys. Chem. B* **2004,** 108, 10408.
27. Behrend, C. J.; Anker, J. N.; Kopelman, R. *Appl. Phys. Lett.* **2004,** 84, 154.
28. Anker, J. N.; Behrend, C.; Kopelman, R. *J. Appl. Phys.* **2003,** 93, 6698.
29. Choi, J.; Zhao, Y.; Zhang, D.; Chien, S.; Lo, Y. H. *Nano Lett.* **2003,** 3, 995.
30. Golestanian, R.; Liverpool, T. B.; Ajdari, A. *Phys. Rev. Lett.* **2005,** 94, 220801.
31. Binks, B. P.; Fletcher, P. D. I. *Langmuir* **2001,** 17, 4708.
32. Nonomura, Y.; Komura, S.; Tsujii, K. *Langmuir* **2004,** 20, 11821.
33. Glaser, N.; Adams, D. J.; Böker, A.; Krausch, G. *Langmuir* **2006,** 22, 5227.
34. Walther, A.; Hoffmann, M.; Müller, A. H. E. *Angew. Chem. Int. Ed.* **2007,** 120, 723.

14. JANUS DISCS

Andreas Walther, Xavier André, Markus Drechsler, Volker Abetz‡, Axel H. E. Müller

Makromolekulare Chemie II and Bayreuther Zentrum für Kolloide und Grenzflächen, Universität Bayreuth, D-95440 Bayreuth, Germany

‡ Institut für Polymerforschung, GKSS-Forschungszentrum Geesthacht GmbH, D-21502 Geesthacht, Germany

Andreas.Walther@uni-bayreuth.de; *Axel.Mueller@uni-bayreuth.de*

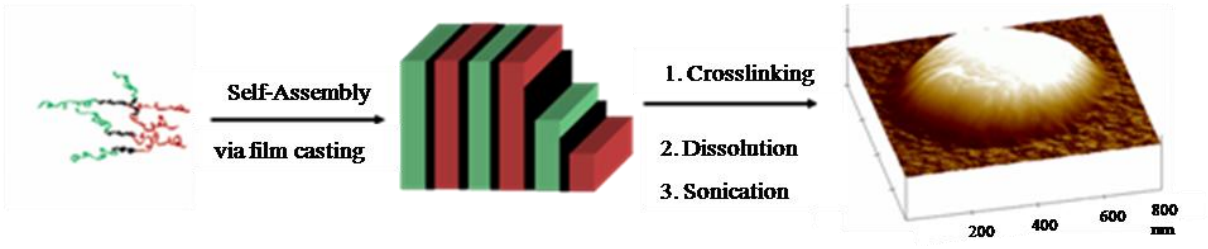

Published in the *Journal of the American Chemical Society*, **2007**, 129, 6187-6198

Abstract

We describe the synthesis and the solution properties of sheet- and disc-like Janus particles, containing an inner crosslinked polybutadiene (PB) layer and two different outer sides of polystyrene (PS) and poly(*tert*-butyl methacrylate) (P*t*BMA). The structures formed upon adsorption of the flat Janus particles onto solid substrates as well as in THF solution are investigated. The Janus discs are obtained in a template-assisted synthetic pathway followed by sonication. Selectively crosslinking the lamellar PB domains in a well-ordered lamellar microphase-separated bulk morphology of polystyrene-*block*-polybutadiene-*block*-poly(*tert*-butyl methacrylate) (SBT) triblock block terpolymers leads to the conservation of the compartmentalization of the two outer blocks. Sonication of the crosslinked block terpolymer templates renders soluble sheet- and disc-like Janus particles, the size of which can be tuned from the micrometer range down to the nanometer scale. Small-angle x-ray scattering, transmission electron microscopy, dynamic light scattering, scanning force microscopy and scanning electron microscopy are used to characterize the template-assisted synthetic process and the solution properties. Cryogenic transmission electron microscopy in THF and TEM of particles, embedded into a photo-crosslinkable silicon oil, indicate a supramolecular aggregation behaviour of the Janus discs in concentrated solutions. Pendant drop tensiometry demonstrates that Janus sheets and discs can be used to stabilize liquid-liquid interfaces, rendering these materials interesting for future applications.

Introduction

In recent years, Janus particles have attracted much attention in nanoscience due to their interesting properties, both for academic as well as for technological reasons.[1-8] In general, Janus structures can be divided into three classes according to their architecture – spherical Janus micelles (3D), two types of Janus cylinders (1D) and Janus sheets or discs (2D), representing the intermediate case of dimensionality (see Scheme 14 - 1). The synthesis of such non-centrosymmetric structures with compartmentalized coronas is a demanding task for the synthetic chemist. Hence, only a few real nanosized polymer-based Janus structures are known in literature.

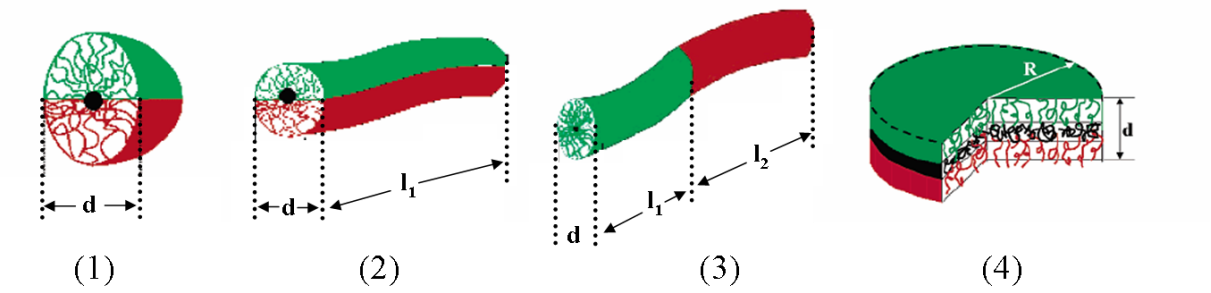

Scheme 14 - 1. Possible Janus architectures with phase-segregated shells: (1) spherical Janus micelle, (2) & (3) two types of Janus cylinders, (4) Janus sheet/disc.

One of the most intensively studied systems is the one concerning the spherical Janus micelles, which are based on template-assisted synthesis using polystyrene-*block*-polybutadiene-*block*-poly(methyl methacrylate) (SBM) block terpolymers. The SBM Janus micelles, as well as their amphiphilic pendants, the hydrolyzed SBMA Janus micelles (MA: methacrylic acid) show interesting hierarchical organization on different length scales. The SBM micelles form larger aggregates in non-selective organic solvents, on a silicon surface[9], and at the air/water interface.[10] The amphiphilic SBMA micelles, obtained after hydrolysis of the PMMA ester groups, also exhibit superstructures and giant particles.[11]

In addition, great efforts have been undertaken to obtain spherical Janus particles from heteroarm star polymers or by using the self-assembly of triblock block terpolymers and heteroarm star polymers in solution.[12, 13] Another self-assembly approach is based on the electrostatic interactions of AB and CD diblock copolymers where B and C form insoluble complexes, e.g. inter-polyelectrolyte complexes, in a solvent for blocks A and D. The first reported attempt has led to vesicles with an asymmetric wall rather than to Janus spheres.[14] Voets et al.[15] recently reported the formation of complex-coacervate core micelles with an asymmetric corona and a slightly anisometric shape. One major drawback of all of these approaches is the fact that the structures need to undergo micropohase segregation of the corona in solution. Consequently, the compartmentalization is not predestined by the template as it is the case for the template-assisted synthesis as presented herein.

Concerning non-spherical nanoscopic Janus architectures the literature is limited to very few examples. For instance, Ishizu et al.[16] synthesized amphiphilic brush-*block*-brush AB-type polymer brushes by a combined grafting through and grafting from process. After polymerizing a PEO macromonomer via ATRP, a second monomer (2-hydroxyethyl methacrylate, HEMA) was added to form the second block. Subsequent esterification with an ATRP initiator and an

additional ATRP of HEMA rendered a Janus type polymer brush with PEO and PHEMA side chains. The polymer brush showed an ellipsoidal shape rather than a cylindrical one, as the degree of polymerization of the backbone was relatively low. A successful approach towards the preparation of Janus cylinders with two hemicylinders of PS and PMMA was reported by Liu et al.[17] After crosslinking the lamella-cylinder (lc) morphology of a suitable SBM block terpolymer and a sonication procedure, very long Janus cylinders with compartmentalized sides could be obtained.

From a theoretical and particularly technological point of view, the remarkable predicted surface activities of Janus structures are interesting. Binks and Fletcher[2] calculated an up to three times higher desorption energy for spherical Janus particles, as compared to particles with a homogenous surface. In the same context, Nonomura et al.[1] recently published results of theoretical calculations about the effect of disc-shaped Janus beads on the interfacial tension. The calculations demonstrated that the adsorption energy of Janus discs can be higher by several orders of magnitude than for ordinary classic surfactants. The promising predictions render Janus structures highly interesting as a novel class of future surfactants, which is of great scientific and industrial interest.

Here, we present for the first time the synthesis of novel disc-shaped Janus particles, composed of two different sides of polystyrene and poly(*tert*-butyl methacrylate). Using scattering and imaging techniques, we show that the particle size can be tuned, that the particles are of true Janus character and that they form supramolecular aggregates in good solvents. Furthermore, the application of these particles to stabilize liquid-liquid interfaces will be demonstrated.

Results and Discussion

Synthesis and Crosslinking

The synthetic pathway to obtain disc-like Janus structures is based on a template-assisted synthesis, involving crosslinking of a bulk film of a polystyrene-*block*-polybutadiene-*block*-poly(*tert*-butyl methacrylate) (SBT) block terpolymer and a subsequent sonication treatment, as outlined in Scheme 14 - 1.

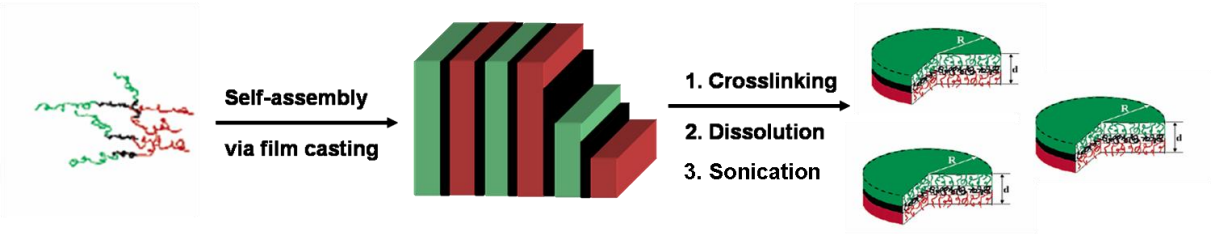

Scheme 14 - 2. Schematic synthesis of Janus discs, based on the selective crosslinking of PB domains of a SBT terpolymer with lamella-lamella (ll) morphology.

For this purpose, several symmetric SBT block terpolymers were synthesized and investigated according to their microphase-separated structures. In the case of SBT, it is known that the desired so-called lamella-lamella (ll) morphology is formed over a wide range of PB fractions as long as the end blocks are of similar volume fractions.[18] The molecular characteristics of the studied SBT block terpolymers, SBT-1 and SBT-2, are summarized in Table 14 - 1.

Table 14 - 1. Molecular Characterization of the SBT block terpolymers.

	Composition[a]	Block DP[b]	10^3 x $M_{n,\,MALS}$ (M_w/M_n)	$R_{g'z}$ [nm] (STD)[c]
SBT-1	$S_{42}B_{10}T_{48}$	$S_{536}B_{246}T_{449}$	133 (1.06)	18.6 (9%)
SBT-2	$S_{45}B_{5}T_{50}$	$S_{575}B_{123}T_{468}$	133 (1.03)	18.6 (13%)

[a] Indices correspond to the weight fractions (in %), as calculated from the ^{1}H NMR spectra (S = polystyrene, B = polybutadiene, T = *tert*-butyl methacrylate). [b] Number-average degree of polymerization of each block. [c] z-average root means square radius of gyration as determined by GPC-MALS measurements (STD = standard deviation).

The number-average molecular weights were kept constant for the two block terpolymers, whereas the inner PB fraction was varied. It was desired to reduce the fraction of PB, based on the assumption that less sonication energy is necessary for a thin inner crosslinked layer in order to obtain soluble products after the crosslinking. The microphase separation was analyzed by transmission electron microscopy (TEM) and small angle x-ray scattering (SAXS). Both terpolymers exhibit lamellar morphologies in the bulk state with alternating lamellae of PS and P*t*BMA, which are separated by a thin lamella of PB (see Figure 14 - 1).

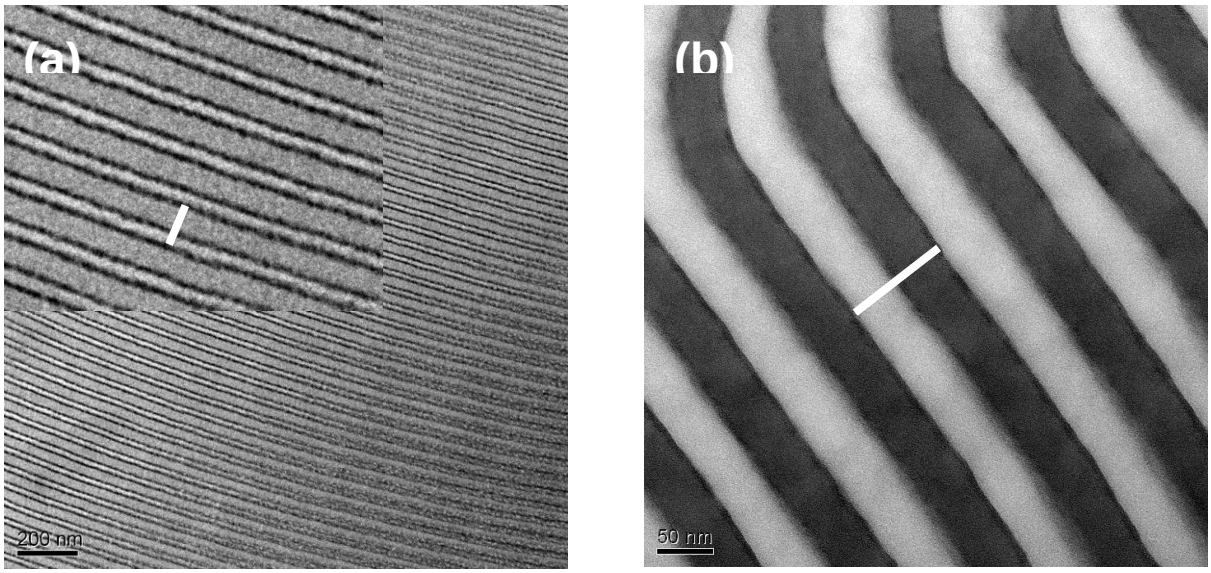

Figure 14 - 1. Transmission electron micrograph of an ultrathin section of SBT-1 (a) and SBT-2 (b) films after staining with OsO_4. The ultrathin film was imaged using standard (a) and carbon coated (b) TEM grids. The white bar indicates the long period of the periodicity of the structure.

Small discontinuities within the PB lamella can be seen in the case of SBT-2 due to the small fraction of PB of only 5 wt%. However, the lamella itself is still continuous and a clear transition to a lamella-cylinder morphology or to a lamella-sphere morphology does not occur. A higher periodicity of the perforations cannot be observed and thus the morphology is best described as irregularly perforated lamella-lamella structure. A clear break-up of the PB layer was observed in the case of a symmetric SBT block terpolymer having a fraction of only 4 wt% of PB (not shown here). The microphase-separated structure of SBT-1 can unambiguously be assigned to a lamella-lamella (ll) morphology. Since it is known that TEM micrographs may not always reflect the true dimensions of the long periods of the structures due to electron-induced degradation and shrinkage of methacrylate blocks, SAXS measurements were performed.[19]

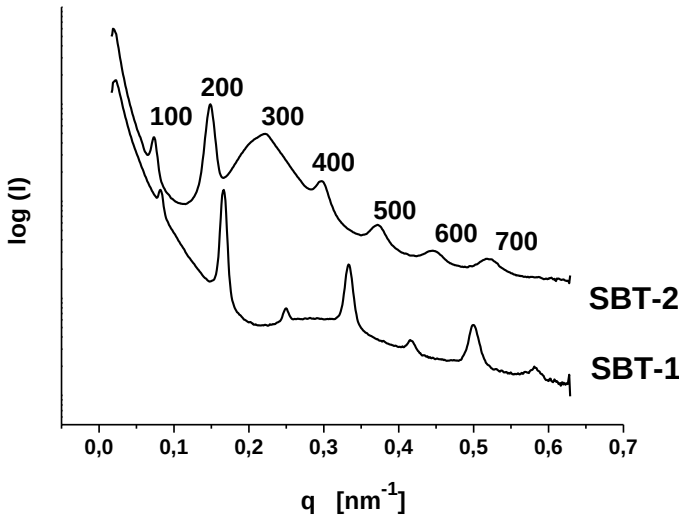

Figure 14 - 2. SAXS diagrams after azimuthal integration of the intensity as a function of the scattering vector q for SBT-2 and SBT-1. The SAXS pattern of SBT-2 was multiplied by 15 to allow a better separation.

Both SAXS patterns exhibit the characteristic peak distributions for lamellar block copolymer structures, meaning the reflections are integer multiples of the first order peak q^* ([100]). The positions of the reflections allow the calculation of the long period, d, of the structures via $d = 2\pi/q^*$. The deduced values are d = 80 nm and d = 86 nm for SBT-1 and SBT-2, corresponding to the ones which were determined by TEM investigations (SBT-1: d = 78 nm; SBT-2: d = 86 nm), when carbon coated grids were used for the imaging process.

In conclusion, both SBT block terpolymers exhibit the desired lamella-lamella morphology which is necessary for the preparation of the flat Janus particles.

The crosslinking of the inner polybutadiene layer preserves the preorientation of the two outer non-centrosymmetric sides, PS and P*t*BMA. The desired Janus particles can be obtained after dissolution of the crosslinked block terpolymer templates by means of sonication. On basis of the determined long periods it is possible to estimate the sheet or disc thickness to be around 35 – 45 nm, resembling a polymer brush-like flat particle.

Two strategies were employed for the crosslinking of the SBT block terpolymer templates. Both "cold vulcanization" by S_2Cl_2, as well as radical crosslinking using AIBN - and its optimization by the thiol-polyene procedure[20-24] – have proven to be effective routes for crosslinking polybutadiene microdomains. The success of the crosslinking strategies was confirmed by TEM, which showed the clear persistence of the lamellar morphologies after crosslinking (see Figure Sup 14 - 1, see supporting information for further details).

Sonication and Solution Properties

Dynamic Light Scattering

After successful crosslinking of the block terpolymer templates with either of the methods mentioned above, the corresponding insoluble fractions were subjected to a sonication procedure in order to obtain soluble Janus discs. Thus, the solutions of swollen crosslinked gels were treated with high energy ultrasound in a temperature-controlled cell until a semi-transparent solution was reached. The effective crosslinking and the persistence of the chemical composition were verified after crosslinking and sonication to coincide with the postulated mechanism of the template-assisted synthesis towards Janus discs (see Supporting Figure Sup 14 - 2 for ^{1}H-NMR characterization).

After this procedure, dynamic light scattering measurements were conducted in order to investigate the sizes of the resulting flat Janus particles and their distribution. Since the appearance of polydisperse and also multimodal distributions was expected using sonication for homogenizing the solutions, the analysis of the normalized field auto-correlation function, $g_1(t)$, was mainly restricted to the use of the CONTIN algorithm. The use of the classical cumulant anaylsis[25], which has the benefit of enabling an estimation of the sample polydispersity via the second cumulant, μ_2, is limited within this work. In the case of multimodal samples or moderately to highly polydisperse samples the series expansion of the cumulant analysis shows only a slow or no convergence at all[26], leading to erroneous results. It may only be applied for samples, whose CONTIN analysis had previously shown a unimodal and relatively narrow distribution.

The investigation of angular dependent scattering data can be used to draw conclusions about the actual shape of particles in solution, both in static as well as in dynamic light scattering. An angular dependence may have several origins: large flexible molecules, anisotropic shapes and polydispersity. For large anisotropic molecules, like rods and disc-shaped molecules, flexion, bending and rotational diffusion occur in addition to the standard translational diffusion. Their contributions to the scattered light are dependent on the wave vector, q, thus inducing an angular dependence. Neither much theoretical nor much experimental work has been reported in the case of disc-like scatterers, which is mainly due to the limited access to free disc-like molecules. A formulation of the dynamic form factor for the intensity of scattered light from thin discs was proposed by Fujime and Kubota and applied to the study of membrane fragments.[27-29] The theoretical expression for the average decay rate for a disc-like scatterer with radius R is given by eq. 1[28]

$$\frac{\Gamma}{q^2} = D + (\frac{R^2}{4})\Theta g_1(qR) + (D' - D'')\left[g_2(qR) - \frac{1}{3} \right] \quad (1)$$

$$\lim_{q \to 0} \frac{\Gamma}{q^2} = D \quad (2)$$

D, D´, D´´ and Θ are the average translational diffusion coefficient, the diffusion coefficients perpendicular and parallel to the disc plane, and the average rotational diffusion coefficient of the disc, respectively. $g_1(qR)$ and $g_2(qR)$ are functions, which can be calculated numerically and depend only on qR. The calculated values can be found elsewhere,[28] in the limit of qR = 0, we find $g_1(qR) = 0$ and $g_2(qR) = 1/3$, so that Γ/q^2 provides the average translational diffusion coefficient upon extrapolation to q = 0 (eq. 2). At larger qR, meaning also larger q^2, additional modes are present.

Figure 14 - 3 displays the normalized field auto-correlation functions, their CONTIN plots as well as the angular dependent scattering data for various samples of Janus discs after different sonication times.

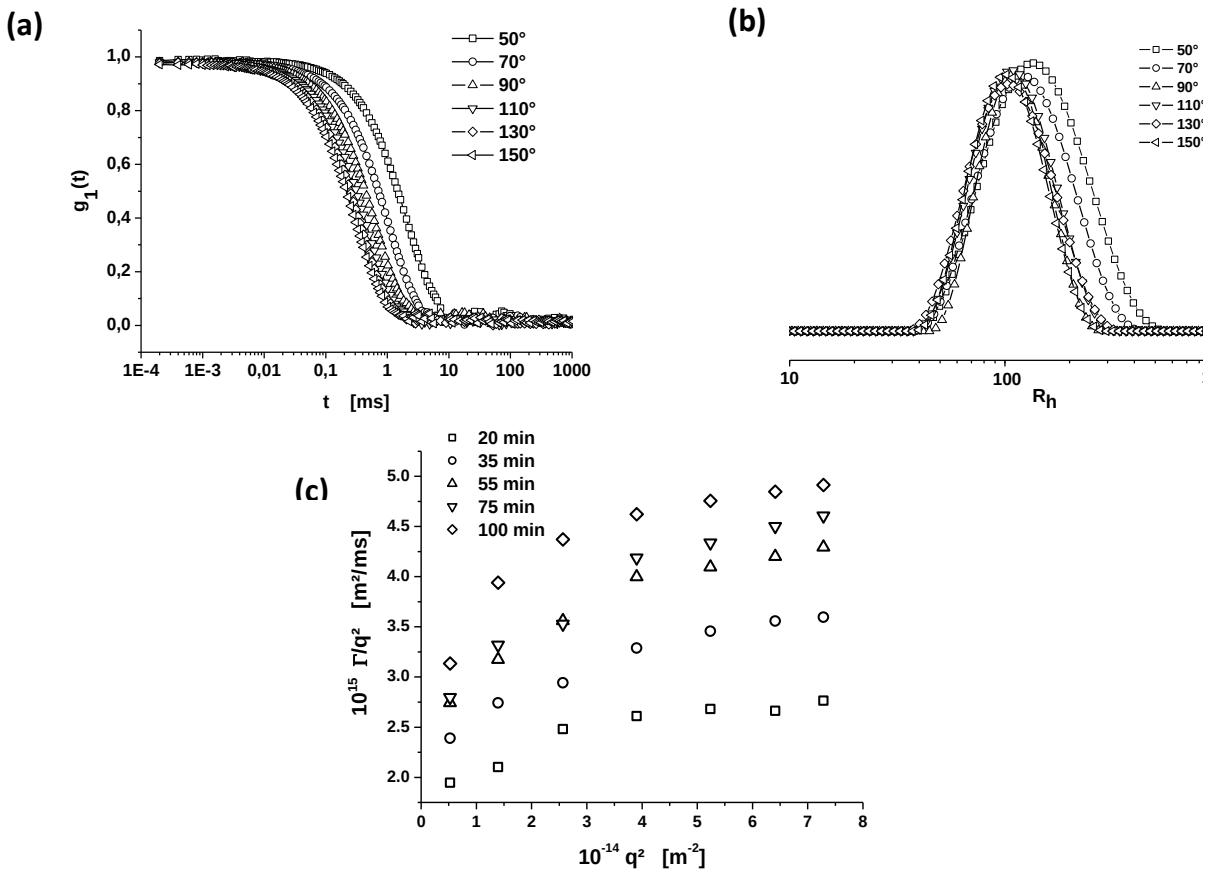

Figure 14 - 3. Normalized field auto-correlation functions (a) and their corresponding CONTIN plots (b) for different angles (SBT-1; 5 wt% AIBN in presence of 5 wt% TRIS, 55 min sonication at 10 % amplitude, measured in THF). (c) Dependence of Γ/q^2 on the squared scattering vector, q^2, for various sonication times.

A shift of the characteristic decay time of the normalized field auto-correlation functions can be observed for the different angles, which translates into different, average decay rates, Γ, diffusion coefficients or apparent hydrodynamic radii in the corresponding CONTIN plots.

All curves presented in Figure 14 - 3c are typical of what one expects for disc-like structures, meaning a curved increase of Γ/q^2 with the squared scattering vector, q^2. This decrease is expected to level off slightly at higher q-values, depending of course on the values of qR. It is worth noting that Kubota et al.[27, 29] and van der Koji et al.[30] found that the polydispersity affects mainly the curvature of the plot of the angular dependent diffusion coefficients of flexible and non-flexible disc-like scatterers, respectively. In conclusion, the obtained scattering data strongly indicates the presence of disc-like scatterers in solution, whose translational diffusion coefficients and apparent hydrodynamic radii can be calculated after extrapolating to zero angle.

In order to further elucidate the size evolution in dependence of the crosslinking method and the sonication energy and duration, DLS measurements at different stages of the sonication and at different sonication energies were performed. Figure 14 - 4 displays the dependence of the apparent hydrodynamic radius, $\langle R_h \rangle_z$ on the sonication duration and the amplitude.

Generally, a characteristic decay of the hydrodynamic radii can be observed with increasing sonication time for all homogenization procedures. The curves follow an exponential decay, indicating that in the beginning of the ultrasound treatment the large particles are fragmented

into significantly smaller ones, causing the rapid decrease. After a certain time (20 - 30 min for SBT-1, 5 – 10 min for SBT-2) the curves show a more asymptotical behaviour. At this stage the particle size decays much more slowly. Consequently, there is some higher resistance to the introduced sonication energy. This resistance is presumably due to the higher mobility of the smaller structures and an accompanying higher resistance and more flexible adaptation to the shock waves produced by the ultrasound. An increase in the sonication amplitude from 10 % to 70 % leads to a much faster disruption of the particles and the plateau is reached earlier. The plateau value is similar for all three sonication amplitudes, however, the lowest one is attained with the highest sonication amplitude.

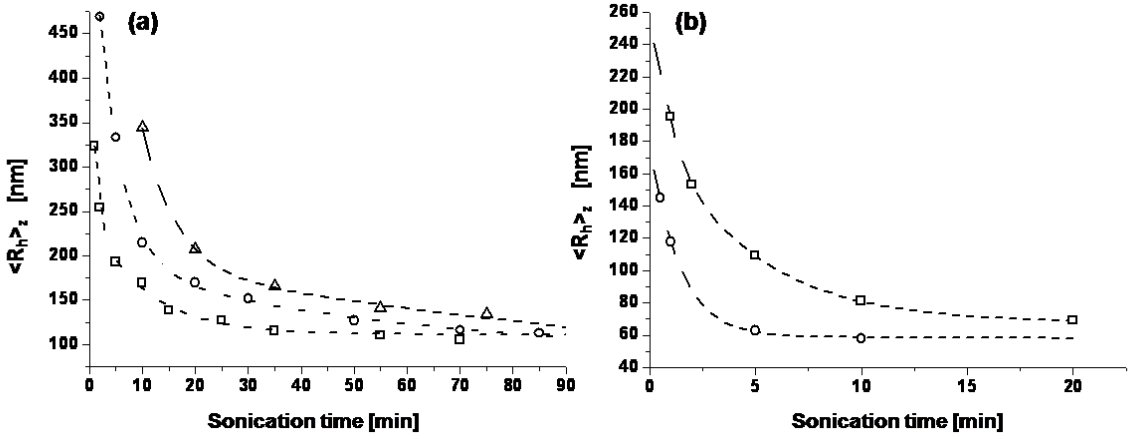

Figure 14 - 4. Dependence of $<R_h>_z$, obtained after extrapolating the angular dependent data to $q^2 \rightarrow 0$, on the sonication power and duration for differently crosslinked block terpolymer templates. Traces for SBT-1 (a) crosslinked with the thiol-polyene process (5 wt% AIBN in presence of 5 wt% TRIS) are shown for different sonication amplitudes (□– 70%, ○ – 30%, △ – 10%). (b) Size evolution for the sonication (30% amplitude) of SBT-2 block terpolymers which were cold vulcanized with sulphur monochloride (□ – 1.5 vol% S_2Cl_2) or crosslinked with the thiol-polyene process (○).

The fits presented in Figure 14 - 4 were performed using a combination of two exponential functions. The ratio of the two decay constants is about 14. Hence one may conclude a kind of two-step mechanism for the particle disruption. The results demonstrate convincingly the facile tunability of the size of the Janus discs. The particle sizes can be adjusted from the micrometer range down to the nanometer level, thus covering a large mesoscopic length scale.

A more detailed look at the different curves reveals further peculiarities between the two different block terpolymer templates. One of the characteristic differences for the sonication of the templates, SBT-1 and SBT-2, is the fact that the former requires longer durations and thus more energy for reaching a solution, which does not show any visible sedimentation. For instance, 300 and 30 seconds are necessary to obtain homogeneous solutions at a sonication amplitude of 30% for SBT-1 and SBT-2 templates, respectively. Since the extent of crosslinking is similar for the radical crosslinking of the two block terpolymer templates, this difference is related to the different fractions of crosslinkable polybutadiene in the two block terpolymers. Secondly, the initial hydrodynamic radii after reaching the solution state for the two kinds of crosslinked block terpolymers are remarkably different, as can be seen from the values for the hydrodynamic radii at short sonication time (0 – 10 min). The hydrodynamic radii for the SBT-2 based Janus particles ($<R_h>_z$ = 140 - 200 nm) are smaller by a factor of two to three than the sizes

obtained for the crosslinked and sonicated SBT-1 block terpolymers ($<R_h>_z$ = 330 - 470 nm). This can be explained considering the very thin, partially discontinuous and not fully crosslinked polybutadiene layer of the SBT-2 block terpolymer. Hence, this template needs much less energy and breaks more frequently, leading to the observation of smaller disc sizes after short sonication time. Values for the hydrodynamic radius much larger than 200 nm cannot be reached using SBT-2. The crosslinked material starts to become soluble at sonication times around 30 s, where the z-average hydrodynamic radius is around 140 - 200 nm, depending on the crosslinking method. A minimum sonication duration of 30 s is yet required in order to solubilize some bigger particles. In addition, the influence of the crosslinking agent, AIBN or S_2Cl_2, can be compared in Figure 14 - 4b. The cold vulcanization leads to the observation of larger particles at all stages of the ultrasound homogenization. This is presumably due to a larger extent of the crosslinking in case of the cold vulcanization and reflects also the morphological changes upon swelling the SBT-2 template in isooctane. TEM investigations had shown a transformation of the perforated into a continuous lamella upon addition of isooctane. Therefore, a more continuous crosslinking can take place during the cold vulcanization.

A further difference between the two block terpolymer templates can be observed with respect to the plateau value. Whereas the hydrodynamic radius for the SBT-1 based flat Janus particle is in the region of 110 – 150 nm, it is only half of it for the SBT-2 based particles. This demonstrates that not only the size of the molecules is important to withstand the mechanical forces of the sonication procedure, but also the thickness of the inner crosslinked layer plays a role. If one assumes a kind of bending modulus for both kinds of disc-like Janus particles, it is obvious that the SBT-1 based particles should have a higher one as the higher content of polybutadiene leads to a tighter network layer within those. Consequently, the mechanical strength and the resistance towards ultrasound are better, explaining the higher value for the plateau.

Mechanism of Particle Disruption

Figure 14 - 5 shows the time-dependent evolution of the normalized field auto-correlation functions and the size distribution for a representative sample of Janus discs (SBT-1, 5 wt% AIBN, 5 wt% TRIS, 30 % amplitude) during the sonication.

The correlation functions show a distinct shift of the characteristic decay time, τ, towards lower values, with increasing duration of the sonication, which correlates with an overall decrease in particle size. The CONTIN plots on the right hand side of Figure 14 - 5 show bimodal distributions for short sonication times (t < 20 min) with peaks at around 150 nm and 600 – 1000 nm.

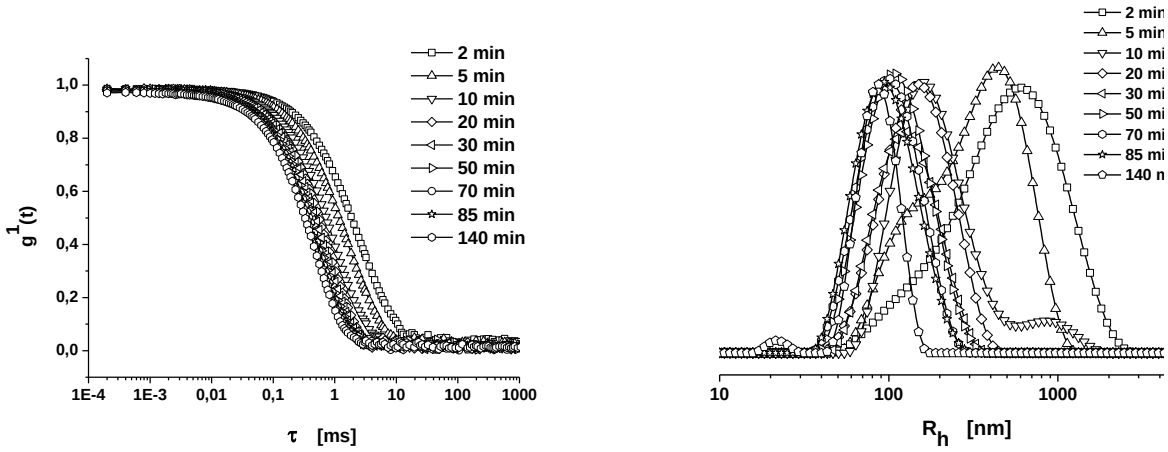

Figure 14 - 5. Normalized field auto-correlation functions (left) at 90° for a Janus disc sample (SBT-1, 5 wt% AIBN, 5 wt% TRIS) which was sonicated at 30 % amplitude. Corresponding size distributions after evaluation with the CONTIN algorithm (right).

It can be seen that the latter peak diminishes during the sonication and vanishes totally for sonication times longer than 20 min. Continuing the sonication for longer than 20 min leads then to a gradual shift of the monomodal peak maximum at $<R_h>_z$ = 80 -120 nm, which can also be seen in the asymptotical behaviour in Figure 14 - 4. The particles are no longer disrupted, but only very small fragments are cut off. Indeed, for very long sonication time (140 min) a peak for very small fragments can appear. A complete disruption of the particles seems to be only possible for particles above a critical threshold value (here around $<R_h>_z$ = 500). The loss of small fragments of the discs does certainly already occur during the early stages of the sonication, but it is invisible as the rapid decrease due to the disruption of large particles dominates the size distribution curves.

This observation is consistent with the above mentioned mechanism, that in the beginning of the sonication the large particles are disrupted very quickly into significantly smaller ones, i.e. they are divided into small parts. A splitting off of small splinters can clearly not account for the rapid decay and the observation of a bimodal distribution of this kind. Instead of the evolution of the size distribution determined here, a gradual shift of the peak should occur and a peak corresponding to very small fragments should arise earlier.

Another phenomenon can be observed during continuing sonication in the plateau region. It can be seen that the size distribution of the Janus discs narrows progressively. Since unimodal distributions can be obtained for longer sonication times, the cumulant analysis can be performed in order to obtain values for the polydispersity indices of the structures. The calculated polydispersities are in the range of 1.3 – 1.1 for sonication times between 20 and 85 min. Consequently, the size distribution is narrowed significantly and Janus discs with moderate size distribution can be obtained by continued sonication.

Visualization

Several imaging techniques were used in order to visualize the resulting disc-like Janus structures. The focus of these investigations was to address the issues, whether the particles aggregate and how the actual shape looks like. In particular one might expect a back-to-back stacking of the particles, i.e. an aggregation of two particles into dimeric superstructures. Furthermore, it is interesting to know, whether the particles possess a more sheet-like character with irregular edges or if they can reach a disc-like appearance.

In general, the particles show a very strong tendency to adsorb onto standard silicon and mica substrates. It was found that the particles tend to aggregate strongly while depositing on the surface. One driving force to create these assemblies is certainly the tendency to minimize energetically unfavourable edges of the flat Janus particles. A good separation can only be obtained when depositing the sample from an ultradilute solution.

Scanning Electron Microscopy

Figure 14 - 6 shows a SEM image of flat Janus particles deposited onto a silicon wafer from a very dilute (0.1 mg/L) $CHCl_3$ solution.

Various discs tend to coalesce and form a continuous film as can be seen on the left-hand side of the image. On the contrary, molecularly dispersed and well-separated particles can be seen on the right-hand side. The size-distribution of these non-aggregated particles resembles those in the solution as determined by DLS of this sample. The particles themselves exhibit a surprisingly circular to ellipsoidal shape. On account of this observation, more attention was drawn on the shape development of the particles on substrates, as well as in solution. In order to gain further information about the particles, especially with respect to their heights and detailed shapes, a thorough scanning force microscopy (SFM) investigation was performed. SFM can further improve the resolution of the Janus particles and resolve more structural details than SEM.

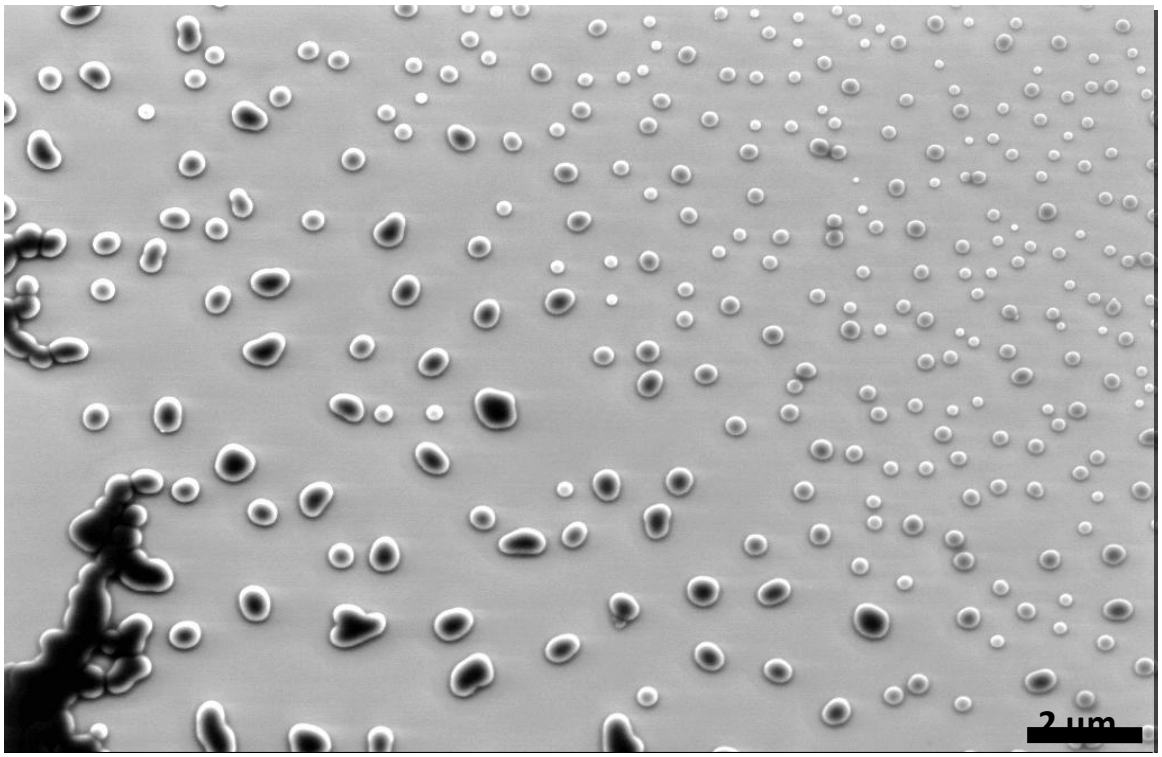

Figure 14 - 6. SEM images obtained from a dip-coated sample of Janus discs (c = 0.1 mg/L in $CHCl_3$; SBT-1, 5 wt% AIBN, 5 wt% TRIS, sonication at 30% amplitude) on silicon (3 kV acceleration voltage).

Scanning Force Microscopy

Several representative SFM images of disc-like Janus structures obtained by crosslinking of the SBT templates via the cold vulcanization or the free radical crosslinking process will be discussed in the following. To the best of our knowledge, this is the first detailed investigation of semi-flexible flat polymeric nanoobjects adsorbed onto surfaces by means of scanning force microscopy.

The images in Figure 14 - 7 reveal a multitude of interesting features. First of all, the discs are round in most of the images as similarly observed by SEM. The inset in Figure 14 - 7b shows the aggregation of two small and more asymmetric particles, confirming the presence of asymmetric objects and the possibility to image those under the applied measurement conditions. The development of round-shaped particles is presumably caused by subjecting the crosslinked material to ultrasound energy. The particles will preferentially break at existing cracks, and protrusions standing out of the main particle will be cut off most easily. These processes lead to a rounding off and “shaving” of the particles. In consequence the particles will develop a round, more disc-like appearance, as can be seen in most of the images.

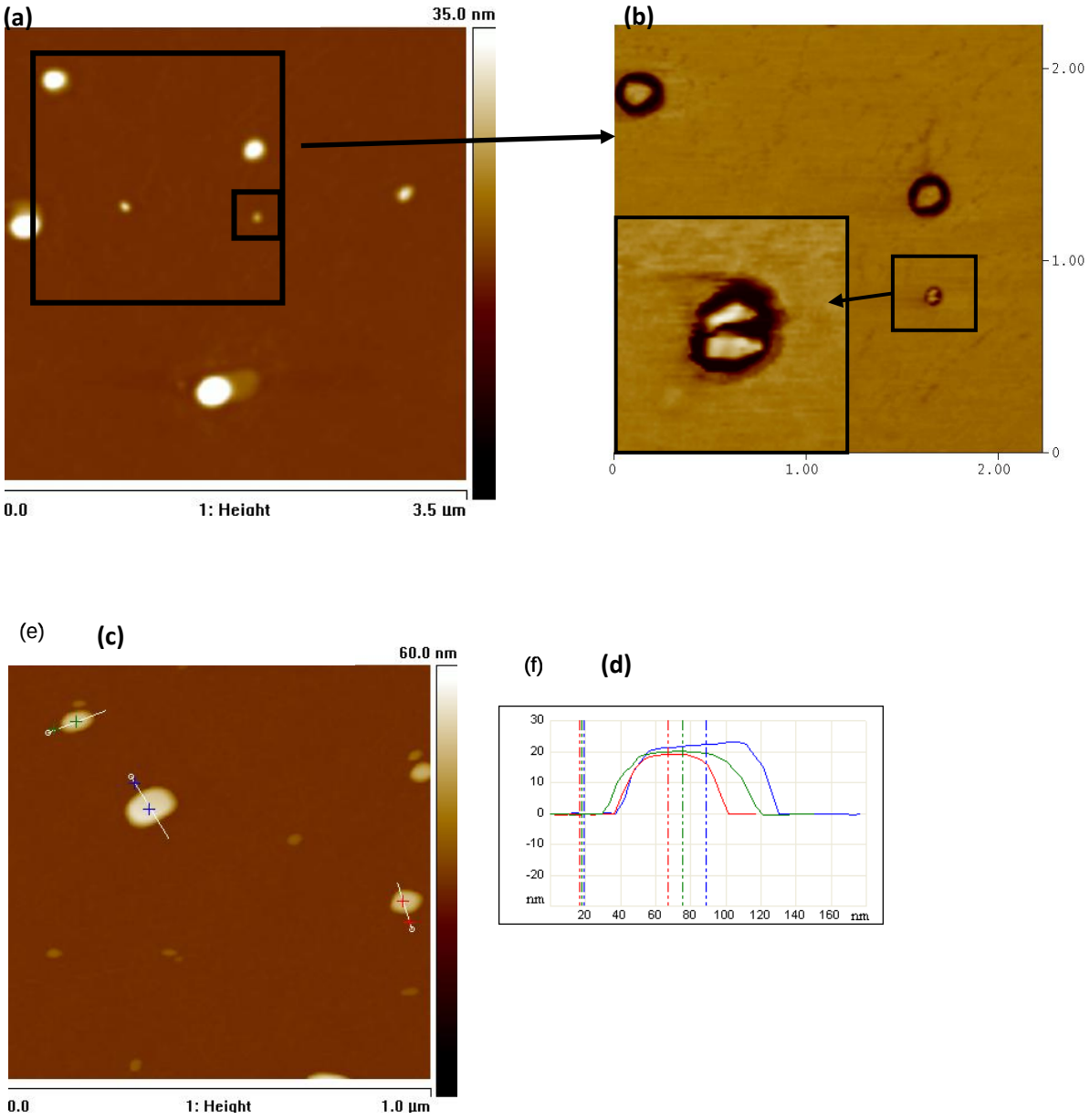

Figure 14 - 7. (a) + (c) SFM height image obtained from a sample of Janus discs (SBT-2, S_2Cl_2, sonication for 20 min at 30% amplitude). (b) Phase image of a part of image (a), containing a further magnified inset. (d) Section analyses corresponding to the lines in image (c). All samples were dip-coated from a $CHCl_3$ solution (c = 0.1 mg/L) onto silicon wafers.

Really anisometric sheet-like structures can only be found in the very beginning of the sonication procedure for the Janus particles based on the SBT-1 template (see Figure 14 - 8 and see supporting information for cryo-TEM images of the early state of sonication). Some potential breaking points are highlighted with arrows in Figure 14 - 8. Breaking the particles at the highlighted crack lines will result in two significantly more spherical particles, in particular for the particle shown on the left-hand side of Figure 14 - 8. This observation strongly supports the aforementioned influence of the sonication treatment and explains the absence of large protrusions and deformed non-circular objects.

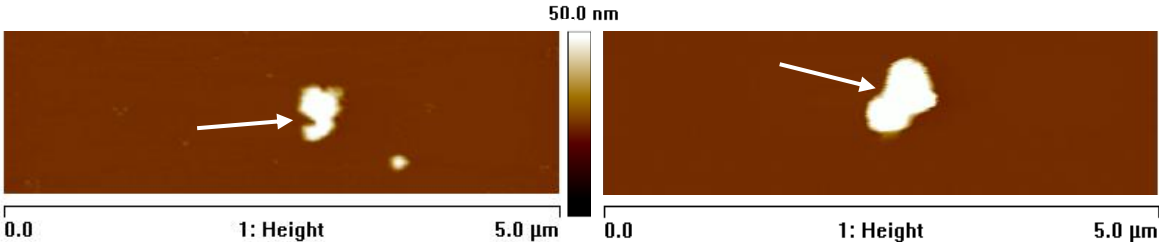

Figure 14 - 8. SFM height images obtained from a sample of Janus sheets (SBT-1, 5 wt% AIBN, 5 wt% TRIS, sonication for 3 min at 30% amplitude) dip-coated from a $CHCl_3$ solution (c = 0.1 mg/L) onto mica. The white arrows highlight potential breaking points of the structures.

Secondly, the phase image in Figure 14 - 7b shows an interesting core-corona contrast for the particles, indicating that the elasticity of the top of the particles is somewhat different from that of the corona. The corona probably consists of spread chains of the underlying side of the Janus disc. Therefore a different material is probed at the outer area of the structure. If there was no coronal segregation, this kind of core-corona structure in the phase contrast would not be expected, as a mixed corona should not give any phase contrast. Due to the polar nature of the substrate and the higher polarity of the P*t*BMA as compared to PS, P*t*BMA is adsorbed to the substrate.

During the thorough analysis of the height profiles of the particles, it was found that many structures show a droplet-shaped section profile. Additionally, a size dependence of the height on the overall particle size could be found. These effects are presumably caused by the rapid drying and the kinetic entrapment of the droplet-like shape which develops during drying for each individual Janus disc (see supporting information for images and further explanation). In order to explore this phenomenon and to prove whether the structures can be kinetically frozen, substrates with formerly deposited Janus discs were either heated to 150 °C in vacuo or annealed in toluene vapour (90 °C) in order to allow a thermal relaxation of the particles. Both methods should provide enough energy to allow a segmental movement and a reorientation of the structures. Figure 14 - 9 shows two representative high-resolution SFM images obtained from such annealing experiments. The images show that several changes developed after the two annealing procedures. The plateau is now very pronounced, in contrast to non-annealed structures, and the height approaches similar values of ca. 28 - 35 nm for all particles, which is a very reasonable value for the disc thickness. Based on the TEM investigations of the uncrosslinked block terpolymer films, values for the disc thickness between 30 – 40 nm are expected. The droplet-like shape changes to a significantly flatter one, which is expected for brush-like disc-shaped object. The plateau itself is totally flat over 150 – 300 nm as can be seen in the two section analyses and the 3D surface plot. Therefore, the kinetically trapped droplet-mimicking structure, induced during the solvent evaporation, is brought much closer to the thermodynamic equilibrium.

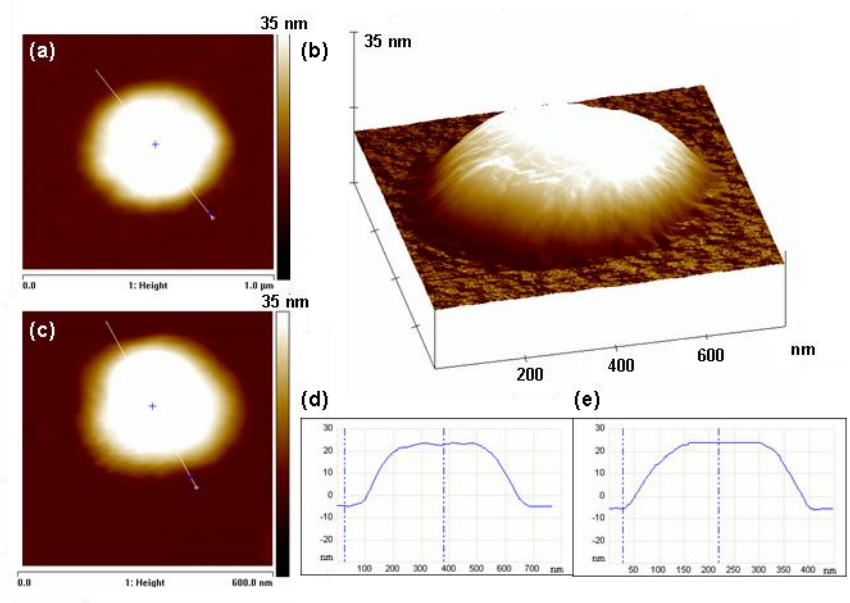

Figure 14 - 9. SFM height image obtained from a sample of Janus discs (SBT-2, 5 wt% AIBN, sonication for 1 min at 30% amplitude) using an ultra-sharp tip (R_{Apex} < 2 nm) for imaging. The sample was dip-coated from a 0.1 mg/L $CHCl_3$ solution onto mica and annealed at 150 °C in vacuo (a) or at 90 °C in toluene vapour (c). (b): 3D surface plot of (a). (d) and (e): Section analyses corresponding to the lines shown in the height images (a) and (c), respectively.

One point , which does not dramatically change upon annealing, is the smooth height increase at the boarder of the Janus discs. Typically, this onset remains in the region of 60 - 120 nm. However, considering the proportions of the polymer chains (e.g. contour length of P*t*BMA; $l_c \approx$ 115 nm) and the strong tendency of the particles to adsorb onto the interfaces (see above), the observed dimensions of the height increase can be understood (see inset in Scheme 14 - Sup-1). It appears that the contributions of the interfacial energy of the system are dominant at the outer regions of the particle, whereas the brush-like behaviour dominates the structure in the centres of the particles. Based on the considerations of the energetic contributions to the system, the appearance of the flat Janus particles on surfaces can now be reasonably understood.

Cryogenic transmission electron microscopy (*cryo*-TEM)

Cryo-TEM was chosen in order to explore the particle shape *in-situ* in solution and to investigate the samples towards the self-assembly into superstructures in concentrated solution. The investigation of particles deposited from solution in the semi-dilute and concentrated regime by SFM or SEM is not possible due to the strong adsorption and aggregation tendency of the particles. Hence it would not be clear whether true aggregates were imaged or whether the assemblies were artificially constructed during the deposition process. Therefore, cryo-TEM investigations in a non-selective organic solvent, THF, were performed for a variety of different samples in the more concentrated regime, typically with concentrations higher than 1 mg/mL. Figure 14 - 10 shows a representative overview of images with aggregated Janus discs (more images can be found in the supporting information).

Despite the low contrast (mass density x specimen thickness) between material and solvent, a layered structure can clearly be seen in the image. Several arrows highlight parts for which distinct layers can be seen most easily. Moreover, the cryo-TEMs convincingly demonstrate the absence of vesicular structures, which could not be ruled out in the beginning of the investigation of flat Janus particles

In order to further elucidate the layered structures, a cross-section analysis is shown in Figure 14 - 10d. The cross section is based on the grey scale originating from the contrast variations within the sample. Two distinct layers can be seen and additionally, the particles show a very flat profile in the centre. This suggests that the particles are indeed flat and that the superstructures are composed of two back-to-back stacked Janus discs. Furthermore, it can be seen that the particles are actually circular and that the above-mentioned mechanism of ultrasound-induced rounding of the particles holds. The aggregation process into superstructures is somewhat surprising as THF is a good solvent for both sides, PS and P*t*BMA. Due to the very good solubility of P*t*BMA in a variety of solvents, we expect that PS forms the inner solvent-swollen part of the assemblies. The driving force for the self-assembly process cannot be readily understood and deserves further investigations in the future.

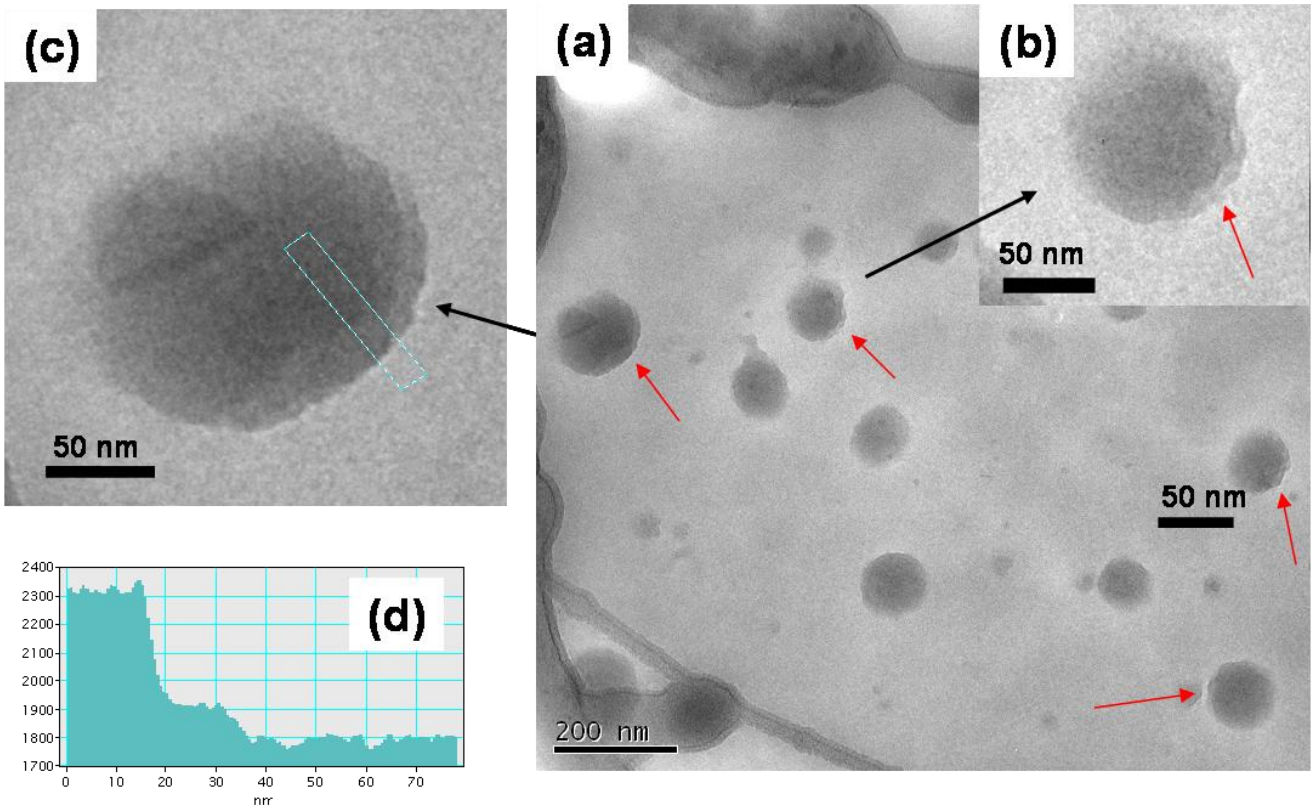

Figure 14 - 10. Cryogenic transmission electron microscopy images of a sample of Janus discs in tetrahydrofuran. The sample was allowed to equilibrate for several weeks at room temperature before imaging. (a) Overview with two magnified images (b) and (c). The red arrows highlight areas in which layered structures can be observed most easily. (d) Cross-section analysis of the bar shown in Figure 14 - (c), demonstrating the layered structure and the flat structure in the inside of the aggregate.

A similar unexpected aggregation into superstructures was demonstrated for the spherical Janus micelles. Therefore, this self-assembly behaviour can be attributed to the unique Janus character of the disc-like particles. In the case investigated here, a time-dependent aggregation process is indicated by the cryo-TEM investigations. For instance, if a sample is analyzed directly after applying high shear stress via passing a 1 µm PTFE filter, mainly molecularly dispersed Janus discs can be observed. In contrast, if the sample is allowed to undergo an aging process (several days), the fraction of aggregates increases significantly. Unfortunately, it is not straightforward to follow this time-dependent process, e.g. by means of DLS or fluorescence correlation spectroscopy, as back-to-back stacking has only a very small influence on the diffusion coefficient. This difference can hardly be measured for a polydisperse system.

In conclusion, the cryo-TEM investigations show convincingly that the particles exist as disc-like structures in solution. Moreover, the Janus discs tend to self-assemble reversibly into loose solvent swollen superstructures in moderately concentrated solution. The structure of those aggregates can be described by back-to-back stacking of the Janus discs.

TEM analysis of Embedded Janus Discs

TEM of embedded Janus discs was done in order to confirm the inherent multicompartment structure and the aggregation of Janus discs into superstructures. The subsequent images were obtained after rapid drying of THF or acetone solutions containing flat Janus particles and a crosslinkable silicon oil. After crosslinking, microtome cutting was performed and the ultrathin sections were stained with OsO4 vapour prior to TEM imaging (see Figure 14 - 11).

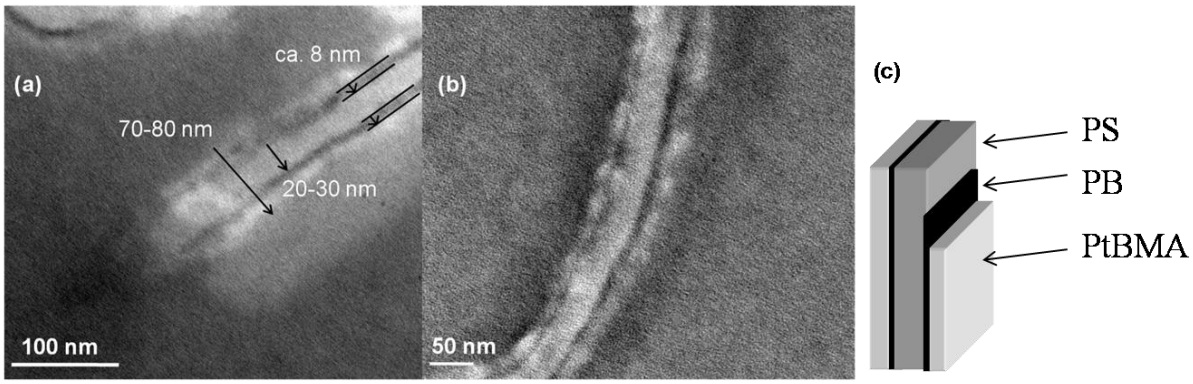

Figure 14 - 11. TEM images of embedded Janus particles (based on the SBT-1 template) after microtome cutting and staining with OsO_4. The particles were embedded from a concentrated solution of THF (a) or acetone (b) in the presence of photo crosslinkable silicon oil. Figure 14 - (c) depicts a schematic representation of the different layers.

Long cylindrical structures can be found within the ultrathin sections. Long cylinders can only originate from flat structures embedded, thus confirming the presence of Janus discs in the solution. A close look at the cross section of the structures reveals the presence of several layers. The structure found corresponds to a back-to-back stacked assembly of the Janus discs with the polystyrene part in the centre. This structure can be found independently of the solvent used. Note that acetone is a non-solvent for polystyrene and thus forces aggregation of the Janus discs into a layered assembly. Since exactly the same structure can be found in the case of THF as solvent for the Janus discs, an aggregation of the Janus discs in the THF solution appears most

likely. The greyscales found for the different layers originate from the elemental composition of the different parts. The thin crosslinked butadiene layer, whose residual double bonds were stained with OsO_4, appears very dark. In contrast, the inner polystyrene layer appears much brighter as almost no OsO_4 is present there. The overall surrounding silicon oil appears slightly darker than the PS part due to the large content of silicon. The P*t*BMA part at the outside is again bright, due to the decomposition of the P*t*BMA in the electron beam. Thus an average contrast originating from degraded P*t*BMA and surrounding silicon oil can be found.

The length scales, as indicated in image (a), correspond closely to what was found from the initial SBT-1 template. Note that the height of the non-aggregated Janus discs was found to be around 30 – 35 nm as imaged by SFM. Thus this value corresponds to half of the thickness found for the back-to-back stacked assembly here. In the experiments it was not possible to image single non-aggregated Janus dics, which is due to the fact that the concentration of the solution is high, typically in the range of (10 – 30 mg/mL). Moreover, during the evaporation of the solvent, the concentration increases dramatically above a critical aggregation concentration. Non-aggregated Janus discs can only be imaged by SFM and SEM at very high dilution.

Besides, image (a) shows the ends of two assembled structures (centre and upper right corner). It can be seen that the assemblies are open at the end and that the polybutadiene layer does not surround and cover the complete inner PS part.

In conclusion, the embedding experiments ultimately confirm a flat multicompartment type architecture and give a strong indication for a self-assembly of the Janus disc in THF.

Behaviour at Liquid-Liquid Interfaces

As already mentioned in the introduction, calculation show that Janus discs should have a much stronger adsorption energy at liquid-liquid interfaces than ordinary low-molecular weight surfactants of similar composition[1] and most likely than homogenous particles of similar size. The herein synthesized Janus discs are ideally suited for investigating this phenomenon experimentally. The predictions for spherical Janus particles were recently verified by Glaser et al.[31] A remarkable decrease of the oil/water interfacial tension was found upon introduction of Janus character into the surface active particles. Janus structures may thus be of great importance as future surfactants.

One way of determining the influence of particles at liquid-liquid interfaces is to analyze the interfacial tension isotherms of a solution of the desired material, e.g. via the pendant drop method. Recording and analyzing the droplet shape of two immiscible liquids, one containing the dissolved material, via a digital camera system provides the time-dependent evolution of the change in interfacial tension. In order to allow a meaningful comparison, the interfacial tension isotherms for the two block terpolymers, SBT-2 and SBT-1, dissolved in cyclohexane, were determined at the immiscible phase boundary of water and cyclohexane. Upon addition of the block terpolymer to the cyclohexane solution the interfacial tension between cyclohexane and water is decreased from ca. 51 mN/m to ca. 30 mN/m. The determined interfacial tension of the pure cyclohexane/water system agrees well with the literature values.[32, 33] The values for both block terpolymers are very close and hence it can be concluded that the inner fraction of polybutadiene plays only a minor role for the reduction of the interfacial tension. In order to see an effect of the crosslinked architectures, the interfacial tension isotherms of the Janus discs are compared to the ones obtained for the block terpolymer solutions Figure 14 - 12.

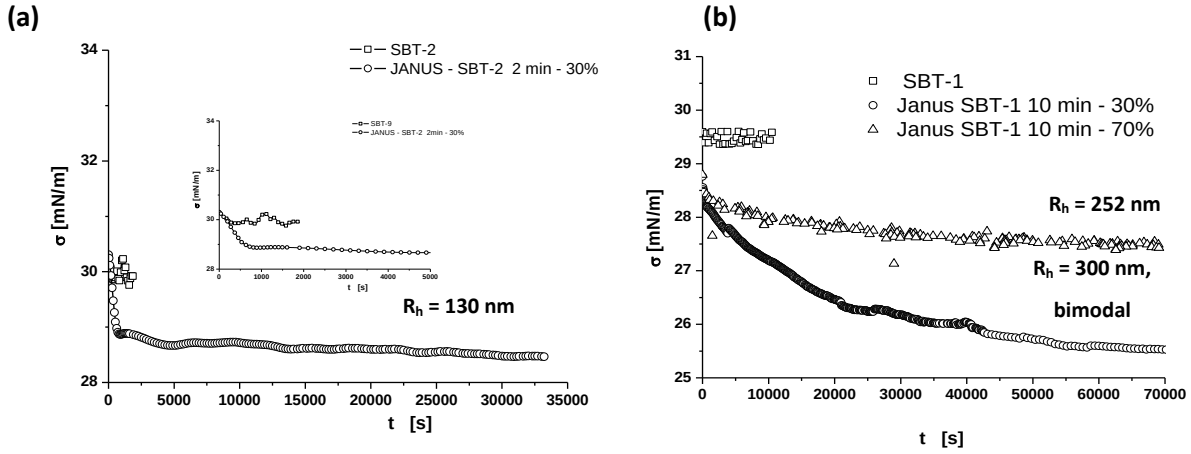

Figure 14 - 12. Interfacial tensíon isotherms of solutions of Janus discs in cyclohexane at the cyclohexane/water interface (c = 1 mg/mL). The isotherms of the block terpolymer precursors are shown for comparison. The z-average hydrodynamic radii of the samples investigates are shown within the diagrams and were obtained by DLS.

A significant decrease of the interfacial tension of the system can be observed for all samples containing the Janus particles. For the SBT-1 based Janus discs two different samples are shown. The one with the higher hydrodynamic radius ($\langle R_h \rangle_z$ = 300 nm) possesses a bimodal size distribution, which is typically obtained at short sonication times (see above). It contains a fraction of relatively large flat Janus sheets (R ≈ 1 - 2 µm). On the contrary, the other sample

shows a monomodal distribution; very large particles are not present in this case. It can be seen that the presence of larger particles leads to a stronger decrease of the interfacial tension and thus it can be concluded that indeed the interfacial tension depends on the disc-size. The lowest decrease of the interfacial tension can be found for the Janus disc sample based on the SBT-2 template, exhibiting the smallest particle size. The interfacial tension isotherms decay more slowly as compared to the pure block terpolymer isotherms. The observed decrease indicates that the systems are of dynamic nature as otherwise no long-lasting time-dependent change would be expected. After reaching the plateau value at longer timescale, the thermodynamically favoured molecules should be placed and oriented at the interface. According to the theory of Nonomura et al.[1], the largest discs adsorb most strongly.

The presented results of the effect of Janus discs on the interfacial tension of a liquid-liquid interface are remarkable and one of the unique features predicted for disc-like Janus particles, in particular under the consideration that the particles themselves are only slightly amphiphilic. Even stronger changes are expected for strongly amphiphilic Janus discs. This novel class of particles is thus of high interest for studies concerning emulsion stabilization, technological formulations or encapsulation of molecules.

Conclusion

We have been able to synthesize for the first time large sheet-like or disc-like Janus particles, consisting of a crosslinked inner polybutadiene layer and two phase-segregated sides of polystyrene and poly(*tert*-butyl methacrylate). The particles can be obtained via a simple template-assisted approach and their size can be tuned from the mesoscopic level to the nanometer scale, typically in the range of several micrometers to hundred nanometers. The size distribution of the Janus discs narrows progressively to moderate values with prolonged homogenization.

A detailed SFM investigation of these novel flat, brush-like polymeric nanoparticles has given a deep insight into the surface structures formed. The appearance of the particles adsorbed onto substrates is governed by a strong interplay between the brush-like behaviour and the interfacial tensions of the system. Due to the introduced ultrasound energy, the sheet-like particles get “shaved” and exhibit circular disc-like outer sides. By means of *cryo*-TEM, which was applied for the first time in THF, it was possible to visualize the aggregation behaviour of the Janus discs *in-situ*. The flat particles self-assemble into superstructures via back-to-back stacking even in good solvents. The aggregation into superstructures and the inherent multicompartment character of the structures could be demonstrated by embedding the Janus discs into a photo-crosslinkable silicon oil and subsequent direct TEM observation of the cross section after microtome cutting and staining.Finally, the effect of Janus discs on the interfacial tension of liquid-liquid interfaces (oil/water) was highlighted, serving as a model system for emulsion stabilization. The Janus particles show a distinct and significant decrease of the interfacial tension as compared to their linear uncrosslinked block terpolymer precursors and are therefore more efficient stabilizing agents. The decrease is most pronounced for the Janus discs with the largest diameters.

Acknowlegments

The authors would like to thank Georg Krausch, Robert Magerle and Nicole Glaser for fruitful discussions as well as Thorsten Goldacker for the synthesis of SBT-2. Furthermore, we are indebted to Astrid Göldel and Clarissa Abetz for numerous TEM and SEM images. Felix Schacher is acknowledged for the microtome cutting. This work was supported by DFG within the ESF SONS-AMPHI Program and by the EU within the Marie Curie RTN POLYAMPHI. Andreas Walther thanks the Bavarian Graduate Support Program for a scholarship.

References

1. Nonomura, Y.; Komura, S.; Tsujii, K. *Langmuir* **2004,** 20, 11821.
2. Binks, B. P.; Fletcher, P. D. I. *Langmuir* **2001,** 17, 4708..
3. Cates, M. E.; Poon, W. C. K.; Clegg, P. S.; Egelhaaf, S. U. 2005-GB2577, 2006003403, 20050701., **2006**.
4. Vanakaras, A. G. *Langmuir* **2006,** 22, 88.
5. Roh, K.-H.; Martin, D. C.; Lahann, J. *Nat. Mater.* **2005,** 4, 759.
6. Perro, A.; Reculusa, S.; Ravaine, S.; Bourgeat-Lami, E.; Duguet, E. *J. Mater. Chem.* **2005,** 15, 3745.
7. Li, Z.; Lee, D.; Rubner, M. F.; Cohen, R. E. *Macromolecules* **2005,** 38, 7876.
8. Shepherd, R. F.; Conrad, J. C.; Rhodes, S. K.; Link, D. R.; Marquez, M.; Weitz, D. A.; Lewis, J. A. *Langmuir* **2006,** 22, 8618.
9. Erhardt, R.; Böker, A.; Zettl, H.; Kaya, H.; Pyckhout-Hintzen, W.; Krausch, G.; Abetz, V.; Müller, A. H. E. *Macromolecules* **2001,** 34, 1069.
10. Xu, H.; Erhardt, R.; Abetz, V.; Müller, A. H. E.; Gödel, W. A. *Langmuir* **2001,** 17, 6787.
11. Erhardt, R.; Zhang, M.; Böker, A.; Zettl, H.; Abetz, C.; Frederik, P.; Krausch, G.; Abetz, V.; Müller, A. H. E. *J. Am. Chem. Soc.* **2003,** 125, 3260.
12. Sfika, V.; Tsitsilianis, C.; Kiriy, A.; Gorodyska, G.; Stamm, M. *Macromolecules* **2004,** 37, 9551.
13. Kiriy, A.; Gorodyska, G.; Minko, S.; Stamm, M.; Tsitsilianis, C. *Macromolecules* **2003,** 36, 8704.
14. Schrage, S.; Sigel, R.; Schlaad, H. *Macromolecules* **2003,** 36, 1417.
15. Voets, I. K.; de Keizer, A.; De Waard, P.; Frederik, P. M.; Bomans, P. H. H.; Schmalz, H.; Walther, A.; King, S. M.; Leermakers, F. A. M.; Cohen Stuart, M. A. *Angew. Chem. Int. Ed.* **2006,** 45, 6673.
16. Ishizu, K.; Satoh, J.; Toyoda, K.; Sogabe, A. *J. Mater. Sci.* **2004,** 39, 4295.
17. Liu, Y.; Abetz, V.; Müller, A. H. E. *Macromolecules* **2003,** 36, 7894.
18. Goldacker, T., PhD Thesis, Bayreuth, Bayreuth, 1999.
19. Breiner, U.; Krappe, U.; Thomas, E. L.; Stadler, R. *Macromolecules* **1998,** 31, 135.
20. Jacobine, A. F., *Radiation Curing in Polymer Science and Technology*. Elsevier Applied Science: London, **1993**; Vol. 3, p 219.
21. Decker, C. *Progress in Polymer Science* **1996,** 21, 593.
22. Decker, C.; Nguyen Thi Viet, T. *Macromol. Chem. Phys.* **1999,** 200, 1965.
23. Decker, C.; Nguyen Thi Viet, T. *Macromol. Chem. Phys.***1999,** 200, 358.
24. Decker, C.; Nguyen Thi Viet, T.; Hien Le, X. *Macromol. Symp.* **1996,** 102, 63.
25. Koppel, D. E. *J. Chem. Phys.* **1972,** 57, 4814.
26. Brown, J. C.; Pusey, P. N. *J. Chem. Phys.* **1975,** 62, 1136.
27. Marque, J.; Ikegami, A.; Kubota, K.; Tominaga, Y.; Fujime, S. *Biophys. J.* **1986,** 50, 139.
28. Fujime, S.; Kubota, K. *Biophys. Chem.* **1985,** 23, 1.

29. Kubota, K.; Tominaga, Y.; Fujime, S.; Otomo, J.; Ikegami, A. *Biophys. Chem.* **1985,** 23, 15.
30. van der Kooij, F. M.; Philipse, A. P.; Dhont, J. K. G. *Langmuir* **2000,** 16, 5317.
31. Glaser, N.; Adams, D. J.; Böker, A.; Krausch, G. *Langmuir* **2006,** 22, 5227.
32. Landfester, K.; Willert, M.; Antonietti, M. *Macromolecules* **2000,** 33, 2370.
33. d'Ans, J.; Lax, E., *Taschenbuch für Chemiker und Physiker*. Springer: Berlin, **1992**; Vol. 4th.

Supporting Information

Experimental Section

Materials

All solvents and reagents were obtained from Merck or Aldrich in p.a. grade and used without further treatment except for the following ones. Zipcone UA was purchased from ABCR. Decane (p.a., Aldrich) and Isooctane (p.a., Aldrich) were treated with sec-butyl lithium and distilled. THF (p.a. Merck) was treated with sec-butyl lithium at low temperatures and distilled. Cyclohexane (Merck) and acetonitrile (Aldrich) were obtained in HPLC grade and used directly.

Synthesis

The anionic polymerization of the polystyrene-*block*-polybutadiene-*block*-poly(*tert*-butyl methacrylate) (SBT) terpolymers was conducted in a similar way as reported elsewhere.[1, 2]

Crosslinking with AIBN / Thiol-Polyene process

AIBN (5 wt%, relative to the mass of the SBT terpolymer), trimethylolpropane mercaptopropionate (TRIS, 0 - 5 wt%) and SBT terpolymer were dissolved in $CHCl_3$ and the film casting process was allowed to take place in a solvent vapour filled desiccator for about two weeks. Afterwards, the film was dried in vacuo at RT for 24 h and crosslinked at 80 °C for 48 h. Subsequently, the film was purified by Soxhlet extraction with THF for 24 h yielding a soluble fraction and an insoluble fraction. The insoluble fraction was subjected to a sonication treatment.

Cold vulcanization

A solvent-cast film was introduced into a reaction vessel and swollen in solvent (decane or isooctane) for a certain period of time (typically: 12 – 48 h). Afterwards, the calculated amount of S_2Cl_2 (typically: 1.5 – 5 vol%) was introduced with a syringe and the crosslinking was allowed to take place for 12 - 48 h at room temperature. After the reaction, the film was washed with several aprotic non-solvents, e.g. acetonitrile and isooctane. Subsequently, the film was purified by Soxhlet extraction with THF for 24 h yielding a soluble and an insoluble fraction. The insoluble fraction was subjected to a sonication treatment.

Sonication

The product underwent ultrasonic treatment using a Branson model-250 digital sonifier, equipped with 1/8 in. diameter tapered microtip, at various amplitudes (200 watt at 100% amplitude). For this purpose, a dispersion of insoluble crosslinked material (c = 0.3 - 1 mg/mL) in THF was allowed to stand at room temperature for several hours to ensure good swelling of the material. Afterwards, it was subjected to the sonication treatment in a temperature controlled

cell. The on/off cycle times were typically in the range of 2s/2s and 2s/10s, depending on the amplitude used.

TEM imaging of embedded Janus discs

10 – 30 mg of Janus discs were dissolved in 1 ml of THF or acetone and added to a vial containing 0.1 – 0.3 mL of Zipcone UA (photo-crosslinkable silicon oil). After rapid evaporation of the solvent, the silicon oil was crosslinked using a standard UV lamp for 1h. Subsequently, the solidified block was microtome cut and the ultrathin sections were stained with OsO_4 prior to TEM imaging.

GPC-MALS measurements were performed at room temperature using a GPC equipped with a Wyatt Technology DAWN DSP-F multi-angle light scattering detector (He-Ne Laser; γ = 632.8 nm) and a Shodex-RI-71 refractive index detector. Three 30 cm PSS SDV columns (104, 105, and 106 Å) were used with THF as eluent at a flow rate of 1 mL/min. Data evaluation was performed with the Astra Software package.

NMR

^{1}H- and ^{13}C-NMR spectra were obtained on a Bruker AC 250 at an operating frequency of 250 MHz and 62.5 MHz, respectively. Various deuterated solvents (Deutero GmbH) were used depending on the solubility of the samples. As an internal standard, the residual proton signal of the deuterated solvent was used.

Dynamic Light Scattering (DLS)

Dynamic light scattering was performed on an ALV DLS/SLS-SP 5022F compact goniometer system with an ALV 5000/E cross-correlator and a He–Ne laser (λ_0 = 632.8 nm). Prior to the light scattering measurements the sample solutions were filtered using Millipore or Roth filters (housing: polypropylene, membrane: polytetrafluoroethylene) with a pore size of 5 μm. All samples were analyzed at high dilution. The data evaluation of the dynamic light scattering measurements was performed with the CONTIN algorithm[3] and the values of the hydrodynamic radii were obtained after extrapolating the angle-dependent scattering data to $q^2 \rightarrow 0$.[4]

Small Angle X-ray Scattering (SAXS).

The SAXS measurements in this work were carried out at the ID02A high-brilliance beamline at the European Synchrotron Radiation Facility (ESRF, Grenoble, France). The operating energy range was 12.5 keV, corresponding to a wavelength of 0.1 nm, at which the highest photon flux is obtained. The detector system with a standard two-dimensional SAXS camera is housed in a 10 m evacuated flight tube. For the experiments an image intensified CCD detector is used, which can handle the full X-ray flux. Prior to data analysis, background scattering was subtracted from the data and corrections were made for spatial distortions and for the detector efficiency. The data evaluation was performed with home-written software.

Scanning Electron Microscopy (SEM)

SEM was performed using a LEO 1530 Gemini instrument equipped with a field emission cathode with a lateral resolution of approximately 2 nm. The acceleration voltage was chosen between 0.5 and 3 kV. Statistical analysis of the size distribution of the particles was performed with ImageJ V1.32 and ImageTool V3.0.

Transmission Electron Microscopy (TEM)

The bulk morphologies of the SBT triblock terpolymer were examined using TEM. Films (around 1 mm thick) were cast from 5% (w/w) solutions in $CHCl_3$ and allowed to evaporate slowly for 2 weeks. The as-cast films were dried for 1 day in vacuum at room temperature and then annealed at 80 °C for 1 - 5 days. Thin sections were cut at room temperature using a Reichert-Jung Ultracut E microtome equipped with a diamond knife. To enhance the electron density contrast between the three blocks, the sections were exposed to OsO_4 vapour for 60 s, which leads to a preferential staining of the polybutadiene block appearing black. Bright-field TEM was performed on Zeiss CEM 902 and LEO 922 OMEGA electron microscopes operated at 80 kV and 200 kV, respectively.

For **cryogenic transmission electron microscopy (cryo-TEM) studies**, a drop of the sample dissolved in THF was put on a lacey transmission electron microscopy (TEM) grid, where most of the liquid was removed with blotting paper, leaving a thin film stretched over the lace. The specimens were instantly vitrifed by rapid immersion into liquid nitrogen and cooled to approximately 90 K by liquid nitrogen in a temperature controlled freezing unit (Zeiss Cryobox, Zeiss NTS GmbH, Oberkochen, Germany). The temperature was monitored and kept constant in the chamber during all of the sample preparation steps. After freezing the specimens, the specimen was inserted into a cryo-transfer holder (CT3500, Gatan, München, Germany) and transferred to a Zeiss EM922 EF-TEM instrument. Examinations were carried out at temperatures around 90 K. The transmission electron microscope was operated at an acceleration voltage of 200 kV. Zero-loss filtered images (ΔE = 0 eV) were taken under reduced dose conditions (100-1000 e/nm^2). All images were registered digitally by a bottom mounted CCD camera system (Ultrascan 1000, Gatan) combined and processed with a digital imaging processing system (Gatan Digital Micrograph 3.9 for GMS 1.4).

Scanning Force Microscopy (SFM)

SFM images were taken on a Digital Instruments Dimension 3100 microscope or on a Veeco Multimode operated in Tapping Mode. The standard silicon nitride probes and super-sharp probes were driven at 3 % offset below their resonance frequencies in the range of 250 - 350 kHz. According to the distributor of the tips, the normal tips and the super sharp tips possess finite tip sizes with radii of 10 - 20 nm and 2 nm, respectively. Offline data processing was done using the Nanoscope Software (V 5.13r10sr1 and V6r2.1) and Gwyddion 1.12.

Pendant Drop Tensiometer isotherms of the interfacial tension were measured on a Dataphysics OCA 20 tensiometer at room temperature. The particle concentration was in the range of 1 mg/ml to 0.1 mg/ml. The shape of the pendant drop was recorded using a CCD camera and the fitting was performed with the Dataphysics software package.

Crosslinking

The crosslinking of the polybutadiene part was accomplished via two ways, the thiol-polyene procedure and by cold vulcanization. The detailed and carefully optimized procedures for the crosslinking of the block terpolymer templates will be published separately. However, a short overview of the experiments is provided in the following.

Cold vulcanization is the reaction of double bonds with S_2Cl_2 in the swollen state. Since the morphologies of the block terpolymers react very sensitively to changes in solvent quality, the conditions were carefully optimized in order to ensure the integrity of the morphology at all stages of the process, i.e. after the addition of swelling solvent and crosslinking agent. Among the suitable solvents and solvent combinations investigated, only decane and isooctane can be used to swell the morphology as they do not alter the microphase-separated structure in any undesired fashion. Additionally, the concentration of the crosslinking agent, S_2Cl_2, may not exceed a certain level, as otherwise an unwanted transition to a core-shell cylinder morphology with P*t*BMA as matrix can take place. However, after careful screening of the experimental conditions, the cold vulcanization was performed successfully.

The alternative crosslinking method using AIBN, or its optimized process, the thiol-polyene reaction,[5] can be performed in a more straightforward manner. According to the work of Decker et al.,[6-9] the crosslinking of polybutadiene domains with AIBN in combination with trimethylolpropane mercaptopropionate (TRIS), a trifunctional crosslinking agent, leads to an increased fraction of insoluble material (thiol-polyene reaction). This is due to the fact, that TRIS can act as transfer agent and is also able to react with the 1,4-polybutadiene moieties which are usually not attacked during a normal radical crosslinking. Hence, it was taken advantage of this beneficial influence and the addition of the trifunctional thiol led to a larger fraction of insoluble material. Before carrying out the crosslinking, TEM images were recorded in order to assure the presence of lamellar morphologies and it was found that film casting in presence of AIBN and TRIS has no influence on the development of the lamellar (ll) morphology. Hence, it is unambiguous that annealing such structures leads to a rapid crosslinking, preserving the microphase-separated morphology. The success of this strategy was confirmed by TEM, which showed the clear persistence of the lamellar morphologies after crosslinking (see Figure Sup 14 - 1).

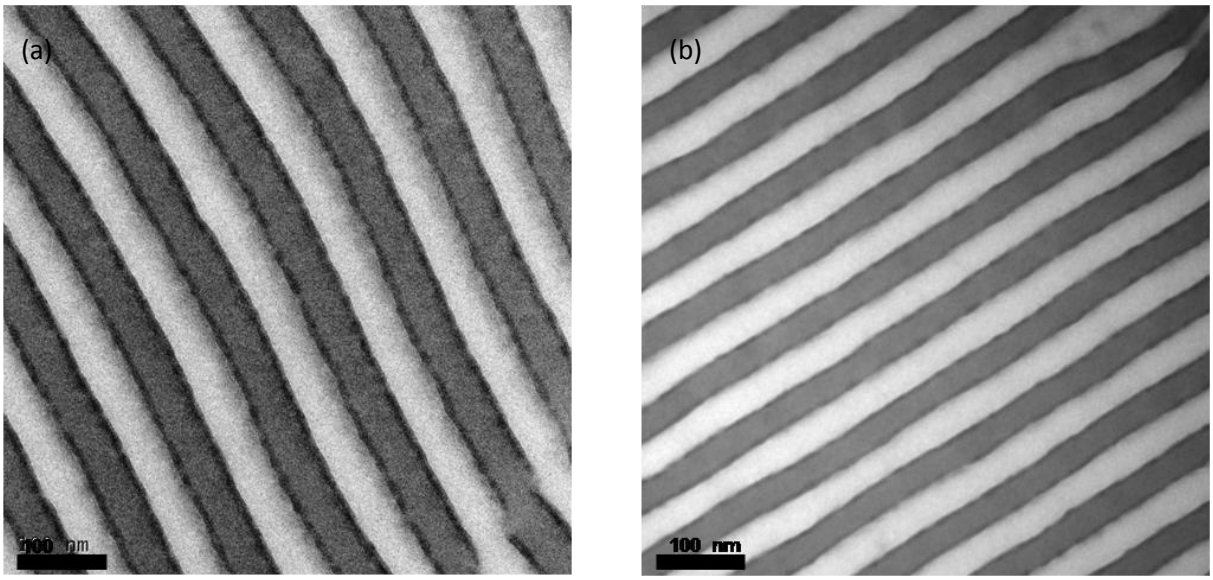

Figure Sup 14 - 1. Transmission electron micrograph of ultrathin sections of SBT-1 films, which were crosslinked with S2Cl2 after swelling in isooctane (a) or an AIBN/TRIS mixture (b). Residual uncrosslinked double bonds were stained with OsO_4 to improve the contrast.

Spectroscopic characterization by ^{1}H-NMR

Spectroscopic characterization of the SBT precursor terpolymer sample and a Janus dics sample obtained after sonication of a template which was crosslinked with 5 wt% AIBN in the presence of 5 wt% TRIS.

Clearly, both spectra show the presence of styrene (a) and *t*-butyl methacrylate units (d) before and after the template-assisted preparation of Janus discs. Herewith, the proposed composition of the outer sides can be confirmed. Additionally, the strong and successful crosslinking of the inner polybutadiene layer of the template can be deduced from the diminishing peaks b and c, corresponding to the unsaturated polybutadiene moieties.

The NMR peaks appear broader after the crosslinking and sonication due to their origin from larger structures with lower flexibility as compared to the initial terpolymer spectrum.

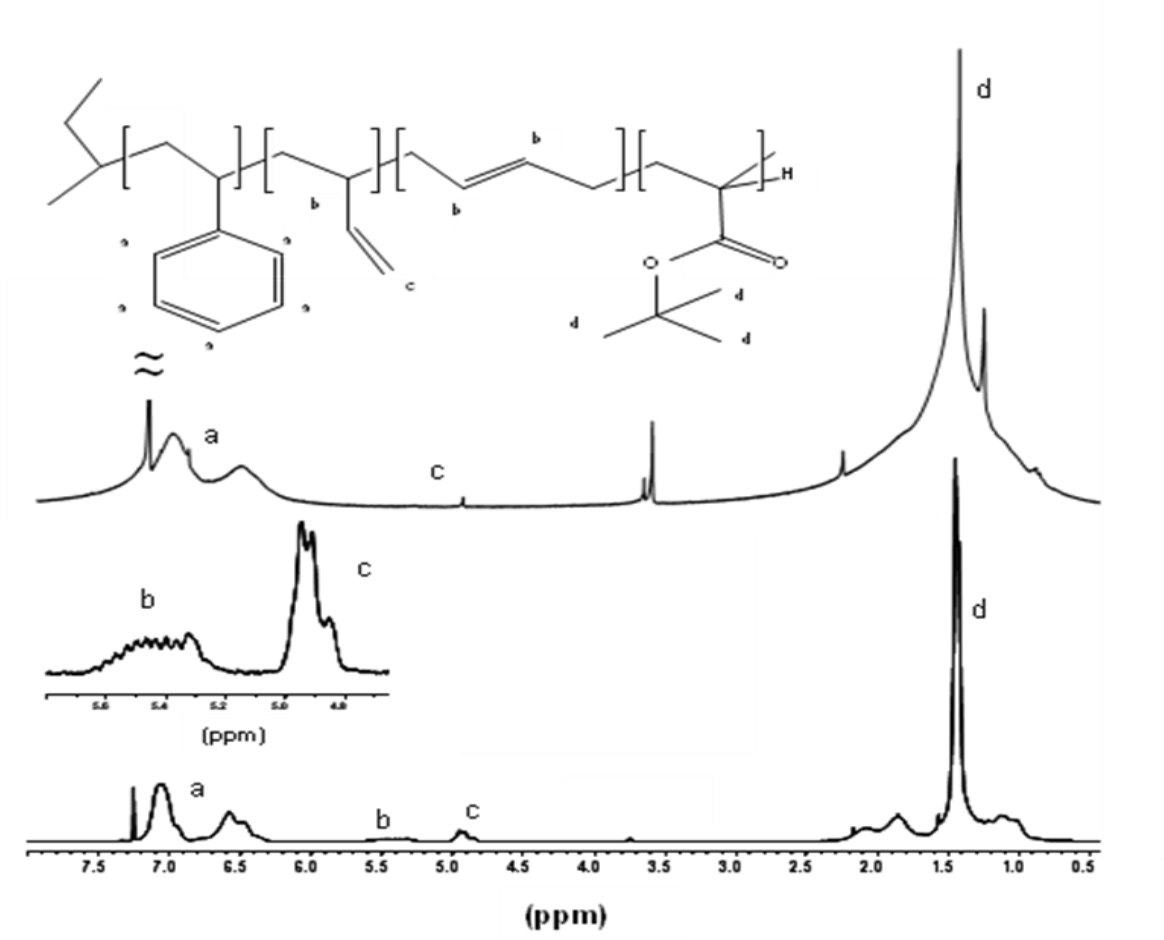

Figure Sup 14 - 2: ^{1}H-NMR spectra of SBT-1 (lower) and a Janus disc sample obtained after sonication of a crosslinked SBT-1 template (upper).

Height dependence of adsorbed Janus discs prior annealing

The height profiles of the particles, which were obtained by section analysis of the SFM height images, reveal an interesting peculiarity. The height profiles exhibit similar shapes, meaning an increase up to a certain level and the development of a plateau (see e.g. Figure 7d in publication). The particles possess high aspect ratios, indicating a very flat geometry. However, during the investigation of various differently crosslinked samples on different substrates it turned out that the plateaus are not always well developed (see Figure Sup 14 - 3). This kind of droplet-shaped appearance was not anticipated for such a polymer brush-like flat particle and deserves further discussion.

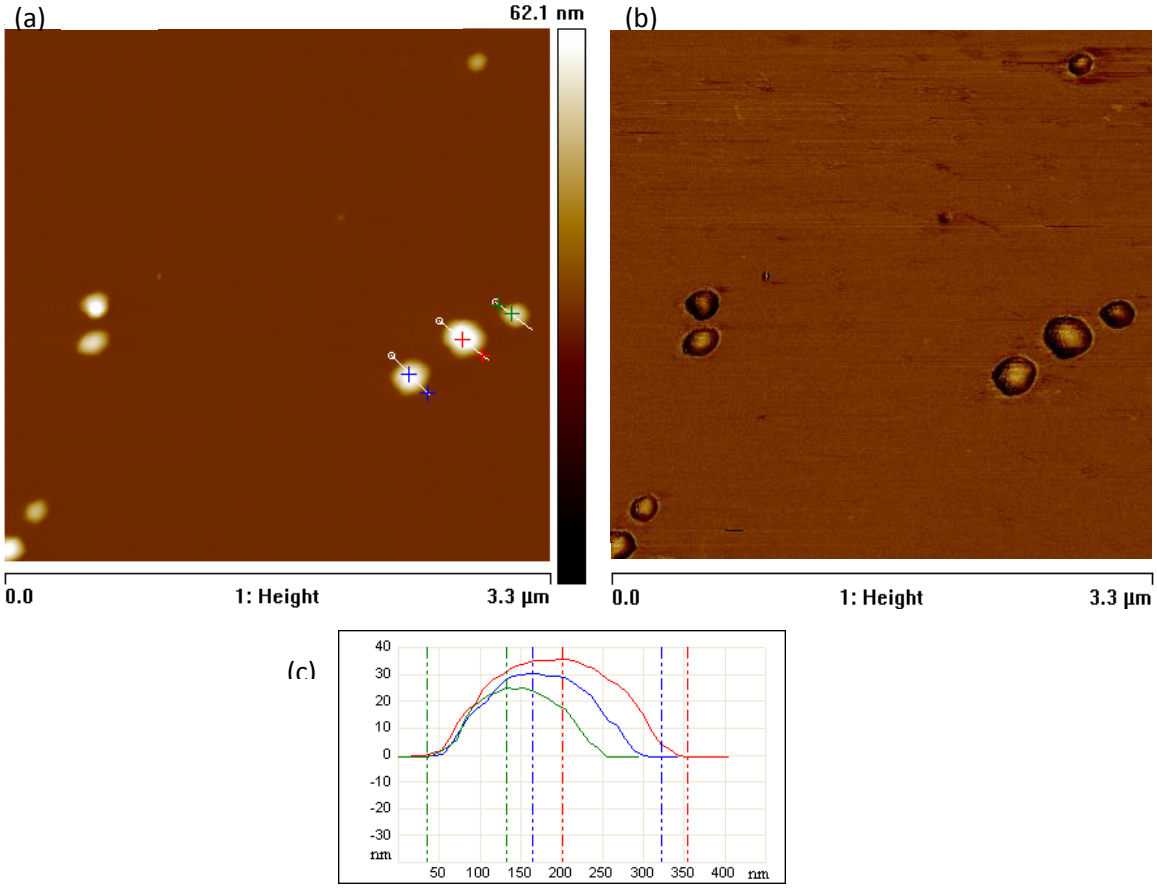

Figure Sup 14 - 3. (a) SFM height image obtained from a sample of Janus discs (SBT-2, 5 wt% AIBN, 5 wt% TRIS, sonication for 5 min at 30% amplitude), dip-coated from a $CHCl_3$ solution (c = 0.1 mg/L) onto mica. (b) Phase image of (a) and (c) section analysis corresponding to the lines shown in image (a).

The phenomenon itself can most frequently be seen for the imaging of samples crosslinked with AIBN using mica as substrate, independent of the block terpolymer template used. This implies an influence of the substrate and of the crosslinking method, resembling the mechanical strength of the material and the surface energy, respectively. The particles shown in Figure Sup 14 - 3 still possess very high aspect ratios, which can clearly not be caused by any kind of spherical particle or collapsed globule. The presence of vesicles, which might be formed by free lamellae, is also highly improbable, as the observed heights and diameters of the particles are generally too low to fulfil the space requirements for a collapsed unilamellar vesicle ($h_{Vesicle}$ = 2 x $h_{Janus\ disc}$ > 45 nm). Additionally, all samples were prepared from ultradilute solutions (c = 0.1 mg/L), for which aggregates are extremely improbable. Therefore, single flat Janus particles are

imaged. A further comparison of the section analyses reveals a dependence of the height of the particles on the overall particle size, meaning that the height increases with rising particle diameter. In order to exclude the presence of any scan artefacts, caused by the finite size of the standard SFM tip (R_{apex} = 10 - 20 nm), images were also recorded with an ultra-sharp tip (R_{apex} < 2 nm) but similar height profiles were found.

In order to explain the droplet-like appearance of a part of these particles, one has to consider the sample deposition process and the resulting interfaces. During the deposition of the Janus discs, drying of the solvent takes place and at the end a solvent-swollen disc-like particle is on top of the surface. At all stages of this process the interfacial energy will try to minimize the liquid-air interface and later on, the interface between air and solvent-swollen particle. The most favourable interfacial shape will be that of a droplet. Therefore, in the end of the drying process, the swollen Janus disc adopts the droplet shape, simply to fulfil the energetic conditions of the system. Upon further drying and complete evaporation of the solvent the object is trapped in the droplet-like shape. Hence the structure is kinetically frozen and may not reorient after complete evaporation of the solvent as the thermal energy is insufficient (see Scheme Sup 14 - 1).

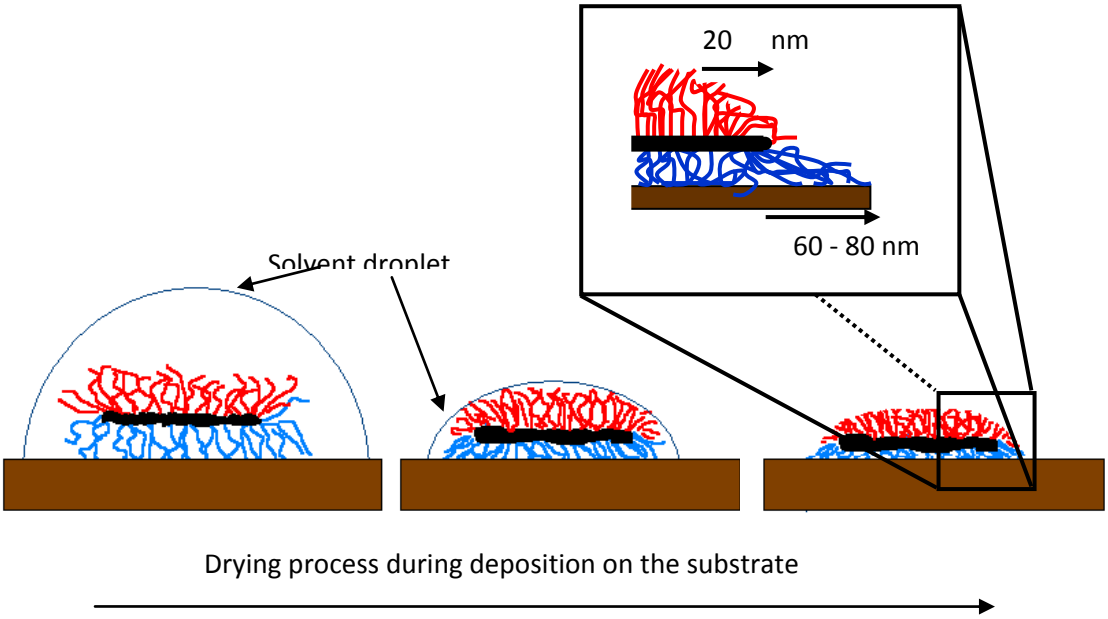

Scheme Sup 14 - 1. Schematic representation of the drying process during deposition of the particles onto the substrate. The red and blue parts indicate PS and P*t*BMA, respectively. The black part corresponds to the inner crosslinked PB layer. The magnified inset displays the expected dimensions of the height increase at an edge of the flat brush-like Janus particle.

This drying mechanism can also account for the observed height dependence of differently sized Janus discs. It is expected that a larger Janus disc causes a larger and thus higher droplet at the end of the drying process, thus explaining the difference in the observed height profiles. It is also important to note that the development of a shape similar to that of a droplet may support the formation of very round and smooth border lines of the particles. Small edges or small protrusions could be hidden, however, for large protrusions this cannot be anticipated.

To minimize the overall interfacial energy of the totally dry system, the pure Janus disc itself (right-hand side in Scheme Sup 14 - 1) also tries to minimize the interfacial area between the upper PS part and air. A smooth edge with a curved and slow increase in the height profile is thus more favourable than a sharp one, which would be expected for such a brush-like flat particle. In conclusion there is a strong energetic competition between the minimization of the interface and the steric repulsion of the brush hairs of the Janus discs. The latter supports a flat orientation with a sharp height increase whereas the former favours a droplet-like appearance.

In order to prove this assumption and to investigate whether the structures are kinetically frozen, substrates with formerly deposited Janus discs were either heated to 150 °C in vacuo or annealed in toluene vapour (90 °C) in order to allow a thermal relaxation of the particles. Both methods should provide enough energy to allow a segmental movement and a reorientation of the structures. The results obtained are presented within the publication (see figure 11 and text).

Cryo-TEM images of very large flat Janus particles at the onset of the sonication

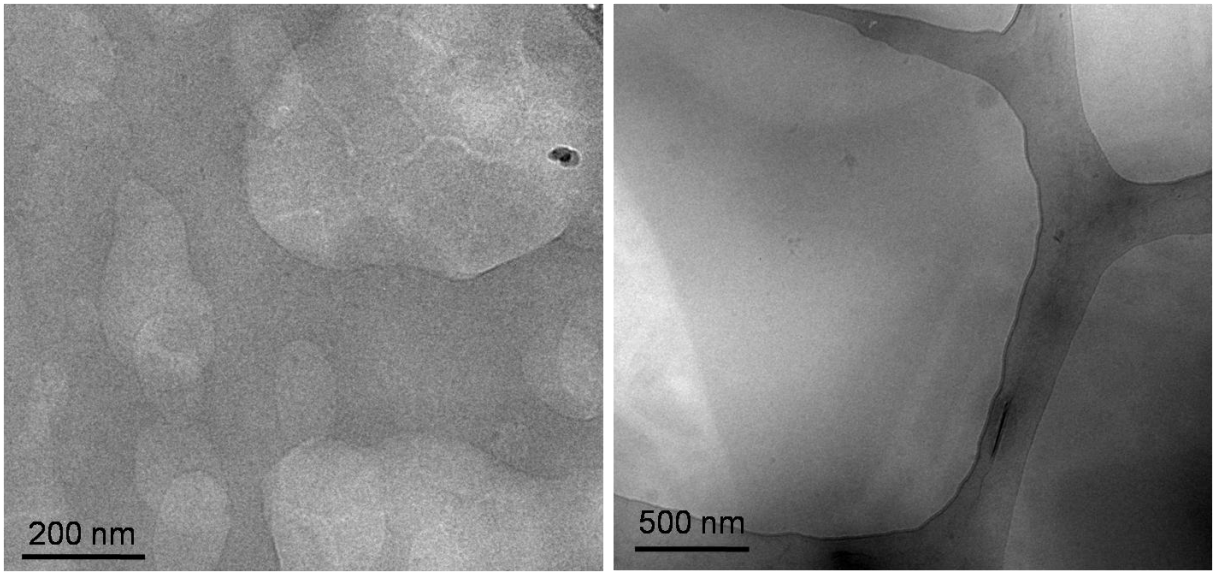

Figure Sup 14 - 4. (a) Cryogenic transmission electron microscopy images of Janus sheets in tetrahydrofuran obtained at the onset of sonication of SBT-2 (left) and SBT-1 (right).

The cryo-TEM image presented on the left above shows a semi-ruptured layer of the crosslinked template, which is characteristic for the beginning of the sonication. At least two layers of the crosslinked template are superimposed onto each other. The image on the right shows a large triangular Janus sheet and some other asymmetric particles on its lower right side (hardly visible). Both samples were filtered prior imaging to remove even larger Janus sheets and some insoluble particles, which can be present at the onset of the homogenization procedure. Similarly semi-ruptured layers and anisometric flat Janus particles cannot be found anymore after prolonged sonication. SFM and cryo-TEM at latter stages show circular particles.

Aggregation of Janus discs into layer-like superstructures via back-to-back stacking

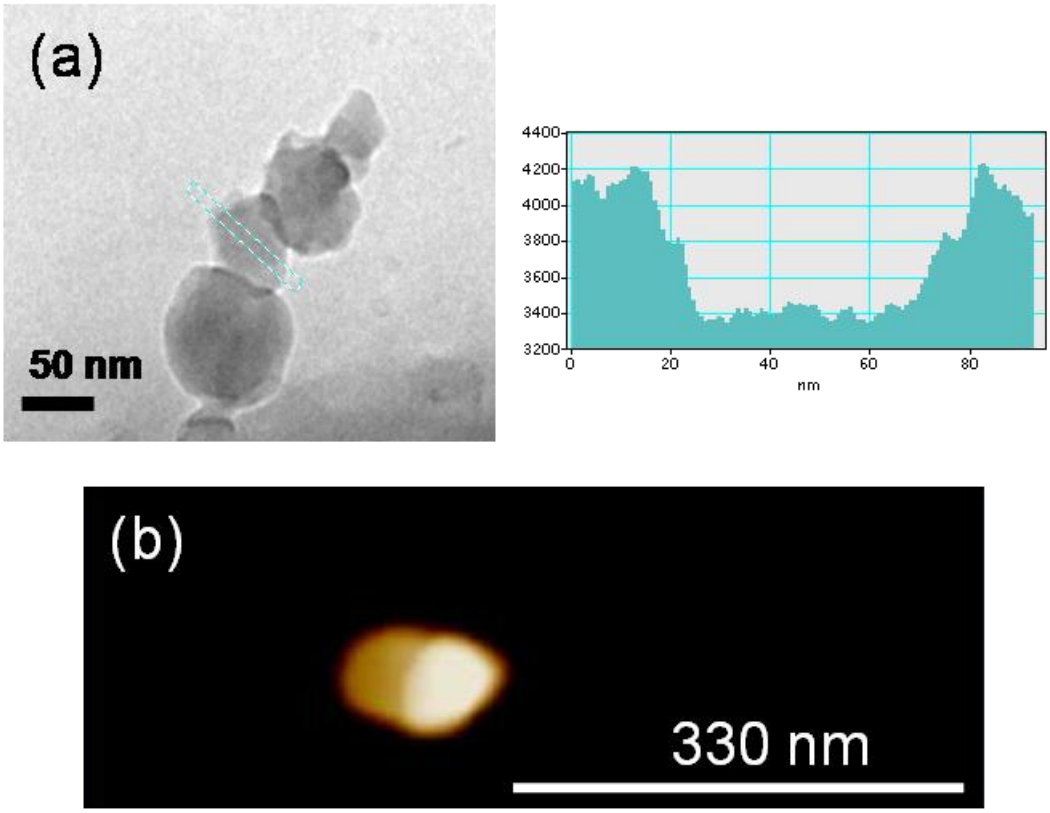

Figure Sup 14 - 5. (a) Cryogenic transmission electron microscopy image of a sample of Janus discs in tetrahydrofuran and its corresponding section analyses. The sample was allowed to equilibrate for several weeks at room temperature before imaging. (b) SFM image of a Janus discs sample (z-scale = 45 nm)

The cryo-TEM image shows the aggregation of several small Janus discs. The only way the assembly and the sticking of the several flat particles can take place is via overlapping of several flat particle sides and back-to-back stacking. The section analysis strongly indicates the presence of two layers and a flat geometry in the inside as can be deduced from the step-like profile at the sides and the flat plateau of the grey-scale analyses, respectively.

The SFM image below exhibits a back-to-back stacked aggregate. A small Janus disc covers one half of a large flat Janus particle below. Note that the observation of back-to-back stacked aggregates via SFM is not straight-forward as deposition can destroy the loose assemblies and as the SFM deposition was usually done at ultrahigh dilution in order to allow a separation of the particles. At these low dilutions the aggregation tendency of the particles is presumably very low.

References

1. Goldacker, T.; Abetz, V.; Stadler, R.; Erukhimovich, I.; Leibler, L., *Nature* **1999,** 398, 137.
2. Auschra, C.; Stadler, R., *Polymer Bulletin* **1993,** 30, 257.
3. Provencher, S. W., *Makromol. Chem.* **1979,** 180, 201.
4. Berne, B. J.; Pecora, R., *Dynamic Light Scattering*. John Wiley & Sons: New York, **1976.**
5. Jacobine, A. F., *Radiation Curing in Polymer Science and Technology*. Elsevier Applied Science: London, 1993; Vol. 3, p 219.

6. Decker, C., *Prog. Polym Sci.* **1996,** 21, 593.
7. Decker, C.; Nguyen Thi Viet, T., *Macromol. Chem. Phys.* **1999,** 200, 1965.
8. Decker, C.; Nguyen Thi Viet, T., *Macromol. Chem. Phys.* **1999,** 200, 358.
9. Decker, C.; Nguyen Thi Viet, T.; Hien Le, X., *Macromol. Symp.* **1996,** 102, 63.

List of Publications

25 **Walther, A.**; Abetz, V; Müller, A. H. E.: Structure-Tunable Bidirectional Hybrid Nanowires Templated by Polymeric Multicompartment Cylinders, *Nat. Nanotech.*, submitted.

24 **Walther, A.**; Drechsler, M.; Abetz, V; Müller, A. H. E.: Self-Assembly of Janus Cylinders into Hierarchical Superstructures, *J. Am. Chem. Soc.*, submitted

23 **Walther, A**.; Müller, A.H.E.: Formation of Hydrophobic Bridges Between Multicompartment Micelles in Water, *Chem. Commun.*, accepted.

22 **Walther, A.**; Drechsler, M.; Müller, A. H. E.: Superstructures of Amphiphilic Janus Discs in Aqueous Medium, *Soft Matter*, in press.

21 **Walther, A**.; Millard, P.-E.; Goldmann, A. S.; Lovesteat, T. M.; Schacher, F.; Barner-Kowollik, C.; Müller, A.H.E.: Bis-Hydrophilic Triblock Terpolymers via RAFT Polymerization: Towards Dynamic Micelles with Tunable Corona Properties, *Macromolecules*, in press.

20 Uchman, M.; Prochazka, K.; Stepanek, M.; Mountrichas, G.; Pispas, S.; Spirkova, M; Walther, A.: pH-Dependent Self-Assembly of Polystyrene-block-Poly((sulfamatecarboxylate)isoprene) Copolymer in Aqueous Media, Langmuir 24, 12017 **(2008)**

19 Pfaff, A.; **Walther, A.**; Lu, Y.; Wittemann, A.; Ballauff, M.; Müller, A.H.E.: Spherical Glycopolymer Brushes, *Polym. Mater. Sci. Eng.* 49, 604 **(2008)**

18 Yuan, J.; Xu, Y.; **Walther, A.**; Bolisetty, S.; Schumacher, M.; Schmalz, H.; Ballauff, M.; Müller, A.H.E.: Water-Soluble Organo-Silica Hybrid Nanowires, *Nat. Mater.*, 7, 718 **(2008)**

17 Retsch, M.; **Walther, A.**; Loos, K.; Müller, A.H.E.: Synthesis of Dense Poly(acrylic acid) brushes and Their Interaction with Amine-Functional Silsesquioxane Nanoparticles, *Langmuir* 24, 9421 **(2008)**

16 **Walther, A**.; André, X.; Göldel, A.; Abetz, V.; Müller, A.H.E.: Controlled Crosslinking of Polybutadiene Containing Terpolymer Templates: A Facile Way towards Complex and Functional Nanostructures, *Polymer* 49, 3217 **(2008)**

15 **Walther, A.**, K. Matussek, Müller, A.H.E.: Engineering Nanostructured Polymer Blends with Controlled Nanoparticle Location using Janus Particles, *ACS Nano,* 2, 1167 **(2008)**

14 **Walther, A.**; Goldmann, A.; Yelamanchili, R.S.; Drechsler, M.; Schmalz, H.; Eisenberg, A.; Müller, A.H.E.: Multiple Morphologies, Phase Transitions and Crosslinking of Crew-Cut Aggregates of Polybutadiene-*block*-Poly(2-vinylpyridine) Diblock Copolymers, *Macromolecules,* 41, 3254 **(2008)**

13 Schmalz, H.; Schmelz, J.; Drechsler, M.; Yuan, J.; **Walther, A.**; Schweimer, K.; Mihut, A. Thermo-Reversible Formation of Wormlike Micelles with a Microphase-Separated Corona from a Semicrystalline Triblock Terpolymer, *Macromolecules*, 41, 3235 **(2008)**

12 **Walther, A**; Müller, A.H.E.: Janus Particles (invited Highlight article), *Soft Matter*, 4, 663 **(2008)**

11 **Walther, A**; Hoffmann, M.; Müller, A.H.E.: Emulsion Polymerization Using Janus Particles as Stabilizers, *Angew. Chem. Int. Ed.* 47, 711 **(2008)**

10 Yelamanchili, R.S.; **Walther, A.**; Müller, A.H.E.; Breu, J.: Core-crosslinked Block Copolymer Nanorods as Templates for Grafting $[SiMo_{12}O_{40}]^{4-}$ Keggin Ions, *Chem. Commun.*, 489 **(2008)**

9 **Walther, A.**; André, X.; Drechsler, M.; Abetz, V.; Müller, A. H. E., Janus Discs, *J. Am. Chem. Soc.*, 129, 6187 **(2007)**

8 Xu, Y.; Becker, H.; Yuan, J.; Burkhardt, M.; Zhang, Y.; **Walther, A**; Bolisetty, S.; Ballauff, M.; Müller, A.H.E.: Double-Grafted Cylindrical Brushes: Synthesis and Characterization of Poly(lauryl methacrylate) Brushes, *Macromol. Chem. Phys.* 208, 1666 **(2007)**

7 Retsch, M.; **Walther, A.**; Loos, K.; Müller, A.H.E.: Synthesis Of Controlled Layers Of Poly(Acrylic Acid) And Their Interaction With Aminofunctional Silsesquioxane Nanoparticles, *Polym. Prepr.,* 48, 795 **(2007)**

6 Schacher, F.; **Walther, A.**; Ruppel, M.; Müller, A.H.E.: Multicompartment Micelles from ABC Triblock Terpolymers, *Polym. Mater. Sci. Eng.* 96, 94 **(2007)**

5 **Walther, A**; André, X.; Drechsler, M.; Abetz, V.; Müller, A.H.E.: Janus Discs: Preparation, Size-Tunability, Visualization, Self-Assembly, *Polym. Mater. Sci. Eng.* 96, 86 **(2007)**

4 Plamper, F.A.; **Walther, A.**; Müller, A.H.E.; Ballauff, M.: Nanoblossoms: Light-Induced Conformational Changes of Cationic Polyelectrolyte Stars in Presence of Multivalent Counterions, *Nano Letters* 7, 167 **(2007)**

3 Voets, I. K.; de Keizer, A.; de Waard, P.; Frederik, P. M.; Bomans P. H. H.; Schmalz, H.; **Walther, A.**; King, S. M.; Leermakers, F. A. M.; Cohen Stuart, M. A.: Double-Faced micelles from water-soluble polymers, *Angew. Chem. Int. Ed.*, 45, 6673 **(2006)**

2 Müller, A.H.E.; **Walther, A.**; Zhang, M.; Mori, H.: Synthesis of Highly Branched Polyelectrolytes and Silica/Polyelectrolyte Hybrids Nanoparticles, *Polym. Mater. Sci. Eng.* 90, 262 **(2004)**

1 Mori, H.; **Walther, A.**; André, X.; Lanzendörfer, M. G.; Müller, A.H.E.: Synthesis of highly branched cationic polyelectrolytes via Self-Condensing Atom Transfer Radical Copolymerization with 2-(Diethylamino)ethyl methacrylate*, Macromolecules*, 37, 2054 **(2004)**

Acknowledgments

First and foremost I would like to thank my supervisor Axel Müller. The relationship between supervisor and student is one of the primary factors influencing a fruitful and enjoyable PhD. Indeed, I have had a great and very productive time throughout the last years. I am particularly grateful to all the opportunities I have been offered. Presenting my work at numerous national and international conferences, having the possibility of spending time overseas and being able to cooperate with a number of groups have been a great experience and enriched my personality and my scientific skills. I owe deep gratitude to Axel Müller for his confidence in letting me develop many projects independently with just as little guidance as necessary. This has helped me a big deal in exploring many different fields of science.

Many thanks go out to the MC^2 group and people from other chairs at Uni Bayreuth who have helped me making this dissertation become reality. The open and direct support from many sides was an enormous help for the fast progress of my PhD. Only the willingness to help and to invest their own time and knowledge into my projects assured the arising publications to be of highest quality. In particular, I want to thank the people who were directly involved, including Xavier Andre, Sabine Wunder, Anja Goldmann, Jiayin Yuan, Markus Ruppel, Kristian Schweimer, Markus Drechsler, Clarissa Abetz, Astrid Göldel, Kerstin Matussek, Benjamin Gössler, Michael Sommer, Pierre Millard, Felix Schacher, Holger Schmalz, Evis Penott-Chang, Sreenath Bolisetty, Nicole Popp, Felix Plamper, Youyong Xu, Sergey Nosov, Manuela Schumacher, Denise Danz, Susanne Erdinger. A special thank you goes to Annette, whose help and actions appear invisible, but actually have a tremendous effect on keeping the lab running. I am also particularly grateful to Gaby Oliver for steering me through the dark regions of university bureaucracy and all the little help here and there.

I would also like thank the various undergraduate students, Martin Hoffman, Andrea Wolf, Thomas Ruhland, Thomas Lunkenbein and Sylvain Catrouillet, who have worked on several individual projects with me. I have benefited from their helping hands and reliable work.

During the past 2.5 years I have profited from various discussions with several scientists. In particular, I would like to thank Volker Abetz, whose comments on manuscripts and research were always very helpful and inspiring. I am also indebted to Ilja Voets, Christopher Barner-Kowollik, Alexander Böker, Matthias Ballauf, Robert Gilbert, Ed Kramer and Bernie Binks for several supportive discussions.

Thanks to Ram Sai Yelamanchili and Josef Breu for collaborating closely on a joint research project. This project helped me to broaden my knowledge of inorganic chemistry.

For the duration of three months, I had the opportunity to perform research at the University of New South Wales in the Centre for Advanced Macromolecular Design (CAMD) in Sydney, Australia. Many thanks go to Christopher Barner-Kowollik, Leonie Barner, Istvan Jacenyik and Tom Davis for hosting me there and organizing this trip. I had an enjoyable and memorable time downunder and was able to get insights into new topics and learned quite some new techniques. In particular I want to mention Raymond Joso, Karina Heredia, Andrew Ah Toy, Tara Lovestead, Till Brüning and Maribel Hernandez-Guerrero, who all contributed to making this stay to such a great memory.

For financial support thank you to the Deutsche Forschungsgemeinschaft (DFG) within the SONS and BIOSONS projects and the European Science Foundation for funding the Marie Curie Research and Training Network “Polyamphi” (MC-RTN Polyamphi). I am also indebted to the Bavarian State for providing me with a fellowship according to the Bavarian Elite Support Program.

Most importantly, thank you to my family for the endless support and helping me to get where I am now. I truly appreciate everything you did, without your help this way would have been much more difficult to go.

Erklärung

Die vorliegende Arbeit wurde von mir selbstständig verfasst und ich habe keine anderen als die angegebenen Hilfsmittel benutzt.

Ferner habe ich nicht versucht, anderweitig mit oder ohne Erfolg eine Dissertation einzureichen oder mich der Doktorprüfung zu unterziehen

Bayreuth, den 30.06.2008

(Andreas Walther)